Investigation into the Nature and Ageing of Tapestry Materials

A thesis submitted to The University of Manchester for the degree of
Doctor of Philosophy
in the Faculty of Engineering and Physical Sciences

2006

Anne-Marei Hacke

School of Materials

Th 26747

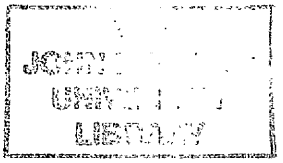

Contents

Abstract **5**
Declaration 6
Copyright Statement 7
Dedication 8
Acknowledgements 9

Chapter 1. Introduction **10**
1.1. MODHT project 10
1.2. Objectives 11
1.2.1. Analysis of natural dyestuffs 11
1.2.2. Analysis of wool and silk 11
1.2.3. Analysis of metal threads 12
1.3. History of tapestries 13
1.4. References 14

Chapter 2. Analytical Methods **19**
2.1. Scanning Electron Microscopy (SEM), Field Emission Gun SEM (FEG-SEM) and Energy Dispersive X-ray Microanalysis (EDX) 19
2.1.1. SEM 19
2.1.2. FEG-SEM 20
2.1.3. EDX 21
2.2. X-ray Photoelectron Spectroscopy (XPS) 21
2.3. Time of Flight Secondary Ion Mass Spectrometry (ToF-SIMS) 24
2.4. X-ray Diffraction (XRD) 26
2.5. References 28

Chapter 3. Historic Samples and Preparation of Models **29**
3.1. Historic tapestry samples: wool, silk and metal threads 29
3.1.1. Patrimonio Nacional Madrid 30
3.1.2. Tournai, Bruges and Brussels 32
3.1.3. Hampton Court Palace 34
3.2. Model tapestry samples 35
3.2.1. Selection of wool and silk yarns 35
3.2.2. Mordanting and dyeing 35
3.2.3. Weaving 43
3.2.4. Accelerated ageing 43
3.3. Model metal thread samples 44
3.4. References 45

Chapter 4. Analysis of Dyestuffs **46**
4.1. Literature review on the classification of natural dyestuffs 46
4.1.1. Anthraquinones 47
4.1.2. Indigoids 47
4.1.3. Flavonoids 48
4.1.4. Neoflavanoids 48
4.1.5. Gallotannins 49
4.2. Literature review on methods for the identification of natural dyestuffs 50
4.2.1. Chemical methods 50
4.2.2. Chromatographic methods 50
4.2.3. Spectroscopic methods 52
4.2.4. Non-Extractive Analysis 53
4.3. Potential of ToF-SIMS for dyestuff identification 54
4.4. Experimental 56
4.4.1. Preparation of dyestuff solutions 57

4.4.2. Mounting of samples and ToF-SIMS analysis conditions 57
4.5. Results 59
4.5.1. Investigation of madder 59
4.5.2. Investigation of cochineal 64
4.5.3. Investigation of brazilwood 66
4.5.4. Investigation of dyer's greenweed 68
4.5.5. Investigation of weld 71
4.5.6. Investigation of young fustic 74
4.5.7. Investigation of oak gall 77
4.5.8. Investigation of alder bark 80
4.5.9. Investigation of indigoids: woad and 6,6'-dibromoindigo 81
4.6. Discussion 85
4.7. Conclusions 87
4.8. References 88

Chapter 5. Analysis of Wool and Silk 92
5.1. Literature review for wool 92
5.1.1. Structure and chemical composition of wool 92
5.1.2. Photochemistry of wool 103
5.1.3. XPS studies of wool 109
5.1.4. SIMS studies of wool 112
5.2. Literature review for silk 114
5.2.1. Structure and chemical composition of silk 114
5.2.2. Photochemistry of silk 116
5.2.3. XPS and SIMS studies of silk 120
5.2.4. The influence of weighting and mordanting on silk and wool 120
5.3. Experimental 123
5.3.1. Tensile strength tests: yarns 123
5.3.2. Tensile strength tests: single fibres 123
5.3.3. Fibre diameter measurements 124
5.3.4. SEM 124
5.3.5. XPS 125
5.3.6. ToF-SIMS 126
5.4. Results and discussion 127
5.4.1. Tensile strength tests: yarns 129
5.4.2. Tensile strength tests: single fibres 142
5.4.3. SEM investigation of fibre surfaces and fracture morphology: wool 146
5.4.4. SEM investigation of fibre surfaces and fracture morphology: silk 156
5.4.5. Investigation of fibre surface chemistry using XPS 161
5.4.6. XPS analysis of wool 162
5.4.7. XPS of wool: interpretation of the C(1s) peak shape 163
5.4.8. XPS of wool: interpretation of the C/O and C/N ratios 169
5.4.9. XPS of wool: interpretation of the N/S and C/S ratios 173
5.4.10. XPS of wool: interpretation of the S(2p) peak shape 174
5.4.11. XPS analysis of silk 177
5.4.12. Investigation if fibre surface chemistry using ToF-SIMS 178
5.4.13. Interpretation of the positive ion ToF-SIMS spectra 178
5.4.14. Interpretation of the negative ion ToF-SIMS spectra 182
5.5. Conclusions 190
5.6. References 193

Chapter 6. Analysis of Metal Threads 201
6.1. Literature review for metal threads 201

6.1.1. Introduction to composition and manufacture of metal threads 201
6.1.2. 'Beaten and Cut' metal threads 202
6.1.3. 'Membrane' metal threads 204
6.1.4. 'Cast, Drawn and Rolled' metal threads 206
6.1.5. Spinning gold 206
6.1.6. Double and triple wrapped metal threads 209
6.1.7. Alloying and gilding methods for metal threads 209
6.1.8. Deterioration and corrosion of metal threads 214
6.1.9. Cleaning of metal threads 218
6.1.10. SEM/EDX studies of metal threads 218
6.2. Experimental 221
6.2.1. Imaging of metal threads 221
6.2.2. Accelerated tarnishing: Oddy tests 221
6.2.3. Detergent treatments 222
6.2.4. Embedding 223
6.2.5. SEM, FEG-SEM and EDX 224
6.2.6. XPS 225
6.2.7. SIMS 226
6.2.8. XRD 227
6.3. Results and discussion 228
6.3.1. Metal thread images and classification 228
6.3.2. Manufacturing techniques 233
6.3.3. Investigation of metal thread corrosion by SEM/EDX 245
6.3.4. Investigation of metal thread corrosion by XPS 249
6.3.5. Investigation of metal thread corrosion by Dynamic SIMS 254
6.3.6. Investigation of metal thread corrosion by XRD 256
6.3.7. Investigation of Oddy test coupons corrosion by SEM/EDX, XPS and XRD 257
6.3.8. Investigation of detergent residues on metals 265
6.4. Conclusions 277
6.5. References 280

Summary **285**

Further Work **288**

Appendices

Appendix to Chapter 4. Analysis of dyestuffs
A. ToF-SIMS spectra of Dyestuffs 289
A.1. Madder 289
A.2. Cochineal 295
A.3. Brazilwood 297
A.4. Dyer's Greenweed 297
A.5. Weld 303
A.6. Young fustic 305
A.7. Oak gall 306
A.8. Alder bark 308
A.9. Woad 309

Appendix to Chapter 5. Analysis of Wool and Silk
B. XPS data of unaged wool 312
B.1. Atomic % and ratios of unaged wool 312
B.2. Relative % of C(1s) peak components and component ratios of unaged wool 314

B.3. Relative % of S(2p) peak components of unaged wool 315
C. XPS data of accelerated aged wool 316
C.1. Atomic % and ratios of accelerated aged wool 316
C.2. Relative % of C(1s) peak components and component ratios of accelerated aged wool 319
C.3. Relative % of S(2p) peak components of accelerated aged wool 320
D. XPS data of historic wool 321
D.1. Atomic % and ratios of historic wool 321
D.2. Relative % of C(1s) peak components and component ratios of historic wool 324
D.3. Relative % of S(2p) peak components of historic wool 325
E. ToF-SIMS spectra of wool 326
E.1. Spectra acquired with a Cs^+ primary ion source 326
E.2. Spectra acquired with a Bi_3^+ primary ion source 342

Appendix to Chapter 6. Analysis of Metal Threads
F. Images of double and triple wrapped metal threads 352
F.1. Double wrapped threads 352
F.2. Triple wrapped threads 353
G. EDX data of metal threads 354
H. Positive dynamic SIMS depth profiles of metal threads 365
H.1. HCP_68E6 exterior 365
H.2. HCP_68E6 interior 365
H.3. HCP_120C3 exterior 366
H.4. HCP_120C3 interior 366
H.5. PNM1_38 exterior 367
H.6. PNM1_38 interior 367
H.7. PNM2_19 exterior 368
H.8. PNM5_24 exterior 368
H.9. BXL2_15 exterior 369
I. XRD patterns of metal threads 370
I.1. HCP_21G3 370
I.2. PNM1_21 370
I.3. PNM2_04 370
I.4. BXL2_11 370
J. XPS data of Oddy tested Ag and Cu coupons 371
J.1. Atomic % of light Oddy tested Ag coupons 371
J.2. Atomic % of light Oddy tested Cu coupons 371
J.3. Atomic % of thermal Oddy tested Ag coupons 372
J.4. Atomic % of thermal Oddy tested Cu coupons 372
J.5. Relative % of S(2p) peak component of light Oddy tested Ag and Cu coupons 373
J.6. Relative % of S(2p) peak component of thermal Oddy tested Ag and Cu coupons 373
K. ToF-SIMS spectra of detergent treated metal coupons and metal threads 374
K.1. ToF-SIMS spectra of silver coupons 374
K.2. ToF-SIMS spectra of copper coupons 379
K.3. ToF-SIMS spectra of metal threads 385

Word count: 83716
(including main text tables and figures but excluding appendices)

Abstract

The study and conservation of tapestries are of vital importance to the preservation of our heritage. Colour fading and metal thread tarnishing are the most obvious signs of tapestry deterioration, yet the degradational processes affecting the tensile properties of the fibres are the determining factors for the lifetime of a tapestry on vertical display. In 2002 an international project on the Monitoring of Damage in Historic Tapestries (MODHT), funded by the European Union, was set up with the overall objective of investigating and evaluating fibre damage with minimum impact, as described in Chapter 1. The work for this thesis was conducted within the context of the MODHT project and included studies on natural dyestuffs, wool and silk fibres and metal threads.

Samples of historic tapestries, dating from the early 15^{th} to the 17^{th} centuries, were studied along with model tapestry fabrics produced to mimic historic tapestries in terms of dye sources, dyeing recipes, wool and silk yarn specifications and fabric structure, detailed in Chapter 2.

The analytical techniques utilised in this thesis are described in Chapter 3 and comprised Scanning Electron Microscopy (SEM) with Energy Dispersive X-ray microanalysis (EDX), X-ray Photoelectron Spectroscopy (XPS), Time of Flight Secondary Ion Mass Spectrometry (ToF-SIMS) and X-ray Diffraction (XRD).

Chapter 4 investigates the applicability of a non-extractive method, ToF-SIMS, for the identification of natural dyes and highlights the potentials and drawbacks of the technique. The analyses were generally successful for dried films of dyebaths and dyes on a paper substrate but less so for dyed textile fibres.

The complex influences of dyeing processes and accelerated ageing, as well as natural ageing, on the mechanical properties, fibre morphologies and surface chemistry of wool and silk were studied, Chapter 5. Particularly interesting results involved the degradative versus protective effects of metal ions and the assessment of the extent of surface sulphur oxidation on wool as a potential marker of damage with direct implications for tensile properties.

Chapter 6 focuses on metal thread classification, composition and corrosion. Additional studies dealt with the influence of wool and silk deterioration on corrosion formation and the adsorption of detergents on metals. Documentation established a variety of extremely rare and intricate metal threads with double and triple layers of silver and silvergilt filaments. New evidence was produced for a combination of rolling and cutting during the manufacture and, for the first time, leaf gilding was unambiguously identified in metal threads.

Declaration

No portion of the work referred to in this thesis has been submitted in support of an application for another degree of qualification of this or any other university or other institute of learning.

Anne-Marei Hacke
March 2006

Copyright Statement

Für Klerma

Acknowledgements

I am indebted to Professor Chris Carr for his continuous support and guidance and I am especially thankful for his inexhaustible enthusiasm in supervising my work.

I am grateful to the European Commission for funding the Monitoring of Damage in Historic Tapestries (MODHT) project under the Fifth Framework Programme, Energy, Environment and Sustainable Development, The City of Tomorrow and Cultural Heritage.

I would like to thank the MODHT team for a successful project and enjoyable meetings in Brussels, Madrid, Hampton Court, Edinburgh, London and Manchester. In particular I would like to thank David Howell, Kathryn Hallett, Anita Quye, David Peggie, Dr Alison Hulme, Professor Hamish McNab, Jan Wouters, Ina Vanden Berghe, Vera Vereecken, Ingrid de Meûter, Dr Marianne Odlyha, Dr Concha Carretero Herrero and Gwynfor Hughes.

I want to express my gratitude to John Edmonds for woad dyings, Bill Barnes for manufacturing gilt threads, Hew Prendergast for chopping alder bark on Christmas day, Dr Karen Finch for allowing me to quote her unpublished translations of Sofus Larsen, Dr Márta Járo and Mary Ballard for fruitful discussions, John Ashton for enabling me to attend a conference in Canberra, Dr Alan Brown, Rob Mitchell and Dr Jean Claude Canry from CSMA Ltd. for SIMS analyses and Neal Fairly for writing CasaXPS and making changes to the software on individual request.

This project could not have been completed without the School of Material's academic, technical and administrative staff and I am particularly grateful for the help I received from Phil Cohen for dyeing, Les Downes for weaving, Trevor Jones for SEM/EDX, Adrian Handley for tensile testing, Dr Chris Wilkins for embedding and cross-sectioning wool and silk, Neil Wardman for embedding and polishing metal thread sections, Michael Faulkner for FEG-SEM, John Walton and Dr Morgan Alexander for XPS, Judith Shackleton for XRD, Simon Williams for looking after my computer, Alison Harvey for FTIR, Dr Jane Batcheller for microscopy and helpful discussions, Christine Craig and Pat Groocock for being organised.

I would like to thank all inhabitants of E-floor, in particular Dion, Shinee, Raimundo, Dharma and Anu for enjoyable tea breaks, lunches and parties.

For their unwavering encouragement and love I wish to thank my family Klaus, Herma, Mila and Bernard, my great friend Paola, and the love of my life Steve.

Chapter 1. Introduction

1.1. MODHT project

Monitoring of Damage in Historic Tapestries (MODHT) was a European project involving the collaboration of curators and conservators, conservation scientists, analytical and textile chemists from different backgrounds and institutions ranging from museums and historic palaces to universities.

Tapestries are among the most valuable cultural heritage in Europe and over the centuries extensive collections have been preserved in varying degrees of physical condition. Tapestries that have been on display, sometimes for several hundred years, will have suffered from obvious colour fading but may seem to have maintained their physical integrity. Yet, unnoticed loss of fibre and fabric strength, due to photodegradation, may lead to structural failure, particularly when these tapestries are removed for cleaning or exhibition. Atmospheric pollutants and climatic influences such as heat and humidity may also affect the fabric.

It is widely accepted that light is the major cause of the degradation in most textile fibres [1]. The main objective of the MODHT project was to establish the nature of the damage in aged tapestry materials and to develop microanalytical techniques to study the tapestry material with minimum impact. Gaining an understanding of the chemical and physical processes involved may aid the prevention of future damage and lead to better conservation methods.

Model tapestries, dyed and woven with the appropriate material and representing historic techniques, were accelerated aged and the degradational changes at the molecular- and macro-levels analysed. Samples from original tapestries from selected European sites were subjected to equivalent analyses and the results compared. By linking this information it was hoped to establish a sensitive system for the objective evaluation of the degradational condition of historic tapestries.

The MODHT project started in April 2002 and was concluded with a conference at Hampton Court Palace held in June 2005. The project was funded by the European Commission under the Fifth Framework Programme, Energy, Environment and Sustainable Development, The City of Tomorrow and Cultural Heritage. The partners were Historic Royal Palaces (HRP), UK; National Museums

of Scotland (NMS), UK; Patrimonio Nacional (PNM), Spain; Konigliches Institut voor het Kunstpatrimonium / Royal Institute for Cultural Heritage (KIK), Belgium; University of Edinburgh (UoE), UK; University of London, Birkbeck College (BBK), UK and University of Manchester (UoM), UK.

Throughout the MODHT project's duration all partners have widely publicised their work in conferences, papers and books [2-27] and as presentations, lectures and seminars [28-37].

1.2. Objectives

Research for this thesis was conducted within the context of the MODHT project and focused on three main areas in particular the analysis of natural dyestuffs, the surface analysis of wool and silk fibres and the general analysis of metal threads.

1.2.1. Analysis of natural dyestuffs

In conservation science various spectroscopic and chromatographic analytical methods are routinely used for the identification of natural dyestuffs on a textile substrate [38]. A shortcoming of almost all techniques is the need for dyestuff extraction prior to analysis. This often requires a relatively large amount of material, which can prove a problem in conservation science when only minute samples are available for analysis. Extraction of dyes from textile fibres can also cause the partial destruction of the dye molecule again complicating identification.

Time of Flight Secondary Ion Mass Spectrometry (ToF-SIMS) is a well suited technique for the analysis of solids, hence eliminating the need for extraction. The identification of natural dyestuffs is a relatively novel application for ToF-SIMS and has not received much attention in conservation science.

This study investigated the applicability of ToF-SIMS for the identification of the colourant components in a range of natural dyes, analogous synthetic chromophores, dyes in solution and dyes on a paper or textile substrate.

1.2.2. Analysis of wool and silk

Historic tapestries are usually significantly faded, but this visual degradation is not the only indicator of ageing [12, 39]. The yarns can lose their mechanical strength to the point where the whole tapestry structure is in danger of disintegration [39].

The extent of fibre degradation is not easy to determine, and sometimes a tapestry that has seemingly maintained its mechanical integrity will crumble under the hands of conservators when taken off the wall. Silk fibres can deteriorate to powder and embrittled wool will break when touched. However, some tapestries of the same age as others that have fallen beyond repair are still in very good condition, demonstrating that assessment of degradational state based on age is not sufficient. Light, humidity and temperature, as well as the textile's history such as washing, handling, storage and display would all have to be taken into account to predict degradation; but to establish and distinguish all these parameters is not usually possible for historic materials. Therefore the MODHT project endeavoured to establish an objective method of assessing the degradational state of historic textile fibres by analytical methods.

In this study the surface chemistry of wool was investigated by X-ray Photoelectron Spectroscopy (XPS) and ToF-SIMS in order to assess the oxidative influences of dyeing procedures and accelerated light ageing. Scanning Electron Microscopy (SEM) visualises structural physical damage of model and historic samples. The results of surface chemical analyses were correlated to tensile strength measurements, as damage at a materials' surface is often the greatest and surface analysis may be a sensitive indicator of overall damage.

1.2.3. Analysis of metal threads

Metal threads in tapestries typically consist of a silver gilt filament wrapped around a silk core [3]. These precious threads were only used in tapestries of the highest quality and the individual threads' fineness and intricacy of structure is intriguing. Sadly today the tarnishing of the metals often blemishes the tapestries' appearance. The influences of the fibrous materials contained in a tapestry on the corrosion of metal threads has not been elucidated and little is known about metal thread manufacturing routes and trade despite the dedication of many publications in conservation science to the study of metal threads [40-42].

However, never before has it been possible to assess such a large quantity of metal threads of similar age and application as in the MODHT project. Nearly 200 samples have been obtained from five different tapestries from three locations in Europe. Although the tapestries were all woven in Belgium during the 16th century the metal threads display a range of structural and degradational differences.

Optical microscopy, Scanning Electron Microscopy / Energy Dispersive X-Ray Microanalysis (SEM/EDX) and Field Emission Gun SEM (FEG-SEM) as well as Dynamic SIMS were utilized for the assessment of dimensional features and alloy composition with the aim of shedding light on the historic manufacturing techniques.

Corrosion products were analysed by SEM/EDX, XPS and X-ray Diffraction (XRD) and compared to accelerated tarnishing tests, which aimed to establish whether the breakdown of differently dyed wool and silk influenced the formation and chemistry of corrosion compounds.

1.3. History of tapestries

The making of tapestry is one of the oldest arts and crafts [43-47]. Figurative textiles found in Egypt date back to as early as 1400 BC. There is evidence that pictorial weaving has been practiced since the antiquity and tapestry making has spread from the East with the crusaders. However, tapestry making in Europe had its climax during the Byzantine to Rococo period, with those tapestries manufactured in the Renaissance usually being regarded as the most beautiful.

From the 15th to the early 17th century the capital of tapestry making was Brussels and its surrounding towns in Flanders. Here the most prominent master weavers and tapestry designers had their workshops. In the middle of the 15th century there were at least fifty master weavers, employing around two thousand people, some as specialists head-makers, arms- and legs-makers or landscape workers, not counting the many children, engaged to do the work, which only tiny hands could do. At that time tapestry making was the town's main industry. In order to control and assure the quality of Flemish gobelins, the tapestry maker's guild in Flanders set up rules and regulations; and in 1528 the town of Brussels introduced a trade-mark [45]. Every tapestry leaving the workshop at Brussels had to be provided with a red shield flanked by two letters B, standing for Brabant – Brussels. Each master weaver was also required to weave his individual mark into the bottom border. This rule was not always followed, which today makes it difficult to identify and differentiate the masters.

The main difference to typical weaving constructions is that the pattern is entirely made up by weft threads, leaving the warp merely as support structure. The weft yarns do not cover the whole width of the fabric but just the pattern area; so that slits occur at colour changes parallel to the warp [46]. The two main techniques used for tapestry manufacture differ in the direction of the warp threads on the machine. The haute-lisse loom, Figure 1.3.1, has vertical warp threads onto which the design outlines and colour changes are traced. By pulling on overhead leashes (French lisse), i.e. strings with loops attached to each warp yarn, the weaver opens the shed through which the pointed bobbin with the coloured weft thread is passed. The work has to be done from the back of the tapestry, but the weaver can step in front of the loom and see how his work is progressing. This is not possible for the other common technique – the weaving on a basse lisse loom, Figure 1.3.1. Here the warp yarns are horizontal and the design cartoon is placed underneath. Foot pedals control the shedding and the weaver can use both hands for inserting the weft, which makes the process faster. When the weaving is completed, the last step is sewing up the loose yarn ends and the slits to give more strength to the fabric structure.

The high warp yarn tension during weaving causes shrinkage when taking the tapestry off the loom. The effect of shrinkage on the design, especially on figures, is less disturbing in horizontal direction than in vertical direction. Therefore it is advantageous that most large-scale tapestries are in a landscape format, so that the warp direction is horizontal to the picture plane.

Figure 1.3.1. Haute Lisse Loom [43]

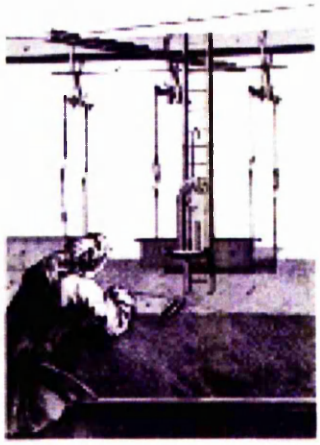

Basse Lisse loom [43]

Originally the colour-scale of tapestries was fairly limited to red, blue, yellow and green, with just a few shades in each colour. The Gothic tapestries did not have any intermittent shades at all and the Renaissance tapestries of Brussels were the first to show pink, mauve and very light blue. In the 15th and 16th century the French and the Flemish weavers perfected the "hachures" technique, which enabled the blending of colours by interlinking the different coloured yarns, so a wide range of colours, shades and blends became possible. Flemish Renaissance gobelins are often rich in gold and silver threads, especially those designed by Bernard van Orley [44]. The base material was almost always wool, which for best quality was imported from England. Wool was allowed to be dyed in the country, often in Arras, though not by the weaver himself but by master dyers [45]. Dyeing in black, which could only be done with iron-oxide was strictly forbidden, because it caused quick decay of the material. It had to be replaced by dark brown or dark blue. Silk was mainly imported from Italy or Spain and also dyed in Spain, while metallic threads often came from Italy or Cyprus [47]. It was not permitted to paint on or embroider in details (e.g. faces) as that was regarded as cheating. The guild carried out regular controls; for example in 1539 a large quantity of tapestries belonging to Willem de Kempeneer, a prominent master-weaver of Brussels was considered of an inferior quality. They were confiscated and de Kempeneer had to pay a fine.

Painters delivered the designs that were reproduced by kartonniers, who brought it to full-scale size and transformed every detail, so it could be used as a model cartoon for weaving. According to Carel van Mander, the most famous tapestry designers in the early 16th century were Bernard van Orley, Pieter Coeck van Aelst, Jan Cornelisz and Vermeyen van Beverwijk. The most renowned weavers were Pieter de Pannemaker and also Willem de Kempeneer, both situated in Brussels. [43-45, 47]

1.4. References

1. Tímár-Balázsy, Á. and D. Eastop, *Chemical Principles of Textile Conservation*, Butterworth-Heinemann (1998) 16-19.
2. Ferreira, E.S.B., A.N. Hulme, H. McNab, and A. Quye, 'The Natural Constituents of Historical Textiles Dyes', *Chemical Society Reviews* **33** (2004) 329-336.
3. Hacke, A.M., C.M. Carr, A. Brown, and D. Howell, 'Investigation into the Nature of Metal Threads in a Renaissance Tapestry and the Cleaning of Tarnished Silver by UV/Ozone (UVO) Treatment', *Journal of Materials Science* **38** (2003) 3307-3314.
4. Hacke, A.M., C.M. Carr, and A. Brown, 'Characterisation of Metal Threads in Renaissance Tapestries', in *Scientific Analysis of Ancient and Historic Textiles: Informing Preservation, Display and Interpretation. AHRB Research Centre for Textile Conservation and Textile Studies First Annual Conference*, Textile Conservation Centre, Winchester Campus, University of Southampton, UK, 13-15 July 2004, ed. R. Janaway and P. Wyeth, Archetype Publications, 71-78.
5. Hallett, K. and D. Howell, 'Size Exclusion Chromatography as a Tool for Monitoring Silk Degradation in Historic Tapestries', in *Scientific Analysis of Ancient and Historic Textiles: Informing Preservation, Display and Interpretation. AHRB Research Centre for Textile Conservation and Textile Studies First Annual Conference*, Textile Conservation Centre, Winchester Campus, University of Southampton, UK, 13-15 July 2004, ed. R. Janaway and P. Wyeth, Archetype Publications, 143-150.
6. Hallett, K. and D. Howell, 'Size Exclusion Chromatography of Silk - Inferring the Tensile Strength and Assessing the Condition of Historic Tapestries', in *Preprints of ICOM Committee for Conservation, 14th Triennial Meeting*, The Hague, Netherlands 2005, In Press.
7. Herrero Carretero, C., 'Flemish Tapestry Weavers Abroad. Emigration and the Founding of Manufacturies in Europe', (ed.) G. Delmarcel, Leuven University Press, Leuven (2002) 227-246.
8. Herrero Carretero, C., 'Tapipes Flamencos en la Coleccion de la Corona de Espana', in *Studies in Western Tapestry. Flemish Tapestry in European and American Collections. Studies in Honour of Guy Delmarcel*, (ed.) K. Brosens, Brepol, Turnhout (2003) 161-170.
9. Herrero Carretero, C., 'Marques d'Importation au XIVe Siecle sur les Tissus Orientaux de Las Huelgas', *Bulletin de Liasion du Centre International d'Etude des Textiles Anciens,*(CIETA) (2004) 81.
10. Herrero Carretero, C., 'La Fortaleza. Cortina de la Colgadura del Dormitorio de Carlos III en el Palacio Nuevo de Madrid', *Reales Sitios* **161** (2004) 52-62.
11. Herrero Carretero, C., 'El Museo de Telas Medievales de Santa Maria la Real de Huelgas. Colecciones Textiles de Patrimonio Nacional', in Vestiduras Ricas. El Monasterio de las Huelgas y su epoca 1170-1340, Palacio Nacional Madrid (2005) 119-138.
12. Howell, D., 'Prioritising Interventive Treatments for Textile Materials', in *Scientific Analysis of Ancient and Historic Textiles: Informing Preservation, Display and Interpretation. AHRB Research Centre for Textile Conservation and Textile Studies First Annual Conference*, Textile Conservation Centre, Winchester Campus, University of Southampton, UK, 13-15 July 2004, ed. R. Janaway and P. Wyeth, Archetype Publications, 69-70.
13. Howell, D., 'Assessment of Damage to Wool and Silk in Model and Historic Tapestries', in *Sustaining Europe's Cultural Heritage: From Research to Policy. 6th European Commission Conference*, Organised by the UCL Centre for Sustainable Heritage and held at the Queen Elizabeth Conference Centre, London, 1-3 September 2004, In Press.
14. Howell, D., 'Planning and Organising a Collaborative Research Project', in *Conservation 2004: Working with the Project Culture. United Kingdom Institute for Conservation Conference*, Merseyside Maritime Museum, Liverpool, UK, 8-9 July 2004, In Press.

15. Howell, D., 'Tapestry Conservation Research - The Big Picture', in *Big Issues: United Kingdom Institute for Conservation (UKIC) Textiles Section 2005 AGM and Forum*, Clothworkers Guild, London 2005, In Press.

16. Hulme, A.N., H. McNab, D.A. Peggie, and A. Quye, 'A Novel Approach to Mordant Identification Using Inductively Coupled Plasma - Mass Spectrometry', in *Dyes in History and Archaeology 23*, Montpelier, France, 4-5 November 2004, Poster.

17. Hulme, A., H. McNab, D.A. Peggie, and A. Quye, 'Negative Ion Electrospray Mass Spectrometry of Neoflavonoids', *Phytochemistry* **66** (23) (2005) 2766-2770.

18. Hulme, A.N., H. McNab, D.A. Peggie, and A. Quye, 'The Application of Liquid Chromatography-Mass Spectrometry and Accelerated Light Ageing for the Analytical Identification of Yellow Flavonoid Dyes in Historical Tapestries', in *Scientific Analysis of Ancient and Historic Textiles: Informing Preservation, Display and Interpretation. AHRB Research Centre for Textile Conservation and Textile Studies First Annual Conference*, Textile Conservation Centre, Winchester Campus, University of Southampton, UK, 13-15 July 2004, ed. R. Janaway and P. Wyeth, Archetype Publications, 208-213.

19. Hulme, A., H. McNab, D.A. Peggie, A. Quye, I. Vanden Berghe, and J. Wouters, 'The Analytical Characterisation of the Main Component Found in Logwood Dyed Textile Samples after Hydrochloric Acid Extraction', in *Preprints of ICOM Committee for Conservation, 14th Triennial Meeting*, The Hague, Netherlands 2005, In Press.

20. Hulme, A.N., H. McNab, D.A. Peggie, A. Quye, I. Vanden Berghe, and J. Wouters, 'The Analytical Characterisation of the Main Component Found in Logwood Dyed Textile Samples after Hydrochloric Acid Extraction', in *ICOM Committee for Conservation*, Amsterdam, Netherlands 2005, In Press.

21. Odlyha, M., Q. Wang, G.M. Foster, J. de Groot, M. Horton, and L. Bozec, 'Monitoring of Damage to Historic Tapestries: The Application of Dynamic Mechanical Thermal Analysis to Model and Historic Tapestries', in *Scientific Analysis of Ancient and Historic Textiles: Informing Preservation, Display and Interpretation. AHRB Research Centre for Textile Conservation and Textile Studies First Annual Conference*, Textile Conservation Centre, Winchester Campus, University of Southampton, UK, 13-15 July 2004, ed. R. Janaway and P. Wyeth, Archetype Publications, 126-134.

22. Odlyha, M., Q. Wang, J. de Groot, G.M. Foster, D. Howell, and R. Larsen, 'Damage Assessment of Historical Tapestries and Parchment: Application of Thermomechanical and other Thermoanalytical Techniques', in *The American Institute for Conservation of Historic and Artistic Works Research and Technical Studies Group*, 13 June 2004, Publication (electronic).

23. Odlyha, M., Q. Wang, J. de Groot, and G.M. Foster, 'Damage Assessment of Tapestry by Micro-Thermal Analysis', in *abstract published in Book of Abstracts of 13th International Congress on Thermal Analysis and Calorimetry (ICTAC)*, Sardinia, Italy 2004, 286.

24. Odlyha, M., 'The Application of Thermoanalytical Techniques to the Preservation of Art and Archaeological Objects', in *Handbook of Thermal Analsis and Calorimetry*, Elsevier (2003) 47-96.

25. Peggie, D.A., A.N. Hulme, H. McNab, and A. Quye, 'The Chemical Characterisation of Aged and Unaged Fibre Samples Dyed with Sawwort (Serratula Tinctoria) Using PDA HPLC and HPLC ESI MS', in *Dyes in History and Archaeology 22*, Riggisberg, 23-24 October 2003, In Press.

26. Quye, A., 'Monitoring of Damage in Historic Tapestries (MODHT)', in *Dyes in History and Archaeology 21* 2002, In Press.

27. Vanden Berghe, I. and J. Wouters, 'Identification and Condition Evaluation of Protein Fibres at the Sub-Microgram Level by Calibrated Amino-Acid Analysis', in *Scientific Analysis of Ancient and Historic Textiles: Informing Preservation, Display and Interpretation. AHRB Research Centre for Textile Conservation and Textile Studies First Annual Conference*, Textile Conservation Centre, Winchester Campus, University of Southampton, UK, 13-15 July 2004, ed. R. Janaway and P. Wyeth, Archetype Publications, 151-158.

28. Hacke, A.M., 'XPS Analysis of Metal Threads in Historic Tapestries', in XPS Users Group Dissemination Meeting, July 2003, University of Manchester (2003).

29. Hacke, A.M., 'Monitoring of Damage in Historic Tapestries', in Department of Textiles and Paper, University of Manchester, Postgraduate Seminar, 4 May 2004, University of Manchester (2004).

30. Hacke, A.M., 'Investigation of XPS S(2p) High Resolution Scans of Historic Wool Fibre Surfaces as a Marker of Degradation', in XPS Users Group Dissemination Meeting, April 2005, University of Manchester (2005).

31. McNab, H., 'The Dyes of Historical Textiles - A Chemist's Perspective', in RSC/UoE Summer school, 1 July 2004, University of Edinburgh (2004).

32. McNab, H., 'The Dyes of Historical Textiles - A Chemist's Perspective', in Seminar, 8 October 2004, University of Northumbria (2004).

33. Odlyha, M., 'Presentation of MODHT Project', in AIC meeting, June 2004, Portland, Oregon (2004).

34. Odlyha, M., 'Presentation of MODHT Project', in *13th International Congress on Thermal Analysis and Calorimetry, Cultural Heritage section (ICTAC)*, Sardinia, Italy 2004.

35. Peggie, D.A., 'Mordants and Dyes: An Historical Perspective', in Organic Postgraduate Seminar Series, 11 November 2004, University of Edinburgh (2004).

36. Peggie, D.A., 'Monitoring of Damage in Historic Tapestries', in Organic Postgraduate Seminar Series, 7 April 2005, University of Edinburgh (2005).

37. Herrero Carretero, C., 'Notas Sobre la Conservacion y Difusion de la Coleccion de Tapices de la Corona de Espana', in Textile Indumentaria: Materias, Tecnicas y Evolucion. Grupo Espanol IIC, Universidad Complutense de Madrid (2003).

38. Verhecken, A., 'A Concise History of Dye Analysis', in *Dyes in History and Archaeology 20*, Amsterdam, Netherlands 2001, ed. J. Kirby, Archetype Publications, 1-22.

39. 'Report on the Conservation Treatment Options for the Tapestry: The Meeting of Abraham and Melchizedek', Hampton Court Palace, Textile Conservation Studios.

40. Braun-Ronsdorf, M., 'Gold and Silver Fabrics from Medieval to Modern Times', *C.I.B.A. Review* **3** (1961) 2-16.

41. Indictor, N., R.J. Koestler, C. Blair, and A.E. Wardwell, 'The Evaluation of Metal Wrappings from Medieval Textiles Using Scanning Electron Microscopy-Energy Dispersive X-Ray Spectrometry', *Textile History* **19** (1) (1988) 3-19.

42. Járó, M., 'Gold Embroidery and Fabrics in Europe: XI-XIV Centuries', *Gold Bulletin* **23** (2) (1990) 40-57.

43. Heinz, D., *Europäische Wandteppiche*, Klinkhardt & Biermann, Braunschweig (1963).

44. Hunter, G.L., *The Practical Book of Tapestries*, J.B. Lippincott Company, Philadelphia & London (1925).

45. Ysselsteyn, D.G.T.v., *Tapestry*, Van Goor Zonen, The Hague, Brussels (1969).

46. Bennet, A.G., *Five Centuries of Tapestry*, Fine Arts Museum of San Francisco, San Francisco 7-22.

47. Campbell, T.P., *Tapestry in the Renaissance, Art and Magnificence*, The Metropolitan Museum of Art, New York (2002).

Chapter 2. Analytical Methods

2.1. Scanning Electron Microscopy (SEM), Field Emission Gun SEM (FEG-SEM) and Energy Dispersive X-ray Microanalysis (EDX)

Electron Microscopy allows high magnification imaging with excellent depth of focus of the surface topography and morphology of a sample [1]. EDX enables compositional analysis of all elements from boron to uranium to a spatial resolution of approximately one micron [1].

2.1.1. SEM

SEM images are formed by scanning an electron beam across a surface and collecting signals, either secondary electrons or back scattered electrons, from the beam-surface interaction. SEM analysis has been used extensively for textile investigations from fibre identification to damage assessment [2, 3]. A typical SEM image of a metal thread surface is shown in Figure 2.1.1.

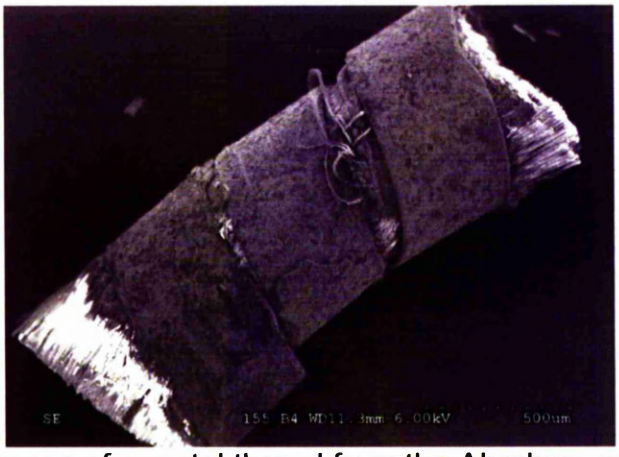

Figure 2.1.1. SEM image of a metal thread from the Abraham and Melchizedek tapestry

An accelerated electron beam, generated by an electron gun (e.g. a thermally emitting tungsten cathode), passes through an adjustable aperture, focused by electromagnetic condenser lenses and scanned across the surface of a specimen held in a vacuum chamber. A current applied to two sets of scan coils deflects the electron beam through an aperture and controls the raster scanning. Magnification is achieved through the ratio of the raster scanned area on the specimen to the area on the cathode ray tube (CRT) screen. The following variable machine settings control the resolution, depth of focus and signal to noise ratio of the final

image: accelerating voltage of the beam, beam current and spot size (controlled through the condenser lens current), aperture size and alignment, astigmatism of the beam and working distance; achieving the best possible image is often a trade-off between these variables.

As the primary electron beam strikes the specimen, backscattered primary electrons, secondary electrons, Auger electrons, X-rays and light photons are emitted. Unscattered and elastically / inelasically scattered electrons pass through the specimen. Some electrons are absorbed into the specimen where they generate a current. Non-conducting samples must therefore be typically gold or carbon coated to dissipate the generated heat and charge. The SEM instrument used in this study is a Hitachi S-3000 N and is equipped with two detectors; a scintillator-photomultiplier type Everhart-Thornley secondary electron detector and a retractable four quadrant solid state backscattered electron detector. Secondary electrons are fewer and of lower energy than backscattered electrons but are emitted from a small region near the surface of the specimen close to the primary electron beam, while back scattered electrons are emitted from a wider and deeper region, thus a secondary electron image will offer higher resolution but less contrast. The number of backscattered electrons which escape the specimen depends on the atomic number of the backscattering atoms; i.e. the higher the atomic number of the atoms in the specimen the higher the number of backscattered electrons from that region and the brighter the image. Therefore backscattered electron images offer not only topographical information but also chemical information through atomic number contrast. An added benefit of the four quadrant solid state detector is that it works in variable pressure. A lower vacuum in the analysis chamber allows charge dissipation without the need of gold or carbon coating for non-conducting samples.

2.1.2. FEG-SEM

Opposed to the commonly used tungsten filament thermal emission gun, the field emission gun possesses a much smaller tip radius and higher emission current density resulting in a higher resolution image and enabling the use of very low accelerating voltages to obtain a true surface image. In this study a Philips XL 30 FEG SEM was used only for cross sectioned metal thread samples.

2.1.3. EDX

X-rays are emitted when a primary electron hits the surface of the specimen and causes the ejection of a secondary electron from one of the orbital shells of an atom. In order for the atom to come back to its stabilised state, an electron from a higher energy orbit fills the resulting gap. During that transition an x-ray photon with characteristic energy and wavelength is emitted. Energy dispersive X-ray microanalysis (EDX) allows the measurement of the characteristic energy and thereby provides information about the chemical elements present on the surface of the specimen. The majority of X-rays are emitted from a relatively wide area from the lower two thirds of the interaction volume of the electron beam, the spatial resolution of X-ray microanalysis is, therefore, relatively poor compared to secondary electron images. A typical EDX spectrum of a metal thread surface is shown in Figure 2.1.2.

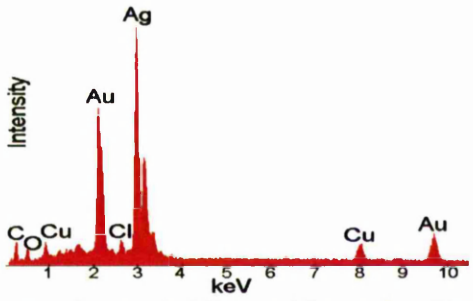

Figure 2.1.2. EDX spectrum of a metal thread from the Daedalus and Icarus tapestry

The Hitachi S-3000 N instrument is equipped with a liquid nitrogen cooled EDAX Sapphire Si(Li) NL2 detector. When incoming X-rays strike the lithium-drifted silicon semi-conductor photoelectrons are generated which in turn generate electron-hole pairs. A strong electric field attracts the electrons and holes to opposite ends of the detector generating a current pulse, the magnitude of which is directly proportional to the number of electron-hole pairs and therefore proportional to the energy of the incoming X-rays.

2.2. X-ray Photoelectron Spectroscopy (XPS)

XPS is a powerful, surface sensitive analysis technique that probes the outer ~2-10 nm of a sample and provides quantitative information about atomic composition and chemical state [4-6]. X-ray photons cause the ejection of photoelectrons upon collision with atoms. The basis of XPS is the analysis of the energy of such

photoelectrons. The binding energy E_B of electrons is specific for each element and its chemical state. The measured kinetic energy E_K of emitted electrons is dependent upon the energy of the incident X-ray photon hν and is therefore converted into the independent measure E_B using the following equation for presentation in a spectrum of intensity versus electron binding energy:

$$E_B = h\nu - E_K - \Phi_{sp}$$

Where Φ_{sp} is the work function of the spectrometer (usually around 5eV).

The electrons from each atomic orbital have certain probabilities of being ejected on collision with X-ray photons. Consequently the spectra of most elements will have a unique set of peaks of approximately constant relative intensities at certain binding energies, which allow unambiguous identification of the elements present.

A typical spectrum of gold is shown in Figure 2.2.1.

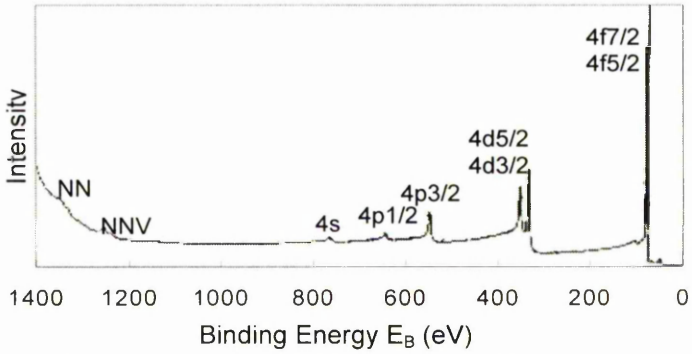

Figure 2.2.1. Monochromated Al Kα spectrum of Au [5]

Paired electrons from the p, d and f subshells become split upon X-ray photon excitation, leading to split peak intensities with definite ratios, Table 2.1.

Table 2.1. Spin-orbit splitting

Subshell	**j value** (total angular momentum quantum number)	**Peak intensity ratio**
s	1/2	-
p	1/2 , 3/2	1:2
d	3/2, 5/2	2:3
f	5/2, 7/2	3:4

In addition to photoelectron emission, relaxation of the excited ions may lead to X-ray fluorescence or emission of Auger electrons. However, these effects contribute little information to the XPS spectra.

The peaks in a spectrum result from 'elastic' photoemission, meaning that no energy loss occurred due to electron collision during ejection. Such energy loss results in 'inelastic' photoemission, which can contribute weak characteristic features to the spectrum but usually adds to the background 'noise'. The 'inelastic mean free path' is defined as the average distance that an electron with a given energy travels between successive inelastic collisions [7]. Therefore the inelastic mean free path controls the sampling depth, which, in general, is in the order of a few nm.

Information about chemical state of the elements can be gained from peak shifts; in general an increase in positive charge of an atom leads to increased binding energy of its electrons. Peak shifts due to electrical charging of the sample during analysis will affect every peak in the same manner; therefore reference is usually made to the C 1s peak which, under neutral conditions, occurs at an E_B of 285 eV.

Quantification in terms of atomic percentage of the elements present on the sample surface is achieved by dividing the peak area by the relative sensitivity factor. Peak areas are determined after appropriate background correction of the spectrum using the linear, Shirley or Tougaard methods [8]. Relative sensitivity factors for all elements can be calculated [9] or determined empirically (usually by the instruments manufacturer, e.g. Kratos sensitivity factors).

The Kratos Axis Ultra XPS instrument has two independent X-ray sources, the monochromatic Al and dual Mg/Al anode. A heated filament causes emission of high energy electrons, which are targeted towards the Al or Mg/Al anode. Transitions from 2p3/2 → 1s and 2p1/2 → 1s generate characteristic Al $K\alpha_{1,2}$ X-rays at 1486.6 eV (or Mg $K\alpha_{1,2}$ at 1253.6 eV).

Bremsstrahlung, satellites, ghost lines and weaker emission of X-rays from additional transitions result in a broadening of the incident X-ray linewidth (0.70 eV and 0.85 eV for Mg $K\alpha_{1,2}$ and Al $K\alpha_{1,2}$, respectively), which ultimately leads to higher background intensity and increased photoelectron linewidth, hence less precise XPS spectra. This can be overcome with monochromated Al Kα X-ray source. Back-diffraction from a quartz crystal is employed to monochromate the X-rays and thereby reduce the linewidth to < 0.3 eV, achieving better signal:noise ratio. However, there can be a considerable loss of X-ray intensity, leading to lower overall signal intensity in the XPS spectrum.

The X-rays are focused either directly from the anode face (dual anode) or by the monochromator onto the sample. Ejected photoelectrons from the sample enter the electron energy analyser system, the concentric hemispherical analyser. Photoelectrons are directed by scan plates through an adjustable aperture and electron-optical lenses and are retarded before entering the hemispherical electron energy analyser. Constant pass energy potentials are applied to the two concentric hemispheres so that injected electrons of a particular (retarded) energy are brought to a focus at the opposite end of the hemisphere. By progressively altering the retardation ratio, electrons of the complete energy range will be scanned and the photoelectron spectrum produced.

On leaving the hemispherical analyser the photoelectrons are detected by a multichannel electron system, consisting of eight independent detectors each of which provides single electron counting. The counts are digitally accumulated and intensity is usually displayed as counts per second (CPS) on the XPS spectrum.

2.3. Time of Flight Secondary Ion Mass Spectrometry (ToF-SIMS)

SIMS is a highly surface sensitive technique that can be used to identify all elements and isotopes from hydrogen to uranium; it allows chemical as well as elemental characterisation of a sample surface [10-12].

In SIMS a surface (usually a solid surface) is bombarded with energetic primary particles; usually primary ions but may also be electrons, neutrons or photons. This causes sputtering, i.e. the emission of secondary particles, which may be single atoms or molecules and molecular fragments, Figure 2.3.1. The mechanism of sputtering and ionisation of the ejected secondary particles is not yet fully understood, but there are various kinetic, electronic and thermodynamic models that try to explain the process [10].

Widely recognized is that the quantity of secondary ion emission and the secondary ion current depends upon the number of primary ions, the primary ion current, the sputtering coefficient, the ionisation probability and the concentration of particles to be studied on the sample surface.

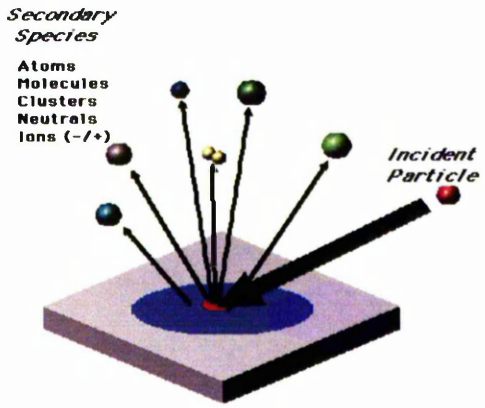

Figure 2.3.1. ToF-SIMS sputtering [13]

The SIMS instrument includes a primary ion source (atom/ ion gun), a vacuum chamber where the sample is placed, a mass analyser and secondary ion detector (e.g. a Time of Flight analyser). The results are processed electronically and the computer software provides spectra of Atomic Mass Units or mass to charge ratio (m/z) versus Intensity.

With the aid of focusing lenses the primary ion beam can be raster scanned across the surface and by collecting secondary ions of a certain mass to charge ratio at each point of the area a chemical image of varying elemental or molecular intensities can be generated.

If the primary ion impact rate is below the accepted threshold level of $1x10^{13}$ ions cm^{-2}, the technique examines a stable surface and the method is known as Static SIMS.

If the primary ion beam is repeatedly scanned across an area the surface will erode over time as the solid lattice structure is disrupted and secondary ions are ejected off the surface layers. Changes of elemental composition with depth can thus be monitored and represented as depth profile graphs of Time versus Intensity for certain elemental or molecular isotopes; this is known as Dynamic SIMS [10-12].

The ToF-SIMS instrument used in this study for the acquisition of spectra in the Static SIMS mode was a PHI 7000 instrument equipped with a pulsed Cs^+ primary ion source (pulse length of 1.25 ns) and Time-of-Flight analyser. Each pulse of the primary ion beam causes the emission of secondary ions which are accelerated to the same kinetic energy. This results in ions of different velocities since heavier ions with the same kinetic energy will travel faster than lighter ions. A high

transmission two-stage grid reflectron time-of-flight mass analyser with a pair of chevron-type multichannel plates with a 10 kV post-acceleration gap is used for ion detection at the end of the flight tube.

The PHI 7000 instrument also comprises a pulsed charge neutraliser for insulating samples. An electron beam (0 - 70 eV) is pulsed out of phase with the primary ion beam to allow the electrons to reach the sample.

Dynamic SIMS analysis was performed on a CAMECA IMS 4f Magnetic Sector SIMS instrument. The instrument is equipped with a Cs^+ primary ion source and a duoplasmatron source for O_2^+, O^- and Ar^+ ions. The primary ion beam can be successively scanned across a well defined surface area, thereby sputter-removing surface layers. The emitted positive and negative secondary ions are analysed in the triple focussing mass spectrometer, generating a depth profile.

2.4. X-ray Diffraction (XRD)

X-Ray Diffraction allows the determination of the crystal structure of a sample [14, 15]. In XRD a sample is irradiated with monochromatic X-rays of known wavelength λ, and these are scattered in all directions upon encounter with atoms. In the case of periodically arranged atoms (crystal) those X-rays, which are scattered off parallel lattice planes and where the angle of incidence θ is equal to the angle of reflection θ, will be totally in phase with one another and their amplitudes add; this is called elastic scattering or diffraction. Most X-rays, however, are scattered in random directions and will be out of phase, partially cancelling one another, Figure 2.4.1.

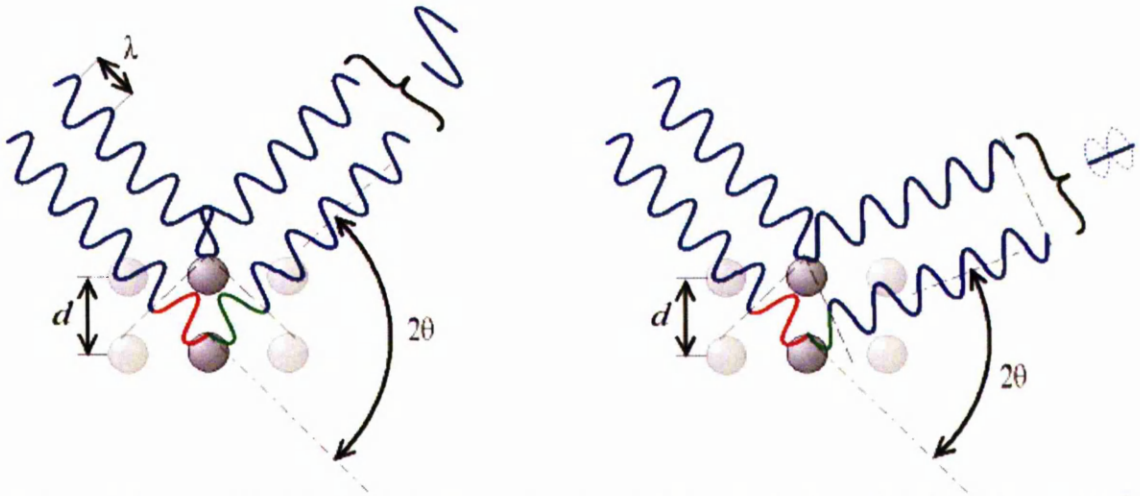

Figure 2.4.1. X-ray scattering causing constructive or destructive interferences [16]

The sample or the detector and/or the X-ray source are rotated relative to one another in order to change the angle of the incident X-ray beam and enable the recording of diffracted X-rays of all crystal lattice planes present.

The angle of elastically scattered X-rays (θ) is measured and the crystal lattice plane *d*-spacings calculated according to Bragg's Law:

$$2d \sin\theta = n\lambda$$

where *n* is an integer, λ is the wavelength of incident X-rays, *d* is the spacing between the planes in the atomic lattice, and θ is the angle between the incident ray and the scattering planes.

The resulting diffraction pattern is represented in a graph of 2-θ versus X-ray intensity. A typical X-ray diffraction pattern for silver is shown in Figure 2.4.2.

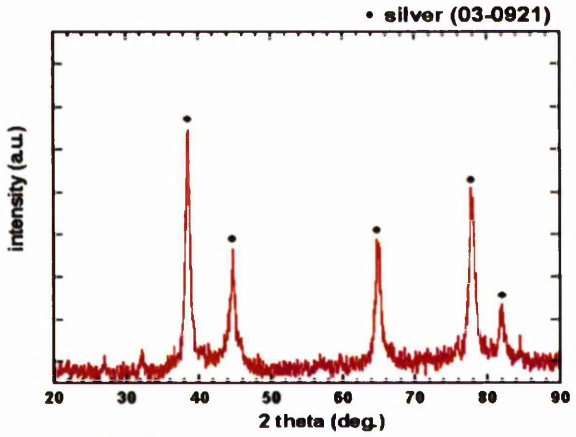

Figure 2.4.2. XRD pattern of silver [17]

In this study XRD was employed to identify corrosion crystals present on metal threads and corroded Ag and Cu coupons.

Analysis of metal threads was performed using a Philips X'Pert MPD instrument capable of glancing incident scan analysis, while Ag and Cu coupons were analysed on a Philips X'Pert APD θ-2-θ system. Both instruments were equipped with a Cu anode X-ray tube.

2.5. References

1. Goldstein, J.I., D.E. Newbury, P. Echlin, D.C. Joy, C. Fiori, and E. Lifshin, *Scanning Electron Microscopy and X-Ray Microanalysis*, Plenum Press, New York, London (1981).
2. Wortmann, F.J. and G. Wortmann, *Scanning Electron Microscopy as a Tool for the Analysis of Woo / Speciality Fibre Blends*, Comett/Eurotex, Guimaraes (1991) 1-97.
3. Hearle, J.W.S., B. Lomas, and W.D. Cooke, *Atlas of Fibre Fracture and Damage to Textiles*, Woodhead Publishing Limited in association with The Textile Institute, Cambridge (1998) 1-468.
4. Briggs, D., *Surface Analysis of Polymers by XPS and Static SIMS*, University Press, Cambridge (1998) 14-47.
5. Moulder, J.F., W.F. Stickle, P.E. Sobol, and K.D. Bomben, *Handbook of X-ray Photoelectron Spectroscopy*, Physical Electronics, Inc., Eden Prairie, Minnesota (1992, 1995) 9-33,128.
6. Watts, F.J., *An Introduction to Surface Analysis by Electron Spectroscopy*, Oxford University Press. Royal Microscopical Society (1990) 1-23.
7. Powell, C.J., A. Jablonski, I.S. Tilinin, S. Tanuma, and D.R. Penn, 'Surface Sensitivity of Auger-Eectron Sectroscopy and X-Ray Photoelectron Spectroscopy', *Journal of Electron Spectroscopy and Related Phenomena* **98-99** (1999) 1-15.
8. Leclerc, G. and J.J. Pireaux, 'The Use of Least Squares for XPS Peak Parameters Estimation. Part 1. Myths and Realities', *Journal of Electron Spectroscopy and Related Phenomena* **71** (2) (1995) 141-164.
9. Scofield, J.H., 'Hartree-Slater Subshell Photoionization Cross-Sections at 1254 and 1487 eV', *Journal of Electron Spectroscopy and Related Phenomena* **8** (2) (1976) 129-137.
10. Briggs, D., A. Brown, and J.C. Vickerman, *Handbook of Static Secondary Ion Mass Spectroscopy*, John Wiley & Sons (1989) 3-15.
11. Cherepin, V.T., *Secondary Ion Mass Spectroscopy of Solid Surfaces*, VNU Science Press BV, Utrecht (1987) 1-92.
12. Vickerman, J.C., A. Brown, and N.M. Reed, eds. *Secondary Ion Mass Spectroscopy. Principles and Applications.* The International Series of Monographs on Chemistry. 1989, Clarendon Press: Oxford. 22.
13. Image from: Basgall, E.J., 'Static ToF-SIMS', http://www.personal.psu.edu/faculty/e/j/ejb11/ (1997).
14. Woolfson, M.M., *An Introduction to X-Ray Chrystallography* 2nd edition, Cambridge University Press (1997) 1-75.
15. Cullity, B.D., *Elements of X-Ray Diffraction*, Addison-Wesley Publishing Company, Inc. (1978) 3-106.
16. Image from: Chan, C.D.N., 'Wikipedia information about Bragg's law on Answers.com', Wikipedia (2005).
17. Image from: Nanotechnologies Inc, 'Products / Silver Nanopowder', http://www.nanoscale.com.

Chapter 3. Historic Samples and Preparation of Models

3.1. Historic tapestry samples: wool, silk and metal threads

Tapestries from the Royal Spanish, Belgian and British collections were selected for sampling by the curators involved in the MODHT project. The tapestries cover a time span from the early 15th to the early 17th centuries and are amongst the most valuable that have survived from these periods.

Small samples of a few mm to a few cm each were cut from knotted ends of yarns at the back of the tapestries, where the supportive lining had been taken off. Great care was taken to ensure the integrity of the tapestry structure was not harmed any further and samples were not taken from floats, which when cut could lead to fraying ends. Only where possible, samples were taken from the face of the tapestries, e.g. from areas that were already broken and had ripped ends of yarns sticking out.

Approximately 30-50 samples were taken from each tapestry comprising of wool and silk yarns of each colour in the design, and where also present, metal threads.

Conservators with expertise for the individual tapestries and sampling sites distinguished between the original weave structure and later restoration work to ensure that samples were taken from the original or if in doubt clearly labelled.

All samples were photographed and the position in the tapestry was documented for later reference. The successively numbered labels of the individual samples contain a code for the identification of the tapestry.

In total 731 samples from 18 different tapestries have been taken during three sampling campaigns in Spain, Belgium and Britain. Details of the individual tapestries that were included in the sampling campaigns are listed below.

3.1.1. Patrimonio Nacional Madrid

A sampling campaign at the Palace in Madrid was carried out in October 2002. In total six tapestries were sampled. The tapestry details and conservation assessments are quoted from the sampling report prepared for MODHT [1].

The Fall of Icarus (PNM1)

(53 were taken)
Brussels, ca. 1545
Design by Cornelius Vermeren or Peter Coeck van Aelst
Woven by Wilhelm van Pannemaker
Material: wool, silk and metal threads
Dimensions: height 357cm, width 518cm
Belongs to a set of five tapestries of the fables of Ovid.
Conservation condition: bad

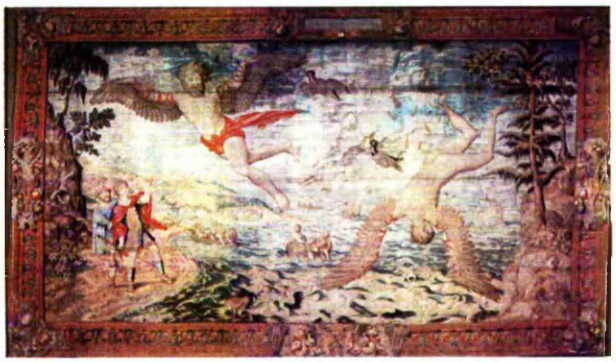

The Abduction of Ganymede (PNM2)

(37 samples taken)
Brussels, ca. 1545
Design by Cornelius Vermeren or Peter Coeck van Aelst
Woven by Wilhelm van Pannemaker
Material: wool, silk and metal threads
Dimensions: height 355cm, width 339cm
Belongs to a set of five tapestries of the fables of Ovid.
Conservation condition: regular

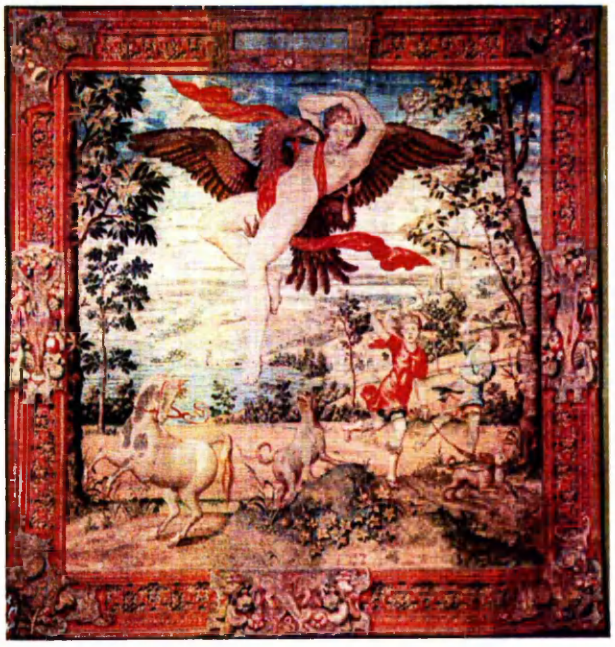

The Sacrifice of Polixena (PNM5)

(41 samples taken)
Brussels, ca. 1545
Design by Cornelius Vermeren or Peter Coeck van Aelst
Woven by Wilhelm van Pannemaker
Material: wool, silk and metal threads
Dimensions: height 355cm, width 587cm
Belongs to a set of five tapestries of the fables of Ovid.
Conservation condition: regular

Rafael and Tobias (PNM7)

(23 samples taken)
Brussels, ca. 1550
Design by Miguel Coxie
Woven by Baltasar van Vlierden
Material: wool and silk
Dimensions: height 494cm, width 810cm
Conservation condition: regular

Atalanta and the Boar of Caledonia (PNM8)

(19 samples taken)
Bruges, ca. 1620
Designer and weaver unknown
Material: wool and silk
Dimensions: height 410cm, width 462cm
Conservation condition: bad

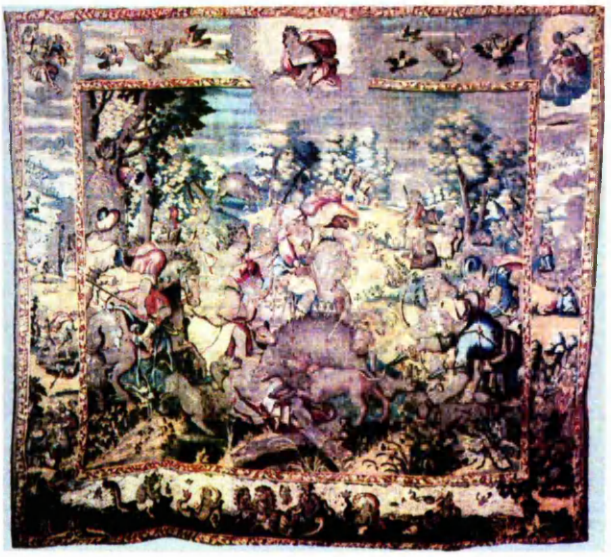

Galerías de emparrados (PNM9)

(26 samples taken)
Antwerp(?) ca. 1660
Designer unknown
Woven by Jacob Wauters
Material: wool and silk
Dimensions: height 132cm, width 163m
Only a fragment is left of the original tapestry.
Conservation condition: regular

3.1.2. Tournai, Bruges and Brussels

A sampling campaign of the Belgian royal collection was performed in February 2003. Samples were taken from tapestries from the cathedral of Tournai (TOU), the Municipal museum and cloister of Holy Mary of the Potterie in Bruges (BRU) and the National Museum in Brussels (BXL) [2].

Story of St. Piatus en Eleutherius (TOU1)

(32 samples taken)
Arras, 1402
Designer unknown
Woven by Pierrot Ferré
Material: wool, 7 warp ends per cm
Dimensions: height 186cm, width 282 cm
Belongs to a set of two tapestries of the story of Eleutherius.
No overall condition assessment

Verdure with the coat of arms of the Brugse Vrije (BRU1)

(19 samples taken)
Bruges, ca. 1530
Designer unknown
Woven by Antoon Segon
Material: wool
4-5 warp ends per cm
Dimensions: 11 fragments: max height 86 cm width 148cm
No overall condition assessment

Mary's Dedication in the Temple (BRU2)

(31 samples taken)
Bruges, 1639
Designer and weaver unknown
Material: wool
5-6 warp ends per cm
Dimensions: height 370 cm, width 422.5 cm
Belongs to a set of two tapestries of the Live of the Virgin.
No overall condition assessment

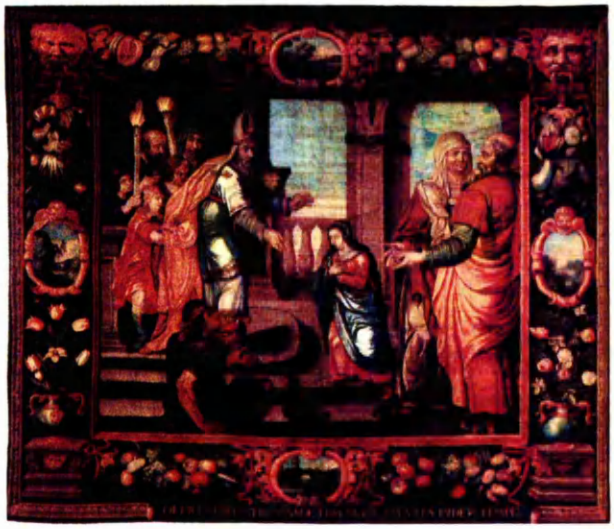

Miracles of the Holy Mary of the Pottery (BRU3)

(28 samples taken)
Bruges, ca. 1630
Designer and weaver unknown
Material: wool, 5 warp ends per cm
Dimensions: height ~170 cm, width ~530cm
Belongs to a set of three tapestries.
No overall condition assessment

Justitia disarmed by Misericordia (BXL1)

(16 samples taken)
Brussels, between 1519-1524
Design and weaver unknown
Material: wool and silk
6-7 warp ends per cm
Dimensions: height 413 cm, width 652 cm
Belongs to a set of four tapestries of the Virtues and Vices.
No overall condition assessment

Christ before Pilate (BXL2)

(43 samples taken)
Brussels, ca. 1520
Design inspired by Albrecht Dürer
Weaver unknown
Material: wool, silk and metal threads
8 warp ends per cm
Dimensions: height 300 cm, width 380 cm
Overall condition is good

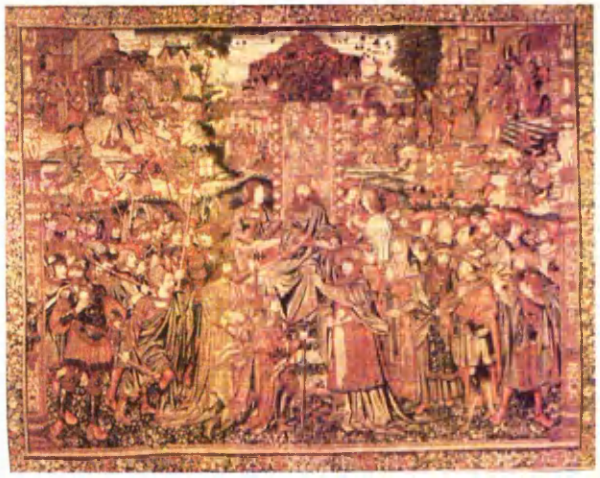

The Legend of Herkenbald (BXL3)

(18 samples taken)
Brussels, 1513
Design by Jan van Roome
Woven by Léon from Brussels
Material: wool
7 warp ends per cm
Dimensions: height 387 cm, width 430 cm
No overall condition assessment

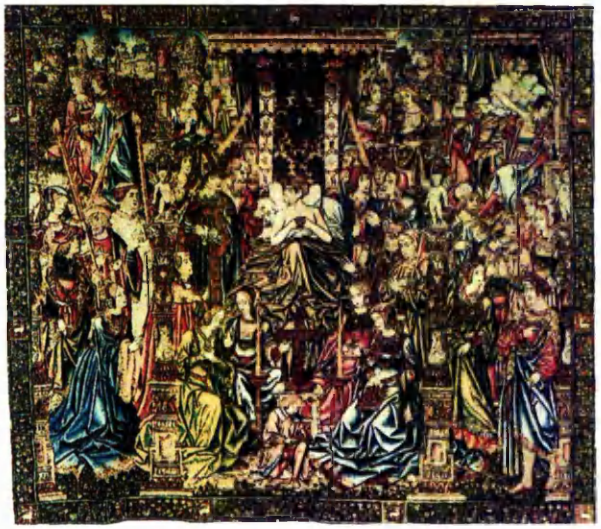

Man and the Seven Sins (BXL4)

(18 samples taken)
Brussels, between 1519-1524
Design and Weaver unknown
Material: wool and silk
6-7 warp ends per cm
Dimensions: height 411cm, width 650 cm
Belongs to a set of four tapestries of the Virtues and Vices.
No overall condition assessment

3.1.3. Hampton Court Palace

The sampling campaign at Hampton Court Palace took place in September 2003. Three tapestries were sampled at that date [3, 4]. Previously taken samples from a tapestry, which is currently undergoing conservation treatment were also included in the analyses for the MODHT project [5].

The Triumph of Time over Fame (HRP 1)

(46 samples taken)
Brussels, ca. 1515
Designer and weaver unknown
Material: wool and silk
Dimensions: height 439cm, width 818cm
Overall condition is weak

Tobias and Raphael taking leave of Tobit (HRP 2)

(67 samples taken)
Brussels, ca. 1544-1546
Designer and weaver unknown
Material: wool, silk and metal threads
Dimensions: height 450cm, width 672cm
Overall condition is weak

The Triumph of Death over Chastity (HRP 3)

(50 samples taken)
Brussels, ca. 1515
Designer and weaver unknown
Material: wool and silk
Dimensions: height 404cm, width 625cm
Overall condition is very poor

Abraham and Melchizedek (HCP)

(164 samples were taken before the start of the MODHT project)
Brussels, ca. 1535
Design by Bernard van Orley
Woven by Willem de Kempeneer
Material: wool, silk and metal threads
Dimensions: height 478cm, width 786cm
Overall condition is very poor

3.2. Model tapestry samples

3.2.1. Selection of wool and silk yarns

For the production of model tapestries it was decided to use the same 3-ply, 158 Tex, English wool yarn from Orme & Co. (manufacturer W & J Whitehead) for warp and weft; the selected silk for weft threads was a 2-ply, 66 Tex, Italian spun silk from H.T. Gaddum & Co. Ltd. These yarns lie well within the range suggested in the literature and, in agreement with HCP textile conservation studio, are believed to represent typical historic samples [6, 7].

The MODHT project partner KIK conducted amino acid analysis of the yarns and confirmed the silk as 100% Bombyx Mori silk and the wool as animal fibres in 95-99% conformity with sheep fibres.

3.2.2. Mordanting and dyeing

The MODHT project partners KIK (Konigliches Institut voor het Kunstpatrimonium / Royal Institute for Cultural Heritage) and NMS (National Museums of Scotland) provided degumming, mordanting and dyeing recipes devised from medieval texts [8, 9].

The selected dyestuffs and auxilliaries and their respective suppliers are listed below.

Oak galls, madder, brazil wood, cochineal and weld were supplied by Verfmolen De Kat, Holland. George Weil Fibrecraft supplied dyer's greenweed, turmeric and sandalwood. Alum, potassium carbonate, ferrous sulphate, iron filings, gum arabic, copper sulphate, copper turnings and tartaric acid were bought from Fisher Chemicals. Bran of wheat was purchased as "Jordan's Natural Wheat Bran". Couched woad was supplied by John Edmonds who cultivates woad plants at Reading University in cooperation with the EU SPINDINGO project. Hew Prendergast from Kew Gardens provided bark from an alder tree and Michel Garcia from the Association Garance, Lauris, Provence, sourced material from a young fustic shrub.

The correct biological source for all dyestuffs was verified by HPLC-PDA analysis, conducted by MODHT project partners at KIK and NMS [10]. A silk degumming trial with potassium carbonate showed a 4% weight loss in the spun silk compared

to a 25% weight loss in raw silk, hence degumming of the spun silk was not required.

All mordantings and dyeings were performed in an open vat or a closed vat. The open vat has a volume of 90 litres; steam heating and temperature controlled heating with an electric element; a hank rotating wince provided constant agitation. The closed vat (Longclose) has a maximum volume of 200 litres and a minimum working volume of 150 litres; steam heating; a reverse flow liquor pump provided constant agitation.

The medieval methods were followed as closely as possible permitted by the equipment and health and safety issues. Parameters such as weight, liquor ratio, pH, temperature and time were controlled and recorded for later reference. The mordanting and dyeing recipes for wool and silk are listed below:

Mordanting and dyeing recipes

Semelwater
The bath was prepared as follows:
Add 2 kg of bran of wheat to 45 l of water, bring to the boil, turn off heat, add 30 l of water and cover vat. Stir every hour (7x) during first day, after 6 days take out 40 l for recipe Red / S1, pH 4.87, add 40 l of hot water, stir and leave for another 24 hours, use 70 l for recipe Red / W1, pH 4.35.

Boil mordant
The bath was prepared as follows:
10 silk hanks (1140 g)
437.5 g alum
Bring 57 l of water to the boil, dissolve alum, pH 3.05, immerse silk, boil for 10 min, take silk out and leave to cool down, immerse silk at room temperature and leave for 10 hours.

Mordanting for Yellow / S1 and S3
The bath was prepared as follows:
9 silk hanks (1025 g)
384.4 g alum
Dissolve alum in hot water, fill vat to 50 l, 38°C, pH 3.49, immerse wool and leave for 20 hours, rinse and dry 3 hanks for Yellow /S3.

Yellow / S1-a-b
The bath was prepared as follows:
10 silk hanks (4 from boil mordant "_a" and 6 from Y / S1 mordant "_b")
1130 g weld
Bring 50 l of water to the boil, add weld and boil for 1.5 hours, pH 6.05.
Transfer 6 hanks from mordanting bath into dye bath without wringing, immerse 4 pre-wetted boil mordanted hanks, boil for 20 min, rinse with hot water.

2nd mordanting for Yellow / S3
The bath was prepared as follows:
3 silk hanks (346 g)
130 g alum

Dissolve alum in hot water, fill bath to 150 l, pH 4.1, 22°C, immerse silk and leave for 16 hours, rinse in cold water.

Yellow / S3-a-b-c-d
The baths were prepared as follows:
7kg dyer's greenweed
150 g K_2CO_3
Dyeing:
(1st) Add 4 kg dyer's greenweed to 150 l of water, boil for 1 hour, pH 6.6, immerse 5 silk hanks (3 from 1st mordanting and 2 boil mordanted) dye at the boil for 30 min, no rinse, leave to dry.
(2nd) Add 3 kg dyer's greenweed to 150 l of water, add K_2CO_3, boil for 1 hour, pH 8.1, immerse all hanks from 1st dyeing for 10 min at the boil, no rinse.
Y/S3_a (boil mordanted and twice dyed); Y/S3_b (mordanted and twice dyed)
(3rd) Immerse 1 pre-dyed (1st and 2nd), boil mordanted hank and 1 unmordanted hank in bath from 2nd dyeing, dye at the boil for 1.5 hours, no rinse.
Y/S3_c (no mordant 3rd dye only); Y/S3_d (boil mordanted and three times dyed)

Mordanting for Yellow / S2
The bath was prepared as follows:
600 g silk (11 hanks)
225 g alum
Dissolve alum in 30 l warm water, 43°C, pH 2.90, immerse silk, leave for 2 hours, 34°C, pH 3.45.

Yellow / S2-a
The bath was prepared as follows:
250 g mordanted silk (7 hanks – 6 for metal threads, l extra)
250 g young fustic "old"
47 g alum
Heat young fustic "old" in 15 l water until boiling point, leave to cool down for 1 hour, 53°C, pH 5.9, add alum and let cool down further, 40°C, pH 3.3, strain 10 l into a clean vessel and immerse silk, pH 3.35, leave for 30 min while stirring, wring and leave to dry.

Yellow / S2-b
The bath was prepared as follows:
100 g mordanted silk (l hank)
100 g young fustic "fresh"
18.75 g alum
Heat young fustic "fresh" in 5 l water until boiling point, leave to cool down for 1 hour, 55°C, pH 5.7, add alum and let cool down further, 40°C, pH 2.9, strain 4 l into a clean vessel and immerse silk, pH 3.1, leave for 30 min while stirring, wring and leave to dry.

Mordanting for Red / S1 and S2
The bath was prepared as follows:
10 silk hanks (1260 g)
315 g alum
Dissolve alum in hot water, fill vat with cold water to make 150 l, 23°C, pH 4.08, immerse silk and leave for 16 hours, rinse until pH of waste water > 6, leave 5 hanks to dry for Red / S1.

Red / S1-a-b-c-d-e
The baths were prepared as follows:
11 silk hanks (5 R / S1 mordanted, 1 boil mordanted, 5 unmordanted)
40 l semelwater
1890 g brazil wood
315 g alum
150 g K_2CO_3
1st dyeing:
To 50 l of water, pH 7.28, 45°C, add 40 l of semelwater, pH 4.85, add brazil wood, heat to 80°C during 6 hours, strain to filter out sludge, boil liquor for 1 hour, take out 45 l and save for 2nd dyeing, leave in 45 l, add 5 l to make 50 l, 90°C, pH 5.45, immerse R / S1 mordanted pre-wetted silk, dye for 20 min, drain, wring.
2nd mordanting:

Dissolve alum in hot water and fill bath with cold water to make 85 l, 33°C, pH 3.51, immerse 10 hanks (5 from 1st dyeing, 5 unmordanted), leave for 16 hours, drain, wring, take 4 hanks out (2 mordant-dye-mordant:: R/S1_b, 2 dyed while 2nd mordant:: R/S1_a).
2nd dyeing and lye treatment:
Mix 10 l of saved dye liquor with 10 l semelwater (pH 4.39) and 30 l water, bring to 90°C, pH 4.95, immerse 6 silk hanks (remaining from 2nd mordanting), dye for 15 min (no visible change in shade, dye liquor is brownish), add 150 g K_2CO_3, pH 10.15, immerse 1 additional silk hank (boil mordanted pre-wetted), dye for 15 min (silk and dye liquor are purple), rinse and wring all 11 hanks.
(2nd mordant - 2nd dye – lye: R/S1_c, 1st mordant – 1st dye - 2nd mordant – 2nd dye – lye: R/S1_d, boil mordant – 2nd dye – lye: R/S1_e)

Red / S2-a-b-c
The baths were prepared as follows:
842 g silk (6+2 hanks)
210.5 g alum
157.5 g madder
400 g potassium carbonate
Mordanting:
Dissolve alum in boiling water, fill up to 50 l with cold water, 48°C, pH 3.50, immerse silk, leave for 20 hours, rinse until pH of waste water has risen >6, drain, take out two hanks and dry.
Dyeing:
Add madder to 50 l hot water, immerse mordanted silk at 90°C, pH 6.58, leave for 20 minutes, pH 5.90, take out two hanks, rinse cold and dry. (R/S2_a)
1st Lye treatment:
Add 50 g potassium carbonate, pH 9.0, leave for 20 minutes, take out two hanks and dry. (R/S2_b)
2nd Lye treatment:
Add 350 g potassium carbonate, pH 10.80, leave for 20 minutes, take out two hanks and dry. (R/S2_c)

Red / S3
The baths were prepared as follows:
5 silk hanks (534 g)
267 g alum
66.75 g NaCl
1 kg copper turnings
133.75 g cochineal
101.5 g gum arabic
101.5 g oak galls
30 g turmeric
Mordanting:
Bring 50 l of water to the boil, dissolve alum and salt, add copper turnings, pH 3.15, turn off heat, immerse silk and leave for 24 hours while cooling down to 22°C, pH 3.97, rinse until pH of waste water > 6.
Dyeing:
Dissolve gum arabic in 35 l warm water, add oak galls, copper turnings, cochineal and turmeric, boil for 2 hours, add water to make 50 l, 70°C, pH 4.8. Immerse silk for 10 min, remove, bring liquor to the boil, immerse silk and boil for 2 hours, wring, leave to dry, rinse when dry.

Oak Gall / S and mordanting for Black / S1_a-b
The bath was prepared as follows:
9 silk hanks (725 g)
725 g oak galls
Immerse silk and oak galls in 50 l water and heat slowly for 20 min until boiling (pH 4.22); boil for 10 min, turn off heat and allow to cool to room temperature over night, wring and rinse.

Black / S1_a-b
The bath was prepared as follows:
6 silk hanks (580 g)
1000 g Fe(II)SO_4
1500 g iron filings
375 g gum arabic

Dissolve Fe(II)SO_4 in 50 l boiling water and add iron filings (pH 4.00), dissolve gum arabic (pH 4.17) immerse 6 pre-wetted oak gall mordanted silk hanks, boil for 30 min, remove and wring, cool for 30 min, take out 3 hanks (Black S1_a), re-immerse 3 hanks (bath has reached pH 3.50), boil for 30 min, remove and wring, cool for 30 min (Black S1_b) rinse all 6 hanks thoroughly in cold water, wring, leave to dry.

Woad dyeing

Blue:

Blue / S1	5 silk hanks
Blue / W1	3 wool hanks

Green:

Green / S1_a	2 boil mordanted, weld dyed silk hanks Y/S1
Green / S1_b	3 mordanted, weld dyed silk hanks Y/S1
Green / S2_a	2 boil mordanted, undyed silk hanks (to be over-dyed by Y/S1)
Green / S2_b	3 mordanted, undyed silk hanks (to be over-dyed by Y/S1)
Green / W1	3 weld dyed wool hanks Y/W1
Green / W2	3 undyed wool hanks (to be over-dyed by Y/W1)

All dyeings in the woad vat were performed by John Edmonds at Chiltern Open-air Museum conforming to medieval practice.
Due to the volume of the vat (30 l) the dyeings were carried out in stages of 3-5 hanks at a time. 2 kg of couched woad were used in total.
Reduction was achieved by bacterial action at 45-50°C and a pH of approximately 8.2-8.5. Wood ash and lime were used to maintain the alkalinity.

Green / S2-a-b
The bath was prepared as follows:
woad dyed silk (5 hanks, 2 boil mordant + 3 normal mordant)
565 g weld
Bring 50 water to the boil, pH 7.40, add weld, boil for 1.5 hour, pH 5.94, immerse prewetted silk, boil for 20 minutes, pH 6.14, cool down for 4 hours, rinse, dry.

Green / W2
The bath was prepared as follows:
500g woad dyed wool (3 hanks)
7.5 g alum
25 g potassium carbonate
250 g weld
Bring 50 water to the boil, pH 7.50, dissolve alum, pH 3.60, immerse prewetted wool, boil for 2 hours, pH 6.02, drain.
Bring 50 water to the boil, pH 7.40, add weld, pH 5.97, add potassium carbonate, pH 7.87, immerse prewetted wool, boil for 1 hour, rinse in warm water, dry.

Yellow / W1
The baths were prepared as follows:
8 wool hanks (1.5 kg)
22.5g alum
75 g K_2CO_3
750 g weld
Mordanting:
Bring 75 l water to the boil, dissolve alum, pH 4, immerse wool and boil for 2 hours, wring out.
Dyeing:
Bring 75 l water to the boil, dissolve K_2CO_3, add weld, pH 10.2, immerse wet wool and boil for 1 hour, wring and rinse with cold and hot water.

Yellow / W2
The baths were prepared as follows:
1 wool hanks (1000 g)
15 g alum
75 g K_2CO_3
2.5 kg dyer's greenweed
Mordanting:

Boil 50 l water, pH 7.2, add alum, pH 3.23, immerse wool, boil for 2 hours, pH 6.0, wring and leave to dry.
Dyeing:
Boil 50 l water, pH 7.4, dissolve K_2CO_3, pH 9.75, add dyer's greenweed, pH 7.33, immerse pre-wetted wool, boil for 1 hour, pH 7.05, wring, rinse in cold water and leave to dry.

Red / W1
The baths were prepared as follows:
6 wool hanks (1000 g)
70 l semelwater
150 g alum
600 g madder
50 g K_2CO_3
Mordanting:
To 50 l of semelwater, pH 4.35, add 150 g alum, dissolve, pH 3.17, immerse wool, bring to the boil and boil for 2 hours, drain, do not wring.
Dyeing:
To 20 l semelwater, pH 4.35, add 30 l of water, add madder, stir and bring up to 40°C, pH 5, immerse wool, raise temperature to 90°C and leave for 3 hours, drain, rinse, wring and leave 3 hanks to dry.
Lye treatment:
In 50 l of water, pH 7.4, dissolve K_2CO_3, pH 10.95, 20°C, immerse 3 hanks and leave for 30 min, rinse.

Red / W2
The baths were prepared as follows:
4 wool hanks (700 g)
70 g oak galls
35 g alum
420 g madder
35 g K_2CO_3
1st mordanting:
Bring 50 l of water to the boil, add oak galls, boil for 30 min, immerse wool and boil for 2 hours, drain bath but do not wring hanks.
2nd mordanting:
Bring 50 l of water to the boil, dissolve alum, immerse wet wool and boil for 2 hours, drain bath, wring hanks.
Dyeing:
Heat 50 l of water to 40°C, add madder, immerse wet wool, bring up to 90°C and keep for 3 hours, wring and rinse, leave 2 hanks to dry.
Lye treatment:
Dissolve K_2CO_3 in hot water, fill vat up to 50 l, pH 10.78, 35°C, immerse 2 wool hanks and leave for 30 min, rinse with hot water.

Red / W3
The baths were prepared as follows:
4 wool hanks (700 g)
105 g alum
175 g brazil wood
50 g K_2CO_3
Mordanting:
Bring 35 l water to the boil, dissolve alum, immerse wool and boil for 1.5 hours, squeeze out.
Dyeing:
Bring 35 l to the boil, add brazil wood, boil for 45 min, refill vat to make 35 l, immerse wool and boil for 1.5 hours, rinse with hot water, leave 2 hanks to dry.
Lye treatment:
Dissolve K_2CO_3 in hot water, fill vat up to 50 l, pH 10.78, 35°C, immerse 2 wool hanks and leave for 30 min, rinse with hot water.

Mordanting for Red / W4 and W5
The bath was prepared as follows:
8 wool hanks (1320 g)

106 g alum
69 g D tartaric acid
30.4 g sandalwood
30.4 g NaCl
Bring 50 l of water to the boil, dissolve alum, tartaric acid and salt, add sandalwood, pH 2.55, immerse wool and boil for 2 hours, turn off heat and leave to cool for 24 hours, remove hanks and do not wring.

Red / W4
The bath was prepared as follows:
4 wool hanks (670 g)
61.75 g starch mixed with water to make 123.5 g starch paste
41.6 g cochineal
10.5 g turmeric
21 g NaCl
Bring 50 l of water to the boil, dissolve starch and salt, add cochineal and turmeric, immerse wool, pH 4.2, boil for 1 hour, rinse in cold water.

Red / W5
The bath was prepared as follows:
4 wool hanks (670 g)
53 g gum arabic
36.2 g cochineal
8.7 g turmeric
1.3 g alum
5.4 g NaCl
Bring 50 l of water to the boil, dissolve gum arabic, alum and salt, add cochineal, immerse wool, boil for 1 hour, rinse in cold water.

Mordanting for Black / W1 and Black / W2
The bath was prepared as follows:
1300 g wool (8 hanks)
1300 g oak galls
Immerse wool in 50 l hot water, 73°C, pH 7.85, (pH goes up to 8.69 due to commercial alkaline scour), remove wool, add oak galls, bring to boil, pH 4.23. Immerse wet wool, boil for 2 hours, drain, cool down, rinse hot and leave to dry.

Black / W1
The baths were prepared as follows:
650 g mordanted wool (4 hanks)
62.5 g $Fe(II)SO_4$
Dyeing:
(1^{st}) Boil 50 l water, pH 7.40, add $Fe(II)SO_4$, pH 4.5, enter prewetted wool, (1^{st}) boil for 30 minutes, remove wool, pH 3.34, let cool down for 40 minutes, take out one hank.
(2^{nd}) Boil 3 hanks for 30 minutes, remove wool, pH unchanged, let cool down for 40 minutes, take out one hank.
(3^{rd}) Boil 2 hanks, for 30 minutes, remove, pH unchanged, let cool down for 40 minutes, rinse all hanks together, dry.

Black / W2
The baths were prepared as follows:
650 g mordanted wool (4 hanks)
975 g $Fe(II)SO_4$
Dyeing:
(1^{st}) Boil 50 l water, pH 7.40, add $Fe(II)SO_4$, pH 4.1, enter prewetted wool, (1^{st}) boil for 30 minutes, remove wool, pH 3.37, let cool down for 40 minutes, take out one hank, rinse.
(2^{nd}) Boil 3 hanks for 30 minutes, remove, pH unchanged, let cool down for 40 minutes, take out one hank, rinse.
(3^{rd}) Boil 2 hanks for 30 minutes, remove, pH 3.39, let cool down for 40 minutes, rinse one hank, dry.

Alder Bark / W and mordanting for Black / W3
The bath was prepared as follows:
1200 g wool (7 hanks)
1800 g alder bark
Boil alder bark in 50 l water, pH 5.70, immerse pre-wetted wool, boil for 2 hours, drain, wring and leave to dry.

Black / W3
The bath was prepared as follows:
685 g wool (4 mordanted hanks)
250 g $Fe(II)SO_4$
Dyeing:
(1^{st}) Boil 50 l water, pH 7.35, add $Fe(II)SO_4$, pH 5, immerse mordanted pre-wetted wool, boil for 40 min, pH 4.40, remove from the dyebath, cool down for 30 min,
(2^{nd}) re-immerse 3 hanks, boil for 40 min, pH 4.20, remove from dyebath, cool down for 30 min,
(3^{rd}) re-immerse 3 hanks, boil for 40 min, pH 4.30, remove from dyebath, cool down for 1 hour, rinse all hanks in cold water until waste water is almost clear.

Oak Gall / W and mordanting for Black / W4
The bath was prepared as follows:
1000 g wool (6 hanks)
1000 g oak galls
Bring 50 l water to the boil, add oak galls, pH 4.30 immerse prewetted wool, boil for 2 hours, drain, cool down, hot rinse, leave to dry.

Black / W4
670 g wool (4 hanks)
The bath was prepared as follows:
109.4 g $Fe(II)SO_4$
109.4 g $Cu(II)SO_4$
Dyeing:
(1^{st}) Boil 50 l water, pH 7.7, add $Cu(II)SO_4$, pH 4.5, add $Fe(II)SO_4$, pH 3.77, immerse prewetted wool, (1^{st}) boil for 30 minutes, remove wool, pH 3.25, let cool down for 40 minutes, take out 1 hank.
(2^{nd}) Boil 3 hanks for 30 minutes, remove wool, pH unchanged, let cool down for 40 minutes, take out one hank.
(3^{rd}) Boil 2 hanks for 30 minutes, remove wool, pH unchanged, let cool down for 40 minutes, rinse all hanks, dry.

Washed / W
The wool was washed twice in excess water for 20 min at 80° C.

Blank dyed / W and Blank dyed with lye / W
The baths were prepared as follows:
1300 g wool (8 hanks)
75 g K_2CO_3
Blank mordanting:
The wool was immersed in 75 l water, pH 7.3 and boiled for 2 hours. The wool was removed from the bath and left to dry.
Blank dyeing:
Boil 4 hanks (blank mordanted) for 1 hour in 75 l water, pH 7.3. Rinse in cold water and dry.
Blank dyeing with lye:
Boil 4 hanks (blank mordanted) for 1 hour in 75 l water with 75 g K_2CO_3, pH 10. Rinse in cold water and dry.

Alum / W
The bath was prepared as follows:
670 g wool (4 hanks)
150 g alum
Boil 50 l water, dissolve alum, pH 3.50, immerse prewetted wool and boil for 1.5 h, wring, rinse and dry.

3.2.3. Weaving

24 wool model tapestry fabrics and 18 silk model tapestry fabrics were woven on a Northrop Single Shuttle loom. Warp and weft yarns had to be reversed to achieve the high weft density typical for the tapestry structure.

Beams were prepared by single-warping for each colour individually. The warp density during weaving was 26.6 ends per cm in wool and 34.6 ends per cm in silk, after taking off the loom the fabric contracted to a warp density of 28 ends per cm in wool and 35 ends per cm in silk. The weft yarn density was 8 picks per cm for. The weft/warp reverse of the structure very closely resembles the historic tapestry weave [6, 7, 11, 12]; therefore in the following, warp will be regarded as weft and vice versa.

Figure 3.2.1 shows the comparable weave structures of a model tapestry sample and a historic 16th century tapestry.

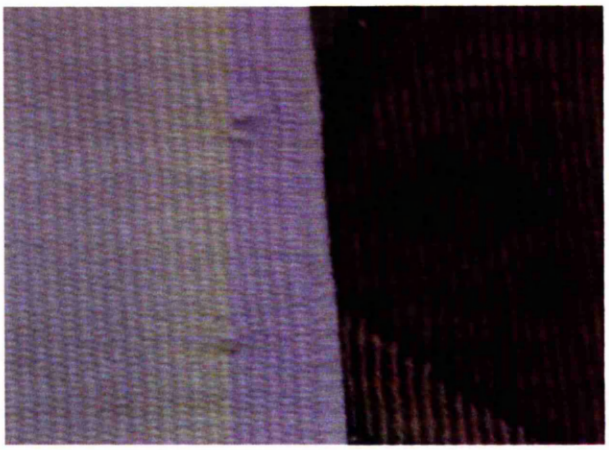

Figure 3.2.1. Photograph illustrating model and historic tapestry weave constructions

3.2.4. Accelerated ageing

Accelerated ageing was carried out by project partner HRP at Hampton Court Palace using a Xenotest-150S light-ageing instrument with an Atlas xenon lamp and a window glass filter with a UV cut-off at 320 nm. The spectral distribution closely matches that of sunlight (CIE 85/1989 [13]) in indoor conditions, Figure 3.2.2. The relative humidity in the sample chamber was monitored and controlled at 65%. The temperature in the sample chamber was uncontrolled but varied between 18 to 22°C during accelerated ageing for MODHT samples. The

illumination in the Xenotest-150S at the sample surface has been estimated at 150,000 lux. Samples are aged for 400 hours to a total exposure of 60 Mega lux hours. This is approximately the equivalent of 400 years exposure under usual museum lighting conditions.

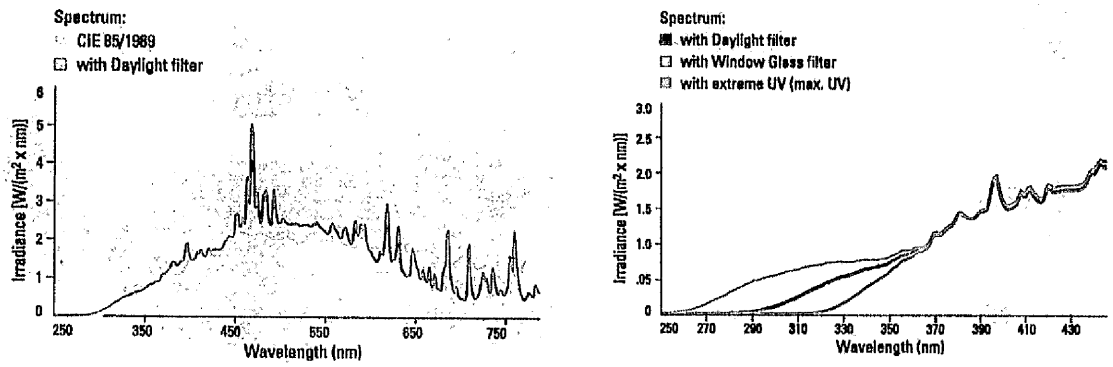

Figure 3.2.2. Atlas xenon lamp spectral distribution with different filters [14]

3.3. Model metal thread samples

Two sets of model metal threads have been produced by Bill Barnes, Goldenthreads, UK.

The silk core was dyed at UMIST using the historically accurate biological dye source and recipe for young fustic.

Six strands of silk were twisted together in Z direction to make the core. 85 μm diameter, electroplated copper – silver (1%) – gold (0.5% & 2%) wire, purchased from Leoni AG, was flattened between steel rollers to make the metal filament.

The threads were spun on a lapping machine, feeding the core through a hollow mandril in the centre of the rotating bobbin holding the metal filament.

3.4. References

1. Herrero Carretero, C., 'La Colección de Tapices de la Corona de España. Selección y Estudio. Propuesta de Análisis de la Herencia Textile Española', Patrimonio Nacional, Madrid (2002).
2. De Meûter, I., 'Sampling in Belgium. 17th-19th February 2003', Royal Museums of Art and History, Brussels (2003).
3. Hallett, K., 'Summaries of Condition Reports on Three Tapestries Selected for Sampling for MODHT Project', Historic Royal Palaces (2005) 1-2.
4. Campbell, T.P., 'Sampling at Hampton Court Palace. Art and display history taken from MODHT report', Historic Royal Palaces (2003).
5. 'Report on the Conservation Treatment Options for the Tapestry: The Meeting of Abraham and Melchizedek', Hampton Court Palace, Textile Conservation Studios.
6. Rapp-Buri and Stucky-Schuerer, *Burgundische Tapisserien*, Hirmer Verlag GmbH (2001) 420.
7. Bilson, T., B. Cooke, and D. Howell, 'Mechanical Aspects of Lining 'Loose Hung' Textiles', in *Fabric of an Exhibition, NAATC (North American Area Textile Conservation)*, Ottowa 1997, 1-14.
8. De Nie, W.L.J., *De Ontwikkeling der Noord-Nederlandsche Textielververij van de Veertiende tot de Achttiende Eeuw*, Transcripts from: Tbouck van Wondre (Brussel, 1513) and manuscripts from early 17th century with dyeing recipes of the Six and Kerspin Family (Holland). Leiden (1937).
9. Edelstein, S.M., *The Plictho of Gioanventura Rosetti.*, The M.I.T. Press, Cambridge (1969; translation of the 1548 (1st) edition).
10. Quye, A., 'Work package 1: report for MODHT 2nd interim meeting', KIK, NMS, Brussels, Edinburgh (2003).
11. Stucky-Schuerer and Rapp-Buri, *Zahm und Wild*, Verlag Philipp von Zabern (1990) 29.
12. Campbell, T.P., *Tapestry in the Renaissance, Art and Magnificence*, The Metropolitan Museum of Art, New York (2002).
13. CIE 85 (1989), 'Technical Report: Solar Spectral Irradiance', CIE Publication No. 85, TC 2.17, International Commission on Illumination.
14. Atlas Material Testing Solutions, 'Product information', www.atlasmtt.de.

Chapter 4. Analysis of Dyestuffs

4.1. Literature review on the classification of natural dyestuffs

Natural dyes and pigments have been used since prehistoric times. Pigmented soils are believed to have been the first sources of colour used by man, as demonstrated by Palaeolithic cave-paintings (15000-9000 BC). Early use of colour on textiles might have been the application of pigmented soils, minerals or soot. However, such colourings are not fast to rinsing and therefore cannot be regarded as textile dyes. Among the earliest archaeological findings of dyed textiles are an Egyptian red border from 3200 BC and mummy wraps dyed with saffron and ochre from 2500 BC. The earliest written record of the use of dyestuffs was found in China and dated to ~ 2600 BC [1].

Colourants used for textiles have been derived from a multitude of natural sources including all parts of plants (e.g. flowers, fruits, leaves, roots, bark and wood), lichen and fungi, insects and molluscs.

The obtained colour as well as the dyeing procedures and fastness properties greatly depend upon the chemical structure of the colourant constituents. These can be classified according to their chromophoric systems as follows [1-4].

- Polyenes: Carotenoids
- Diaryloylmethanes: Curcumin
- Benzoquinones
- Naphthoquinones
- Anthraquinones
- Indigoids
- Flavonoids
- Neoflavanoids
- Anthocyanides
- Gallotannins
- Lichen and Fungi

In addition H. Schweppe lists insoluble redwoods, xanthenes, benzophenones, basic quaternary ammonium compounds, condensed proanthocyanidines, naphthalene derivatives, chlorophyll, natural inorganic pigments and natural colourants with partially known or unknown constituents [1].

The most important natural dyestuffs used historically in tapestry production belonged to the groups of anthraquinones, indigoids, flavonoids, neoflavanoids, and gallotannins. Correspondingly the dyes investigated in this study belong to these groups. Their occurrence, chemistry and properties are discussed below.

4.1.1. Anthraquinones

The most important natural red dyes belong to the anthraquinone group. They are found in the roots of many plants as well as in insects and animals. Anthraquinone dyes generally require mordants for fixation. The dyes have good lightfastness and good washfastness due to the formation of complexes with metal salts. The roots of madder and the kermes or cochineal insect are sources of the most famous anthraquinone dyes. The earliest mention of kermes has been identified in the Bible book of Exodus, where references are made to scarlet coloured linen. The popular madder dye 'Turkey red' was a Near Eastern process which yielded the most brilliant red. The process involved up to 20 steps and until the early 19th century great efforts were undertaken to master the procedure and introduce it in Europe.

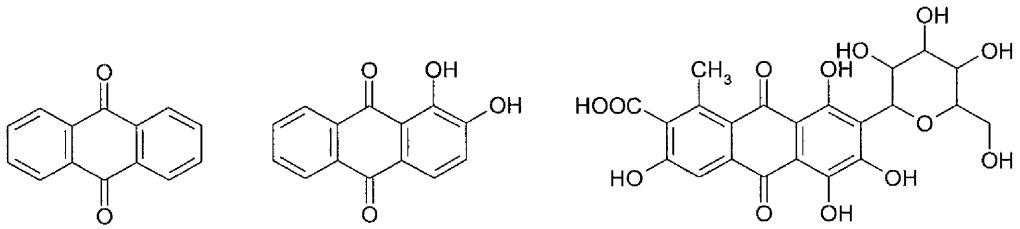

Scheme 4.1.1. Structure of anthraquinone, alizarin (from madder) and carminic acid (from kermes)

4.1.2. Indigoids

Indigo and Tyrian purple are some of the oldest and most important textile dyestuffs. Indigo is found in many plants, the most important being the European woad and the Asian indigofera tinctoria. Tyrian purple was probably the most famous and precious dyestuff in antiquity, some evidence indicates that it had already been used in the late Bronze age (13th cent. BC). Precursors of the red to purple dyes are obtained from the glands of various molluscs, the most important being hexaplex trunculus (old name is murex trunculus).

Indigoids are vat dyes, meaning that the water insoluble molecule has to be reduced to convert it into its soluble 'leuco' form. Historically that process was achieved by fermentation and enzymatic hydrolysis. The leuco form has affinity for textile fibres and can be reoxidised to yield its colour. The water insoluble nature of indigoids provides very good washfastness.

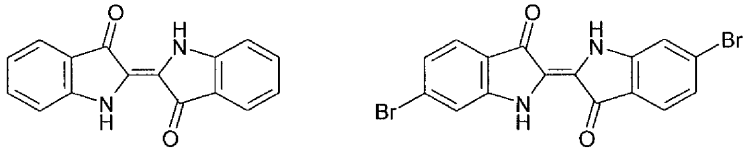

Scheme 4.1.2. Structure of indigotin (from woad) and 6,6 dibromoindigo (from hexaplex trunculus)

4.1.3. Flavonoids

Most natural yellow dyes are flavonoids and their main chromophores are based on flavone and flavonol ; further chromophores are isoflavone, flavanone, chalcone and aurone.

Well known plants that contain flavonoids and can be used for textile dyeing are weld, young fustic, dyer's greenweed, sawwort and camomile. Within the plants colourant constituents are often present as glycosides, which are hydrolysed in the dyebath. In most cases the dyeing procedure requires mordants to produce brilliant shades of yellow and improve the very variable light and washfastness properties. In general flavones are more resistant to photo-oxidation than flavonols.

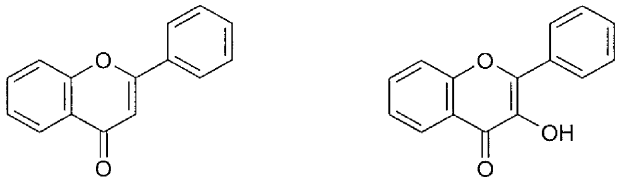

Scheme 4.1.3. Structure of flavone and flavonol

4.1.4. Neoflavanoids

Brazilwood and logwood are neoflavanoids, which despite their fugitive character were very common and popular dyestuffs. In fact Cabral named the country 'Brazil' on account of its vast forests of brazilwood when he and his companions landed

on the east coast of South America in 1500. The trees contain colourless compounds, which oxidise to give deep shades of red or blue in the case of logwood. Neoflavanoids are mordant dyestuffs and depending on the metal salt and pH of the dyebath various shades of red and blue can be achieved. The basic structure is shown in Scheme 4.1.4 , while Scheme 4.1.5 shows the parent and oxidised colourant constituents of Brazilwood.

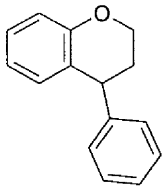

Scheme 4.1.4. Structure of neoflavan

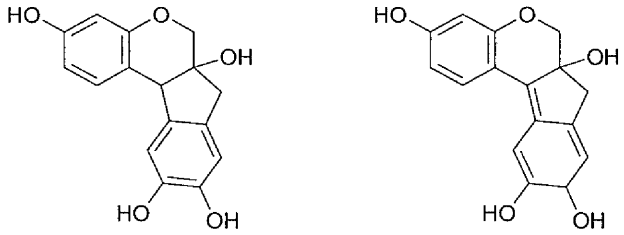

Scheme 4.1.5. Structure of brazilin (colourless) and brazilein (oxidised form; coloured)

4.1.5. Gallotannins

Gallotannins were originally used in leather processing but have also found application as mordants and, in combination with ferrous sulfate, as inks and dyestuffs for grey, brown and black.

Gallotannins can be found in the leaves, fruits, bark and wood of several trees and lower plants. However the chief source of gallotannins are galls, pathological growths on leaves, buds and twigs caused by the eggs of insects of the wasp family.

Gallotannins are usually large molecules containing gallic acid residues with ester linkages. Scheme 4.1.6 shows gallic acid and an example of a gallotannin compound contained in allepogalls, where the number and position of gallic acid residues and hydroxyl groups can vary.

It was found that free gallic acid residues in the dyebath reduce Fe(III) to Fe(II) and form a soluble iron-II-gallate. Hence, the capability to dye deep shades of black is decreased for those gallotannins containing free gallic acid.

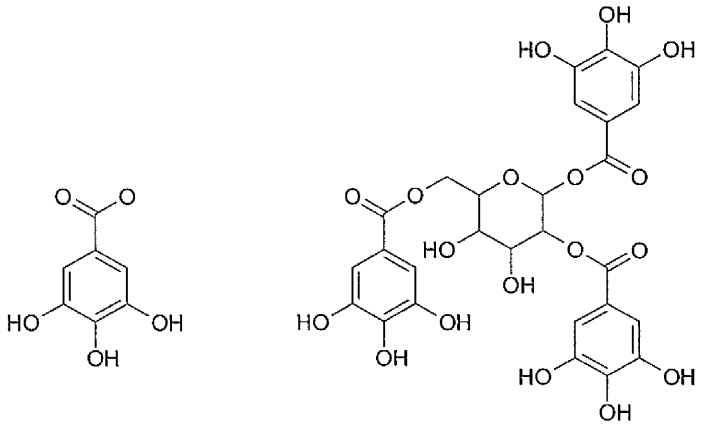

Scheme 4.1.6. Structure of gallic acid and gallotannin of allepogalls (*Quercus infectoria*)

4.2. Literature review on methods for the identification of natural dyestuffs

A comprehensive review of chemical, chromatographic and spectroscopic methods for the analysis of natural dyestuffs was written by Helmut Schweppe [1], in less detail by Bhattacharyya and Vairagi [5] and most recently by André Verhecken [6].

4.2.1. Chemical methods

Before the development of sophisticated instruments for the analysis of organic compounds, dyestuff identification was carried out based on the visual assessment of substrate, shade and depth of colour and the capability of various solvents to extract the dye. By judging the colour of extracts with water, ethanol, glacial acetic acid, ammonia and sulphuric acid the general class of most natural dyestuffs can be identified. For example fibres dyed with madder will not extract in water, ethanol or ammonia but extracts with glacial acetic acid are yellow and extracts with sulphuric acid are brown-red; while fibres dyed with brazilwood will yield a yellow extract in water, glacial acetic acid and sulphuric acid and a red extract in ammonia, ethanol does not cause extraction of brazilwood [1].

4.2.2. Chromatographic methods

The extracts of dyestuffs usually contain several chromophoric components; only the separation of these components can yield an unambiguous identification of the dye source. This can be achieved with various chromatographic methods [1].

First trials with chromatographic methods to separate dyes were already undertaken towards the end of the 19th century [7]. However, with the advent of Paper Chromatography (PC) the analysis improved. In PC the extracted dyestuff is applied to a stationary phase (paper, cellulose) which is partially immersed in a mobile phase (solvent). As the solvent spreads through the paper it causes the separation of the components of the sample according to how strongly they adsorb to the stationary phase versus how much they interact with the mobile phase. Various solvents and paper coatings have been used to make the method more versatile [1].

A further chromatographic method was invented in 1951. Thin Layer Chromatography (TLC) works on the same principle as paper chromatography, however the stationary phase is usually a thin coating of silica gel, aluminium oxide, polyamide, cellulose, acetylcellulose or diatomaceous earth on plates of glass, aluminium or polyester. For the separation of natural dyestuffs coatings of polyamide and in some cases silica gel were found to work best [1]. A comparison of the relative positions, colour and UV fluorescence (UV-Vis spectrophotometry) of the separated sample components with those of standard dyestuffs will in many cases lead to the identification of the unknown sample [1].

The establishment of High Performance Liquid Chromatography (HPLC) in 1966 led to better separation of sample components and offered even greater possibilities for the unequivocal identification of dyestuffs. In HPLC the flow of the mobile phase is pressure controlled as it moves through the stationary phase, defined as the immobile packing material in a column. The high resolution of HPLC is due to the controlled and continuous flow rate, high plate number (small particle size and long column), uniformity / quality of column material, accurate low volume sample injectors and sensitive low volume detectors. The introduction of diode array detectors greatly improved the performance of HPLC and made it possible to distinguish between similar plant dyes and insect dyes of different origins and families [8, 9] . In the 1960's some attempts were undertaken to use

Gas Chromatography (GC) for the identification of dyestuffs. Anthraquinone and flavonoid dyestuffs have been identified using GC, however, HPLC often linked with a diode array detector in order to fully characterise the dye's uv/visible absorption is the preferred and most widely used method [1, 5, 6, 8-15].

4.2.3. Spectroscopic methods

Additional approaches for the identification of dyestuffs are spectroscopic methods. It was found that the general class of dyestuffs in solution could be identified with absorption and transmission spectroscopy in the visual region and the ultraviolet region (UV/Vis Spectroscopy) as well as by Fluorescence Spectroscopy [6, 16]. However, it has not been possible to distinguish between different plants that contain the same class of dyestuffs. Infrared Spectroscopy and the more sensitive Fourier Transform Infrared Spectroscopy (FTIR) allow the determination of functional groups and, by comparison with standard spectra, the identification of dyes and pigments. The methods generally require the separation of all side products other than the dyestuff from the sample solution [1, 6].

Various mass spectrometric techniques have been applied successfully for the identification of dyes [9, 12, 15, 17, 18]. In particular the combination of Liquid Chromatography with Ion Trap Mass Spectrometry (LC-Ion-Trap-MS) [12, 15], High Resolution and Electrospray Mass Spectrometry [17, 18].

However, in all of these techniques extraction of the dyestuff from the fibre using various solvents and extraction protocols is required. The extraction process itself may be destructive and is not always quantitative for all chromophores in a dye mixture. Solvents can cause partial destruction or chemical alteration of chromophores during the extraction process or storage. The removal of samples and destructive testing of art and historical works is controversial. Wherever possible analysis techniques are being optimised to reduce samples sizes and the demand for in-situ analysis is great and has received much attention in conservation science.

4.2.4. Non-Extractive analysis

X-ray Fluorescence (XRF), Proton Induced X-ray Emission (PIXE) and Raman Spectroscopic methods are now routinely used for in-situ analysis of inks and pigments on manuscripts and paintings [19-28]. While these techniques are

excellent for the analysis of inorganic pigments and metals used in lake (insoluble mixtures of dyes with mineral binders), the identification of organic dyes is not possible with XRF and PIXE. Although Raman Spectroscopy yields molecular information and dyes can be analysed on the basis of their functional groups, the unambiguous identification is usually hampered by the high background of organic material from the substrate or paint binders and additives. A few studies on textiles have employed analytical methods that do not require the extraction of dyestuff or mordants [29-35], using Raman spectroscopy or Fluorimetry for the analysis of dyes and X-ray analytical techniques for the identification of metallic mordants. However, these techniques usually require large sample sizes, a disadvantage in conservation science where sample sizes are often in the microgram region. Wouters identifies Raman Micro-spectroscopy and Raman Fourier transform systems as potentially successful instrumentation in possible future developments in the analysis of organic dyes [36]. Nevertheless, at present there are no established in-situ methods for the analysis of natural dyes.

In recent years several researchers have investigated the applicability of Mass Spectrometric techniques that do not require extraction for the identification of natural dyestuffs. In particular, Time of Flight Secondary Ion Mass Spectrometry (ToF-SIMS) has been successfully employed to study iron-gall inks on paper and woad dyed wool [37] , while SIMS has been utilized in a study of the complexation sites of alizarin aluminium lakes [38]. UV Laser Time of Flight Matrix Assisted Laser Desorption Ionization Mass Spectrometry (ToF MALDI MS) has been shown to successfully identify Prussian Blue pigments (ferric ferrocyanide and the more modern phthalocyanine blue), the yellow pigment lead chromate as well as the dyestuff carminic acid from carmine alum lake in paint-on-paper samples [39]. A study employing MALDI and Electrospray Ionisation (ESI) MS has also proved the applicability of the techniques for the identification of carminic acid dye in a linseed oil and dammar resin matrix as paint on canvas [40]. A recent project "Molecular Aspects of Ageing in Painted Works of Art" (MOLART) has investigated various Laser Desorption Mass Spectrometric (LDMS) techniques for the identification of natural organic pigments and explored Imaging Secondary Ion Mass Spectrometry for the analysis of inorganic pigments and paint binding media [41-43]. Analysis of anthraquinones, flavonoids and indigoids was moderately successful. The LDMS technique was able to identify some but could not

distinguish all flavonoids present in yellow dyes and although anthraquinones, especially alizarin, could be identified, the analysis of anthraquinones in aged paint cross sections was reported to have failed. Nevertheless some promising results were obtained from the analysis of indigo and weld dyed wool fibres [41, 44, 45]. All of these studies suggest the potential effectiveness of the evolving mass spectrometric methods for dye analysis without extraction. However, none has given sufficient results on the analysis of natural dyes and in particular natural dyes applied to textile fibres, hence; there remains a strong uncertainty in the identification of unknown dyestuffs. As yet no method has been established as the most useful and much work remains before any mass spectrometric method could find common practical application in conservation science.

4.3. Potential of ToF-SIMS for dyestuff identification

SIMS is a powerful analysis technique capable of gaining atomic and molecular information from solid samples with the further advantage of minimal fragmentation of molecular ions facilitating their identification. The technique has been described in more detail in Chapter 2. section 2.3. In static mode the SIMS technique is classed as non-destructive as statistically every point in the analysed area is struck only once by the scanning primary ion beam and no perceptible damage occurs to the analysed sample surface. Analysis takes place in ultra-high vacuum, which presents a drawback as only small objects can be placed wholly into the analysis chamber, and in most cases a small sample must be taken for analysis. However, the option of reducing the area of analysis to a few μm^2 allows the analysis of single fibres, the removal of which does not cause any perceptible loss of material even to an intact textile. The Time of Flight analyser provides the high sensitivity required in static SIMS and a wide mass range. This is especially useful for the analysis of large molecules and compounds such as some anthraquinone dyestuffs and their metal mordant complexes.

SIMS has been successfully applied for the characterisation of synthetic organic dyes as layers deposited on Ag or Si substrates. Lenaerts et al. studied the influence of substrates, dye layer thickness and primary ion source on the secondary ion yield [46, 47]. Organic synthetic dyes have also been characterised on filter paper substrates in a study by Scheifers et al. who concluded that cationic

dye classes can be identified according to their low mass fragments and the particular dye may be identified by higher mass fragments or it's intact cation [48]. Goschnick et al. employed SIMS to analyse afterchrome dyed wool and investigated the distribution of chromium oxidation states from fibre surface to bulk [49]. ToF-SIMS has also found application in forensic research in a study of inks and printing colourants on paper [50]. All studies emphasize the high sensitivity of the SIMS technique and its powerful potential for the identification of organic dyes.

Few SIMS studies have been conducted on natural dyes and pigments. Boon et al. used Imaging SIMS for the investigation of elemental distribution in paint cross sections [42]. Sanyova employed the SIMS technique to study the complexation sites of aluminium with the anthraquinone dye alizarin [38]. Model and historic iron gall inks and their degradation products have been successfully characterised by Delamare and Repoux [37]. Their study also included ToF-SIMS analysis of woad dyed wool at intermediate dyeing steps, however, the obtained spectra did not permit unequivocal conclusions.

The SIMS and in particular ToF-SIMS powerful analysis capabilities and the above mentioned studies on synthetic organic and some natural dyes suggest the technique has the potential for in-situ dyestuff identification.

Therefore the present study was undertaken to investigate the applicability of Time of Flight Secondary Ion Mass Spectrometry (ToF-SIMS) for the identification of some natural dyestuffs.

4.4. Experimental

ToF-SIMS spectra were obtained from synthetic chromophores, known to be the colourant constituents of natural dyestuffs, as well as dried films of prepared dyebath solutions and dye on a paper or textile substrate. Film samples were also characterised from dyebaths "exhausted" onto untreated and alum mordanted wool in order to investigate possible changes in relative concentration of colourant constituents due to extended boiling time of the dyebath or differential dye uptake by the wool. Furthermore, ToF-SIMS analysis was also performed on cross sections of dyed wool fibres as well the intact surfaces of dyed wool and silk fibres.

4.4.1. Preparation of dyestuff solutions

Dyebaths were prepared for ToF-SIMS analysis of (a) un-exhausted dyebaths, (b) exhausted dyebaths and (c) dyebaths applied to filter paper. The preparation of the dyebaths is summarized in Table 4.4.1. The dyebaths were left to boil (or at 90°C for madder) for time (1) before the first samples of dyebaths were taken by filtering a small amount through silica (dyebath preparations a & b) or a single drop of the dyebath was applied to cellulose filter paper (dyebath preparations c). Subsequently prewetted wool was immersed in the dyebaths (b) and left to boil (or at 90°C) for time (2); the dyed wool was removed and samples of the partially exhausted dyebaths taken. Prewetted alum mordanted wool was then immersed in the partially exhausted dyebaths and dyed at the boil (or at 90°C) for time (3) before dyebath samples were taken.

Table 4.4.1. Preparation of dyebaths

Dyebath	analysis stage	dyestuff	lye (K_2CO_3)	water (tap)	temperature	time (min) (1)	time (min) (2)	unmordanted wool	time (min) (3)	alum mordanted wool	pH (prior to exhaustion)
Madder	a	2.0 g		250 ml	90°C	60					6.5
	b	2.0 g		250 ml	90°C	20	30	3 g	30	3 g	6.0
	c	1.2 g		100 ml	90°C	30					6.5
Madder + K_2CO_3	a	2.0 g	0.3 g	250 ml	90°C	60					9.2
	b	2.0 g	0.3 g	250 ml	90°C	20	30	3 g	30	3 g	8.8
	c	1.2 g	0.1 g	100 ml	90°C	30					7.3
Cochineal	a	2.0 g		250 ml	boil	60					5.6
	c	0.8 g		100 ml	boil	30					6.4
Cochineal + K_2CO_3	c	0.8 g	0.1 g	100 ml	boil	30					7.7
Brazilwood	a	5.0 g		250 ml	boil	60					6.5
Brazilwood + K_2CO_3	a	5.0 g	0.3 g	250 ml	boil	60					8.6
Dyer's Greenweed	a	5.0 g		250 ml	boil	60					5.6
	b	5.0 g		250 ml	boil	20	30	2 g	30	2 g	5.8
Dyer's Greenweed + K_2CO_3	a	5.0 g	0.3 g	250 ml	boil	60					8.4
	b	5.0 g	0.3 g	250 ml	boil	20	30	2 g	30	2 g	8.2
Weld	c	1.0 g		100 ml	boil	30					5.8
Weld + K_2CO_3	c	1.0 g	0.1 g	100 ml	boil	30					7.9
Young Fustic	a	5.0 g		250 ml	boil	10					5.3
	b	5.0 g		250 ml	boil	20	30	5 g	30	5 g	5.6
Oak Gall	a	5.0 g		250 ml	boil	20					3.5
	c	2.0 g		100 ml	boil	30					3.9
Alder Bark	a	5.0 g		250 ml	boil	60					5.2
$Fe(II)SO_4$	c	0.1 g		100 ml	boil	30					3.1

4.4.2. Mounting of samples and ToF-SIMS analysis conditions

ToF-SIMS analysis was conducted on synthetic colourant components and natural dyestuff powder, fresh and exhausted dyebaths as well as surfaces and cross sections of dyed wool and silk fibres. Table 4.4.2 summarizes the analyses which have been performed for each dyestuff.

Dyestuff powders were mounted on adhesive tape while dyebaths were dried as thin films on aluminium foil. Wool and silk fibres or resin embedded fibre cross sections were clamped on ToF-SIMS sample stubs.

ToF-SIMS spectra of mass range 0-1000 in positive and negative ion mode were acquired on a PHI 7000 instrument. Analysis was performed under static conditions using a Cs^+ primary ion source at 8 keV with a pulse length of 1.25 ns. A pulsed electron flood source (50-70 eV) was used for charge compensation on the textile samples.

Spectra of the cross sectioned dyed wool fibres and additional spectra of the dyebaths madder, madder + K_2CO_3, dyer's greenweed, dyer's greenweed + K_2CO_3 and powdered woad were acquired on an Ion-ToF ToF-SIMS 5 instrument using a Au_1^+ primary ion source. In the case of cross sections further spectra were acquired using a Au_3^+ primary ion source. Spectra were obtained in negative and positive ion mode over a mass range of 0-1000. For cross-sectioned samples the area of analysis was 84 μm^2 and primary ion dose was $3.37^* 10^8$, while dyebath samples were analysed at an area of 100 μm^2 and primary ion dose of $4.99^* 10^8$.

Table 4.4.2. ToF-SIMS analyses performed for various dyestuffs

Dyestuff / Tannin	**synthetic chromophore**	**dyebath**	**dyebath exhausted with wool**	**dyebath exhausted with alum wool**	**dye on filter paper**	**dye on alum filter paper**	**dyed silk (surface)**	**dyed wool (surface)**	**dyed wool (cross section)**
Madder	x	x	x	x	x	x		x	x
Madder + K_2CO_3		x	x	x	x	x	x	x	
Cochineal	x	x			x	x	x	x	
Cochineal + K_2CO_3					x	x			
Brazilwood		x							
Brazilwood + K_2CO_3		x							
Dyer's Greenweed		x	x	x					
Dyer's Greenweed + K_2CO_3		x	x	x					x
Weld					x	x			
Weld + K_2CO_3					x	x		x	
Young Fustic		x	x	x					
Oak Gall		x			x				
Oak Gall + $Fe(II)SO_4$					x				
Alder Bark		x							
Woad	x						x	x	x

4.5. Results

The results of ToF-SIMS analyses of synthetic components, natural dyestuff powders, dyebaths and fibres are listed and discussed collectively under the appropriate natural dyestuff.

All obtained ToF-SIMS spectra in their appropriate mass range are represented in the Appendix sections A.1. to A.9. Example spectra illustrating the principal peaks are also shown in this chapter.

4.5.1. Investigation of madder

Figure 4.5.1. Rubia tinctorum L.[51]2]

Madder used to be widely cultivated throughout Europe, Asia and the Americas. It is a sturdy annual plant, 50-80 cm high, whose roots can be dried and used for dyeing. Various shades of red can be acquired, depending on the mordant used.

At least eight different species of madder have been identified, each with slight variations in the relative concentrations of their colourant constituents. Variations in colourant constituents also occur due to season and age of the plants. Rubia tinctorum L. is the most common madder plant, Figure 4.5.1.

Madder belongs to the anthraquinone dyes. 23 different anthraquinones and 5 O-glycosides have been identified in the roots of the plant. The most important chromophores are alizarin, purpurin, pseudopurpurin, purpuroxanthin, munjistin and rubiadin; these are shown in Scheme 4.5.1 [1].

Of the colourant constituents only alizarin was analysed as a synthetic chromophore. Figure 4.5.2 shows the negative and positive ToF-SIMS spectra with clear peaks at m/z = 239^-, 240^- and 241^+, 242^+ for the negative and positive alizarin ions and isotopes, respectively. Figure 4.5.3 shows ToF-SIMS spectra of the madder dyebaths without and with the addition of lye (K_2CO_3) with

assignments listed in Table 4.5.1. In contrast to the analysis of synthetic alizarin where the major peaks were present in both negative and positive spectra, the anthraquinone peaks for madder in the dyebaths were exclusively present in the negative spectra. The predominant peak for madder is the m/z = 239^- ion alizarin, while the predominant peak in the spectrum for madder with lye is the peak assigned to rubiadin (m/z = 253^-). Further shifts in relative intensities due to the addition of lye were noted in the group of ions at m/z = 500^- to 550^-, as well as the absence of alizarin ester in the madder/lye dyebath, due to the instability of the ester bond to alkaline hydrolysis [52].

Madder dyebaths both with and without lye have also been analysed using $Au1^+$ as primary ion source; the spectra showed the same principal peaks in comparable relative intensities as was observed in the dyebaths' spectra using a Cs^+ primary ion source.

ToF-SIMS spectra of exhausted madder and madder/lye dyebaths have been obtained. Overall, the same peaks as listed in Table 4.5.1 were also observed for exhausted dyebaths; no significant changes in relative intensities were noted.

ToF-SIMS analysis of the surface of madder dyed wool and silk has been performed (samples Red/W1, Red/W1_wl and Red/S2_b dyeing recipes are listed in Chapter 3, section 3.2.2.). It has not been possible to detect any peaks relating to anthraquinone compounds. Analysis of a yarn cross-section of sample Red/W1 did also not produce peaks clearly identifiable as madder chromophores or its derivatives. Peaks at m/z = 239^- and 223^- were present in the ToF-SIMS spectrum of the madder dyed wool cross section but may be related to contamination rather than alizarin and its derivative because the negative ion spectra of cross-sectioned Dyer's Greenweed dyed wool and woad dyed wool also showed the peaks at m/z = 223^- as well as m/z = 239^-, respectively, see ToF-SIMS spectra in the appendix.

Madder and madder/lye dyebaths were also analysed on filter paper substrates with and without prior impregnation with alum mordant. The main peaks observed were the same as those identified on spectra of dyebaths on aluminium foil substrate although the recorded intensities were 10-100 times lower.

Alizarin
Molecular formula = $C_{14}H_8O_4$
Molecular weight = 240.211

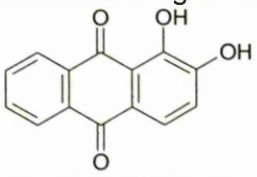

Purpurin
Molecular formula = $C_{14}H_8O_5$
Molecular weight = 256.210

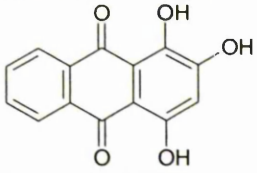

Pseudopurpurin
Molecular formula = $C_{15}H_8O_7$
Molecular weight = 300.23

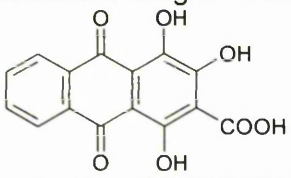

Purpuroxanthin
Molecular formula = $C_{14}H_8O_4$
Molecular weight = 240.211

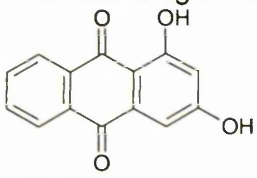

Munjistin
Molecular formula = $C_{15}H_8O_6$
Molecular weight = 284.220

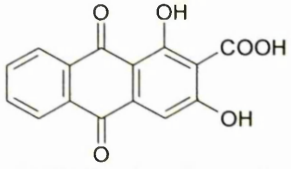

Rubiadin
Molecular formula = $C_{15}H_{10}O_4$
Molecular weight = 254.238

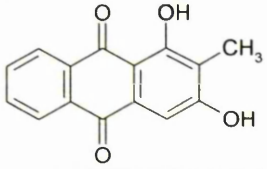

Scheme 4.5.1. Structures of chromophores of madder

Alizarin synthetic chromophore negative ion spectrum : Cs^+ primary ion source

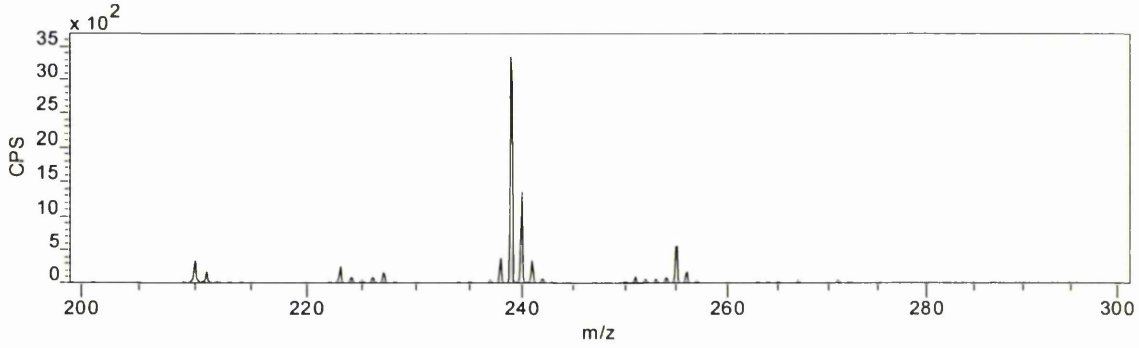

Alizarin synthetic chromophore positive ion spectrum : Cs^+ primary ion source

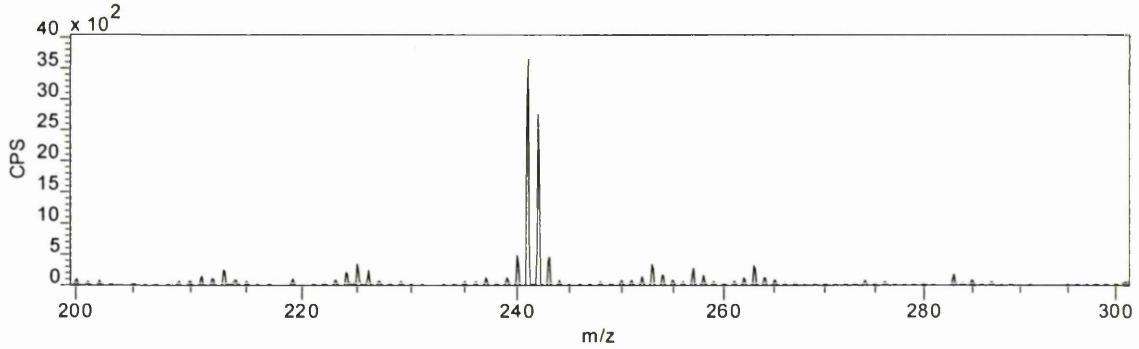

Figure 4.5.2. Negative and positive ion ToF-SIMS spectra of synthetic alizarin

Madder dyebath negative ion spectrum : Cs^+ primary ion source

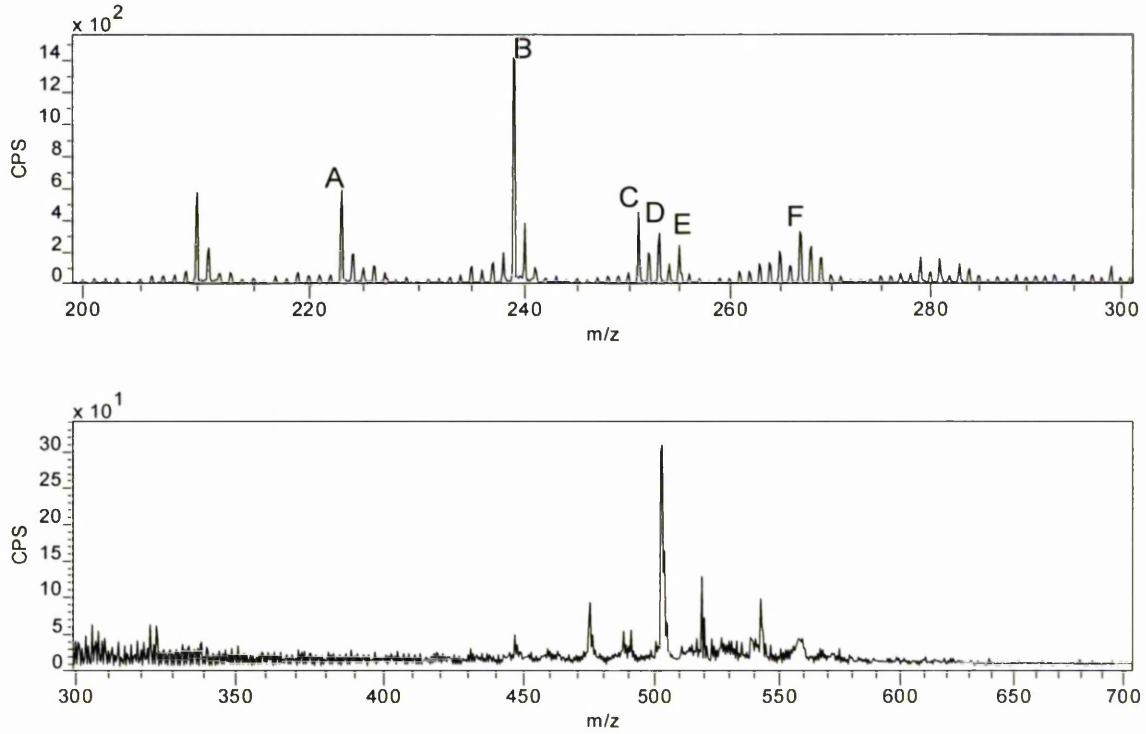

Madder/lye dyebath negative ion spectrum : Cs^+ primary ion source

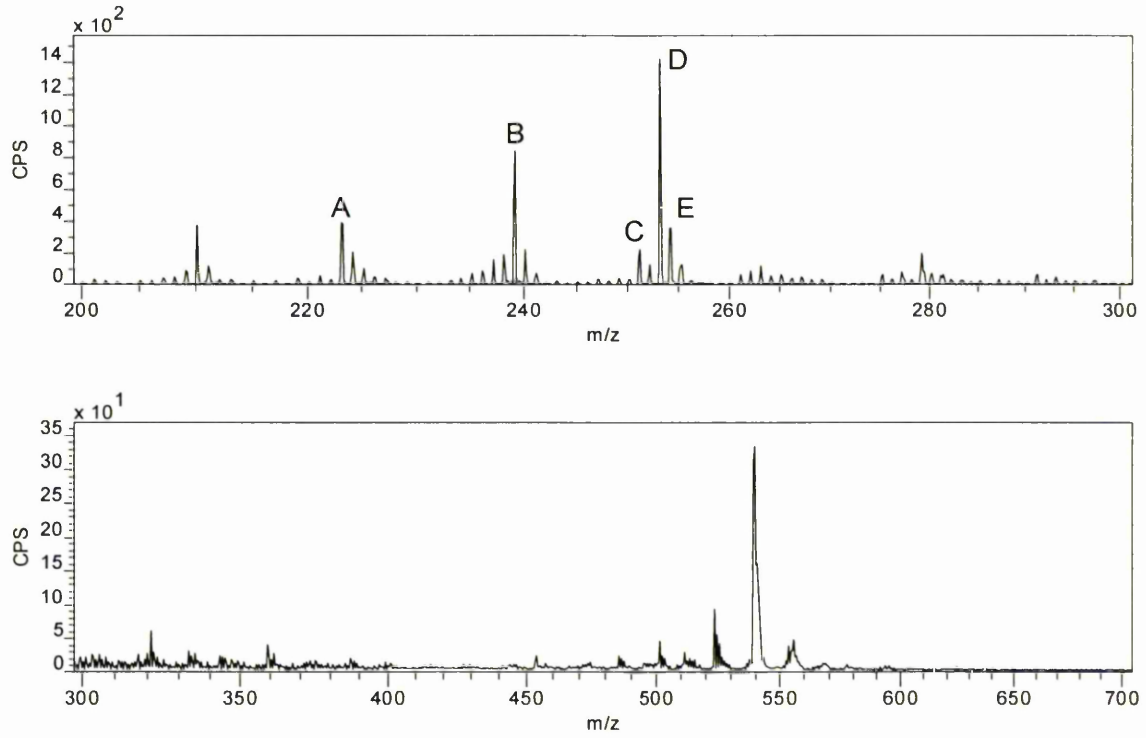

Figure 4.5.3. Negative ion ToF-SIMS spectra of Madder and Madder/lye dyebaths

Table 4.5.1. ToF-SIMS assignments for madder compounds

m/z		Assignment	Molecular ion structure	dyebaths	dyebaths applied to paper	dyebaths + K_2CO_3	dyebaths + K_2CO_3 applied to paper
223$^-$	A	alizarin derivative	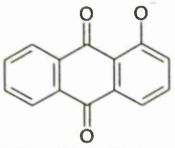	•	•	•	•
239$^-$	B	alizarin	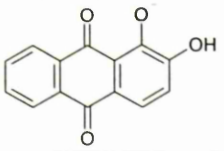	•	•	•	•
251$^-$	C	rubiadin derivative	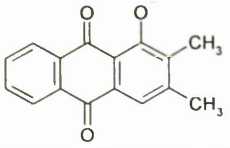	•	•	•	•
253$^-$	D	rubiadin	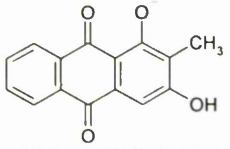	•	•	•	•
255$^-$	E	purpurin	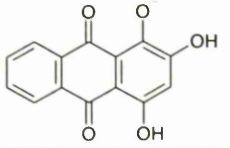	•		•	
267$^-$	F	alizarin ester	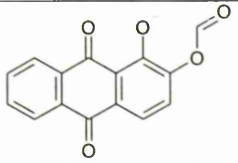	•			

• Ion intensity present

4.5.2. Investigation of cochineal

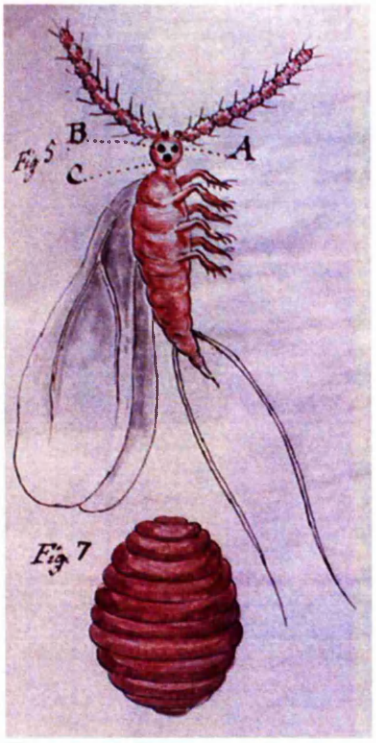

Figure 4.5.4. Cochineal (male and female insects) [53]4]

Cochineal is an anthraquinone dyestuff extracted from dried pregnant female scale insects. There are several species of cochineal insects, the most important being the American cochineal, followed by the Armenian cochineal and the Polish cochineal. All cochineal dyes have the major colourant constituent carminic acid. Related scale insect dyes are extracted from kermes and lac, whose main chromophores are kermesic acid and laccaic acid, respectively. Kermes is native to the Mediterranean and has been used as a dyestuff since Roman times or earlier. In the 16th century Spaniards introduced the American cochineal in Europe which had a greater concentration of colourant constituents and eventually completely replaced the use of kermes in Europe. In addition to carminic acid the American cochineal also contains traces of flavokermesic acid and kermesic acid, Scheme 4.5.2.

In ToF-SIMS analysis of synthetic carminic acid a clear peak at m/z = 491$^-$ was observed in the negative spectrum, Figure 4.5.5. Clusters of peaks also occurred at m/z = 309$^-$ to 313$^-$, 325$^-$ to 327$^-$, 337$^-$ to 339$^-$, 353$^-$, 418$^-$, 447$^-$ and 473$^-$ to 475$^-$; most of these peaks were also observed in the negative ToF-SIMS spectrum of cochineal in the dyebath, Figure 4.5.6, it was therefore assumed that they are anthraquinone derivatives of carminic acid. The peak cluster at m/z = 309$^-$ to 313$^-$ could possibly be attributed to kermesic acid. However, none of the other peaks could be assigned to specific compounds. In the dyebath spectrum the peak for carminic acid at m/z = 491$^-$ was relatively small and the predominant peak occurred at m/z = 381$^-$. It was not possible to identify peaks relating to cochineal chromophores in ToF-SIMS analysis of cochineal dyebaths on filter paper (with and without lye) or cochineal dyed wool and silk surfaces (samples Red / W4 and Red / S3), possibly due to migration of chromophoric species into the subsurface.

Carminic acid
Molecular weight: 492.40

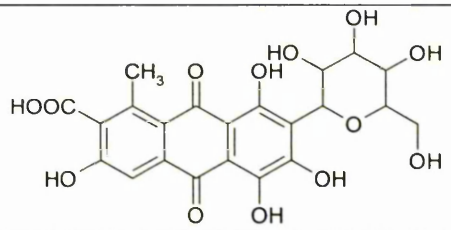

Flavokermesic acid
Molecular weight: 314.25

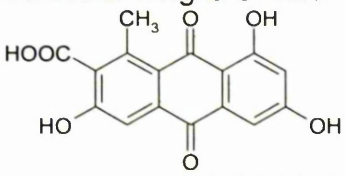

Kermesic acid
Molecular weight: 330.25

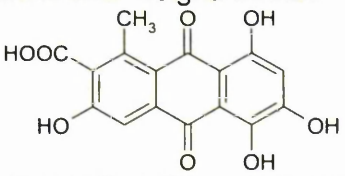

Scheme 4.5.2. Structure of chromophores of cochineal

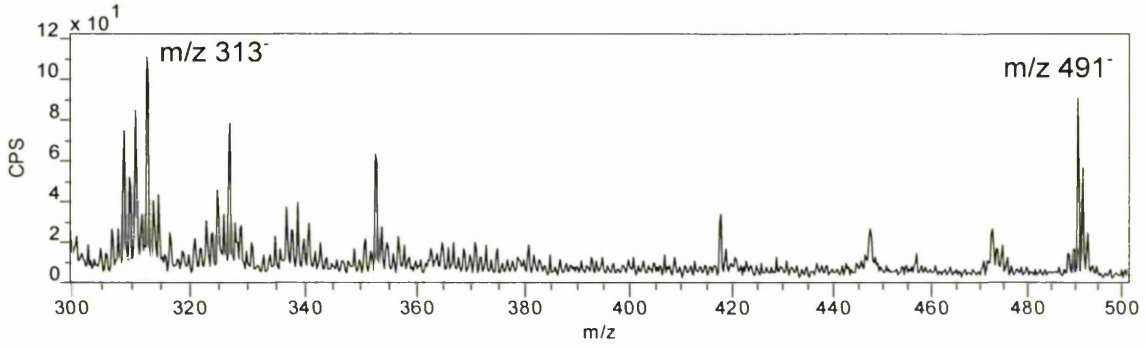

Figure 4.5.5. Negative ion ToF-SIMS spectrum of synthetic carminic acid : Cs^+ primary ion source

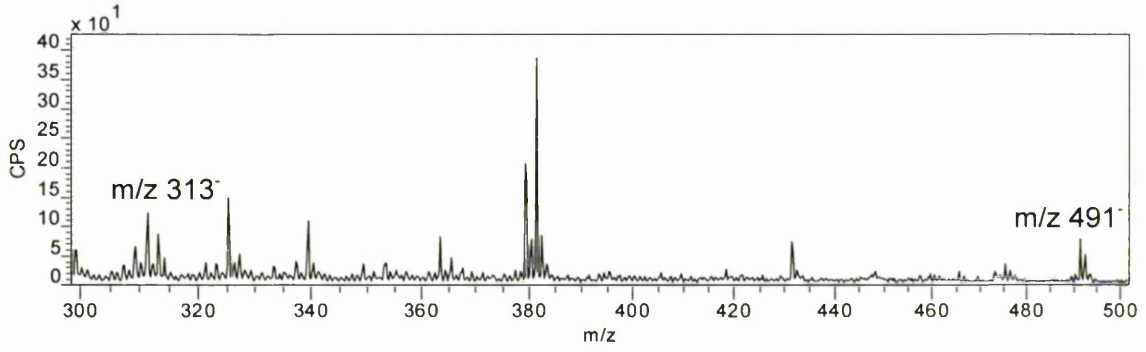

Figure 4.5.6. Negative ion ToF-SIMS spectrum of cochineal dyebath : Cs^+ primary ion source

4.5.3. Investigation of brazilwood

Figure 4.5.7. Caesalpinia [54]5]

The heartwood of several red wood trees of the *caesalpinia* family is used for dyeing; all are neoflavanoid dyestuffs and contain brazilin, which oxidises to the chromophore brazilein, Scheme 4.1.5.

The term brazilwood is specific for *caesalpinia brasiliens L. – Leguminosae*, other red wood trees used for dyeing include sappan wood, fernambuco wood, peachwood and braziletto wood.

Dyebaths of brazilwood without and with the addition of lye were ToF-SIMS analysed. Negative ToF-SIMS spectra are shown in Figure 4.5.8. A peak attributable to brazilein (m/z = 283^-) was only observed in the negative spectrum of the brazilwood dyebath without lye. In the comparable spectrum for brazilwood with lye a peak of similar intensity was observed at m/z = 281-, which could be attributed to brazilein with the replacement of one hydroxyl group by a methyl group, Table 4.5.2. However, these peaks were not the predominant peaks of the spectra; peaks with higher intensities were observed at m/z = 303^-, 229^-, 227^-, 211^- and lower molecular weights; no assignments were made for these peaks.

Brazilwood dyebath negative ion spectrum : Cs^+ primary ion source

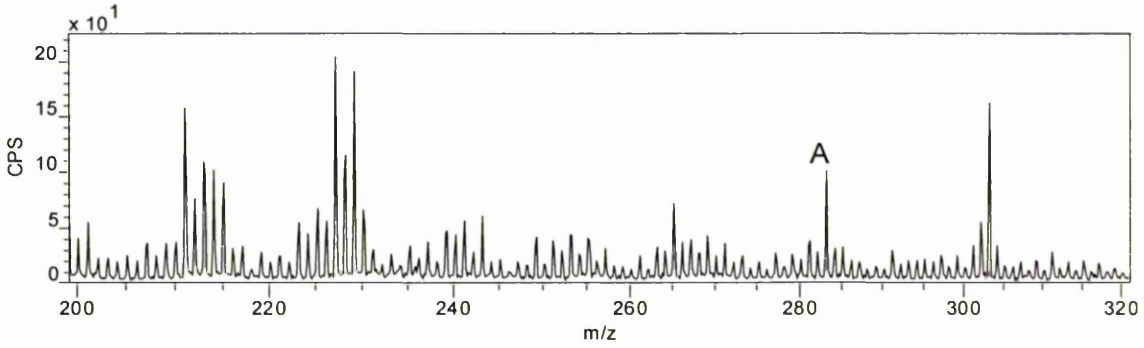

Brazilwood/lye dyebath negative ion spectrum : Cs^+ primary ion source

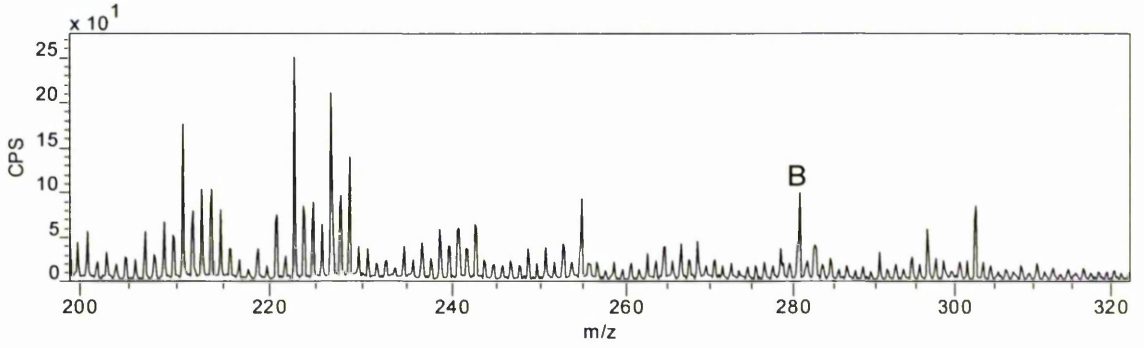

Figure 4.5.8. Negative ion ToF-SIMS spectra of Brazilwood dyebaths

Table 4.5.2. ToF-SIMS assignments for Brazilwood

m/z		Assignment	Molecular ion structure	dyebaths	dyebaths + K_2CO_3
283$^-$	A	brazilein	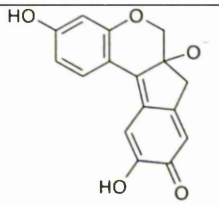	•	
281$^-$	B	brazilein derivative	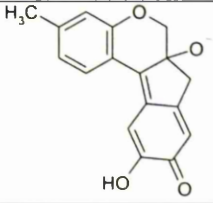		•

• Ion intensity present

4.5.4. Investigation of dyer's greenweed

Figure 4.5.9. Genista tinctoria L. [55]6]

Dyer's greenweed (Genista tinctoria L.) is a shrubby plant native to Britain, Central and Southern Europe and established in North America. Its flowers, leaves and small twigs can be used for dyeing on mordanted wool. It produces a bright yellow colour, which can be modified to give brown or olive green when treated with ferrous sulfate or copper sulfate respectively [1].

The dyestuff belongs to the flavonoid group with its major colourant constituents being luteolin and genistein.

Luteolin and genistein are also the principal peaks observed in the negative ToF-SIMS spectrum of the Dyer's greenweed (DGW) dyebath, Figure 4.5.10. In addition to luteolin and genistein the positive spectrum also exhibits peaks assigned to genistein methyl ether, luteolin methyl ether and some unidentified peaks at m/z = 213^+, 245^+ and 249^+.

Of the chromophoric peaks found in the spectra of DGW dyebath only genistein at m/z = 269^- was observed at low intensity in the DGW with lye (DGW/lye) spectra. A dominant peak at m/z = 255^- was assigned to flavanone, however, this assignment is tentative because the common contaminant palmitic acid appears at the same mass to charge ratio and, though weak, signals at m/z = 255^- have been noted in spectra of non-flavonoid dyebaths and in particular dyebaths applied to filter paper. A group of peaks at m/z = 277^- to 283^- appeared on all DGW/lye spectra and was assigned to luteolin with its hydroxyl groups replaced by methyl groups. All assignments are listed in Table 4.5.3.

DGW and DGW/lye were also analysed using a $Au1^+$ primary ion source; the results were comparable to those obtained using Cs^+ as primary ions with the same principal peaks in similar relative intensities.

ToF-SIMS spectra of exhausted DGW and DGW/lye dyebaths have been obtained. In general, the same peaks as listed in Figure 4.5.10 and Table 4.5.3 were also observed for exhausted dyebaths.

DGW/lye dyed wool (Yellow/W2_wl) was analysed in cross section, however, no peaks were identified as chromophores or their derivatives.

Dyer's greenweed dyebath negative ion spectrum : Cs^+ primary ion source

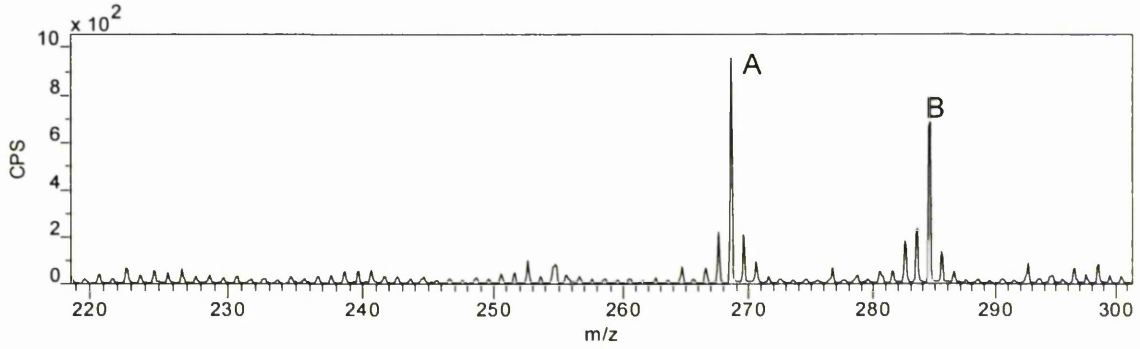

Dyer's greenweed dyebath positive ion spectrum : Cs^+ primary ion source

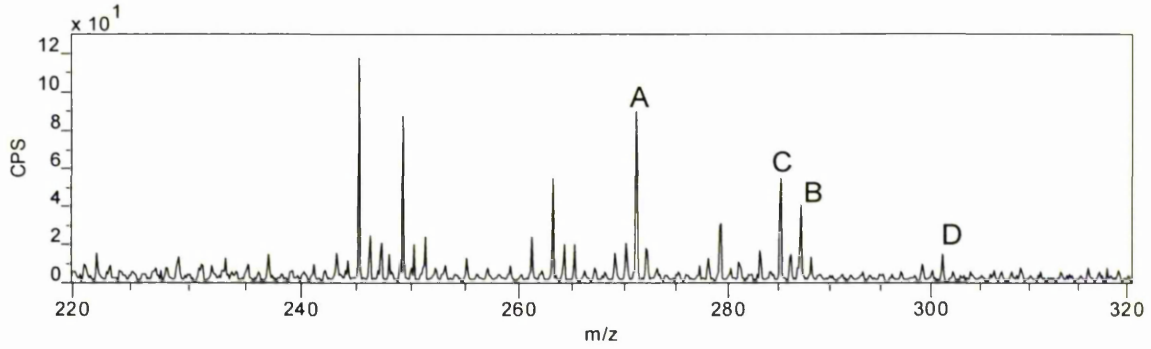

Dyer's greenweed with lye dyebath negative ion spectrum : Cs^+ primary ion source

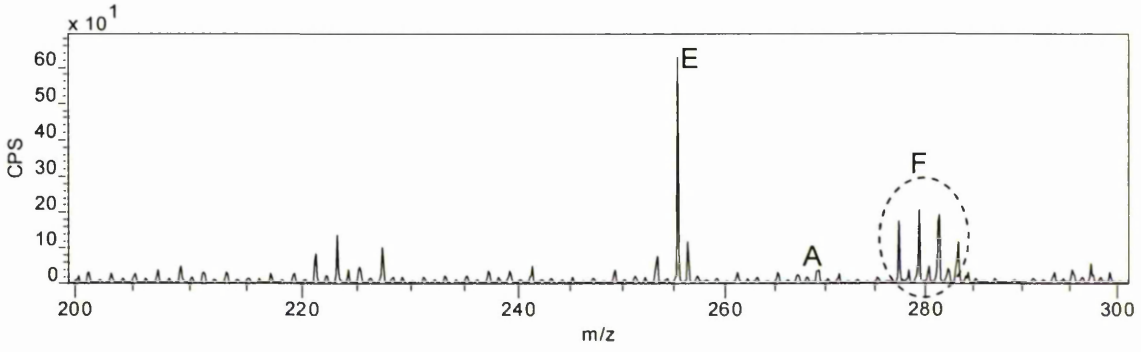

Figure 4.5.10. Negative and positive ion ToF-SIMS spectra of dyebaths of Dyer's greenweed and Dyer's greenweed with lye

Table 4.5.3. ToF-SIMS assignments of DGW compounds

m/z		Assignment	Molecular ion structure	dyebaths	dyebaths + K_2CO_3
255^-	E	flavanone	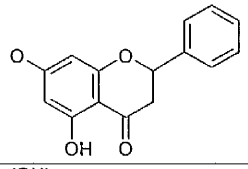		•
269^- 271^+	A	genistein	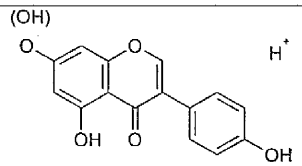	•	•
277^- to 283^-	F	luteolin derivatives	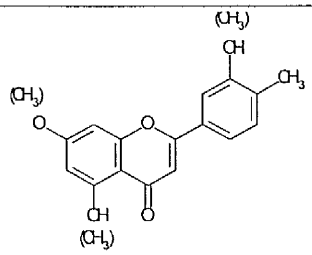		•
285^- 287^+	B	luteolin	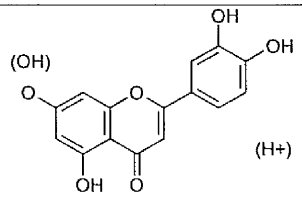	•	
285^+	C	genistein methyl ether	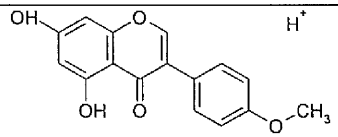	•	
301^+	D	luteolin methyl ether	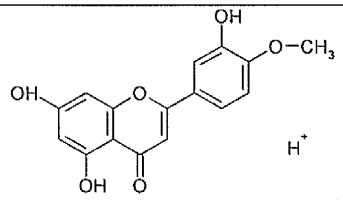	•	

• Ion intensity present

4.5.5. Investigation of weld

Figure 4.5.11. Reseda luteola L. [56]7]

Weld (Reseda luteola L.) is a biennial plant, native to Central and Southern Europe that grows to 50 to 150 cm height and produces pale yellow flowers. The whole plant can be used for dyeing; especially the seeds are rich in chromophores.

Weld, as one of the oldest yellow dyestuffs, was cultivated throughout Europe. It was already known in Antiquity and remained the most important yellow dyestuff in Europe until the discovery of the Americas and the subsequent import of dyestuffs with higher concentrations of chromophores.

Dyed on alum mordanted wool or silk, weld yields bright lemon- yellow shades. Olive or brown shades can be achieved with copper or iron mordants respectively. The light fastness is generally considered to be good [1].

Weld belongs to the group of flavonoid dyestuffs with its main colourant constituent being luteolin; small amounts of apigenin, isorhamnetin and a glycoside of kaempferol are also present, Scheme 4.5.3.

ToF-SIMS spectra were obtained from weld and weld with lye dyebaths on filter paper substrate only. The dominant peaks in the higher mass range in both positive and negative mode occurred at m/z = 287^+ and 285^-, respectively, and were attributed to luteolin. Apigenin was also identified in the positive spectra only at m/z = 271^+. Further high intensity signals were noted at m/z = 255^-, possibly attributable to flavanone, and an unassigned peak at m/z = 221^-. Overall the same peaks were observed for weld dyebaths and weld/lye dyebaths. Positive and negative ToF-SIMS spectra showing the aforementioned peaks are represented in Figure 4.5.12. Assignments are listed in Table 4.5.4.

ToF-SIMS spectra were also obtained from weld dyed wool fibre surfaces; however, the analysis was unsuccessful in detecting the chromophores.

Luteolin Molecular weight: 286.24 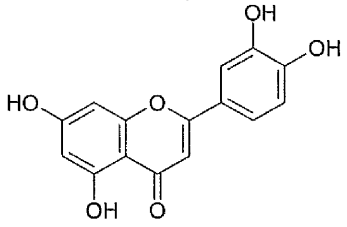	Apigenin Molecular weight: 270.24 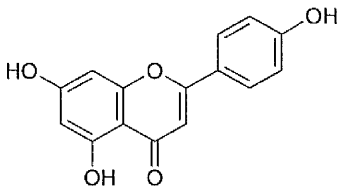
Isorhamnetin Molecular weight: 300.27 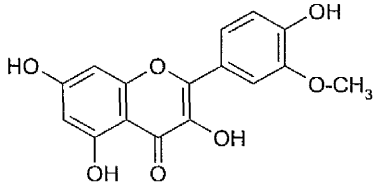	Kaemperol 3-glycoside-7-rhamnoside Molecular weight: 578.53 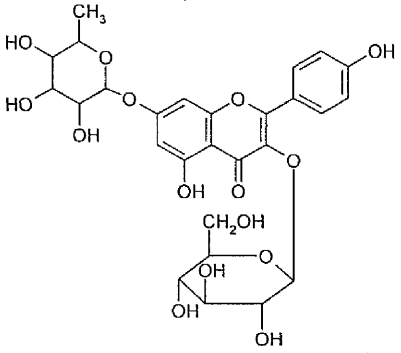

Scheme 4.5.3. Structures of chromophores of weld

Weld/lye dye on filter paper positive ion spectrum : Cs^+ primary ion source

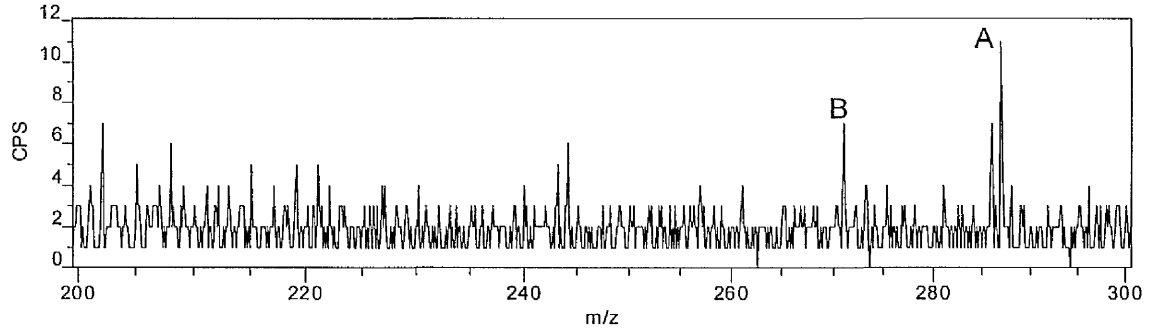

Weld/lye dye on filter paper negative ion spectrum : Cs^+ primary ion source

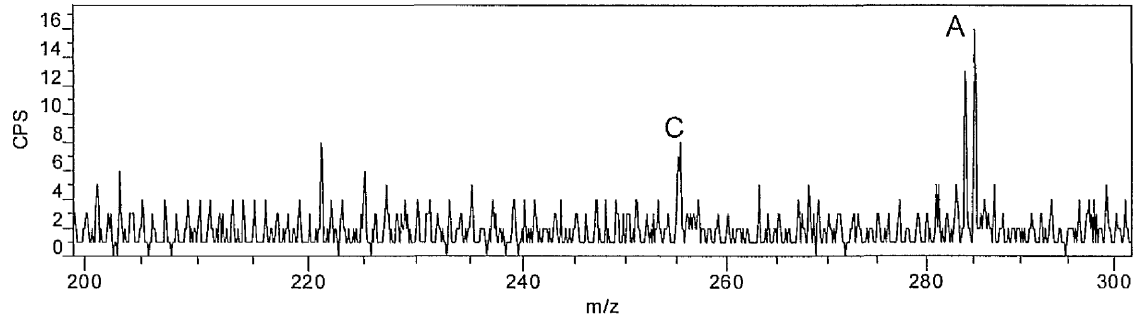

Figure 4.5.12. Positive and negative ToF-SIMS spectra of weld/lye on filter paper

Table 4.5.4. ToF-SIMS assignments for Weld

m/z		Assignment	Molecular ion structure	dyebath on filler paper	dyebaths + K_2CO_3 on filter paper	dyebaths on alum filter paper	dyebaths + K_2CO_3 on alum filter paper
255^-	C	flavanone	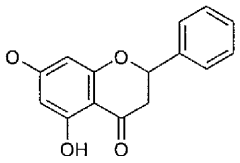	•	•		
271^+	B	apigenin	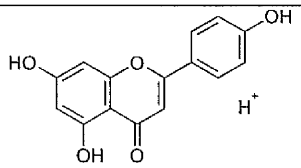	•	•	•	
285^- 287^+	A	luteolin	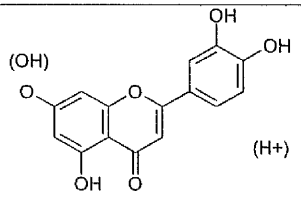	•	•	•	•

• Ion intensity present

4.5.6. Investigation of young fustic

Figure 4.5.13. Cotinus coggygria [57]8]

Young fustic (cotinus coggygria) is a bushy tree up to 3 m in height and native to southern Europe, the Mediterranean, and various regions in Asia.

Its leaves contain tannins and were sometimes used for dyeing black on iron mordanted wool.

In particular the heartwood of young fustic is used for dyeing, it contains yellow flavonoid chromophores, fisetin, myrcetin, fustin and sulfuretin, Scheme 4.5.4 [1, 4].

The silk cores of metal threads were often dyed with young fustic, which is a mordant dyestuff and gives deep shades of yellow-orange and even red, yet with poor lightfastness.

ToF-SIMS analysis of the dyebath indicated the presence of sulfuretin and fisetin and / or fustin, which has the same molecular weight as fisetin. Negative and positive ToF-SIMS spectra are shown in Figure 4.5.14. In the positive spectrum sulfuretin and fisetin were also present with Na^+ and K^+ ions. Assignments are listed in Table 4.5.5. Fisetin and myrcetin are regarded as the main colourant constituents of young fustic [4], therefore the relatively high intensity of sulfuretin and the absence of a peak for myrcetin were surprising.

ToF-SIMS spectra of exhausted young fustic dyebaths have been obtained; overall the intensities for the chromophoric peaks were similar to those observed for the non-exhausted dyebath.

Fisetin
Molecular weight: 286.236

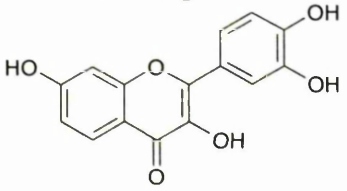

Fustin
Molecular weight: 286.236

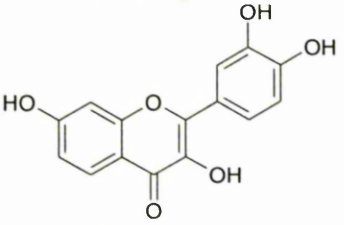

Myrcetin
Molecular weight: 318.24

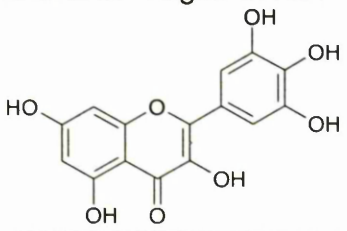

Sulfuretin
Molecular weight: 270.237

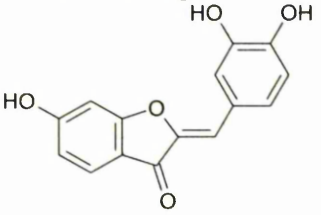

Scheme 4.5.4. Structures of chromophores of Young fustic

Young fustic dyebath negative ion spectrum : Cs^+ primary ion source

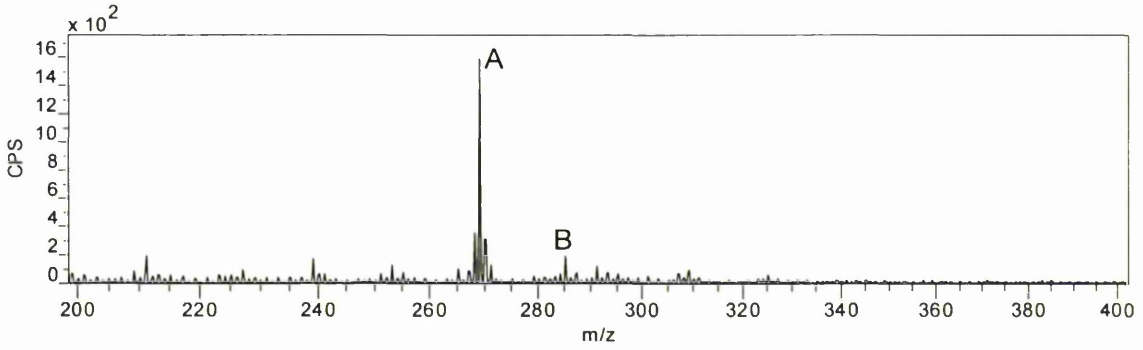

Young fustic dyebath positive ion spectrum : Cs^+ primary ion source

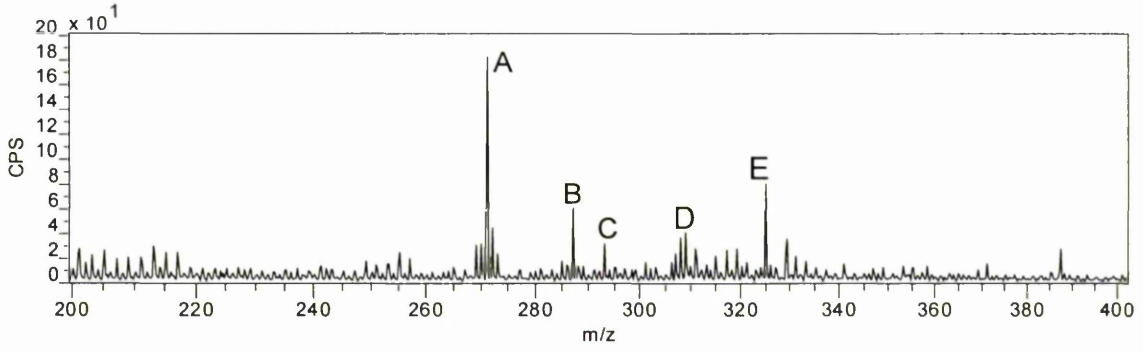

Figure 4.5.14. Negative and positive ion ToF-SIMS spectra of young fustic dyebath

Table 4.5.5. ToF-SIMS assignments for Young fustic

m/z		Assignment	Molecular ion structure	dyebaths
269^- 271^+	A	sulfuretin	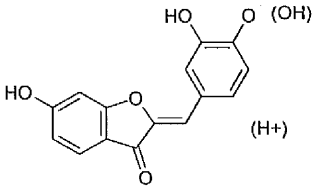	•
285^- 287^+	B	fisetin and/or fustin	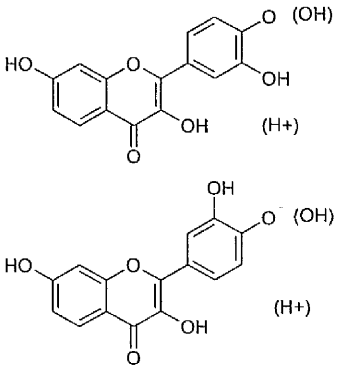	•
293^+	C	sulfuretin + Na^+		•
309^+	D	sulfuretin + K^+ and/or fisetin (or fustin) + Na^+		•
325^+	E	fisetin (or fustin) + K^+		•

• Ion intensity present

4.5.7. Investigation of oak gall

Figure 4.5.15. Oak gall [58]9]

Oak galls are globular growths on the twigs of the dyer's oak, *Quercus infectoria* OLIV., caused by irritations due to the deposition of eggs by the gall-wasp, *Cynips Gallae tinctoriae* OLIV.

Oak galls and other gallotannin containing galls, e.g. sumach galls were traditionally used in the leather industry and in combination with iron (II) sulfate as black ink and textile dyestuffs. The principal constituents of oak galls are 50 to 70 % gallotannic acid and 2 to 4 % gallic acid, ellagic acid, sugar and starch [59], Figure 4.5.16.

An unknown peak at m/z = 130^+ and a gallic acid derivative peak at m/z = 153^+, exhibited high intensities in the positive ToF-SIMS spectrum of the oak gall dyebath, Scheme 4.5.5.

The negative ion ToF-SIMS spectrum of the oak gall dyebath, Scheme 4.5.5, exhibited peaks, which could be assigned to gallic acid (m/z = 169^-) and ellagic acid (m/z = 301^-). The peak assignments are listed in Table 4.5.6. A high intensity peak at m/z = 124^- was previously observed by Delamare and Repoux and assigned to $C_6H_4O_3$ [37]. Another high intensity peak at m/z = 517^- could possibly be due to large gallotannin residues, the structure of which could not be established.

ToF-SIMS spectra were also obtained from oak gall dyebath on filter paper and oak gall with ferrous sulphate dyebath on filter paper. The analyses showed essentially the same peaks as were detected from the oak gall dyebath on aluminium foil substrate. However, no peaks were identified for the Fe^+ ion or iron containing species.

Gallic acid
Molecular
weight: 170.10

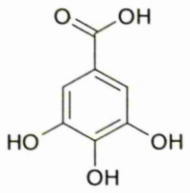

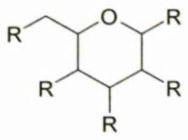

R = gallic acid residues or OH

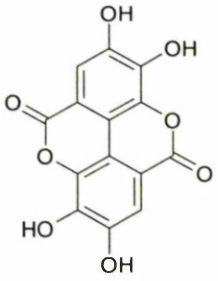

Ellagic acid
Molecular
weight: 302.20

Scheme 4.5.5. Positive and negative ion ToF-SIMS spectra of Oak gall dyebath

Oak gall bath positive ion spectrum : Cs^+ primary ion source

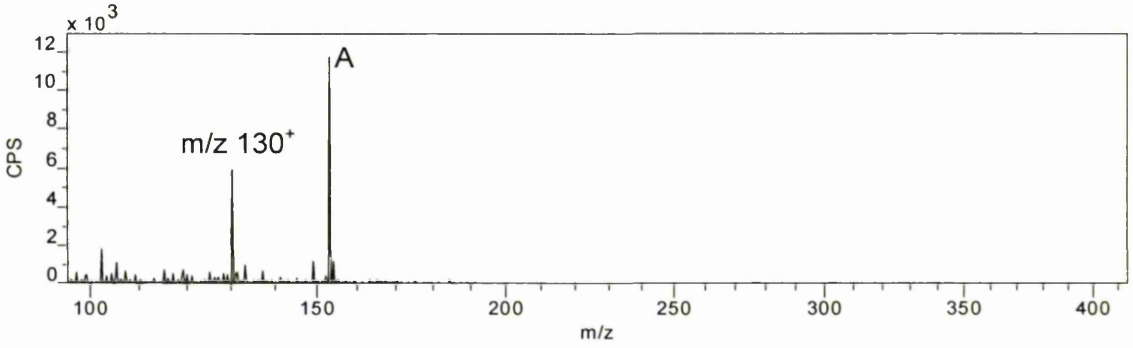

Oak gall bath negative ion spectrum : Cs^+ primary ion source

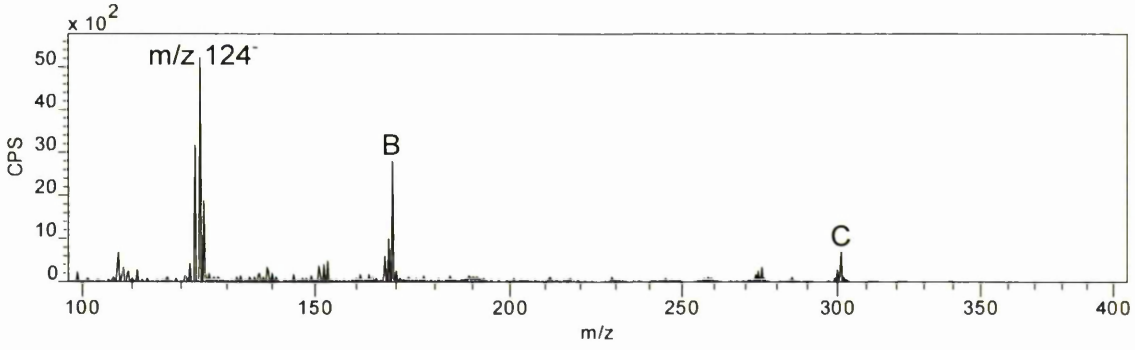

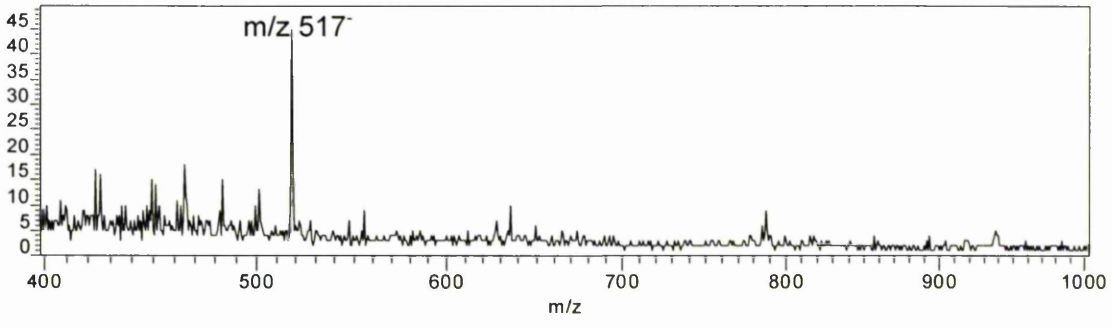

Figure 4.5.16. Structures of Gallic acid, gallotannin and ellagic acid

Table 4.5.6. ToF-SIMS assignments for Oak gall

m/z		Assignment	Molecular ion structure	dyebaths	dyebaths applied to paper	dyebaths + $Fe(II)SO_4$ applied to paper
153^+	A	gallic acid derivative	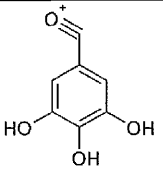	•	•	•
169^-	B	gallic acid	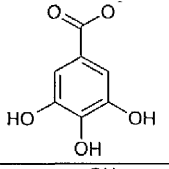	•	•	•
301^-	C	ellagic acid	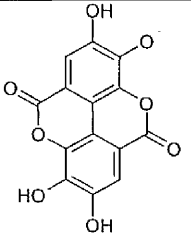	•	•	•

• Ion intensity present

4.5.8. Investigation of alder bark

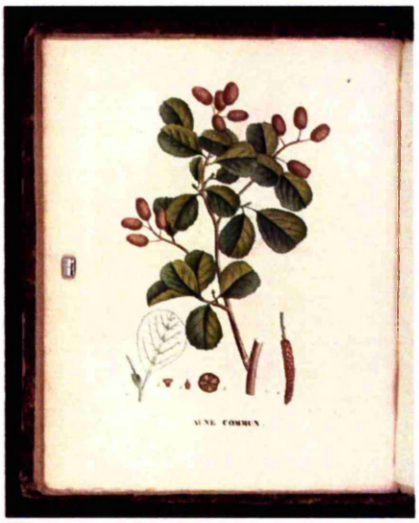

Figure 4.5.17. Alder (*Alnus glutinosa*) [60]1]

The alder tree is native throughout Europe, Asia and North America. Its bark is used for dyeing brown shades and in combination with iron (II) sulfate deep black shades. The bark contains ~20% tannins and some flavonoid (quercetin-3-galactoside) and possibly anthraquinone (emodin) dyestuffs [1].

ToF-SIMS analysis of alder bark dyebath was unsuccessful, as no molecular assignments could be made for the expected species. The most pronounced peaks occurred at m/z = 109^-, 121^-, 104^+ and 123^+ as shown in Figure 4.5.18.

Alder bark bath negative ion spectrum : Cs^+ primary ion source

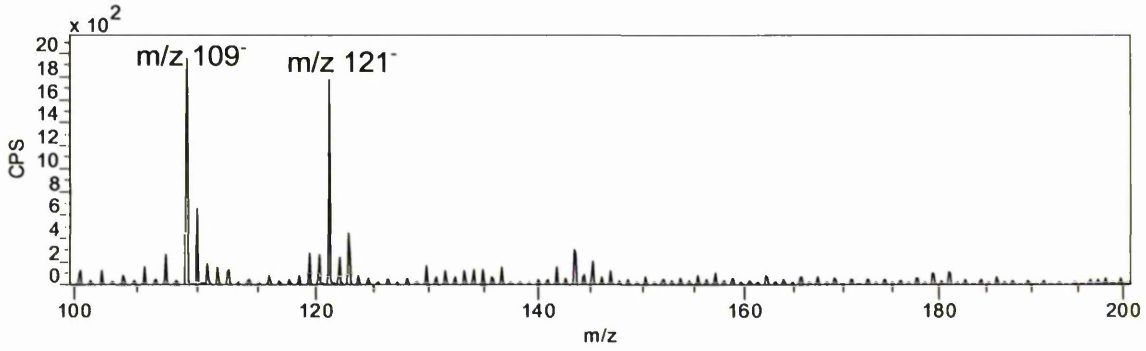

Alder bark bath positive ion spectrum : Cs^+ primary ion source

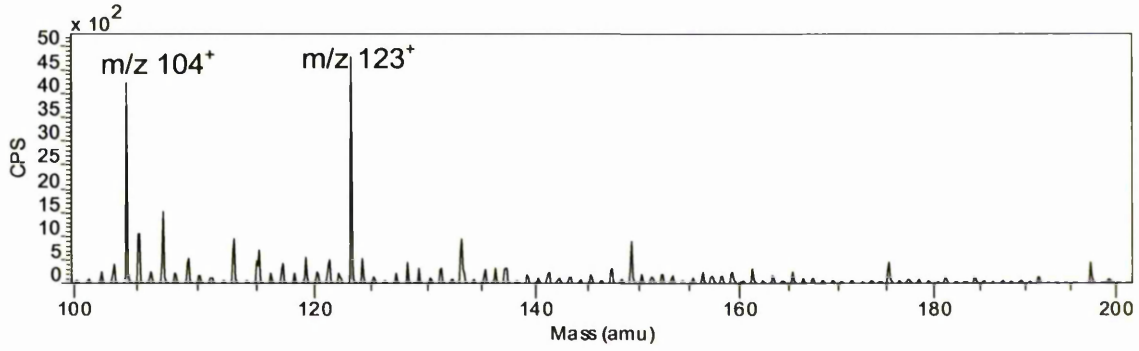

Figure 4.5.18. Negative and positive ion spectra of Alder bark dyebath

4.5.9. Investigation of indigoids: woad and 6,6'-dibromoindigo

Figure 4.5.19. Woad (*Isatis tinctoria*) [61]2]

Woad is a biennial plant, 1-1.5 meters tall with yellow flowers in its second year. It probably came from south-eastern Europe and south-western Russia but trade and its tendencies to become a noxious weed caused it to spread through most of Europe and many parts of Asia, Africa and America.

Woad has been known and used as a colourant since pre-biblical times, e.g. both Plinius and Caesar mentioned that woad was used as body and face paint in Britain.

Large scale cultivation of woad was widespread in the 13th century in Italy, France and Germany. Until the 16th century woad was the most important blue dyestuff and cultivation only declined due to the import of indigo (*indigofera tinctoria*) from India and later the synthetic production of indigo by Bayer. Commercial cultivation and processing of woad eventually ceased in the 19th century.

Figure 4.5.20. Processing of woad [61]2]

Woad leaves contain isatan B which releases the indigo precursor isatin during the fermentation process. In addition, woad leaves also contain the flavonoids quercetin and campherol. The leaves were harvested in the first year and crushed into a paste by a horse drawn mill. Woad balls were formed out of the paste and dried in the sun. This is shown in an 18th century drawing in Figure 4.5.20. The dried woad balls were broken up and fermented, the fermentation product was known as couched woad. Dyers would add bran, lime, wood ash and sometimes stale urine to the couched woad in the dyebath to adjust the pH to 8.5-9 and prompt the enzymatic reduction of the indigo chromophore into its soluble leuco form. This could take several days where the vat had to be kept at a certain temperature and be regularly stirred. Once the vat was reduced cloth could be dyed by repeatedly immersing and oxidising it on air.

The reduced and colourless (leuco) form of indigo adsorbs onto the fibre where it turns blue upon oxidation.

Depending on fibre type and indigo particle size woad dyed textiles exhibit greatly varying degrees of light-fastness from poor to very good [62].

Another dyestuff belonging to the chemical class of indigoids is Tyrian Purple, containing 6,6' dibromoindigo, which is the oxidised extract of the glands of various molluscs, e.g. hexaplex trunculus, yielding red to deep purple shades. The preparation of the glands of the molluscs was a lengthy process involving salting and fermentation over several days.

Thousands of molluscs were needed for extraction and dyeing with Tyrian purple making it an extremely expensive procedure. The use of the dye had its peak in Antiquity and was gradually replaced by cheaper alternatives of dyeing purple by overdyeing blue and red shades. There is no evidence that Tyrian purple had been used in tapestry production therefore the dye was not used in the preparation of MODHT model tapestry material. However, due to the similarity of the chromophore with the common indigo from woad, the synthetic form of the dye, 6,6' dibromoindigo was included in the ToF-SIMS analyses. The spectra showed very strong signals for dibromoindigo and bromoindigo in both positive and negative ion mode, Figure 4.5.21, as well as high intensity signals for Br^- at m/z = 79^- and 81^-, see appendix.

ToF-SIMS spectra were also obtained from powdered woad and woad dyed wool and silk fibre surfaces as well as woad dyed wool cross section. Powdered woad showed high intensity peaks for indigotin in both positive and negative ToF-SIMS spectra with the characteristic peaks occurring at m/z 263^+ and 261^-, Figure 4.5.22. Indigotin on wool surfaces (samples Blue / W1 and Green / W2) was also identified in positive and negative mode, Figure 4.5.23 and Figure 4.5.24, with the signal being strongest in positive mode; while the accelerated aged wool (sample Blue / W1_aged), the woad dyed wool cross section and the woad dyed silk sample (Blue / S1) did not yield any chromophoric peaks.

6,6'-Dibromoindigo synthetic chromophore positive ion spectrum: Cs^+ primary ion source

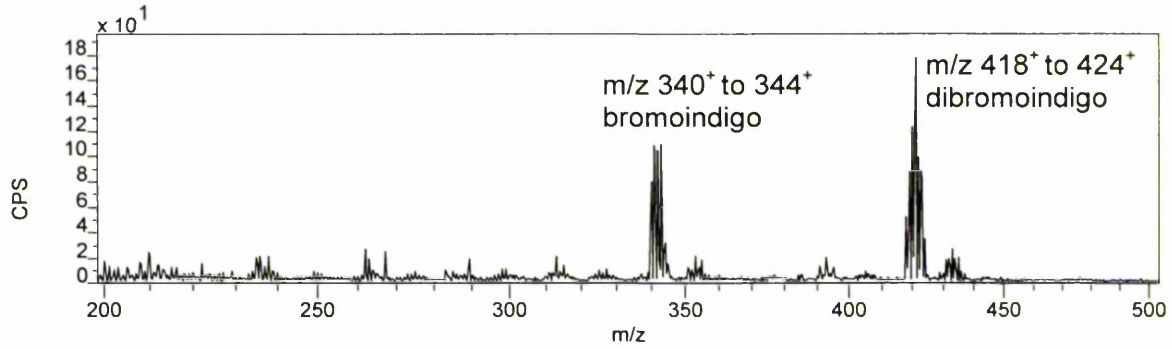

6,6'-Dibromoindigo synthetic chromophore negative ion spectrum: Cs^+ primary ion source

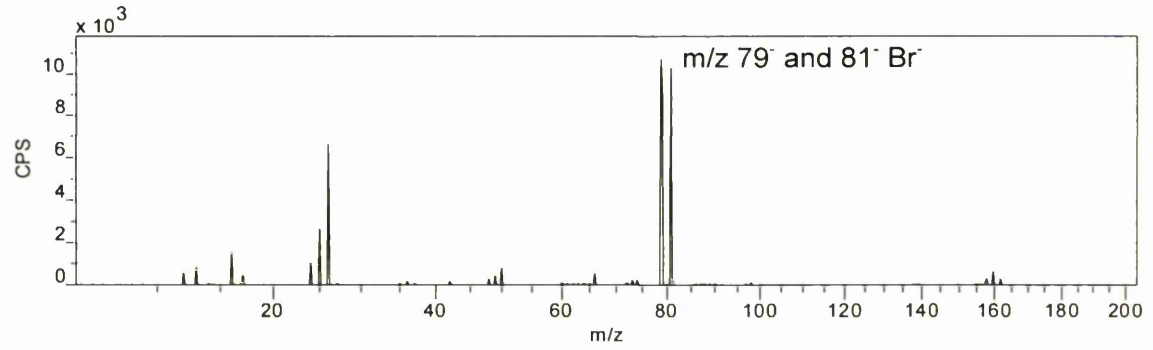

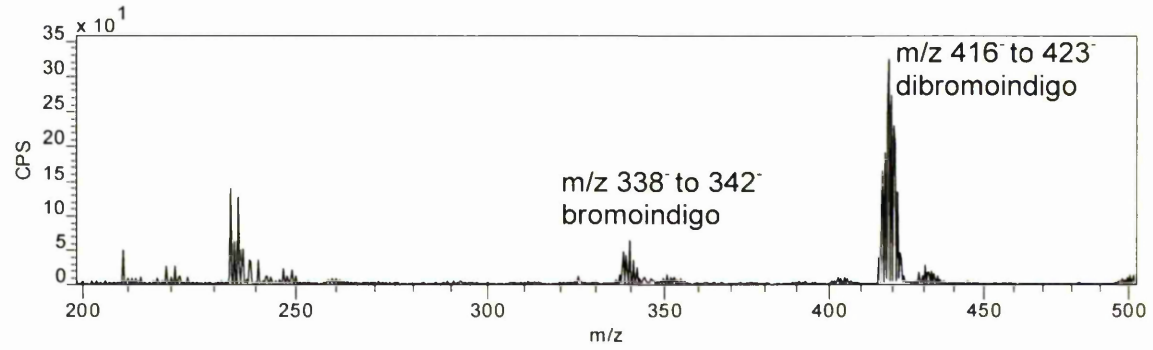

Figure 4.5.21. Positive and negative ion ToF-SIMS spectra of 6,6' Dibromoindigo

Woad powder dispersion positive ion spectrum : Au_1^+ primary ion source

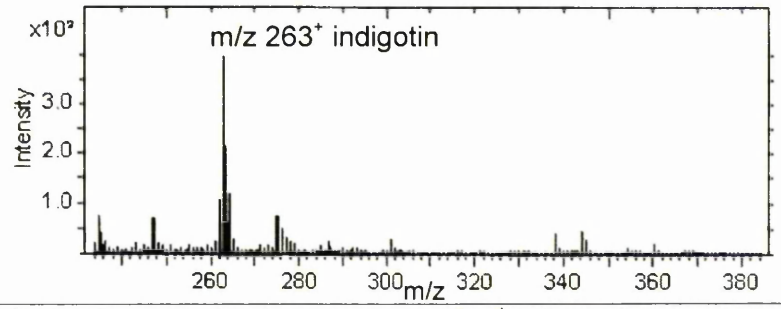

Woad powder dispersion negative ion spectrum : Au_1^+ primary ion source

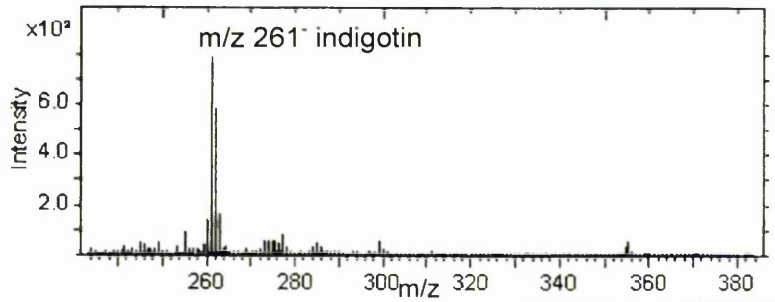

Figure 4.5.22. Positive and negative ion ToF-SIMS spectra of powdered woad

Woad dyed wool (Blue/W1) positive ion spectrum : Cs^+ primary ion source

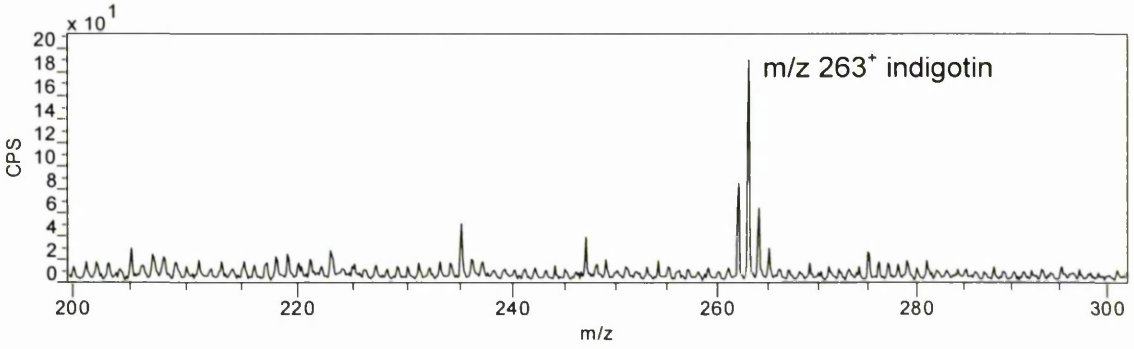

Woad dyed wool (Blue/W1) negative ion spectrum : Cs^+ primary ion source

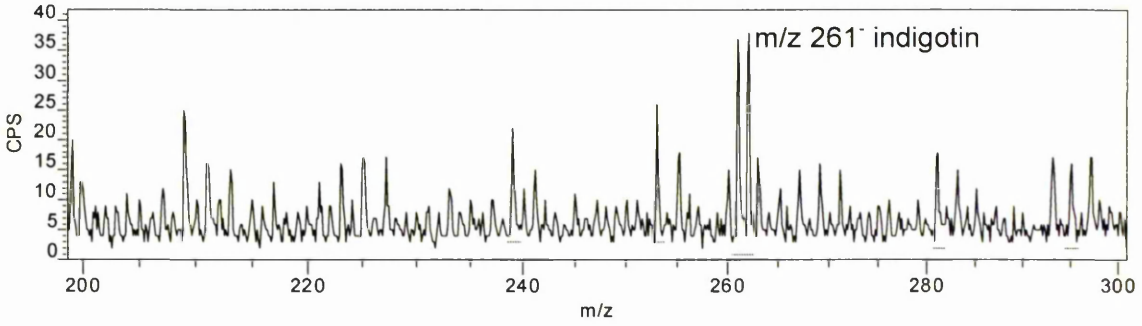

Figure 4.5.23. Positive and negative ion ToF-SIMS spectra of woad dyed wool

Woad and weld dyed wool (Green/W2) positive ion spectrum : Cs^+ primary ion source

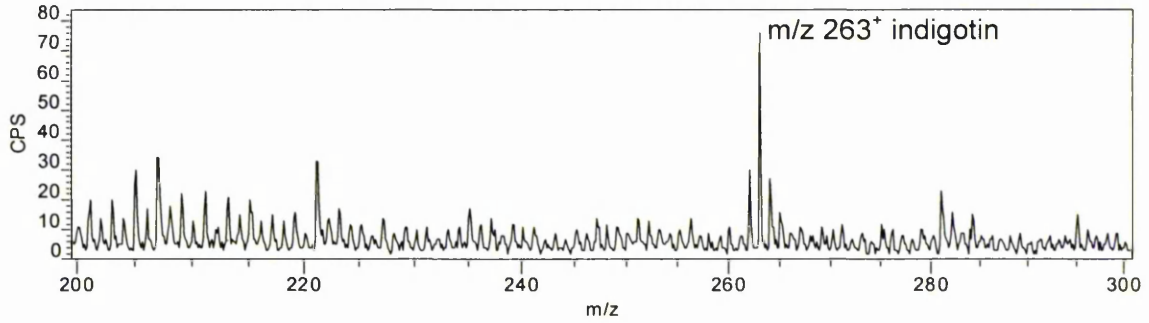

Woad and weld dyed wool (Green/W2) negative ion spectrum : Cs^+ primary ion source

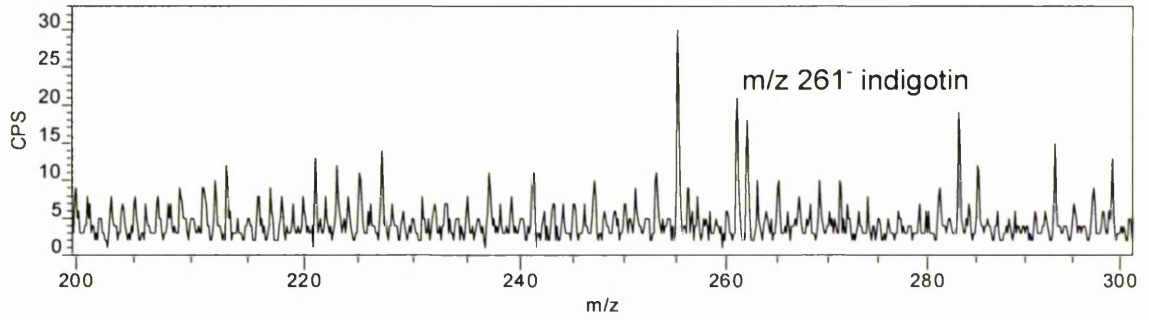

Figure 4.5.24. Positive and negative ion ToF-SIMS spectra of woad and weld dyed wool

4.6. Discussion

Signals attributable to the dye chromophores and derivatives were identified on all ToF-SIMS spectra of dyebaths and exhausted dyebaths, with the exception of alder bark. There were no significant variations of relative signal intensities due to exhaustion of the dyebaths, while the addition of lye (K_2CO_3) to the dyebaths caused considerable changes in the chromophores detected. In particular a replacement of hydroxyl by methyl groups under the addition of lye was observed on chromophores in the dyer's greenweed and brazilwood dyebaths.

The similarities of non-exhausted and exhausted dyebath spectra show that, under the conditions applied, relatively little exhaustion took place, i.e. the dyeing of wool samples did not deplete the dyebaths of chromophores. Furthermore, it suggests that parameters such as temperature treatment and time do not influence the relative abundance of chromophores in the dyebath, while the changes observed in the dyebath spectra due to the addition of K_2CO_3 highlight the difficulty of identifying a 'fingerprint' spectrum that could be used to characterise the dyestuff,

since dye recipes vary greatly in pH and other additives may also influence the presence and relative intensities of chromophores. In addition, the identical mass to charge ratios for different chromophores, in particular the flavonoids sulfuretin, genistein and apigenin (m/z = 269^- and 271^+) and fisetin, fustin and luteolin (m/z = 285^- and 287^+) may also provide difficulties in the identification of unknown dyestuffs.

The main colourant constituents of young fustic are fisetin and myrcetin (molecular mass 318.24) and to a lesser extent fustin (molecular mass 286.24) and sulfuretin. The absence of a signal for myrcetin and the relatively low intensity of fisetin / fustin (m/z = 285^-) compared to the signal for sulfuretin (m/z = 269^-) were, therefore, surprising. A possible explanation is the loss of three hydroxyl groups from myrcetin and one hydroxyl group from fisetin during desorption / ionisation leading to an increased peak at m/z = 269^-. The same principle may be applied to dyer's greenweed where the peak for genistein (m/z = 269^- and 271^+) may be increased due to a loss of hydroxyl groups from luteolin (m/z = 285^- and 287^+).

Several chromophore derivatives have been proposed as assignments for dominant peaks in the mass spectra. However, at this stage it cannot be distinguished whether these fragmented chromophore molecules are intrinsically present in the dyebath or were formed due to ionisation processes during ToF-SIMS analysis.

Madder and dyer's greenweed dyebaths, both with and without lye were also analysed using $Au1^+$ as primary ion source. The major peaks attributed to chromophores were the same as observed on the spectra acquired using a Cs^+ primary ion source. The relative intensities of principal peaks were also found to be similar in the two analysis techniques.

Analysis of the dyes applied to filter paper was successful for madder, weld and oak gall, while cochineal did not produce peaks identifiable as chromophores. In the analyses of oak gall bath and oak gall on paper as well as oak gall with ferrous sulphate on paper a set of peaks was detected in each case and attributed to gallic acid and derivative and ellagic acid. This is in good concordance with Delamare and Repoux's findings [37]. In most dyebath and dye on filter paper spectra the peaks attributed to chromophores were of high relative intensities with peaks attributed to impurities or cellulosic fragment molecules of the paper being

of lower intensities. This suggests a good ionisation probability for dyestuff molecules and implies the usefulness of the technique for samples where the dyestuff is present on the surface.

Surface analysis of silk dyed with madder, cochineal or woad and wool dyed with madder, cochineal or weld did not allow identification of the chromophores, while wool fibres dyed with woad yielded the indigotin peak at m/z 261^- and 263^+. This was attributed to the ring dyeing properties of woad, as opposed to the deeper penetration of the madder, cochineal and weld dyes. However, the analysis of three dyed wool samples (madder, DGW and woad) in cross-section was also not successful. The potential detection of dyestuff in wool fibre cross-sections was hampered due to contamination from the resin. All embedded and cross-sectioned wool samples showed high intensities of polyethylene contamination peaks (m/z = 105^+, 115^+, 128^+, 147^+) and silicon containing contamination peaks (m/z = 207^+, 221^+, 281^+, 323-327^+ and m/z = 163^-, 223^-, 237^-).

4.7. Conclusions

The study showed that several of the chromophores present in natural dyestuffs such as madder, dyer's greenweed, young fustic and weld can be identified by ToF-SIMS analysis of dried films of dyebaths and applied to a paper substrate. Analysis of brazilwood and cochineal were less distinct with the principal chromophore signals being of lower intensity than other peaks in the same mass region. Oak gall yielded peaks attributable to gallic acid and ellagic acid, known to be the principal building blocks of gallotannins. This could be of use in the identification of inks on paper, which often consist of the combination of tannins with ferrous sulphate.

Both Cs^+ and Au_1^+ primary ion sources were shown to successfully desorb and ionise the chromophoric species from dyebath films.

Indigo was identified in powdered woad as well as on the surface of dyed wool fibres while the detection of other dyes on wool and silk fibres failed. This may be due to the penetration of dyes into the bulk of the fibres, whereas indigo exhibits ring dyeing properties and can therefore be detected on the fibre surface. Cross-sections of dyed wool were also examined but the detection of chromophores was not successful, probably due to contamination from the embedding resin.

The study confirms the potential of the ToF-SIMS technique for dyestuff identification without extraction and using small sample sizes in the micron region. However, drawbacks of the technique have also been highlighted such as the requirement for the dyestuff to be on the immediate surface, ToF-SIMS' sensitivity towards contamination, overlapping mass to charge ratios of different chromophores and varying relative intensities and chromophoric contents following dyebath additives or fluctuations in pH. Nevertheless, it was demonstrated that ToF-SIMS analysis may enable unequivocal identification of natural dyes due to its ability to desorb and ionise whole chromophoric species.

4.8. References

1. Schweppe, H., *Handbuch der Naturfarbstoffe*, Nikol Verlagsgesellschaft mbH & Co. KG, Hamburg (1993).
2. Sekar, N., 'Natural Colourants - An Introduction', *Colourage* **46** (7) (1999) 57-60.
3. Travis, T., 'Madder Red - A Revolutionary Colour', *Chemistry & Industry* **1** (1994) 28.
4. Ferreira, E.S.B., A. Hulme, H. McNab, and A. Quye, 'The Natural Constituents of Historical Dyes', *Chemical Society Reviews* **33** (6) (2004) 329 - 336.
5. Bhattacharyya, N. and S. Vairagi, 'Natural Dye -- Its Authenticity and Identification', *Colourage* **49** (4) (2002) 45-53.
6. Verhecken, A., 'A Concise History of Dye Analysis', in *Dyes in History and Archaeology 20*, Amsterdam, Netherlands 2001, ed. J. Kirby, Archetype Publications, 1-22.
7. Paterson, D., 'Capillarity of Aniline Colours: Its Application in Detection Mixed Colouring Matters', *Journal of the Society of Dyers and Colourists* **9** (6) (1893) 110-111.
8. Wouters, J. and A. Verhecken, 'The Coccid Insect Dyes: HPLC and Computerized Diode-Array Analysis of Dyed Yarns', *Studies in Conservation* **34** (4) (1989) 189-200.
9. Ferreira, E.S.B., A. Quye, H. McNab, A. Hulme, J. Wouters, and J.J. Boon, 'Development of Analytical Techniques for the Study of Natural Yellow Dyes in Historic Textiles', in *Dyes in History and Archaeology 16/17* 1997/98, 179-186.
10. Wouters, J. and A. Verhecken, 'High-Performance Liquid Chromatography of Blue and Purple Indigoid Natural Dyes', *Journal of the Society of Dyers and Colourists* **107** (7-8) (1991) 266-269.
11. Wouters, J., 'High Performance Liquid Chromatography of Anthraquinones: Analysis of Plant and Insect Extracts and Dyed Textiles', *Studies in Conservation* **30** (3) (1985) 119-128.
12. Ferreira, E.S.B., A. Quye, A.N. Hulme, and H. McNab, 'LC–Ion Trap MS and PDA–HPLC – Complementary Techniques in the Analysis of Flavonoid Dyes in Historical Textiles: The Case Study of an 18th-Century Herald's Tabard', in *Dyes in History and Archaeology 19*, National Museums of Scotland, Edinburgh, October 2000, ed. J. Kirby, 13-18.
13. Koren, Z.C., 'HPLC analysis of the Natural Scale Insect, Madder and Indigo Dyes', *Journal of the Society of Dyers and Colourists* **110** (9) (1994) 273-277.
14. Maugard, T., E. Enaud, P. Choisy, and M.D. Legoy, 'Identification of an Indigo Precursor from Leaves of Isatis Tinctoria (Woad)', *Phytochemistry* **58** (6) (2001) 897-904.

15. Ferreira, E.S.B., A. Quye, H. McNab, and A. Hulme, 'Photo-oxidation Products of Quercetin and Morin as markers for the Charaterisation of Natural Flavonoid Yellow Dyes in Ancient Textiles', in *Dyes in History and Archaeology 18* 1999, 63-72.

16. Park, J. and J. Shore, 'Estimation of Dyes in Solution by Transmission Measurements', *Journal of the Society of Dyers and Colourists* **102** (11) (1986) 330-335.

17. McGovern, P.E., J. Lazar, and R.H. Michel, 'The Analysis of Indigoid Dyes by Mass Spectrometry', *Journal of the Society of Dyers and Colourists* **106** (1) (1990) 22-25.

18. Puchalska, M., M. Orlinska, M.A. Ackacha, K. Polec-Pawlak, and M. Jarosz, 'Identification of Anthraquinone Coloring Matters in Natural Red Dyes by Electrospray Mass Spectrometry Coupled to Capillary Electrophoresis', *Journal of Mass Spectrometry* **38** (12) (2003) 1252-1258.

19. Grassi, N., A. Migliori, P.A. Mando, and H.C. del Castillo, 'Identification of Lapis-Lazuli Pigments in Paint Layers by PIGE Measurements', *Nuclear Instruments & Methods in Physics Research Section B- Beam Interactions with Materials and Atoms* **219-20** (2004) 48-52.

20. Denker, A. and J. Opitz-Coutureau, 'Paintings - High-Energy Protons Detect Pigments and Paint- Layers', *Nuclear Instruments & Methods in Physics Research Section B- Beam Interactions with Materials and Atoms* **213** (2004) 677-682.

21. Gilbert, B., S. Denoel, G. Weber, and D. Allart, 'Analysis of Green Copper Pigments in Illuminated Manuscripts by Micro-Raman Spectroscopy', *Analyst* **128** (10) (2003) 1213-1217.

22. Neelmeijer, C. and M. Mader, 'The Merits of Particle Induced X-Ray Emission in Revealing Painting Techniques', *Nuclear Instruments & Methods in Physics Research Section B-Beam Interactions with Materials and Atoms* **189** (2002) 293-302.

23. Andalo, C., M. Bicchieri, P. Bocchini, G. Casu, G.C. Galletti, P.A. Mando, M. Nardone, A. Sodo, and M.P. Zappala, 'The beautiful "Trionfo d'Amore" Attributed to Botticelli: A Chemical Characterisation by Proton-Induced X-Ray Emission and Micro-Raman Spectroscopy', *Analytica Chimica Acta* **429** (2) (2001) 279-286.

24. Neelmeijer, C., I. Brissaud, T. Calligaro, G. Demortier, A. Hautojarvi, M. Mader, L. Martinot, M. Schreiner, T. Tuurnala, and G. Weber, 'Paintings - A Challenge for XRF and PIXE Analysis', *X-Ray Spectrometry* **29** (1) (2000) 101-110.

25. Bell, I.M., R.J.H. Clark, and P.J. Gibbs, 'Raman spectroscopic library of natural and synthetic pigments (pre-similar to 1850 AD)', *Spectrochimica Acta Part a-Molecular and Biomolecular Spectroscopy* **53** (12) (1997) 2159-2179.

26. Mando, P.A., 'Advantages and Limitations of External Beams in Applications to Arts and Archaeology, Geology and Environmental-Problems', *Nuclear Instruments & Methods in Physics Research Section B- Beam Interactions with Materials and Atoms* **85** (1-4) (1994) 815-823.

27. Derbyshire, A. and R. Withnall, 'Pigment Analysis of Portrait Miniatures Using Raman Microscopy', *Journal of Raman Spectroscopy* **30** (1999) 185-188.

28. Burgio, L., J.H. Clark, and P.J. Gibbs, 'Pigment Identification Studies In Situ of Javanese, Thai, Korean, Chinese and Uighur Manuscripts by Raman Microscopy', *Journal of Raman Spectroscopy* **30** (1999) 181-184.

29. Green, L.R. and V.D. Daniels, 'Identification of Mordants Using Analytical Techniques', in *Dyes in History and Archaeology 9* 1990, 10-14.

30. Williams, E.T. and N. Indictor, 'Detection of Metallic Mordants on Textiles by Particle-Induced X-Ray Emission', *Scanning Electron Microsc.* **3** (1986) 847-850.

31. Coupry, C., G. Sagon, and P. Gorguet Ballesteros, 'Raman Spectroscopic Investigation of Blue Contemporary Textiles', *Journal of Raman Spectroscopy* **28** (2-3) (1997) 85-89.

32. White, P., N. Burke, and E. Wagner, 'Coloured Evidence - The Use of SERS for the Forensic Examination of Colourants', in *Federation of Analytical Chemistry and Spectroscopy Societies*, Nashville, Tennessee 2000.

33. Koestler, R.J., R. Sheryll, and N. Indictor, 'Identification of Dyeing Mordants and Related Substances on Textile Fibers: A Preliminary Study Using Energy Dispersive X-Ray Spectrometry', *Studies in Conservation* **30** (2) (1985) 58-62.

34. Járó, M., Á. Tímár-Balázsy, and L. Kriston, 'X-Ray Diffraction Investigation of the Pigments of Printed Textiles. Scientific Examination of Works of Art', ICOM Committee for Conservation (1987).

35. Lanterna, G. and I. Tosini, 'Le Indagne sui Coloranti e gli Ausiliari di Tintura della Serie di Arazzi della Passione (Analyses of Dyes and Colorants in the Series of Tapestries of the Passion in the Basilica of San Marco in Venice)', *Note di Restauro* **7** (1995) 129-134.

36. Wouters, J., 'Possible Future Developments in the Analysis of Organic Dyes', in *Dyes in History and Archaeology 20*, Amsterdam, Netherlands 2001, ed. J. Kirby, Archetype Publications, 23-29.

37. Delamare, F. and M. Repoux, 'Studying Dyes by Time of Flight Secondary Ion Mass Spectrometry', in *Dyes in History and Archaeology 20*, Netherlands Institute for Cultural Heritage, Amsterdam, 1-2 November 2001, 39-50.

38. Sanyova, J., 'Spectroscopic Studies (SIMS, ESI-MS, FTIR) on the Structure of Anthraquinone-Aluminium Complexes', in *Dyes in History and Archaeology 21*, Avignon, 10-12 October 2002, Poster.

39. Grim, D.M. and J. Allison, 'Identification of Colorants as Used in Watercolor and Oil Paintings by UV Laser Desorption Mass Spectrometry', *International Journal of Mass Spectrometry* **222** (1-3) (2003) 85-99.

40. Maier, M.S., S.D. Parera, and A.M. Seldes, 'Matrix-Assisted Laser Desorption and Electrospray Ionization Mass Spectrometry of Carminic Acid Isolated from Cochineal', *International Journal of Mass Spectrometry* **232** (3) (2004) 225-229.

41. Ed. Clarke, M. and J. Boon, 'A Multidisciplinary NWO PRIORITEIT Project on Molecular Aspects of Ageing in Painted Works of Art; Final Report and Highlights', FOM Institute AMOLF, Amsterdam (1995-2002).

42. Boon, J.J., K. Keune, J. van der Weerd, M. Geldof, and J.R.J. van Asperen de Boer, 'Imaging Microspectroscopic, Secondary Ion Mass Spectrometric and Electron Microscopic Studies on Discolored and Partially Discolored Smalt in Cross-Sections of 16th Century Paintings', *Chimia* **55** (11) (2001) 952-960.

43. Keune, K. and J.J. Boon, 'Imaging Secondary Ion Mass Spectrometry of a Paint Cross Section Taken from an Early Netherlandish Painting by Rogier van der Weyden', *Analytical Chemistry* **76** (5) (2004) 1374 - 1385.

44. Wyplosz, N., R.M.A. Heeren, G.v. Rooij, and J.J. Boon, 'Analysis of Natural Organic Pigments by Laser Desorption Mass Spectrometry (LDMS): A Preliminary Study to Spatially Resolved Mass Spectrometry', in *Dyes in History and Archaeology* 1999, ed. J. Kirby, 187-198.

45. Wyplosz, N., *Laser Desorption Mass Spectrometric Studies of Artists' Organic Pigments*, Ph.D., FOM Institue for Atomic and Molecular Physics, University of Amsterdam, Amsterdam, (2003).

46. Lenaerts, J., L. Van Vaeck, and R. Gijbels, 'Secondary Ion Formation of Low Molecular Weight Organic Dyes in Time-of-Flight Static Secondary Ion Mass Spectrometry', *Rapid Communications in Mass Spectrometry* **17** (2003) 2115-2124.

47. Lenaerts, J., L. Van Vaeck, R. Gijbels, and J. Van Luppen, 'Comparison of Mono- and Polyatomic Primary Ions for the Characterization of Organic Dye Overlayers with Static Secondary Ion Mass Spectrometry', *Rapid Communications in Mass Spectrometry* **18** (3) (2004) 257-264.

48. Scheifers, S.M., S. Verma, and R.G. Cooks, 'Characterization of Organic Dyes by Secondary Ion Mass Spectrometry', *Analytical Chemistry* **55** (14) (1983) 2260-2266.

49. Goschnick, J., M. Lipp, H.-J. Ache, H. Thomas, R. Kaufmann, R. Peters, and H. Höcker, 'Afterchrome Dyeing of Wool. Part B -Characterisation of Chromium-Treated Wool by Secondary Particle Mass Spectrometry', *Journal of the Society of Dyers and Colourists* **108** (1992) 191-194.

50. Pachuta, S.J. and J.S. Staral, 'Nondestructive Analysis of Colorants on Paper by Time-of-Flight secondary Ion Mass Spectrometry', *Analytical Chemistry* **66** (2) (1994) 276-284.

51. Image from: Köhler, F.E., 'Medizinal-Pflanzen in naturgetreuen Abbildungen mit kurz erläuterndem Texte : Atlas zur Pharmacopoea', 1995-2003 Missouri Botanical Garden, http://ridgwaydb.mobot.org/mobot/rarebooks/ (1883-1914).

52. Bruice, T.C. and T.H. Fife, 'Hydroxyl Group Catalysis. III.1 The Nature of Neighboring Hydroxyl Group Assistance in the Alkaline Hydrolysis of the Ester Bond', *Journal of the American Chemical Society* **84** (1962) 1973-1979.

53. Image from: Phipps, E., F. Zaharia, and N. Shibayama, 'Conservation and Technical Study of a Colonial Andean Tapestry', in Met Objectives, Spring 2004, Volume 5, No. 2, www.metmuseum.org, Joseph Alzate y Ramirez, Memoria sobre la naturaleza, cultivo y beneficio del la grana. . . , 1777. Ayer Ms. 1031, The Newberry Library, Chicago. This plate appears in the late-eighteenth-century work of a Mexican priest, Alzate y Remirez, on the nature, cultivation, and usefulness of the cochineal insect.

54. Image from: Kress, H., 'Brazilwood, Caesalpinia Echtinata', http://www.ibiblio.org.

55. Image from: Grieve, M., *A Modern Herbal*, Web edition of printed version: Dover edition, published in 1971 unabridged republication of original publication by Harcourt, Brace & Company www.botanical.com (1931).

56. Image from: Lindmans, C.A.M., 'Bilder ur Nordens Flora', http://www.vobam.se/lindmanal.htm (1917-1926).

57. Image from: Jacquin, N.J., 'Floræ Austriacæ, Sive, Plantarum Selectarum in Austriæ Archiducatu', Missouri Botanical Garden,1995-2003 http://ridgwaydb.mobot.org/mobot/rarebooks/ (1773-1778).

58. Image from: Eusman, E. and B. Reißland, 'The Iron Gall Ink Corrosion Website', European Commission of Preservation and Access in Amsterdam, Museum Boijmans van Beuningen in Rotterdam, Netherlands Institute of Cultural Heritage in Amsterdam, Algemeen Rijksarchief in The Hague, and the Teyler Museum in Haarlem http://www.knaw.nl/ecpa/ink/index.html.

59. Kress, H., 'The British Pharmaceutical Codex', http://www.ibiblio.org/herbmed Council of the Pharmaceutical Society of Great Britain, 1911 (2001-2004).

60. Image from: Saint-Hilaire, J., 'Traité des Arbres Forestiers', 1995-2003 Missouri Botanical Garden http://ridgwaydb.mobot.org/mobot/rarebooks/Paris (1824).

61. Image from: Schreber, D.G., 'Historische, Physische und Öconomische Beschreibung des Waidtes, Halle', Deutsches Museum · 80306 München http://www.deutsches-museum.de/bib/entdeckt/alt_buch/text1198.htm (1752).

62. Daniels, V., 'How Lightfast is Indigo?...' in *Dyes in History and Archaeology 23*, Montpellier 2004, In Press.

Chapter 5. Analysis of Wool and Silk

5.1. Literature review for wool

5.1.1. Structure and chemical composition of wool

Wool fibres consist of mainly two types of cells, the cortical and the cuticle cells. However, coarser wool fibres may contain another type of cell, the 'medulla' cells, which run centrally along the fibre axis often forming vacuoles [1-7].

The cuticle is subdivided into epi-, exo- and endocuticle and forms scales surrounding the cortical, which itself is composed of paracortex and orthocortex, Figure 5.1.1.. The individual para- and orthocortical cells are composed of macrofibrils in a surrounding substance of nuclear remnants and intermacrofibrillar material and are enclosed in the cell membrane complex. Macrofibrils contain bundles of keratin intermediate filaments (IF, formerly called microfibrils) packed in an amorphous matrix (keratin associated proteins, KAP). These intermediate filaments are a partial helical arrangement of several left-handed coiled coil protofilaments of which each comprises two right-handed (α-helix) polypeptide chains, Figure 5.1.2. A polypeptide chain is represented in Scheme 5.1.1, with the sequence of amino acids linked in the polypeptide chain defining the protein type. The nature of the proteins and individual morphological features of the wool fibre are discussed below in more detail.

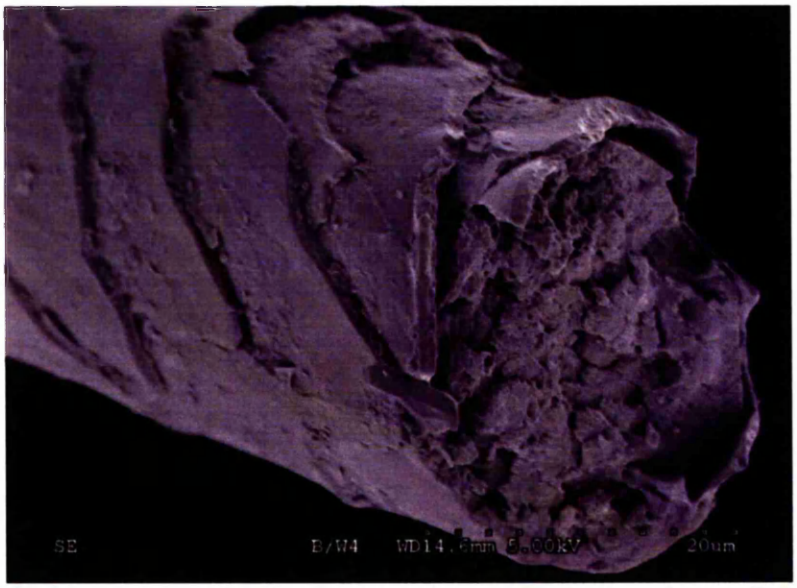

Figure 5.1.1. SEM micrograph of a fractured wool fibre showing cuticle cells surrounding the cortex

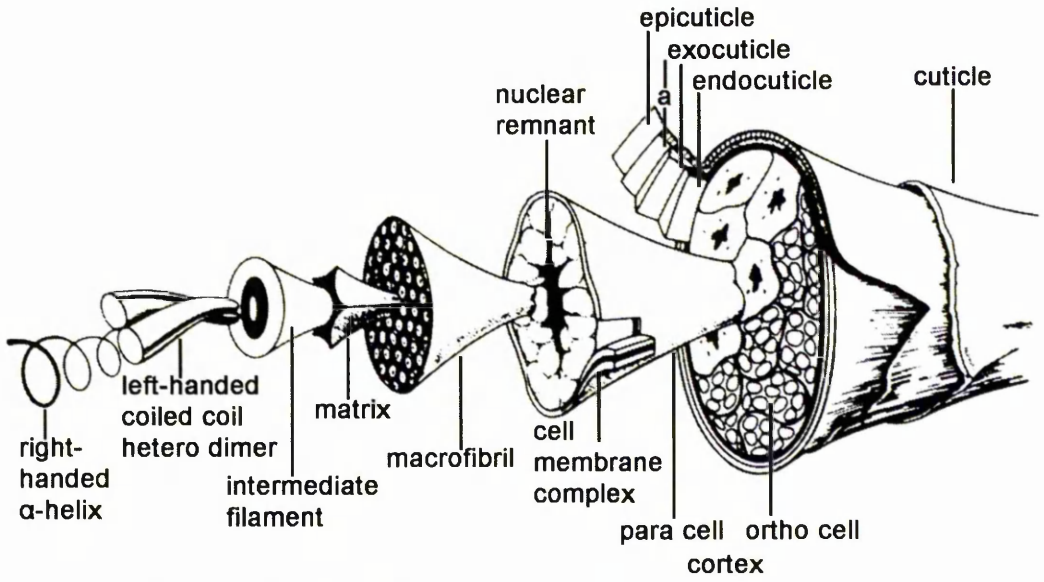

Figure 5.1.2. Morphology of a fine wool fibre [1]

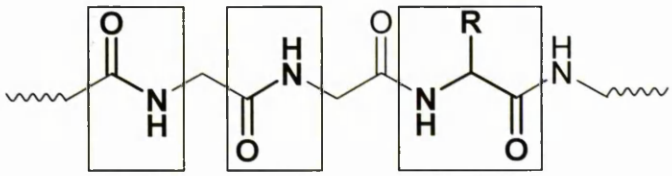

Scheme 5.1.1. Polypeptide chain

By weight wool consists of approximately 97% keratinous protein characterised by an overall high sulphur content, 2% non-proteinaceous material and 1% inorganic material [7]. Around fifty to one hundred different proteins have been identified in the wool fibre and are classified into groups and families as outlined in the following sections. In addition wool contains mainly waxy lipids, polysaccharides, nucleic acids, carbohydrates and mineral salts [1, 7].

Wool proteins are composed of mainly 21 amino acids, Table 5.1.1, with variations in amino acid content due to deviations in analysis parameters, breed of sheep, diet [8], climate and other external influences.

Table 5.1.1. Amino acid compositions of wool fibres

Amino Acid	Residue Percentage			
Alanine	5.2	4.5	5.4	5.8
Arginine	6.2	6.5	6.9	7.7
Aspartic acid (a)	5.9	5.4	6.6	6.9
Glutamic acid (b)	11.1	11.1	11.9	12.1
Glycine	8.6	7.5	8.2	7.0
Cysteine (c)	13.1	10.2	10.0	10.7
Histidine	0.8	0.6	0.8	0.7
Isoleucine	3.0	2.5	3.1	3.3
Leucine	7.2	6.3	7.7	7.9
Lysine	2.7	2.1	2.8	3.4
Methionine	0.5	0.4	0.4	0.6
Phenylalanine	2.5	2.7	2.8	2.6
Proline	6.6	6.9	7.2	6.4
Serine	10.8	9.4	10.5	10.0
Threonine	6.5	6.0	6.3	6.0
Tryptophan	(d)	(d)	(d)	(d)
Tyrosine	3.8	3.8	3.7	3.2
Valine	5.7	4.6	5.7	5.8
NH_3	(e)	9.6	(e)	(e)
Reference	[3]	[2]	[6]	[8]

(a) Includes asparagine
(b) Includes glutamine
(c) Contributes to cystine
(d) The value cannot be obtained by acid hydrolysis method
(e) value NH_3 was not included

Scheme 5.1.2 shows the structure and nature of the amino acid residues. Both basic and acidic residues are present in approximately equal concentrations, hence accounting for the amphoteric nature of wool.

Various types of chemical bonds can exist between the amino acid groups of neighbouring polypeptide chains; i.e. covalent di-sulphide cystine links between two cysteine residues, hydrophobic interactions between two non-polar hydrocarbon residues, isopeptide and ionic bonds between basic and acidic groups and hydrogen bonds between amino and carboxyl groups in the amino acid residues as well as between –CO and –NH groups of the backbone peptide chains, Scheme 5.1.3.

The combined effects of covalent and non-covalent links between the peptide chains control the fibre properties, in particular the chemical solubility and the tensile strength. Above all the high amount of covalent cystine links in keratin accounts for its stability and relatively low solubility [4].

acidic residues

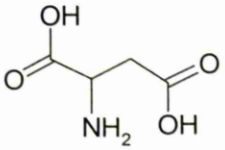

aspartic acid

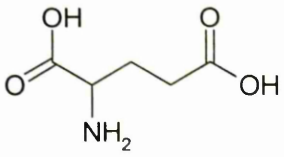

glutamic acid

basic residues

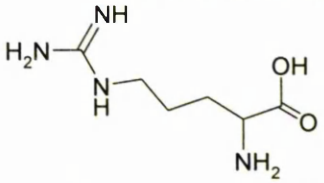

arginine

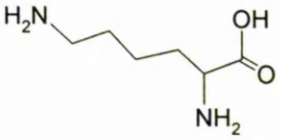

lysine

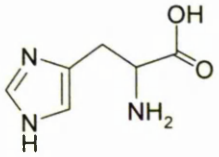

histidine

non-polar hydrocarbon residues

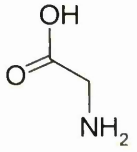

glycine

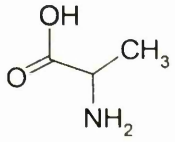

alanine

phenylalanine

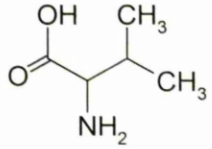

valine

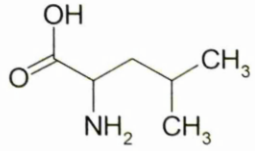

leucine

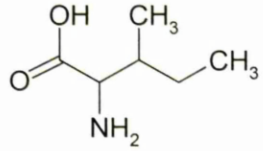

isoleucine

polar residues

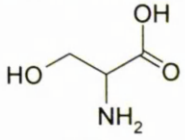

serine

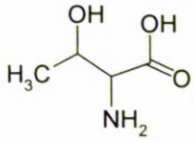

threonine

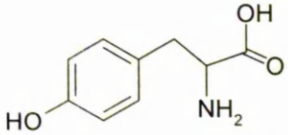

tyrosine

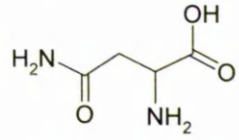

asparagine

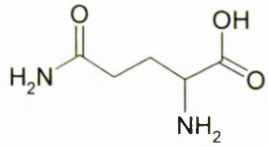

glutamine

heterocyclic residues

tryptophan

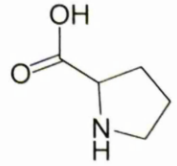

proline

sulphur containing residues

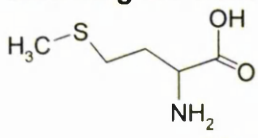

methionine

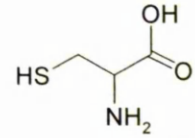

cysteine

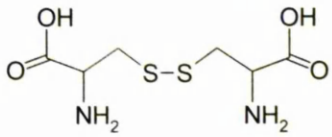

cystine

Scheme 5.1.2. Amino acid residues in wool polypeptide structure

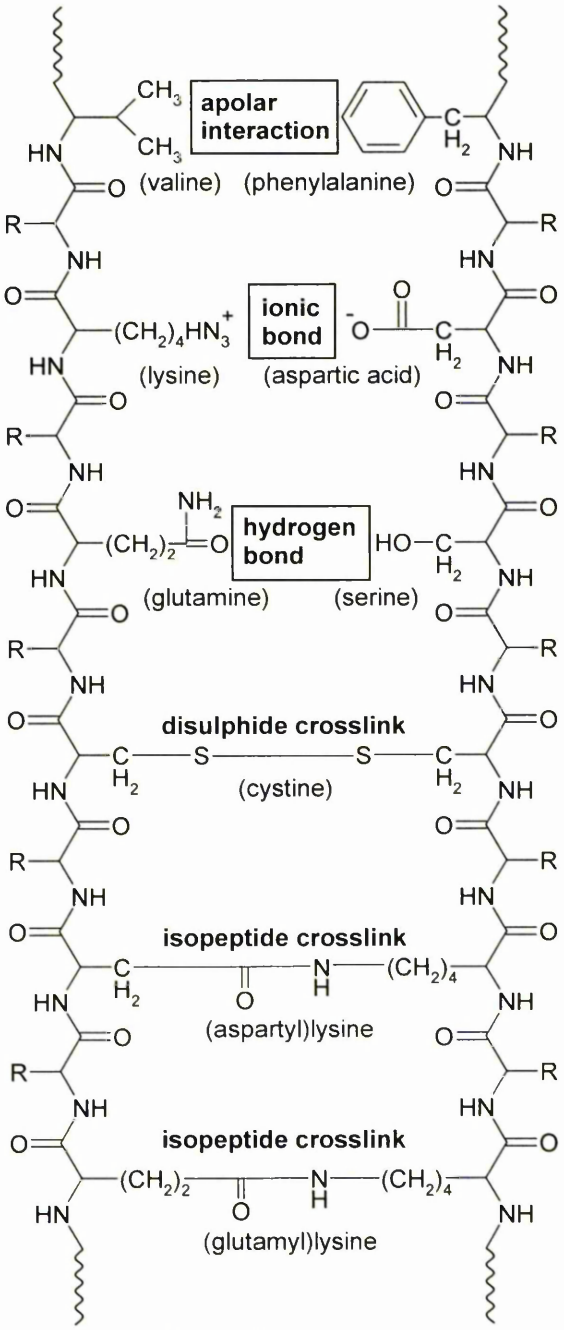

Scheme 5.1.3. Amino acid bond formation [1]

Proteinaceous material

According to their relative amino acid compositions and sequences, the keratinous proteins of wool have been classified as illustrated in Table 5.1.2. The keratin intermediate filament proteins are particularly rich in those amino acids which contribute to the α-helix formation, i.e. the acidic and the basic residues. The cysteine-rich proteins (KAP1-5 & 9-12) contain mainly cystine, proline, serine and threonine and, according to an out-dated nomenclature, can be subdivided into

high-sulphur proteins (KAP1-3 with 12-30 mol% cysteine) and ultrahigh-sulphur proteins (KAP4, 5, 9-12 with 30-41 mol% cysteine) of which KAP5 and KAP10 have been shown to contain a high amount of glycine-rich repeats and are specifically located in the cuticle cells. KAP4 and KAP12 are particular to paracortical cells, while those proteins high in glycine and tyrosine (KAP6-9) are predominantly present in the orthocortex. In addition to glycine and tyrosine, KAP7 and KAP8 in particular , contain mainly serine and phenylalanine but very little cystine, which renders them more susceptible to chemical dissolution due to the low number of covalent disulphide crosslinks between protein chains [1-3, 6, 9].

Table 5.1.2. Wool keratin protein families; adapted from [9]

Group		Family		Number of proteins
Keratin intermediate filament proteins	Low-sulphur	K1 (IF type I)	Microfibrils	4
		K2 (IF type II)	Microfibrils	4
Keratin associated proteins (Matrix)	Cysteine-rich (high-sulphur)	KAP1		several
		KAP2		~ 10
		KAP3		4
	Cysteine-rich (ultrahigh-sulphur)	KAP4	Paracortex	several
		KAP5	Cuticle	several
		KAP9		>= 3
		KAP10	Cuticle	>= 3
		KAP11		>= 1
		KAP12	Paracortex	several
	Glycine / tyrosine-rich	KAP6	Orthocortex	~ 10
		KAP7	Orthocortex	1
		KAP8	Orthocortex	1

Non-proteinaceous material

The very small amount (~ 1-2 wt%) of non-proteinaceous material of wool is primarily accounted for by straight-chain saturated and mono-unsaturated fatty acids of various lengths between C_7 and C_{26}, as well as sterols, glycerides and other types of lipids. Lipids are present in the intercellular regions throughout the fibre and, in particular the branched C_{21} fatty acid (18-methyleicosanoic acid), on or near the fibre surface, which accounts for its hydrophobic nature. It has been shown that removal or modification of the outer layer of lipids increases the wettability of the fibres and therefore improves dyeability [10].

Inorganic material

Approximately 1 wt% of wool was found to be inorganic material consisting of potassium, sodium, calcium, aluminium, iron, silicon dioxide, sulfate, carbonate and traces of phosphorus pentoxide and chloride [7].

Cuticle cells

The outer layer of the wool fibre is made up of scales, which overlap each other from root to tip. Each scale is a cuticle cell and depending on the breed of sheep and coarseness of the wool fibre, the surrounding scale layer can be up to 15 cells thick, but is usually only one cell [1]. Depending on the fineness of the wool fibre, the cuticle cells vary greatly in shape and size; the commonly cited dimension of 20 x 30 x 1 μm gives just a rough estimation [11]. Each cuticle cell is constituted of several layers, namely the endocuticle, the exocuticle with its A-layer and a surrounding third layer, a resistant membrane. However, there is much controversy about the nature and depth of that outermost surface membrane of the wool fibre [3]. Figure 5.1.3 shows a model for the sublayers of the cuticle cell.

A matrix structure of lipids contained within proteinaceous material has been suggested, as well as a layered structure with a continuous surface layer of lipids covalently bound to the proteins [3, 12]. The terms epicuticle, fibre cuticle surface membrane (FCUSM), β-layer and lipid- or F-layer, have all been used to describe parts of the outermost surface of the wool fibre, while it has also been suggested that such a membrane is non-existent and its verification in the Allwörden reaction be part of the deteriorated A-layer [11]. This was disputed by Swift and Smith, who, through TEM investigations, presented evidence of the existence of the epicuticle [13].

However, generally accepted is the model of a lipid monolayer (18-MEA) covalently bound to an underlying layer of heavily crosslinked protein (outer β-layer, epicuticle), rich in cystine, cysteine and with high contents of isopeptide bond forming lysine and glutamine [14]. Investigations by Brack et al. suggested that part of the bound surface lipids are contained within the outer β-layer [15]. The so-called "inner layer" is thought to be chemically similar to the epicuticle [13]. The region between two overlapping cuticle cells is considered part of the cell membrane complex and consists of a proteinaceous δ-layer [16] between two β-layers, which are thought to contain covalently bound fatty acids in a protein matrix [13]. Swift and Holmes investigated the epicuticle of human hair by electron microscopy and measured its thickness at 2.5 nm, suggesting that the epicuticle is identical with the lipid layer of the cell membrane complex [17]. Later Swift and Smith measured the epicuticle of wool fibres to be 13 nm and the covalently bound surface lipids 8 nm in thickness [13], while Jones et al. gave values of 2 to 7 nm

for the whole surface membrane [3], with the surface lipid component being 0.4 - 0.9 nm [18, 19].

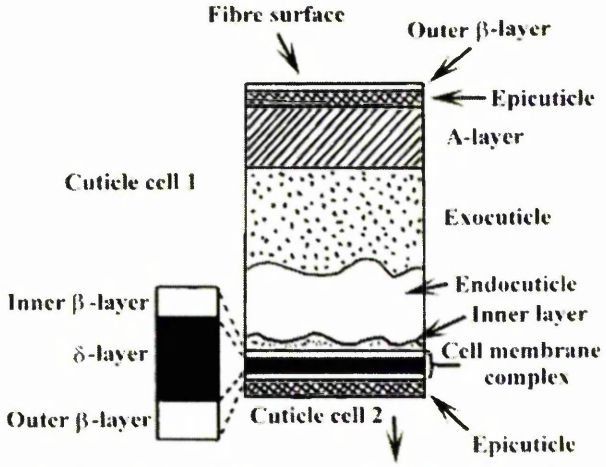

Figure 5.1.3. Schematic diagram of the layered structure of a mammalian cuticle cell [13]

The amino acid composition of the cuticular sublayers differs mainly in cystine content. Overall the cuticle cells are rich in high-sulphur proteins (KAP5 and KAP10) and poor in α-helix forming low-sulphur proteins (cuticle-specific IF keratin [9]), therefore the molecular conformation of cuticle cells is believed to be amorphous with a high amount of disulphide crosslinking. Staining tests of fibre cross-sections with ammoniacal silver showed that the amount of cystine in the cuticle layers increased in the order: cell membrane complex (β- and δ-layer), endocuticle, exocuticle, A-layer, epicuticle [13]. Alike the thickness of the epicuticle, its amino acid composition is also contentious. Residue percentages for cysteine stated by several researchers vary from 11.5%[20], 12%[21], 21%[12], 25-33%[18], 35%[19] to ~37.5%[13]. Table 5.1.3 shows the amino acid composition of the wool cuticle components as found by some researchers.

The most recent studies, employing XPS and SIMS analyses agree on the high level of sulphur in the epicuticle (~35% cysteine residues) and the thin surface lipid layer (~0.9nm) [19, 22]. No values for other amino acids were given but earlier studies had a good correlation of results [20, 21]. A "corrected" version of these results is shown in Table 5.1.4, where all amino acid percentages were relatively lowered to accommodate for 35% cysteine.

Table 5.1.3. Amino Acid composition of wool fibre cuticle Cu, exocuticle Exo, epicuticle Epi and high-sulphur protein of the cuticle HSCU

Amino Acid	Residue Percentage							
	Cu	Exo	Cu	Exo	Cu	Epi	HSCU	Epi
Alanine	5.7	5.4	5.8	6.4	5.7	4.6	6.1	4.6
Arginine	4.8	4.7	4.3	4.8	4.8	4.3	5.0	4.3
Aspartic acid	3.6	2.1	3.5	2.1	4.2	5.8	1.3	5.8
Glutamic acid	8.9	8.2	8.7	8.6	9.2	10.7	7.4	10.7
Glycine	8.5	8.5	8.2	8.6	9.6	15.4	4.4	15.4
Cysteine (a)	14.4	18.2	14.8	18.6	14.0	11.5	20.0	11.9
Histidine	1.0	0.7	0.8	0.5	1.0	1.0	0.4	1.0
Isoleucine	2.4	1.9	2.7	2.9	2.6	2.5	1.4	2.5
Leucine	5.7	4.3	6.1	4.6	6.2	5.5	5.0	5.5
Lysine	2.7	2.0	2.7	2.1	2.9	4.8	0.8	4.8
Methionine	0.4	0.2	0.3	0.2	0.4	0.03	0.0..	-
Phenylalanine	1.6	1.0	1.7	1.2	1.9	1.8	0.7	1.9
Proline	11.5	13.5	10.5	12.4	9.0	5.8	14.9	5.8
Serine	14.6	15.5	14.3	11.8	13.7	13.7	15.9	13.7
Threonine	4.8	4.6	4.4	3.9	5.0	3.6	5.2	3.6
Tryptophan							0.1	
Tyrosine	2.6	2.0	2.8	2.0	2.9	2.7	1.9	2.1
Valine	6.4	6.8	7.5	8.2	6.5	5.7	7.8	5.7
Citrulline			0.3	-				0.9
Ornithine			0.2	-				
References	[23]		[24]		[20]		[25]	[21]

(a) Contributes to cystine
(b) The value cannot be obtained on acid hydrolysates

Table 5.1.4. Assumed amino acid composition of epicuticle and β-layer

Amino Acid	Residue Percentage
Alanine	3.4
Arginine	3.2
Aspartic acid	4.3
Glutamic acid	7.9
Glycine	11.4
Cysteine (a)	35.0
Histidine	0.7
Isoleucine	1.8
Leucine	4.1
Lysine	3.5
Methionine	0.0
Phenylalanine	1.3
Proline	4.3
Serine	10.1
Threonine	2.7
Tryptophan	0.0
Tyrosine	2.0
Valine	4.2

(a) Contributes to cystine

The covalently bound fatty acids on the outermost wool surface and the fatty acids contained in the β-layer consist of mainly 18-methyleicosanoic acid, palmitic acid, stearic acid and oleic acid [14, 26]. Their concentrations and carbon chain lengths

are represented in Table 5.1.5. These surface lipids account for the high hydrophobicity of wool fibres [1-3, 5].

18-MEA binds to cysteine residue of proteins by thioester linkage and less commonly to serine or threonine residues by oxygen ester linkage [14]. Dai et al. suggested that the lipids on the wool surface are tilted at an angle of 30° to the surface normal [27]. Taking the tilt into account the suggested thickness of the lipid layer of <1nm is plausible [18, 19]. Others suggested a folding of the lipid chains to accommodate the thinness of the lipid layer [28]. A lipid layer thickness of 8 nm, as measured by Swift and Smith [13] seems unlikely because of the ability to detect the underlying proteinaceous nitrogen and sulphur with the surface sensitive techniques XPS and SIMS, as demonstrated in numerous studies [14, 15, 18, 19, 27, 29-51].

Table 5.1.5. Bound lipids on wool top [14]

Fatty acid	**Molecular formula (including thioester linkage to cysteine)**	**Concentration (%)**	**Molecular length (of C chain only)**
palmitic C16	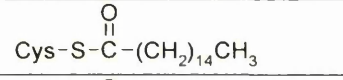	14.4 +/- 1.5	1.89nm
oleic C18:1	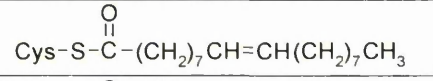	7.7 +/- 1	
stearic C18	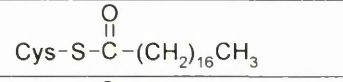	11.1 +/- 1.2	2.14nm
18-MEA	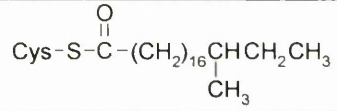	68.4 +/- 1.9	2.39nm

Cortical cells

The cortex forms the body of the wool fibre and is subdivided into ortho-, para- and sometimes meso-cortical cells. Individual cortical cells are spindle shaped and approximately 100 µm long and 3-6 µm wide, they are closely packed in a matrix of cell membrane complex and arranged parallel to the fibre axis. The cells contain bundles of macrofibrils separated from each other by intermacrofibrillar matrix material, the distribution of which differs between the ortho-, para- and mesocortical cells. Intermacrofibrillar material is concentrated in specific regions between the macrofibrils in para- and mesocortical cells, while in orthocortical cells it is distributed more evenly around the macrofibrillar boundaries. This renders the orthocortex more prone to hydrolysis and chemical attack because due to the

small number of covalent crosslinks, the Intermacrofibrillar material is easily swollen and offers pathways for chemical reagents [52].

The macrofibrils contain rod-like packages of mainly crystalline intermediate filaments (IF), of approximately 10 nm diameter, constituted of low-sulphur keratin intermediate filament type I and type II proteins in an amorphous matrix of keratin associated proteins (KAP). Amino acid sequencing has shown that two α-helical protein molecules (keratin IF type I and type II) are coiled together to form highly organised hetero dimers which exhibit four crystalline regions interrupted by three amorphous regions and ending in amorphous domains with a N-terminus and a C-terminus. The majority of cysteine residues in IF proteins are concentrated in the amorphous end domains of the peptide chain, allowing for extensive disulphide crosslinking with the surrounding KAP matrix [9].

The arrangement of intermediate filaments in the macrofibrils of the orthocortex is believed to hold a twist, giving a 'whorl' shape in cross-section. The intermediate filaments in the mesocortex are arranged in a hexagonal pattern, while the intermediate filaments in the paracortex are largely randomly distributed. In addition, the proportion of intermediate filaments to matrix material differs in the various cortical cells. Being richer in ultrahigh-sulphur KAP4 and KAP12 matrix material, the paracortical cells contain more disulphide crosslinks than the orthocortex, which is richer IF proteins and high glycine / high tyrosine KAP6, 7, 8 proteins.

The arrangement of para- and orthocortical cells is bilateral in most wool fibres. However, it can also be cylindrical or even random in coarser wool. Sometimes medulla cells are present in the centre of the fibre and mesocortical cells are arranged at the boundary between ortho- and paracortex [1-3].

Cell membrane complex (CMC)

The CMC separates the cuticle cells from the cortex and the individual cortical cells from each other; as a result the CMC forms the only continuous phase in the wool fibre, which makes it especially important for the fibre's physical and chemical properties even though it accounts for only ~ 4-6% of the total mass of the wool fibre [16]. The CMC provides intercellular adhesion, though it has been shown that the CMC has relatively low mechanical strength and is the first

component of the wool fibre to fail under biaxial and torsional stresses, leading to 'fibrillation' [53].

The CMC is a ca. 20 nm thick, layered structure composed of KAP proteins, non-proteinaceous material (lipids) and a much disputed chemically resistant membrane, which envelops each cell, including the cuticular cells, although it has been suggested that the intercellular material between the cuticle cells varies from the intercellular material between cortical cells [16]. However, neither the composition of the intercellular cement protein (δ-layer) nor the constitution of the chemically resistant protein is fully understood. The intercellular cement protein is believed to contain high levels of glycine, tyrosine and phenylalanine and very low amounts of cystine, hence the small number of cystine disulphide crosslinks account for the easy swelling properties of the CMC [6]. The membrane contains the same amount of cystine linkages as the overall composition of wool, which therefore does not offer an explanation for its high resistance to chemical attack. However, it has been suggested that steric hindrance of the disulphide links of the high amount of isopeptide crosslinks between glutamic or aspartic acids and lysine in the chemically resistant protein may contribute to its higher stability [3, 16].

Lipid material consisting of free fatty acids, cholesterols, ceramides and glycerides within the CMC forms layers (β-layers) between the chemically resistant membrane on the immediate outside of cells and the KAP layer (δ-layer) in the centre of the CMC; Figure 5.1.3 omits the resistant membrane. The lipid material is believed to be arranged in a bilayer lamellar structure of 5-8 nm width with solid crystalline and liquid crystalline phases which undergo transition to solely liquid crystalline above body temperature [54]. However, it has also been suggested that the histological feature identified as the β-layer is identical with the resistant membrane [55].

5.1.2. Photochemistry of wool

UV and visible light irradiation of wool causes photo-yellowing, -bleaching and –tendering. In order to undergo photo-physical or -chemical reactions the chromophores in the protein have to absorb incident light.

Light induced excitation of a chromophore in the ground state causes an energy transition to the singlet state (e.g. excitation of tryptophan: $^1Trp_0 \xrightarrow{h\nu} {}^1Trp^*$). The

excess energy of which can be deactivated through a number of possible pathways. Dissipation through internal vibrational relaxation or the emission of a photon (wool fluorescence [56]) are photophysical processes that do not alter the chemical nature of the absorbing molecule. A rearrangement of electrons such as intersystem crossing of the first singlet excited state to the triplet state ($^1Trp^* \rightarrow {}^3Trp^*$) and subsequent energy transfer to another molecule (e.g. from $^3Trp^*$ to $^3O_2 \rightarrow {}^1O_2^*$) can lead to the formation of excited oxygen which may trigger the photolysis of certain amino acids [57, 58]. The photodegradation of tryptophan leads to the formation of the kynurenine and other yellow kynurenine derivatives [59]. Most of the radiation energy absorbed by tyrosine is transferred to tryptophan and thus augments the pathway leading to singlet oxygen which in turn initiates photo-oxidation of tyrosine [57].

Photodegradation reactions have been shown to involve various sulphur and carbon centred free radical species as well as singlet oxygen [60]. It was stated that sulphur radicals may only be generated from cystine residues adjacent to a tyrosine residue, where energy of electron transfer from the excited tyrosine to cystine cleaves the disulphide link [60, 61]. Carbon radicals are preferentially produced at tryptophan, tyrosine, phenylalanine and histidine residues [62]; but their detailed structures have not yet been identified [61].

It has also been shown that irradiation of wool causes the formation of crosslinks involving the tryptophan residues [62]; possibly between tryptophan and histidine; and that the oxidation of tyrosine increases crosslinking in the form of bityrosine [60].

The effect of various excitation wavelengths on the properties of wool has been studied by many researchers and it was found that wavelengths between 290 nm and 310 nm are mainly responsible for photo-yellowing while photo-bleaching occurs at wavelengths above 400 nm (particularly 400-460 nm). The tendering of wool is mainly, but not exclusively, caused by radiation below 300 nm [63-65].

The measured UV absorption spectrum of a merino wool fibre compared to the absorption spectrum as expected from the calculation of the amino acid composition of wool is shown in Figure 5.1.4.

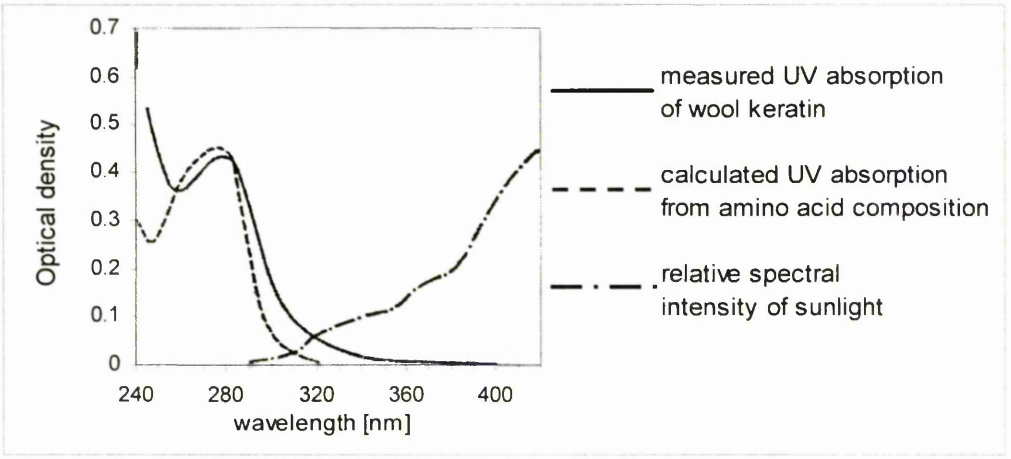

Figure 5.1.4. UV absorption spectrum of wool and spectral intensity of sunlight [57]

The chromophores mainly responsible for absorption in the 250-300 nm region are the most photoactive residues in amino acids and include disulphide bonds in cystine and the aromatic residues of tyrosine, tryptophan and phenylalanine. Maximum light absorption occurs at the following wavelengths: ~250 nm for disulphide groups in cystine residues, 257 nm for phenylalanine, 275 nm for tyrosine and 280 nm for tryptophan [66, 67]. The calculated and measured light absorption curves in Figure 5.1.4 show a discrepancy at wavelengths > 290 nm; the responsible chromophores for the additional measured light absorption are mainly unknown but thought to comprise photo degradation products of amino acids and possibly impurities in the wool [60].

The absorption of light >310 nm is especially interesting for this study because the historic tapestries, whilst on display, received irradiation from sunlight behind window glass which filters the lower wavelength UV light. Correspondingly, the MODHT model tapestry samples have been accelerated aged using a Xenon lamp with a UV filter yielding a similar spectral distribution as sunlight behind window glass.

Absorption at ~ 320 nm was tentatively attributed to glyoxylic and pyruvic acids, the degradation products of peptide chain fission at the alanine and glycine residues [60]. It was also suggested that irradiation of wool at 320 nm causes the degradation of the tryptophan radical tryptophyl, generating yellow degradation products which absorb light at 350-500 nm and are, in turn, degraded by radiation between 380 nm and 500 nm [61]. The free sulphur radical $RCH_2S^{\cdot}$ has been shown to absorb light at 600 nm. This corresponds to a broad absorption peak in

Lennox' measured absorption curve of desiccated, UV irradiated and P_2O_5 dried wool; the absorption in the visible region gradually disappeared when the wool was allowed to equilibrate with moist air, Figure 5.1.5 [68].

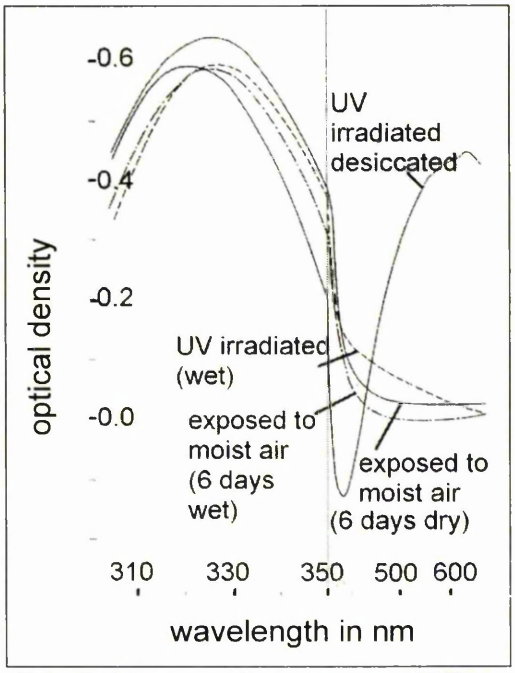

Figure 5.1.5. UV and visible light absorption by wool [68].

Photo-yellowing and photo-bleaching of wool

The tryptophan degradation product kynurenine is bright yellow and, along with the yellow/brown bityrosine and coloured degradation products of the amino acid histidine, has been identified as responsible the photo-yellowing effect of wool [69]. Asquith et al. also claimed that cystine and methionine form yellow products upon degradation both in the presence and absence of oxygen [70]. However, Milligan states that the amino acids cystine and methionine do not degrade to form coloured products [64]. Holt and Milligan investigated carbonyl formation in irradiated wool and concluded that the increase in carbonyl group content is not directly related to wool yellowing [71]. They could show that the photo-oxidation of the side chains of serine, threonine and cystine led to the production of carbonyl derivatives [72]. Irradiation of dry wool in the absence of oxygen produces a green discolouration which may be caused by cystyl radicals and rapidly disappears upon exposure to oxygen [67, 73].

The photo-bleaching effect of wool occurs on exposure to near blue light radiation (>400 nm), hence the yellower the wool the greater is the absorbance of blue light

and the more rapid is the photo-bleaching action [74], which is thought to be due to the destruction of fugitive yellowing chromophores, possibly accompanied by the generation of fluorescent derivatives [61, 75]. Simpson found that acidic treatment of wool shortened the period of photo-bleaching and quickened the onset of photo-yellowing, while neutral or slightly alkaline conditions slowed down the photo-bleaching and the photo-yellowing effect of wool upon exposure to sunlight [75].

Photo-tendering of wool

Disulphide bond breakdown of cystine together with main chain breakdown is mainly responsible for the photo-tendering of wool [60, 64, 65, 71, 72, 74, 76, 77].

Baumann stated that during photo-oxidative degradation of wool reactions cause decomposition of side chains and scission of the main peptide chain, which lead to the formation of new end-groups [76]. Scheme 5.1.4 shows the photo-oxidative cleavage of the main peptide chain at the NC^{α} bond leading to α-keto acids, as proposed by Meybeck and Meybeck [78]. Milligan noted that photo-tendering is mainly caused by the scission of the protein chains and the oxidation of cystine to cysteic acid breaking the disulphide crosslinks between the protein chains [65]. Scheme 5.1.5 shows three possible reaction pathways involving either S-S or C-S fission and leading to the formation of cysteic acid via intermediate products, of which cystine monoxide (I), cystine dioxide (II), cysteine sulfinic acid (III) and cysteine sulphonate (IV) have been detected [79]. However, all of the intermediate oxidation products are unstable and eventually hydrolyse to cystine and cysteic acid.

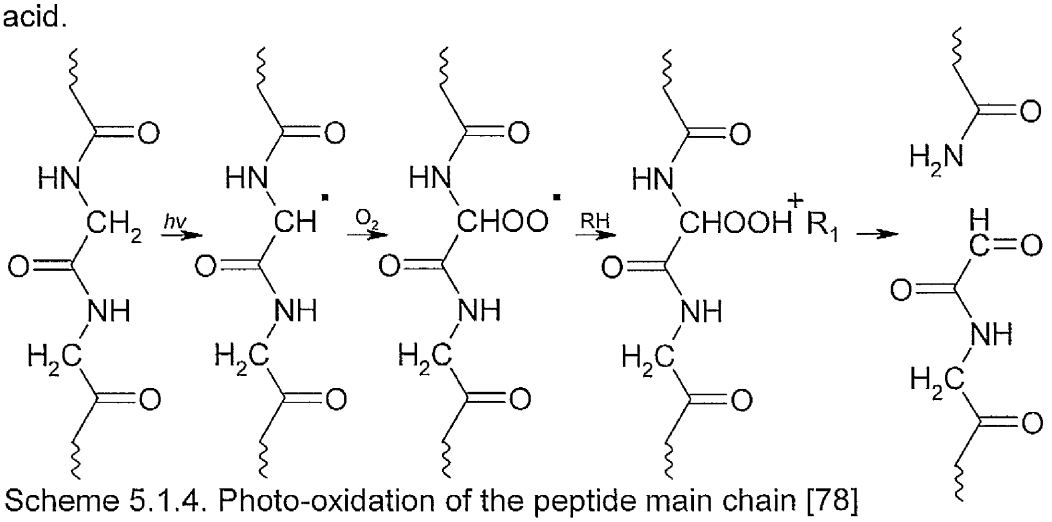

Scheme 5.1.4. Photo-oxidation of the peptide main chain [78]

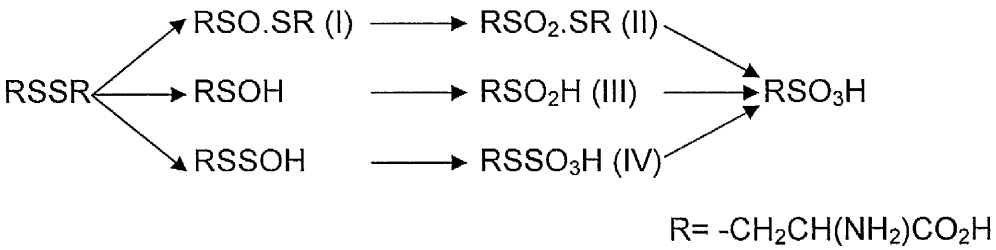

Scheme 5.1.5. Oxidation of cystine di-sulphide to cysteic acid [79]

Weatherall showed that carbon dioxide was lost from wool on irradiation with light of wavelengths up to 365 nm; it was suggested that carboxyl groups are formed in irradiated wool but they are themselves susceptible to loss by photolysis. It was also shown that in photo-tendered wool the cystine content dropped while the cysteic acid level rose; histidine and tyrosine levels also decreased while ammonia increased [77]. This was confirmed by Milligan, and by Nicholls who found that during photochemical reaction tryptophan, histidine and cystine suffered the most degradation followed by tyrosine, phenylalanine and methionine which also suffered significant losses [64, 74]. Main chain breakdown at the alanine and glycine residues led to the formation of pyruvic and glyoxylic acids [64, 74]. Other α-keto acids suggested that breakdown occured adjacent to several different amino acid residues such as proline, serine, threonine, glutamic acid and tyrosine [60, 71]. Holt and Milligan showed that photo-oxidation of wool leads to an increase in carbonyl groups and identified carbonyl derivatives of serine, threonine and cystine amino acids [72]. UV and simulated sunlight irradiation of the surface lipid layer has been found to remove covalently bound fatty acids and increase the surface carbonyl and carboxyl content through oxidation of fatty acids [10, 35, 42, 47, 49, 80].

Körner stated that during photo-oxidation of 18-MEA the hydrogen atom in position 18 is cleaved off and a tertiary radical formed, which may react with oxygen to form a hydroperoxide according to Scheme 5.1.6 [26].

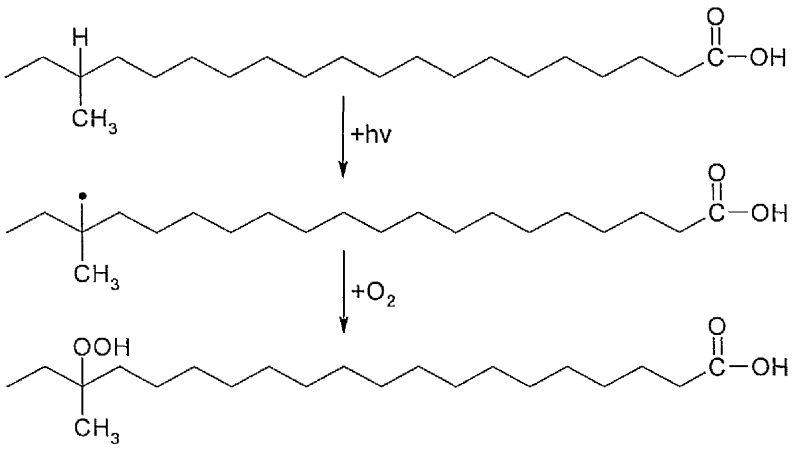

Scheme 5.1.6. Photosensitized oxidation of 18-methyl-eicosanoic acid [26]

5.1.3. XPS studies of wool

XPS has been employed to study the chemistry of the wool surface since the early 1970's [29, 30]. Millard was the first to report the chemical state changes observed on the oxidised wool surface. He identified the main sulphur S(2p) peak at 164 eV as cystine and suggested a sulfate ion or other S^{6+} species for the shifted S(2p) peak at 168 eV following Corona discharge treatment [29]. Millard also identified oxidative shifts to higher binding energies in the O(1s), N(1s) and C(1s) peaks in plasma treated wool. He assigned three components of the C(1s) peak to aliphatic carbon at 285 eV, carbon with a single bond to oxygen at 286.5 eV and carbonyl carbon at 288.5 eV [30]. In addition to the previously identified C(1s) components Bradley et al. suggested a peak shift of +0.7 eV for carbon bound to nitrogen relative to the main hydrocarbon peak [35].

Later Bradley and Mathieson made a more detailed assignment of components in the C(1s) peaks of untreated and UV oxidised wool, Table 5.1.6 [42].

Table 5.1.6. peak assignments for the C(1s) components in wool [42]

Binding Energy	Peak shift	Peak assignment
285.5 eV	0 ev	C-C / C-H
287 eV	1.5 eV	C-N
288.5 eV	3 eV	N-C=O
287.5	2 eV	N-C-O (in oxidised wool only)
289.5	4 eV	COOH / COOR (in oxidised wool only)

In a recent study employing XPS on wool Molina et al. suggested a fifth peak component on the lower binding energy side of C(1s) for adventitious carbon [51]. However, this broadening of the C(1s) peak had previously been attributed to sample charging [46].

Carr et al. attributed the S(2p) peak at 168eV to cysteic acid [31] and, in a study on copper treated wool [33], to Bunte salt. Following treatment with *t*-butoxide, Carr et al. observed a 0.7 eV shift of the S(2p) peak to lower binding energy, which they tentatively attributed to the conversion of cystine to lanthionine residues [18]. Intermediate oxidation products such as sulfenic acid, sulfinic acid and perthiocysteine were suggested to cause the broad and asymmetric S(2p) peak shape observed after alkali treatment [18]. A broadening of the S(2p) peak accompanied by a decrease in intensity was also observed by Kidd et al. after gaseous fluorination treatment; this was attributed to loss of sulphur and the formation of more than one oxidation product [38]. Baumann et al. identified intermediate oxidation products of cystyl residues on the wool surface after various wet treatments [81]. Monoxycystyl residues with a binding energy of 165.5 eV and sulphinic acid residues at 167 eV were detected after oxidative treatments under acidic conditions, specifically performic acid, hydrogen peroxide and chlorination with sodium hypochlorite treatment. No intermediate oxidation products were detected after oxidative treatments under alkaline conditions; this was attributed to the low hydrolytical stability of monoxy- and dioxycystyl residues under alkaline conditions [81, 82].

Information about the presence of a surface lipid layer can be obtained through the relative atomic percentages of carbon and nitrogen; a high C/N ratio reflects the presence of carbon-rich material, i.e. lipids on the immediate surface [18]. An XPS investigation of the weathered tips of wool fibres showed lower C/N and S/N ratios than were found for the base of fibre, indicating a loss of covalently bound lipids and loss of sulphur due to weathering. Also, a high proportion (30%) of oxidised sulphur was detected in the weathered tips [15].

Using the Auger peaks Ward et al. observed a higher C/N ratio than calculated from the photoelectron peaks, this was attributed to a hydrocarbon outer surface layer, because the escape depth for Auger electrons is ~1 nm compared to an escape depth of ~4 nm for photoelectrons. Working on the assumption of a

uniform surface, they estimated a thickness of 0.9 nm +/- 0.4 nm for the surface lipid layer [19].

Brack et al. studied the adsorption of surfactants on the wool fibre surface by examining the changes in the C(1s) peak shape and variations in the C/N ratios [45]. Presence of surfactants on the sample surface should increase C/N because the underlying proteinaceous nitrogen would not be detected.

In a study on the influence of water at elevated temperatures (50-100°C) on the wool fibre surface Brack et al. found that such treatment caused only minimal oxidation of sulphur but significant decrease in the surface lipid content [46]. However, this was only observed after solvent extraction of the water treated fibres. Before solvent extraction the C/N ratio actually increased, indicating that carbonaceous material dissolved from within the fibre deposited on the surface [46].

Carr et al. studied wool and hair protein fractions and used the N/S ratio to calculate the sulphur content of the epicuticle to be 9% by weight, which corresponds to 25-35 mol% cysteine residues [18]. This was confirmed by Ward et al. who estimated 35 mol% content of half-cystine (cysteine) residue in the surface protein [19] and Dowling et al. who found the sulphur content of the untreated wool surface was 8.7% by weight and the sulphur content of the cortex was 2% [34].

In a study employing methyl mercuric iodide reaction with wool Carr et al. calculated a free sulfhydryl content of 140 µmol/g of epicuticle protein, which gives the same ratio of sulfhydryl groups to total sulphur on the surface and the bulk of the fibre [32].

Tillin et al. reacted wool with hexafluoroacetone and subsequently analysed the wool surface and bulk (powdered wool). Through calculation of the F/N ratios they concluded that proteinaceous reactive sites in the epicuticle are less accessible for reaction than reactive sites in the cortex [83].

Bradley et al. employed XPS to study the oxidative effect of UV/Ozone treatment and oxygen plasma treatment on the wool fibre surface. They showed that the treatments led to oxidation of di-sulphide links to sulphonic acid groups and proteinaceous carbon to carbonyl functional groups [35, 36, 43]. In studies by Shao et al. the relative increase in the higher binding energy part of the C(1s) peak

(287-289 eV) was also attributed to the formation of carboxylic acid groups during UV/Ozone treatment [10, 49].

Klausen et al. [39], Brack et al. [15] and most recently Molina et al. [51] used semi quantitative deconvolution of the C(1s) peak to show that oxidative treatments (oxygen plasma [39], potassium hydroxide and potassium *t*-butoxide [15] and water vapour plasma) result in the oxidation and subsequent removal of the surface lipid layer. The proteinaceous components of the C(1s) peak (C-O, C-N, C=O) increased while the hydrocarbon, i.e. lipid component decreased. A similar approach was taken by Dai et al. who used the ratios of the curve fitted C(1s) components to study the effect of oxygen plasma treatment on self-assembled monolayers as a model for the wool fibre surface [27]. They concluded that carbon oxidation and C-C bond scission occurred prior to complete removal of the lipid molecule from the wool surface [27].

5.1.4. SIMS studies of wool

Ward et al. compared the positive ion Static SIMS spectra of wool to those of pure protein and polyethylene [19]. Pure protein showed nitrogen containing even mass numbered peaks at m/z 18^+, 28^+ , 30^+, 42^+, 44^+, 56^+ and 70^+, whereas both wool and polyethylene exhibited uneven mass numbered peaks. This was attributed to a saturated hydrocarbon surface on the wool fibre, namely the lipid layer; with characteristic peaks at m/z 27^+, 29^+, 41^+, 43^+, 55^+ and 57^+. After treating the wool with *tert*-butoxide those peaks attributed to protein increased while the hydrocarbon peaks decreased, showing that the treatment caused the partial removal of the lipid layer [15, 19]. Ward et al. suggested that SIMS has a greater sensitivity towards lipids compared to protein, explaining the relatively high intensity of hydrocarbon peaks even after lipid removal [19]. ToF-SIMS peaks in the higher mass range at m/z 311^-, 325^- and 341^- were attributed to the lipid chains $C_{19}H_{39}COO^-$, $C_{20}H_{41}COO^-$ and $C_{20}H_{40}OHCOO^-$ with the peaks at m/z 341^- and 325^- being associated with the methyl branched C_{21} fatty acid (18MEA) [19]. This was disputed by Peet et al. who suggested that 18MEA was primarily bound via thioester linkages and assigned the ion $C_{20}H_{41}COS^-$ for the peak occurring at m/z 341^- [84]. A more detailed assignment of lipid peaks was given by Shao et al. [44].

Table 5.1.7. Lipid peak assignment in ToF-SIMS spectra [44, 85]

Fatty acid species		**SIMS peak (a.m.u.)**	**relative fatty acid concentrations (%)**
18-MEA	$C_{20}H_{41}COS^-$	341	40.2
	$C_{20}H_{41}COO^-$	325	8.6
Eicosanoic acid	$C_{19}H_{39}COS^-$	326	13.7
	$C_{19}H_{39}COO^-$	311	2.9
	$C_{18}H_{37}COS^-$	313	8.5
	$C_{18}H_{37}COO^-$	297	overlap with oleic acid
Stearic acid	$C_{17}H_{35}COS^-$	299	3.6
	$C_{17}H_{35}COO^-$	283	3.4
Oleic acid	$C_{17}H_{33}COS^-$	297	4.3
	$C_{17}H_{33}COO^-$	281	2.1
	$C_{16}H_{33}COS^-$	285	4.2
	$C_{16}H_{33}COO^-$	269	2.3
Palmitic acid	$C_{15}H_{31}COS^-$	271	3.9
	$C_{15}H_{31}COO^-$	255	2.4

The relative decrease or absence of lipid signals after oxidative treatments has been used to evaluate the extent of removal of the lipid layer after chlorination, plasma treatment, permonosulfuric acid treatment, exposure to UV/Ozone and hydrogen peroxide bleaching [44, 47, 85].

In addition, Shao et al. attributed the signals at m/z 80^- and 81^- present in the oxidised wool spectrum to sulphonic acid SO_3^- and SO_3H respectively [44].

Brack at al. studied the adsorption and rinsing behaviour of surfactants on the wool fibre surface and showed that nonyl phenol ethoxylates are strongly bond to the fibre surface [45] . While Volooj et al. studied the adsorption behaviour of protein softeners [85].

Volooj et al. calculated the relative concentrations of fatty acids on the merino wool fibre surface using the ratio $I_A/(I_A+I_{42})$ where I_A is the intensity of the respective lipid ions and I_{42} is the wool surface characteristic signal at m/z 42^- corresponding to $^-N=C=O$ [85], Table 5.1.7.

5.2. Literature review for silk

5.2.1. Structure and chemical composition of silk

Silk is the cocoon fibre produced by the larvae of a variety of insects and spiders [86-91]. The commercially most useful silk stems from the domesticated Bombyx mori silkworm. The glands of the larva produce two fibroin filaments, which are bound together by the protein gum sericin into a single thread.

Before silk is employed for any textile application it is degummed in order to achieve a finer, more lustrous filament by completely removing the sericin. Sericin is soluble in boiling water, dilute aqueous alkaline and acid solutions. These treatments as well as enzymic methods can be used for degumming [86].

The degummed silk filament of the Bombyx mori family is approximately triangular in cross section with a diameter of 10-20 μm and a fine twist. The length of the filament depends on the quality of the cocoon and the reeling method and can be up to 500-800 m. The surface of the filament is very smooth, Figure 5.2.1.

Figure 5.2.1. SEM micrograph of silk filament cross-section and surface

Each silk fibre is believed to consist of 20-30 bundles of orientated fibrils. The individual fibrils are approximately 10 nm in diameter and 350 nm in length and grouped in concentric rings [87].

Silk is mainly constituted of 18 different amino acids in two major sequences, which form a 'heavy' polypeptide (H-chain) and a 'light' polypeptide (L-chain), Table 5.2.1. More than 80% of the silk fibroin consists of the three amino acids glycine, alanine and serine in an approximate 3:2:1 ratio [88]. Chemical structures of the amino acid residues are shown in Scheme 5.1.2.

The sequence of both the heavy and the light chain have been fully characterised [92, 93]. The H-chain was found to be 5253 residues long with a molecular weight of 391367 Da [92]. Approximately 90% of the H-chain is made up of low complexity regions where glycine (G) takes up alternate positions with mainly alanine (A), some serine (S) and tyrosine (Y) and, to a low extent, valine and threonine. The most abundant repeat units are the hexapaptides GAGAGS (432 copies) and GAGAGY (120 copies). Other amino acid residues are present in regions of higher complexity. The H-chain contains five cysteine residues located near the N- and C-termini, only one cysteine residue of the H-chain forms a disulphide bond with the L-chain [92]. The L-chain consists of 262 amino acid residues in comparatively complex sequence and has an approximate molecular weight of 25800 Da [93]. It contains three cysteine residues of which two form an intramolecular cystine disulphide bridge and the other, near the C-terminus, offers the possibility of a disulphide linkage with the H-chain. The molar ratio was suggested to be 1:1. More than half of the total amino acid content of silk fibroin is accounted for by glycine, alanine and serine, though the amino acid composition of the two molecular chains differs considerably, Table 5.2.1 [86].

Table 5.2.1. Amino acid composition of silk fibroin

	Residue percentage				
Amino acid	**Fibre**	**Fibre**	**Fibre**	**H-chain**	**L-chain**
Glycine	43.7	43.7	44.6	49.4	9.2
Alanine	30.3	29.3	29.4	29.8	14.2
Serine	9.9	10.7	12.1	11.3	9.0
Tyrosine	5.2	5.5	5.2	4.6	2.8
Valine	1.8	2.4	2.2	2.0	6.4
Aspartic acid/Asn	1.5	1.8	1.3	0.7	14.8
Glutamic acid/ Gln	1.2	1.2	1.0	0.7	9.2
Threonie	0.7	0.9	0.9	0.5	3.0
Phenylalanine	1.2	0.9	0.6	0.4	2.7
Isoleucine	0.8	0.7	0.7	0.1	7.8
Leucine	0.7	0.6	0.5	0.1	7.5
Arginine	0.9	0.5	0.5	0.2	4.5
Lysine	0.2	0.3	0.3	0.1	1.2
Proline	0.4	n.s.	0.4	0.3	3.2
Histidine	0.4	n.s.	0.1	0.1	2.3
Methionine	0.9	n.s.	0.1	n.s.	0.4
Tryptophan	n.s.	n.s.	0.1	n.s.	n.s.
Cysteine	n.s.	n.s.	0.2	n.s.	1.40
Reference	[89]	[90]	[86]	[86]	[86]

n.s. = not stated

On the macromolecular level silk is composed of amorphous and crystalline regions, the latter of which are constituted of β-pleated sheets held together by hydrogen bonds as shown in Figure 5.2.2. The crystalline regions are made up of irregular stacking of H-chain molecules, which run along the fibre axis in antiparrallel–antipolar packing. The DNA sequence for the crystalline regions is assumed to lead mainly to GAGAGS [91]. The L-chain is not associated with crystalline regions in the molecular structure. It is assumed that the amorphous regions contain those parts of the polypeptide molecule with bulkier side chains such as tyrosine. The occurrence of α-helical arrangement of the molecular chains in amorphous regions has been suggested but was later discounted [86].

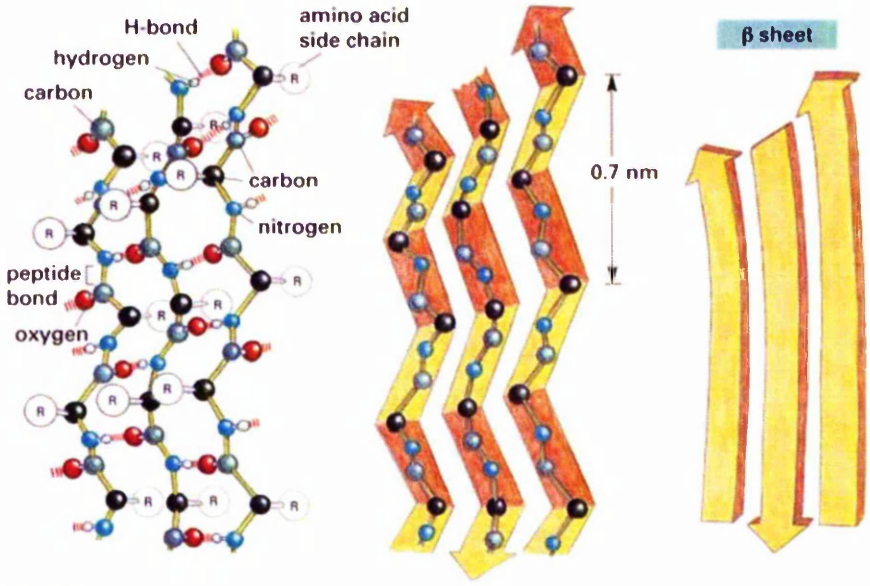

Figure 5.2.2. Antipolar-antiparallel model of the β-sheet structure with hydrogen bonds [94]

5.2.2. Photochemistry of silk

Silk of all natural textile fibres is the most susceptible to degradational changes induced by light radiation, especially of the UV range. Physical and chemical changes due to the photo-degradation of silk lead to yellowing and tendering of the fibres [86].

The absorption spectrum of silk shows a maximum at 280 nm due to the principal light absorbing groups in the fibroin protein, the aromatic amino acids tyrosine, tryptophan and phenylalanine [47, 90].

Becker and Tuross examined the morphology of silk exposed to UV light and observed that radiation between 230 nm – 285 nm caused fusion of adjacent silk fibres similar to a 'melting' process [90].

Photo-yellowing of silk

Initial yellowing has been related to a decrease in the isoelectric point of silk and was attributed to the oxidation of side chains at the fibre surface, in particular the photo-oxidation of tyrosine and tryptophan [69, 86, 95].

Photo-tendering of silk

Initial degradational breakdown is thought to be due to the cleaving of hydrogen bonds, which is followed by oxidation of tyrosine and the eventual fission of the polypeptide chain at the C-N position and at the tyrosine residues [86].

Numerous researchers have investigated the alteration of tensile properties of silk due to physical and chemical degradation [87, 89, 90, 96-100]. Gogoi studied the effect of UV radiation on silk fabric and found that tensile strength, abrasion resistance, crease recovery, bending and flexural rigidity decreased with extended exposure. In addition, the effect was found to be stronger in wet fabric than in dry fabric [98]. Tsukada and Hirabayashi found that UV irradiated silk experienced significant decreases in elongation and tensile strength; the percentage change observed in elongation was more rapid and proceeded further than the change in strength [96]. This was confirmed by Hansen and Ginell, who conducted light ageing experiments on silk and found that the breaking load was the tensile property least susceptible to photo-degradational change. Initial degradation seemed to occur linearly but with increased exposure to radiation the degradation levelled out following an exponential model [97]. Similarly, heat ageing experiments at 150°C showed that silk decomposed rapidly following a linear trend in decrease of tensile strength on a logarithmic scale [99].

Bresee and Goodyear attributed overall degradational changes in aged silk fibres to both hydrolytic and oxidative reactions [87]. Hydrolysis may have occurred during dyeing or washing treatments of the fabric, while oxidation could be induced by photo-reaction or due to oxidising agents present in the fabric itself or the

environment. Losses in tensile strength were associated with hydrolytic polymer chain scission, while the reduction of elongation and elasticity in aged silk fibres was attributed to oxidative formation of new intra- and inter-molecular crosslinks.

Several studies have shown that silk released nitrogen containing gases upon photolysis [89, 90, 101, 102]. Early investigations by Harris showed that photo-degradation of silk was mainly due to oxidation and accompanied by the formation of 'ammonia' nitrogen, while degradation due to hydrolysis was accompanied by the formation of 'amino' nitrogen [102]. Yanagi et al. and Hirabayashi et al. showed that UV irradiation of silk caused weight loss of the fibre due to emission of ammonia gas [89, 101]. Becker and Tuross investigated the loss of amino acids due to photo-degradation [90]. Employing ion exchange HPLC analysis of hydrolysates from silk irradiated at varying UV wavelengths, it was found that the percentage loss of amino acids increased with decreasing wavelength. Tyrosine exhibited the largest percentage loss. This was accompanied by an increase in the amount of hydrolysable ammonia in the irradiated silk.

In general the acidic, ionizable and hydroxylated amino acids were lost at faster rates than the aliphatic amino acids, with glycine and alanine being the most stable. All amino acids apart from isoleucine, leucine and phenylalanine exhibited a UV dependency in their rates of degradation, i.e. the higher the UV content or the lower the wavelength of the incident radiation the faster the decomposition of amino acids. Initial photo-degradation occurred selectively in the amorphous regions but as exposure time and dose increased degradation became more random and affected the whole fibroin matrix including peptide bond scission in crystalline and amorphous regions [90].

Following these findings, Becker at al. investigated the possibility of using HPLC analysis of the remaining amino acid content in historic silk fibres as an indicator for their state of degradation [88]. It was assumed that degradation started with the loss of those amino acids with large side chains, i.e. the amorphous parts of the protein and eventually proceeded to the crystalline regions, hence the further the protein was degraded the more material was hydrolysable from crystalline parts. Thus the ratio of extracts from crystalline versus amorphous regions was determined from the ratio of neutral to acidic amino acids. Comparison of data acquired from tensile strength tests and total amino acid recovery confirmed the correlation between age, strength loss and loss of amino acids, Figure 5.2.3.

Becker et al. concluded that the "analysis of the extractable proteinaceous material from silk fabrics is a useful tool in determining the state of protein preservation".

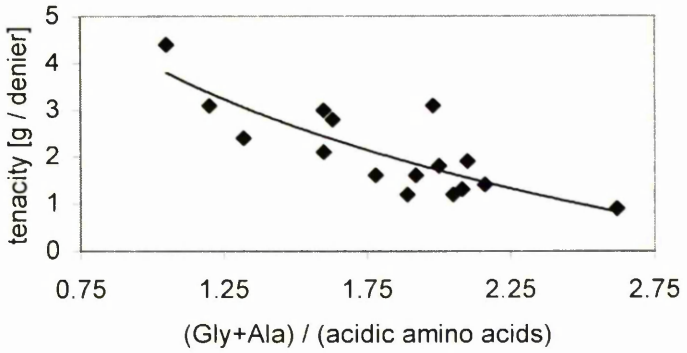

Figure 5.2.3. Correlation of strength loss and ratio of loss of amino acids from crystalline to amorphous regions [88]

Tsukada and Hirabayashi had previously suggested that the degree of crystallinity of silk did not change upon exposure to UV light [96]. Refractive index measurements suggested that no structural changes occurred in irradiated silk but a slight decrease in degree of molecular orientation, which was related to a decrease in relative viscosity. This was attributed to the disintegration of fibroin molecules and highly orientated β sheet structures becoming disordered under the influence of UV radiation.

A decrease in intrinsic viscosity was confirmed by Yanagi et al. who performed artificial ageing experiments with γ-rays [89]. However, comparative thermal analysis of original old silk samples and artificially γ-ray aged silk showed that both had opposite effects on the macromolecular structure of the silk fibre. The degree of crystallinity in γ-ray aged silk decreased, whereas crystallinity in old silk apparently increased or rather crystalline regions remained intact while amino acids in amorphous regions decomposed, thus altering the crystallinity ratio.

Irradiation with UV light was also found to cause weight loss, which was larger in amorphous regions than in crystalline regions and was mainly due to considerable loss of tyrosine and phenylalanine [89].

In addition, Shao et al. proposed that, in unexposed silk, crystalline regions dominated in the fibre bulk, while outer layers of the fibre became increasingly less ordered [47]. XPS analysis of silk suggested that the carbon concentration at the surface was higher than in the bulk fibre, this was attributed to an amorphous outer layer containing a higher amount of the carbon rich tyrosine residue.

Following artificial ageing experiments with UV radiation, Shao et al. suggested that the amorphous surface layer of the silk filament was modified / removed.

5.2.3. XPS and SIMS studies of silk

Shao et al. employed XPS and SIMS for the study of silk fibres [47, 103]. They observed a higher C/N ratio on the surface than was expected from bulk analysis and attributed it to a higher concentration of the carbon rich amino acid tyrosine on the surface. Tyrosine is predominantly present in the amorphous regions of the silk fibre, which is consistent with the model describing a highly orientated core, which becomes progressively less ordered towards the outer layers of the silk fibre. Sulphur was shown to be predominantly present in cysteic acid form, even on the unoxidised silk surface; UV/Ozone treatment caused the disappearance of the S(2p) peak as well as a decrease in carbon and relative increases in oxygen and nitrogen. This was attributed to the oxidative removal of the outer amorphous layer of the silk fibre [103]. The effect of simulated sunlight was suggested to be similar to the effect of UV/Ozone on silk [103].

5.2.4. The influence of weighting and mordanting on silk and wool

Most natural dyestuffs require a mordant in the form of metal salts or tannic acids to increase their substantivity for the fibre. The application of various salts of metals such as Al, Cu, Fe, Zn and Sn creates different shades and depths of shade of colour, as well as increased wash- and light-fastness. However, light fastness tests on mordanted and unmordanted dyed wool and silk showed that the mordanted samples underwent greater relative change in colour and shade because due to mordanting dyed wool and silk had a deeper initial shade in colour and therefore increased light absorbance [100].

To increase the weight, handle and drape properties of silk, inorganic salts of Al, Fe, Pb, Sn or Zn of up to 300% of weight of fabric have been applied in the past [99]. Ballard et al. employed EDX for the analysis of weighting material on historic silks [104, 105]. The presence of S, Fe, Ca, Si and Al was identified in all analysed samples and Sn, Cl, K and Na in most samples. The sulphur content was generally higher than could be accounted for by cysteine or methionine or sulphur

containing dyestuffs, and treatment with sulphuric acid was suggested as the source of the excess sulphur.

This common practice of metallic 'weighting' of silk is generally believed to increase the susceptibility of historic silk textiles to degradation [86]. To date there is no routine conservation treatment for textiles impregnated with excess metal ions, with the general recommendation being to store these textiles in the dark, avoid high relative humidity and high temperatures, as well as wet or dry cleaning [106].

Although there is apparently an extensive literature encompassing the interactions of metals with fibres there is still much debate regarding the influence of metal ion absorption on the tensile properties of wool and silk and their subsequent effect on ageing processes. Metal ions may bind to carboxylate, amino, thiol and sulphonate groups thereby imparting a strengthening effect to the fibre through crosslinking of neighbouring peptide chains in the amorphous regions or, conversely, a weakening effect through disruption of the molecular β-sheet structure of silk or the α-helical arrangement of wool in the crystalline regions [107-109]. The effect of metal ion adsorption on silk has been studied by Shimizu and by Hojo and Shirai [107, 108]. Metal complexes with silk protein were believed to form at the N, O and S ligand atoms of the main chain and side chains [107]. Shimizu showed that metal cations adsorbed onto silk and formed ion bonds with terminal carboxylic groups and, with increasing pH, terminal amino groups also became adsorption sites; as represented in Scheme 5.2.1.

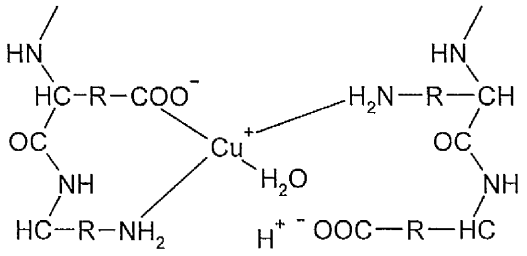

Scheme 5.2.1. Metal complex formation. Ion bonding of Cu(II) and silk [108]

The tensile strength and chemical degradation of historic weighted silks [110-112] and the application of various metal ions, sometimes in combination with dyestuffs, and their effects on the tensile properties of wool and silk, following artificial ageing, has been previously studied but with conflicting conclusions obtained by the various workers [100, 107, 108, 113, 114].

An early investigation by Appel and Jessup of accelerated and natural ageing of weighted silk showed that the decrease in tensile strength cannot be correlated to the amount of metal ion absorbed by the fabric as some heavily weighted silks showed lower strength losses than less weighted fabrics [110]. Kuruppillai found that the stability of silk to light was greatest at around pH 10 but decreased rapidly above pH 11 or below pH 3. Weighting of silk decreased its pH and thereby increased its sensitivity to photo-degradation [99].

Hojo and Shirai reported increased thermal stability as well as increasing tensile strength but decreased elongation of silk following treatment with cupric, ferrous and aluminium ions [107]. It was found that thermolysis of peptides started at the –NH- link therefore metal complex formation with the N amino ligands increased thermo stability of the protein. Likewise, Shimizu mentions an increase in silk tensile strength due to absorption of nickel and cobalt ions [108]. In contrast, Needles et al. found the tensile strength and strain reduced for silk mordanted with alum, chromium, copper, iron and tin and dyed with alizarin, brazilin and carminic acid, while wool, which underwent the same treatments, showed increased elongation for all mordants except chromium, with the tensile strength values generally increasing for iron and chromium mordanted wool, but decreasing for tin and alum mordanted wool [100]. Alternatively Smith et al. found the tensile strength increased for alum mordanted and dyed wool [114].

According to Needles et al. the photo-degradation of chromium mordanted wool and tin and iron mordanted wool and silk was increased, while copper mordanted silk showed greater stability to photo-degradation [100]. Similarly, Shimizu stated that copper, nickel and manganese had a photo-protective effect on silk while the absorption of zinc, iron and chromium ions accelerated photo-degradation [108]. Indictor and Ballard also state that iron mordants seem particularly corrosive to fibres [115]. Smith et al. reported decreased tensile strength and strain for artificially light aged iron and copper mordanted and dyed wool but found the degradation was substantially reduced for alum mordanted wool [114]. In another study the same research group found photo-protective effects not only for alum treated wool but also for chromium, iron, lanthanum, uranyl and zirconyl treated wool [113].

On the whole, the influence of metal ion adsorption on silk and wool is variable and depends greatly on the oxidation states of the metal, the pH, relative amount

of metal and application procedure as well as possible additive/synergistic effects with chromophores. Metal complex formation may occur with ligand atoms of the protein side chains or with main chain amine as well as with dyestuffs present in the fibre. Thermolysis and photolysis properties are greatly affected by the stabilising action of metal ion bond formation, as well as the destabilising action of acid hydrolysis or oxidative effects during treatment, and the oxidative catalytic action of metal ions within the fibre.

5.3. Experimental

5.3.1. Tensile strength tests: yarns

Influences of dyestuffs and dyeing procedures as well as the effect of accelerated ageing were evaluated through tensile strength measurements of wool and silk yarns. Where possible, any observed differences in comparison to the tensile strength values of untreated yarn samples were correlated to dyestuffs, auxiliaries and procedures.

The tests were performed on an Instron Series IX Automated Materials Testing System using a gauge length of 50 mm. The samples were slack-mounted and the tests were carried out at a constant rate of extension of 250 mm/min using a load cell of 1 kN. All samples were conditioned at 23°C and 50% relative humidity for at least 24 hours prior to testing. Results presented are the average of a minimum of ten replicate measurements. The maximum load before sample rupture was recorded in cN. Strain at maximum is the apparent elongation as the percentage increase in length based on the gauge length.

5.3.2. Tensile strength tests: single fibres

Samples of unaged, accelerated aged and historic single wool fibres were mounted on card board strips over a 6 mm Ø punched hole using epoxy resin. The crimp of the wool fibres was straightened during mounting applying minimal pre-tension. All samples were conditioned at 23°C and 50% relative humidity for at least 24 hours prior to testing. The card board strips were fastened between the clamps of a Series IX Automated Materials Testing System aligning the 6 mm gauge length with the punched hole. The cardboard on either side of the wool fibre was clipped prior to testing. The constant rate of extension was set at 2.4 mm/min using a load cell of 10 N. Approximately 50 specimens were prepared and tested

for each sample, discarding all specimens which showed fibre fracture inside the epoxy resin or obvious fibre slippage. The strain at maximum in % and the maximum load (mN) before sample rupture were recorded.

Figure 5.3.1. Mounted and tensile strength tested wool fibre

5.3.3. Fibre diameter measurements

Average wool fibre diameters were obtained for the single fibre tensile tested samples, given that sufficient sampling material was left. 1-2 mm of approximately 100 fibres were mounted in paraffin on a microscope slide. The samples were viewed under an Olympus Microscope fitted with a JVC Colour Video Camera TK-107OE producing live images on a computer screen at approximately 1130 x magnification. The image analysis software Image-Pro Plus 5.1 was utilized to obtain diameter measurements of 100 different fibres and export the results into Microsoft Excel for calculation of the average and standard deviation.

5.3.4. SEM

SEM images were obtained to study the influence of dyeing procedures and accelerated ageing in wool and silk surfaces and cross sections after fracture.

All wool and silk fibre samples were mounted with adhesive copper tape. For fibre surface analysis thread samples of ~2.5 cm were mounted on SEM ring stubs, while the samples for fracture morphology analysis were mounted in SEM clamp stubs with ~1-2 mm free length. Fibre samples were gold coated to reduce image distortions through charging.

Instrumental settings

The Hitachi SEM S-3000N system was used in this study, and unless otherwise stated, the secondary electron detector, a medium aperture, working distance of approximately 12 mm and 5 keV accelerating voltage were used for all samples. Detector ID, sample name, working distance, accelerating voltage and the appropriate scale bar were recorded on each SEM micrograph. On average ten images of different areas of each sample have been obtained but only few representative images were chosen for presentation in this thesis.

The back scatter detector was employed for fibre surface analysis to minimise problems encountered through charging due to the longer sample length. The shorter free sample length for fracture morphology analysis ensured quick charge dissipation and facilitated the use of the secondary electron detector.

5.3.5. XPS

XPS was employed for the analysis of wool and silk fibres from model and original tapestry samples to study the surface chemical changes occurring during accelerated and natural ageing. Copper screw plates were used to clamp the yarn and fabric samples onto the sample bar. Due to their small size some historic samples had to be mounted using adhesive tape. Otherwise mounting with adhesive tape was avoided due to possible sample contamination with silicon residues.

Initially historic wool samples were XPS analysed as received, however, the spectra revealed significant amounts of carbon and silicon contamination. Two non-swelling solvents, acetone and heptane, were assessed as cleaning agents and heptane appeared to successfully reduce surface contamination, as indicated by a decrease in the carbon and silicon signals and an increase in oxygen, nitrogen and sulphur intensities, Table 5.3.1. Heptane extraction was therefore performed separately for each sample in clean glass vials. The samples were treated at room temperature under constant agitation for 40 minutes exchanging the heptane four times.

Table 5.3.1. Averaged XPS results of a historic wool sample before and after heptane extraction

Sample	Atomic %						
	O 1s	N 1s	C 1s	S 2p	Ca 2p	Si 2p	Al 2p
HRP1_1	15.8	4.2	73.1	1.7	1.1	2.3	1.8
HRP1_1 heptane	18.9	6.4	67.8	2.4	1.5	2.0	1.1

Instrumental settings

The Kratos Axis Ultra X-ray photoelectron spectrometer was used in this study. Wide scans of 900-0 or 600-0 eV binding energy were taken of each sample using the Al Kα monochromator X-ray source and resolution pass energy 160 eV. The analysed area was approximately 300 x 800 μm on all samples (lens mode hybrid and slot aperture). Other instrumental settings were 10 mA current, 15 kV anode HT, 0.4 eV step, 600-1000 ms dwell time and 1-2 sweeps per sample. High

resolution survey scans of the C(1s), O(1s), N(1s), S(2p) and Al(2p) peaks were obtained using resolution pass energy 20 eV, 0.1 eV step and all other settings as above.

Due to the insulating nature of wool and silk fibres the charge neutraliser was on during all sample analyses.

Data processing

Two or three different areas were analysed on each sample and the data processed using Casa XPS 2.2.67 software. Quantification was carried out using Scofield sensitivity factors and transmission functions. A linear background was used for all peaks and if curve fitting was performed with more than one component the full width half maximum values were constrained to differ by no more than 0.5. The results given in this thesis state the average relative atomic percentages and elemental ratios as calculated for different areas on the same sample.

5.3.6. ToF-SIMS

ToF-SIMS analysis was carried out to study the influence of dyeing procedures and accelerated and natural ageing on wool and silk, in particular lipid removal and sulphur oxidation on the wool surfaces.

ToF-SIMS spectra of wool and silk surfaces were obtained in positive and negative ion mode in a mass range of 0-1000 using a PHI 7000 instrument. Analysis was performed under static conditions using a Cs^+ primary ion source, operated at 8 keV with a pulse length of 1.25 ns. A pulsed electron flood source (50-70 eV) was used for charge compensation. Typical acquisition times were 95 s. Further analyses of wool surfaces were carried out on an ION-TOF ToF-SIMS 5 instrument equipped with a bismuth primary ion source. High resolution mass spectra were collected from sample areas measuring 0.1mm x 0.1mm using Bi_3^+ ion bombardment.

The data was processed using Casa XPS 2.2.67 software. All spectra were calibrated from time bins to mass bins using the CH and C_2H peak positions for negative ion spectra, and CH_3 and C_2H_3 peak positions for positive ion spectra. Semi-quantification was performed by measuring relative peak areas.

5.4. Results and discussion

Stress-strain curves for wool and silk have typical shapes characteristic of the fibres' morphological and molecular structures [116-121]. The onset to the stress-strain curves for yarns shows a relatively shallow slope which is attributed to tension building up in the yarn, inter-fibre slippage and, in the case of wool, de-crimping of the fibres; in Figure 5.4.1 the end of this region is marked with $Yarn_{(S)}$ for silk and $Yarn_{(W)}$ for wool. Both wool and silk exhibit a Hookean region, i.e. an elastic region where stress and strain increase linearly and the deformation (strain) is completely, and immediately, recoverable on release of tension (load). The slope of the curve in the Hookean region is termed the initial elastic modulus, $E_{(W)}$ and $E_{(S)}$ in Figure 5.4.1, and is distinctive for the stiffness of the material with silk exhibiting a steeper slope, i.e. higher stiffness, than wool. The stress and strain in the Hookean region are accounted for by the stretching of bond angles and bond spacings without rupture. Further increase of stress or strain into the yield region, Figure 5.4.1 $Yield_{(w)}$ and $Yield_{(S)}$, leads to elastic and plastic deformation of the molecular structure of the materials. In wool this is mainly attributed to the extension of the crystalline regions in the intermediate filaments from the α-helix protein structure into β-pleated sheets (α-β transition) and proceeds with little increase in stress. In silk the crystalline structure is already fully extended and the yield-stress causes the stretching of amorphous regions which, due to being restrained by the high overall crystallinity of silk (65-70 %), are relatively immobile. Excessive stress causes the crystalline regions in silk to slide past each other with hydrogen bonds being broken [122]. Similar to the deformation in the Hookean region, the elastic deformation in the yield region is also reversible for wool but depends on moisture content, temperature and time. Fibres extended to a constant strain for long times will eventually reach equilibrium through the re-formation of bonds, i.e. the fibre relaxes thereby decreasing the force needed to maintain the constant strain. Such plastic deformation is recoverable (temporary set) if the newly formed bonds, e.g. salt links, hydrogen bonds and van der Waals interactions, are broken and re-formed in their original positions; this occurs slowly at high relative humidity (> 60%) and almost immediately in water. However, plastic deformation is irrecoverable (permanent set) if it is due to the re-formation of covalent bonds between the protein chains, e.g. thiol disulphide interchange reactions in wool occurring in water at 100°C [116].

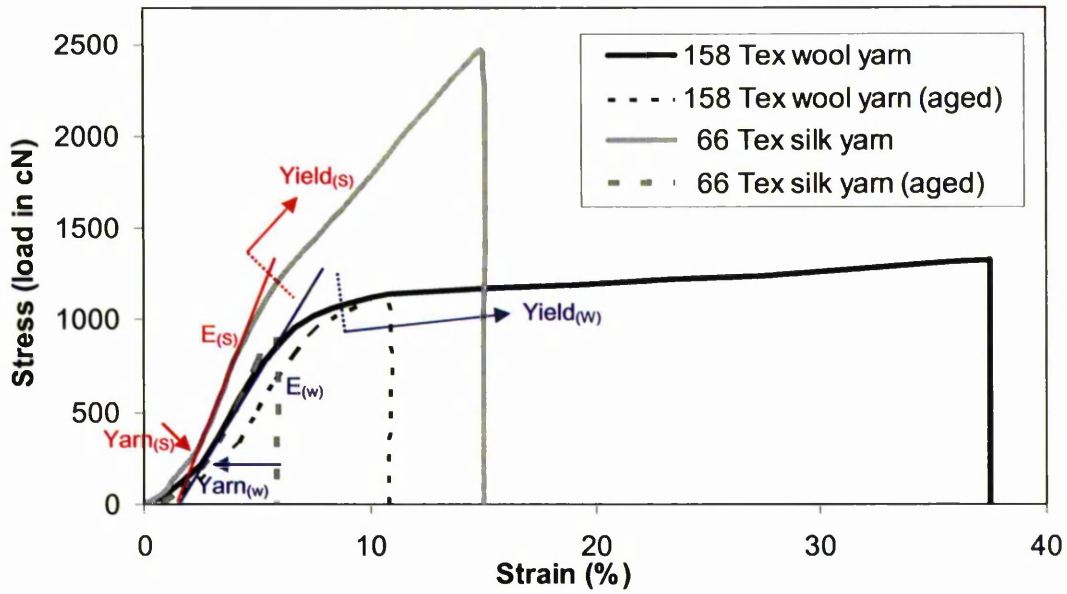

Figure 5.4.1. Stress-strain curves for unaged and aged wool and silk yarn

Wool fibres exhibit a post-yield region where the stress increases at a higher rate, the onset of this region lies around 30% strain for unaged untreated fibres, Figure 5.4.2. The yield and post-yield regions were indistinguishable in the stress-strain curves of yarns, Figure 5.4.1, due to the stresses and strains not being equally distributed amongst all fibres.

There are various models aiming to explain the reason for the stress increase in the post-yield region [116-119]. Wortmann and Zahn accredit the fibre stiffening to the α-β transition of the disulphide crosslinked segments of the intermediate filaments, while the matrix is assumed to behave as a thixotropic gel undergoing a transition into the sol state (free flowing) and contributing equally to the yield and the post-yield regions [118]. Feughelman describes a model whereby disulphide crosslinked protein globules of the matrix become jammed between the intermediate filaments as they contract upon extension, thereby obstructing further α-β transition of the intermediate filaments and increasing the stress [117]. Hearle, on the other hand, assumes the matrix to be a continuous covalently cross-linked network and attributed the stiffening of the fibre in the post-yield region to a stiffening of the matrix at high strains (>30%), while the intermediate filament α-β transition is assumed to proceed without additional increase in stress [119]. The three models also disagree on the cause of rupture of wool fibres. Wortmann and Zahn as well as Feughelman suggest the intermediate filaments as starting points of rupture while in Hearle's model rupture starts in the matrix [119].

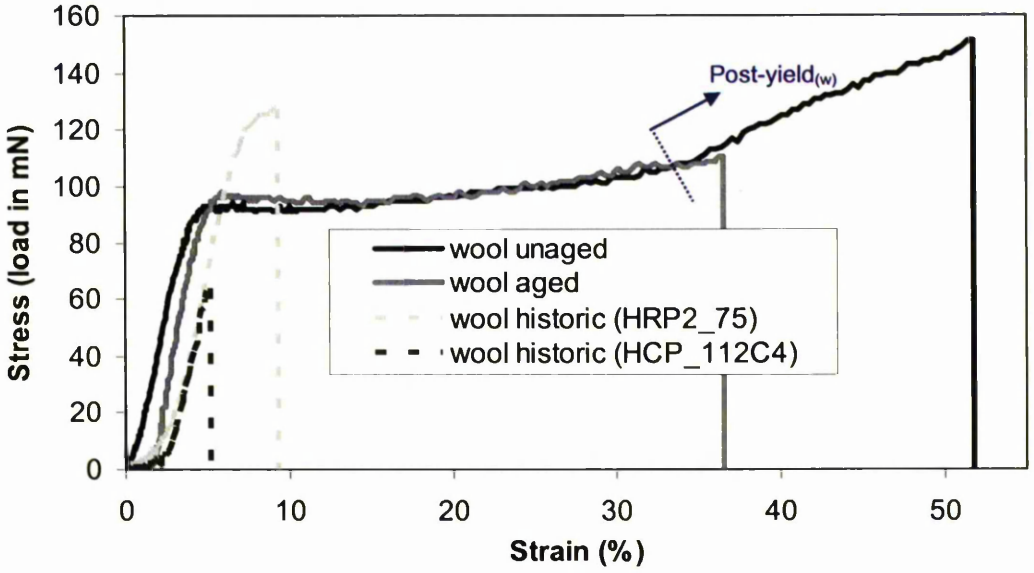

Figure 5.4.2. Stress-strain curves of single wool fibre tensile tests

Figure 5.4.1 and Figure 5.4.2 show typical stress-strain curves as obtained in the tensile tests on unaged and accelerated aged yarns as well as unaged, accelerated aged and historic fibres. In general accelerated aged yarns and fibres followed the curves of the unaged samples but ruptured at a lower strain and, consequently, lower stress. Especially the silk samples showed large reductions in strain, often breaking before the onset of the yield region. Similarly, many historic wool samples ruptured at strains within the Hookean region, indicating that ageing has caused extensive changes in the cross-linking structure of the proteins, inhibiting the extension of the matrix and α-β transition of intermediate filaments.

5.4.1. Tensile strength tests: yarns

Tensile strength tests were conducted on unaged and accelerated aged wool and silk yarns. Undyed wool and silk yarns were light aged for 200, 400, 600 and 800 hours to monitor the progression of loss of tensile strength. The results are represented in Figures 5.4.3 and 5.4.4. The silk yarn is initially stronger than the wool but the maximum load decreases more rapidly and after 400 hours ageing is lower than the value for wool. The load decreases in an almost linear fashion for both wool and silk, while the strain has a more rapid initial decrease followed by a levelling of the curves after 400 hours ageing, demonstrated in Figure 5.4.4.

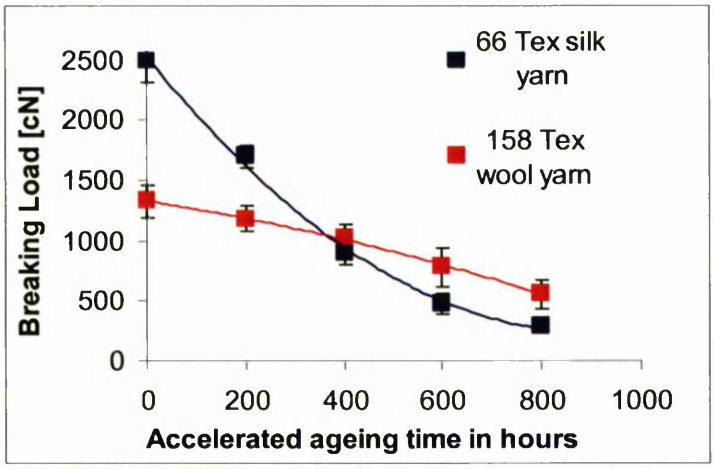

Figure 5.4.3. Tensile breaking load of wool and silk following light ageing

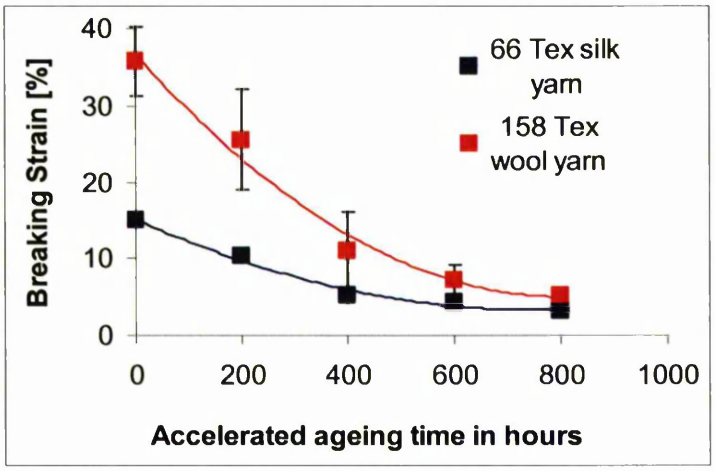

Figure 5.4.4. Tensile breaking strain of wool and silk following light ageing

After 800 hours ageing the point of total failure of the silk yarn was nearly reached with many samples being too weak to withstand the pressure of the clamps in the tensile strength tester.

The level of accelerated ageing chosen for all MODHT model samples was 400 hours in the Xenotest as this is the calculated equivalent of 400 years exposure to sunlight behind window glass or, in other words, 400 years exposure to museum lighting conditions which, as a model, corresponds to the age of the historic tapestries included in the MODHT project (15^{th} to 17^{th} century). A small number of dyed wool and silk samples was also aged for 800 hours. The results are listed in Tables 5.4.1 and 5.4.2 and represented in Figures 5.4.5 and 5.4.6. For ease of interpretation error bars have been added to the undyed samples only, but these represent typical values obtained for undyed as well as dyed samples. The tests were repeated several times for the undyed unaged and aged samples to show

the variations in tensile properties that can be expected. Data regions prescribed by the standard deviations for undyed samples are indicated as ovals. Standard deviations for wool yarns are considerably greater than for silk with average values of 8.9% and 17.6% for unaged wool load and strain, respectively, compared to 5.9% and 5.5% for unaged silk load and strain, respectively. This is ascribed to the greater evenness of the silk yarns due to their straight filament fibres, while wool comprises comparatively shorter staple length and crimped fibres causing more slippage during tensile testing and a generally bulkier, more irregular yarn.

Examination of Figure 5.4.5 and Table 5.4.1 shows that all wool dyeing procedures lead to a decrease in strain, while alum mordanting without subsequent dyeing leads to an increase in strain. The decreases in strain noted for brazilwood, woad, madder and alder bark dyeings are small and lie within the standard deviation region of undyed wool; cochineal dyeings had a generally lower strain than undyed wool; while weld, oak gall, dyer's greenweed, woad+weld and most of the black dyeings experienced significant decreases in strain.

Changes in breaking force values were not as apparent; the dyeings with brazilwood, woad, madder, alder bark, oak gall and the black dyeings exhibited breaking loads slightly above the average breaking load for undyed wool, yet within the region of standard deviation, only the alum mordanted wool showed a significant increase in load, while the weld dyed and blank dyed with lye samples exhibited a decrease in load.

After 400 hours and 800 hours ageing most of the dyed wool samples show similar tensile test results as the undyed wool; exceptions being the alum mordanted and some of the black dyed samples.

Examination of Figure 5.4.6 and Table 5.4.2, on the other hand, shows that dyeing procedures of the silk samples do not greatly influence the initial tensile properties with all tested samples falling within the region of standard deviation of the undyed silk. Disparities between differently dyed samples emerge only upon ageing.

Effects such as alkaline hydrolysis, absorption of metal ions and influences of dye chromophores may be responsible for the observed differences in tensile properties and are discussed below.

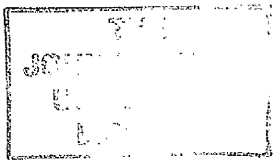

Table 5.4.1. Tensile strength values for wool samples

Mordant and dyestuff	Sample name	unaged wool yarn				400 hours aged wool yarn				800 hours aged wool yarn			
		Breaking Load (cN)	Standard Deviation	Breaking Strain (%)	Repeats	Breaking Load (cN)	Standard Deviation	Breaking Strain (%)	Repeats	Breaking Load (cN)	Standard Deviation	Breaking Strain (%)	Repeats
	undyed/W	**1241**	101	**36.5**	21	**1132**	80	**13.7**	15	**553**	121	**5.2**	15
	undyed/W	**1219**	90	**36.7**	15	**1063**	104	**9.8**	15				
	undyed/W	**1271**	109	**35.9**	20	**1013**	99	**9**	22				
	undyed/W	**1330**	135	**35.8**	15	**1023**	109	**11**	16				
	undyed/W	**1285**	144	**39.3**	16								
	undyed/W	**1240**	74	**35**	8								
	undyed/W	**1256**	110	**35.5**	10								
	undyed/W	**1287**	137	**39.3**	10								
	undyed/W	**1302**	138	**37.3**	15								
	undyed/W	**1249**	82	**35.7**	16								
"	blank dyed/W	**1152**	85	**32.9**	18	**1144**	164	**15.3**	15				
	blank dyed/W_wl	**997**	103	**20.2**	19	**910**	94	**10.3**	15				
alum	alum/W	**1560**	128	**40.5**	15	**1334**	102	**28.6**	15				
alder bark	alder bark/W	**1335**	132	**34.4**	15	**1235**	116	**12.1**	15				
oak gall	oak gall/W	**1309**	114	**21.3**	20	**1102**	107	**8.3**	20				
oak gall + $FeSO_4$	black/W1	**1334**	114	**26.2**	20	**1103**	101	**10.3**	20				
	black/W2	**1364**	108	**28.6**	19	**1126**	118	**10.8**	20	**753**	170	**9.3**	12
	black/W2	**1307**	132	**24.9**	15								
alder bark + $FeSO_4$	black/W3	**1305**	96	**34.4**	20	**621**	129	**7**	19				
	black/W3	**1329**	121	**31.3**	20	**712**	130	**5.9**	15				

Continuation of Table 5.4.1. Tensile strength values for wool samples

Mordant and dyestuff	Sample name	unaged wool yarn				400 hours aged wool yarn				800 hours aged wool yarn			
		Breaking Load (cN)	Standard Deviation	Breaking Strain (%)	Repeats	Breaking Load (cN)	Standard Deviation	Breaking Strain (%)	Repeats	Breaking Load (cN)	Standard Deviation	Breaking Strain (%)	Repeats
oak gall + $FeSO_4$ + $CuSO_4$	black/W4	**1265**	156	**23.2**	20	**1153**	94	**11**	20	**927**	121	**9.9**	18
	black/W4	**1288**	114	**24.8**	15								
woad	blue/W1	**1346**	85	**35.1**	14	**1010**	121	**8.1**	15				
	blue/W1	**1373**	134	**34.6**	15					**550**	132	**4.9**	17
	blue/W1_dark	**1325**	133	**33.6**	20	**1040**	109	**10.6**	20				
	blue/W1_pale	**1332**	132	**34.8**	20	**959**	107	**9.6**	20				
alum + weld + woad	green/W1	**1240**	119	**20.3**	30	**958**	118	**7.9**	15				
	green/W2	**1310**	118	**29.3**	20	**1067**	105	**9.7**	15				
alum + madder	red/W1	**1396**	108	**32.9**	15	**981**	128	**9.1**	15	**490**	154	**4.8**	17
	red/W1	**1348**	143	**32.7**	15								
	red/W1_wl	**1280**	59	**32.4**	15	**1165**	118	**11.1**	15				
alum + oak gall + madder	red/W2	**1473**	91	**35.4**	15	**1167**	121	**10.4**	15				
alum + brazilwood	red/W3_wl	**1360**	114	**35.8**	20	**1056**	141	**10.1**	15				
alum + cochineal	red/W4	**1265**	86	**29.3**	30	**866**	125	**7.7**	15	**399**	74	**5.2**	17
	red/W4	**1339**	123	**33.4**	15								
	red/W5	**1262**	105	**28.8**	15	**1047**	107	**11.9**	15				
alum + weld	yellow/W1	**1138**	133	**20.6**	21	**1104**	158	**12**	15	**527**	146	**5.7**	13
	yellow/W1	**1164**	103	**24.1**	15								
alum + dyer's greenweed	yellow/W2	**1280**	140	**25.5**	20	**1069**	117	**9.4**	15	**660**	161	**5.9**	16
	yellow/W2	**1213**	146	**26.6**	15								

Table 5.4.2. Tensile strength values for silk samples

Mordant and dyestuff	Sample name	unaged silk yarn				400 hours aged silk yarn				800 hours aged silk yarn			
		Breaking Load (cN)	Standard Deviation	Breaking Strain (%)	Standard Deviation	Breaking Load (cN)	Standard Deviation	Breaking Strain (%)	Standard Deviation	Breaking Load (cN)	Standard Deviation	Breaking Strain (%)	Standard Deviation
-	undyed/S	**2493**	180	**14.9**	0.9	**896**	103	**5.1**	0.5	**278**	50	**3.2**	0.8
	undyed/S	**2387**	101	**16.1**	1.0	**930**	76	**5.8**	0.6				
	undyed/S	**2184**	70	**15.6**	1.0	**796**	96	**4.4**	0.6				
	undyed/S	**2265**	102	**15.3**	0.7								
	undyed/S	**2509**	176	**15.5**	0.7								
	undyed/S	**2296**	88	**14.8**	0.9								
	undyed/S	**2355**	152	**16.4**	1.0								
	undyed/S	**2180**	132	**15.2**	1.3								
Alum	alum/S	**2301**	96	**15.2**	0.8	**847**	47	**4.3**	0.4				
Oak gall + $Fe(II)SO_4$	black/S1a	**2245**	147	**14.2**	0.8					**996**	168	**7.2**	1.0
	black/S1a	**2240**	155	**15.2**	1.0								
	black/S1b	**2395**	170	**14.9**	1.2	**1633**	143	**10**	1.7				
Woad	blue/S_dark	**2304**	132	**15.6**	0.8	**643**	98	**5.7**	0.8				
	blue/S_medium	**2340**	192	**14.0**	0.9								
	blue/S_medium	**2286**	159	**16.0**	0.9								
	blue/S_pale	**2189**	142	**15.8**	1.0	**388**	94	**5.8**	0.7	**150**	37	**1.4**	0.4
Alum + weld + woad	green/S1_b	**2486**	114	**16.3**	0.8	**619**	62	**5.6**	0.6				
	green/S2_b	**2350**	82	**16.4**	0.8	**738**	101	**6.8**	0.9				

Mordant and dyestuff	Sample name	Repeats	Repeats	Repeats
		unaged silk yarn	400 hours aged silk yarn	800 hours aged silk yarn
-	undyed/S	10	10	10
	undyed/S	10	10	
	undyed/S	10	10	
	undyed/S	15		
	undyed/S	10		
	undyed/S	10		
	undyed/S	10		
	undyed/S	12		
Alum	alum/S	10	10	
Oak gall + $Fe(II)SO_4$	black/S1a	10		10
	black/S1a	10		
	black/S1b	10	10	
Woad	blue/S_dark	15	8	
	blue/S_medium	10		
	blue/S_medium	10		
	blue/S_pale	10	10	10
Alum + weld + woad	green/S1_b	10	10	
	green/S2_b	10	10	

Continuation of Table 5.4.2. Tensile strength values for silk samples

Mordant and dyestuff	Sample name	unaged silk yarn				400 hours aged silk yarn				800 hours aged silk yarn			
		Breaking Load (cN)	Standard Deviation	Breaking Strain (%)	Standard Deviation	Breaking Load (cN)	Standard Deviation	Breaking Strain (%)	Standard Deviation	Breaking Load (cN)	Standard Deviation	Breaking Strain (%)	Standard Deviation
alum + madder	red/S2_a	**2245**	143	**14.6**	0.7					**160**	46	**6.2**	1.3
	red/S2_b	**2309**	190	**14.8**	0.8								
	red/S2_c	**2263**	123	**15.7**	1.5								
alum + brazilwood	red/S1_b	**2449**	159	**15.6**	0.7	**621**	91	**5.6**	0.7				
	red/S1_c	**2468**	112	**16.4**	0.7	**1074**	91	**6.7**	0.4				
	red/S1_d	**2345**	132	**16.0**	0.7	**880**	61	**4.9**	0.5				
	red/S1_e	**2259**	160	**15.2**	0.7	**951**	68	**6.3**	0.6				
alum + cochineal	red/S3	**2319**	187	**15.4**	0.8					**507**	95	**6.4**	2.8
	red/S3	**2286**	165	**16.6**	0.8	**861**	128	**8.4**	1.6				
alum + weld	yellow/S1_a	**2471**	122	**17.0**	0.9	**1039**	81	**6.8**	1.2				
	yellow/S1_b	**2276**	140	**15.3**	1.3					**217**	38	**3.7**	0.9
	yellow/S1_b	**2288**	103	**16.0**	0.8								
alum + dyer's greenweed	yellow/S2_a	**2285**	98	**15.3**	0.7	**657**	104	**4.1**	0.6				
	yellow/S2_b	**2265**	136	**14.8**	0.6	**839**	75	**4.9**	0.6				
	yellow/S2_c	**2216**	74	**15.0**	0.9								
alum + young fustic	yellow/S3_a	**2331**	145	**16.2**	0.6								
	yellow/S3_b	**2377**	228	**16.0**	0.5	**719**	77	**5.9**	0.6				
	yellow/S3_c	**2320**	130	**15.6**	0.6	**715**	60	**6.1**	0.9				

Mordant and dyestuff	Sample name	Repeats					
		unaged silk yarn	400 hours aged silk yarn	800 hours aged silk yarn			
alum + madder	red/S2_a	10		10			
	red/S2_b	10					
	red/S2_c	10					
alum + brazilwood	red/S1_b	15	10				
	red/S1_c	10	10				
	red/S1_d	10	10				
	red/S1_e	15	10				
alum + cochineal	red/S3	10		10			
	red/S3	10	10				
alum + weld	yellow/S1_a	10					
	yellow/S1_b	10		10			
	yellow/S1_b	10					
alum + dyer's greenweed	yellow/S2_a	10	10				
	yellow/S2_b	10	10				
	yellow/S2_c	10					
alum + young fustic	yellow/S3_a	11					
	yellow/S3_b	10	10				
	yellow/S3_c	10	10				

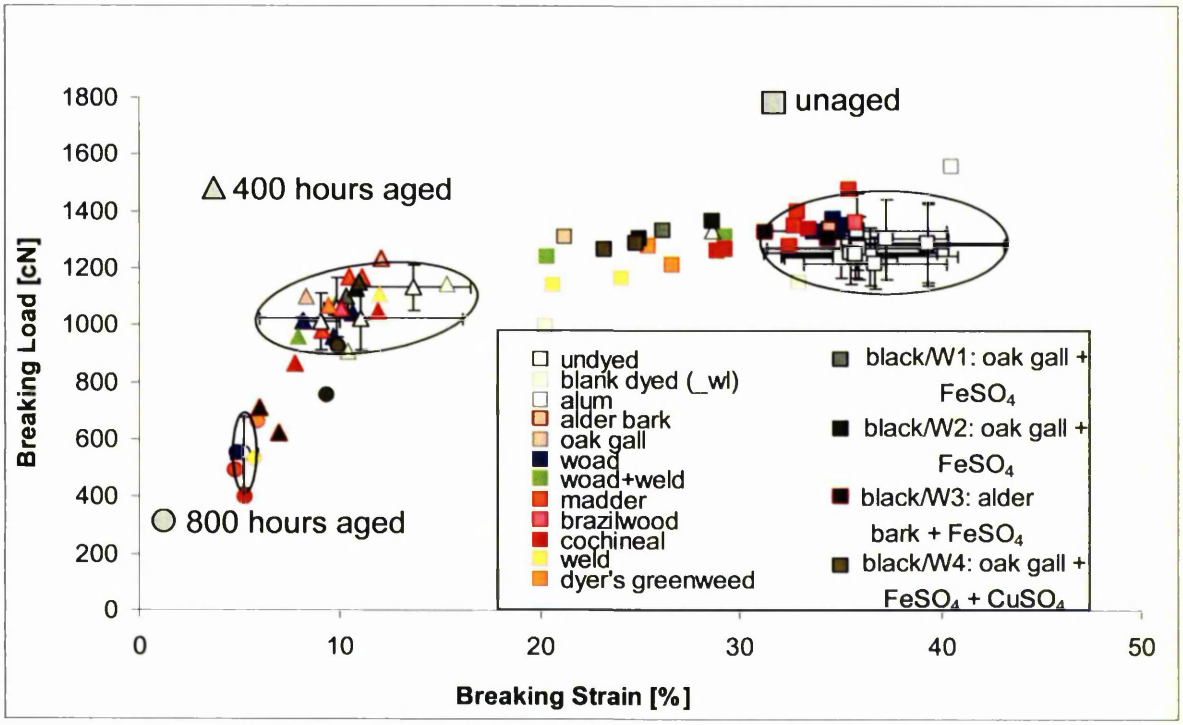

Figure 5.4.5. Tensile strength of unaged and light aged wool

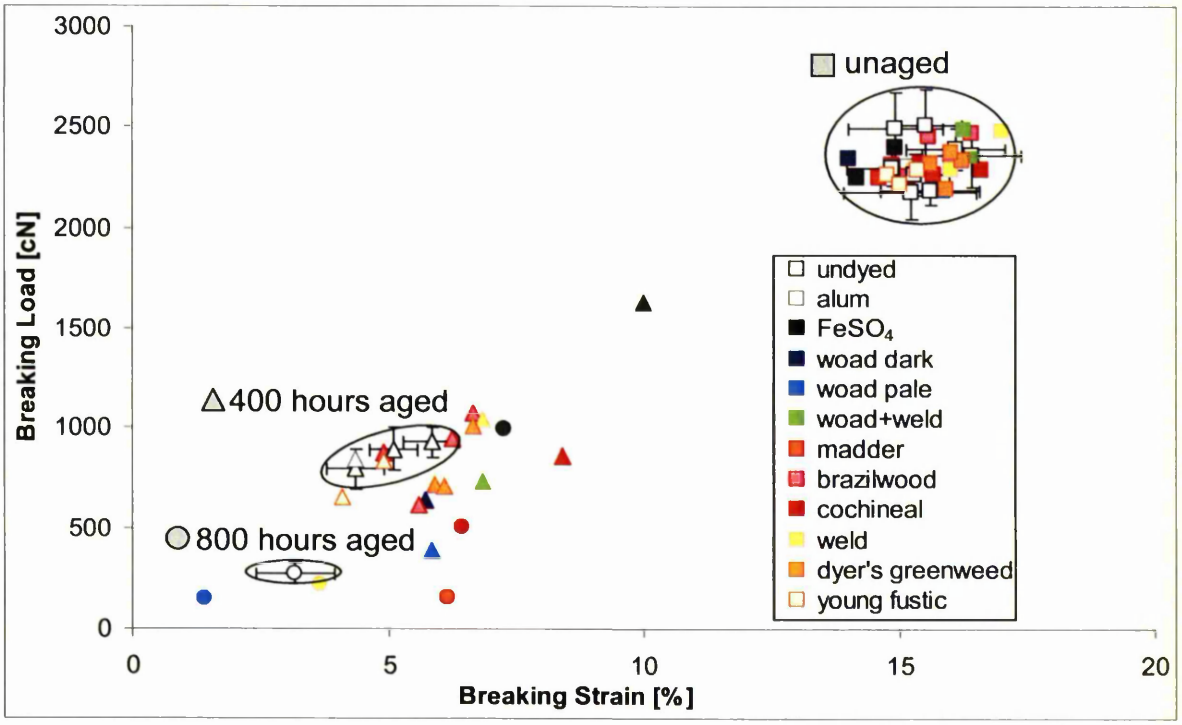

Figure 5.4.6. Tensile strength of unaged and light aged silk

Alkali hydrolysis

The decreased tensile strength of the samples dyed with weld and woad+weld (yellow/W1 and green/W1) was attributed to the severe alkali treatment these samples received (2 hours boiling at pH 10). The dyeing procedure for sample green/W2 was similar, though less K_2CO_3 was employed and, in the final treatment, pH was only around 8, which explains the lower changes in tensile properties. The degradative action of a high pH due to the addition of K_2CO_3 to the dyebath was confirmed in the low tensile strength of the blank dyed with lye sample which received the same treatment as the weld dyed yellow/W1 sample but without the dyestuff in the dyebath. Severe yellowing was noted in the blank dyed with lye sample; this alkali-yellowing of wool has been attributed to the destruction and conversion of cystine, serine and threonine into coloured residues [123].

Both the weld and the blank dyed with lye samples showed similar tensile properties as the undyed wool following 400 and 800 hours ageing. None of the silk dyeings were performed at similar alkalinity, therefore the effect was not observed in silk samples. Alkaline conditions partially destroy several amino acids with simultaneous formation of new amino acids, the predominant ones being the conversion of cystine into lanthionine and cystine together with lysine into lysinoalanine.

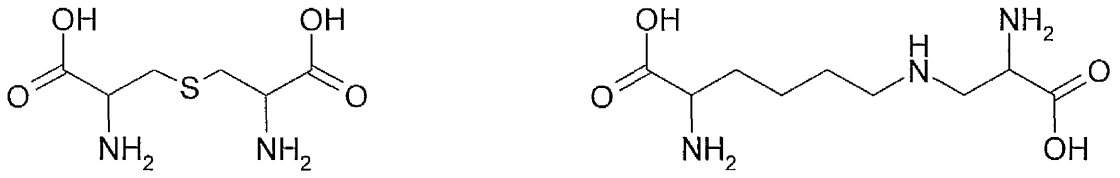

Scheme 5.4.1. Chemical structures of lanthionine and lysinoalanine [123]

It was found that alkali treament introduces new inter-chain crosslinks, probably through the formation of lysinoalanine [123]; thereby decreasing the extensibility of the fibre. Severe alkali treatment of wool has been shown to decrease the sulphur content due to release of sulfide and sulfate [123], with the scission of di-sulphide bonds contributing toward a decrease in breaking strength. Sulphur containing amino acids are predominantly present in amorphous regions and this loss of material from amorphous regions increases the relative abundance of crystalline regions. The release of ammonia following alkali treatment was attributed to hydrolysis of amide groups and peptide bonds [123]; again contributing towards a

decrease in breaking force. This is exacerbated by the rupture of ionic bonds between amino acids of adjacent peptide chains in crystalline regions where basic and acidic amino acids dominate. Approximately 25% by weight of the wool fibre is constituted of salt linkage forming amino acids, namely the basic residues arginine, lysine and histidine and the carboxylic residues aspartic and glutamic acid. In acidic and alkaline solutions these salt linkages between di-amino and di-carboxylic acids break [4].

Metal ion absorption

The alum mordanted wool stands out as the only sample which experienced a marked increase in both breaking force and strain following treatment. The strengthening effect of the alum mordant on wool can also be observed after ageing, where the alum sample exhibits the highest strain and load values by a large margin. The strengthening effect may be attributable to metal complexing. Hartley found that aluminium ions bind to carboxylate and sulphonate groups by ionic bonds and to a lesser extent to non-specific sites by Van der Waals forces, while amino or thiol groups are not involved in binding absorbed aluminium in wool [109]. Carboxylate ions in wool are predominantly present in the crystalline regions, i.e. regions with high concentrations of aspartic acid and glutamic acid, the only carboxyl group containing amino acids in wool. However, carboxylate ions may also form along the oxidised backbone chain of peptides, see Scheme 5.1.4. Photo-oxidation of the peptide main chain Sulphonate groups are only present in oxidised wool where free thiol groups or cleaved cystine links have been converted into cysteic acid, see Scheme 5.1.5. Within the wool morphology high amounts of sulphur containing amino acids (primarily cysteine and some methionine) are present in the amorphous regions of the cortex and the epicuticle.

Miller and Smith showed that the treatment of wool with aluminium salts has a photo-protective effect [113]. Smith et al. also reported an increase in breaking force for alum mordanted wool and attributed the effect to covalent metal crosslinks formed between carboxyl groups of adjacent polypeptide chains [114]. The linking metal ions were suggested to possess hydroxyl or oxohydroxyl ligands, which, during the dyeing procedure, react with the carboxyl groups of the protein chains, leaving the metal ion free to complex with the dye chromophore [114]. This results in a decrease in crosslinks between neighbouring protein chains and

ultimately leads to a decrease in tensile strength as can be observed in all alum mordanted dyed samples, Figure 5.4.5. In addition, the removal of aluminium ions during washing or dyeing also reduces the amount of inter chain crosslinks and leads to a loss in tensile strength. This was confirmed by Hartley who showed that aluminium ions preferably bind to hydroxyl ions rather that carboxylate or sulphonate groups leading to the gradual removal of aluminium during washing or dyeing [109].

Conversely, the alum mordanted silk did not show changes in tensile properties after treatment or ageing. This may be due to the alum treatment of silk taking place at room temperature opposed to alum mordanting of wool at the boil.

The black dyed wool showed decreased strain but unaltered breaking force; especially the sample dyed with iron sulphate and copper sulphate showed significant loss of extensibility. Upon ageing, however, the three black dyed samples with oak gall mordant show tensile properties similar to undyed wool, i.e. the relative loss of breaking load and strain was lowered, while the sample dyed with an alder bark tannin and ferrous sulphate showed increased loss of strain and especially load. The lower rate of decrease of tensile properties for oak gall mordanted, ferrous sulphate and copper sulphate dyed wool upon ageing was also observed after 800 hours ageing where the samples black/W2 and black/W4 exhibit higher load and strain values than the undyed or any other dyed wool, Table 5.4.1 and Figure 5.4.5.

This protective effect of oak gall mordanting with ferrous sulphate dyeing was similarly observed in silk where the Black / S1 samples showed considerably lower rates of decrease in load and strain than any other silk samples after 400 and 800 hours ageing, Table 5.4.2 and Figure 5.4.6.

The absorption of ferric and especially cupric ions by wool and silk has been studied by several researchers [33, 108, 114, 124-132]. The studies agree that the dominant binding sites for Fe(II) and Cu(II) ions are the carboxylate groups of aspartic and glutamic acids, according to Scheme 5.4.2 and the following reaction schemes [132]:

$$R\text{-}COOH + Cu^{2+} \rightleftharpoons R\text{-}COOCu^{+} + H^{+}$$

$$R\text{-}COOH + R\text{-}COOCu^{+} \rightleftharpoons R\text{-}COO\text{-}Cu\text{-}OOC\text{-}R + H^{+}$$

Where R is wool (aspartyl and glutamyl residues)

Scheme 5.4.2. Proposed Cu(II) ion complexes with wool [125]

The complexation of copper with carboxyl groups led to a green colour of the wool, which changed to brown upon extended boiling time in water [126]. The unstable brown products were ascribed to copper sulfide (CuS_x, where $1<x<2$) which formed due to the reaction of copper ions with hydrogen sulfide (H_2S) which in turn is produced during the hydrolysis of wool cystine disulfide bonds in boiling water [126, 128]. Shimizu suggests that with increasing pH (up to pH 6) further binding sites are offered by deprotonated amino groups [108]. Copper-nitrogen complex formation in methylated mohair was proposed by Guthrie and Laurie [124] and Kokot et al. [127] who showed that Cu(II) treatment under high pH led to blue-purple to grey coloured wool. Smith at al., Carr et al. and Masri and Friedman state that Cu(II) ions additionally bind with sulphonate groups present in oxidised wool and generated due to the ability of Cu(II) to catalyse oxidation of sulfhydryl groups, increasing the amount of absorbed metal ions [33, 114, 131].

The sample black/W4 dyed with an oak gall mordant and ferrous sulphate and copper sulphate has a dark green colour suggesting that the primary binding site for Cu ions are carboxyl residues.

Similar to alum mordanting the treatment with ferrous sulphate and copper sulphate leads to metal complexes between adjacent protein chains, however, in contrast to the immediate strengthening effect of alum the Fe(II) and Cu(II) treated wool shows only decreased strain. The strengthening effect can only be observed after ageing, where tensile properties for both wool and silk treated with oak gall and Fe(II) or Cu(II) are higher than those obtained for undyed wool and silk. These results correlate well with findings by Miller and Smith, and Smith at al. who reported lower losses in tensile strength for wool treated with aluminium ions, cupric ions and ferric ions compared to untreated wool following irradiation [113, 114]. Similarly wool treated with aluminium ions or cupric ions and dyed with weld or madder showed increased tensile strength. It was suggested that this effect was due to a reverse reaction of the metal ions bound to cysteic acid, initiating sulphur

radicals which cause reformation of the disulphuide crosslinks, thereby strengthening the fibre [114]. Figure 5.4.6 shows a slight strengthening of the cochineal dyed silk following 400 hours and 800 hours ageing; this may be due to copper ion complexing as copper turnings were used in the dyebath. Smith's explanation of reformation of disulphide links, however, would not hold for silk as sulphur containing amino acids are limited.

Wool treated with ferric ions and dyed with weld or madder, on the other hand, showed substantial losses in tensile strength; Smith et al. attributed this to the loss of metal-protein crosslinks during dyeing and additional bond cleavage initiated by free radicals produced by the excited dye chromophores [114]. Accepting this explanation the disparities in tensile properties between the samples dyed with oak gall and alder bark tannins in combination with ferrous sulphate can be rationalized. Alder bark contains some flavonoid and anthraquinone dyestuffs in addition to tannins [133]; these may act as photosensitizing agents in conjunction with the ferric ions, leading to the increased degradation of the black/W3 samples, Figure 5.4.5

It is well known in textile conservation that the characteristic dark outlines of figures in Renaissance tapestries woven in shades of black or brown wool disintegrate over time, leaving the bare warp yarns [134, 135]. In the 16th century the dyer's guild even prohibited the use of the black dyestuff because it caused quick decay of the material [136]. This is usually attributed to the oxidative action of ferrous sulphate dyeing; however, the above mentioned results propose that ferrous sulphate dyeing is particularly oxidative in conjunction with other dyestuffs, suggesting that the dark outlines in tapestries were in fact combination dyeings with an iron mordant rather than dyeings using ferrous sulphate on its own.

Dyestuff chromophores

Flavonoids are known anti-oxidants [137]; it may therefore be assumed that dyestuffs with flavonoid chromophores such as weld, dyer's greenweed and young fustic exert some protection from oxidative photodegradation of the fibre. While anthraquinones are oxidising agents, leading to the assumption that dyestuffs such as madder and cochineal would increase photodegradation. The phototendering action of anthraquinoid dyes was mentioned in a review by Leaver

[138]. While Miller and Smith mention a photo-protective action of yellow dyes which may be due to a screening action of the yellow colour having a large extinction coefficient in the particularly damaging spectral region of blue light [113]. Yet, contrary to these assumptions no significant differences were observed in the rates of loss of tensile strength and strain for the flavonoid and anthraquinone dyed wool and silk yarns, Figures 5.4.5 and 5.4.6. This confirms Allen and McKellar's work, who state that the photosensitising action of dyes and pigments is virtually non-existent for wool fibres [139].

5.4.2. Tensile strength tests: single fibres

Single fibre tensile strength tests were performed in order to achieve direct measurements of tensile properties of historic samples. In addition, the yarn properties such as Tex value and twist do not influence test results of single fibres making it a practical method for the comparison of samples from different sources.

Wool fibres show great variability in diameter, hence the standard deviations were expected to be considerably higher than standard deviations in tensile strength tests on yarns; the obtained average values were 47% standard deviation for load at maximum and 58% for strain at maximum. To evaluate whether the differences observed were statistically significant the 95% confidence range were calculated according to:

$$\text{Confidence range} = \overline{x} +/- t_{(\alpha/2,\nu)}\, s /\sqrt{n}$$

Where $\overline{x}$ = sample mean (average load or strain values); s = standard deviation calculated for average load or strain values; n = sample size (number of repeats); $t_{(\alpha/2,n-1)}$ = Student's t distribution value for a two-sided test with $\alpha = 0.05$ for 95% confidence level and $\nu = n-1$ (degree of freedom). The *t* value varied from 2.014 to 2.101 for degrees of freedom between 45 and 18 [140].

The averaged results of the fibre diameter measurements, main dye sources of historic fibres and all single fibre tensile strength tests with standard deviations, 95% confidence range and number of repeats are listed in Table 5.4.3. The load-strain values with standard deviations are represented in Figure 5.4.7, while Figure 5.4.8 shows the load-strain values with 95% confidence range demonstrating that the tensile values obtained for the unaged wool samples and the respective accelerated aged samples are different despite the large overlaps of standard

deviation regions. The single fibre tensile strength values of unaged and accelerated aged wool reflect the results of tensile strength tests on yarns; with the alum mordanted sample showing higher strain than the blank dyed wool with lye and the accelerated aged samples being considerably weaker than the comparative unaged wool samples, Figure 5.4.8. This confirms the validity of the method, allowing evaluation of tensile strength by multiple single fibre measurements.

The historic fibres show widespread breaking strength and strain values with many samples rupturing in or near the Hookean region (~ < 5%) indicating the extensive cross-linking of intermediate filaments hindering the α-β transition. In addition, the lowest load values (~ < 100 mN) signify the most extensive degradation of the amorphous network between the intermediate filaments. No more than three samples of each tapestry were analysed which is insufficient data to indicate degradational differences between individual tapestries. Nevertheless, the tapestries from the Belgian and British sampling sites (BRU, BXL, HCP and HRP) had comparatively more samples with low strains than the tapestries sampled in Spain (PNM) suggesting that the latter are in a better state of preservation.

However, Figure 5.4.9 shows that the tensile values, in particular the average load values, decrease with decreasing average fibre diameter which may lead to misinterpretation of the tensile values in Table 5.4.3. This error could be reduced if the fibre diameters were measured for each single fibre test and the tensile values normalized.

Table 5.4.3. Single fibre tensile strength results for wool

Sample name	Main dye source *	Mean Diameter (100 repeats)	Standard Deviation	Breaking Load (mN)	Standard Deviation	95% confidence range	Breaking Strain (%)	Standard Deviation	95% confidence range	Repeats n; (degree of freedom v = n-1)
Unaged fibres										
undyed/W	-	**28.1**	7.0	**145.6**	59.9	17.8	**45.2**	15.2	4.5	46
alum/W	-	**27.5**	7.3	**143.2**	62.5	20.0	**50.2**	10.8	3.5	40
blank dyed/W_wl	-	**26.4**	5.7	**117.7**	41.9	14.6	**38.4**	15.9	5.5	34
Accelerated aged fibres										
undyed/W	-	-	-	**111.2**	43.4	14.7	**30.2**	15.7	5.3	36
alum/W	-	-	-	**117.4**	56.4	19.1	**34.2**	17.8	6.0	36
blank dyed/W_wl	-	-	-	**79.8**	43.0	15.0	**4.2**	1.6	0.6	34
Historic fibres										
BRU1_8	i/f	**28.5**	10.5	**75.1**	27.9	11.8	**4.4**	2.3	1.0	24
BRU1_10	m/w	n.a.	-	**123.2**	39.8	17.2	**6.9**	3.9	1.7	23
BRU2_23	m	n.a.	-	**142.8**	59.0	22.9	**18.0**	15.4	6.0	28
BXL1_5	m	n.a.	-	**173.6**	87.0	27.1	**3.8**	0.9	0.3	42
BXL3_3	r	n.a.	-	**105.3**	65.0	23.8	**3.4**	1.4	0.5	31
HCP_112C4	n.a.	**25.1**	5.9	**68.0**	27.6	9.9	**4.3**	1.8	0.7	32
HCP_33G4	n.a.	**30.6**	6.9	**138.1**	33.7	13.3	**29.9**	10.0	4.0	27
HRP2_21	i	**34.6**	9.5	**125.8**	51.8	21.4	**5.0**	2.5	1.0	25
HRP2_38	w/i	**29.7**	9.0	**107.4**	59.4	25.1	**9.3**	8.7	3.7	24
HRP2_75	w/i	**30.8**	8.7	**125.0**	61.6	22.2	**6.1**	3.6	1.3	32
HRP3_19	n.a.	**31.3**	7.3	**95.6**	50.3	16.8	**5.1**	1.9	0.6	37
PNM1_17	m	n.a.	-	**109.6**	58.4	21.8	**4.4**	1.6	0.6	30
PNM1_47	r/f	n.a.	-	**130.3**	62.9	19.6	**13.2**	12.1	3.8	42
PNM2_20	m/b	**31.0**	9.9	**146.0**	64.7	21.6	**13.4**	10.9	3.6	37
PNM2_27	c	n.a.	-	**52.2**	34.4	14.2	**10.1**	8.2	3.4	25
PNM5_15	m/b	n.a.	-	**155.5**	90.9	31.2	**25.3**	14.4	4.9	35
PNM7_7	r	n.a.	-	**109.3**	60.0	20.0	**4.5**	4.4	1.5	37
PNM9_13 (front)	n.a.	**33.6**	11.9	**213.4**	94.9	30.7	**19.0**	16.3	5.3	39
PNM9_2 (front)	f	n.a.	-	**181.9**	88.8	42.8	**28.1**	18.1	8.7	19
PNM9_20	w/i	n.a.	-	**151.7**	77.4	24.8	**8.1**	8.5	2.7	40

* Dyestuff analysis was performed by MODHT partners at the National Museums of Scotland and University of Edinburgh

i: indigoid; f: flavonoid; m: madder; w: weld; r:rubiacea; b: brazilwwod; c: cochineal (Mexican)

n.a. not alanysed; fibre diameters were not measured if sample material was not sufficient

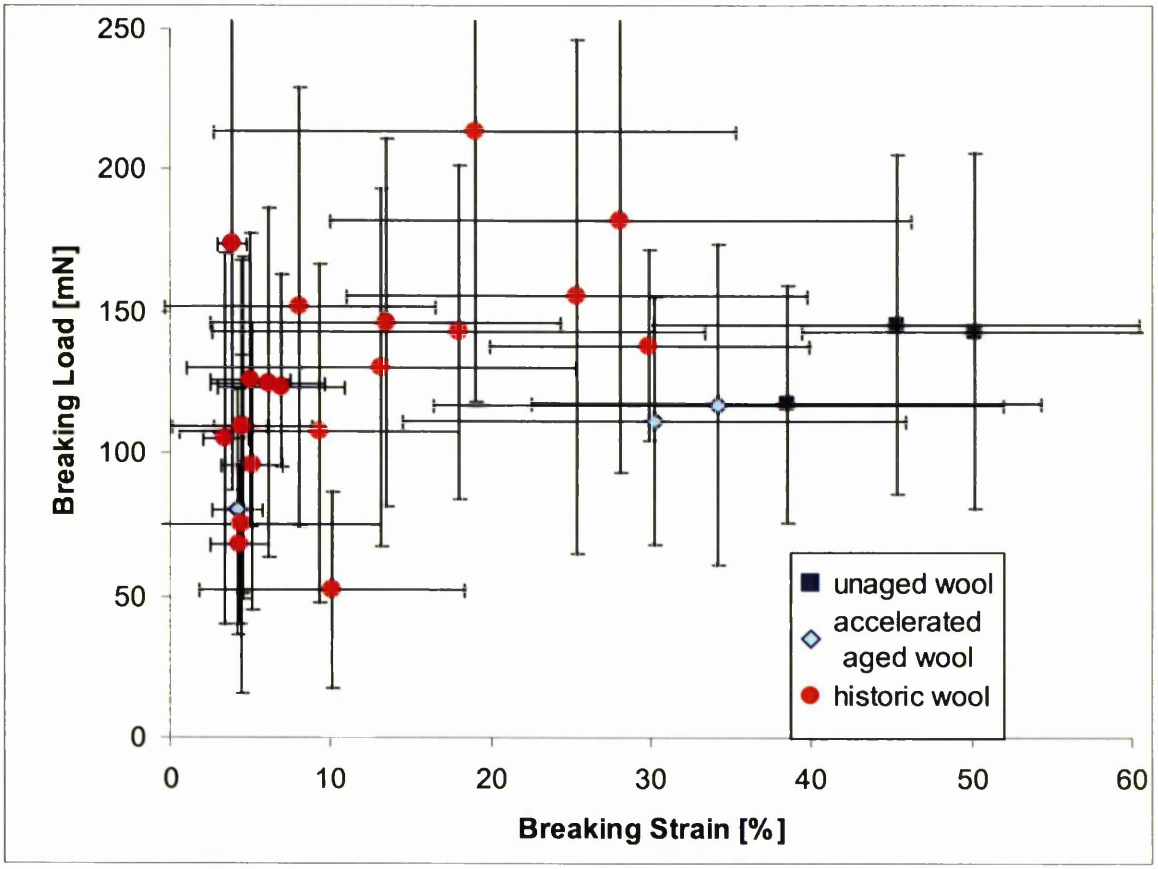

Figure 5.4.7. Single fibre tensile strength results with standard deviations

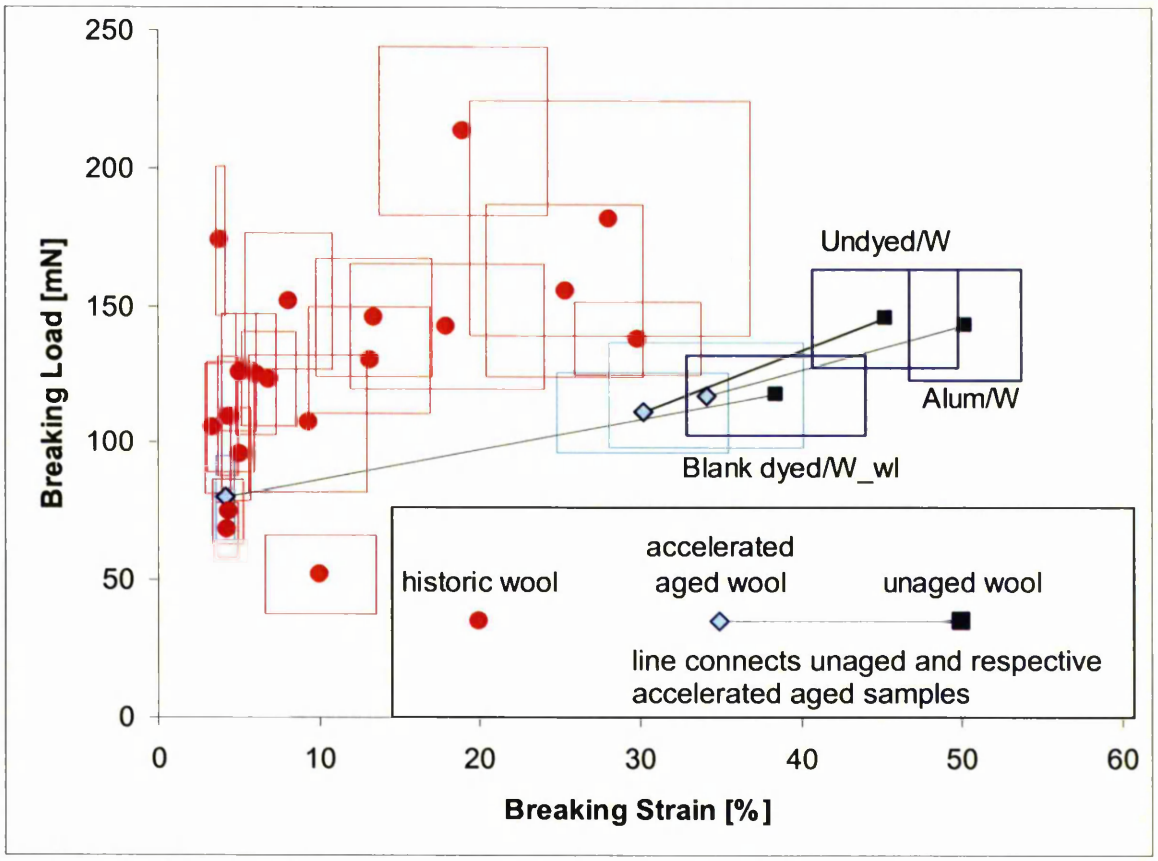

Figure 5.4.8. Single fibre tensile strength results with 95% confidence range

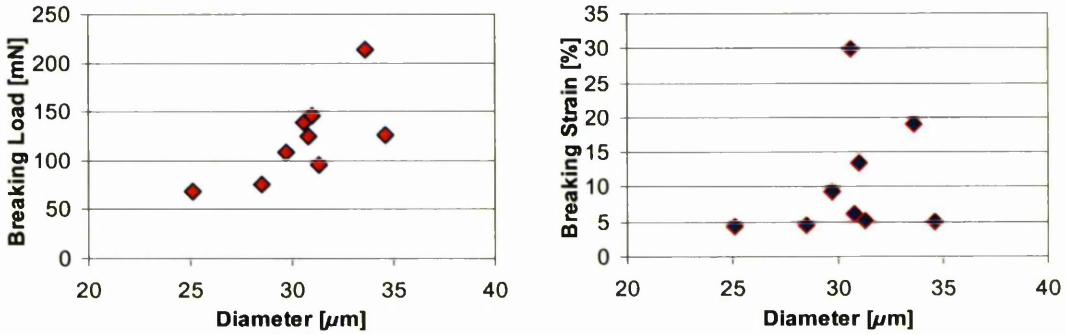

Figure 5.4.9. Relationship between tensile values and fibre diameter for historic samples

5.4.3. SEM investigation of fibre surfaces and fracture morphology: wool

SEM micrographs of wool and silk fibre surfaces and fibre fractures have been obtained for the assessment of fibre damage due to mordanting and dyeing procedures as well as natural and accelerated ageing.

Surface morphology of wool

The SEM micrographs of undyed and dyed wool surfaces, Figure 5.4.10 and Figure 5.4.11, show that none of the dyestuffs or dyeing procedures had a detrimental influence on the wool surface in terms of scale loss or damage. All samples were subjected to a final rinse after dyeing procedures, however, some surface residue was left, in particular where insoluble plant matter was present in the dyebath and deposited on the fibre surfaces.

The accelerated aged fibres showed severe longitudinal cracks, Figure 5.4.12, on the exposed front side of the model tapestry fabrics and in particular on the crowns of the weave structure. The fibres on the back of the tapestry weave and the lower lying points of yarn cross-over received less light during accelerated ageing and did not develop cracks. This is confirmed in Figure 5.4.13 which shows light microscopy images of accelerated aged model tapestry fabric in cross section. The fibres on the front of the weave are faded and show cracks that penetrate deep into the fibre cortex while the fibres on the back appear undamaged.

The cracks mirror the spindle shaped morphology of the macrofibrils, splitting through the cuticle cells and opening the fibrillar structure of the wool cortex, see Figure 5.4.13. This may indicate that the cell membrane complex (CMC) disintegrated due to accelerated ageing, leaving the fibrils without their girding

matrix and thereby reducing the intercellular adhesion. The KAP (keratin associated protein) part of the CMC contains a high proportion of the amino acids glycine, tyrosine, phenylalanine, serine and glutamic acid. Especially tyrosine and phenylalanine are prone to photodegradation due to the high light absorption of their aromatic structures. However, disintegration of the CMC should also affect the cuticle adhesion to the cortex, yet the cracks split cuticle cells lengthwise while the cuticle adhesion to the cortex seemed to remain intact. No difference was observed on the extent of scale flaking in unaged and accelerated aged samples.

The structure of the cracks leading from the surface to the interior may suggest that they formed due to a rapid drying out causing the surface to shrink while the bulk is still swollen with absorbed water. However, the temperature in the accelerated ageing chamber was ambient, although uncontrolled. According to the MODHT partner at Hampton Court Palace Textile Conservation Studio, where the ageing of model materials was performed, no heating of the sample surfaces was observed and the temperature in the ageing chamber was monitored to vary between 18 to 22°C with a controlled relative humidity of 65%, making a thermal effect unlikely. In order to investigate this wool samples were placed in an oven at 110°C for up to 38 days, yet SEM micrographs of the thermally aged wool did not show any cracking. Neither did wool samples aged for 300 hours in a weatherometer using a mercury lamp show cracking (see Experimental section of Chapter 6. Analysis of Metal Threads 6.2.2. Accelerated tarnishing: Oddy tests). It is therefore most probable that the observed cracking is caused by the particular spectral distribution of the xenon lamp. Only one study was found in the literature that used xenon arc irradiation on keratin fibres, but microscopic investigation of surface damage was not undertaken [141]. Gamez-Garcia [142-144] and Swift [145] investigated the cuticle damage and longitudinal as well as transverse cracking structures of hair fibres caused by torsional stresses, extensional stresses and circumferential stresses due to wetting and blow-drying of hair; yet none of the cracking structures discussed in these papers resemble the cracks observed in this study, Figure 5.4.12, and the mechanism of their formation is as yet not understood.

Figure 5.4.10. Undyed wool fibre surface

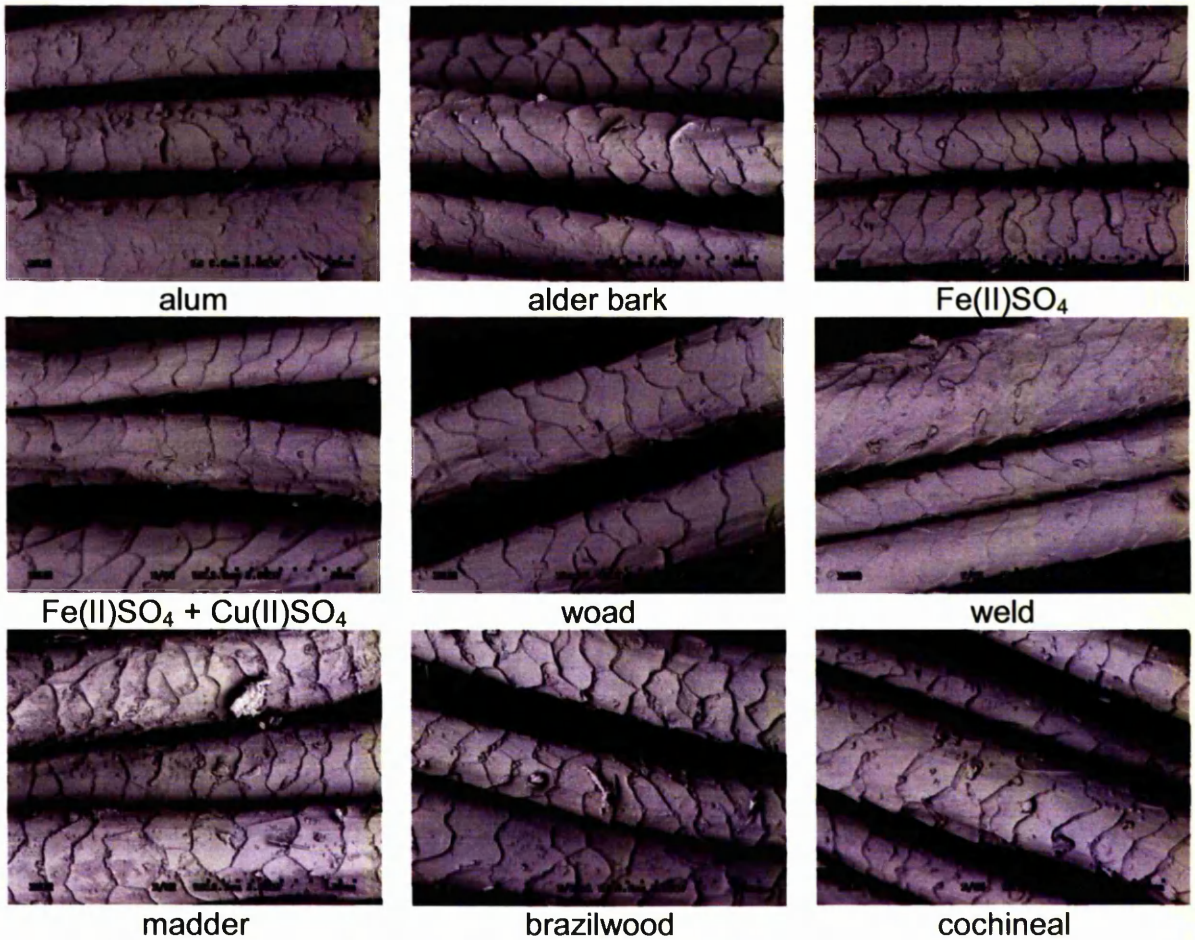

Figure 5.4.11. Mordanted and dyed wool fibre surfaces

Figure 5.4.12. Accelerated aged wool fibre surfaces

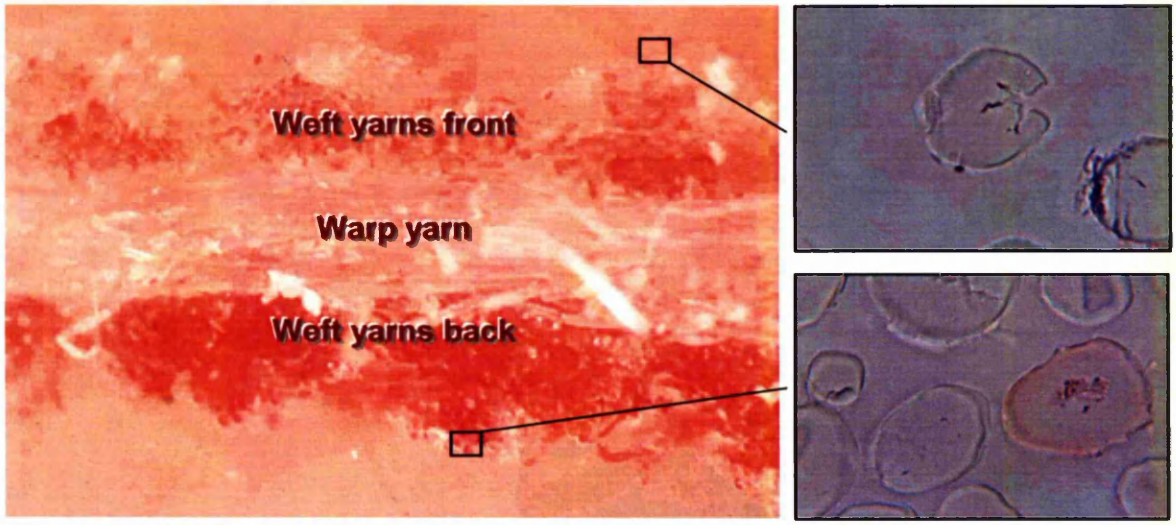

Figure 5.4.13. Cross section of accelerated aged brazilwood dyed model tapestry

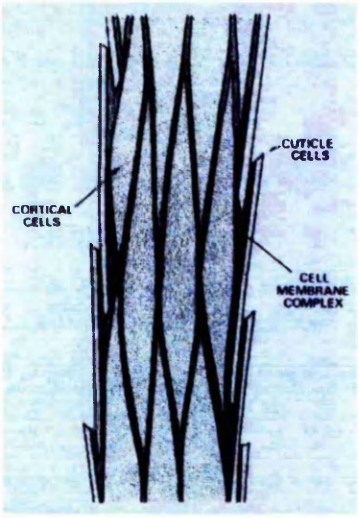

Figure 5.4.14. Schematic model of cortical cell arrangement in the wool fibre [16]

Figure 5.4.15 shows SEM images of wool fibres taken from the back of historic tapestries, while Figure 5.4.16 shows fibres from the front of historic tapestries. The surface morphology of the fibres from the back appears largely undamaged with some scale loss and the onset of transverse cracks apparent in samples HCP 108C4, BXL1_5 and HCP 112C4 respectively. The fibres taken from the front of tapestries show more severe damage in particular transverse cracking (b, f, h and i), scale ablation (c and e) and fine longitudinal cracks (d). However, the majority of fibres from both the back and front of the historic tapestries appeared undamaged with their scale structure mostly intact.

Transverse cracks, as observed in some historic fibres, are a sign of embrittlement, where the composite structure of cuticle cells, cortex and cell membrane complex has lost its flexibility and extensibility and subsequently cracks upon bending or stretching. This embrittlement may be caused by the formation of crosslinks during degradation [60, 62].

The differences in cracking pattern observed in the accelerated aged and historic fibres may lead to criticism of the validity of the ageing regime used in the MODHT project. Nevertheless, the results of chemical analyses such as amino acid analysis, FTIR Spectroscopy and XPS show the same trends of degradational change for accelerated aged model and historic wool, thereby supporting the accelerated ageing regime as a suitable model [146-148].

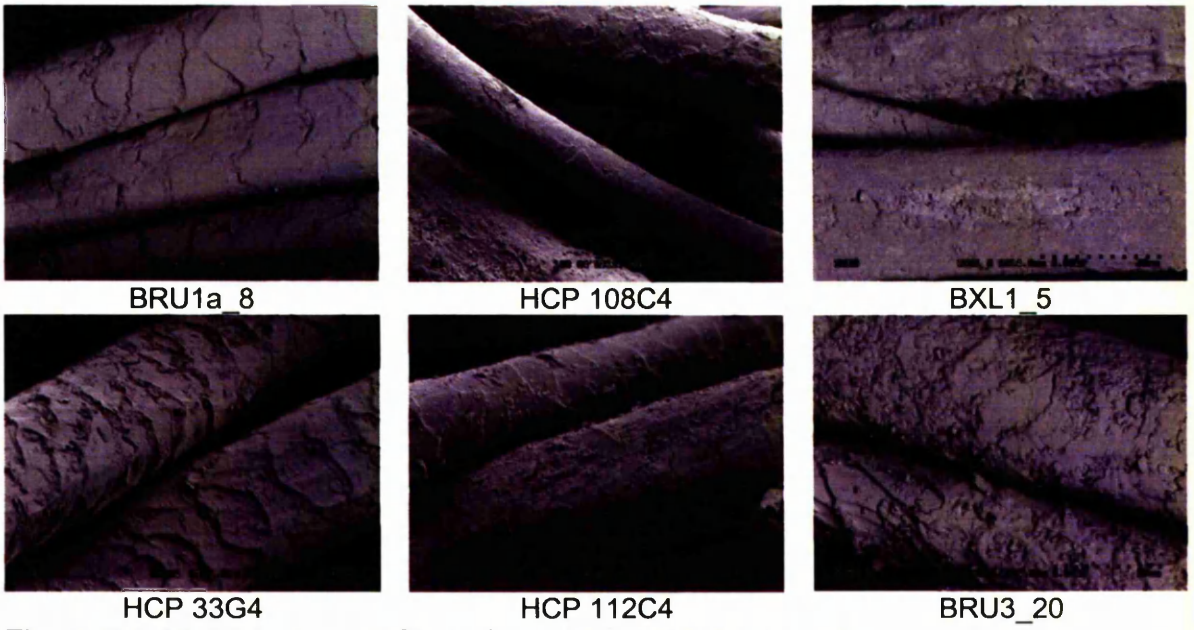

Figure 5.4.15. Historic wool fibres from the back of tapestries

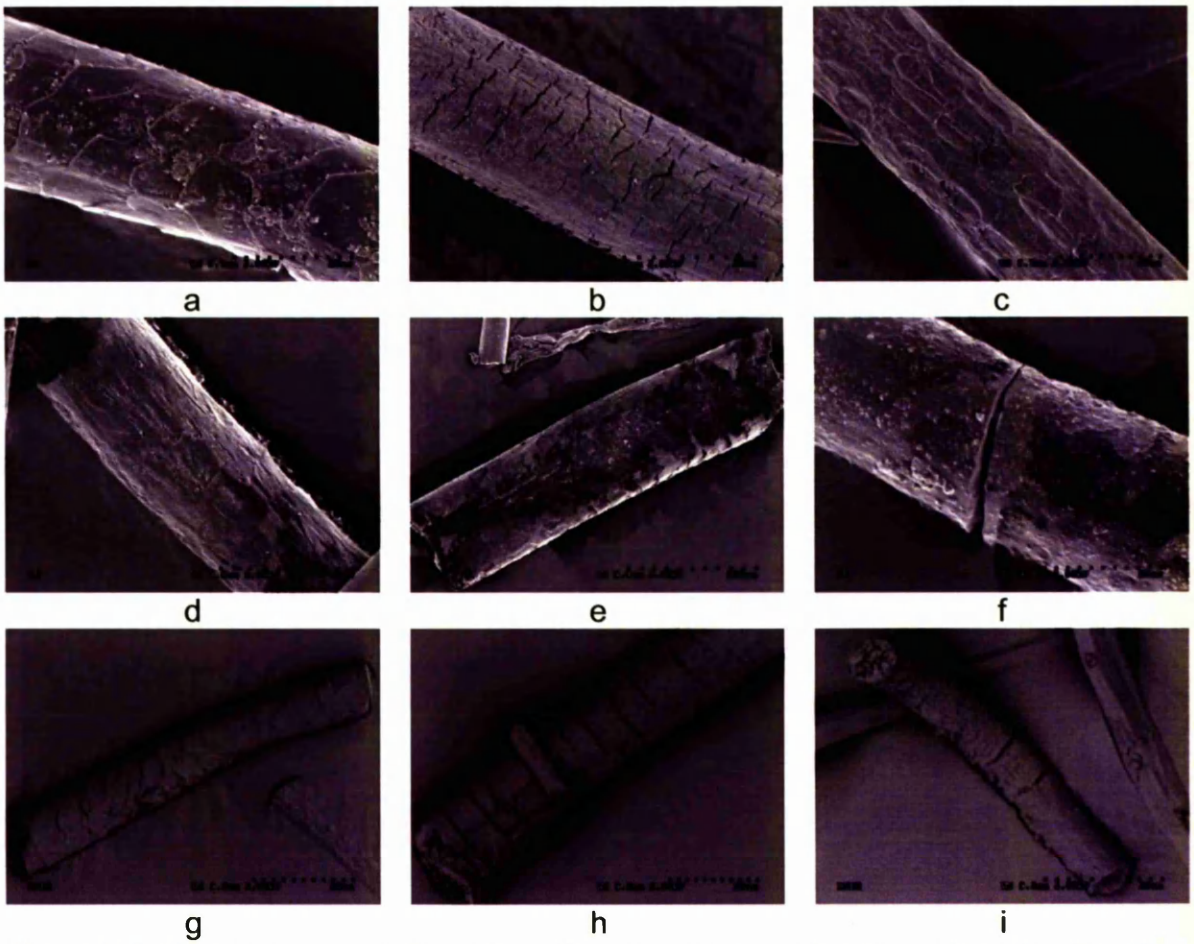

Figure 5.4.16. Historic wool fibres from the front of tapestries from Hampton Court Palace. "Romance" Tapestry (a-f); "Abraham and Melchizedek" Tapestry (g-i)

Fracture morphology of wool

Fractured morphologies were investigated on fibres taken from tensile strength tested samples. The fractures were assessed according to Hearle's classification [149] which is schematically represented in Figure 5.4.17.

Hearle et al. proposed that the most common fracture morphology of untreated wool was granular [149]. However, axial step breaks were also frequently found. It was suggested that generally the axial splits ran between the ortho- and the para-cortex and existed before the transverse splits occurred, leading to step breaks. Radial breaks usually started from a pre-existing flaw at a point between the cortex and the cuticle cells. Fibrillated multiple split breaks were mainly found in abraded textiles and biaxial rotation fatigue tests, which caused loss of fibrillar cohesion through internal hysteresis [77, 149].

In the present analysis many different forms of fracture morphologies were observed. Most samples exhibited a variety of breaks including brittle, radial, granular, axial and fibrillar breaks; examples of the various types of fractures are represented in Figure 5.4.18. The most commonly found fractures were a combination of granular and radial and were similar to the fractures found in undyed wool. Some fibrillar multiple split ends were found, but it was likely that they were naturally occurring ends, with fibrillation being due to abrasion as proposed by Weatherall [77].

Fracture type			Fracture morphology and initiation
1	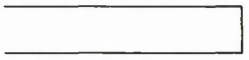	brittle	Fracture exhibits a smooth break perpendicular to fibre axis.
2	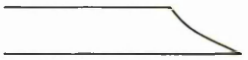	ductile / radial	Fracture propagates from surface flaw and travels radially through fibre.
3	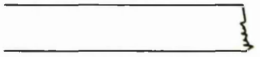	granular / fibrillar	Moderate loss of interfibrillar cohesion causes a break of rough surface appearance, defined by groups of morphological units.
4	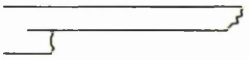	axial step	Fracture starts as a radial crack, then changes direction and follows an axial split along fibre axis and ends in another radial crack.
5		fibrillar	Major loss of interfibrillar cohesion causes independent breaks of morphological units.
6		fibrillar / multiple split	Fibre flexing and biaxial rotation and loss of interfibrillar cohesion cause multiple split breaks resulting in a frayed appearance of the end.
7		high-speed melt	Plastic deformation due to high-speed breaks in synthetic (esp. nylon) fibres leads to 'mushroom' shaped ends.
8		axial split	Highly oriented fibres with high axial cohesion but lower transverse cohesion exhibit split breaks along crystalline configurations; mostly encountered in high-modulus synthetic fibres.

Figure 5.4.17. Fibre fracture morphologies [149]

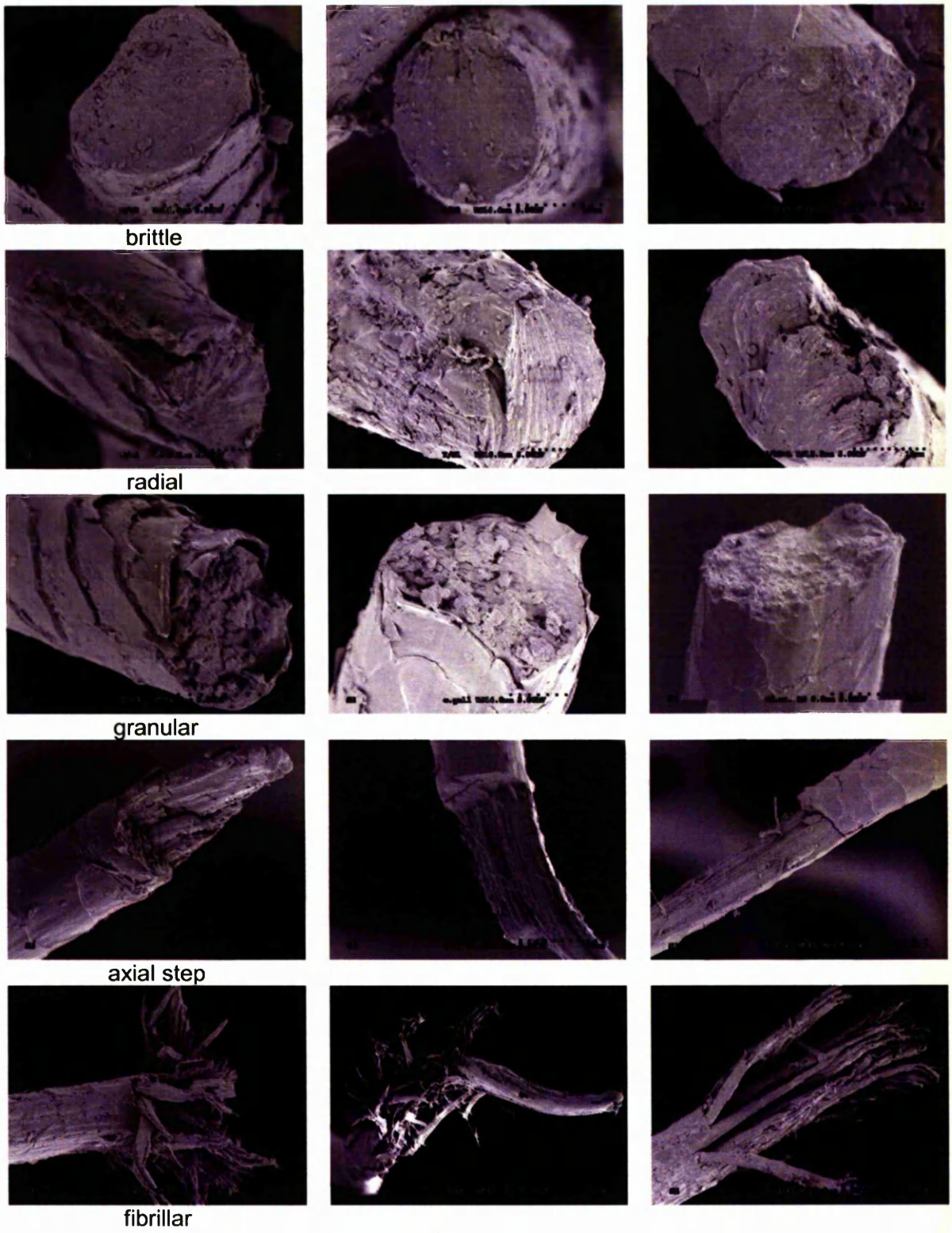

Figure 5.4.18. Wool fibre fracture morphologies

170 SEM images of tensile tested wool fibre fractures have been obtained and classified, see Table 5.4.4. The higher number of brittle breaks observed in the unaged black wool samples dyed with ferrous sulphate tentatively suggests that the dyeing caused an increase in brittle breaks due to metal complex formation. On the other hand the slight increase in brittle breaks may also be due to the acidity of the dyebath and the prolonged dyeing times used in the recipes for black dyeings of wool, see Chapter 3. section 3.2. Mordanting and dyeing. As according to Weatherall, wool which has been modified by partial acid hydrolysis showed a decreased tendency to fracture with fibrillation due to increased degree of crosslinking [77].

Simpson and Page found that physical changes due to photodegradation led to a decrease in breaking strength and extension and eventually brittle fracture morphology of wool fibres [150]. In addition, Weatherall proposed that the brittle, smooth fracture morphology as observed in photo-degraded wool was due to alteration in the nature of crosslinking of the protein chains [77]. SEM investigations of the fracture morphologies of unaged, accelerated aged and historic wool fibres were expected to reveal significant differences; it was therefore surprising to find a similar distribution of fracture types, see Figure 5.4.19 and Table 5.4.4.

Table 5.4.4. Fracture morphologies observed in tensile tested wool samples

Sample	brittle	radial	granular	granular / radial	axial step	fibrillar	other	Total
undyed	2	3	10	6			1	22
blank dyed	1		2	1				4
blank dyed with lye	2	1	4					7
blue W1 (woad)			6		1			7
yellow W1 (weld)		1	4	2				7
green W1 (weld + woad)		1	5			1	1	8
green W2 (woad + weld)	1	2	2				1	6
oak gall	1		3	2	1	3	1	11
red W1 (madder)	2	1	3	2				8
red W1 with lye (madder)	1	1	2		1	1		6
red W3 with lye (brazilwood)	2	2	2	2			1	9
black W1 (ferrous sulphate)	4		2		3	1		10
black W2 (ferrous sulphate)	4	3	5			1	1	14
black W4 (ferrous & copper sulphate)	1		6	1	1			9
Total #	**21**	**15**	**56**	**16**	**7**	**7**	**6**	**106**
Total %	**19.8**	**14.2**	**52.8**	**15.1**	**6.6**	**6.6**	**5.7**	
undyed aged (200 hours)	4		1					5
undyed aged (400 hours)		1	9	2	3			15
undyed aged (600 hours)	3				1	2	1	7
blank dyed aged (400 hours)	2	1	2					5
blank dyed with lye aged (400 hours)	2	1						3
yellow W1 aged (400 hours)			2		1		2	5
black W2 aged (400 hours)	1		2	1		2		6
Total #	**12**	**3**	**16**	**3**	**5**	**4**	**3**	**41**
Total %	**29.3**	**7.3**	**39.0**	**7.3**	**12.2**	**9.8**	**7.3**	
hist. BXL1_5		3		2				5
hist. HRP2_21		2	1	1	1		1	6
hist. HRP2_38		2	2	1	1			6
hist. HRP2_75		3	2	1				6
Total #		**10**	**5**	**5**	**2**		**1**	**23**
Total %		**43.5**	**21.7**	**21.7**	**8.7**		**4.3**	

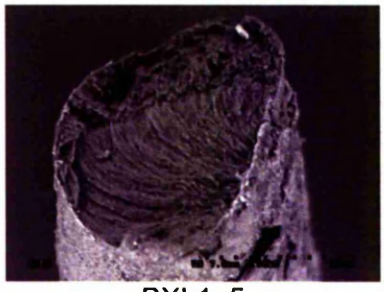

BXL1_5

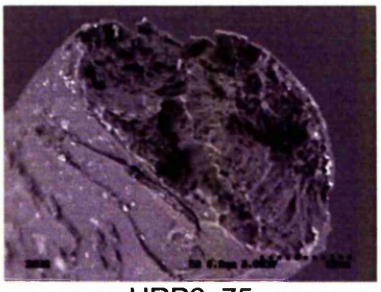

HRP2_75

HRP2_75

Figure 5.4.19. Radial and granular fracture morphologies of historic wool fibres

5.4.4. SEM investigation of fibre surfaces and fracture morphology: silk

Surface morphology of silk

The surface of undyed, unaged silk fibres was found to be mainly smooth but frequently exhibited flaws such as thickening of the diameter as represented in Figure 5.4.20. The dyeing and mordanting of silk caused some surface damage in the form of fine strips of material peeling off the surface. This surface damage was observed on all dyed and mordanted samples and also varied within the same sample with some areas appearing undamaged and others showing extensive peeling. The effect appears to be caused by either mechanical action during the dyeing process or additives in the dyebaths, i.e. mordants and dyestuffs, rather than pH conditions. Given that tests of pH treatments of silk in small scale blank dyebaths under the addition of alum or K_2CO_3 at pH 4, 7.5, 10 and 11.4 for two hours at the boil did not show the same damage, Figure 5.4.21.

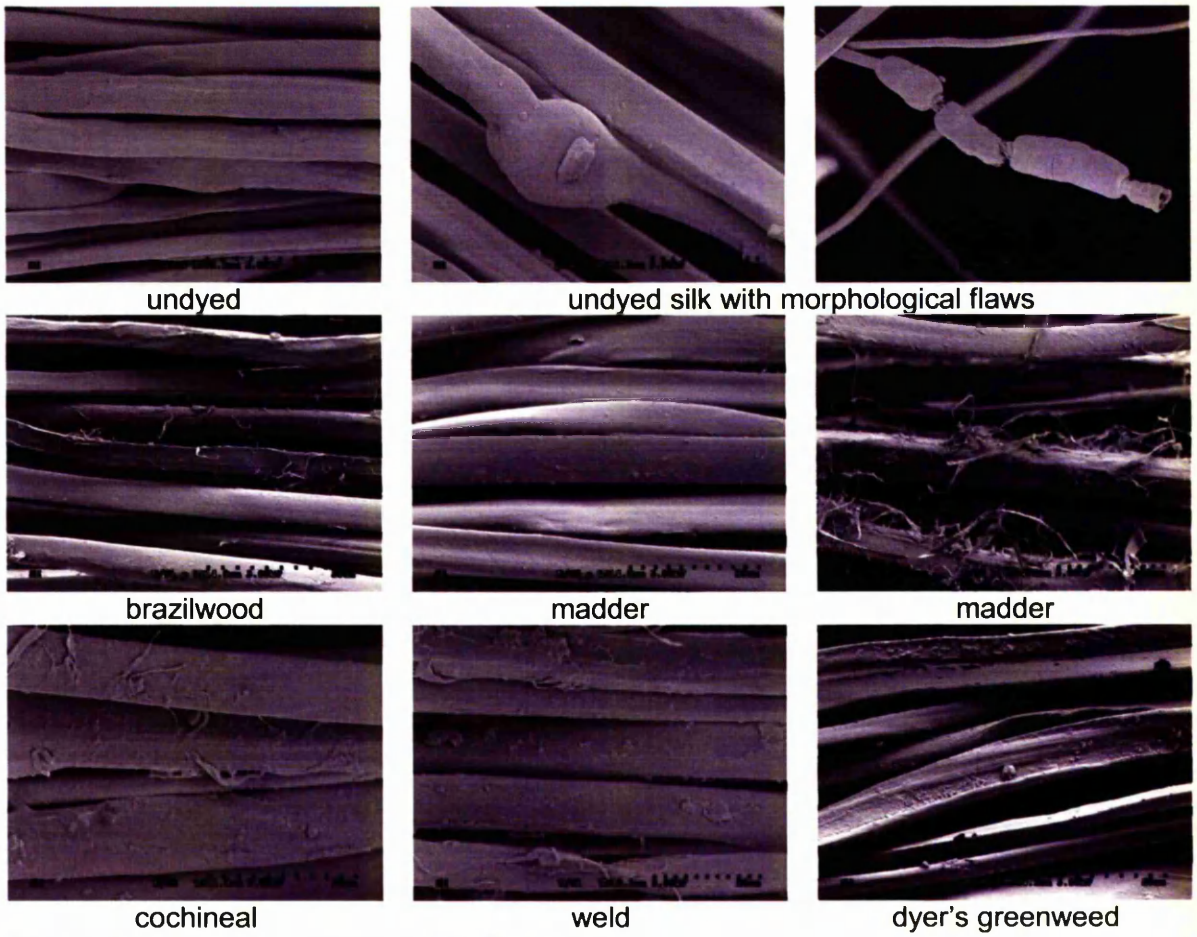

Figure 5.4.20. Undyed and dyed silk fibre surfaces

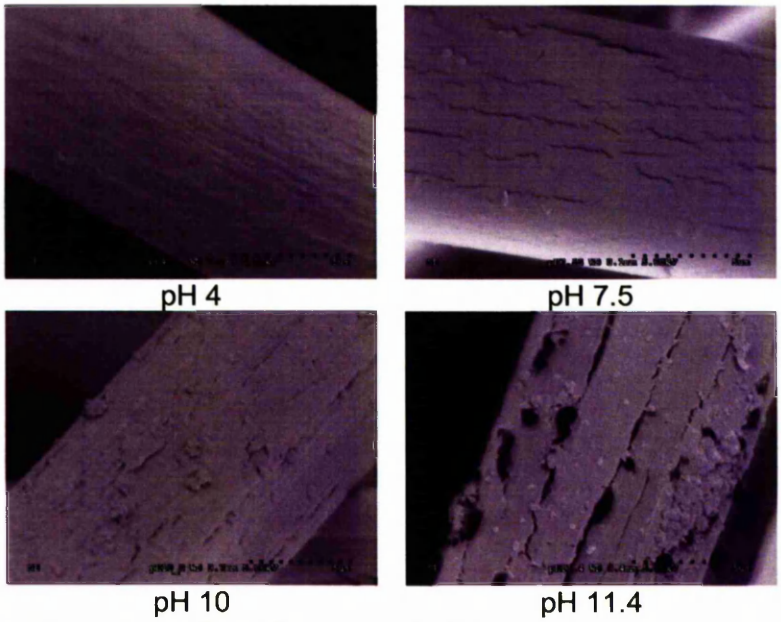

Figure 5.4.21. pH treated silk surface morphology

The surface morphologies of accelerated aged and historic silk fibres are represented in Figures 5.4.22 and 5.4.23. In contrast to the observations made for wool samples, the cracking patterns for silk are very similar, with both accelerated and natural ageing leading to mainly longitudinal cracks and some transverse cracks in historic samples only. However, similar to historic wool, the majority of fibres in historic silk samples showed no sign of surface damage, exhibiting the smooth morphology of unaged and undyed silk.

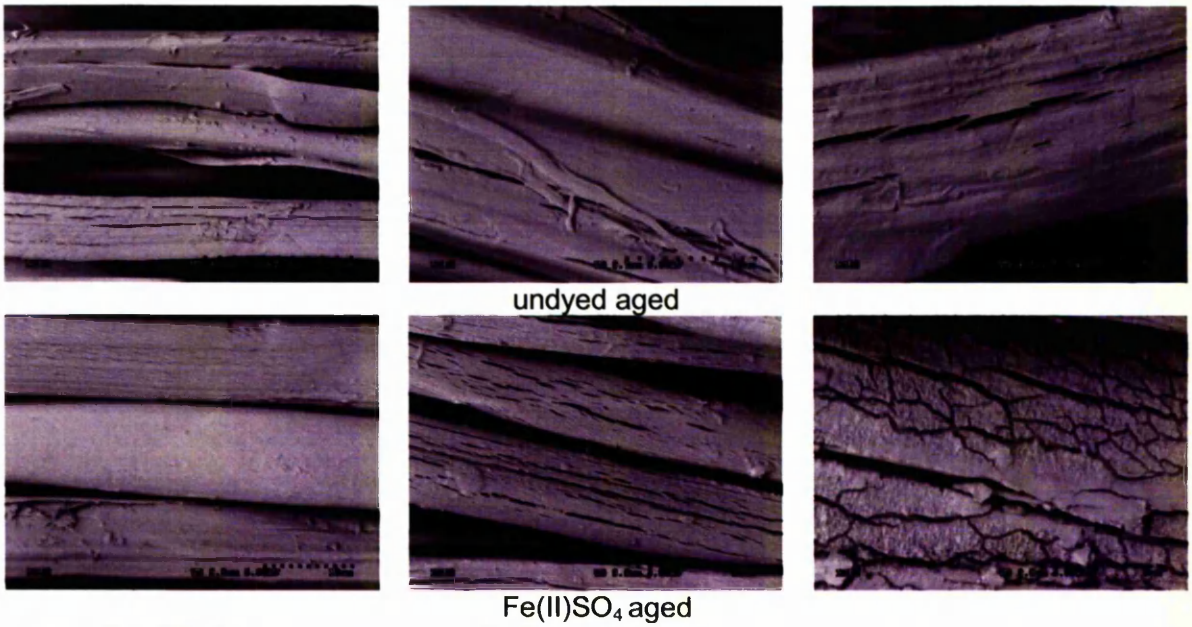

Figure 5.4.22. Accelerated aged silk fibre surfaces

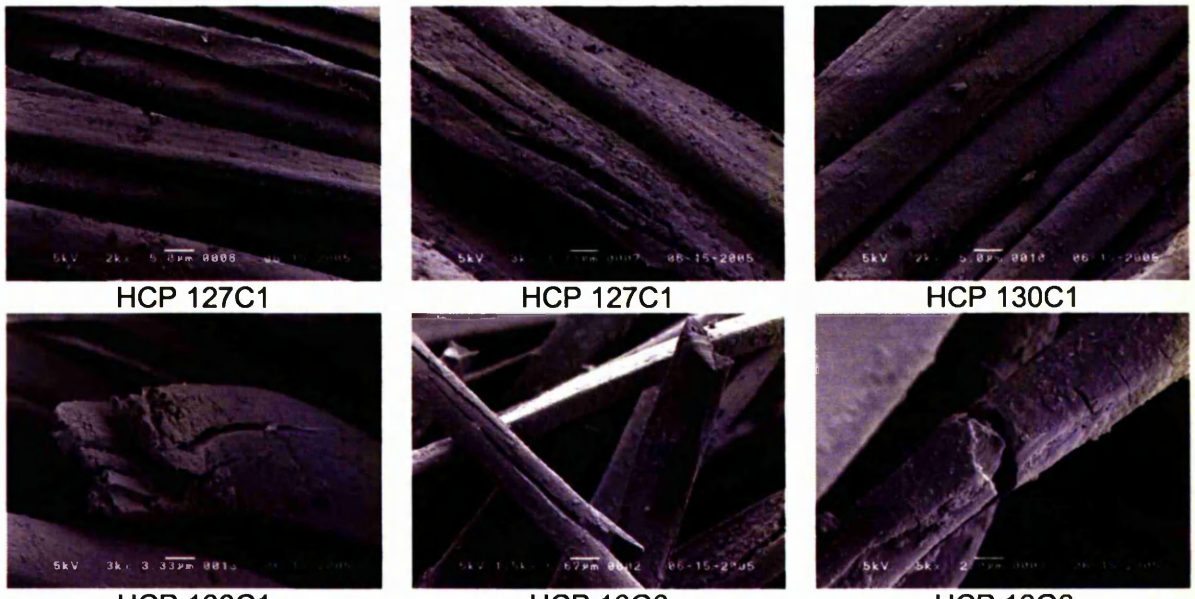

HCP 127C1 HCP 127C1 HCP 130C1

HCP 130C1 HCP 16G6 HCP 16G6

Figure 5.4.23. Historic silk fibre surfaces

Fracture morphology of silk

SEM micrographs of fracture morphologies were obtained from unaged and accelerated aged silk fibres only, as historic silk fibres were not tensile strength tested. The findings were expected to be similar to those found in work conducted by several researchers in the field of fracture morphology of photo-degraded wool and silk [77, 87, 149-151]. Hearle et al. state that tensile breaks of silk are granular in nature; however, one of the two example images in the "Atlas of fibre fracture" shows a combination break of granular and radial [149]. Bresee and Goodyear employed SEM to study the fracture morphology of historic silk samples (1880-1980) in comparison to untreated and accelerated heat- and light-aged silk samples [87]. In the analysis of untreated silk, Bresee and Goodyear found only few breaks, which were due to loss of interfibrillar cohesion and large internal voids. The majority of untreated silk samples exhibited breaks, which propagated from a flaw in the surface and ran diagonally through the fibre diameter leaving a tail end on both sides [87]. According to Hearle's classification of fracture morphology, Figure 5.4.17 [149], these breaks should have been termed 'radial', whereas Bresee and Goodyear referred to the breaks as 'axial split'. This was misleading because the splits did not actually run along the fibre axis or any macrospcopic morphological unit but rather broke through fibrils. Heat ageing for 6h at 60°C resulted in a shift in majority from 'radial' breaks to fibrillar breaks indicating a greater loss of interfibrillar cohesion than found in untreated samples.

In addition, heat aged samples appeared to show an increase in brittle breaks and a decrease in ductile breaks. Light ageing on the other hand apparently increased the number of 'radial' breaks from 50% as found in untreated silk to 70% of fractures, while no brittle breaks were found in accelerated photo-degraded silk. This was attributed to the surface damaging effect of light leading to increased surface flaws which prompted 'radial' breaks [87]. Bresee and Goodyear did not observe any independent fibrillar breaks in historic samples, suggesting that interfibrillar cohesion, i.e. hydrogen bonding was still strong in the historic silk. However, in historic samples the most common type of fracture was 'granular' and attributed to a moderate loss of interfibrillar cohesion and there seemed to be no difference in the number of ductile and brittle breaks in historic samples compared to untreated modern samples, suggesting that natural ageing processes in silk cause loss of interfibrillar cohesion rather than embrittlement [87]. In contrast to Bresee and Goodyear's proposition, Cooke and Howell observed mainly brittle breaks during the analysis of ancient silk textiles and the effect was attributed to embrittlement during photo-degradation [151].

The investigations of fracture morphologies for the MODHT project showed mainly combinations of radial and granular breaks and some axial step breaks in both unaged and accelerated aged samples, while brittle or fibrillated fractures were not observed, Figure 5.4.24 and Table 5.4.5. The analysis also showed that many fibres failed at the point of morphological flaws leading to breaks, which appeared reminiscent of plastic deformation as observed in high-speed rupture of melt-spun fibres but were due to inherent imperfections in the fibres, compare Figure 5.4.20 and Figure 5.4.17, fracture type 7.

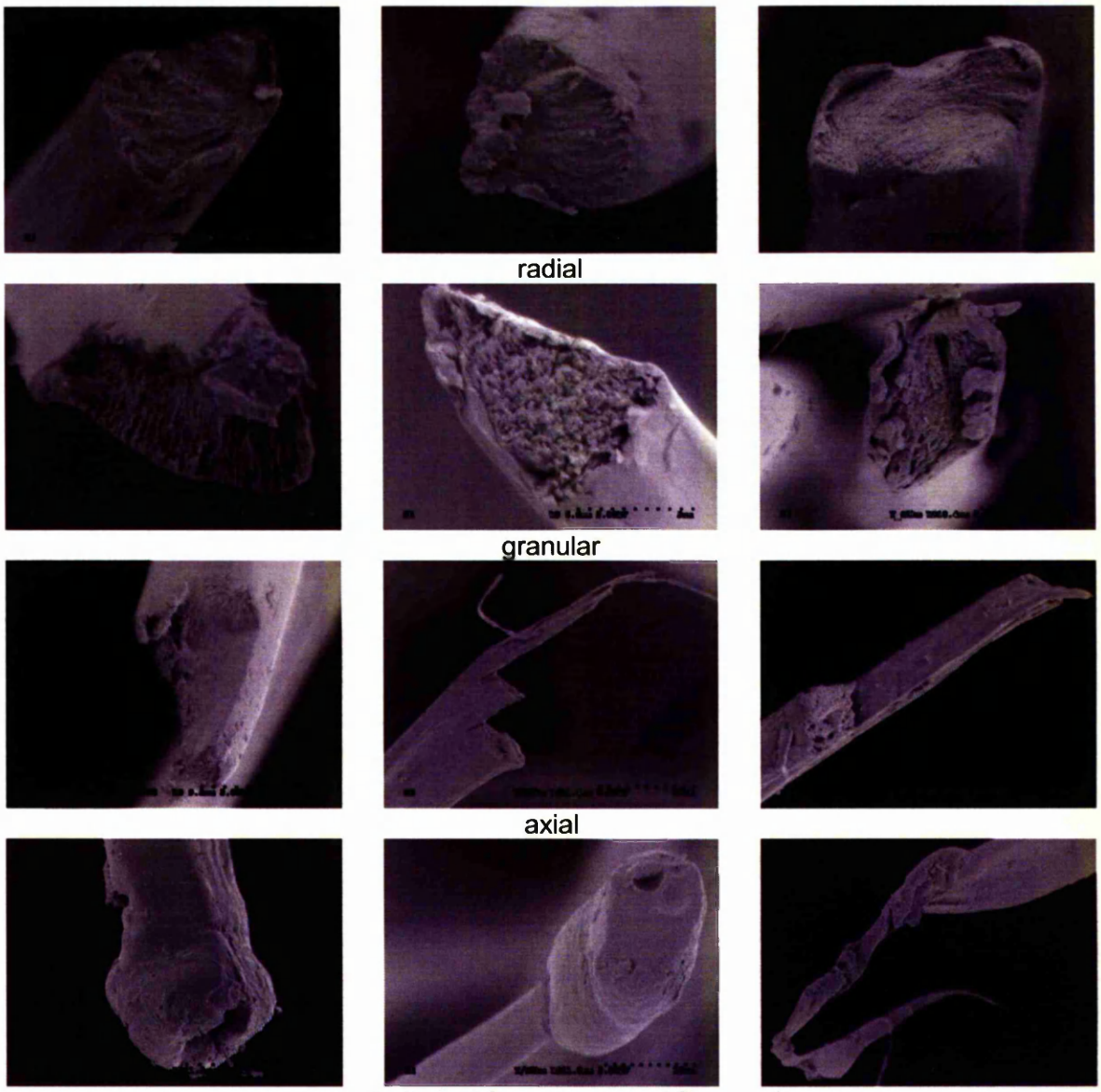

Figure 5.4.24. Silk fibre fracture morphologies

Table 5.4.5. Fracture morphologies observed in tensile tested silk samples

Sample	radial	granular	granular /radial	axial step	other	Total
undyed	2	8	3	2	2	17
alum		3			5	8
yellow S1 (weld)		4				4
yellow S3 (dyer's greenweed)		2	2	2	7	13
red S1 (brazilwood)	1		3			4
red S3 (cochineal)	1		1	2	1	5
black S1 (ferrous sulphate)		4		1		5
Total #	**4**	**21**	**9**	**7**	**15**	**56**
Total %	**7.1**	**37.5**	**16.1**	**12.5**	**26.8**	
undyed aged (400 hours)		3		1	1	5
black S1 aged (400 hours)	3	1		1		5
Total #	**3**	**4**	**0**	**2**	**1**	**10**
Total %	**30**	**40**	**0**	**20**	**10**	

5.4.5. Investigation of fibre surface chemistry using XPS

XPS has been used extensively for the study of the wool surface [10, 15, 18, 19, 27, 29-51, 81, 152] but only few studies were found on silk [47, 103]. While many studies concentrated on the effect of oxidative treatments, namely alcoholic alkali solutions [15], Corona discharge [29, 37], UV/ Ozone [10, 35, 36, 42, 43, 47, 49, 50, 103], various plasma treatments [27, 30, 36, 39, 44, 51, 152] and other shrink proofing and bleaching treatments [31, 33, 38, 44, 48, 81], only one study briefly mentioned the influence of simulated sunlight [103] , see section 5.1. XPS studies of wool and 5.2. XPS and SIMS studies of silk.

This study investigates the effects of accelerated ageing with simulated sunlight on wool dyed with various natural dyes in comparisons with historic wool fibres. XPS analysis of silk was performed on few undyed unaged and accelerated aged samples only and the results briefly discussed.

The main peaks expected from XP spectra of both wool and silk correspond to oxygen O(1s) 531eV, nitrogen N(1s) 400eV, carbon C(1s) 289-285eV and sulphur S(2p) 168-164eV. Figure 5.4.25 shows a typical XP spectrum of the unmodified wool surface.

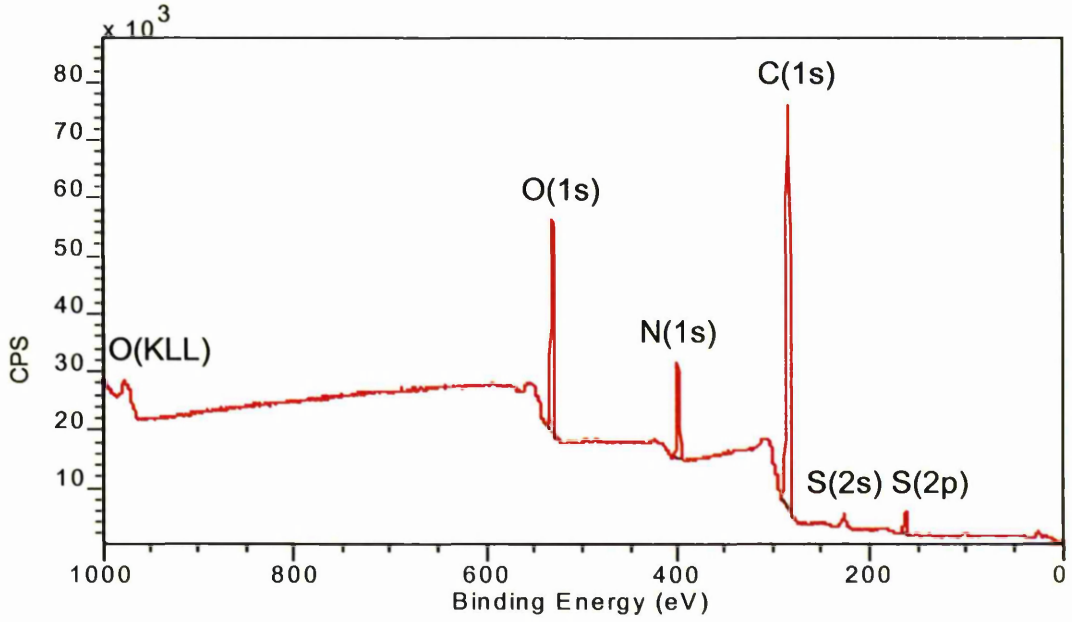

Figure 5.4.25. XP spectrum of wool surface

5.4.6. XPS analysis of wool

Some dyed unaged and accelerated aged samples have been found to contain small amounts of silicon Si(2p), calcium Ca(2p) and phosphorus P(2p) these contaminations originate from processing and handling. Depending on the dyestuffs and mordants used some aluminium Al(2p), copper Cu(2p) and iron Fe(2p) has also been detected. Traces of tin Sn(3d) were identified on a few samples and most likely derived from contamination present in the analysis chamber of the instrument. Tables listing quantified XPS data of all samples analysed are represented in the appendix sections B, C and D. The results of multiple analyses of the same samples have been averaged and are listed in the appropriate sections below.

Information about the oxidative and degradational state of the analysed fibres was gained from the following features of the quantified XP spectra:

- Carbon C(1s) peak shape and relative ratios of components;
- Carbon to oxygen ratio C/O;
- Carbon to nitrogen ratio C/N;
- Carbon to sulphur ratio C/S;
- Nitrogen to sulphur ratio N/S;
- Sulphur S(2p) peak relative percentage of oxidised component.

Data from the literature on XPS analysis of untreated wool and silk regarding relative atomic % and elemental ratios has been summarised in Table 5.4.6. Reference to these data will be made in the following sections by comparison with the respective ratios as observed in the present study.

Table 5.4.6. XPS data of untreated wool and silk fibres

Elemental ratios and atomic %		O/C	C/O	C/N	N/S	C/S	C	O	N	S
Wool	[31]	0.16	6.25	10						
	[34]	0.19	5.26	12.5	2.7	32.2				
	[19]	0.2	5	6.9	3.3	23				
	[35, 36]	0.15	6.72	12.8	2.3	29.4	79.3	11.8	6.2	2.7
	[37]	0.16	6.39	6.4	2.4	26.9	77.9	12.2	6.9	2.9
	[36]	0.16	6.28	8.6	2.8	24.5	76.0	12.1	8.8	3.1
	[38]	0.14	7.09	7.1	4.9	34.8	80.1	11.3	6.2	2.3
	[15]			9.9	4					
	[46]	0.17	5.86	9.5	4	38.4	76.8	13.1	8.1	2.0
	[48]	0.16	6.25	9.1	2.7	24.6	76.3	12.2	8.4	3.1
	[51]	0.18	5.68	12.0	2.4	28.4	76.7	13.5	6.4	2.7
Silk	[103]	0.34	2.90	4.8	44.7	214	64.2	22.1	13.4	0.3

5.4.7. XPS of wool: interpretation of the C(1s) peak shape

With the aim of facilitating the visual interpretation of the C(1s) peak shapes two model C(1s) peaks shapes were established. Because neither the thickness of the lipid layer nor the content of lipids in the β-layer has been unambiguously identified, it has not been attempted to establish a theoretical XPS C(1s) peak shape for the total wool surface but rather two separate C(1s) peak shapes for protein and lipids.

In order to establish the theoretical XPS C(1s) peak shape for a homogenous surface consisting of epicuticle and β-layer proteinaceous material only, all possible carbon atom configurations were counted in each amino acid and multiplied by the respective residue percentage, see Table 5.1.4. Assumed amino acid composition of epicuticle and β-layer. Approximated peak shifts were deduced from the Beamson and Briggs XPS of Polymers Database [153] and are in accordance with above mentioned references of XPS on wool and silk. Carbon configurations, which result in similar peak shifts, are shown in Table 5.4.7. Their relative concentrations were added and the results shown in Table 5.4.8. C(1s) peak shifts and carbon configurations for the four fatty acids 18-MEA, palmitic, stearic and oleic acid are represented in Table 5.4.9 together with their respective percentage assuming the concentrations given in Table 5.1.5, page 101. Theoretical XPS C(1s) peak shapes corresponding to the data of Tables 5.4.8 and 5.4.9 are shown in Figure 5.4.26. A Gaussian-Lorentzian (50) peak shape with full-width-half-maximum value of 1.2 was chosen for the synthetic components because it offered best peak fit in actual C(1s) high-resolution spectra of wool surfaces. Wool surfaces with a homogenous and very thick lipid layer (>5nm) or a contaminant hydrocarbon surface layer would exhibit a C(1s) peak shape similar to Figure 5.4.26 (b) while the C(1s) shape for wool depleted of all lipids would look like Figure 5.4.26 (a).

Table 5.4.7. XPS C1s peak shift eV for all carbon configurations in keratin protein

~ -0.4 eV	0 eV	~ 0.4-0.5 eV	~ 1.2-1.6 eV	~ 3 eV	~ 4.3 eV
(C,H),C-**C**=C	C-**C**H_2-C	S-**C**H_2-S	C,N-**C**H-C	C,N-**C**=O	C,HO-**C**=O
(C,H),C-**C**=C Phenol	C-**C**H_3	C-**C**H_2-S	C,N-**C**H-N	N,N-**C**=N	
(C,H),C-**C**=C Pyrrole	C-**C**H-C,C	N-**C**$H_{(2)}$-C Pyrrolidine	C-**C**H_2-OH		
	(C,H),N-**C**=C Imidazole	C-**C**H_2-OH	C-**C**H-C,OH		
	N-**C**H=C Pyrrole		C,HO-**C**=C Phenol		
	C -**C**$H_{(2)}$-C Pyrrolidine				

Table 5.4.8: Theoretical XPS C(1s) peak shift percentages for wool surface protein

0 eV peak shift %	24.9 %	
~ -0.4 eV peak shift %	4.65 %	**42.4 %**
~ 0.4-0.5 eV peak shift %	12.9 %	
~ 1.2-1.6 eV peak shift %	**28.2 %**	
~ 3 eV peak shift %	**26.3 %**	
~ 4.3 eV peak shift %	**3.1 %**	
total	100 %	

Table 5.4.9: Theoretical XPS C 1s peak shift percentages for wool surface lipids

0 eV (CH,CH2,CH3)	~0 eV S-**C**H=O	~ -0.4 eV C-**C**H=C	~ 4.3 eV C,HO-**C**=O
88.71 %	5.25 %	0.80 %	**5.25 %**
	94.75 %		

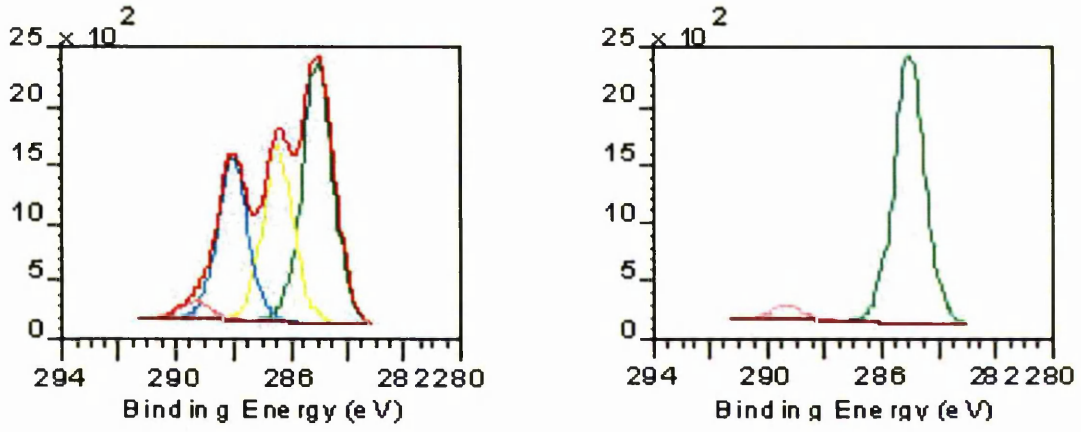

(a) wool surface protein (b) wool surface lipids

colours of components correspond to tables above

Figure 5.4.26. Theoretical C(1s) peak shapes of wool surface protein and lipids

Photo-oxidation of the wool surface has previously been found to oxidise and remove fatty acids [10, 26, 35, 42, 47, 49, 80], thereby increasing the signal intensity of carbonyl and carboxyl group components with shifts in binding energy of ~3eV and ~4eV respectively. This is exemplified in Figure 5.4.27, which shows the curve fitted C(1s) spectra of a wool sample before and after irradiation (accelerated ageing). For all undyed and dyed model wool tapestry samples the relative percentage of the hydrocarbon base peak at 285 eV was reduced from an average of 58% to an average of 47% while the carbon-nitrogen, carbonyl and carboxylic peak components underwent relative increases. These changes in the C(1s) peak confirm the irradiation induced oxidation and eventual loss of hydrocarbon material, i.e. lipids from the wool surface.

Averaged values of the relative percentages of C(1s) components of unaged, accelerated aged and historic wool are represented in Tables 5.4.10 and 5.4.11.

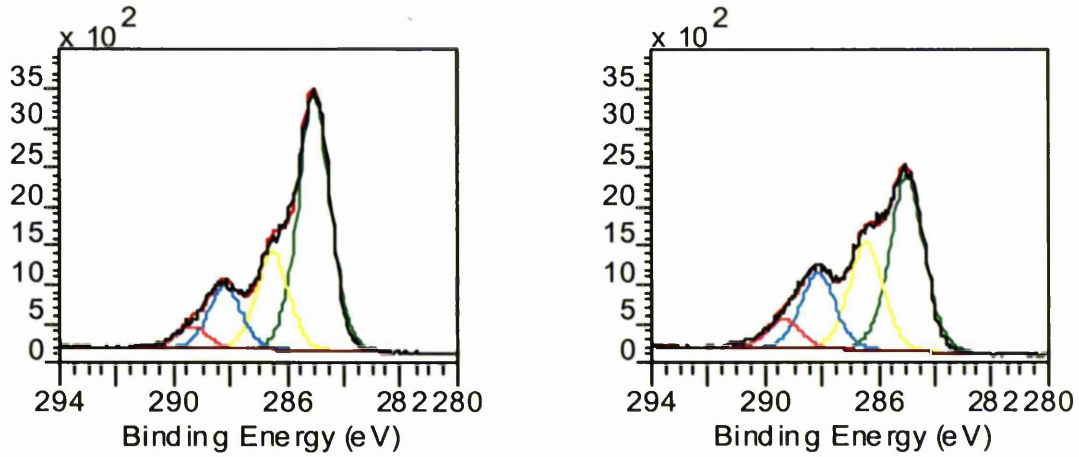

unaged (Red/W3_wl) aged (Red/W3_wl)

Figure 5.4.27. C(1s) spectra of brazil dyed, unaged and aged wool

Table 5.4.10. Average XPS results of model wool fabrics

Sample	Relative % of C(1s) peak components				Component ratios	
	Hydro-carbon 185 ev	Carbon-nitrogen ~186.3 eV	Carbonyl ~188 eV	Carboxyl ~189 eV	CH/CN	CH/CO
Undyed	62.67	21.88	12.89	2.56	2.89	4.09
Undyed aged	46.41	27.79	19.51	6.29	1.67	1.82
Blank dyed	69.12	17.48	11.55	1.85	3.96	5.16
Blank dyed_wl	58.67	25.93	11.57	3.82	2.26	3.81
Alum	62.99	22.84	11.63	2.53	2.76	4.45
Alder bark	67.84	19.74	11.34	1.08	3.44	5.46
Alder bark aged	42.74	32.38	16.96	7.92	1.32	1.72
Oak gall	52.77	26.96	15.52	4.75	2.17	2.66
Oak gall aged	47.72	28.74	17.52	6.02	1.66	2.04
Oak gall aged (back)	50.16	28.81	15.99	5.04	1.74	2.38
Black/W1	64.90	19.96	12.64	2.50	3.25	4.29
Black/W1 aged	43.21	29.18	21.75	5.86	1.48	1.57
Black/W2	37.84	27.66	25.50	9.01	1.37	1.10
Black/W2 aged	43.35	29.34	19.28	8.03	1.48	1.66
Black/W3	54.86	27.10	12.78	5.26	2.02	3.04
Black/W3 aged	40.51	29.33	23.71	6.46	1.38	1.35
Black/W4	56.43	25.12	13.77	4.68	2.26	3.10
Black/W4 aged	47.76	28.54	16.80	6.91	1.68	2.07
Blue/W1	61.01	21.50	12.58	4.91	2.84	3.49
Blue/W1 aged	34.74	29.55	25.67	10.04	1.18	0.97
Green/W1	49.83	29.02	15.76	5.39	1.72	2.39
Green/W1 aged	34.89	29.27	26.92	8.92	1.19	0.99
Green/W2	59.15	23.40	13.45	4.00	2.59	3.60
Green/W2 aged	44.22	28.77	22.50	4.51	1.54	1.64
Red/W1	59.09	24.88	12.21	3.82	2.37	3.69
Red/W1 aged	52.87	24.93	17.15	5.04	2.16	2.44
Red/W1_wl	52.64	26.83	15.20	5.32	2.01	2.73
Red/W1_wl aged	43.78	27.97	20.60	7.65	1.57	1.56
Red/W1_wl aged (back)	47.13	26.25	18.26	8.36	1.83	1.85
Red/W2	59.24	24.74	12.28	3.74	2.39	3.70
Red/W2_wl	46.72	26.75	19.98	6.55	1.75	1.76
Red/W2_wl aged	40.80	31.17	21.83	6.20	1.31	1.46
Red/W3_wl	64.01	23.18	10.32	2.49	2.76	5.00
Red/W3_wl aged	45.09	27.78	19.66	7.47	1.62	1.66
Red/W3_wl aged (back)	52.82	26.18	15.43	5.57	2.02	2.52
Red/W4	65.87	21.00	11.20	1.92	3.14	5.02
Red/W4 aged	58.26	29.06	11.11	1.57	2.00	4.60
Red/W5	53.15	28.51	14.03	4.31	1.90	2.92
Red/W5 aged	49.22	28.05	15.63	7.10	1.75	2.17
Red/W5 aged (back)	56.04	24.46	14.48	5.03	2.29	2.87
Yellow/W1	57.95	22.75	14.16	5.14	2.58	3.01
Yellow/W1 aged	42.30	29.12	22.08	6.50	1.45	1.48
Yellow/W2	54.97	25.70	14.66	4.67	2.26	3.14
Yellow/W2 aged	53.89	25.68	14.88	5.54	2.10	2.64
Yellow/W2 aged (back)	52.24	28.46	14.09	5.21	1.86	2.71

Table 5.4.11. Average XPS results of heptane extracted historic wool samples

Sample	Relative % of C(1s) peak components				Component ratios	
	Hydrocarbon 185 ev	Carbon-nitrogen ~186.3 eV	Carbonyl ~188 eV	Carboxyl ~189 eV	CH/CN	CH/CO
BRU2_23	54.9	27.3	12.9	4.9	2.0	3.1
HCP 115_C4	41.5	30.4	19.6	8.5	1.4	1.5
HCP 18_G4	63.5	21.3	10.1	5.1	3.0	4.2
HCP 90_D4	38.9	28.3	23.7	9.1	1.4	1.2
HRP1_1	51.7	27.5	14.0	6.8	1.9	2.5
HRP1_22	62.3	21.9	14.1	1.7	2.8	4.0
HRP1_46	42.5	32.5	17.9	7.1	1.3	1.7
HRP2_21	47.5	28.4	16.2	7.9	1.7	2.0
HRP2_38	50.7	27.0	12.7	9.6	1.9	2.3
HRP2_62	47.8	29.3	18.5	4.4	1.6	2.1
HRP3_19	55.3	25.9	13.2	5.6	2.1	3.0
PNM2_27	57.2	24.8	13.0	5.0	2.3	3.2
PNM5_15	51.5	27.8	13.9	6.8	2.0	2.5
PNM7_7	54.5	24.7	15.5	5.4	2.2	2.6
PNM9_13	46.5	31.2	15.8	6.5	1.5	2.1
PNM9_20	50.2	27.8	14.5	7.5	1.8	2.3

In order to measure the change in C(1s) peak shape the ratio of hydrocarbon to oxidised carbon {CH/CO = hydrocarbon 285 eV / (carbonyl ~288 eV + carboxylic ~289 eV)} and the ratio of hydrocarbon to carbon-nitrogen {CH/CN = hydrocarbon 285 eV / carbon-nitrogen ~286.3 eV} was calculated for all samples, Tables 5.4.10 and 5.4.11. The CH/CO ratio was found to drop from an average of 3.5 to 2, while the CH/CN ratio decreased on average from 2.5 to 1.7 due to accelerated ageing. These measures were found to possess a crude correlation with the tensile strength value strain, Figure 5.4.28. Though widespread, the data points of unaged wool generally show increasing strain with increasing CH/CO and CH/CN values while examination of the data points of accelerated aged wool shows no indication of a trend within the cluster. Therefore, the calculations of ratios of the C(1s) peak components may give an indication of processing induced damage in modern wool caused by a variety of parameters such as time, temperature, alkalinity or acidity as well as the mordants or dyestuffs but the values do not yield information about tensile properties after accelerated ageing.

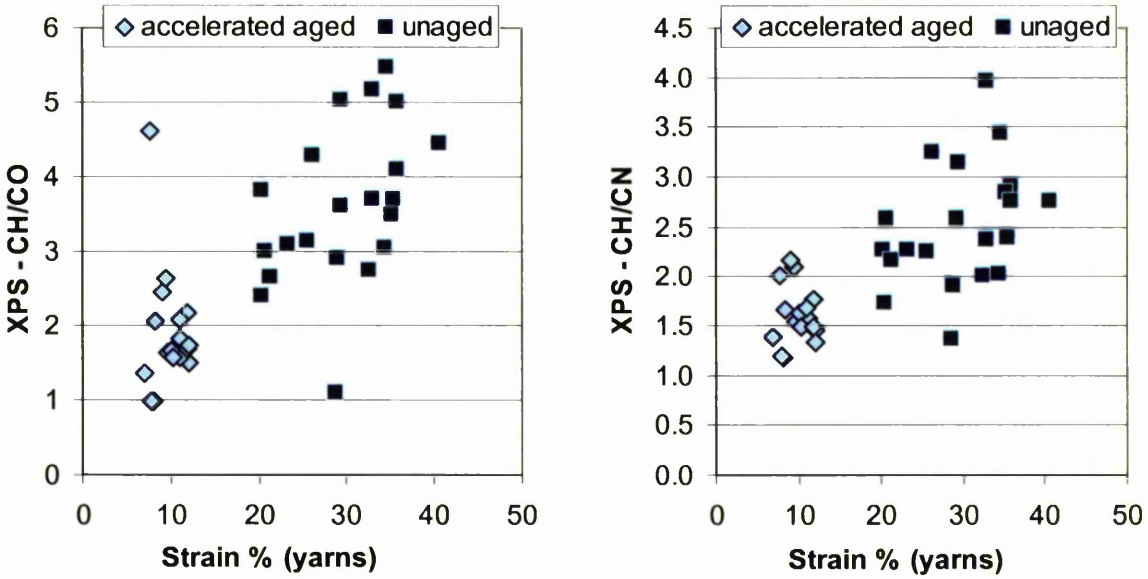

Figure 5.4.28. Correlation between ratio of C(1s) peak components and tensile strain

An assessment of the C(1s) peak components of historic wool fibres showed that they are similar in shape to those of accelerated aged wool with an average relative hydrocarbon peak intensity of 51% and an average CH/CO ratio of 2.5 and CH/CN ratio of 1.9, Figure 5.4.29. Hence, leaving the yarn structure (Tex and twist) out of consideration, it could be assumed that the historic samples have similar tensile strain as the accelerated aged samples. However, as discussed above these values only give a general indication of degradation and are not sensitive markers of damage.

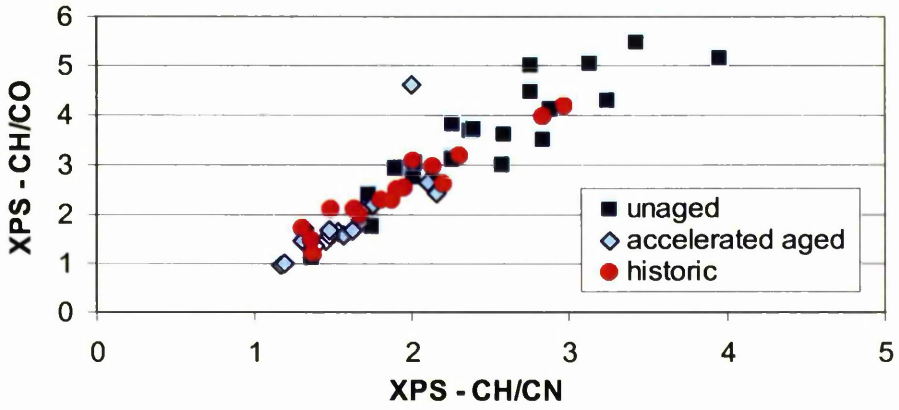

Figure 5.4.29. Ratios of XPS C(1s) peak components

5.4.8. XPS of wool: interpretation of the C/O and C/N ratios

The ratios of atomic % carbon, oxygen, nitrogen and sulphur have been averaged from multiple analyses points on each sample and are listed in Table 5.4.12. Similar to the components ratios of the C(1s) peak, the total atomic % carbon to oxygen ratio (C/O) and carbon to nitrogen ratio (C/N) reflect the extent of oxidation and surface lipid removal. An increase in total surface oxygen content will decrease C/O and also lead to a peak broadening or peak shift of those elements, which accommodate the additional oxygen, i.e. initially C(1s) and eventually N(1s) and S(2p). The more of the lipids are cleaved and removed the more of the underlying proteinaceous nitrogen will be accessible to XPS detection, thereby decreasing the C/N ratio.

Table 5.4.12. Average elemental ratios from XPS analysis of model wool fabrics

Sample	Unaged				Accelerated aged			
	C/O	C/N	C/S	N/S	C/O	C/N	C/S	N/S
Undyed	6.8	10.2	23.1	2.3	3.8	7.0	33.7	4.8
Blank dyed	6.2	10.4	30.2	2.9	2.7	5.6	42.0	7.4
Blank dyed_wl	5.5	11.6	43.3	3.7				
Alum	3.6	11.2	19.0	1.7	1.9	6.4	14.4	2.2
Alder bark	5.4	10.4	29.2	2.8	2.9	7.3	44.5	6.1
Oak gall	5.3	12.8	25.5	2.0	3.4	9.7	86.6	8.7
Black/W1	4.9	10.9	27.2	2.5	2.3	5.8	31.9	5.5
Black/W2	3.4	12.6	33.2	2.6	3.1	10.1	28.9	3.2
Black/W3	4.3	9.7	24.2	2.5	2.5	5.0	34.2	6.8
Black/W4	4.4	10.3	27.6	2.7	3.3	8.0	29.7	3.8
Blue/W1	5.3	9.0	23.1	2.6	2.8	5.6	36.4	6.5
Green/W1	3.9	8.8	22.8	2.6	2.2	4.9	31.2	6.3
Green/W2	5.3	11.5	27.3	2.4	2.7	6.3	72.4	11.4
Red/W1	5.4	9.9	26.2	2.7	3.0	6.6	42.4	6.8
Red/W1_wl	5.1	9.1	23.9	2.6	3.1	5.3	42.1	7.9
Red/W2	6.0	13.0	25.6	2.0	3.2	6.7	43.8	6.6
Red/W2_wl	4.3	11.1	28.2	2.5	2.3	5.8	47.5	8.1
Red/W3_wl	4.2	13.0	31.7	2.4	3.2	7.7	27.5	3.6
Red/W4	6.8	13.6	24.2	1.8	4.0	8.8	62.7	7.1
Red/W5	5.5	9.9	27.1	2.7	3.3	8.0	48.5	6.1
Yellow/W1	4.3	10.2	22.3	2.2	2.4	5.8	28.4	4.9
Yellow/W2	5.3	10.9	26.7	2.5	2.9	8.6	42.9	5.0

Table 5.4.13. Average elemental ratios from XPS analysis of heptane extracted historic wool samples

Sample	C/O	C/N	C/S	N/S
BRU2_23	1.8	11.0	22.3	2.0
HCP 115_C4	2.5	10.6	31.2	3.0
HCP 18_G4	3.5	18.7	49.7	2.7
HCP 90_C4	2.4	12.3	35.8	2.9
HRP1_1	3.6	10.8	29.0	2.7
HRP1_21	2.5	7.2	26.2	3.6
HRP1_22	3.4	10.8	28.9	2.7
HRP1_46	2.4	8.4	20.8	2.5
HRP2_21	2.0	9.7	51.6	5.3
HRP2_38	2.6	7.8	24.6	3.1
HRP2_61	2.4	9.5	39.7	4.2
HRP2_62	2.3	6.9	57.4	8.3
HRP3_19	1.5	14.1	12.9	0.9
PNM2_27	1.6	14.0	26.7	1.9
PNM5_15	2.3	13.5	34.2	2.5
PNM7_7	1.8	8.3	15.8	1.9
PNM9_13	1.9	9.9	19.0	1.9
PNM9_20	1.8	9.4	24.3	2.6

For the dyed unaged wool fabrics the average C/O ratio was 4.8 and decreased to 2.9 in accelerated aged wool; average C/N values decreased from 10.8 to 7.3. The C/O values found in the literature were generally > 5 and < 7.1 while the C/N values showed greater variety between 6.4 to 12.4, Table 5.4.6. The relatively higher surface oxygen content of MODHT model tapestry samples indicates that some oxidation and possibly lipid removal has taken place during the dyeing procedure. This is consistent with the postulation that the data summarised from the literature was collected from untreated (possibly scoured) wool and confirmed by the higher average C/O value of undyed unaged wool; C/O = 6.8 decreasing to 3.8 after accelerated ageing.

In general accelerated aged wool has similar C/O values but higher C/N values than the theoretical atomic % ratios for epicuticle keratin without any lipid contribution, which are C/O = 2.8 and C/N = 3.3; calculated from the epicuticle amino acid composition as shown in Table 5.1.4, Figure 5.4.30. It follows that accelerated ageing has reduced but not substantially removed the surface carbon, i.e. lipid layer, but caused the formation of carbonyl and carboxyl groups which partially account for the additional oxygen and the low C/O ratio.

It was expected to find a good correlation between the C/O and C/N ratios as both are indicators of lipid removal, however, C/O also shows oxidation without lipid removal and it is this phenomenon which appears to prevail during the dyeing and mordanting processes. Therefore a plot of C/O against C/N does not indicate a

trend within the unaged samples, yet for the accelerated aged samples the values correlate and C/O decreases with decreasing C/N, Figure 5.4.30. This indicates that most dyeing and mordanting processes had a negligible effect on the surface chemistry of wool after accelerated ageing, yet significantly affected the surface chemistry of wool before ageing. The C/N ratios of historic fibres were generally in the same range as C/N of accelerated aged fibres while the C/O values for historic fibres were slightly lower, Figure 5.4.30, indicating similar surface carbon content but further surface oxidation. ToF-SIMS analysis revealed a complete loss of surface lipids for the historic wool (see Investigation of fibre surface chemistry using ToF-SIMS, page178). The high C/N values, i.e. relative to C/N of epicuticle amino acids, may be partially explicable due to the photo-oxidative loss of nitrogen containing basic amino acids arginine, lysine and histidine, however, the bulk of excess carbon is probably due to contamination; see hydrocarbon signals in ToF-SIMS analysis.

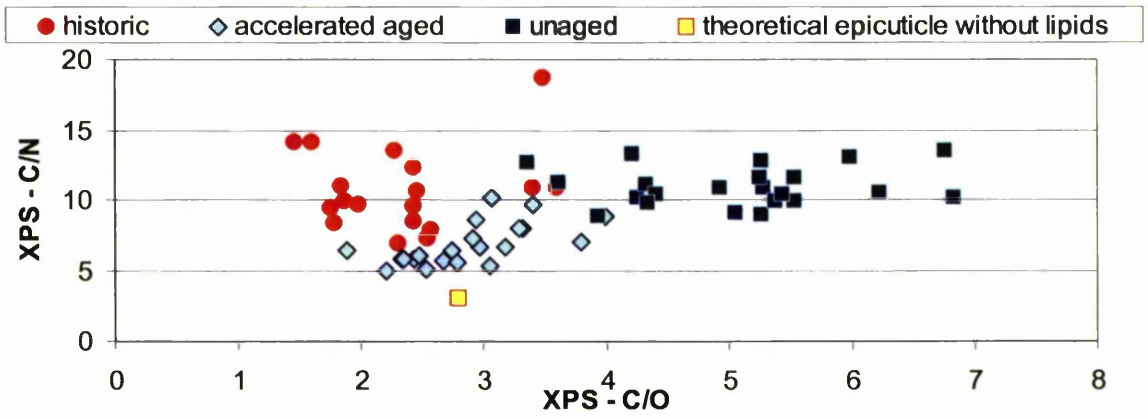

Figure 5.4.30. Correlation between C/O and C/N ratios

Figure 5.4.31 shows the average C/O and C/N ratios calculated for all analysed model wool fabrics and arranged by decreasing C/O ratio of unaged samples. Undyed wool exhibits the highest C/O value, showing the least surface oxidation, while the four black dyed samples, Yellow/W1, Green/W1 and the red samples with lye are located towards the right hand side of the graph indicating significant processing induced oxidation. This can be attributed to the severe dyebath conditions, i.e. high alkalinity for Yellow/W1, Green/W1 and the lye (K_2CO_3) treatments and prolonged dyeing time at low pH for the black recipes.

Further examination of Figure 5.4.31 shows that accelerated ageing caused the C/O ratios to decrease by varying amounts, generally, the higher the initial C/O the

higher the decrease and the lower the initial C/O the lower the further decrease, resulting in a reduced spread of C/O values in accelerated aged samples. This was also observed in tensile strength tests where the initial variations of unaged wool samples diminished after ageing, Figure 5.4.5.

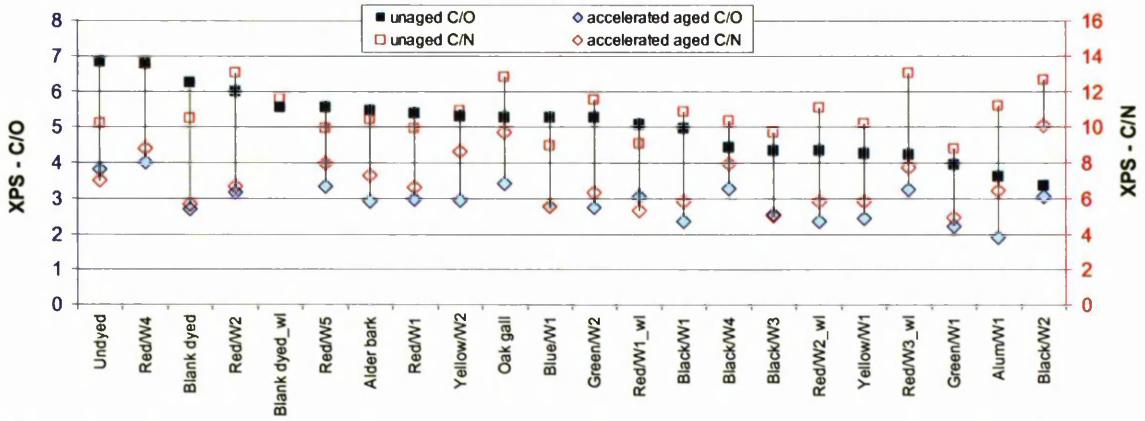

Figure 5.4.31. C/O and C/N ratios of unaged and accelerated aged wool fabrics

Accordingly, the plot of C/O ratio against tensile strain shows a simple correlation for the unaged samples but is reduced to a cluster without any particular trend for the accelerated aged wool, Figure 5.4.32. Therefore, the C/O value may be a useful indicator of the general degradational state of wool fibres, in particular for processing induced degradation of modern fibres, but it lacks the sensitivity for discrimination between accelerated aged wool. The C/N is lower for accelerated aged wool than for unaged wool but within these groups the value does not show any correlation with tensile strain, making it an ineffective indicator of damage.

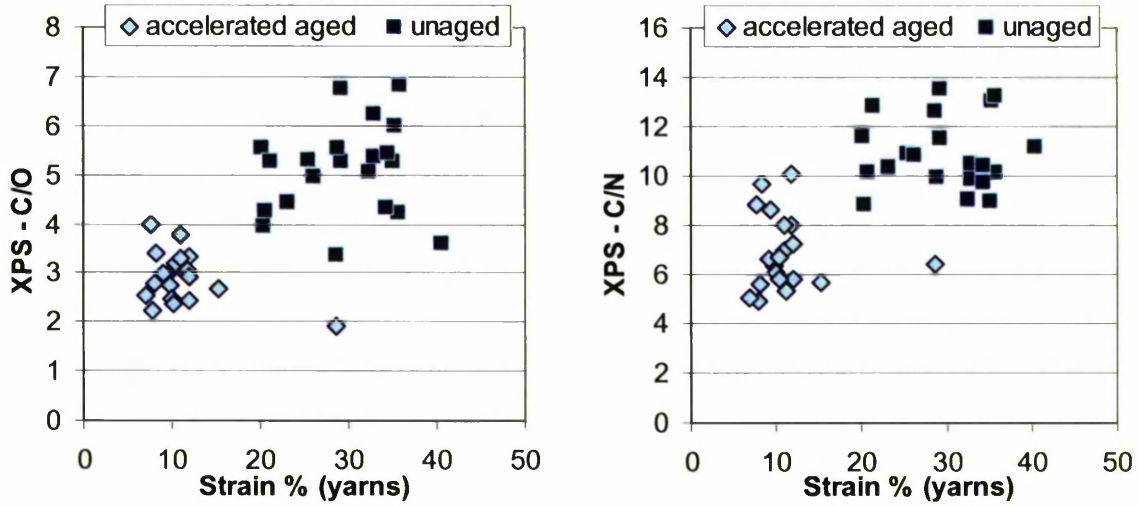

Figure 5.4.32. Correlation between atomic % ratios C/O and C/N with tensile strain

5.4.9. XPS of wool: interpretation of the N/S and C/S ratios

Both the nitrogen and the sulphur signal originate from the proteinaceous part of the wool surface. The N/S and C/S ratios of unaged, accelerated aged and historic wool are listed in Tables 5.4.12 and 5.4.13. The theoretical N/S and C/S ratios as calculated from the epicuticle composition, Table 5.1.4, are N/S = 3.4 and C/S = 11.1, however, the C/S ratio for the wool surface is much higher due to carbon contribution from the lipid layer. In this study the average N/S ratio for unaged wool fibres was 2.5 and increased to 6.1 following accelerated ageing, demonstrating significant depletion of sulphur. Similarly, the average C/S ratio increased from 26.9 to 41.5, again indicating sulphur depletion as well as insignificant lipid removal, which would lead to a lower hydrocarbon and higher sulphur contribution. Both the N/S and C/S ratios for unaged wool are in the same range as the respective values found in the literature on XPS analysis of untreated wool, Table 5.4.6. The N/S and C/S ratios of most historic fibres were similar to those found for unaged wool, Table 5.4.14.

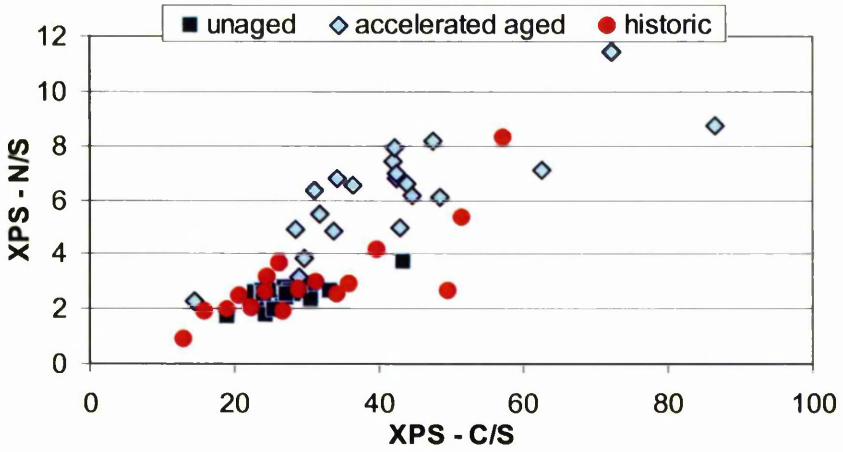

Table 5.4.14. Correlation between N/S and C/S ratios

This could suggest that accelerated ageing caused further depletion of sulphur than natural ageing. However, the total sulphur content on most historic and accelerated aged fibres was similar, on average 2.3 and 2.1 atomic % respectively; while the total nitrogen was considerably lower on historic fibres, on average 6 atomic % opposed to 8.8 atomic % on accelerated aged fibres. Likewise, the total carbon content was lower on historic fibres than on accelerated aged fibres, possibly due to the loss of the lipid layer.

5.4.10. XPS of wool: interpretation of the S(2p) peak shape

Sulphur in wool is present in the amino acid cysteine and its disulphide form cystine as well as in thioester linkages of lipids on the epicuticle surface. The covalent cystine disulphide bonds play a major role in the mechanical strength of wool fibres. Photo-oxidation causes the scission of these bonds and formation of cysteic acid, see Scheme 5.1.5, page 108. Thereby sulphur undergoes a transition in oxidative state from S^{2+} to S^{6+}. In the XP spectrum this is reflected in the S(2p) shift to higher binding energy from S^{2+} at 164 eV to S^{6+} at 168 eV. This is exemplified in Figure 5.4.33. The S(2p) spectra were curve fitted using Gaussian-Lorentzian (50) peak shape and full width half maximum values between 1.3-1.8. Due to spin orbit splitting each peak consists of two components, S(2p) 3/2 and S(2p) 1/2. Their relative ratio is always 2:1 with a gap in binding energy of 1.2 eV.

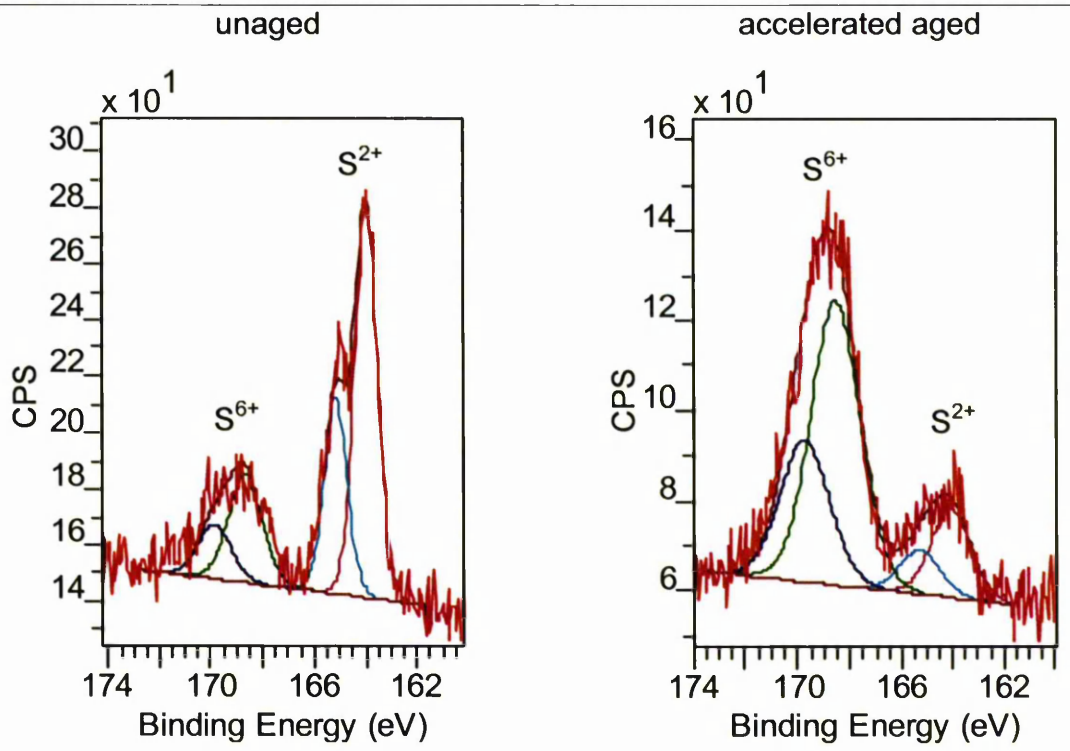

Figure 5.4.33. XPS high resolution sulphur S(2p) spectra of wool

The relative percentages of the S(2p) components were calculated from high resolution spectra as well as wide scans. In most cases the results differed by <5% and were averaged. For samples with differences > 5% the components of the less noisy and better resolution peak were measured and the other disregarded. Results from multiple analyses of the same samples were averaged

and the values given in Table 5.4.15. On average 17% of the surface sulphur is oxidised on unaged samples. The relatively high content of oxidised sulphur on Alum /W is most probably due to residues from the mordanting procedure with alum ($AlK(SO_4)_2$). The proportion of oxidised sulphur increased to an average of 74% due to accelerated ageing and 82% due to natural ageing.

Table 5.4.15. XPS S(2p) results of model and historic wool in total atomic % (S) and relative % of peak components (S^{2+} and S^{6+})

Sample	unaged			accelerated aged			Sample	historic		
	S	S^{2+}	S^{6+}	S	S^{2+}	S^{6+}		S	S^{2+}	S^{6+}
Undyed	3.3	89.2	10.8	2.1	26.6	73.4	BRU1a_8	1.3	23.5	76.5
Blank dyed	2.6	87.6	12.4	1.5	27.3	72.7	BRU2_23	2.5	13.7	86.3
Blank dyed_wl	1.8	81.5	18.5				BRU3_15	2.0	4.2	95.8
Alum	3.6	60.9	39.1	3.8	8.7	91.3	BXL1_5	4.9	1.1	98.9
Alder bark	2.6	84.1	15.9	1.5	25.4	74.6	HCP 112_C4	2.0	23.8	76.2
Oak gall	3.1	92.1	7.9	1.1	38.6	61.4	HCP 115_C4	2.0	16.2	83.8
Black/W1	2.7	90.9	9.1	1.9	31.0	69.0	HCP 126_C1	0.8	27.1	72.9
Black/W2	2.2	62.1	37.9	2.3	25.4	74.6	HCP 133_C1	0.3	21.6	78.4
Black/W3	3.0	87.8	12.2	1.8	22.6	77.4	HCP 157_B6	0.5	17.8	82.2
Black/W4	2.6	82.1	17.9	2.3	30.7	69.3	HCP 18_G4	1.4	34.5	65.5
Blue/W1	3.2	79.3	20.7	1.7	23.2	76.8	HCP 33_G4	2.3	29.8	70.2
Green/W1	3.0	79.2	20.8	1.8	22.0	78.0	HCP 45_F4	1.7	26.1	73.9
Green/W2	2.8	82.5	17.5	0.9	21.2	78.8	HCP 56_E1	1.9	24.8	75.2
Red/W1	2.9	87.0	13.0	1.6	34.0	66.0	HCP 90_D4	1.8	32.9	67.1
Red/W1_wl	3.1	86.8	13.2	1.5	28.1	71.9	HRP1_1	2.4	19.4	80.6
Red/W2	3.0	89.1	10.9	1.5	21.4	78.6	HRP1_21	2.4	25.0	75.0
Red/W2_wl	2.6			1.3	21.7	78.3	HRP1_22	1.8	24.4	75.6
Red/W3_wl	2.3	74.3	25.7	2.4	21.5	78.5	HRP1_3	0.6	17.4	82.6
Red/W4	3.2	88.7	11.3	1.2	26.5	73.5	HRP1_46	3.0	36.6	63.4
Red/W5	2.8	86.2	13.8	1.4	32.3	67.7	HRP2_21	1.1	24.3	75.7
Yellow/W1	3.1	82.7	16.3	2.1	22.6	77.4	HRP2_38	2.5	22.0	78.0
Yellow/W2	2.8	84.0	16.0	1.6	32.8	67.2	HRP2_61	1.6	33.3	66.7
							HRP2_62	1.1	22.1	77.9
							HRP3_19	4.1	2.1	97.9
							PNM2_27	2.1	7.1	92.9
							PNM5_15	1.8	17.9	82.1
							PNM7_7	3.4	15.9	84.1
							PNM9_13	3.0	7.7	92.3
							PNM9_20	2.3	12.4	87.6

The oxidised S(2p) % of historic samples is in the same range as that of accelerated aged samples and clearly distinct from the value for unaged wool, which suggests this value as a good indicator of general degradational state. Furthermore, the quantification of surface sulphur of wool is less affected by contamination than the quantification of carbon as was confirmed by the similarities between the XPS S(2p) analysis results of uncleaned and heptane extracted historic samples. In contrast to the carbon ratios which showed great disparities with considerably higher C/O, C/N and C/S values for historic samples

which had not been heptane extracted, see tables of XPS results in the appendix sections D.1. and D.3.

A plot of oxidised S(2p) % against yarn tensile strain shows an overall trend but does not have the sensitivity to distinguish between samples within the clusters of unaged and accelerated aged wool, Figure 5.4.34. However, a plot of oxidised S(2p) % against tensile strain measured in single fibre tensile strength tests suggests a more direct correlation of increasing relative percent oxidised sulphur with decreasing strain, Figure 5.4.35.

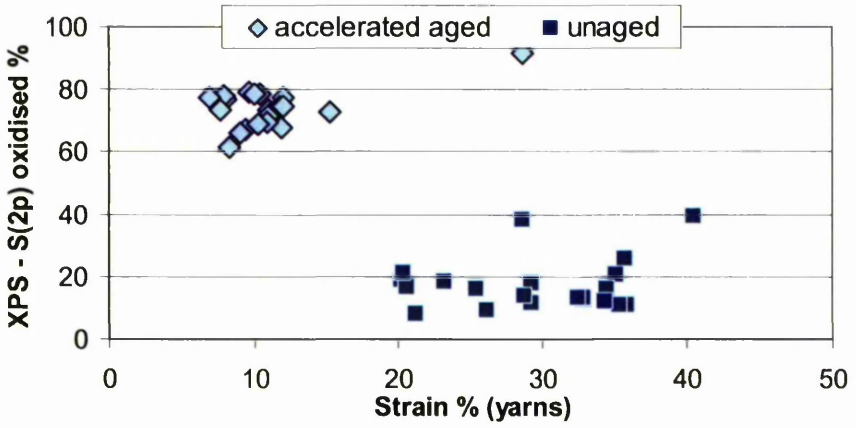

Figure 5.4.34. Correlation between relative % oxidised sulphur and tensile strain

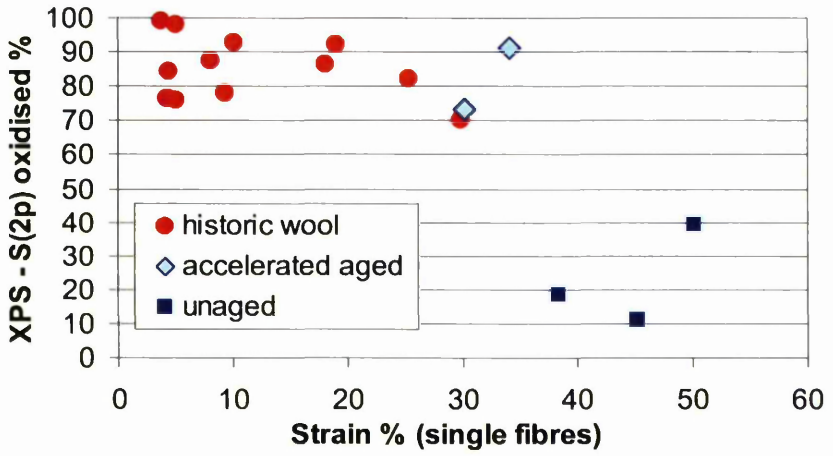

Figure 5.4.35. Correlation between relative % oxidised sulphur and tensile strain

5.4.11. XPS analysis of silk

XPS analysis for this study focused on wool fibres and only few samples of undyed silk were analysed. It was decided to concentrate the XPS analyses on wool fibres because the sulphur rich keratin protein allows the quantification of the oxidised sulphur peak component which was identified as the most promising indicator of fibre degradation. Sulphur concentration in silk fibroin is inherently too small making unambiguous quantification of its individual peak components unfeasible. The use of carbon ratios as damage indicators was also investigated for wool fibres but these values are susceptible to contamination.

The quantified atomic % and elemental ratios are listed in Table 5.4.16. The obtained results varied from the values given in the literature [103], Table 5.4.6. In particular nitrogen and oxygen were present in lower concentrations and carbon showed higher concentration. It is unclear whether this is due to carbonaceous contamination or an intrinsic difference in the analysed silk.

The nitrogen to sulphur ratio increased upon accelerated ageing, indicating the depletion of sulphur. Surface sulphur was in its oxidised form even before accelerated ageing, Figure 5.4.36 (b); this is consistent with Shao's findings [103].

Accelerated ageing also caused changes in the carbon to oxygen ratio and the carbon peak shape reflecting the increase in carbonyl and carboxyl groups, Figure 5.4.36 (a). The carbon peak components were not quantified because XPS high resolution scans of the silk surfaces suffered from charging.

The total carbon atomic % and the carbon to nitrogen ratio experienced a decrease due to accelerated ageing; this has previously been attributed to the oxidative removal of amorphous material from the silk surface which contains high amounts of the carbon rich amino acid tyrosine, [103].

Table 5.4.16. XPS results of model silk fabric

Sample	O1s	N1s	C1s	S2p	Si2p	Ca2p	C/O	C/N	C/S	N/S
Unaged	16.7	3.4	73.1	0.4	4.8	1.6	4.4	21.6	182.4	8.5
Unaged	16.8	3.6	73.1	0.3	4.7	1.6	4.4	20.5	219.4	10.7
Accelerated aged (back)	19.4	4.1	70.1	0.3	4.6	1.6	3.6	17.2	258.5	15.1
Accelerated aged (back)	19.1	4.1	70.0	0.4	4.8	1.6	3.7	17.2	188.1	10.9
Accelerated aged (front)	23.8	7.4	60.7	0.4	6.9	0.8	2.5	8.2	150.1	18.3
Accelerated aged (front)	24.0	7.6	60.2	0.5	7.1	0.7	2.5	7.9	125.9	15.9

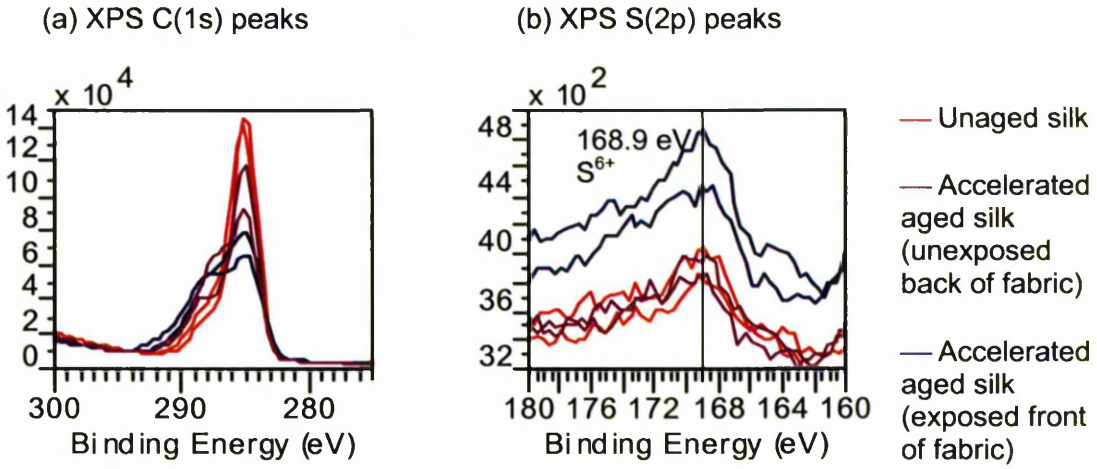

Figure 5.4.36. Carbon and sulphur peaks of unaged and accelerated aged silk

5.4.12. Investigation of fibre surface chemistry using ToF-SIMS

Unaged, accelerated aged and historic wool samples were analysed by ToF-SIMS to study the influence of some dyeing processes and accelerated / natural ageing on the lipid layer and sulphur containing residues as well as the potential of the technique for the identification of natural dyes on the fibre surfaces. This latter aspect was discussed in Chapter 4. Analysis of Dyestuffs.

ToF-SIMS spectra were acquired on two different instruments using a caesium mono-atomic primary ion beam and a bismuth cluster primary ion beam. Cluster ion sources achieve higher secondary ion yields than mono-atomic ion primary sources and the Bi_3^+ cluster ion appears to be especially efficient in the analysis of organic samples [154, 155]. The semi-quantification of the mass spectra acquired with the different primary ion sources is, therefore, not directly comparable but similar trends were noted and are discussed below. All ToF-SIMS spectra of wool are represented in the appendix sections E.1. and E.2.

5.4.13. Interpretation of the positive ion ToF-SIMS spectra

A typical positive ion ToF-SIMS spectrum of wool is represented in Figure 5.4.37. Hydrocarbon species in the region m/z 15^+ to 69^+ as well as sodium and potassium at m/z 23^+ and m/z 39^+ were present on all unaged, accelerated aged and historic wool samples, with sample HCP 90_D4 showing exceptionally high intensity for Na^+ and accordingly low intensities for the hydrocarbon species. The peak area ratios of Na^+ to hydrocarbon indicated a marked increase of Na^+ at the

wool surface after accelerated ageing, possibly caused by sodium ion migration from the bulk of the fibre, Table 5.4.17. XPS analysis also showed the presence of sodium on several historic wool samples although sodium was not detected in XPS analysis of unaged and accelerated aged wool. However, the primary XPS peak for sodium is Na(1s) and occurs at 1072 eV and with that lies outside the scan range used for all unaged and accelerated aged samples and most historic samples, which was generally 0-1000 eV.

Ward et al., and Brack at al. demonstrated that nitrogen containing compounds associated with protein show even mass numbered peaks at m/z 18^+, 28^+ , 30^+, 42^+, 44^+, 56^+ and 70^+ in the ToF-SIMS spectrum of lipid depleted wool [15, 19]. In this study the area ratios of the protein series to the hydrocarbon series stayed comparatively constant after accelerated ageing but showed higher values for the historic samples (for samples analysed with a Cs^+ primary ion beam only), indicating further surface hydrocarbon, i.e. lipid, depletion in the historic wool making the bulk protein more accessible to ToF-SIMS analysis, Table 5.4.17.

Wool wax contains significant quantities of cholesterol which is readily detectable by ToF-SIMS analysis at m/z 369^+, attributed to its fragmentation ion $[M\text{-}OH]^+$ ($C_{27}H_{45}$) [156, 157]. The signal was present in all spectra of model unaged and aged samples but was not detected on the historic samples with the exception of HRP1_1. Table 5.4.17 shows the peak area ratio of cholesterol relative to the total ion intensity. All samples analysed with a Cs^+ primary ion beam show a clear reduction in the signal intensity due to accelerated ageing, while with the Bi_3^+ analyses the trend is somewhat unclear, with the Undyed and the Red/W1_wl samples showing an increase in the m/z 369^+ ion and the Yellow/W1 showing a decrease after ageing. The reason for these discrepancies is unknown and was especially surprising due to the clearer cholesterol signal in the Bi_3^+ primary ion analyses as compared to the Cs^+ primary ion analyses where the m/z 369^+ ion was surrounded by similarly intense signals at one mass unit interval from m/z 364^+ to 371^+ and further peak clusters between m/z 300^+ - 400^+, Figure 5.4.37 and Figure 5.4.38.

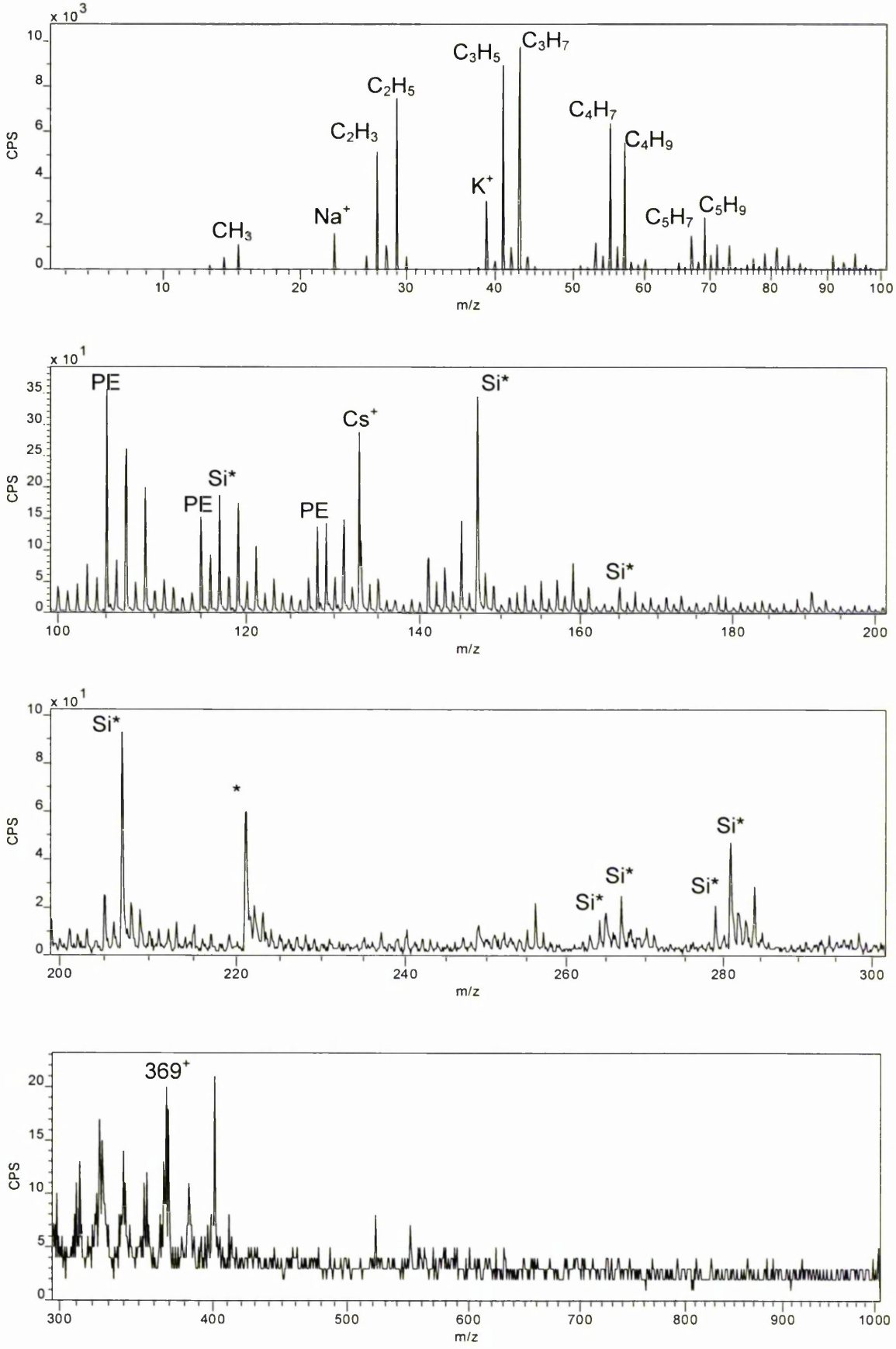

Figure 5.4.37. Positive ion ToF-SIMS spectrum of unaged undyed wool: Cs^+ primary ion analysis

Cs^+ primary ion analysis

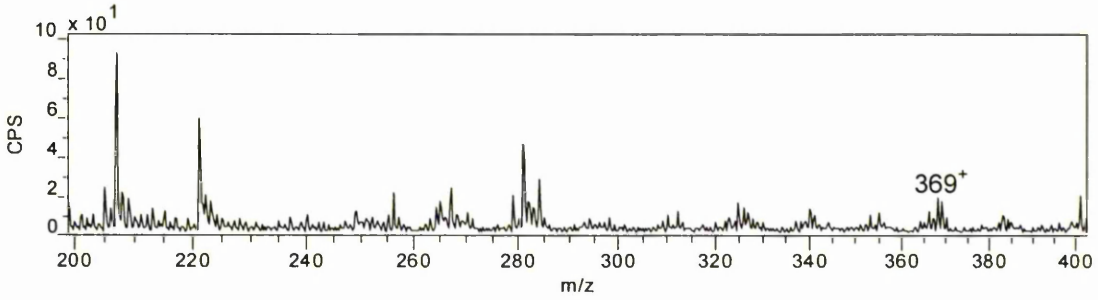

Bi_3^+ primary ion analysis

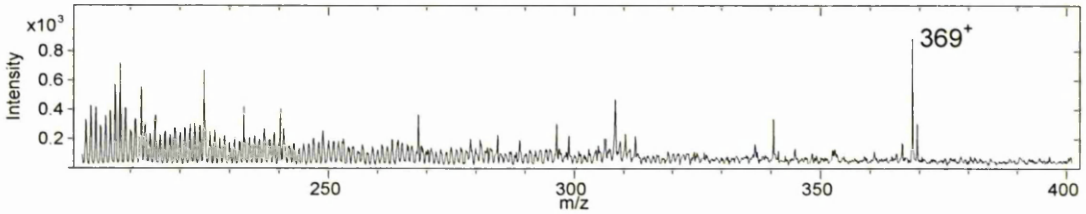

Figure 5.4.38. Positive ion spectra of undyed wool showing the cholesterol signal

Table 5.4.17. Peak area ratios of sodium, protein associated peaks and cholesterol

Sample		Unaged	Accelerated aged	Unaged	Accelerated aged	Unaged	Accelerated aged
		100 x Na / Σ hydrocarbon*		100 x Σ protein* / Σ hydrocarbon*		10^4 x sterol*/ total	
Model wool tapestry fabrics	Undyed	7.5	n.a.	11.0	n.a.	4.3	n.a.
	Undyed	4.6	18.3	11.1	9.8	3.8	1.0
	Undyed	30.5	41.1	41.5	50.6	5.0	5.8
	Alum	0.5	19.1	11.2	10.0	2.9	0.8
	Red/W4	0.2	1.6	10.8	11.2	6.4	2.5
	Blue/W1	1.2	5.6	9.7	12.0	2.0	1.2
	Green/W2	0.9	16.9	12.2	93.7	1.9	12.7
	Yellow/W1	0.7	n.a.	12.4	n.a.	3.1	n.a.
	Yellow/W1	12.1	37.8	76.3	87.6	5.7	1.6
	Red/W1	1.0	54.6	12.9	90.4	2.4	0.7
	Red/W1_wl	15.6	15.1	72.3	55.7	5.4	7.2
Historic wool samples	HCP 90_D4	146.4		15.8		n.d.	
	HRP 2_61	1.0		22.5		n.d.	
	HRP1_21	8.0		16.8		n.d.	
	HRP1_1	10.6		51.0		8.0	
	HCP_115C4	23.8		49.4		n.d.	

n.a. : Sample was not analysed; n.d. : Signal was not detected
protein* : Peak areas of m/z 18^+, 28^+, 30^+, 42^+, 44^+, 56^+ & 70^+
hydrocarbon* : Peak areas of m/z 13^+, 27^+, 29^+, 41^+, 43^+, 55^+, 57^+ & 69^+
sterol* : Peak area of m/z 369^+ cholesterol $[M\text{-}OH]^+$

= Samples analysed with a Bi_3^+ cluster primary ion source.
= Samples analysed with a Cs^+ primary ion source.

Polyethylene contamination (PE) has been identified from peaks at m/z 105^+, 115^+, 128^+ and 165^+ on most samples. Similarly, peaks at m/z 28^+, 73^+, 147^+, 207^+, 221^+, 265^+, 267^+, 279^+, 281^+, 323^+-329^+, 339^+, 341^+ and 355^+ were present on most samples and were attributed to silicon contaminations (donated Si* in Figure 5.4.37); possibly in the form of polydimethyl siloxane (PDMS) on some samples, which in addition to peaks at m/z 73^+, 147^+, 207^+, 221^+ and 281^+ showed a peak at m/z 117^+ [158, 159]. Further contamination identified on many spectra was attributed to dimethyl dialkyl quaternary ammonium with characteristic peaks at m/z 494^+, 522^+ and 550^+.

Samples Blue/W1 and Green/W2 had a high intensity peak at m/z 263^+. This has been assigned to indigotin from the dye stuff woad. This peak, however, was not present on the accelerated aged Blue/W1 sample, indicating that the light ageing process destroyed indigotin from the surface; this was supported by the observed colour fading. Similarly, indigotin was detected in the negative ion ToF-SIMS spectra of the unaged Blue/W1 and Green/W2 at m/z 261^- and 262^- but was not observed in the accelerated aged Blue/W1 sample. Both the unaged and accelerated aged cochineal dyed samples (Red/W4) exhibited a high intensity peak at m/z 497^+. The mass is close to that of cochineal's principal chromophore carminic acid (mass = 492). However, none of the other carminic acid containing samples (synthetic carminic acid, cochineal dyed silk, cochineal dyebath or cochineal on paper) showed similar peaks. The signal at m/z 497^+ is, therefore, attributed to an unidentified contamination, see Chapter 4. Analysis of Dyestuffs.

5.4.14. Interpretation of the negative ion ToF-SIMS spectra

A negative ion ToF-SIMS spectrum of unaged undyed wool is represented in Figure 5.4.39. In the low mass region peaks for CH^-, O^-, OH^- and C_2H^- are predominant for all samples. Furthermore, characteristic signals at m/z 42^- corresponding to $C{=}N{=}O^-$ and peaks at m/z 32^-, 33^-, 80^-, 96^- and 97^- attributed to the sulphur species S^-, SH^-, SO_3^-, SO_4^- and HSO_4^-, respectively have been observed on all wool spectra. However, the oxidised sulphur species SO_3^- and $(H)SO_4^-$ showed near background level intensities for the Cs^+ primary ion analyses of samples Yellow/W1, Red/W1_wl and the historic wool sample HCP_90_D4; while all other historic wool samples clearly showed the presence of

the oxidised sulphur species on the surface. An increase in the oxidised sulphur species SO_3^- , generally accompanied by a decrease in the non-oxidised sulphur SH^- , relative to the CNO^- signal intensity was noted for all accelerated aged samples compared to the respective unaged samples, Table 5.4.18.

Many unidentified but low intensity peaks were observed in the mass region 100-200, with peaks at m/z $121^-/122^-$, 149^-, 163^- and 183^- frequently occurring.

A signal at m/z 265^- commonly attributed to dodecyl sulphate has been detected on approximately half of all model wool samples and on all tested historic wool samples with the exception of HCP_90D4. This residual detergent contamination possibly originates from washing of the tapestries during conservation treatment; whereas, on the model samples, it may stem from the manufacturers scouring procedure and may have been partially removed during the dyeing processes.

Table 5.4.18. Peak area ratios of sulphur species

Sample		Unaged	Accelerated aged	Unaged	Accelerated aged
		100 x SH^-/CNO^-		100 x SO_3^-/CNO^-	
Model wool tapestry fabrics	Undyed	63.2	n.a.	59.7	n.a.
	Undyed	54.6	48.7	54.5	104.5
	Undyed	41.5	40.8	74.8	115.8
	Alum	68.9	58.3	89.3	111.0
	Red/W4	56.8	57.6	64.5	90.5
	Blue/W1	99.6	79.0	105.2	121.4
	Green/W2	75.7	14.3	99.0	70.8
	Yellow/W1	9.0	n.a.	6.4	n.a.
	Yellow/W1	32.4	16.9	100.0	110.3
	Red/W1	80.0	8.5	46.5	93.7
	Red/W1_wl	64.9	77.7	65.3	125.8
Historic wool samples	HCP_90D4	78.5		14.8	
	HRP 2_61	17.4		105.5	
	HRP1_21	64.2		119.5	
	HRP1_1	10.9		79.9	
	HCP_115C4	11.6		74.3	

n.a. : Sample was not analysed

= Samples analysed with a Bi_3^+ cluster primary ion source.

= Samples analysed with a Cs^+ primary ion source.

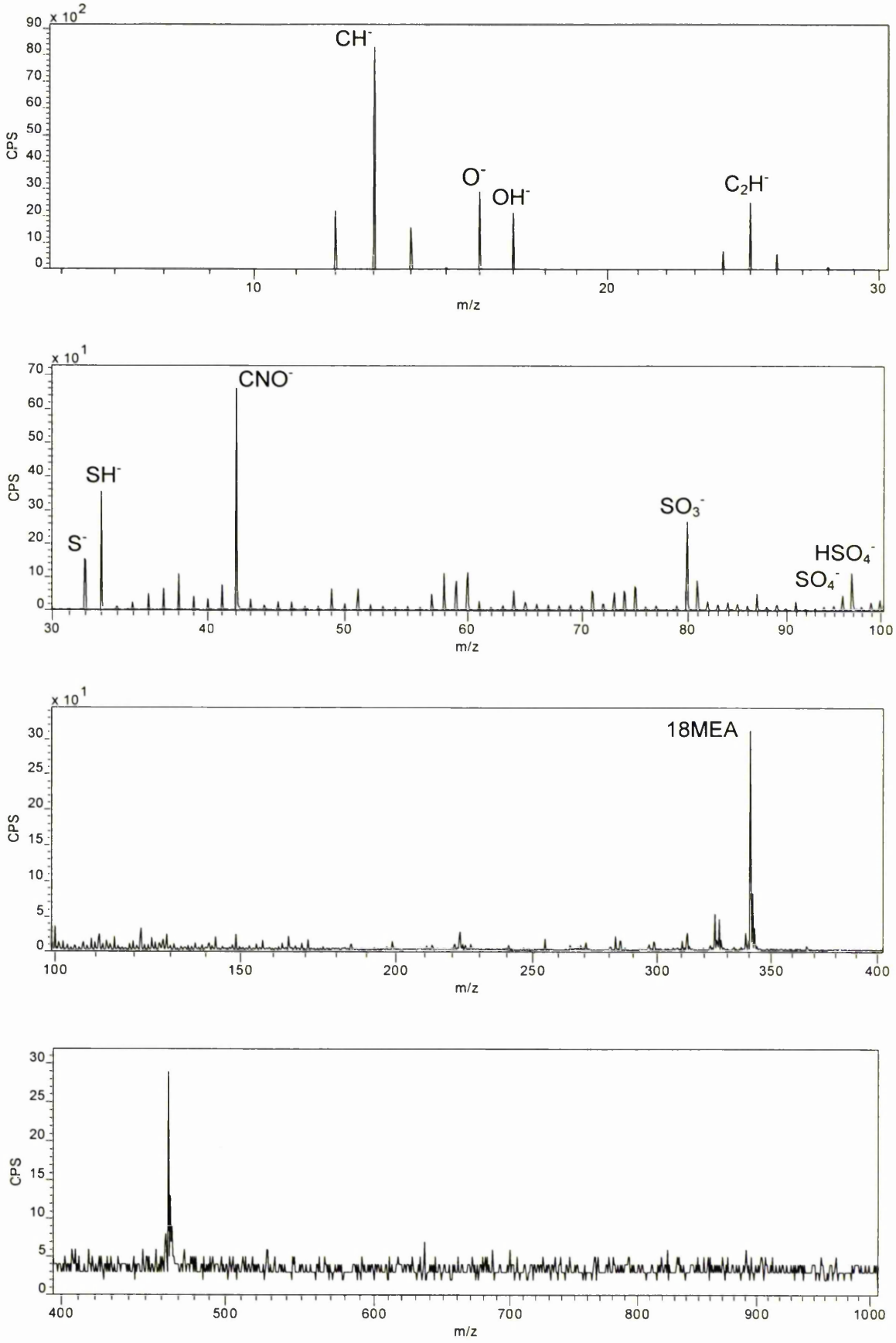

Figure 5.4.39. Negative ion ToF-SIMS spectrum of unaged undyed wool : Cs^+ primary ion source

The major peaks associated with lipids, i.e. stearic acid, oleic acid, eicosanoic acid and methyleicosanoic acid (18MEA) in their carboxylic and thiocarboxylic forms have been observed on all unaged and accelerated aged wool samples with the exception of sample Yellow/W1 where 18MEA was not detected on the unaged sample (Cs^+ primary ion analysis) and the aged sample (Bi_3^+ primary ion analysis). 18MEA was also not detected on the analysed historic wool samples, Table 5.4.19. For the unaged model tapestry sample Yellow/W1 the absence or relatively low intensity of the 18MEA signal (Cs^+ and Bi_3^+ analyses, respectively) can be attributed to the severe dyeing procedure, which involved treatment at high pH at high temperatures. The absence of lipid signals on all historic wool spectra suggests the destruction and complete removal of surface lipids due to natural ageing. Generally, accelerated ageing also caused a decrease in the surface lipid signal intensities. Peak area ratios of the predominant lipid 18MEA relative to the CNO^- signal and the total signal intensity are shown in Table 5.4.19.

Table 5.4.19. Peak area ratios of 18MEA

Sample		Unaged	Accelerated aged	Unaged	Accelerated aged
		100 x 18MEA/CNO^-		100 x 18MEA/Total*	
Model wool tapestry fabrics	Undyed	89.5	n.a.	1.80	n.a.
	Undyed	20.6	75.4	0.73	1.68
	Undyed	68.6	11.4	1.32	0.58
	Alum	95.1	54.9	1.57	0.85
	Red/W4	122.2	123.0	2.57	2.45
	Blue/W1	59.5	49.2	0.66	0.42
	Green/W2	46.4	2.1	0.68	0.04
	Yellow/W1	n.d.	n.a.	n.d.	n.a.
	Yellow/W1	11.4	n.d.	0.15	n.d.
	Red/W1	49.5	1.0	0.76	0.04
	Red/W1_wl	160.5	72.1	2.36	0.52
Historic wool samples	HCP 90_D4	n.d.			
	HRP 2_61	n.d.			
	HRP1_21	n.d.			
	HRP1_1	n.d.			
	HCP_115C4	n.d.			

n.a. : Sample was not analysed
n.d. : 18MEA was not detected
Total*: Total area of m/z 0-1000

= Samples analysed with a Bi_3^+ cluster primary ion source.
= Samples analysed with a Cs^+ primary ion source.

For all Bi_3^+ primary ion analyses the accelerated aged samples show a distinct reduction in the 18MEA signal relative to the respective unaged samples, with 18MEA being reduced to below the detection limit for the weld dyed sample (Yellow/W1). The trend is not as clear, however, for the samples analysed with a

Cs^+ primary ion beam. The ratios decreased for the alum mordanted and woad dyed wool samples (Alum and Blue/W1), stayed comparatively constant for cochineal dyed wool (Red/W4) and increased for the undyed wool sample.

Cs^+ primary ion analyses did not show any lipid signals for those samples where a signal for 18MEA was absent, while the Bi_3^+ primary ion analyses showed signals for other lipids, in particular the carboxylic 18MEA at m/z 325^- and carboxylic eicosanoic acid at m/z 311^-, as well as a signal at m/z 339^-. This latter signal was always present as a minor component in the peak cluster around 18MEA at m/z 341^-. Table 5.4.20 shows that the signal at m/z 325^- was generally present at a higher intensity than signals at m/z 311^- and 339^- and all three signals experienced reduction due to accelerated ageing.

Table 5.4.20. Area ratios of lipid associated peaks

Sample		Unaged	Accelerated aged	Unaged	Accelerated aged	Unaged	Accelerated aged
		100 x (m/z 339^-) / Total*		100 x (m/z 325^-) / Total*		100 x (m/z 311^-) / Total*	
Model wool tapestry fabrics	Undyed	0.20	n.a.	0.34	n.a.	0.11	n.a.
	Undyed	0.30	0.17	0.73	0.53	0.20	0.19
	Undyed	0.13	0.13	0.24	0.24	0.08	0.14
	Alum	0.12	0.07	0.29	0.28	0.08	0.04
	Red/W4	0.30	0.21	0.72	0.72	0.24	0.26
	Blue/W1	0.59	0.35	0.54	0.37	0.21	0.13
	Green/W2	0.17	0.05	0.31	0.09	0.10	0.06
	Yellow/W1	n.d.	n.a.	n.d.	n.a.	n.d.	n.a.
	Yellow/W1	0.11	0.06	0.15	0.07	0.11	0.06
	Red/W1	0.10	0.05	0.19	0.06	0.07	0.06
	Red/W1_wl	0.13	0.05	0.30	0.09	0.10	0.06
Historic wool samples	HCP 90_D4	n.d.		n.d.		n.d.	
	HRP 2_61	n.d.		n.d.		n.d.	
	HRP1_21	n.d.		n.d.		n.d.	
	HRP1_1	0.06		0.06		0.05	
	HCP_115C4	0.06		0.05		0.06	

n.a. : Sample was not analysed; n.d. : Signal was not detected
Total* : Total area from m/z 0-1000

= Samples analysed with a Bi_3^+ cluster primary ion source.
= Samples analysed with a Cs^+ primary ion source.

For the Bi_3^+ primary ion analyses the relative decrease of peak intensities following accelerated ageing was highest for the 18MEA peak at m/z 341^-, while m/z 339^-, 325^- and 311^- showed lower decreases, Table 5.4.21. However, peaks at m/z 339^- in conjunction with m/z 325^- and 311^- may also be attributed to alkylbenzene

sulfonate surfactant contamination with alkyl chain lengths of C_{13}, C_{12} and C_{11}. As the mass to charge ratios of the aforementioned fatty acids and the surfactant are identical, unambiguous identification would only be possible by high resolution mass spectral analysis.

Table 5.4.21. Rate of decrease in lipids due to accelerated ageing calculated from Bi_3^+ primary ion analysed unaged and aged samples

Samples	$(x)_{un}$ / $Total_{un}$ / $(x)_{ag}$ / $Total_{ag}$			
	x = m/z 341$^-$	x = m/z 339$^-$	x = m/z 325$^-$	x = m/z 311$^-$
Undyed	2.28	1.02	1.01	0.55
Yellow/W1	∞	1.89	2.29	2.04
Red/W1_wl	4.49	2.55	3.24	1.65

$(x)_{un, ag}$: Lipid peak area on unaged and aged sample
$Total_{un, ag}$: Total area from m/z 0-1000 on unaged and aged sample

The results support the above stated hypothesis that accelerated ageing reduces the surface lipid content but does not cause complete lipid removal, see section 5.4.8. XPS of wool: interpretation of the C/O and C/N ratios. Furthermore, the findings indicate that the oxygen ester bound 18MEA and eicosanoic acids may be more resistant to photo-oxidative degradation than the thioester bound 18MEA wool lipid.

For all Cs^+ primary ion analyses, with the exceptions of the unaged and accelerated aged Blue/W1 samples, those samples which showed the major lipid peaks also showed a series of peaks with 14 mass units intervals from m/z 129$^-$ to 325$^-$; with m/z 325$^-$, 311$^-$, 297$^-$, 283$^-$, 269$^-$ and 255$^-$ being associated with the major saturated carboxylic fatty acids and the repeating pattern of peaks suggesting a further nine fatty acids with a CH_2 stepwise decrease in chain lengths, Figure 5.4.40. The two aforementioned wool samples which did not show the peak series at m/z 129$^-$ to 141$^-$ (unaged and accelerated aged Blue/W1) both exhibited a strong signal at m/z 183$^-$ followed by series of low intensity peaks at 14 mass units intervals from m/z 183$^-$ to 337$^-$. The peak at m/z 281$^-$ has previously been attributed to the unsaturated carboxylic oleic acid and the regular pattern of peaks observed in this study suggests that these peaks are also associated with different chain lengths unsaturated carboxylic fatty acids, Figure 5.4.41. The additional saturated peak series was also observed on the undyed unaged, Red/W1_wl unaged and aged and the Yellow/W1 aged samples analysed with the Bi_3^+ primary ion source, while the unsaturated series was detected on the Yellow/W1 unaged and, less obvious, on the Yellow/W1 aged, undyed aged and Green/W2 aged samples. Sample Red/W1 aged and the historic samples did not exhibit either of

the additional fatty acid series. The suggested additional peak assignments for fatty acids are listed together with previously identified fatty acids in Table 5.4.22. Whether these additional fatty acids originated through desorption and ionisation processes during ToF-SIMS analysis or are inherent to the wool surface is not clear.

Table 5.4.22. Fatty acids identified in the ToF-SIMS spectra of wool surfaces

Fatty acid species	**Trivial Name**	**Chemical Formula**	**SIMS peak (m/z)** **• saturated series** *** unsaturated series** xxx previously assigned [19, 44, 84, 85] **xxx proposed assignment**
Docosanoic acid		$C_{21}H_{41}COO^-$	337 *
18MEA		$C_{19}H_{39}COS^-$	341
		$C_{22}H_{43}COO^-$	325 •
Heneicosanoic acid		$C_{20}H_{39}COO^-$	323 *
Eicosanoic acid	Arachidic acid	$C_{19}H_{39}COS^-$	327
		$C_{21}H_{41}COO^-$	311 •
		$C_{19}H_{37}COO^-$	309 *
Nonadecanoic acid		$C_{18}H_{37}COS^-$	313
		$C_{20}H_{39}COO^-$	297 •
		$C_{18}H_{35}COO^-$	295 *
Octadecanoic acid	Stearic acid	$C_{17}H_{35}COS^-$	299
		$C_{19}H_{37}COO^-$	283 •
	Oleic acid	$C_{17}H_{33}COS^-$	297
		$C_{19}H_{35}COO^-$	281 *
Heptadecanoic acid		$C_{16}H_{33}COS^-$	285
		$C_{18}H_{35}COO^-$	269 •
		$C_{16}H_{31}COO^-$	267 *
Hexadecanoic acid	Palmitic acid	$C_{15}H_{31}COS^-$	271
		$C_{17}H_{33}COO^-$	255 •
		$C_{15}H_{29}COO^-$	253 *
Pentadecanoic acid		$C_{14}H_{29}COO^-$	241 •
		$C_{14}H_{27}COO^-$	239 *
Butadecanoic acid	Myristic acid	$C_{13}H_{27}COO^-$	227 •
		$C_{13}H_{25}COO^-$	225 *
Tridecanoic acid		$C_{12}H_{25}COO^-$	213 •
		$C_{12}H_{23}COO^-$	211 *
Propadecanoic acid	Lauric acid	$C_{11}H_{23}COO^-$	199 •
		$C_{11}H_{21}COO^-$	197 *
Undecanoic acid		$C_{10}H_{21}COO^-$	185 •
		$C_{10}H_{19}COO^-$	183 *
Decanoic acid	Capric acid	$C_9H_{19}COO^-$	171 •
Nonanoic acid		$C_8H_{17}COO^-$	157 •
Octanoic acid	Caprylic acid	$C_7H_{15}COO^-$	143 •
Heptanoic acid		$C_6H_{13}COO^-$	129 •

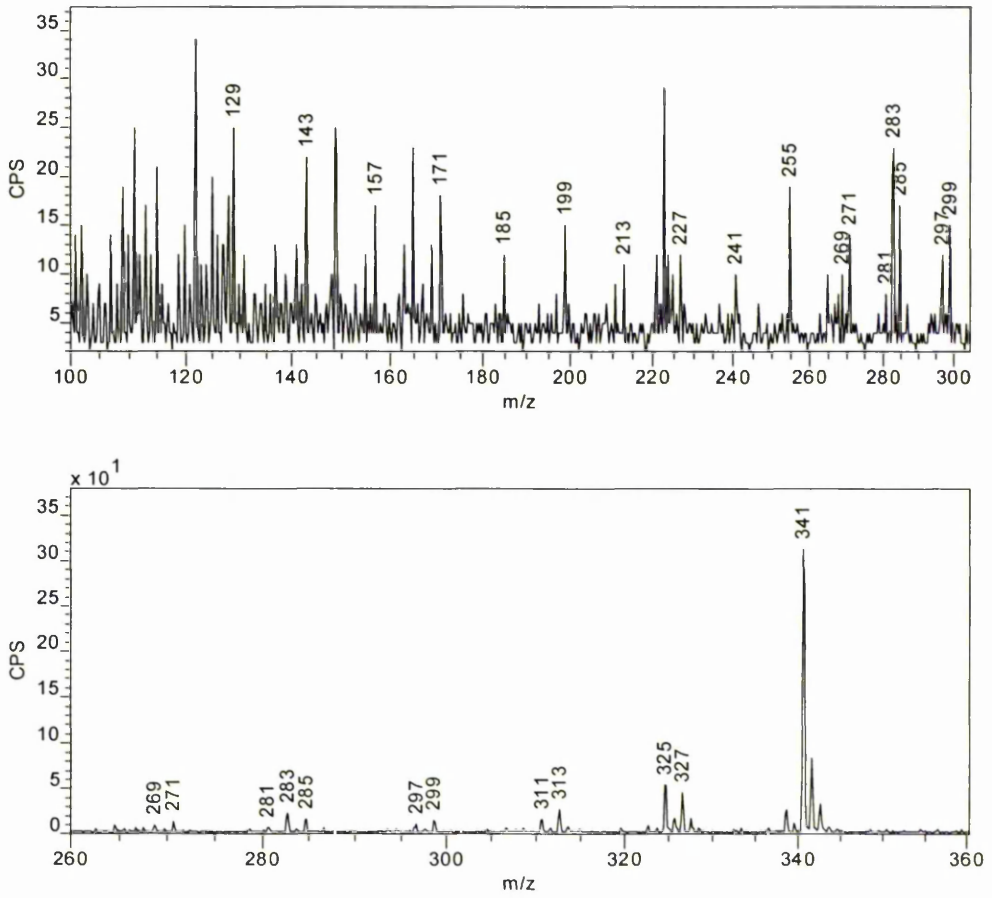

Figure 5.4.40. Negative ion ToF-SIMS spectra of unaged wool showing the saturated fatty acid series

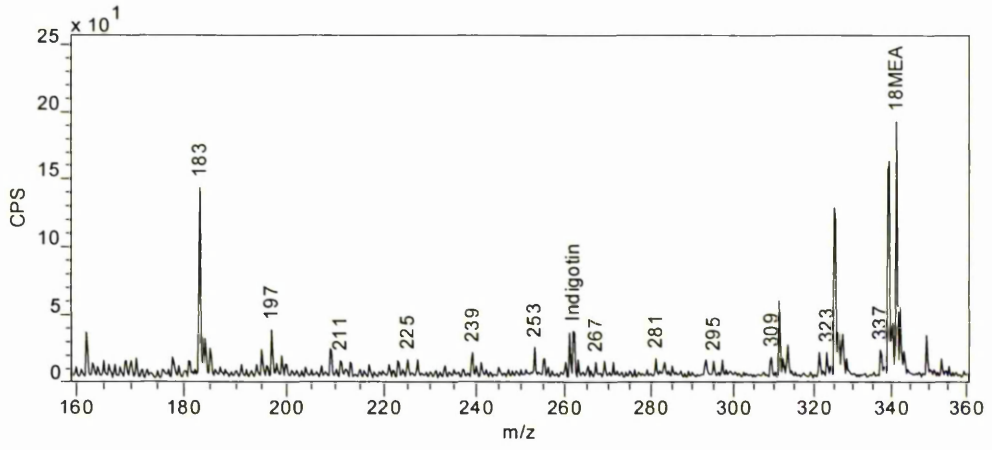

Figure 5.4.41. Negative ion ToF-SIMS spectrum of Blue/W1 showing the unsaturated fatty acid series

5.5. Conclusions

Wool and silk yarns have been mordanted and dyed according to historic recipes and woven into tapestry structures which closely resemble historic tapestry weaves. Model tapestry fabrics were accelerated aged with simulated sunlight and their surface and fracture morphology as well as surface chemistry compared to historic samples and where possible linked to tensile strength values obtained from tensile tests of yarns and single fibres.

Tensile strength tests showed that many mordanting and dyeing procedures had a strong influence on the initial tensile properties of wool but, on the whole, did not significantly affect the extent of degradation due to subsequent accelerated ageing. Alkali hydrolysis was attributed to the initial losses in tensile strength and extensibility of wool dyed at high pH, in particular the weld dyeings. Effects of metal ion complexing were discussed in terms of the changes observed in tensile properties of wool and silk treated with aluminium, iron and copper ions. Especially alum mordanting was identified to have a strengthening effect while dyeings with weld and dyers greenweed, oak gall mordanting and black dyeing procedures significantly weakened the fibres. In contrast, tensile properties of silk were largely unaffected by dyeing and mordanting procedures but showed greater variability after accelerated ageing. The black ferrous sulphate dyeings with an oak gall mordant were found to initially weaken the fibres but impart a photo-protective effect, resulting in a lower rate of degradation in accelerated ageing for both wool and silk.

A method for single fibre tensile strength testing suitable for the small sample sizes of historic wool was devised and successfully tested.

SEM analysis of the surface of dyed wool showed that none of the dyestuffs had a detrimental effect on the scale structure. SEM micrographs of accelerated aged wool fibres showed substantial damage in the form of longitudinal cracks, these cracks were not observed on historic fibres and their origin is as yet unknown although some evidence for visible light irradiation damage rather than thermal damage was given. The surface morphologies of historic fibres were mainly indistinguishable from modern fibres, with intact scale structures. However, some fibres, in particular samples taken from the front of historic tapestries, showed transverse cracks and scale flaking to the extent of complete loss of scales.

A wide range of fracture morphologies was observed in all wool samples with radial and granular breaks being predominant. A possible increase in brittle breaks was observed for the samples dyed with the highest amount of ferrous sulphate and was attributed to metal complex formation. Fracture morphologies of historic wool fibres showed a similar distribution of fracture types as unaged and accelerated aged fibres.

Surface morphology analysis of silk fibres indicated that all dyeing procedures caused localised surface damage in the form of peeling of thin strips of material off the otherwise smooth surface. Both accelerated aged and historic fibres showed areas with longitudinal cracks and some transverse cracks observed on historic silk only. Fracture morphologies were found to be mainly radial and granular with some axial step breaks and in contrast to expectations brittle breaks were not observed in either unaged or accelerated aged silk.

Though interesting and informative, SEM analysis was found to be too subjective and equivocal as a suitable method for objective damage assessment of historic fibres due to the similarities observed between unaged and historic fibres and the irregularities observed within samples, i.e. many unaged and historic fibres were indistinguishable by their surface and fracture morphologies and most samples exhibited areas with and without visible damage, making an objective assessment of extent and type of damage unfeasible.

XPS analysis has been performed on unaged and accelerated aged wool and historic fibres. The effects of mordant and dye treatments and accelerated ageing were evaluated by comparison of relative elemental ratios and changes in the carbon and sulphur peak shapes. Surface oxidation and lipid removal were reflected in decreasing ratios of carbon to oxygen, carbon to nitrogen and the hydrocarbon to oxidised carbon peak components. The carbon to oxygen ratio in particular showed good correlation with tensile strain for the unaged wool samples, indicating processing induced damage. None of the carbon ratios, however, possessed the sensitivity to distinguish between accelerated aged samples when plotted against tensile properties.

The quantification of oxidised sulphur relative to non-oxidised sulphur is theoretically linked to tensile strength since the covalent disulphide bonds in wool rupture on oxidation and thereby decrease the fibre's cohesion. The oxidised

percentage of surface sulphur was found to be similar for accelerated aged and historic wool and clearly distinct from unaged wool. The value showed the same simple correlation with yarn tensile strain as was identified for the carbon ratios, yet assessment of the relationship between oxidised sulphur percentage with strain from single fibre tensile strength tests showed improved correlation and suggests the usefulness of the parameter as a marker of damage for historic wool fibres. A further advantage of the quantification of sulphur is its relatively low susceptibility to contamination compared to quantification of carbon, as carbonaceous contaminants prevail.

The carbon to sulphur ratios and the similarly low atomic % of sulphur on accelerated aged and historic samples signified comparable loss of sulphur due to accelerated and natural ageing, while the carbon to nitrogen and nitrogen to sulphur ratios and the relatively low atomic % of nitrogen on historic samples suggested a higher loss of nitrogen due to natural ageing as compared to accelerated ageing.

XPS analysis of undyed unaged and accelerated aged silk also showed surface oxidation and removal of carbonaceous material, possibly a tyrosine rich amorphous layer, due to accelerated ageing. Surface sulphur was found to be present in its oxidised state even before accelerated ageing and experienced a decrease relative to nitrogen which showed increased signal intensities after accelerated ageing.

ToF-SIMS analysis confirmed the relative increase of oxidised sulphur species, i.e. cysteic acid, on the accelerated aged and historic wool surfaces. Accelerated ageing was shown to reduce the relative amount of fatty acids, in particular the major wool lipid 18MEA which was not detected on historic wool samples indicating the further degradation of the historic wool compared to the accelerated aged wool. Analysis with a Bi_3^+ primary ion beam indicated the presence of some oxygen-ester bound lipids on samples which were depleted of 18MEA, suggesting their increased resistance to degradation over the thioester bound 18MEA. Additional peaks attributable to series of saturated and unsaturated fatty acids have been identified at lower masses than the previously established wool lipid assignments.

5.6. References

1. Rippon, J.A., 'The Structure of Wool', in *Wool Dyeing*, (ed.) D.M. Lewis, Society of Dyers and Colourists (1992) 1-51.
2. Maclaren, J.A. and B. Milligan, *Wool Science - The Chemical Reactivity of the Wool Fibre*, Science Press (1981) 1-16.
3. Jones, L.N., D.E. Rivett, and D.J. Tucker, 'Wool And Related Mammalian Fibres', in *Handbook of Fibre Chemistry*, (ed.) M. Lewin and E.M. Pearce, Marcel Dekker, Inc., New York (1998) 378.
4. Speakman, J.B., 'The chemistry of wool and related fibres', *Journal of the Textile Institute* **32** (1941) T83-T108.
5. Leeder, J.D., L.A. Holt, J.A. Rippon, and I.W. Stapleton, 'Diffusion of Dyes and Other Reagents Into the Wool Fibre', in *Proceedings of the 8th International Wool Textile Research Conference, Vol.VI*, Christchurch, New Zealand, 7-14 Feb. 1990, ed. G.H. Crawshaw, Wool Research Organisation of New Zealand, 227-238.
6. Leeder, J.D. and R.C. Marshall, 'Readily-Extracted Proteins from Merino Wool', *Textile Research Journal* **52** (4) (1982) 245-249.
7. Zahn, H., F.J. Wortmann, and H. Höcker, 'Chemistry and the Structure of Wool', *Chemie in Unserer Zeit* **31** (6) (1997) 280-290.
8. Gillespie, J.M., A. Broad, and P.J. Reis, 'Further Study on the Dietary-Regulated Biosynthesis of High-Sulphur Wool Proteins', *Biochemical Journal* **112** (1969) 41-49.
9. Powell, B.C., 'The Keratin Proteins and Genes of Wool and Hair', *International Journal of Sheep and Wool Science* **44** (2) (1996) 100-118.
10. Shao, J., C.J. Hawkyard, and C.M. Carr, 'Investigation into the Effect of UV/Ozone Treatments on the Dyeability and Printability of Wool', *Journal of the Society of Dyers and Colourists* **113** (4) (1997) 126-131.
11. Phan, K.-H., H. Thomas, and E. Heine, 'Structure of the Cuticle of Fine Wool Fibres', in *Proceedings of the 9th International Wool Textile Research Conference, Vol. II*, Biella, Italy, 28 June - 5 July 1995, International Wool Secretariat, 19-30.
12. Allen, C.F., S.A. Dobrowski, P.T. Speakman, and E.V. Truter, 'Evidence for Lipid and Filamentous Protein in Allworden Membrane', in *Proceedings of the 7th International Wool Textile Research Conference, Vol. I*, Tokyo, August 1985, Society of Fiber Science and Technology, 143-151.
13. Swift, J.A. and J.R. Smith, 'Microscopical Investigations on the Epicuticle of Mammalian Keratin Fibres', *Journal of Microscopy* **204** (3) (2001) 203-211.
14. Jones, L.N. and D.E. Rivett, 'The Role of 18-Methyleicosanoic Acid in the Structure and Formation of Mammalian Hair Fibres', *Micron* **28** (6) (1997) 469-485.
15. Brack, N., R. Lamb, D. Pham, and P. Turner, 'XPS and SIMS Investigation of Covalently Bound Lipid on the Wool Fibre Surface', *Surface and Interface Analysis* **24** (10) (1996) 704-710.
16. Leeder, J.D., 'The Cell Membrane Complex and its Influence on the Properties of the Wool Fibre', *Wool Science Review* **63** (October) (1986) 1-35.
17. Swift, J.A. and A.W. Holmes, 'Degradation of Human Hair by Papain', *Textile Research Journal* **35** (11) (1965) 1014.
18. Carr, C.M., I.H. Leaver, and A.E. Hughes, 'X-ray Photoelectron Spectroscopy Study of the Wool Fibre Surface', *Textile Research Journal* **56** (7) (1986) 457-461.
19. Ward, R.J., H.A. Willis, G.A. George, G.B. Guise, R.J. Denning, D.J. Evans, and R.D. Short, 'Surface-Analysis of Wool by X-Ray Photoelectron-Spectroscopy and Static Secondary-Ion Mass-Spectrometry', *Textile Research Journal* **63** (6) (1993) 362-368.
20. Nakamusa, Y., Y. Hatayama, T. Okazaki, H. Ito, and A. Watanabe, 'Surface Properties of Wool Cuticle as Compared with those of Gelatine Film', in *Proceedings of the 6th International Wool Textile Research Conference, Vol. II*, Pretoria, 26 Aug.-3 Sept. 1980, CSIR, 273-284.

21. King, N.L.R. and J.H. Bradbury, 'The Chemical Composition of Wool, V: The Epicuticle', *Australian Journal of Biological Sciences* **21** (1968) 375-384.

22. Carr, C.M., I.H. Leaver, and A.E. Hughes, 'X-ray Photoelectron Spectroscopy Study of the Wool Fibre Surface', *Textile Research Journal* **56** (1986) 457-461.

23. Bauters, M. and P. Ponchel, 'Behaviour of the Exo and Endo Cuticle at the Time of Various Treatments on Wool', in *Proceedings of the 6th International Wool Textile Research Conference, Vol. II*, Pretoria, 26 Aug.-3 Sept. 1980, CSIR, 309-321.

24. Knott, J., M. Belly, and H. Zahn, 'Seperation of Cuticle from Wool by Mechanical Treatments', in *Proceedings of the 6th International Wool Textile Research Conference, Vol. II*, Pretoria, 26 Aug.-3 Sept. 1980, CSIR, 93-107.

25. Ley, K.F. and W.G. Crewther, 'The Proteins of Wool Cuticle', in *Proceedings of the 6th International Wool Textile Research Conference, Vol. II*, Pretoria, 26 Aug.-3 Sept. 1980, CSIR, 13-28.

26. Körner, A., H. Schmidt, T. Merten, S. Peters, H. Thomas, and H. Höcker, 'Changes in the Content of 18-MEA in Wool after UV-Irradiation and Corona Treatment', in *Proceedings of the 9th International Wool Textile Research Conference, Vol. II*, Biella, Italy, 28 June - 5 July 1995, International Wool Secretariat, 414-419.

27. Dai, X.J., F.M. Elms, and G.A. George, 'Mechanism for the Plasma Oxidation of Wool Fiber Surfaces from XPS Studies Of Self-Assembled Monolayers', *Journal of Applied Polymer Science* **80** (9) (2001) 1461-1469.

28. Zahn, H., H. Messinger, and H. Höcker, 'Covalently Linked Fatty Acids at the Surface of Wool: Part of Cuticle Cell Envelope', *Textile Research Journal* **64** (9) (1994) 554-555.

29. Millard, M.M., 'Analysis of the Surface Oxidized Wool Fibre by X-ray Electron Spectrometry', *Analytical Chemistry* **44** (1972) 828-829.

30. Millard, M.M., 'Surface Analysis of Plasma Treated Wool Fibres by X-ray Photoelctron Spectrometry', in *Proceedings of the 5th International Wool Textile Research Conference, Vol. II*, Aachen, Germany, 2-11 September 1975, ed. K. Ziegler, Deutsches Wollforschungsinstitut, 44-53.

31. Carr, C.M., S.F. Ho, D.W. Lewis, E.D. Owen, and M.W. Roberts, 'Photoelectron Spectroscopy and the Surface Chemistry of Wool', *Journal of the Textile Institute* **76** (6) (1985) 419-424.

32. Carr, C.M., I.H. Leaver, and A.E. Hughes, 'Detection and Analysis by XPS of Sulfhydryl Groups at the Surface of Wool Fibers', *Textile Research Journal* **56** (3) (1986) 216-17.

33. Carr, C.M., J.C. Evans, and M.W. Roberts, 'An X-ray Photoelectron and Electron Spin Resonance Study of Wool Treated with Aqueous Solutions of Chromium and Copper Ions', *Textile Research Journal* **57** (1987) 109-113.

34. Dowling, L.M., L.N. Jones, I.H. Leaver, and A.E. Hughes, 'TEM and X-Ray Photoelectron Spectroscopic Studies of Wool Fibers after Cuticle Removal', *Textile Research Journal* **58** (11) (1988) 640-5.

35. Bradley, R.H., I.L. Clackson, and D.E. Sykes, 'UV Ozone Modification of Wool Fiber Surfaces', *Applied Surface Science* **72** (2) (1993) 143-147.

36. Bradley, R.H., I.L. Clackson, and D.E. Sykes, 'XPS of Oxidized Wool Fiber Surfaces', *Surface and Interface Analysis* **22** (1994) 497-501.

37. Carr, C.M., K.J. Dodd, M.A. Connors, A. Henderson, and J. Vickerman, 'The Effect of Corona Treatments on the Hygral Expansion of Wool Worsted Fabrics', *Journal of the Society of Dyers and Colourists* **110** (12) (1994) 383-6.

38. Kidd, B., C.M. Carr, K.J. Dodd, J. Vickerman, and K. Byrne, 'X-Ray Photoelectron Spectroscopic Study of Wool Modified by Gaseous Fluorine', *Textile Research Journal* **65** (9) (1995) 504-506.

39. Klausen, T., H. Thomas, and H. Höcker, 'Influence of Oxygen Plasma Treatment on the Chemical and Morphological Changes of the Wool Fibre Surface', in *Proceedings of the 9th International Wool Textile Research Conference, Vol. II*, Biella, Italy, 28 June - 5 July 1995, International Wool Secretariat, 241-248.

40. Horr, T.J., 'Determining the Lipid Layer Thickness on Wool Fiber Surfaces Using XPS', *Textile Research Journal* **66** (2) (1996) 122-122.

41. StJohn, H.A.W. and G.A. George, 'Determining the Lipid Layer Thickness on Wool Fiber Surfaces Using XPS - Reply', *Textile Research Journal* **66** (2) (1996) 122-122.

42. Bradley, R.H. and I. Mathieson, 'Chemical Interactions of Ultraviolet Light with Wool Fiber Surfaces', *Journal of Colloid and Interface Science* **194** (2) (1997) 338-343.

43. Bradley, R.H., I. Mathieson, and K.M. Byrne, 'Spectroscopic Studies of Modified Wool Fiber Surfaces', *Journal of Materials Chemistry* **7** (12) (1997) 2477-2482.

44. Shao, J., D.C. Jones, R. Mitchell, J.C. Vickerman, and C.M. Carr, 'Time-of-Flight Secondary-Ion-Mass Spectrometric (ToF-SIMS) and X-Ray Photoelectron Spectroscopic (XPS) Analyses of the Surface Lipids of Wool', *Journal of the Textile Institute* **88** (4) (1997) 317-324.

45. Brack, N., R. Lamb, D. Pham, and P. Turner, 'Nonionic Surfactants and the Wool Fibre Surface', *Colloids and Surfaces, A: Physicochemical and Engineering Aspects* **146** (1-3) (1999) 405-415.

46. Brack, N., R.N. Lamb, D. Pham, T. Phillips, and P. Turner, 'Effect of Water at Elevated Temperatures on the Wool Fibre Surface', *Surface and Interface Analysis* **27** (12) (1999) 1050-1054.

47. Shao, J., C.M. Carr, C.P. Rowlands, and J. Walton, 'XPS, SIMS, and ESR studies of UV/ozone-irradiated silk and wool', *Journal of the Textile Institute* **90** (4) (1999) 459-468.

48. El-Sayed, H., A. Kantouch, E. Heine, and H. Höcker, 'Developing a Zero-AOX Shrink-Resist Process for Wool. Part 1: Preliminary Results', *Coloration Technology* **117** (4) (2001) 234-238.

49. Shao, J., J. Liu, and C.M. Carr, 'Investigation into the Synergistic Effect between UV/Ozone Exposure and Peroxide Pad-Batch Bleaching on the Printability of Wool', *Coloration Technology* **117** (5) (2001) 270-275.

50. Xin, J.H., R. Zhu, J. Hua, and J. Shen, 'Surface Modification and Low Temperature Dyeing Properties of Wool Treated by UV Radiation', *Coloration Technology* **118** (4) (2002) 169-173.

51. Molina, R., P. Jovancic, D. Jocic, E. Bertran, and P. Erra, 'Surface Characterization of Keratin Fibres Treated by Water Vapour Plasma', *Surface and Interface Analysis* **35** (2) (2003) 128-135.

52. Wortmann, F.J., G. Wortmann, and H. Zahn, 'Pathways for Dye Diffusion in Wool Fibers', *Textile Research Journal* **67** (10) (1997) 720-724.

53. Anderson, C.A., D.S. Taylor, and J.D. Leeder, 'Role of Torsional Forces in Morphological Breakdown of Wool Fibers during Abrasion', *Wear* **21** (1) (1972) 115-127.

54. Fonollosa, J., L. Campos, M. Marti, A. de la Maza, J.L. Parra, and L. Coderch, 'X-ray Diffraction Analysis of Internal Wool Lipids', *Chemistry and Physics of Lipids* **130** (2) (2004) 159-166.

55. Leeder, J.D., D.G. Bishop, and L.N. Jones, 'Internal Lipids of Wool Fibers', *Textile Research Journal* **53** (7) (1983) 402-407.

56. Melhuish, W.H. and G.J. Smith, 'The Effect of Temperature on Tryptophan Luminescence in Wool Keratin', in *Proceedings of the 8th International Wool Textile Research Conference, Vol. IV*, Christchurch, New Zealand, 7-14 Feb. 1990, ed. G.H. Crawshaw, Wool Research Organisation of New Zealand, 288-296.

57. Nicholls, C.H. and M.T. Pailthorpe, 'Primary Reactions in the Photoyellowing of Wool Keratin', *Journal of the Textile Institute* **67** (1) (1976) 397-403.

58. Nilsson, R., P.B. Merkel, and D.R. Kearns, 'Unambiguous Evidence for the Participation of Singlet Oxygen in Photodynamic Oxidation of Amino Acids', *Photochemistry and Photobiology* **16** (1972) 117-124.

59. Schäfer, K., D. Goddinger, and H. Höcker, 'Photodegradation of Tryptophan in Wool', *Journal of the Society of Dyers and Colourists* **113** (12) (1997) 350-355.

60. Smith, G.J., 'New Trends in Photobiology (Invited Review) Photodegradation of Keratin and other Structural Proteins', *Journal of Photochemistry and Photobiology B-Biology* **27** (1995) 187-198.

61. Davidson, R.S., 'The Photodegradation of Some Naturally Occurring Polymers', *Journal of Photochemistry and Photobiology B-Biology* **33** (1) (1996) 3-25.

62. Holt, L.A., B. Milligan, and D.E. Rivett, 'The Role of Tryptophan in the Photochemical Crosslinking of Peptides and Proteins', in *Proceedings of the 5th International Wool Textile Research Conference, Vol. II*, Aachen, Germany, 2-11 September 1975, ed. K. Ziegler, Deutsches Wollforschungsinstitut, 559-569.

63. Holt, L.A. and P.J. Waters, 'Factors Affecting the Degradation of Wool by Light - Wavelength, Temperature, Moisture Content', in *Proceedings of the 7th International Wool Textile Research Conference, Vol IV*, Tokyo, August 1985, Society of Fiber Science and Technology, 1-10.

64. Milligan, B., 'Sunlight Yellowing of White Wool: A Complex Problem', in *Proceedings of the 6th International Wool Textile Research Conference, Vol. V*, Pretoria, 26 Aug. - 3 Sept. 1980, CSIR, 167-181.

65. Milligan, B., 'The Degradation of Automotive Upholstery Fabrics by Light and Heat', *Review of Progress in Coloration* **16** (1986) 1-7.

66. Lewis, D.M., 'Some Aspects of the Photochemisry of Fibrous Proteins', *Colourage* **36** (4) (1989) 25-31.

67. Church, J.S. and K.R. Millington, 'Photodegradation of Wool Keratin .1. Vibrational Spectroscopic Studies', *Biospectroscopy* **2** (4) (1996) 249-258.

68. Lennox, F.G., 'A Spectrophotometric Study of Yellowing in Wool Fabric', *Journal of the Textile Institute* **51** (Conference May 24) (1960) T1193-T1209.

69. Holt, L.A., B. Milligan, and W.E. Savige, 'Photoyellowing of Wool and Silk: the Effect of Converting Tryptophan to Oxindolylalanine Residues', *Journal of the Textile Institute* **68** (3) (1977) 124-126.

70. Asquith, R.S., L. Hirst, and D.E. Rivett, 'A Study of the UV Yellowing of Amino Acid, Peptides and Soluble Proteins', *Textile Research Journal* **40** (3) (1970) 285-289.

71. Holt, L.A. and B. Milligan, 'The Formation of Carbonyl Groups During Irradiation of Wool and its Relevance to Photoyellowing', *Textile Research Journal* **47** (9) (1977) 620-624.

72. Holt, L.A. and B. Milligan, 'Photo-Oxidation of the Serine, Threonine, and Cystine Side-Chains of Wool to Carbonyl Derivatives', *Textile Research Journal* **50** (6) (1980) 387-391.

73. El-Zaher, N.A. and M.N. Micheal, 'Time Optimization of Ultraviolet-Ozone Pretreatment for Improving Wool Fabrics Properties', *Journal of Applied Polymer Science* **85** (7) (2002) 1469-1476.

74. Nicholls, C.H., 'Photodegradation and Photoyellowing of Wool', in *Developments in Polymer Photochemistry*, (ed.) N.S. Allen, Applied Science Publishers (1980) 125-144.

75. Simpson, W.S., 'The Influence of pH on the Reflectance and Photostability of Wool to Sunlight', *Journal of the Textile Institute* **78** (5) (1987) 430-438.

76. Baumann, H., 'The Effect of Reactive Dyes on the Main-Chain Scission of Wool on Exposure to Light', *Journal of the Society of Dyers and Colourists* **90** (9) (1974) 326-328.

77. Weatherall, J.L., 'The Tendering of Wool by Light', in *Proceedings of the 5th International Wool Textile Research Conference, Vol. II*, Aachen, Germany, 2-11 September 1975, ed. K. Ziegler, Deutsches Wollforschungsinstitut, 580-589.

78. Meybeck, A. and J. Meybeck, 'Photo-Oxidation of the Peptide Group. II. Solid State Peptides and Polyaminoacids', *Photochemistry and Photobiology* **6** (5) (1967) 365-378.

79. Maclaren, J.A. and B. Milligan, *Wool Science - The Chemical Reactivity of the Wool Fibre*, Science Press (1981) 53-62.

80. Jones, D.C., C.M. Carr, W.D. Cooke, R. Mitchell, and J.C. Vickerman, 'The Photodegradation of Wool and Wool Blend Fabrics in Relation to Their Use in Automotive Upholstery', in *Proceedings of the 9th International Wool Textile Research Conference, Vol. IV*, Biella, Italy, 28 June - 5 July 1995, International Wool Secretariat, 245-256.

81. Baumann, H., L.D. Setiawan, and D. Gribbin, 'Surface Studies of Keratin Fibers and Related Model Compounds Using ESCA. 2 - Intermediate Oxidation Products of Cystyl Residues on Keratin Fiber Surfaces and their Hydrolytical Stability', *Surface and Interface Analysis* **8** (5) (1986) 219-25.

82. Setiawan, L.D., H. Baumann, and D. Gribbin, 'Surface Studies of Keratin Fibers and Related Model Compounds Using ESCA', *Surface and Interface Analysis* **7** (4) (1985) 188-195.

83. Tillin, S.J., A.E. Pavlath, S.H. Zeronian, and A.G. Pittmann, 'An ESCA Study of the Surface and Interior Reactive Sites in Wool Fibers', *Textile Research Journal* **50** (12) (1980) 724-7.

84. Peet, D.J., R.E.H. Wettenhall, and D.E. Rivett, 'The Chemistry of the Cuticle Surface of Keratin Fibres', *Textile Research Journal* **65** (1) (1995) 58-59.

85. Volooj, S., C.M. Carr, R. Mitchell, and J.C. Vickerman, 'Time-of-Flight Secondary Ion Mass Spectrometry (ToF-SIMS) Analysis of the Bleaching of Keratin Fibres and the Application of Cationic Alkyl Protein Softeners to Bleached Cashmere', *Surface and Interface Analysis* **29** (7) (2000) 422-430.

86. Robson, R.M., 'Silk: Composition, Structure , and Properties', in *Handbook of Fibre Chemistry*, (ed.) E.M. Pearce, Marcel Dekker, Inc., New York (1998) 415-464.

87. Bresee, R.R. and G.E. Goodyear, 'Fractography of Historic Silk Fibers', in *Historic Textile and Paper Materials* 1986, ed. H.L. Needles and S.H. Zeronian, American Chemical Society, 95-109.

88. Becker, M.A., Y. Magoshi, T. Sakai, and N.C. Tuross, 'Chemical and Physical Properties of Old Silk Fabrics + Biochemical Analysis of 17 Japanese Silk Kimono Lining Fabrics', *Studies in Conservation* **42** (1) (1997) 27-37.

89. Yanagi, Y., Y. Kondo, and K. Hirabayashi, 'Deterioration of Silk Fabrics and their Crystallinity', *Textile Research Journal* **70** (10) (2000) 871-875.

90. Becker, M.A. and N.C. Tuross, 'Initial Changes Found in Bombyx Mori Silk Fibroin', in *Silk Polymers: Materials Science and Biotechnology*, Charlottesville, Virginia, Jan. 28-29 1993, ed. D. Kaplan, et al., American Chemical Scociety, 252-269.

91. Takahashi, Y., 'Crystal Structure of Silk of Bombyx Mori', in *Silk Polymers: Materials Science and Biotechnology*, Charlottesville, Virginia, Jan. 28-29 1993, ed. D. Kaplan, et al., American Chemical Scociety, 168-175.

92. Zhou, C.-Z., F. Confalonieri, N. Medina, Y. Zivanovic, C. Esnault, T. Yang, M. Jacquet, J. Janin, M. Duguet, R. Perasso, and Z.-G. Li, 'Fine Organization of Bombyx Mori Fibroin Heavy Chain Gene', *Nucleic Acids Research* **28** (12) (2000) 2413–2419.

93. Yamaguchi, K., Y. Kikuchi, T. Takagi, A. Kikuchi, F. Oyama, K. Shimura, and S. Mizuno, 'Primary Structure of the Silk Fibroin Light Chain Determined by cDNA Sequencing and Peptide Analysis', *Journal of Molecular Biology* **210** (1) (1989) 127-139.

94. Image from: Garland Science, 'Essential Cell Biology', http://fig.cox.miami.edu (2004).

95. Das, S., 'Photodegradation and Yellowing of Silk', *Indian Textile Journal* **102** (8) (1992) 52-53.

96. Tsukada, M. and K. Hirabayashi, 'Change of Silk Fibroin Structure by Ultraviolet Radiation', *Journal of Polymer Science. Polymer Letters Edition* **18** (7) (1980) 507-511.

97. Hansen, E.F. and W.S. Ginell, 'The Conservation of Silk with Paylene-C', in *Historic Textile and Paper Materials II* 1989, ed. S.H. Zeronian and H.L. Needles, American Chemical Society, 108-133.

98. Gogoi, S., B. Baruah, and C.R. Sarkar, 'Effect of Ultra Violet Light on Silk Fabric', *Colourage* **46** (2) (1999) 23-30.

99. Kuruppillai, R.V., S.P. Hersh, and P.A. Tucker, 'Degradation of Silk by Heat and Light', in *Historic Textile and Paper Materials* 1986, ed. H.L. Needles and S.H. Zeronian, American Chemical Society, 111-127.

100. Needles, H.L., V. Cassman, and M.J. Collins, 'Mordanted, Natural-Dyes Wool and Silk Fabrics. Light and Burial-Induced Changes in the Color and Tensile Properties', in *Historic Textile and Paper Materials* 1986, ed. H.L. Needles and S.H. Zeronian, American Chemical Society, 199-210.

101. Hirabayashi, K., Y. Yanagi, S. Kawakami, K. Okuyama, and W. Hu, *Journal of Sericultural Science of Japan* **56** (1) (1987) 18-22.

102. Harris, M., 'The Photchemical Decomposition of Silk', *American Dyestuff Reporter* **23** (1934) 403-405.

103. Shao, J., J. Liu, J. Zheng, and C.M. Carr, 'X-Ray Photoelectron Spectroscopic Study of Silk Fibroin Surface', *Polymer International* **51** (12) (2002) 1479-1483.

104. Ballard, M., R.J. Koestler, C. Blair, C. Santamaria, and N. Indictor, 'Historic Silk Flags from Harrisburg', in *Historic Textile and Paper Materials II* 1989, ed. S.H. Zeronian and H.L. Needles, American Chemical Society, 134-142.

105. Ballard, M., R.J. Koestler, and N. Indictor, 'Weighted Silks Observed Using Energy Dispersive X-Ray Spectrometry', *Scanning Electron Microscopy* **II** (1986) 499-506.

106. Tímár-Balázsy, Á. and D. Eastop, *Chemical Principles of Textile Conservation*, Butterworth-Heinemann (1998) 105.

107. Hojo, N. and H. Shirai, 'Metal Complexes of Silk Protein', in *Structure of Silk Yarn. Part B: Chemical Structure and Processing of Silk Yarn*, (ed.) N. Hojo and D. Mahadevappa, Science Publishers, Inc., Enfield NH USA, Plymouth UK (2000) 135-157.

108. Shimizu, F., 'Adsorption Behaviour of Metal Ions on Silk and Their Effect on the Photo-Degradation of the Silk', in *Structure of Silk Yarn. Part B: Chemical Structure and Processing of Silk Yarn*, (ed.) N. Hojo and D. Mahadevappa, Science Publishers, Inc., Enfield NH USA, Plymouth UK (2000) 159-172.

109. Hartley, F.R., 'Uptake of Aluminium by Wool', *Australian Journal of Chemistry* **21** (4) (1968) 1013-1022.

110. Appel, W.M.D. and D.A. Jessup, 'Accelerated ageing test for weighted silk', *Journal of Research of the National Bureau of Standards* **15** (1935) 601-608. (Summary in: Leon, A., A.H. Geiger, and H. Geiger, 'Mitteilungen aus verschiedenen Gebieten', Naturwissenschaften (Historical Archive) 24 (38) (1936) 606 - 608).

111. Miller, J.E. and B.M. Reagan, 'Degradation in Weighted and Unweighted Historic Silks', *Journal of the American Institute for Conservation* **28** (2) (1989) 97-115.

112. Garside, P., L. Sophia, and P. Wyeth, 'Characterization of Historic Silk by Polarized Attenuated Total Reflectance Fourier Transform Infrared Spectroscopy for Informed Conservation', *Applied Spectroscopy* **59** (10) (2005) 1242-1247.

113. Miller, I.J. and G.J. Smith, 'Protection against Phototendering of Wool by Metal-Salts and Mordanted Dyes', *Journal of the Society of Dyers and Colourists* **111** (4) (1995) 103-106.

114. Smith, G.J., I.J. Miller, and V. Daniels, 'Phototendering of Wool Sensitized by Naturally Occurring Polyphenolic Dyes', *Journal of Photochemistry and Photobiology A-Chemistry* **169** (2) (2005) 147-152.

115. Indictor, N. and M. Ballard, 'The Effects of Ageing on Textiles that Contain Metal: Implications for Analyses', in *International Restorer Seminar*, Veszprem, Hungary: National Centre of Museums, 1-10 July 1989 1990, ed. M. Járó, Eri, Istvan, 67-75.

116. Feughelman, M., *Mechanical Properties and Structure of Alpha-Keratin Fibres*, UNiversity of New South Wales Press, Sydney (1997) 1-148.

117. Feughelman, M., 'Natural Protein Fibers', *Journal of Applied Polymer Science* **83** (3) (2002) 489-507.

118. Wortmann, F.J. and H. Zahn, 'The Stress / Strain Curve of alpha-Keratin Fibers and the Structure of the Intermediate Filament', *Textile Research Journal* **64** (12) (1994) 737-743.

119. Hearle, J.W.S., 'A Critical Review of the Structural Mechanics of Wool and Hair Fibres', *International Journal of Biological Macromolecules* **27** (2000) 123-138.

120. Pérez-Rigueiro, J., C. Viney, J. Llorca, and M. Elices, 'Silkworm Silk as an Engineering Material', *Journal of Applied Polymer Science* **70** (12) (1998) 2439-2447.

121. Pérez-Rigueiro, J., C. Viney, J. Llorca, and M. Elices, 'Mechanical Properties of Single-Brin Silkworm Silk', *Journal of Applied Polymer Science* **75** (10) (2000) 1270-1277.

122. Gohl, E.P.G., *Textile Science* 2nd edition, Longman Cheshire Pty Limited, Melbourne (1983) 68-88.

123. Maclaren, J.A. and B. Milligan, *Wool Science - The Chemical Reactivity of the Wool Fibre*, Science Press (1981) 89-105.

124. Guthrie, R.E. and S.H. Laurie, 'The Binding of Copper (II) to Mohair Keratin', *Australian Journal of Chemistry* **21** (1968) 2437-2443.

125. Kokot, S., M. Feughelman, and R.M. Golding, 'An Electron Spin Resonance Study of the Copper (II) Interaction with Wool-Keratin. Part I: An Interpretation and the Properties of a Copper (II) / Wool ESR Spectrum', *Textile Research Journal* **42** (12) (1972) 704-708.

126. Kokot, S., M. Feughelman, and R.M. Golding, 'An Electron Spin Resonance Study of the Copper (II) Interaction with Wool-Keratin. Part II: The Nature of the Copper (II) Interaction with Wool-Keratin', *Textile Research Journal* **43** (3) (1973) 146-153.

127. Kokot, S., 'Sites for Cu(II) Stabilization in Wool Keratin', *Textile Research Journal* **63** (3) (1993) 159-161.

128. Kokot, S., J. Cheng, and N. Gill, 'Comparative-Study of Metal-Ion Interactions with Wool Keratin Using Chemometrics', *Analyst* **119** (4) (1994) 677-681.

129. Sheffield, A. and M.J. Doyle, 'Uptake of Copper(II) by Wool', *Textile Research Journal* **75** (3) (2005) 203-207.

130. Brady, P.R., G.N. Freeland, R.J. Hine, and Hoskinso.Rm, 'Absorption of Certain Metal-Ions by Wool Fibers', *Textile Research Journal* **44** (10) (1974) 733-735.

131. Masri, M.S. and M. Friedman, 'Effect of Chemical Modification of Wool on Metal-Ion Binding', *Journal of Applied Polymer Science* **18** (8) (1974) 2367-2377.

132. Fukatsu, K., 'Formation of Copper(II)-Wool Keratin Complexes', *Textile Research Journal* **58** (2) (1988) 91-96.

133. Schweppe, H., *Handbuch der Naturfarbstoffe*, Nikol Verlagsgesellschaft mbH & Co. KG, Hamburg (1993).

134. Jakobiec, W., 'Weaving the Story of Tobias', *CCI Newsletter* **23** (1999) www.cci-icc.gc.ca.

135. Lemberg, M., 'The Problem of Brown Wool in Medieval Tapestries: The Restoration of the Fourth Caesar Tapestry', in *Studies in Textile History, in Memory of Harold B. Burnham*, (ed.) V. Gervers, Royal Ontario Museum, Toronto, Canada (1977) 178-183.

136. Ysselsteyn, D.G.T.v., *Tapestry*, Van Goor Zonen, The Hague, Brussels (1969).

137. Pietta, P.-G., 'Flavonoids as Antioxidants', *Journal of Natural Products* **63** (7) (2000) 1035 - 1042.

138. Leaver, I.H., 'Photooxidation and Photoreduction of Dyes in Polymers', in *Photochemistry of Dyed and Pigmented Polymers*, (ed.) A.K. Allen and J.F. McKellar, Applied Science Publishers, London (1980) 161-245.

139. Allen, A.K. and J.F. McKellar, 'Photosensitised Degradation of Polymers by Dyes and Pigments', in *Photochemistry of Dyed and Pigmented Polymers*, (ed.) A.K. Allen and J.F. McKellar, Applied Science Publishers, London (1980) 247-284.

140. NIST/SEMATECH, 'e-Handbook of Statistical Methods', http://www.itl.nist.gov/div898/handbook/ Section 1.3.6.7. Exploratory Data Analysis / Tables for Probability Distributions (2006).

141. Terashima, M., T. Imai, Y. Chonan, and K. Shirai, 'Evaluation of the Deterioration in Mink Hair under Xenon Arc Irradiation by Fourier Transform Infrared (FTIR) Microspectroscopy', *Sen-I Gakkaishi* **54** (7) (1998) 354-359.

142. Gamez-Garcia, M., 'The Cracking of Human Hair Cuticles by Cyclical Thermal Stresses', *Journal of Cosmetic Science* **49** (3) (1998) 141-153.

143. Gamez-Garcia, M., 'Cuticle Decementation and Cuticle Buckling Produced by Poisson Contraction on the Cuticular Envelope of Human Hair', *Journal of Cosmetic Science* **49** (4) (1998) 213-222.

144. Gamez-Garcia, M., 'Plastic Yielding and Fracture of Human Hair Cuticles by Cyclical Torsion Stresses', *Journal of Cosmetic Science* **50** (2) (1999) 69-77.

145. Swift, J.A., 'The Mechanics of Fracture of Human Hair', *International Journal of Cosmetic Science* **21** (4) (1999) 227-239.

146. Carr, C.M., A.M. Hacke, J. Wouters, I. Vanden Berghe, K. Hallett, M. Odlyha, A. Quye, H. McNab, A. Hulme, D.A. Peggie, and C. Herrero Carretero, 'Unpublished Presentations', in *Monitoring of Damage in Historic Tapestries, End of Project Workshop*, Hampton Court Palace, 20-21 June 2005.

147. Vanden Berghe, I. and J. Wouters, 'Identification and Condition Evaluation of Protein Fibres at the Sub-Microgram Level by Calibrated Amino-Acid Analysis', in *Scientific Analysis of Ancient and Historic Textiles: Informing Preservation, Display and Interpretation. AHRB Research Centre for Textile Conservation and Textile Studies First Annual Conference*, Textile Conservation Centre, Winchester Campus, University of Southampton, UK, 13-15 July 2004, ed. R. Janaway and P. Wyeth, Archetype Publications, 151-158.

148. Hacke, A.M. and C.M. Carr, 'Investigation into the Nature and Degradation of Historical Wool Tapestries', in *Proceedings of the 11th International Wool Textile Research Conference*, Leeds, UK, 4-9 Sept. 2005, In Press.

149. Hearle, J.W.S., B. Lomas, and W.D. Cooke, *Atlas of fibre fracture and damage to textiles* 2nd, Woodhead Publishing Limited in association with The Textile Institute, Cambridge (1998) 18, 138-151.

150. Simpson, W.S. and C.T. Page, 'Inhibition of Light Tendering of Wool', in *Proceedings of the 6th International Wool Textile Research Conference, Vol. V*, Pretoria, 26 Aug.-3 Sept. 1980, CSIR, 183-193.

151. Cooke, W.D. and D. Howell, 'Diagnosis of Deterioration in a Tapestry Using Scanning Electron Microscopy', *The Conservator* **12** (1988) 47-51.

152. Jovancic, P., D. Jocic, R. Molina, M.R. Julia, and P. Erra, 'The Combined Low-Temperature Plasma/Enzyme Wool Shrink-Resist Treatment', *AATCC Review* **3** (2) (2003) 25-28.

153. Beamson, G. and D. Briggs, 'The XPS of Polymers Database', SurfaceSpectra Ltd (2002).

154. Cheng, J. and N. Winograd, 'Looking at Surfaces with Cluster Ion Beams', *Materials Today* **9** (1-2) (2006) 50-51.

155. Touboul, D., F. Kollmer, E. Niehuis, A. Brunelle, and O. Laprevote, 'Improvement of Biological Time-of-Flight-Secondary Ion Mass Spectrometry Imaging with a Bismuth Cluster Ion Source', *Journal of the American Society for Mass Spectrometry* **16** (10) (2005) 1608-1618.

156. Batcheller, J., A.M. Hacke, R. Mitchell, and C.M. Carr, 'Investigation into the Nature of Historical Tapestries Using Time of Flight Secondary Ion Mass Spectrometry (ToF-SIMS)', in *SIMS XV, The 15th International Conference on Secondary Ion Mass Spectrometry*, Manchester, UK, 12-16 September 2005, Accepted for publication in Journal of Applied Surface Science.

157. Nygrena, H., K. Börnera, P. Malmberga, and B. Hagenhoff, 'Localization of Cholesterol in Rat Cerebellum with Imaging TOF-SIMS', in *SIMS XV, The 15th International Conference on Secondary Ion Mass Spectrometry*, Manchester, UK, 12-16 September 2005.

158. Steele, A., J.K.W. Toporske, R. Avci, C. Agee, and D.S. McKay, 'Investigation into the Contamination of Lunar return Material. Part 1. Surface Analysis and Imaging Investigations', in *32nd Lunar and Planetary Science Conference*, Houston, Texas, USA 2001, Lunar and Planetary Institute (pdf online), 1674.pdf.

159. Keune, K. and J.J. Boon, 'Enhancement of the Static SIMS Secondary Ion Yields of Lipid Moieties by Ultrathin Gold Coating of Aged Oil Paint Surfaces', *Surface and Interface Analysis* **36** (13) (2004) 1620-1628.

Chapter 6. Analysis of Metal Threads

6.1. Literature review for metal threads

6.1.1. Introduction to composition and manufacture of metal threads

Several studies on the history and provenance [1-5], structural and elemental composition [3, 6-12] and manufacturing methods [11-16] have described five categories for the incorporation of metal in textiles, Table 6.1.1.

Table 6.1.1. Categories for the inclusion of metal in textiles

I.	Metal applied (with adhesive) to already woven fabric
II.	Metal wire or flattened strips
III.	Metal wire or strips wound around a fibre core
IV.	Metallic surface applied (with adhesive) to an organic wrapping wound around fibre core
V.	Metallic surface applied (with adhesive) to organic strips

Metal threads may have been manufactured in the Middle East as long ago as the 3rd millennium BC. By the 5th century BC tapestries with metal threads were woven in the Eastern Mediterranean [7]. One of the earliest accounts of the use of metal threads stems from the Old Testament, Exodus, Chapter 39: *"...and made the holy garments for Aaron... And he made the ephod (vestment) of gold, blue and purple, and scarlet and fine twined linen. And they did beat the gold into thin plates, and cut it into wires, to work it in the blue, and in the purple..."*.

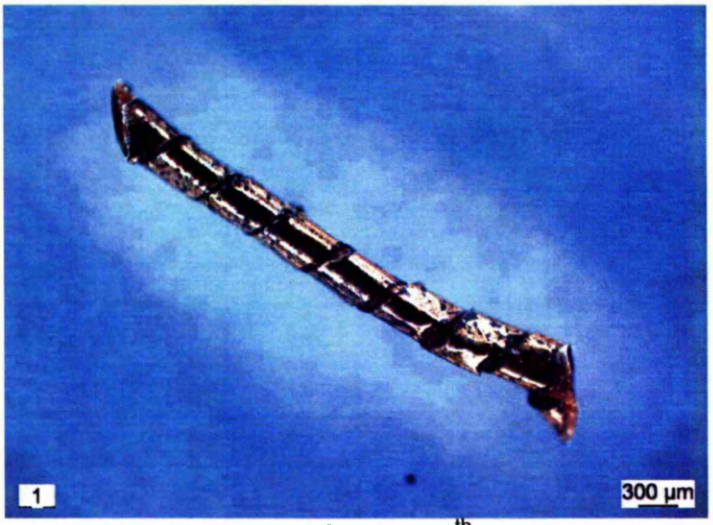

Figure 6.1.1. Category III metal thread from a 16th century tapestry

6.1.2. 'Beaten and Cut' metal threads

It is believed that the earliest metal threads were of the so called 'beaten and cut' type where blocks of gold or single-sided gilt silver were beaten into thin sheets and subsequently cut into filaments. These could be incorporated into textiles as category II or III threads, Table 6.1.1., a technique that was presumably already used in ancient Egypt [11]. According to Járó in Europe in the 5th to 8th centuries metallic decorations on textiles were mostly strips cut from gold foils that were directly incorporated into the textile by weave or embroidery techniques, though some early examples of metal threads with a fibrous core and metallic wrapping have been found [4, 11]. Geijer and Thomas describe an early 3rd century textile fragment found in a Roman sarcophagus in Hungary. The tapestry weave contained gold threads with a silk core of brownish-red or purple colour [17]. Another example of early wound metal threads are the 4th century remains of gold filament wrappings from a grave of a woman at London's Spitalfield market [18]. At that time category III threads might have been imported from the East. The technique of wrapping 'beaten and cut' gold strip around a silk core was the most common during the 9th and 10th centuries, with some late examples of pure gold threads being found in the 11th and 12th century Hungarian coronation mantle and coronation vestments [19] and some early examples of gilt silver threads being found in a 10th century German relic pouch [11]. Gilt silver foil was produced from the 9th century but its use for solid metal filaments became wide spread only in the 11th or 12th century [15, 19]. During the 11th century these threads were made in England, suggesting that the method was known in Europe before that date. The geographical assignment for manufacturing centres and the methods used for gilding the silver are not certain.

The making of palm-sized gold foils has been described in some ancient and medieval manuscripts, e.g. Papyrus Leiden (Egyptian hieroglyphs), Old Testament (Exodus, Chapter 39), Lucca manuscript (8th century) and Theophilus Presbyter's Schedula Diversarum Artium (12th century). The gold foils may have been joined to longer foils which were then cut into narrow strips for winding around a fibrous core. Indeed, Theophilus Presbyter is said to describe a method of soldering silver and gold foils together and hammering them into bands for cutting into narrow strips [20]. It is not unanimously identified what type of tool was utilized for the cutting of gold strips, nor is the method of winding the metal filament around the fibrous core recognized [4]. However, Karen Finch's unpublished translation of

a Danish book by Sofus Larsen (1939) gives detailed descriptions of the processes involved in the production of precious metal threads [21]. The following quotes are courtesy of Karen Finch.

> Late Longobardian (6th -8th century) Latin document, found in Lucca by L.A. Muratori – Antiquitates Italiae Medii Aevi, in Bibliotheca Capituli Canonicorum Lucensium: *"How to prepare a gold leaf of a consistency fit to make gold thread. Beat a long thin bar of gold and when it has been beaten out lengthways, fold it and beat the double thickness together. Do not beat on the fold. Open the gold and fold it in three layers, beat it again till it gets the desired size, measure it, even it out with a wooden mallet and then make the one piece into three leaves of three handbreadth in length. Trim with a pair of long thin very fine scissors. Next put the leaves on top of each other and stretch them with an iron hammer (sic) in this way the leaves shall be of the same size. Heat an oven with charcoal and put the leaves in until they are heated through. Throw water over them to make them lustrous and colour them with a solution of vinegar and (dragant). Use a feather to distribute the solution between the leaves. Wash in clean water and separate the leaves for drying. Rub them when dry with goat's hair and cut into strips. 12 strips for embroidery should be equal in weight to 15 strips for weaving."* [21]
>
> Descriptions of techniques for the preparation of gilded lamella by Vanoccio Biringuccio, 'Pirotechnia', Venice 1540 and Etienne Binet (pseudonym Francois Réne), 'Essay des Merveilles de Nature', Rouen, 1622: *"First the gold and silver to be used had to be refined to perfection and the silver made into a narrow bar ready for gilding on one side only. The preparations had to follow specific rules to ensure that the gilding would last, beginning with meticulous cleaning of both the silver bar and the gold leaf. With the fusion successfully achieved came the really difficult task of beating the gilded bar into leaf. The bar would be put on a special anvil in a wooden frame shaped according to whether it was going to be flattened lengthways or sideways. Often the bar had to be annealed several times before it reached a certain stage, when it would be folded. The beating continued till the double leaf reached the desired size. The leaf was never beaten on the gilded side, which throughout was protected between layers of paper of fine cloth or parchment. Sometimes, despite the most careful preparations, the gold would turn mat and the work would then be scrapped. When the beating was successfully accomplished, the thin gilded leaves of exactly similar size would be handed over to the women cutters, whose expertise with their curiously shaped scissors turned the leaf into not quite millimetre wide lamella ready for spinning. {...} The final purpose of this great and elaborate work is the fine and polite delusion of making a gold thread that will cover 200 times as much silver and silk as its weight in gold and yet seem to be made wholly of gold."* [21]

6.1.3. 'Membrane' metal threads

In the 11th or 12th centuries membrane threads consisting of a gilt or silvered membrane filament wound around a core of linen, silk or cotton (category IV and V, Table 6.1.1.) became commonly available. Membrane threads were more flexible than solid metal threads, thus facilitating the weaving and in addition reducing the weight and the cost of gold fabrics. The so called "Cyprus gold" began to spread from Byzantium, western Asian or north African regions by trade coming through the ports of Cyprus [1, 7]. Levantine traders of the eleventh century introduced the "Cypriot gold" also known as "skin gold" or "membrane gold" and occasionally mentioned in inventories as "brocatum ad aurum de opere cyprese", "opus cyprese", "aurum filatum cyprese" or "or de chypre", while "Aurum filatum de opere Romanie" is a membrane metal thread from Byzantium distinguished by the use of a yellow silk core, lower gold content and narrower filament width than the Cyprus gold [1]. However, the term "Cyprus Gold" is contentious and may refer to a type of gold thread with a copper bulk; in fact the word copper itself is derived from the Greek word for the island "Kupros" due to its abundance of copper mines [22]. This is also supported by a 16th century source cited in Karen Finch's translation [21].

> H.O. Hildebrandt, 'Sveriges Medeltid' Part I and II, Stockholm 1884-1898 quotes a Swedish embroiderer Lambertus employed by Hans Brask, Bishop of Linköping 1524: *"Insegold is the best among spun gold and the best of insegold is spun on red silk, because it holds its colour. One Inse should weigh 2 Lods (Cologne weight) with that which is wound on reed weighing as much less as the weight of the reed. That which is spun on yellow silk soon loses its colour. Insegold sold in bundles weigh more. Insegold is gold laid on silver. Insegold and silver thread is priced at the same rate. Cyprian gold is laid on copper and always wound on reed whether spun on yellow or red silk and is often sold as insegold, but Cyprian gold is gold under and over. Fine thread is best (because of being longer). Cologne gold is not spun on silk but on other fibres and does not tolerate water. It is bought in bundles of a dozen. It is never on reed but always sold in long bundles. Cologne gold has under (it) a white membrane."* [21]

Membrane threads were first manufactured in Asia and imported into Europe from the 11th century. By the 13th or 14th century membrane thread production was also taken up in Europe [12]. In most cases the membranes consisted of animal gut or leather, only in China and Japan membrane threads had a paper substrate. A type of membrane thread developed in China by the 14th century was made from gilt mulberry paper [7]. The cellulosic or proteinaceous membranes were gilt with

pure gold or an alloy, usually in the form of a thin sheet but sometimes as a powder, probably employing some sort of an adhesive, the composition of which has not been identified.

During the analysis of some Japanese metal threads Kohara et al. identified haematite (α-Fe_2O_3) by X-ray diffraction patterns and suggested its employment as part of the adhesive medium for fixing the metal foil to the paper substrate [23]. De Reyer et al. employed microscopy and DNA amplification for the analysis of the substrates of membrane threads. The results suggested that leather and intestine tissue from different animal species were used for the substrate and animal glue or fat for the adhesive material for gilding [24]. Indictor et al. suggested that copper may have been employed as part of the adhesive material joining the metal layer to the substrate [8]. When the gilding was done with gold powder a microscopic investigation usually reveals a less shiny and rather crumbly surface [4]. An examination of membrane gilding techniques suggested that in the case of powder gilding it was prepared by grinding filed metal [15].

The adornment of textiles with 'beaten and cut' gilt-silver threads and the cheaper membrane threads became increasingly popular and from the 13th or 14th centuries the thread was not only imported but also produced in European workshops [12]. The Papal record of gifts to churches and monasteries, the "Liber pontificalis" of 1295, gives one in four fabrics as being decorated with precious metals [1]. 13th century gold threads from Paris often consisted of the pure metal unalloyed. In 1250 the statutes of the Paris trade mention the prohibition on penalty of a fine for gold and silver beaters "batteurs d'or et d'argent" to make use of inferior metal alloys such as too high a concentration of silver or copper in gold or any use of tin in silver as these would soon render the thread unsightly. In Cologne a guild of woman gold spinners has been recorded since 1397. Following the growing demand for gold and silver threads during the 14th century silk towns such as Lucca, Venice and Florence set up their own gold spinning establishments. The production of membrane gold and silver threads was the standard one in most of Europe from the 13th century onwards [1]. Especially the terms "Lucca gold" and "Cologne gold" became generic terms for membrane threads [25].

6.1.4. 'Cast, Drawn and Rolled' metal threads

Towards the end of the 14th century production centres in Italy and Spain returned to the earlier solid metal filaments but with the advance of wire making technique it became easier to produce such solid metal filaments of the so called 'cast, drawn and rolled' type [1]. Rods of silver were gilded and drawn into wires which were then flattened between rollers and wound around a fibrous core, usually of yellow or white silk for gilt or silver threads, respectively; though metal threads with a linen, cotton, animal hair or sinew core have also been reported [1, 3, 13, 26, 27].

According to Darrah this manufacturing method possibly spread from Persia throughout Europe and the thread known as "aurum battutum" was produced in Paris and Cologne as early as 1250 and 1347 respectively, with manufacture in England established by 1500 [7]. However, there may be some confusion as the term "aurum battutum" suggests the older method of 'beaten and cut' threads also referred to as "or battu" or "aurum platinum" [21].

The method of drawing wire probably originated in the Near East and after the 11th century spread to Europe and the Far East. Earlier methods of wire production include the hammering or twisting of cut strips from a flat metal sheet [3]. Oddy [14] described early methods of wire making; hammering, block-twisting, strip-drawing and strip-twisting being used before the invention of the draw-plate facilitated the manufacture of metal wires by drawing it through a series of dies of decreasing diameter. There is much controversy as to where and when the draw-plate was first used. Some claim that ancient Persian wires from the 5th century B.C. or wires from Helenistic times (3rd to 2nd centuries B.C.) were already drawn but fail to provide substantive evidence. Only marks left by the process of manufacture such as longitudinal striations from die holes or helical seams from twisting can attest to the technique that was used. However, the earliest archaeological evidence of draw-plates date to the Viking period (9th or 10th century A.D.) and the earliest historical reference to draw-plates is by Theophilus in the 12th century A.D. [14, 28].

Karen Finch's translation of Sofus Larsen describes the processes of wire drawing according to 16th century documents and wire flattening according to 18th century documents [21].

> Vanoccio Biringuccio, 'Pirotechnia', Venice 1540 and Tomaso Garzoni da Bagnocaullos Encyclopaedia, 'La Piazza Univaersale de Tutte le Professione del Monde', Venice 1585: *"Gold wire drawing fell in three parts, each requiring special tools. The work began on a coarse pulling machine with a gold or gilded bar abouth eight inches across. The bar was first hammered into a rounded shape at the top and then pulled till it had a diameter about the size of a little finger. Next the rod was transferred to the pulling table where it was further reduced to the size of a fine knitting needle. The third part consisted of pulling this wire through the ever reducing holes of a drawplate or series of drawplates set between two turntables."* [21]
>
> J.S. Halle, 'Werkstätte der Heutigen Künste', 1761 and Lejisugo, 'Vollkommener und Gründlicher Bericht von Gold und Silber-Draht-Ziehen', 1744: *"They describe a machine consisting of a solid square wooden frame bearing two steelrollers hung in round iron shafts and with the lower one turned by a crank. The steel rollers were set independently and pressure could be exerted from a lever set above as well as by heavy weight hung below. When the crank was turned the wire would come off one bobbin onto a steel spring, from where it could glide between the rollers and come out on the other side flat and lustrous and ready for winding on to the other bobbin."* [21]

Járó et al. stated that in European textiles metal threads made of double-sided gilt silver strips, i.e. 'cast, drawn and rolled' were used from the 16th century onwards [29, 30]. Parallel striations were detected on a metal strip from an excavated 16th century bonnet and suggested that it was made by wire drawing and flattening [29, 30]. Following the analyses of a large number of gilt silver metal threads dating from 1400-1900 Tronner et al. stated that the change from single- to double-sided gilding of metal strips occurred around 1650 [31]. The data given by Montegut et al. support the hypothesis that double sided gilt metal strips (cast, drawn and rolled) were used only from the late 15th or the 16th centuries onwards. Threads pre-dating the 16th century are of the 'beaten and cut' or membrane type [5]. By the end of the 16th century membrane threads were no more used in Europe [15]. Garside studied metal thread samples dating from the 15th to the 19th centuries. The results agree with the general finding that membrane threads were still used in the 15th century but are not found in later European textiles [32, 33].

In the 18th century the so called Nuremberg thread became a popular, cheaper type of metal thread. It was manufactured from a copper rod which was thinly silvered and gilt and subsequently cast, drawn and rolled into a filament for spinning around a fibrous core [13]. Traces of nickel, zinc, chromium and tin were frequently found in these threads [13].

6.1.5. Spinning gold

'Beaten and cut' as well as 'membrane' metal threads were spun from discontinuous lamellas and a process describing the spinning of approximately 30 cm long lamellas around a silk core with the aid of a drop spindle is given in Karen Finch's translation [21].

> Etienne Binet (pseudonym Francois Réne), 'Essay des Merveilles de Nature', Rouen, 1622: *"The spinner holds the end of a skein of yellow silk placed on a bobbin stand in front of her and wears a thimble with several lateral grooves on her left index finger. In one of these grooves is placed – silver side down – a gold lamella. With her right hand the spinner keeps the spindle in motion while spinning the lamella around the silk. The lamella is spun so close that it covers the silk core with no sign of either its silver underside of the silk. All is made into an entity so firm and thin that it appears as gold only even though the silk thread by itself was thicker than this new gold thread, which is pressed together with spindle and thumb."* [21]

In contrast to the relatively short 'beaten and cut' and 'membrane' metal filaments or lamellas, the length of 'cast, drawn and rolled' metal filaments is determined only by the length of the drawn wire, thus making a continuous spinning process possible, where the silk core and the metal filament are reeled from separate cones and combined in the spinning. This is illustrated in a copperplate engraving from "Etwas für Alle", Part II, by Abraham a Sancta Clara, Würzburg, 1711, Figure 6.1.2.

Figure 6.1.2. Woman spinning gold thread [1]

6.1.6. Double and triple wrapped metal threads

Metal threads with double and even triple wrappings have been found in four out of the five tapestries containing metal threads which were analysed within the MODHT project [34, 35].

Previously, metal threads with multiple wrapping have rarely been mentioned in the literature. Two double wrapped gilt leather substrate metal threads with linen and cotton cores were found in a 14th century Near Eastern textile [8]. Montegut mentions one double wrapped thread from late 15th century Spain or Italy, possibly Venice [5], while Indictor identified one double wrapped metal thread of Indian origin [3].

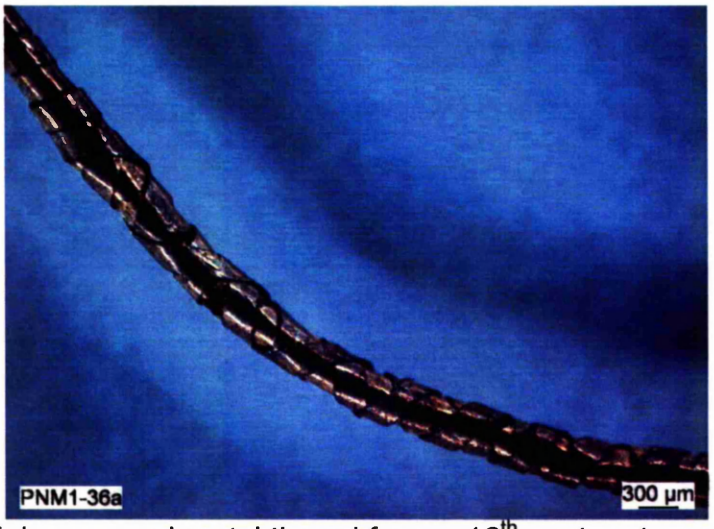

Figure 6.1.3. Triple wrapped metal thread from a 16th century tapestry

6.1.7. Alloying and gilding methods for metal threads

Several methods for gilding are discussed in the literature, these include hammering, welding, soldering and fire-gilding as well as leaf gilding with adhesives and powder gilding for membrane threads in particular. Járó et al. suggest that fire-gilding was used later than the alternative methods of hammering metal layers together or gilding by welding or soldering [29]. In contrast to the alloying of gold to silver with heat, the methods of beating or drawing the metal filament may cause the bulk silver to 'show through' the thin gold layer on the surface more obviously [36]. Kentish Barnes described a method of gilding rods of silver for wire drawing involving a solid bar of silver of approximately 1.5 inches in diameter which was surface cleaned and polished before laying onto gold leaf and rolling the bar until covered in at least one layer of gold leaf. The bar was then

wrapped in paper and heated in a charcoal fire until the gold firmly adhered to the silver surface [37]. Soldering of gold to silver with the aid of a copper containing soldering material is said to have been described by Theophilus Presbyter in the 12th century and Járó mentions malachite, a copper carbonate, as a possible soldering material because it would reduce the melting point of silver and copper [12, 19]. Járó and Toth state that the so-called 'Or de Milan' is produced from a single-sided gilt silver block employing fire-gilding with gold mercury amalgam for the application of the gold layer to the silver bulk. This technique involves the application of a gold mercury amalgam to a block of silver, causing the surface dissolution of silver to aid the bonding with gold and the subsequent evaporation of the mercury by heating the sample in a furnace [16, 32]. Depending on the temperature and length of time of heating both welding and fire-gilding produce a gradient diffusion layer of gold silver alloy [16], which have been shown to vary between 2 µm and 10 µm in thickness [2]. Hardin and Duffield analysed allegedly 'cast, drawn and rolled' Persian metal threads [6]. The presence of mercury, as established by X-ray energy dispersive technique, on a silver metal filament with a thin gold coating was attributed to the fire-gilding method employing a mercury amalgam. Another suggested possibility for the presence of mercury may be that it is a remnant from the gold mining process. Járó and Toth support this view, stating that the mercury was employed for the refining of gold, therefore its presence does not indicate the use of gold amalgam for the gilding [16]. Hoke and Petrascheck-Heim also noted that mercury was used in the silver-gilding process in gold amalgam and claimed that the presence of mercury increases the diffusion of silver and gold between the two layers [2].

Diffusion of metal between the layers has been investigated by several researchers. Skals, describing metal threads found in a Danish 12th or 13th century textile, attributed a high concentration of silver (24%) in the gold layer to either a very thin gilding or to metal diffusion during corrosion [26]. Employing XPS analysis on a 17th century metal thread Howell et al. observed a surface migration of silver through the gold overlayer [38]. Járó et at. attributed the diffused interface between the gold and silver layers to an alloy formation during gilding [15]. Indictor et al. mentioned 'surface enrichment' of the metal strips and attributed the effect to preferential silver migration into the fibrous core leaving a higher concentration of gold in the alloy [8]. The presence of migratory metals in the fibrous core has been noted previously and can obscure / complicate the determination of metallic

mordants in the core fibres [2, 3, 9, 39, 40]. However, the presence of aluminium and iron has usually been attributed to mordants [3, 5].

The detection of trace impurities or alloy materials in the metal filaments has indicated that in metal threads of European origin, copper was already used by the 15th century. It was most likely employed for the 'strengthening effect' it lends to silver and gold. Most silver 'cast, drawn and rolled' filaments were shown to have a higher proportion of silver to copper than comparable silver-gilt filaments. Lead and iron were commonly found as traces in the 'cast, drawn and rolled' metal filaments [7]. Allegedly gold from the Caucasus contained palladium, however, Hoke and Petrascheck-Heim have found palladium in very few metal threads [2].

It has been suggested that there is a link between provenance of the metal thread and variations in copper concentration in the silver alloy. It is now generally believed that the silver to copper ratio in European gilt-silver metal threads is considerably lower than in the more pure gilt-silver threads of Oriental origin [2]. However, it should be noted that in the Middle Ages Arab weavers controlled the silk production in Sicily and Spain, hence for this time period these regions can be counted for as belonging to the 'Orient'.

It has also been stated that homogeneity determination of the metal alloy could reveal information about manufacture and provenance of the metal thread [2]. High homogeneity is usually found in Oriental metal thread production. With EDX analysis homogeneity may be quantified according to the rate of increase in standard deviation from measurements taken at one point compared to the standard deviation of measurements taken at different points. A fivefold increase denominates 'high' homogeneity, a fifteen fold increase or more stands for 'low' homogeneity, while 'medium' homogeneity lies between those thresholds.

The association of provenance with metal ratios and homogeneity has been taken up and examined by various researchers. Garside found the copper content was between 5% and 15% in the European samples but only traces of copper were found in the Middle Eastern and Oriental threads [32]. Indictor et al. stated that the gold to silver ratio may be used as a tentative indicator of metal thread provenance. Threads consisting of a metal alloy of silver and gold are assigned to European origin, with those threads exhibiting more gold than silver being found in Spain only. Very high purity metal filaments may indicate Near Eastern manufacture [8, 9]. In addition Indictor et al. noted that the determination of the

copper content can be used as an indicator for purity of metals [8, 9]. However, Indictor and Koestler did doubt the efficacy of the association of metal homogeneity to provenance of manufacture because homogeneity is greatly affected by wear and corrosion [39]. In a study of Persian metal threads Hardin and Duffield did not find evidence for the linking of EDX results to provenance of metal threads [6]. Using trace impurities and alloy compositions as an indicator of provenance of manufacture may also be hampered by the wide-spread practice of recycling of precious metals for use in precious objects production [41].

Literature data for European category III metal threads has been averaged and is summarised in Table 6.1.2.

A metal thread database including information about provenance, condition and all experimentally obtained values has recently been established by Tronner et al. [31]. Statistical evaluation using principal component analysis indicated strong positive correlation for some obvious data such as apparent gold concentration and gold layer thickness, damage of textile and damage of object, damage of metal and observed corrosion. However, no obvious trend in the dimensions of the metal strips could be identified over the centuries. Nevertheless more interesting correlation was found between width of metal strip and thickness of gold layer. However, the date and origin of the threads and colours of the silk cores could not be correlated to any variables.

Table 6.1.2. Literature data for European category III metal threads

Silver metal threads				
Reference:	[34]	[32, 33]	[7, 13]	[5]
Diameter of thread	500-750 µm	n.s.	n.s.	310 µm
Core material	silk	silk	n.s.	n.s.
Core colour	white	white	n.s.	n.s.
Core twist*	i.d.	Z	n.s.	n.s.
Width of metal strip	250-500 µm	90-300 µm	n.s.	230 µm
Thickness of metal strip	n.s.	10-35 µm	n.s.	12.5 µm
Direction of wrapping	S	Z (Oriental) S (European)	n.s.	S
Copper concentration in silver bulk	n.s.	up to 20%	~2-5%	2%
Gold concentration in silver bulk	n.s.	n.s.	~0-6%	n.s.
Origin	Brussels	Cologne	England / Italy	Florence
Date	16th C	15th C	17th–18th C	15th C
Production method **	B.C. or C.D.R.	B.C.	C.D.R.	B.C. or C.D.R.

Silver gilt metal threads						
Reference:	[11]	[34]	[32, 33]	[31]	[5]	[2]
Diameter of thread	n.s.	250-1000 µm	n.s.	n.s.	170-500 µm	120-360 µm
Core material	silk	silk	silk	n.s.	silk	n.s.
Core colour	white / gray	light to dark yellow	yellow	n.s.	n.s.	n.s.
Core twist*	n.s.	i.d.	S or i.d.	n.s.	i.d. or S 1- or 2-ply	n.s.
Width of metal strip	200 µm	250-500 µm	90-300 µm	290-300 µm	270-580 µm	200-350 µm
Thickness of metal strip	25 µm	n.s.	10-35 µm	15-21 µm	5-12 µm	20 µm
Direction of wrapping	S	S	n.s.	n.s.	S	n.s.
Thickness of gold layer	3-5 µm	40 nm	1-4 µm	60-70 nm	n.s.	5 µm
Gilding method	welding or fire-gilding	n.s.	n.s.	n.s.	n.s.	n.s.
Copper concentration in silver bulk	0.6 %	9-30%	5-17%	n.s.	3-17%	n.s.
Origin	German	Brussels	Cologne	n.s.	Italy	n.s.
Date	10th C	16th C	15th C	15th-17th C	15th-16th C	n.s.
production method **	B.C.	B.C. or C.D.R.	B.C.	n.s.	B.C. or C.D.R.	B.C.

n.s. = not stated
* i.d. = indiscernible
** B.C. = beaten and cut; C.D.R. = cast, drawn and rolled

6.1.8. Deterioration and corrosion of metal threads

The factors affecting the general condition of textiles containing metals is well reviewed by Indictor and Ballard [36]. The quality of manufacture in particular the composition and homogeneity of the metals, the spacing of wrappings on the threads, the fineness and treatment of the core fibres and the tightness of the weave greatly influence the longevity of the textile as a whole; though the major factor for the condition of a textile will always be its history. The purpose it served, and the consequent wear and tear, will cause mainly physical deterioration processes such as tension, stress, abrasion, compression, folding, twisting etc. While the atmospheric and environmental conditions it was exposed to during use, display, storage or disposal and possible biological attack may initiate the final chemical and / or biological deterioration processes.

The deterioration of metal threads in tapestries can be of a physical nature, i.e. abrasion of the thin gold layer or breakage of metal coils in folds or other areas of tension but since the handling of tapestries is usually limited most damage is due to chemical attack, i.e. corrosion. The nature of the corrosion products on metal threads has not been investigated widely. It is generally agreed that the major corrosion products are sulphur and chlorine containing residues [6, 34, 42]. To the author's knowledge no study on metal thread corrosion has been published which employed X-ray diffraction or another technique capable of identifying the corrosion crystal formation.

In the following, general aspects of silver and copper corrosion are discussed. Silver corrosion products are predominantly acanthite (Ag_2S) and chlorargyrite (AgCl) and to a lesser extent silver oxide Ag_2O and silver sulfate Ag_2SO_4 [43-45]. Copper exposed to the atmosphere undergoes a patination process in three to four stages; the initial corrosion products are reddish-brown and turn black with further corrosion, the terminal corrosion state is the greenish-blue brochantite ($Cu_4(SO_4)(OH)_6$) [45]. Other major copper corrosion products include various copper sulfate salts as well as cuprite (Cu_2O) as the initial corrosion product and, depending on atmospheric pollutants, chalcocite (Cu_2S), atacamite ($Cu_2Cl(OH)_3$) and, especially indoors, copper carboxylates [45]. Copper has a higher reactivity than silver and is therefore preferentially corroded in silver copper alloys [45].

Sulphur oxides from air pollution are assumed to be the most likely source for sulphur [6]. In general, the most abundant sulphurous compound in the

atmosphere is carbonyl sulphide (COS) followed by sulphur dioxide (SO_2) and, in small concentrations, carbon disulfide (CS_2) and hydrogen sulphide (H_2S). COS and H_2S rapidly tarnish silver and copper especially in a humid atmosphere, while SO_2 and CS_2 cause only very slow formation of corrosion products [44, 46]. COS is a common pollutant produced from fossil fuel combustion but it is also released during the degradation of keratinous protein such as hair and wool; therefore metal museum objects should never be stored near wool. Dubus et al. showed that silver in display cases lined with wool have an increased corrosion rate [43]. It has also been suggested that gases released during the degradation of the silk core material form a major source for sulphur [2]. This view is rebutted due to the minimal amount of sulphur containing amino acids in the silk fibroin.

Chlorine containing corrosion products may be derived from the salt used in dyeing of the core fibres or contamination from excessive handling or perspiration. For metals in coastal regions the atmospheric content of chlorine salts was suggested as a cause for corrosion growth [32].

Gold has very low reactivity and is therefore corrosion resistant. However, cracks and voids in the gold surface or the precipitation of silver or copper through a gold layer will inevitably lead to corrosion growth, which can sometimes cover the whole layer. Corrosion formation starts at the exposed surface of the metal where the three-dimensional lattice structure has unsaturated valences. When these are filled with atoms of approximately the same size as the metal atoms the lattice can be completed and inhibits further reaction. Therefore a thin corrosion layer such as silver oxide (Ag_2O) or copper oxide (Cu_2O) can be regarded as corrosion protective [42]. A reaction with sulphide or chloride ions can only take place when the oxide layer is destroyed. Again this can happen through chemical or physical means such as cleaning. Once the oxide layer is damaged the metal surface will be more prone to further corrosion [42, 47]. Silver ions are highly mobile which can cause silver sulfide growth over inert surfaces, i.e. sulfide corrosion can creep over a gold layer [42, 48]. It has been observed that silver sulfide does not grow as a continuous film but instead forms an inhomogeneous layer which grows rapidly at impurity sites and areas where the silver crystal lattice is not in its (111) plane, i.e. at steps and facets [45, 48]. The formation of silver and copper corrosion products occurs only in the presence of oxygen and moisture. Adsorbed water of three monolayers in thickness shows bulk water properties where the first monolayer forms hydroxide bonds with the metal surface and the subsequent layers have

high mobility and random orientation. Metal ions are dissolved from the solid surface by proton or ligand induced metal dissolution in electrochemical reactions involving an anodic and a cathodic reaction [45].

$$Me \rightarrow Me^{n+} + ne^- \text{ (anode reaction, metal dissolution)}$$

$$1/2O_2 + H^+ + 2e^- \rightarrow OH^- \text{ (cathode reaction, oxygen reduction)}$$

The anodic dissolution of metal ions can proceed via a proton exchange reaction where a H^+ ion protonates a hydroxyl group bound to a metal atom which can subsequently leave the solid surface as an aquo-metal ion [45].

$$Cu\text{-}OH + H^+ \rightarrow Cu\text{-}OH_2^+ \rightarrow Cu^+ + H_2O$$

surface oxide dissolution of aquo-metal ion dissolved Cu ion

The dissolved metal ion can form ion pairs with dissolved atmospheric constituents which will eventually precipitate into a solid phase [45].

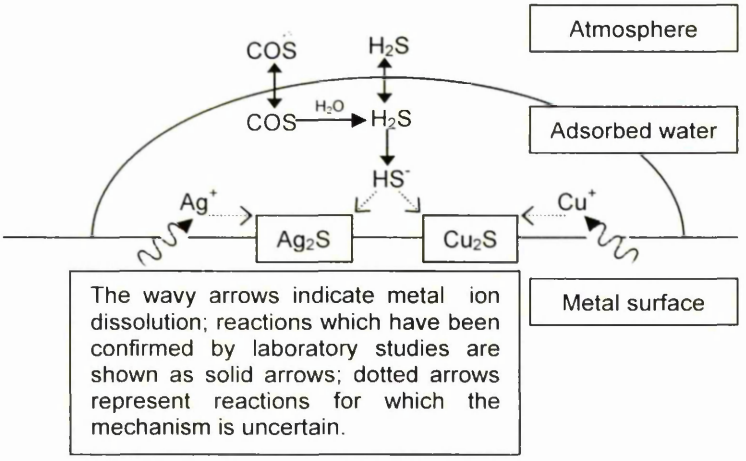

Figure 6.1.4. Schematic representation of the processes involved in corrosion formation

Usually silver sulfide is black but Járó suggested that reddish appearance of some corroded silver-gold alloy metal threads was due to finely distributed silver sulphide residues on the surface. The exposure of a clean silver-gold alloy foil to dry air containing sulphur gases under laboratory conditions resulted in a similar discolouration [49]. The morphological appearance of sulphide corrosion crystals was described as 'trees', 'bushes', 'needles' , 'cauliflower' and more general 'black spots' in the case of copper sulphides [49-51]; silver sulphide crystals have been described as 'dendrites' breaking the gold layer [2], 'whiskers', 'black fuzzies', 'flower-or tree-shaped' and 'mushroom-shaped bubbles' [49, 52]. These descriptions are very subjective but there seems to be a general distinction

between sharp crystals and rounded crystals. The cause for the different growth behaviour of the sulphide crystals is not known. Bennett et al. observed that silver sulphide initially grew as 'nearly spherical clumps' and formed 'needles' after the corrosion layer exceeded 16 nm average thickness [48]. Franey at al. suggested that these 'mounds' or 'clumps' coalesce at an average thickness of ten monolayers and thereby impede further corrosion [44]. In contrast, Dubus et al. noted a linear increase of Ag_2S corrosion but a retardation of the AgCl corrosion rate, i.e. a protective effect of a AgCl layer [53]. This finding is inconsistent with Járó's statement that "silver chloride does not create a protective layer on the surface of silver, the metal can completely transform to silver chloride" [42].

Corrosion damage appears to create not only deposits but also holes on the surface of some metal filaments [6]. Delamination and differences in the cracking structure were attributed to either stress-corrosion causes or the manufacturing technique. To explain the multi-layered appearance of some delaminated metal strips Járó and Toth suggest a manufacturing method involving folding and stretching of a metal foil or strip before it is cut into narrower strips for winding [49]. Hardin and Duffield also observed such delamination damage on some supposedly 'cast, drawn and rolled' metal filaments and thus suggested a different manufacturing type such as the joining of thin foil by hammering and subsequent cutting into strips [6]. Corrosion growth through cracks in the gilt layer and the flaking off of corrosion layers is also mentioned by Garside and Rogerson [32, 33]. Van Langh et al. reported silver sulphide corrosion in a stratified layer with stratifications of 200-1250 nm thickness [54].

Silver chloride corrosion is often found on metal objects from excavations. Silver chloride itself is white so the greyish or black appearance of the corrosion layer is attributed to finely distributed silver powder from disintegrated silver chloride or is due to transformation into silver sulphide on the surface [49].

Salts formed by the release of silver and copper ions in electrochemical processes are known to have a fungicidal effect and may have a protective effect on textiles under burial conditions [55].

6.1.9. Cleaning of metal threads

Several workers have investigated the cleaning of metal threads. Howell tested electrochemical reduction, electrolytical reduction and ultra-sonic treatment [56]. The methods proved not successful and even detrimental to the thread. Mechanical cleaning with a glass bristle brush was ruled out because it would damage the textile fibres and scratch the metal surface leaving it even more accessible to further corrosion. An aqueous or acetone solution of 3% formic acid and 2% thiourea showed good results in removing the corrosion but leaving the gold layer intact; furthermore the method appeared harmless to the fibres [56]. Járó found that Howell's silver dip treatment could not clean tarnished metal foil while an alteration of the recipe to 12% thiourea and 30% citric acid proved successful but both methods would be degradative towards the silk core [49].

Degrigny et al. investigated the cleaning of metal threads with various Nd3+:YAG lasers and achieved good results in the removal of corrosion products [57]. However, side effects of laser cleaning included a loss of brightness and lustre of the metal and possible changes in shade of colour, i.e. a white or gilt appearance of silver. The re-corrosion rates of laser cleaned metal threads and the possible damaging effects of laser irradiation on adjacent textile fibres were not investigated [57].

Sipos and Gondar provide photographical documentation of the effect of various mechanical and chemical treatments for the cleaning of metal threads. The general conclusion is that treatments can be harmful to fibres and metal and re-corrosion cannot be prevented after cleaning [47].

6.1.10. SEM/EDX studies of metal threads

For studies on the measurements and compositional structure of metal threads some workers have made use of Energy Dispersive X-ray Fluorescence (EDXRF) [7, 13] or X-ray Diffractometry (XRD) [23] but most studies have utilised Scanning Electron Microscopy coupled with Energy Dispersive X-ray microanalysis (SEM/EDX) [2-6, 8-10, 15, 16, 23, 26, 29-33, 39, 40, 49, 56, 58]. Recently some criticism on the accuracy of quantitative EDX analysis has arisen. Nord and Tronner point out that many EDX analyses of metal concentrations of the thin gold layer may be adversely compromised by the usage of too high an accelerating voltage, which leads to the inclusion of some of the bulk metal in the compositional

analysis [31, 40]. According to their analyses the surface gilding contains only low amounts of other metals but varies in thickness due to imperfect manufacturing, wear and / or unsuitable cleaning methods. Spectra should be obtained using the lowest possible accelerating voltage to achieve a low penetration depth of the electron beam. 4 kV is suggested as a suitable accelerating voltage because it only slightly exceeds the adsorption limits for gold silver and copper which lie at 2.307 keV (AuM_{IV}), 3.810 keV (AgL_I) and 1.100 keV (CuL_I). Table 6.1.3 illustrates that too high an accelerating voltage could distort the results for thin pure gold layers [31].

Table 6.1.3. EDX analysis of silver gilt layers [31]

Real thickness of gold layer over silver bulk in µm (obtained through sputtering)	Lowest accelerating voltage for which the silver AgL peak could be observed in kV	Apparent gold concentration in wt% as determined at various accelerating voltages (the true gold concentration in the gold layer is always 100%)			Accelerating voltage in kV for which the standard gold layer thickness (µm) equals the maximum Monte Carlo penetration depth in gold
		20kV	25kV	30kV	
0.021	4	8	6	5	2
0.042	5.5	18	15	13	4
0.060	6.8	28	25	22	5
0.080	8	40	34	32	6.5
0.102	9	57	47	42	7
0.120	11	66	57	51	8
0.171	16	90	84	78	11
0.221	20	99	94	87	12.5
0.283	25	100	100	100	16.5

The values for the experimental accelerating voltage allowing observation of the AgL peak are more or less 50% higher than the Monte Carlo simulation calculated values. This indicates that the characteristic X-rays for AgL are predominantly generated at about two-thirds of the maximum penetration depth. Using the following two diagrams, Figure 6.1.5 and Figure 6.1.6, with EDX analysis the gold layer thickness for gilt silver strips can be estimated; though results will always be obstructed by surface corrosion, micro-cracks, metal alloys and diffusion between the silver bulk and the gold layer.

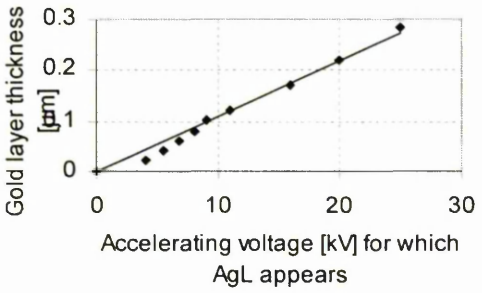

Figure 6.1.5. Accelerating voltage for which silver peak appears, for different gold layer thicknesses [31]

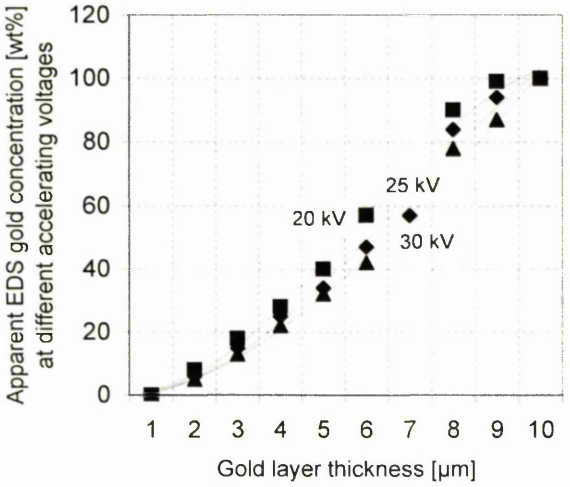

Figure 6.1.6. Apparent gold concentration at different kV versus true gold layer thickness [31]

Results obtained by Tronner et al. show that the gold layers are usually extremely thin, virtually always <1µm and often <0.1µm.

The analysis of cross sections can reveal information about the morphology and manufacture of the metal strip but in the case of a layered structure compositional analysis must be viewed critically because it is likely that the drop-shaped volume of the electron beam is wider than the individual layers. The migration of silver ions into the gold layer and vice versa and the presence of micro cracks in the surface gilding caused by the manufacturing technique or by corrosion stresses may also interfere with the analysis [31, 40].

Nord and Tronner found the surface sensitive AES (Auger Electron Spectroscopy) to be most useful in the quantitative analysis of metal composition. X-ray Photoelectron Spectroscopy (XPS) and Secondary Ion Mass Spectroscopy (SIMS) are mentioned as potentially valuable techniques for the analysis of metal threads [40]. So far only two studies on metal threads have employed XPS and ToF-SIMS [34, 38].

6.2. Experimental

6.2.1. Imaging of metal threads

All metal thread samples received from the sampling campaigns in Spain, Belgium and Great Britain were documented as digital images using a Leica DC 3000 camera coupled to a microscope and Leica IM 1000 software, capable of superposition image assembly, which allows up to 30 images of different levels of depth of focus to be assembled into one image.

The images were used to establish structural features such as silver or gold appearance of filament, level of corrosion, number of wrapping layers and direction of winding of the filaments, colour, twist and ply of the core fibres and dimensional features such as diameter of the thread, width of filament and number of coils per unit length. According to these features the metal threads were assigned into groups and the images were used to select samples for further analysis with SEM/EDX, XPS, SIMS and XRD.

6.2.2. Accelerated tarnishing: Oddy tests

Silver and copper coupons, 5 x 10 x 0.25 mm, > 99.9 % purity (from Aldrich Chemical Company), were cut and a pin hole punched in each. The coupons were cleaned successively in propanol, hexane, chloroform and methanol for 10 minutes in an ultrasonic cleaner. Silver and copper coupons were incubated under thermal or light Oddy test conditions indicated below with the following wool and silk samples:

Dye	Wool	Silk
• -	Undyed	Undyed
• -	Alum*	Alum*
• Weld	Yellow/W1	Yellow/S1_b
• Woad	Blue/W1	Blue/S1
• Brazilwood	Red/W3_wl	Red/S1_d
• Madder	Red/W1_wl	Red/S2_b

* Alum mordanted wool and silk was included in the thermal Oddy test only.

Thermal Oddy test

0.2 g of wool or silk yarn was placed in the bottom of a test tube together with Durham tubes (6.5 x 30 mm) filled with deionised water. Silver and copper coupons were suspended from the top of the test tube using nylon wire and the tubes sealed with a stopper and tape. Ten yarn samples and one control were incubated at 60°C for 4 weeks. The test setup is shown in Figure 6.2.1.

Light Oddy test

Ten wool and silk fabrics, 4 x 5 cm, were stapled to a cardboard backing and placed in glass cells (2 x 5 x 15 cm) along with tubes, 6.5 x 120 mm, filled with deionised water. Silver and copper coupons were suspended from the top of the cells containing the fabric pieces and one control sample containing only the tube with deionised water. The coupons were shielded from direct irradiation with cardboard placed around the top of the sealed cells. The fabric samples were irradiated for 300 hours using an OSRAM 400 W HQ (MB-U) mercury lamp in a Microscal Ltd. Mark V Light Fastness Tester. The cells were equipped with a circulating water cooling system maintaining the temperature at 27-29 °C.

Figure 6.2.1. Thermal Oddy test setup

6.2.3. Detergent treatments

Clean and corroded silver and copper coupons, taken from the Oddy tests, as well as model metal threads and historic metal threads were treated with detergent solutions based on the textile cleaning procedures used at the Textile Conservation Studio at Hampton Court Palace [59]. Nonylphenol ethoxylate detergents have been phased out in Europe due to their environmentally harmful oestrogenic degradation products. However, in particular in America and Australia, these detergents (e.g. Synperonic N) are still being used widely in conservation treatments (see internet discussion forums such as Conservation DistList and TEXCONS). A nonylphenol ethoxylate detergent (Tergitol-NP9) has therefore

been included in this study. The anionic detergent Sodium Dodecyl Sulfate was obtained in 99% and 98% purity.

The treatment solutions were prepared as follows:

• Untreated	no treatment
• H_2O	deionised water only
• SDS 99%	0.25 g Sodium Dodecyl Sulfate 99% in 500 ml deionised water
• SDS 98%	0.25 g Sodium Dodecyl Sulfate 98% in 500 ml deionised water
• SDS+T-NP9	0.25 g SDS 99% + 1 g Tergitol-NP9 in 500 ml deionised water
• T-NP9	1 g Tergitol-NP9 in 500 ml deionised water

The metal coupons and metal threads were immersed in separate beakers each and treated at room temperature for one hour under constant agitation. They were subsequently rinsed in excess deionised water for one hour, replacing the rinsing water every 20 min, and finally air dried. All samples as well as the pure detergents were analysed by ToF-SIMS with the analysis conditions listed under section 6.2.7. Experimental: SIMS.

Table 6.2.1 lists all samples used in this study; marked with '+' or the respective sample name if the treatment was carried out and marked with '-' if the treatment was omitted. Sample PNM1_24 was treated with SDS 99% but the ToF-SIMS analysis failed, marked (+). The pre-cleaning procedure and corrosion conditions used for silver and copper coupons are described above, see Accelerated tarnishing: Thermal Oddy test. The production of model metal threads and the origin of historic metal threads are described in Chapter 3. sections 3.1. Historic tapestry samples and 3.3. Model metal thread samples.

Table 6.2.1. Samples used in detergent treatments

Treatment	Silver		Copper		Metal threads			
	Clean	Corroded	Clean	Corroded	Model	PNM1_24	PNM2_17	PNM5_24
Untreated	+	-	+	-	+	+	+	+
H_2O	+	Green/W2	+	Green/W2	-	-	-	-
SDS 99%	+	Red/W3_wl	+	Red/W3_wl	+	(+)	+	+
SDS 98%	+	-	+	-	-	-	-	-
T-NP9 + SDS	+	Alum/W	+	Alum/W	+	+	+	+
T-NP9	+	Red/W5	+	Red/W5	+	+	+	+

6.2.4. Embedding

Three metal thread samples were embedded and cross sectioned for FEG-SEM/EDX analysis. The samples were taken from different tapestries and different groups:

Sample	Group
HCP 28G6	Double wrapped
PNM1_36	Triple wrapped
PNM5_06	Gilt medium diameter

The samples were embedded using Struer's Epofix Epoxy resin and sectioned using Struer's Accutom 5 with a diamond cutting blade. Sections were obtained in cross-section and length-section of the metal threads. The sections were ground using P120, P400, P600 and P1200 grinding papers and subsequently polished using 6 µm diamond paste on Texmet cloth, 1 µm and ¼ µm diamond paste on Microcloth and finally 1/20 µm colloidal silica Metpret on Microcloth. Lubricating fluid Kemet type OS was used for all polishing stages.

6.2.5. SEM, FEG-SEM and EDX

SEM images were obtained for the investigation of manufacturing methods of metal threads and the corrosion morphology of metal threads and Oddy tested Ag and Cu coupons. The metal threads chosen for SEM analysis are listed below:

Sample	Group	Sample	Group
HCP 49F5	Gilt large diameter	BXL 2_06	Corroded gilt medium diameter
HCP 6E5	Gilt large diameter	HCP 169A2	Corroded gilt medium diameter
HCP 71E5	Gilt large diameter	HCP 119C3	Gilt small diameter
HCP 95D6	Gilt large diameter	HCP 31G5	Gilt small diameter
HCP 161A6	Corroded gilt large diameter	HCP 96D6	Gilt small diameter
HCP 72E4	Corroded gilt large diameter	PNM 1_06	Gilt small diameter
BXL 2_04	Gilt medium diameter	PNM 1_24	Gilt small diameter
BXL 2_19	Gilt medium diameter	PNM 2_02	Gilt small diameter
BXL 2_22	Gilt medium diameter	PNM 2_06	Gilt small diameter
BXL 2_36	Gilt medium diameter	PNM 2_19	Gilt small diameter
HCP 46F6	Gilt medium diameter	PNM 5_24	Gilt small diameter
HCP 51F5	Gilt medium diameter	BXL 2_15	Corroded gilt small diameter
PNM 1_03	Gilt medium diameter	HCP 140B6	Silver
PNM 1_38	Gilt medium diameter	PNM 1_01	Silver
PNM 2_17	Gilt medium diameter	PNM 2_18	Silver
PNM 5_06	Gilt medium diameter	PNM 5_09	Silver
PNM 5_26	Gilt medium diameter	HCP 28G6	Double wrapped
PNM 5_30	Gilt medium diameter	PNM 1_36	Triple wrapped
PNM 5_41	Gilt medium diameter	BXL 2_24	Restoration
BXL 2_05	Corroded gilt medium diameter	BXL 2_07	Restoration

Samples were mounted on carbon adhesive tape, metal threads were mounted either as whole threads, unwound filaments or embedded sections. EDX analysis was performed on both sides of the metal threads for the analysis of alloy composition and corrosion compounds.

Instrumental settings

The Hitachi SEM S-3000 N system equipped with a scintillator-photomultiplier type Everhart-Thornley secondary electron detector, a retractable four quadrant solid

state backscattered electron detector and a liquid nitrogen cooled EDAX Sapphire Si(Li) NL2 detector was used in this study. Unless otherwise stated, the secondary electron detector, a medium aperture, approximately 40 spot size, working distance of < 5 mm and 5 keV accelerating voltage were used for SEM imaging. Detector ID, sample name, working distance, accelerating voltage and the appropriate scale bar were recorded on each SEM micrograph. EDX spectra were obtained at 15 mm working distance, large aperture and at varying spot sizes and accelerating voltages (7-30 keV).

The FEG-SEM instrument used for the analysis of embedded metal thread cross/length-sections was a Phillips XL30 FEG equipped with a SDD3 Röntec silicone drift diode detector for EDX analysis, an Everhart Thornley secondary electron detector and a Si diode backscatter detector. Images and EDX spectra were obtained using 10 mm working distance, the backscatter detector and X-ray detector respectively and varying accelerating voltages (5-20 kV).

6.2.6. XPS

XPS was utilised for the analysis of seven metal threads as well as Oddy tested silver and copper coupons to study the elemental composition on the surface of metal threads and the nature of corrosion compounds. The analysed metal threads and their respective groups were:

Sample	Group	Sample	Group
HCP 155B4	Corroded gilt medium diameter	PNM2_06	Gilt small diameter
HCP 72E4	Corroded gilt large diameter	PNM2_19	Corroded gilt small diameter
PNM1_38	Gilt medium diameter	PNM5_24	Gilt small diameter
PNM1_45	Gilt small diameter		

Instrumental settings

The Kratos Axis Ultra X-ray photoelectron spectrometer was used in this study. Wide scans of 1000-0 eV binding energy were taken of metal thread and metal coupon samples using the Al Kα monochromator X-ray source and resolution pass energy of 160 eV. The analysed area was approximately 300 x 800 µm on Ag and Cu coupons (lens mode hybrid and slot aperture) and, due to smaller sample size, 220 x 220 µm on metal threads (lens mode 1 and 110 µm aperture). Other instrumental settings were 10 mA current, 15 kV anode HT, 0.4 eV step, 600-1000 ms dwell time and 1-2 sweeps per sample. Depending on the sample high

resolution survey scans of the Ag(3d), Cu(2p), Au(4f), C(1s), O(1s), N(1s), Cl(2p) and S(2p) peaks were obtained using resolution pass energy of 20 eV, 0.1 eV step and all other settings as above. One sample was argon ion etched (PNM5_24) using a differentially pumped argon ion gun at 4 kV beam energy for 25, 50 and 75 seconds.

Data processing

One to three different areas were analysed on each sample and the data processed using Casa XPS 2.2.67 software. Quantification was carried out using Scofield sensitivity factors and transmission functions. A linear background was used for all peaks and if curve fitting was performed with more than one component the full width half maximum values were constrained to differ by no more than 0.5. The results given in this report state the average relative atomic percentages and elemental ratios as calculated for different areas on the same sample.

6.2.7. SIMS

Dynamic SIMS was employed for surface analysis and depth profiling of metal thread filaments for the investigation of manufacturing technique and corrosion products, while static ToF-SIMS was used for the investigation of residues on metal threads and coupons following detergent treatment.

Surface spectra and depth profiles were obtained from the following metal threads:

Sample	Group	Sample	Group
HCP 68E6	Gilt small diameter	PNM2_19	Corroded gilt small diameter
HCP 120C3	Gilt medium diameter	PNM5_24	Gilt small diameter
PNM1_38	Gilt medium diameter	BXL2_15	Corroded gilt small diameter

Dynamic SIMS analysis was performed on a CAMECA IMS 4f Magnetic Sector SIMS instrument. The Cs^+ primary ion beam was operated at 10 keV, with a beam current of 1 nA and for depth profiles 2 – 15 nA. The areas analysed were approximately 200 x 200 µm, Figure 6.2.2. Typical acquisition times were 200-400 seconds for spectra and 1000-4000 seconds for depth profiles, depending on the achieved analysis depth. A reference crater was measured using a Dektak Profilometer; subsequent depth calibrations were made based on the reference crater measurement, using a sputter rate factor. The approximate depth of analysis into the subsurface was 0.25 – 2 µm.

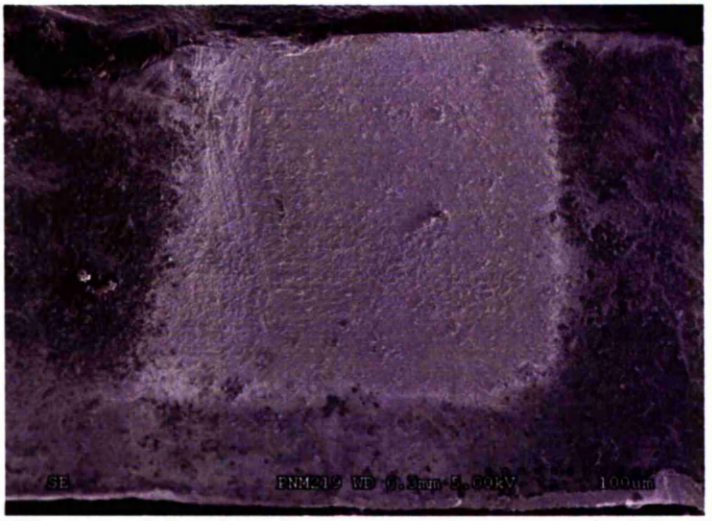

Figure 6.2.2. SIMS crater following depth analysis of sample PNM2_19

Silver and copper coupons and metal threads from detergent treatments as well as the pure detergents were analysed by ToF-SIMS using a PHI 7000 ToF-SIMS Instrument with a Cs^+ primary ion source at 8 keV beam current. The area of analysis was 350 μm^2 and high resolution surface mass spectra were obtained in positive and negative ion mode over the mass range 0 -1000 amu. The pure detergents were analysed as dried spots on copper tape (detergent SDS 99%) and silver foil (detergent Tergitol-NP9).

6.2.8. XRD

XRD analysis was performed for the investigation of the corrosion products on the following six metal threads and four metal coupons:

Sample	Metal thread group	Metal coupons
HCP 161A6	corroded gilt large diameter	Silver - Oddy thermal incubated with undyed wool
HCP 169A2	corroded gilt medium diameter	Silver - Oddy light incubated with undyed wool
HCP 21G3	silver small diameter	Copper - Oddy thermal incubated with undyed wool
PNM1_21	corroded gilt medium diameter	Copper - Oddy light incubated with undyed wool
PNM2_04	silver medium diameter	
BXL2_11	corroded gilt small diameter	

The analysis of metal threads was performed on a Philips X'Pert MPD instrument. The samples were mounted on glass slides, carefully positioning the top of the curvature of the metal thread in the X-ray beam. Due to the small sample size and to avoid beam penetration into the sample bulk, glancing incidence diffraction with a thin film collimator was employed. Silver and copper coupons were analysed on a Philips X'Pert APD system using $\theta 2\theta$ diffraction. Both instruments were equipped with a Cu anode X-ray tube and the scan range was 10-85°2θ for all samples.

6.3. Results and discussion

6.3.1. Metal threads images and classification

All metal threads were of category III, Table 6.1.1. Categories for the inclusion of metal in textiles, i.e. solid metal filaments wound around a fibrous core, which was found to be silk in all samples with the exception of a number of restoration threads with cotton core fibres. The silk core was white or light yellow for silver threads and dyed in darker yellow shades for gilt threads; the core fibres usually exhibited a low twist in the opposite direction to the metal filament. The wrapping direction of the metal filaments was S in all single wrapped samples with the exception of one single wrapped sample from the "Abraham and Melchizedek" tapestry (sample HCP 19G3 gilt medium diameter thread) and three restoration threads from the "Christ before Pilate" tapestry (samples BXL 2_01/_18/_20) which exhibited Z directional winding. The metal filaments of the double and triple wrapped threads showed combinations of S and Z winding. According to appearance of metal, level of corrosion and thread diameter, all metal thread samples were assigned into groups, which are listed in Table 6.3.1. Figures 6.3.2 to 6.3.10 show representative images of samples of each group (note: scale bars on BXL2 images are incorrect). The thread diameter, width of metal foil and number of coils per 5 mm thread were measured manually through digital imaging analysis. All µm measurements were rounded to the nearest 50 due to the relative imprecision of the measurement technique. The metal strip width and number of coils per unit length were found to vary with thread diameter. Large diameter threads (≥ 650 µm) generally have wider metal strips and fewer coils than medium (< 650 > 350 µm) or small diameter threads (≤ 350 µm), which show the finest metal strip width and the most coils per unit length. The relationship between diameter, width and coil number was also observed in the silver threads, Figure 6.3.1.

The relative amounts of samples per group gave some indication of overall quality of metal threads used for the different tapestries. All five tapestries were manufactured in Brussels at approximately the same time (1520-1545).

Due to the large number of samples only few representative samples were analysed with SEM/EDX, XPS, ToF-SIMS and XRD.

Table 6.3.1. Groups of metal thread samples

Group	Number of samples in tapestry					
	HCP	PNM1	PNM2	PNM5	BXL2	Total
Gilt large diameter (≥650 µm)	14 / 4	- / -	- / -	- / -	- / -	14 / 4
Gilt medium diameter (< 650 > 350 µm)	26 / 12	3 / 3	3 / -	5 / -	8 / 4	45 / 19
Gilt small diameter (≤350µm)	12 / 3	6 / 4	6 / 3	3 / -	- / 2	27 / 12
Silver	-/26	-/4	-/4	1/-	-	1/34
Double wrapped	7/5	2/2	1/1	-/1	-	10/9
Triple wrapped	-	1/-	-	1/2	-	2/2
Restoration	-	-	-/1	-	4/3	4/4
No assignment	2/1	2/0	-	1/-	-	7/1
Total number of samples in tapestry	112	27	19	14	21	193

x / x = # samples with little or no corrosion / # heavily corroded samples

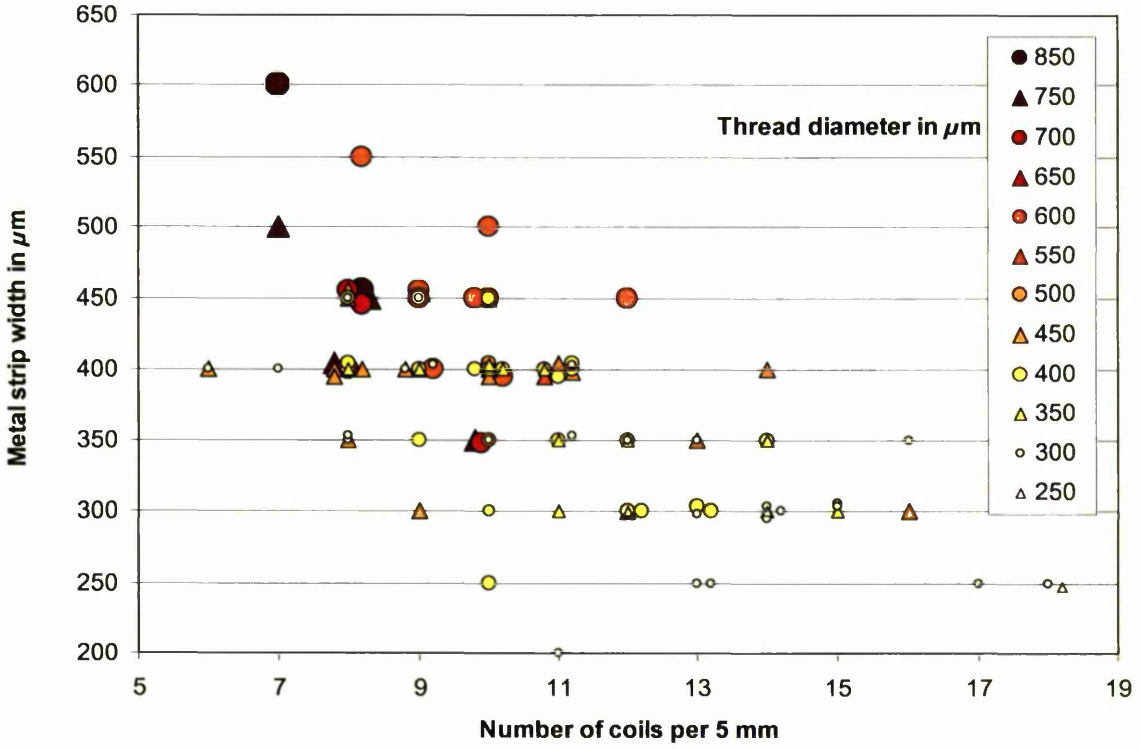

Figure 6.3.1. Relationship of metal thread diameter, metal strip width and number of coils per unit length of metal thread (114 samples; overlapping data points were artificially spread)


HCP 71E5

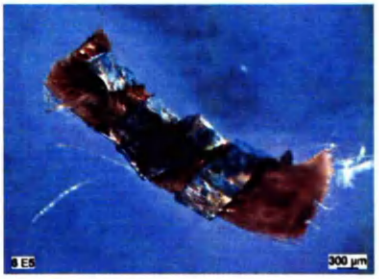
HCP 06E5

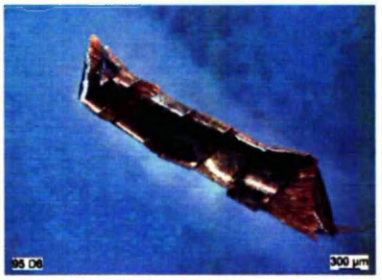
HCP 95D6

Figure 6.3.2. Gilt large diameter metal threads

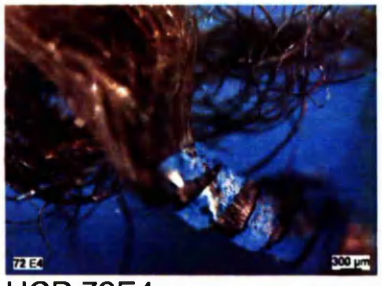
HCP 72E4


HCP 161A6


HCP 137C6

Figure 6.3.3. Corroded gilt large diameter metal threads


HCP 51F5

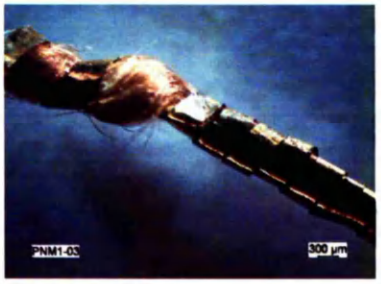
PNM 1_03


PNM 5_26

Figure 6.3.4. Gilt medium diameter metal threads

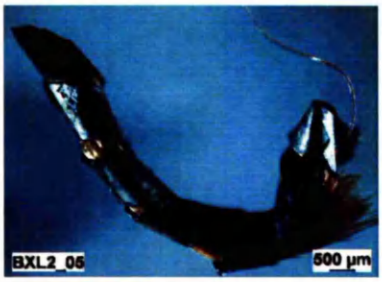
BXL 2_05

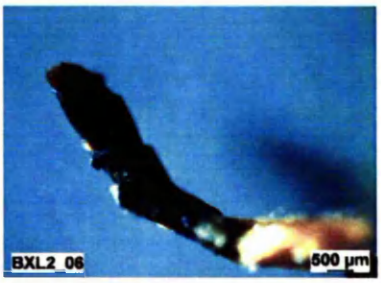
BXL 2_06

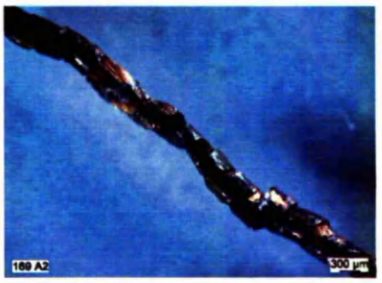
HCP 169A2

Figure 6.3.5. Corroded gilt medium diameter metal threads


HCP 31G5


PNM 1_24

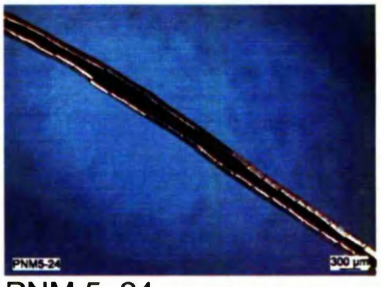
PNM 5_24

Figure 6.3.6. Gilt small diameter metal threads

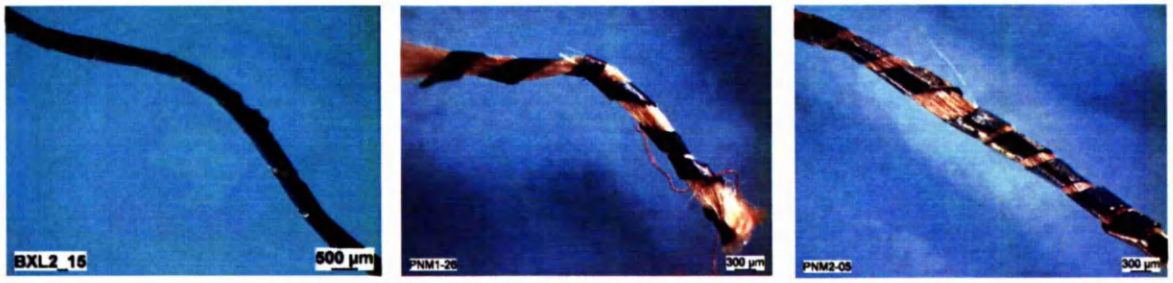

BXL 2_15 PNM 1_26 PNM 2_05

Figure 6.3.7. Corroded gilt small diameter metal threads

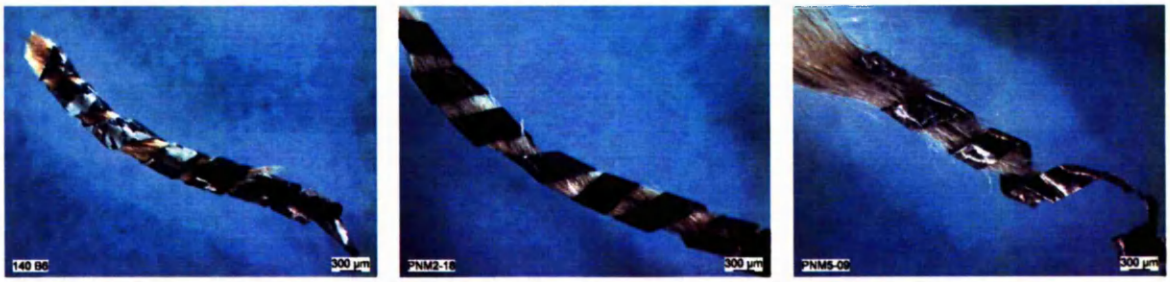

HCP 140B6 PNM 2_18 PNM 5_09

Figure 6.3.8. Silver metal threads (all diameters)

HCP 28G6 HCP 64E6 PNM 5_04

Figure 6.3.9. Double wrapped metal threads

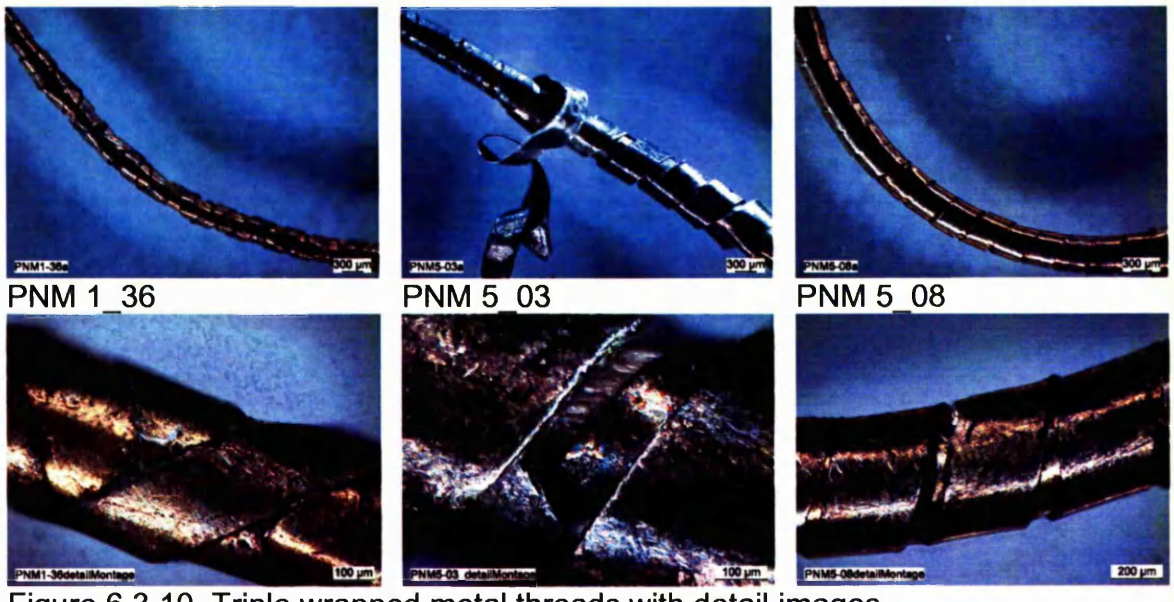

PNM 1_36 PNM 5_03 PNM 5_08

Figure 6.3.10. Triple wrapped metal threads with detail images

The double and triple wrapped metal threads are unusual examples of overt wealth and are regarded as the highest quality precious metal threads. Along with the double and triple wrapped threads, the group of small diameter threads seemed the most intricate in manufacture; extremely fine and so tightly wrapped that the silk core was hardly visible through the gaps between the metal filament coils and thus represent very high quality metal threads.

A third of all samples taken from the BXL2 "Christ before Pilate" tapestry were restoration threads and the remaining samples were gilt small to medium diameter threads with partially heavily corroded filaments. No samples with double or triple wrappings were observed in this tapestry, suggesting that the choice of metal threads used in this tapestry was of lower quality than the metal threads used in the other tapestries. HCP "Abraham and Melchizedek" is the only tapestry which exhibited large diameter threads; the tapestry also showed the highest relative amount of silver threads with almost a quarter of all HCP samples being silver. The three PNM tapestries (PNM1, 2 & 5) belong to the same set of the "Fables of Ovid" and it was assumed that the same type of metal threads were used throughout, this was also reflected in the similar distribution of relative amounts of samples per group. The rare triple wrapped threads were exclusively found in the PNM tapestries which also showed high relative amounts of double wrapped threads and small diameter threads. This indicates that the metal threads incorporated in the PNM tapestries are of the highest quality.

However, the HCP, BXL2, PNM1 and PNM2 tapestries all contained approximately 50% heavily corroded samples, while PNM5 exhibited only very few corroded samples, Table 6.3.1. This was most likely due to the history of the tapestries, i.e. the length of time of display and conditions of storage. The tapestries "The Fall of Icarus" (PNM1) and "The Abduction of Ganymede" (PNM2) have been on permanent display for at least the last fifty years in "Palacio de San Ildefonso, Sala Tapices Fabulas de Ovidio", while the tapestry "The Sacrifice of Polixena" (PNM5) was in storage in "Palacio Real de Madrid, Almacen de Tapices" accounting for the better preservation of its metal threads.

The discontinuous spinning process used for 'beaten and cut' metal threads may lead to an overlap of adjoining metal lamellas. These 'false' double wrapped threads would exhibit the same winding direction for the inner and outer metal lamellas. As can be seen from Table 6.3.2 most samples identified as double or

triple wrapped threads showed a second or third layer of metal in opposite winding direction to the underlying layer, see also images of double and triple wrapped threads in the appendix sections F.1. and F.2. The four triple wrapped threads exhibited S over Z over S winding while there were eight double wrapped samples with S over Z winding, four samples with Z over S winding, three samples with an indiscernible winding direction of the inner layer and two samples showing S over S winding. The two latter samples (PNM 2_03 and PNM 2_16) also showed the same filament widths for both inner and outer layers, i.e. 300 µm. This suggests that they are samples of single wrapped threads showing the region of overlap from the joining of one metal lamella to the next during the spinning process.

Table 6.3.2. Dimensional features of double and triple wrapped threads

	Sample	Group	Ø µm	3rd layer (outer)			2nd layer			1st layer (inner)		
				#	w	d	#	w	d	#	w	d
Double wrapped	HCP 67-E6	Gilt large	900	-	-	-	10	400	S	x	500	Z
	HCP 136-C6	Gilt large	750	-	-	-	x	400	S	10	400	Z
	HCP 153-B6	Gilt large	700	-	-	-	x	450	S	x	250	Z
	HCP103-D6	Gilt large	650	-	-	-	12	350	S	x	x	Z
	HCP 73-E4	Gilt medium	600	-	-	-	16	250	S	x	400	x
	HCP _X_	Gilt medium	500	-	-	-	x	450	Z	x	300	S
	HCP 167-A3	Gilt medium	450	-	-	-	x	400	S	x	x	x
	HCP 43-F6	Gilt medium	450	-	-	-	x	300	Z	9	300	S
	HCP 64-E6	Gilt medium	450	-	-	-	10	300	Z	14	300	S
	HCP 69-E6	Gilt medium	450	-	-	-	x	400	S	x	400	Z
	HCP 28-G6	Gilt medium	400	-	-	-	10	350	Z	12	300	S
	HCP 94-D6	Silver large	700	-	-	-	x	400	S	8	400	Z
	PNM1-46	Gilt medium	500	-	-	-	x	350	S	x	350	x
	PNM1-10	Gilt medium	450	-	-	-	x	450	Z	15	400	S
	PNM1-08	Gilt medium	400	-	-	-	12	400	Z	x	x	S
	PNM1-49	Silver medium	450	-	-	-	8	350	S	11	350	Z
	PNM2-03	Gilt medium	400	-	-	-	x	300	S	14	300	S
	PNM2-16	Silver medium	400	-	-	-	x	300	S	10	300	S
	PNM5-04	Gilt medium	400	-	-	-	10	300	S	8	200	Z
Triple wrapped	PNM1-36	Gilt small	350	8	200	S	11	200	Z	11	200	S
	PNM5-03	Silver medium	600	8	450	S	7	450	Z	8	450	S
	PNM5-05	Silver medium	700	8	400	S	x	400	Z	x	400	S
	PNM5-08	Gilt medium	500	12	350	S	x	x	Z	x	x	S

#: number of coils per 5 mm
w: approximate width of metal filament in µm
d: direction of metal wrapping
x: indiscernible

6.3.2. Manufacturing techniques

Establishing the manufacturing technique is often made by means of SEM analysis of the edges of metal filaments [7, 11, 12, 19]. Sharp angles with tool marks left from cutting indicate 'beaten and cut' threads, while smooth and round

edges and longitudinal striations are characteristic for 'cast, drawn and rolled' threads. However, SEM analysis of model metal threads, produced from flattened (rolled) wires, see Chapter 3. section 3.3., showed that this characterisation can be misleading. The edges on the model metal thread filaments were also often rough with sharp angles, Figure 6.3.11. Therefore, the determination of the manufacturing technique must include the analysis of the metal filaments' exterior and interior sides to ascertain single- or double- sided gilding, indicative of 'beaten and cut' or 'cast, drawn and rolled' manufacture respectively.

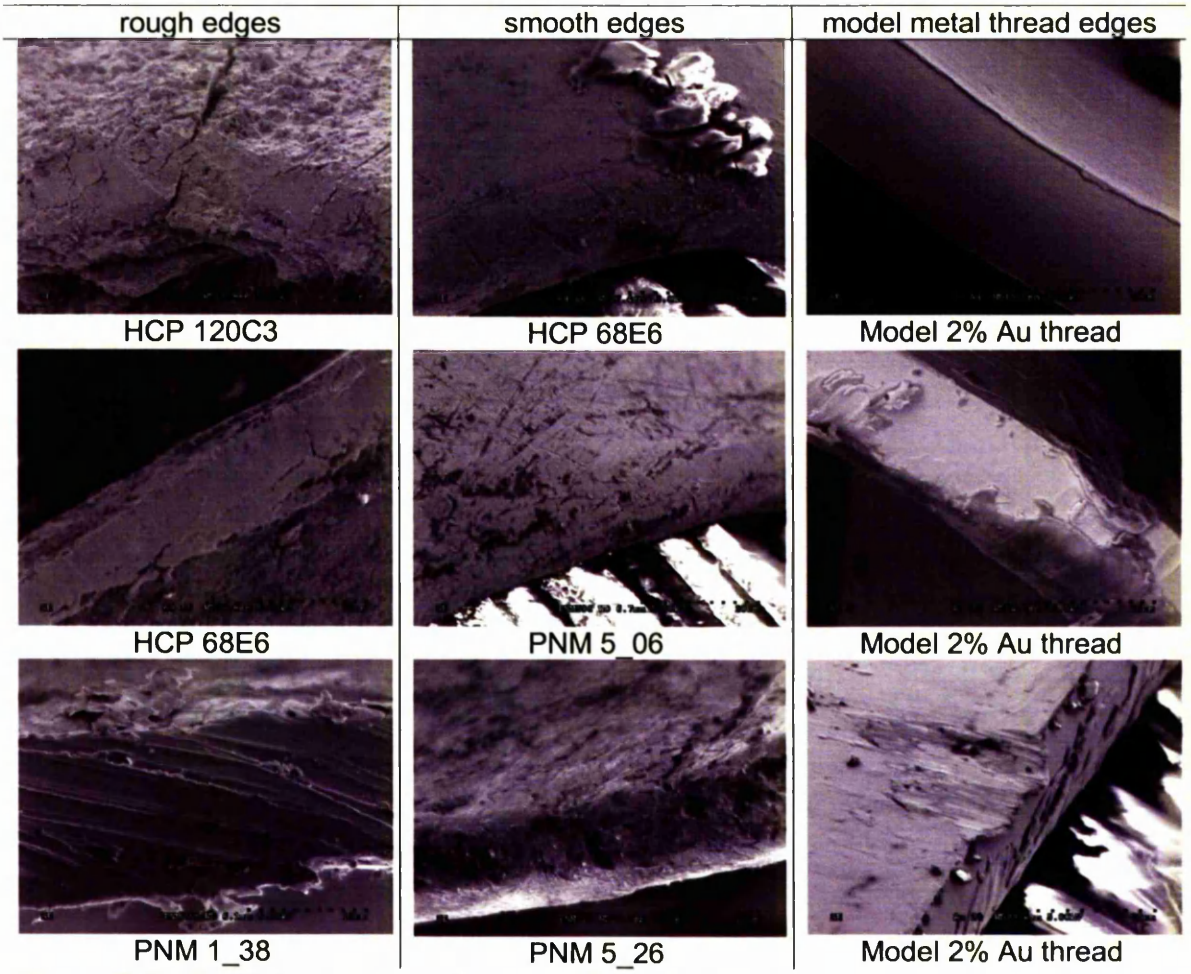

Figure 6.3.11. Historic and model metal filament edges

Forty-one metal thread samples were analysed by EDX; for most samples multiple spectra were obtained at varying accelerating voltages from several analysis points on the exterior and interior sides of the metal filament. The complete dataset of all EDX analyses of metal threads is listed in the appendix section G, while Table 6.3.3 gives a summary of the results, showing the highest gold concentration measured at any point on the sample and the averaged results from multiple analysis points at low accelerating voltages (7-10 kV), i.e. near the sample surface, and at high accelerating voltages (20-30 kV), i.e. close to bulk analysis.

Table 6.3.3. Averaged EDX data of metal threads in weight %

Sample	Group*	Highest Au concentration kV 07-20 wt. %			Exterior kV 07-10 wt. %			Exterior kV 20-30 wt. %			Interior kV 07-10 wt. %			Interior kV 20-30 wt. %		
		Ag	Cu	Au	Ag	Cu	Au	Ag	Cu	Au	Ag	Cu	Au	Ag	Cu	Au
HCP 49F5	L	18	3	79	42	7	51	68	5	27	88	12		93	7	
HCP 6E5	L	27	7	66	74	10	16	75	11	14	83	17		90	10	
HCP 71E5	L	27	3	70	41	3	55	74	6	20	96	4		94	6	
HCP 95D6	L	23	3	74	34	4	63	63	10	28	95	5		95	5	
HCP161A6	Lc	24	3	72	86	3	11	87	6	7	93	7		85	15	
HCP 72E4	Lc	44	7	49	51	18	31	68	7	25	79	21		91	9	
BXL 2_04	M	30	7	62	40	14	46	63	8	29	76	24		90	10	
BXL 2_19	M	25	6	69	64	24	12	49	11	40	71	29		91	9	
BXL 2_22	M	21	6	73	32	10	58	57	6	37	87	13		93	7	
BXL 2_36	M	12	3	85	53	14	33	67	7	27	75	25		92	8	
HCP 46F6	M	20	11	70	30	9	62	79	5	16	85	15		92	8	
HCP 51F5	M	33	3	64	43	4	53	64	5	31	89	11		94	6	
PNM 1_03	M	34	11	56	34	11	56	68	6	26	84	16		88	12	
PNM 1_38	M	30	18	52	32	17	51	81	6	13				90	10	
PNM 2_17	M	25	6	69	49	8	43	74	7	19	88	12		94	6	
PNM 5_06	M	31	1	68	34	5	61	69	5	26	90	10		93	7	
PNM 5_26	M	21	7	72	33	8	59	76	6	18	81	19		92	8	
PNM 5_30	M	18	3	79	32	6	62	65	7	27	83	17		92	8	
PNM 5_41	M	13	5	83	45	9	46	62	7	31	90	10		92	8	
BXL 2_06	Mc	14	5	81	48	12	41	59	6	35	87	13		93	7	
BXL 2_05	Mc	21	5	74	77	11	12	77	9	14	85	15		90	10	
HCP169A2	Mc	14	10	76	79	6	15	88	7	5	79	21		87	13	
HCP119C3	S	21	5	74	56	6	38	66	4	30	73	27		91	9	
HCP 31G5	S	21	2	77	41	4	55	77	4	19	83	17		94	6	
HCP 96D6	S	11	3	85	32	7	61	62	5	33	76	24		93	7	
PNM 1_06	S							72	5	23				89	11	
PNM 1_24	S	22	5	73	32	7	61	59	6	35	87	13		92	8	
PNM 2_02	S	24	19	56	43	14	43				81	19		92	8	
PNM 2_06	S	37	11	52	63	20	17	67	10	23	75	25		88	12	
PNM 2_19	S	32	23	45	33	25	41	74	9	17				92	8	
PNM 5_24	S	36	19	45	51	16	33	76	7	17	91	9		92	8	
BXL 2_15	Sc	82	0	18	86	0	14	98	0	2				91	3	6
HCP140B6	Ag				98	2	0	95	5	0	95	5		94	6	
PNM 1_01	Ag							94	6					94	6	
PNM 2_18	Ag							90	10	0				90	10	
PNM 5_09	Ag				90	10	0	91	9	0	89	11		93	7	
HCP 28G6	2x	45	2	53										96	4	
PNM 1_36	3x	34	3	63										92	8	
BXL 2_14	R	11	52	37	43	54	3	92	1	6	95	2	3	92	3	6
BXL 2_24	R							97	3							
						Cu	Zn		Cu	Zn		Cu	Zn		Cu	Zn
BXL 2_07	R					67	33		86	14		67	33		86	14

* L: Gilt large diameter; Lc: Corroded gilt large diameter; M: Gilt medium diameter; Mc: Corroded gilt medium diameter; S: Gilt small diameter; Sc: Corroded gilt small diameter; Ag: Silver; 2x: Double wrapped; 3x: Triple wrapped; R: Restoration

The results show that all but one of the analysed gilt small, medium and large diameter threads are gilt on one side only suggesting the 'beaten and cut' manufacturing route. Sample BXL 2_15 showed some gold on the interior of the metal filament which is indicative of 'cast, drawn and rolled' manufacture. The 'cast, drawn and rolled' method is a relatively modern production pathway with the change over from 'beaten and cut' threads occurring between the late 15th or 16th century to the 17th century. The five tapestries with metal threads analysed in this project were produced in Brussels around 1520 (BXL2), 1535 (HCP) and 1545 (PNM series). The early production date of the BXL2 tapestry and the similarity with EDX analysis results of the restoration thread BXL 2_14, Table 6.3.3, suggest that sample BXL 2_15 is also a restoration thread and therewith a later inclusion in the tapestry. Sample BXL2_07 was already identified as a restoration thread during sampling due to its position and weave construction within the tapestry design and its unusual black core fibres. SEM images of cross-sections suggested that the core fibres consisted of mercerized cotton, implying that the thread was not manufactured before the mid 19th century when John Mercer invented the alkali treatment to impart strength, lustre and improved dyeability to cotton fibres, Figure 6.3.12 [60]. EDX analysis showed that the metal filament contained brass, i.e. a copper-zinc alloy, with the zinc content being higher on the surfaces of the metal filament than in its bulk, indicating that the filament was produced by the 'Pinchbeck' method, a technique invented by Christopher Pinchbeck in the early 18th century whereby a copper object is being passed through zinc vapour to convert its surface into brass to create a resemblance of gold [16].

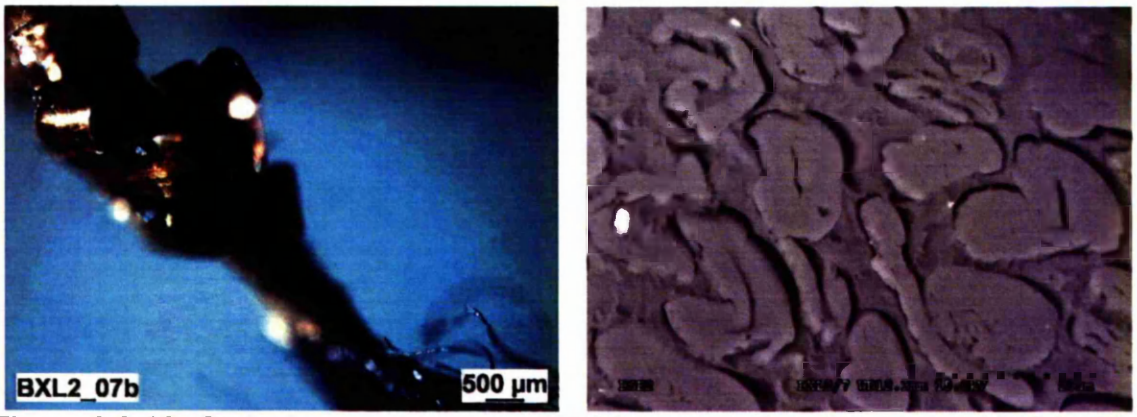

Figure 6.3.12. Optical microscopy and SEM (cross-sectional) images of BXL2_07

The highest gold concentration measured on any metal thread was 85 wt.% (samples BXL 2_36 and HCP 96D6) this may indicate that the gilding was performed with alloyed gold containing silver and copper. However, it may also be due to precipitation of silver and copper ions from the bulk into the gold layer or due to the thinness of the gold layer and the penetration of the electron beam into the silver-copper bulk. An indication for precipitation of copper ions is given by the generally higher copper concentration close to the sample surface compared to the sample bulk, i.e. EDX analysis of the interior sides at low and high accelerating voltages respectively, Table 6.3.3. This is also exemplified in Figure 6.3.13 which shows the relative wt.% of copper as determined by 'depth' analysis using increasing accelerating voltages from 7 to 30 kV at the same area of analysis. Four out of six samples showed higher copper concentrations at lower accelerating voltages, i.e. close to the sample surface while the two samples with the lowest copper concentration (~ 5 wt.%) exhibited a relatively homogenous copper concentration with depth. Analogous 'depth' analysis of the exterior of metal threads is represented in Figure 6.3.14. The gold concentrations are at a maximum at 7-10 kV and decrease with increasing accelerating voltage, the silver concentrations follow the reverse trend with increasing concentrations at increasing accelerating voltages, while the copper concentrations remain relatively constant. This indicates a higher relative proportion of copper in the gold layer compared to silver in the gold layer and suggests either the predominant precipitation of copper over silver or the initial inclusion of a higher percentage of copper in the gold used for gilding.

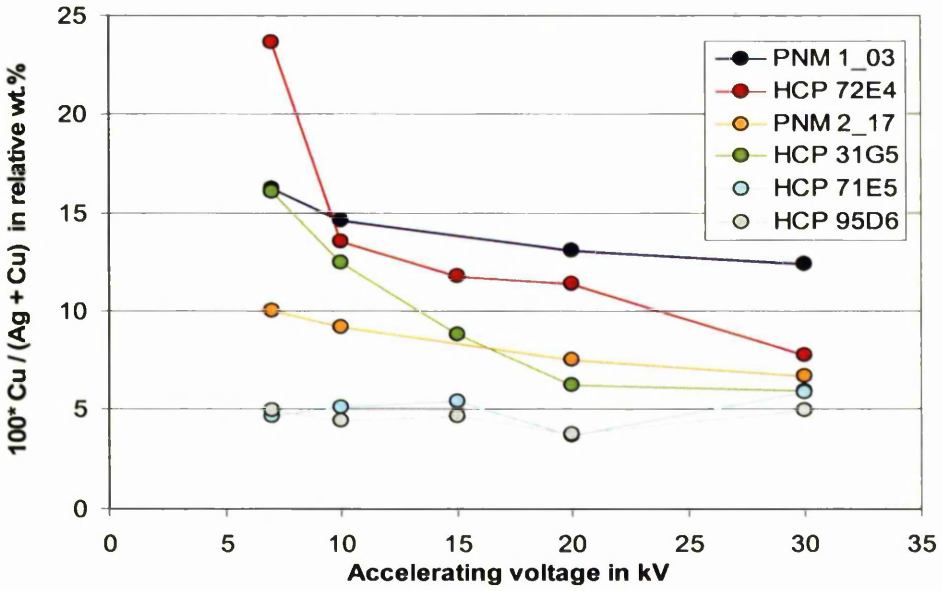

Figure 6.3.13. EDX 'depth' analysis of the interior of metal thread filaments

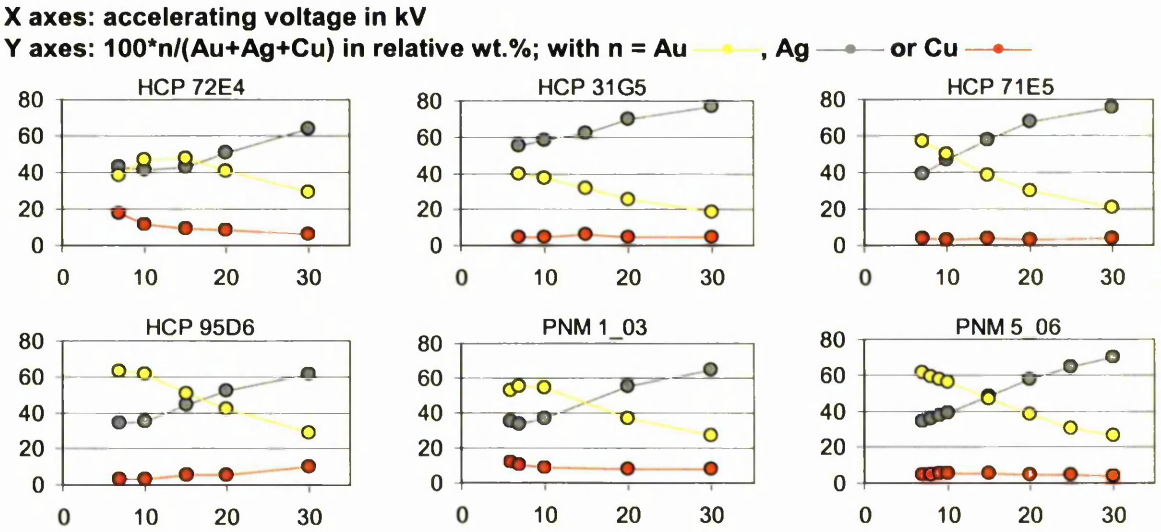

Figure 6.3.14. EDX 'depth' analysis of the exterior of metal thread filaments

Copper ion migration was also observed on the semi-quantitative depth profiles obtained by dynamic SIMS analysis. Most profiles showed mirroring silver and copper lines, i.e. the surface copper concentration was high and decreased with increasing silver concentration until the surface etching reached the bulk region where the silver and copper lines levelled at their respective concentrations. Typical SIMS depth profiles of the exterior and the interior of a metal thread filament are shown in Figure 6.3.15 and Figure 6.3.16. All obtained SIMS depth profiles are represented in the appendix sections H.1. to H.9. Figure 6.3.16 exemplifies a 'sub-surface enrichment' phenomenon observed in a third of all analysed samples where the copper concentration shows a minimum just below the initial surface maximum. This silver 'enriched' region can be attributed to the depletion of copper through ion migration to the surface where copper corrosion products formed.

The exterior of sample HCP 68E6 showed its gold maximum at approximately 20 nm depth and its minimum, i.e. bulk or background concentration, at ~ 80 nm. This was representative of all analysed samples which showed gold maxima at or below 100 nm and interface regions down to a maximum of 500 nm depth. These extremely thin gold layers are consistent with other recent studies on metal threads which revealed lower gold layer thicknesses than previously proposed [40, 61].

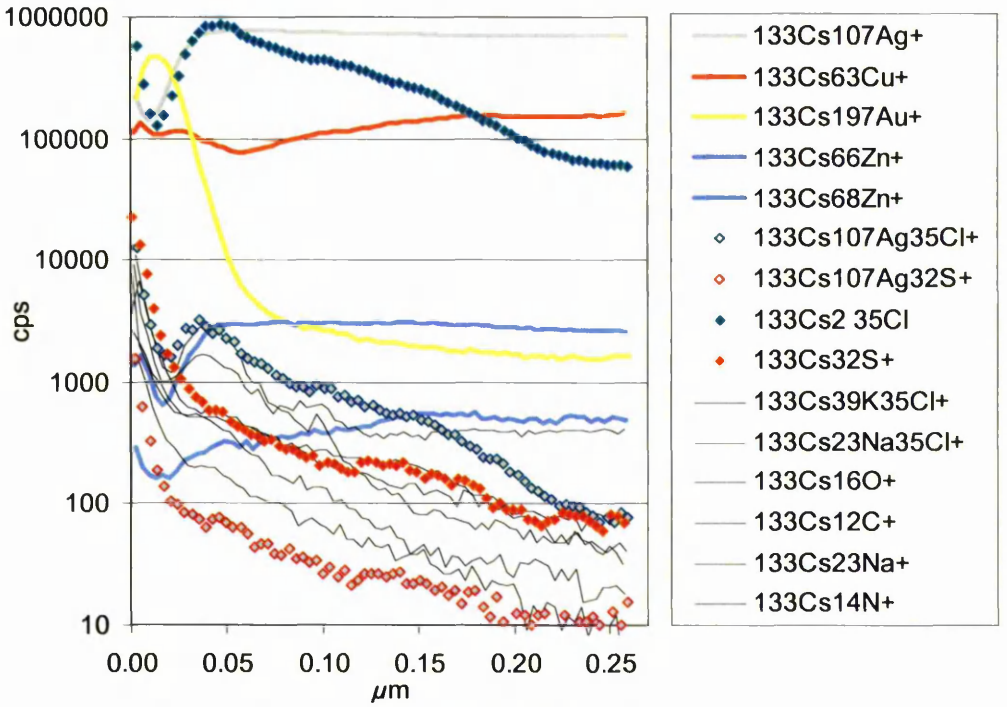

Figure 6.3.15. Positive SIMS depth profile of the exterior of HCP 68E6

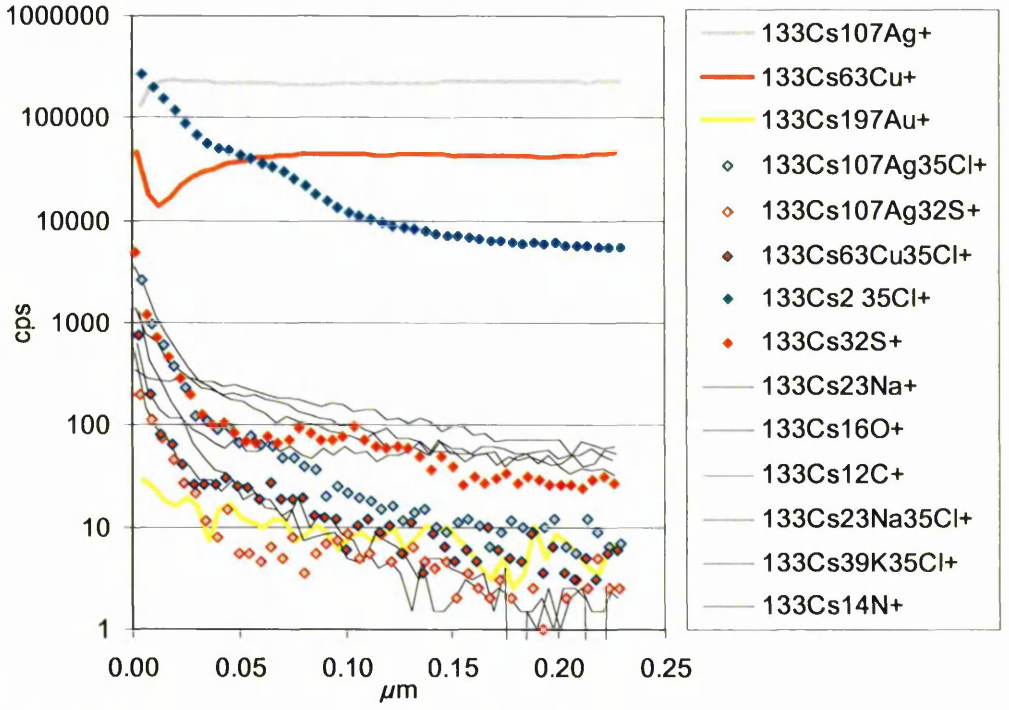

Figure 6.3.16. Positive SIMS depth profile of the interior of HCP 68E6

The surface or near surface silver enrichment phenomenon described above has been long noted in numismatics and has been attributed to segregation during casting or annealing, chemical treatment such as pickling in acids or blanching, wearing and/or corrosion [62]. Beck et al. could show in a recent publication that surface silver enrichment of silver-copper alloys may also occur during the

fabrication of the alloy due to phase separation in the cooling process [62]. However, this can only take place if the alloy is cooled under equilibrium conditions, i.e. if the silver-rich phase and the copper-rich phase have enough time to separate during cooling and if the alloy contains enough copper to allow for phase separation [63]. This is represented in the equilibrium phase diagram in Figure 6.3.17. The overall alloy composition is given in Ag wt% along the lower x-axis and in Ag at% along the upper x-axis. Silver can accommodate approximately 9 wt% copper without separating into two phases, similarly copper can take up to 8 wt% silver in a single phase alloy in equilibrium. The lowest melting point of any silver-copper alloy is the eutectic temperature (779°C) for the eutectic phase consisting of 72 wt% Ag and 28 wt% copper. Alloys with a lower silver content (to the left of the eutectic composition) will possess grains of a copper-rich phase (92 wt% Cu and 8 wt% Ag) surrounded by the eutectic phase, while alloys with a high silver content possess grains of a silver-rich phase (91 wt% Ag and 9 wt% Cu) surrounded by the eutectic phase.

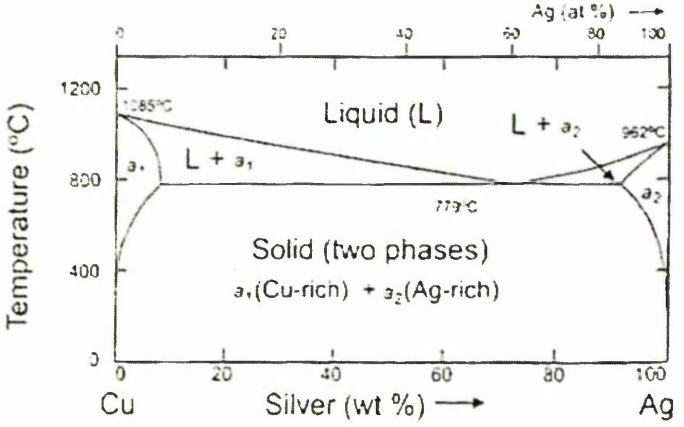

Figure 6.3.17. Equilibrium phase diagram for copper and silver [63]

Rapid cooling of molten silver-copper alloys does not allow enough time for diffusion of silver and copper atoms thus phase separation cannot occur. The resulting single phase alloy is softer and more malleable than two phase alloys. Subsequent heat treatment or natural ageing over very long times can allow precipitation and thereby phase separation; i.e. so called age hardening [63].

In order to investigate the manufacturing method of the metal thread filaments' bulk alloys, highly polished cross sections were analysed using a Field Emission Gun Scanning Electron Microscope (FEG-SEM) in Backscatter mode to distinguish individual grains and grain boundaries through atomic number contrast.

The three analysed metal thread filaments consisted of single phase alloys as no grains could be distinguished; instead the metal sections had a uniform but porous appearance as shown in Figure 6.3.18. EDX analysis showed that the copper content in the silver bulk was generally < 9 wt%, see Table 6.3.3 and appendix section G, which explains the single phase alloy. It may be that the gold- and silversmiths deliberately included only a small amount of copper in silver-copper alloy in order to attain a flexible metal for the inclusion in textiles. On the other hand, rapid cooling may have been employed to achieve the same effect which would also account for the inclusion of pores in the metal bulk.

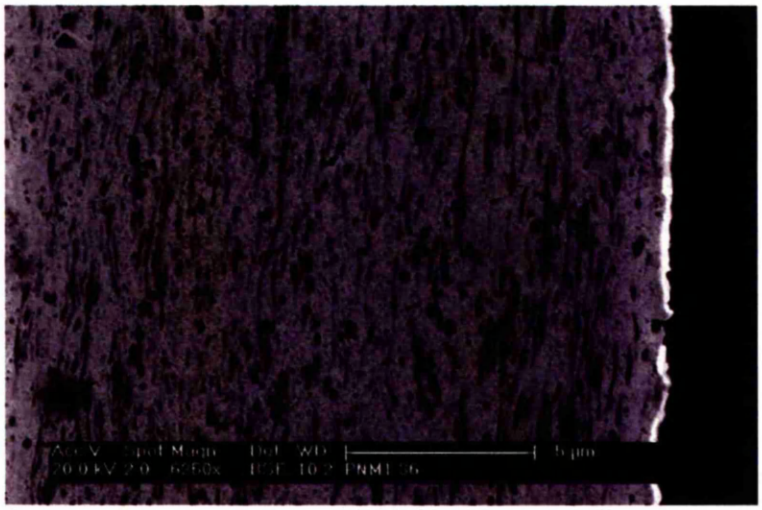

Figure 6.3.18. Porous length section of PNM1_36 metal filament

The pores in the metal bulk were compressed during the further processing of the metal sheets or rods into thin foil or wire. Beating of a metal sheet would compress the pores equally in all directions while the drawing of a wire would stretch the pores lengthwise. Since all analysed metal filament were gilt on one side only it was expected to observe similarly sized and shaped pores in the length sections and cross sections. Yet, stretched pores were observed in the length sections and were particularly noticeable in sample PNM5_06 as shown in Figure 6.3.19. This metal thread sample also showed a groove running parallel with the filament which provides further evidence of rolling rather than beating, Figure 6.3.20. However, since the filaments are single gilt it is unlikely that they were produced from drawn wire. Rolling of metal sheets may have been employed for the thinning into foils before cutting into filaments. Evidence of cutting was detected on the cross sections of the edges of metal filaments which showed signs of pressure applied from the direction of the non-gilt side (interior), i.e. stretched pores from the interior to the exterior, Figure 6.3.21.

Cross sections | Length sections

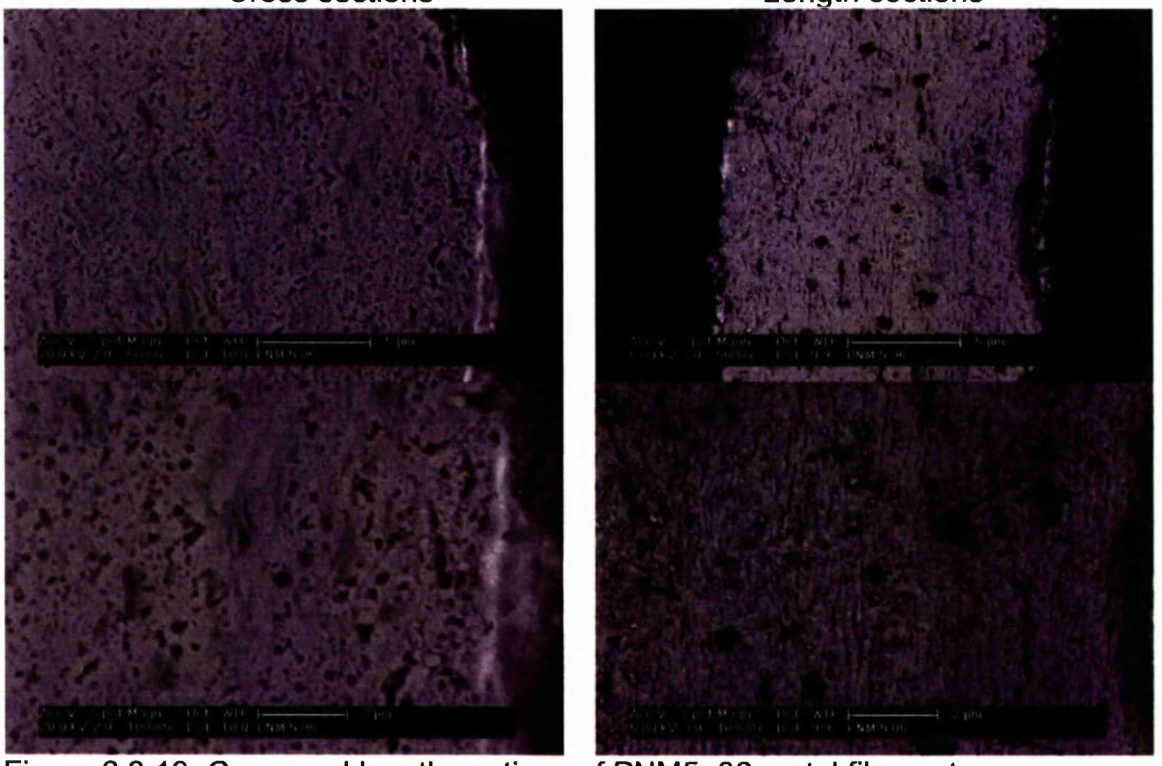

Figure 6.3.19. Cross and length sections of PNM5_06 metal filament

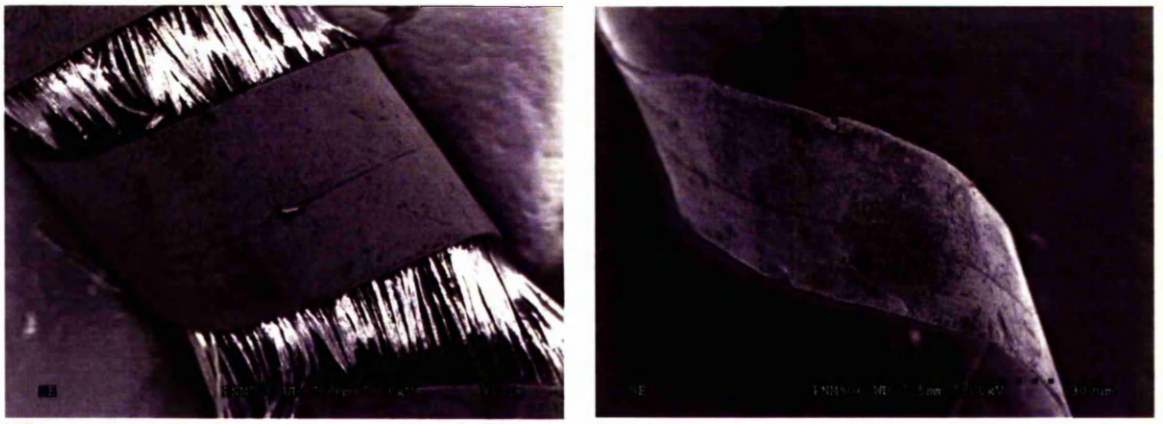

Figure 6.3.20. Striation on PNM5_06

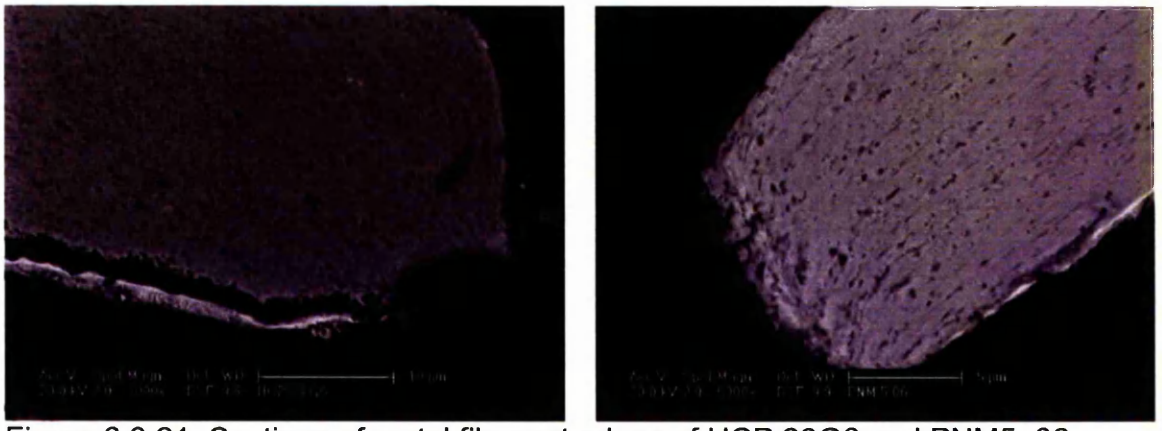

Figure 6.3.21. Sections of metal filament edges of HCP 28G6 and PNM5_06

The FEG-SEM cross sections were also used for measuring the thickness of the metal filaments and the thickness of the gold layers. The filaments of the three investigated threads were found to be approximately 20 μm thick and showed gold layer thicknesses of approximately 200-300 nm, Figure 6.3.22 and Figure 6.3.23. The Backscattered images showed very clear contrast between the gold layers and the silver-copper bulk with no signs of a diffusion zone. This suggests the leaf gilding technique, which is further confirmed through the partial delamination of gold layers on all samples and the presence of overlapping gold leaves on samples PNM1_36 and PNM5_06, Figure 6.3.24 and Figure 6.3.25. Delamination has previously been suggested to signify manufacturing technique, for example folding and stretching of a metal foil or strip prior to cutting into narrower strips for winding [49], or joining of thin foils by hammering and subsequent cutting into strips [6].

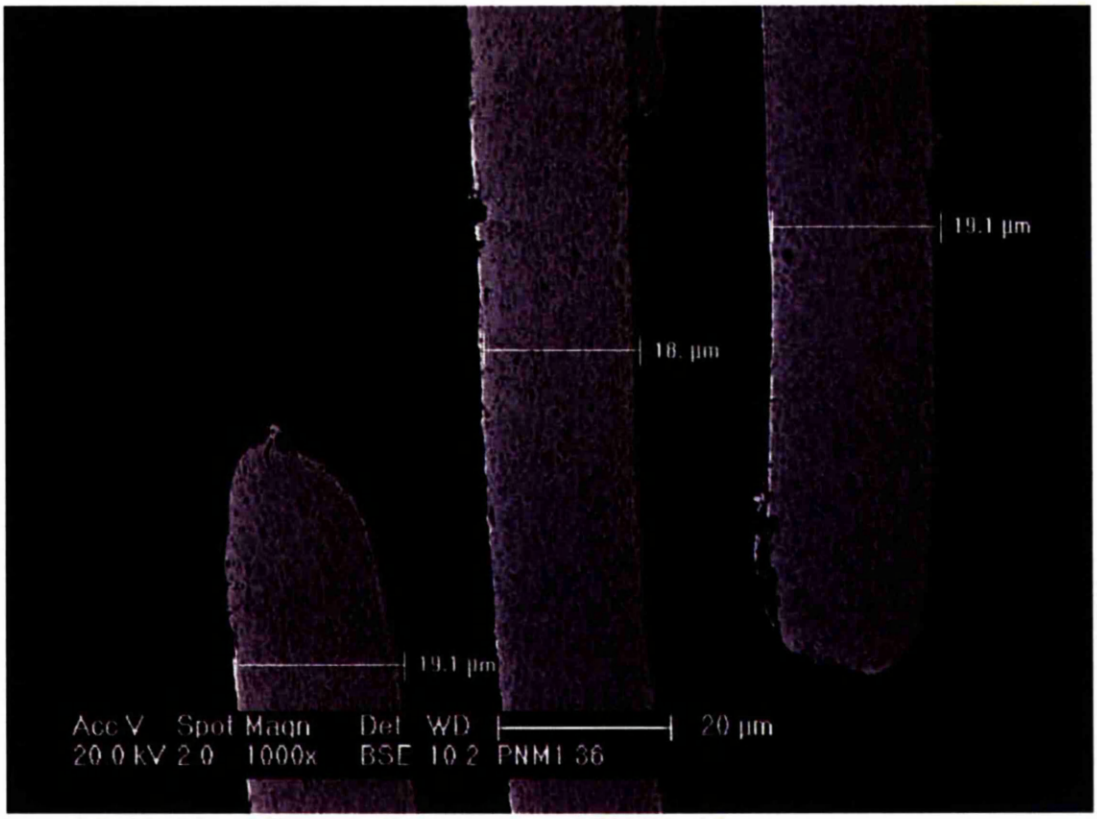

Figure 6.3.22. Metal filament thicknesses of PNM1_36

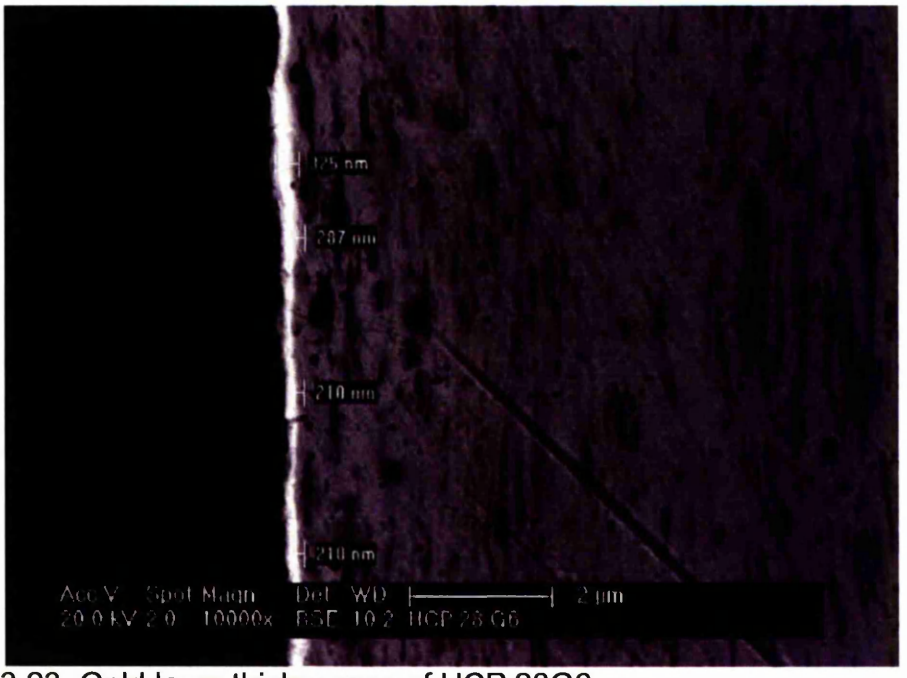

Figure 6.3.23. Gold layer thicknesses of HCP 28G6

Figure 6.3.24. Delaminating gold layer of HCP 28G6

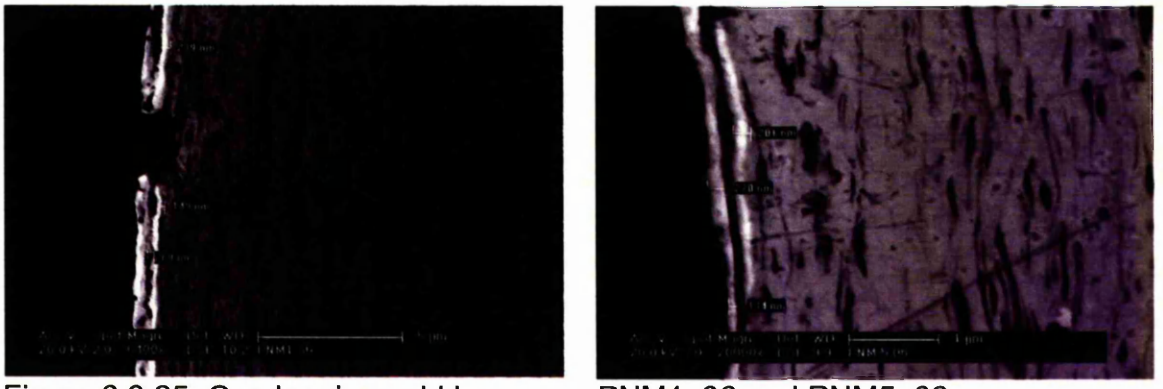

Figure 6.3.25. Overlapping gold leaves on PNM1_36 and PNM5_06

6.3.3. Investigation of metal thread corrosion by SEM/EDX

Approximately 50% of all metal thread samples were heavily corroded, Table 6.3.1. Corrosion morphologies have been investigated by SEM, while the composition of corrosion products was studied by EDX, XPS, SIMS and XRD analyses.

The majority of corrosion morphologies on metal threads were found to be rounded crystals, often joined into a continuous layer, with corrosion cracking, flaking and delamination also being observed on most samples. Figure 6.3.26 to Figure 6.3.28 show typical morphologies of corrosion products and their delamination observed on heavily corroded metal threads as well as initial corrosion growth over gilt layers; see HCP 46F6 and PNM5_30 in Figure 6.3.28. Cross sections of metal thread filaments in Figure 6.3.27 illustrate thick corrosion layers detaching from the bulk metal and corrosion pitting or tunnelling causing the disintegration of the metal bulk.

EDX analyses of corrosion products indicated high levels of sulphur and, in some cases, chlorine as well as increased levels of carbon and oxygen; see EDX results listed in the appendix section G. The nature of the delamination of corrosion products was investigated by analysing adjacent areas of delaminated and underlying layers on the same sample. The areas of analyses are indicated in Figure 6.3.28 and the results are listed in Table 6.3.4.

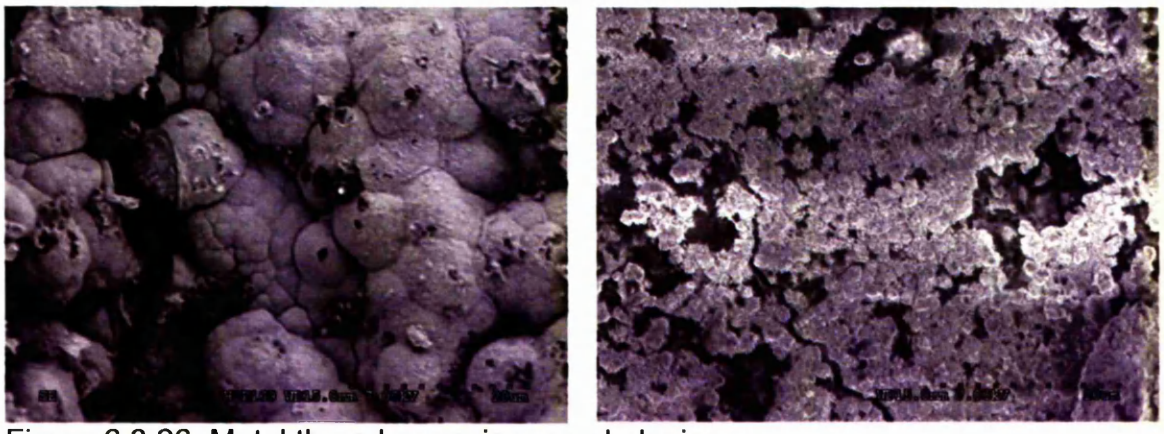

Figure 6.3.26. Metal thread corrosion morphologies

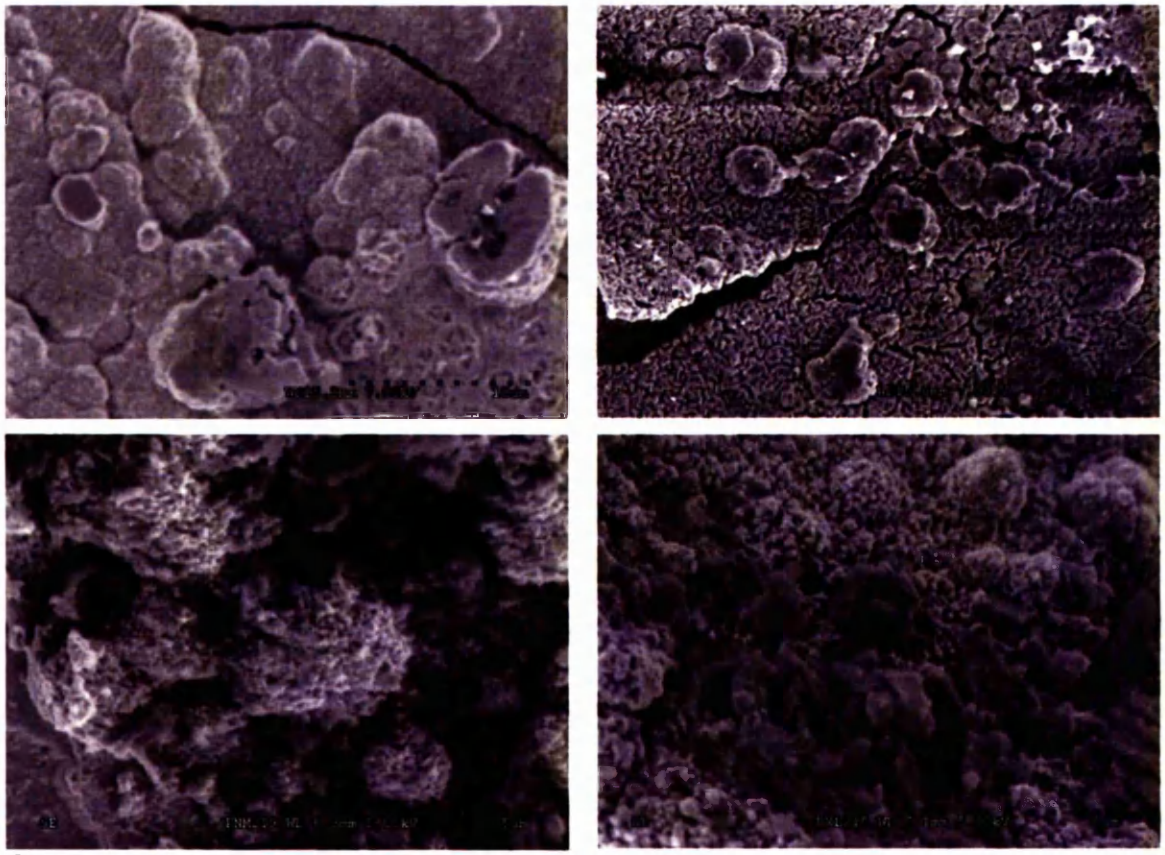

Continuation of Figure 6.3.26. Metal thread corrosion morphologies

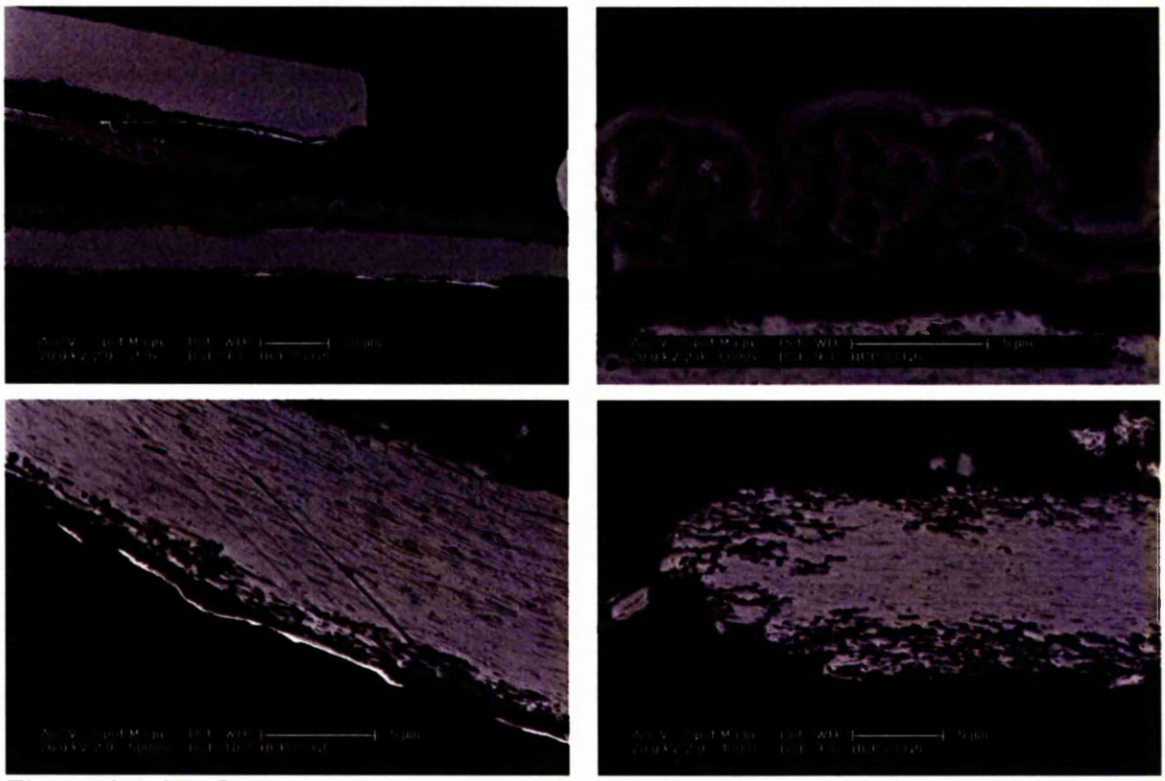

Figure 6.3.27. Cross sections of metal thread corrosion morphologies

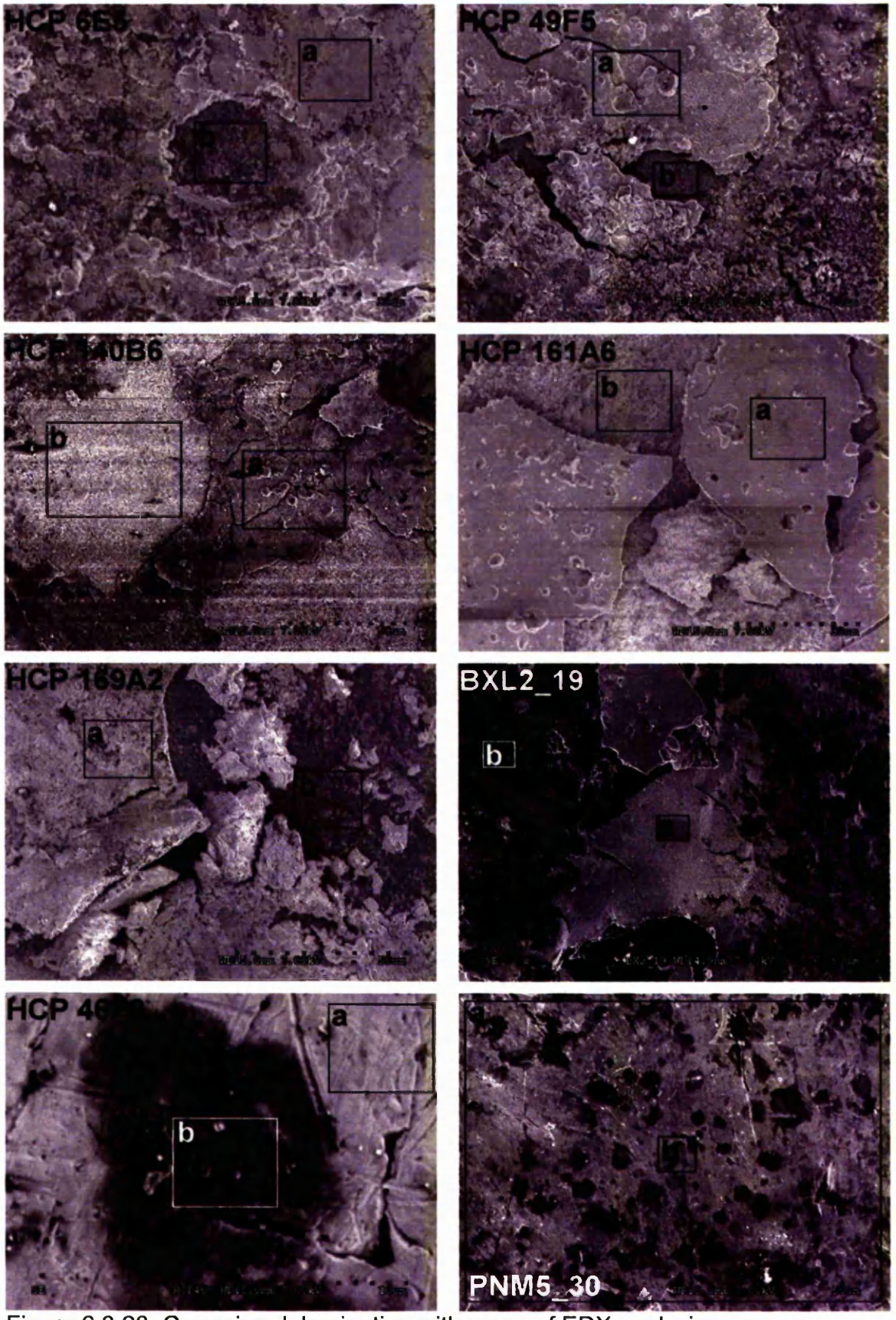

Figure 6.3.28. Corrosion delamination with areas of EDX analysis

Table 6.3.4. EDX results of delaminated corrosion products

Sample * x / y	Image	** Atomic %							100*n/(Ag+Cu+Au)						
		AgL	CuL	AuM	C K	O K	S K	ClK	n=Ag	n=Cu	n=Au	n=C	n=O	n=S	n=Cl
HCP 6E5	a	36	8	-	39	2	12	1	82	18	-	89	6	27	1
L / i	b	11	7	-	74	3	4	0	62	38	-	411	19	24	1
HCP 49F5	a	38	6	-	25	6	17	7	86	14	-	56	13	37	16
L / e	b	29	15	-	43	7	4	-	67	33	-	99	17	8	-
HCP 140B6	a	38	2	-	36	7	15	1	96	4	-	91	17	39	3
Ag / i	b	68	2	-	19	5	1	-	97	3	-	27	8	2	-
HCP 161A6	a	50	1	-	19	4	25	-	97	3	-	37	8	49	-
Lc / i	b	33	10	-	22	28	6	-	78	22	-	51	66	15	-
HCP 169A2	a	26	4	-	40	12	1	16	86	14	-	132	41	4	55
Mc / e	b	9	9	-	66	7	2	6	51	49	-	356	36	9	35
BXL 2_19	a	41	1	1	31	4	21	0	95	2	2	72	8	49	1
M / e	b	20	9	0	63	6	2	-	68	32	0	217	20	7	-
HCP 46F6	a	8	7	16	62	5	2	-	26	24	50	200	18	6	-
M / e	b	8	9	11	63	6	2	-	28	32	40	224	21	8	-
PNM 5_30	a	8	4	16	54	14	1	1	29	14	57	190	47	5	4
M / e	b	4	6	8	73	8	1	-	23	32	45	411	44	6	-

* x = group L = Gilt large; Ag = Silver; Lc = Gilt large corroded; Mc = Gilt medium corroded; M = Gilt medium
* y = side i = interior; e = exterior
**At.% = - Element was not detected
**At.% = 0 Element relative atomic % < 0.5

In most cases layer 'b' contained significantly increased levels of copper, with the highest relative level detected in sample HCP 169A2 which showed 49% copper as relative atomic % of metallic components only. As well as the increased copper levels an increase in the carbon levels was noted in the 'b' layer, while layer 'a' showed relatively high levels of silver and sulphur and, for samples HCP 49F5 and HCP 169A2, high levels of chlorine. Samples HCP 46F6 and PNM5_30 differ in that they do not show corrosion delamination but show only patches of initial corrosion growth over the exterior gold layer. These patches show similarities with the 'b' layer of delaminated samples in their high relative copper and carbon contents. These results suggest corrosion growth in at least two major stages where the initial corrosion is predominantly copper corrosion, possibly copper carbonates and copper sulfide, followed by silver corrosion growth, possibly silver sulfide, which adheres only loosely to the underlying corrosion and is prone to delamination.

Sample HCP 140B6 does not show the above mentioned characteristics as both the 'a' and 'b' layers contain similar relative amounts of silver and copper and, in contrast to all other samples, the 'a' layer contains more carbon than the 'b' layer.

6.3.4. Investigation of metal thread corrosion by XPS

XPS analysis was performed on few samples only as the surface sensitive nature of the analysis technique resulted in low signal intensities for the elements of interest, i.e. the metallic components, sulphur and chlorine, while contamination peaks for carbon and oxygen dominated the spectra, thereby limiting the value of the information gained. Contaminant reduction by solvent extraction of the samples prior to analysis was not carried out due to the fragility and brittleness of corrosion products and the potential solubility of corrosion products, e.g. copper sulfates.

Table 6.3.5 lists the results obtained from XPS analyses of metal threads. Approximately 80-95 % of the surface composition is made up of carbon and oxygen, which is primarily attributed to surface contamination rather than corrosion products. Consistent with the results obtained from EDX analysis XPS confirmed the high relative levels of copper on the immediate surface of metal thread samples. The maximum intensity of copper relative to silver was observed on the exterior of sample PNM2_06 where 100*Cu/(Ag+Cu) = 88.6 atomic %, equivalent to 82.1 weight %. Surface etching with an argon ion beam for up to 75 seconds was performed on sample PNM5_24. The metallic components silver, copper and gold as well as the residues attributed to corrosion products sulphur and chlorine increased with increasing etching time, while the contaminants carbon and oxygen decreased. An estimation of depth was not made but the remaining high levels of carbon and oxygen and the continued increase of sulphur and chlorine suggest that surface etching under the conditions applied removed only a few nanometres of surface material and may be a useful method of surface cleaning for XPS analysis. Samples PNM2_19 and PNM5_24 showed peaks for lead and zinc, respectively, and these were attributed to either surface contamination through dust deposition or metallic inclusions in the silver-copper bulk present at levels below the detection limit by EDX analysis.

Table 6.3.5. XPS results for metal threads

Sample	Group*/ Side**	Atomic %											
		Ag(3d)	Cu 2p)	Au(4f)	C(1s)	O(1s)	Si(2p)	Cl(2p)	Si(2s)	Ca(2p)	N(1s)	Pb(4f)	Zn(2p)
HCP 155B4	Mc/e	6.5	2.2	-	70.5	15.2	-	2.9	-	-	2.7	-	-
HCP 72E4	Lc/e	0.3	1.7	-	82.3	12.4	-	-	-	-	3.3	-	-
PNM1_38	M/e	2.2	2.0	0.2	69.2	18.5	0.9	0.6	5.1	0.3	1.0	-	-
	M/i	1.5	2.5	-	62.7	23.0	0.7	0.4	6.6	0.6	1.9	-	-
PNM1_45	Sc/e	1.6	0.4	-	70.3	26.2	-	-	-	-	1.5	-	-
PNM2_06	S/e	0.5	2.8	-	60.9	29.9	2.3	0.8	-	-	2.7	-	-
PNM2_19	Sc/e	2.4	3.5	0.1	61.2	22.5	1.1	0.9	5.0	0.4	2.9	0.1	-
	Sc/i	4.6	6.8		55.7	25.4	2.5	0.9	0.3	0.2	3.4	0.1	-
PNM5_24	S/e	1.6	1.6	0.1	72.6	19.1	1.2	2.0	1.4	-	0.4	-	0.2
	S/e$^+$25	4.0	5.1	0.6	65.3	14.9	3.4	3.1	0.9	-	1.6	-	1.2
	S/e$^+$50	6.2	6.6	0.8	64.0	13.4	3.5	3.1	0.7	-	0.7	-	1.0
	S/e$^+$75	6.9	7.3	0.8	58.4	11.5	4.6	3.7	1.7	-	4.9	-	0.3

Group*: Mc = Gilt medium corroded; Lc = Gilt large corroded; M = Gilt medium; Sc = Gilt small corroded; S = Gilt small
Side**: e = exterior; i = interior
e$^+$ = Exterior surface was argon ion etched for 25 seconds, 50 seconds and 75 seconds

Figure 6.3.29 and Figure 6.3.30 show the high resolution scans for carbon and oxygen of sample PNM2_19 and graphs of the C(1s) and O(1s) theoretical binding energies for various compounds [64]. The principal carbon peak occurs at 285 eV and is attributed to hydrocarbon contamination; smaller signal intensities at higher binding energies may arise from carbon bound to nitrogen, sulphur, chlorine or oxygen, e.g. carboxyls and possibly carbonates. Oxygen only exhibits one relatively broad peak which may contain several smaller peaks attributable to various chemical states such as metal oxides, hydroxides, carbonates or sulfates. However, as the overall peak is featureless it is not possible to make chemical state assignments for oxygen and the fitted peaks shown in Figure 6.3.30 are only exemplars.

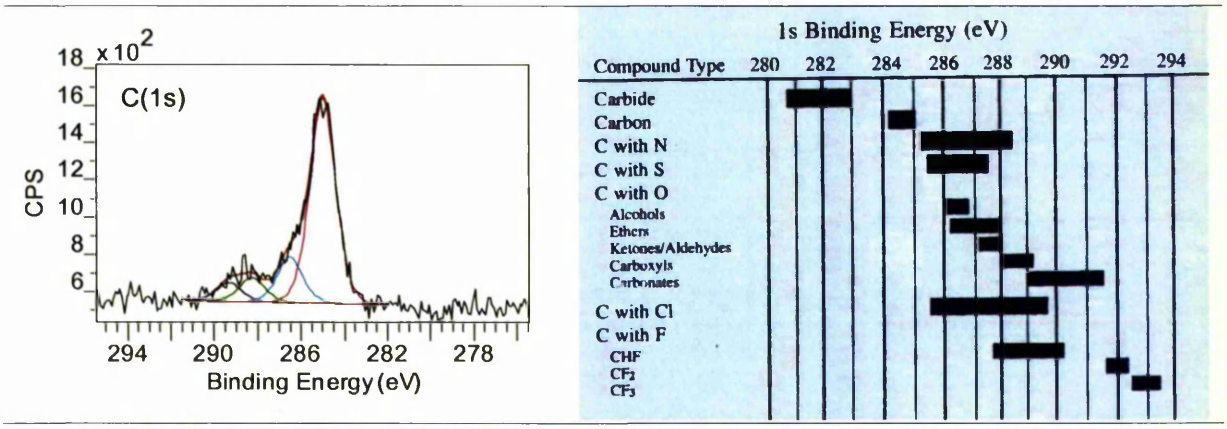

Figure 6.3.29. Metal thread PNM2_19 exterior, XPS C(1s) high resolution scan and binding energies [64]

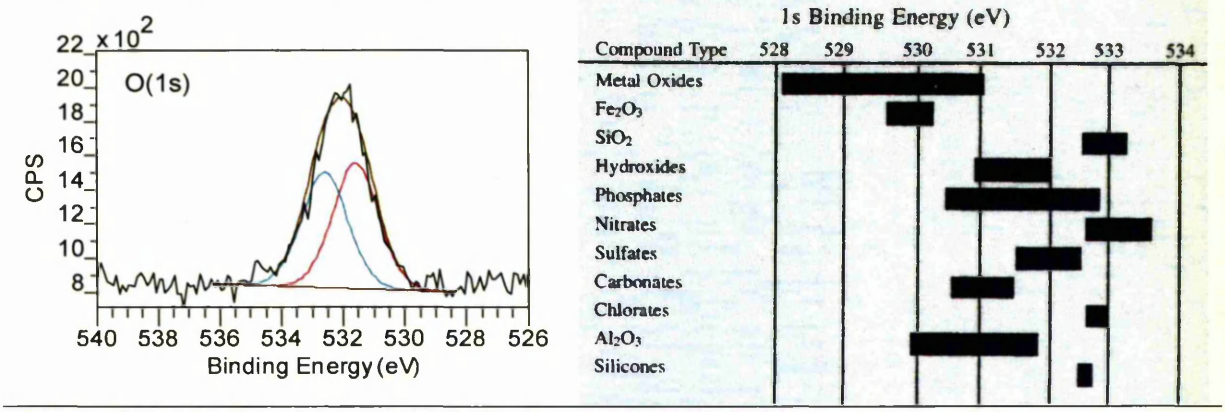

Figure 6.3.30. Metal thread PNM2_19 exterior, XPS O(1s) high resolution scan and binding energies [64]

The principal XPS peaks for sulphur and chlorine are S(2p) and Cl(2p), respectively, and exhibit spin orbit splitting, i.e. the 2p peak consists of two peaks, namely $2p_{1/2}$ and $2p_{3/2}$ with a fixed 1:2 area ratio and fixed binding energy difference of 1.2 eV for sulphur $2p_{1/2}$ and $2p_{3/2}$ and 1.6 eV for chlorine $2p_{1/2}$ and $2p_{3/2}$. The split peaks are peak fitted and represented in Figure 6.3.31. Sulphur 2p exhibits two major peaks at ~ 164 eV and 169 eV. This partial shift to higher binding energy signifies the presence of sulphur in at least two chemical states most likely attributable to sulfide and sulfate corrosion products.

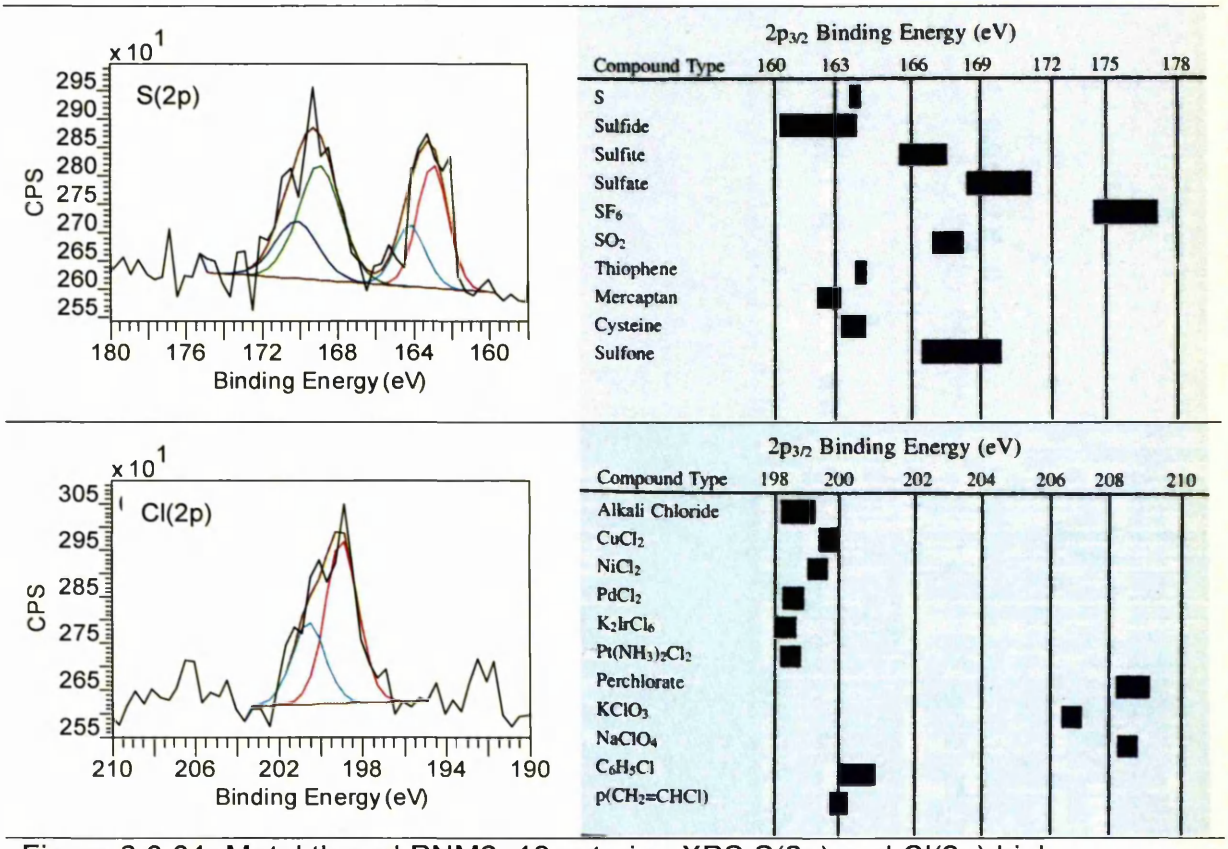

Figure 6.3.31. Metal thread PNM2_19 exterior, XPS S(2p) and Cl(2p) high resolution scans and binding energies [64]

Figure 6.3.32 and Figure 6.3.33 show the principal peaks of copper Cu(2p), silver Ag(3d) and gold Au(4f) with spin orbit splitting of the copper signal into Cu($2p_{1/2}$) and ($2p_{3/2}$), the silver signal into Ag($3d_{3/2}$) and ($3d_{5/2}$) and the gold signal into Au($4f_{5/2}$) and ($4f_{7/2}$). The fixed peak intensity ratio for split 2p peaks is 1:2, for 3d peaks it is 2:3 for 4f peaks 3:4. The binding energy differences for split peaks are Cu 2p ΔeV = 19.9 eV, Ag 3d ΔeV = 6 eV and Au 4f ΔeV = 3.7 eV. The Cu 2p 3/2 peak has its maximum at ~ 932 eV and may be attributed to Cu, Cu_2S, CuS, CuCl or C_2O. A very small peak broadening at the higher energy side of the Cu 2p peaks may arise from $CuCl_2$, CuO, $Cu(OH)_2$ or $CuSO_4$ residues. The Ag 3d 5/2 peak occurs at ~ 368.5 eV which fits the approximate binding energy regions of most corrosion products and does not allow distinction between silver sulfides and silver sulfates. Gold shows its Au($4f_{7/2}$) peak at ~ 84 eV corresponding to the primary Au peak as stated in the graph of theoretical binding energies of gold compounds.

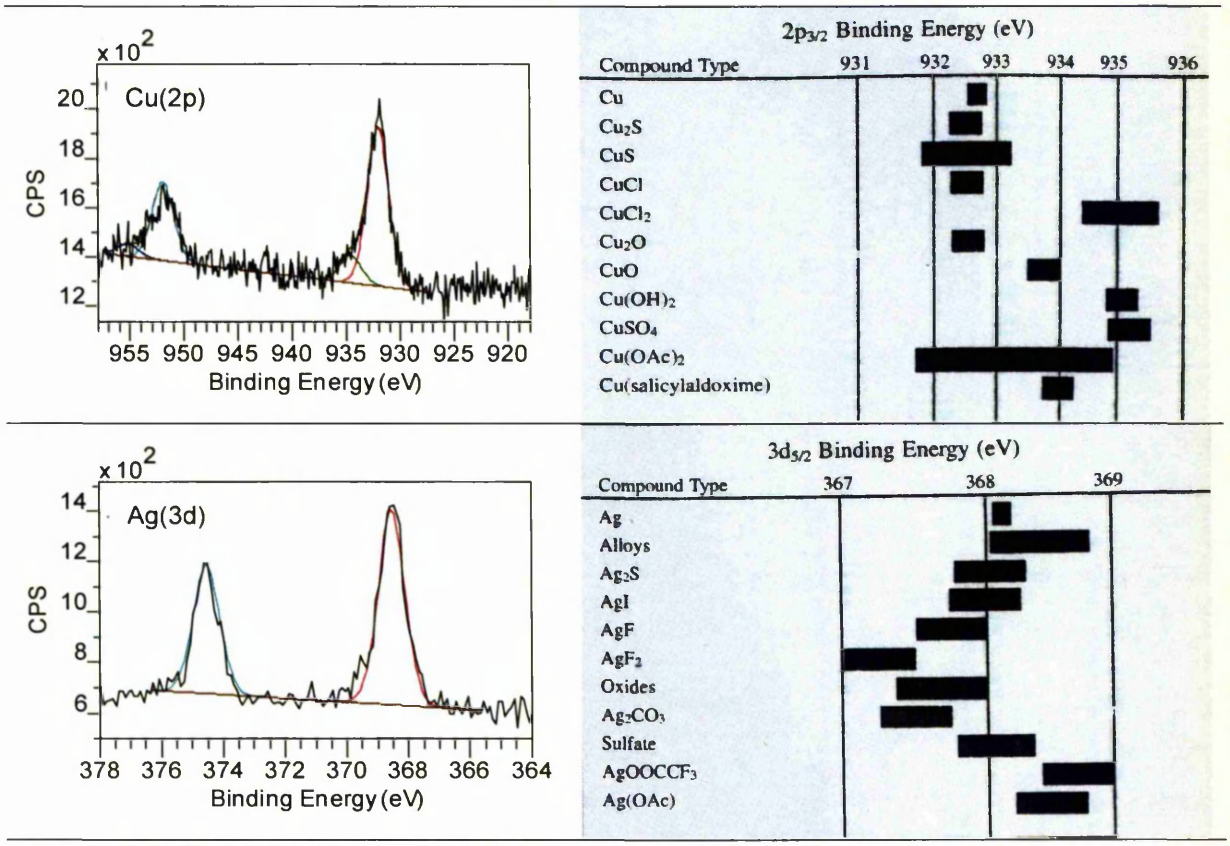

Figure 6.3.32. Metal thread PNM2_19 exterior, XPS Cu(2p) and Ag(3d) high resolution scans and binding energies [64]

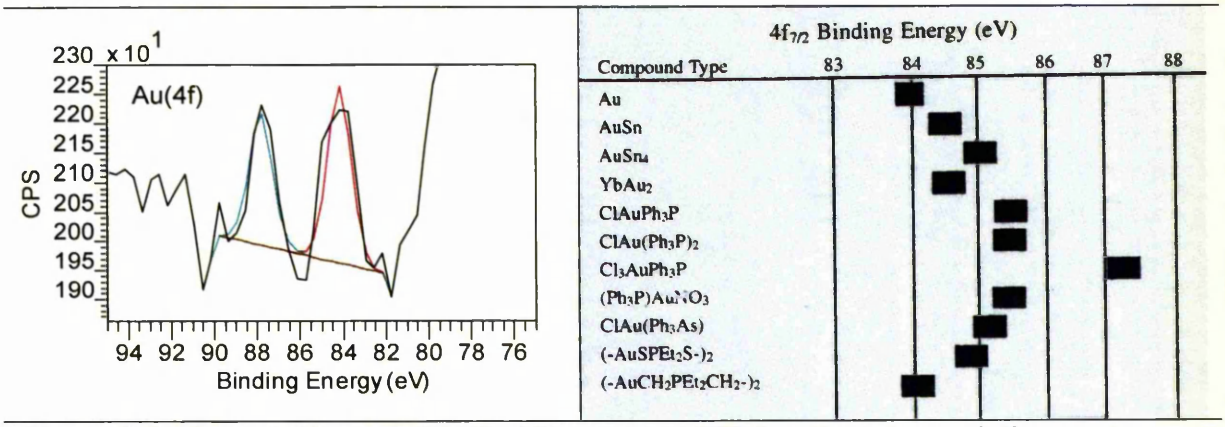

Figure 6.3.33. Metal thread PNM2_19 exterior, XPS Au(4f) high resolution scan and binding energies [64]

On the example of sample PNM2_19 Figure 6.3.29 to Figure 6.3.33 show the peak fitted signals for most elements detected on metal threads; peaks for silicon, calcium, nitrogen, lead and zinc have been omitted because these signals are attributed to contamination rather than corrosion. The peak positions and observed peak shapes are representative of all analysed metal thread samples with the exception of the sulphur peak which showed variations in the relative signal intensities for its two chemical states, i.e. sulfide and sulfate. Quantification for the fitted sulphur peak components has not been performed due to the low and noisy signal intensities, however, the variation in the intensities for sulfide (~164 eV) and sulfate (~169 eV) observed on metal threads are represented in Figure 6.3.34, indicating the presence of different corrosion products in variable relative intensities on metal threads of similar origins.

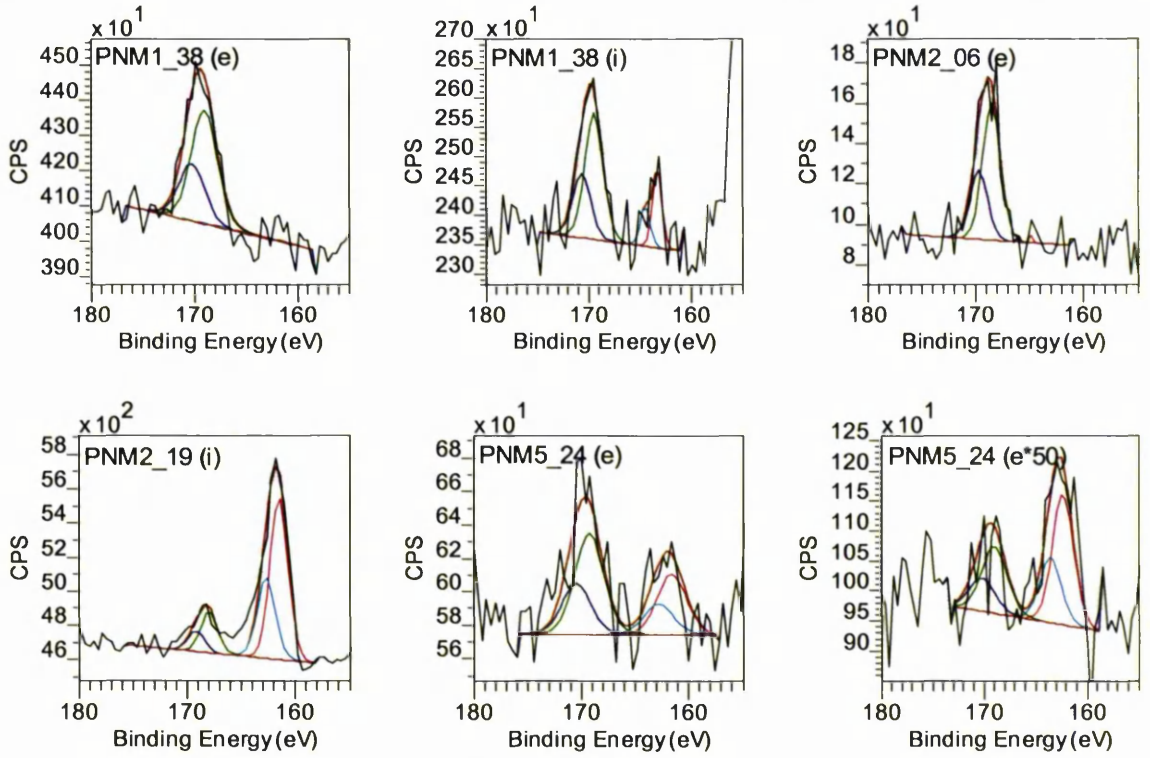

Figure 6.3.34. XPS S(2p) scans of metal threads

6.3.5. Investigation of metal thread corrosion by Dynamic SIMS

SIMS depth profiling was employed for the investigation of manufacturing technique as discussed above. Positive and negative ion mass spectra were obtained from the non-etched surfaces before depth profiling. Typical positive and negative ion mass spectra are represented in Figure 6.3.35 and Figure 6.3.36 with the identified peaks marked. It can be seen that both silver and copper yield intense peaks in the positive spectrum while gold is primarily detected in the negative spectrum; this is due to the ionization potentials (IP) and electron affinities (EA) of the metals which are (Me{IP; EA}) Cu{7.73eV;1.23eV}, Ag{7.58eV;1.30eV} and Au{9.23eV; 2.31eV} [65]. IP is the energy necessary to remove an electron from the neutral atom while EA is the energy released when an electron is added to a neutral atom. Elements with a low IP are readily detected in positive ion mass spectra while elements with high EA have a high negative ion yield.

Previous studies on silver tarnish by SIMS and ultra low energy SIMS identified surface species such as SO_3^-, S_2^-, S^-, Cl^-, O^- and organic hydrocarbon residues [66] and various simple silver and copper compounds with carbon, sulphur or

oxygen [67]. Most of these species were also detected on the analysed metal threads and may be attributed to corrosion. The absence of peaks for larger molecules such as sulfate or carbonate corrosion products is possibly due to the instability of such products to the Cs^+ ion beam during desorption ionisation.

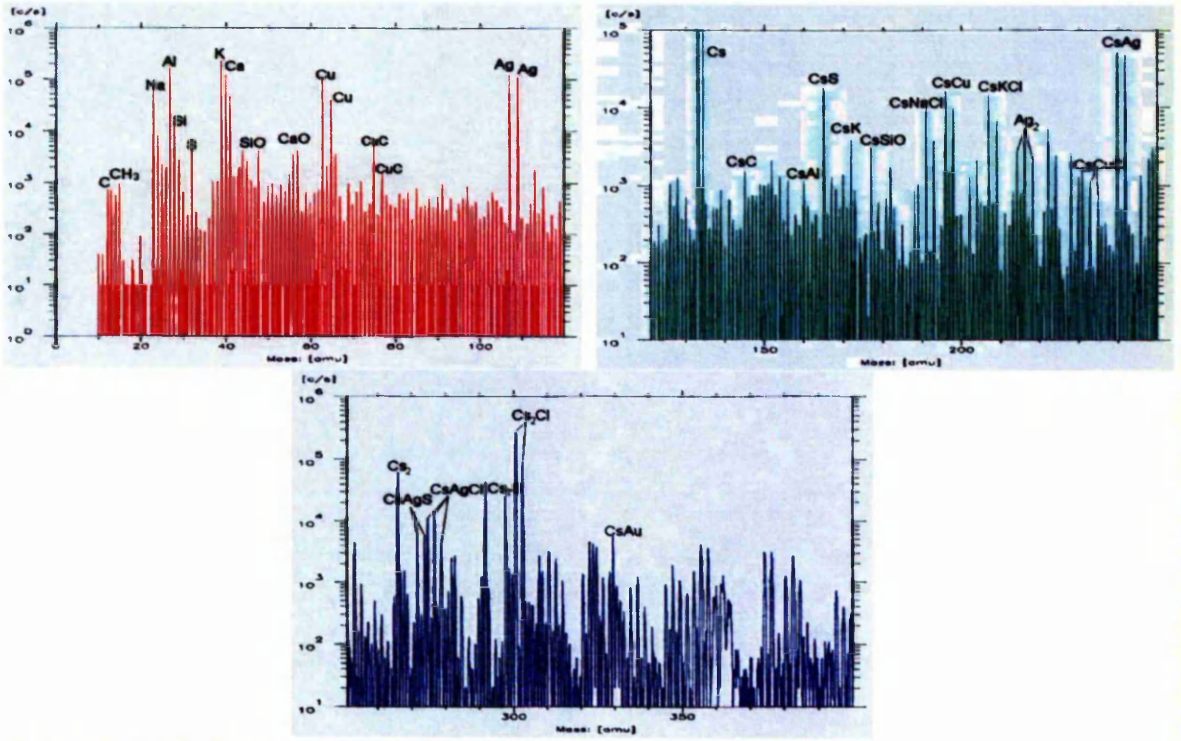

Figure 6.3.35. Positive SIMS spectrum of the exterior of HCP 120C3

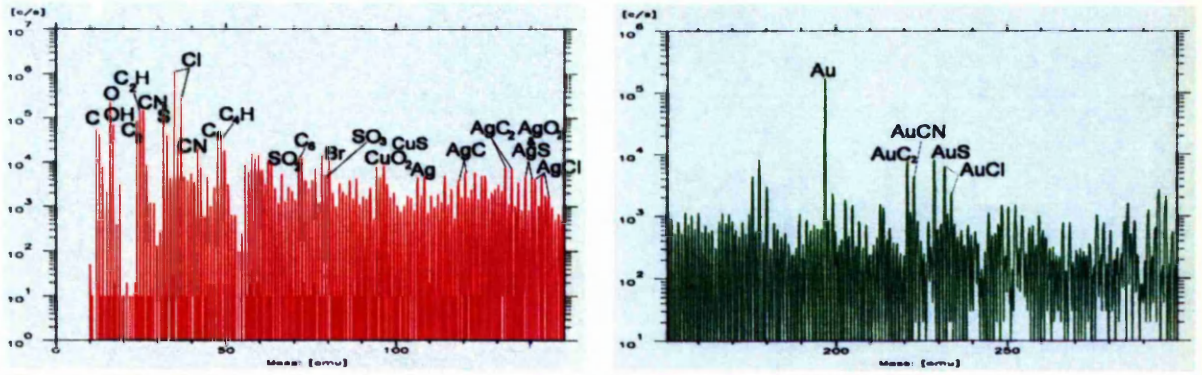

Figure 6.3.36. Negative SIMS spectrum of the exterior of HCP 68E6

6.3.6. Investigation of metal thread corrosion by XRD

X-ray diffraction is commonly used for the identification of corrosion crystals on museum objects [53]; but to the author's knowledge, has never before been applied to metal thread corrosion analysis, possibly due to the difficulties involved in the accurate positioning of the small and uneven samples in the X-ray beam. Complications were also encountered in the present investigation where six metal threads were analysed. The X-ray diffraction of one sample failed, three samples gave such low intensity signals that only the silver diffraction pattern could be identified while the analysis of two metal threads was successful and allowed the unambiguous identification of the corrosion products acanthite and chlorargyrite, Figure 6.3.37, and the tentative identification of digenite, Figure 6.3.38. XRD patterns of the other metal threads are represented in the appendix sections I.1. to I.4.

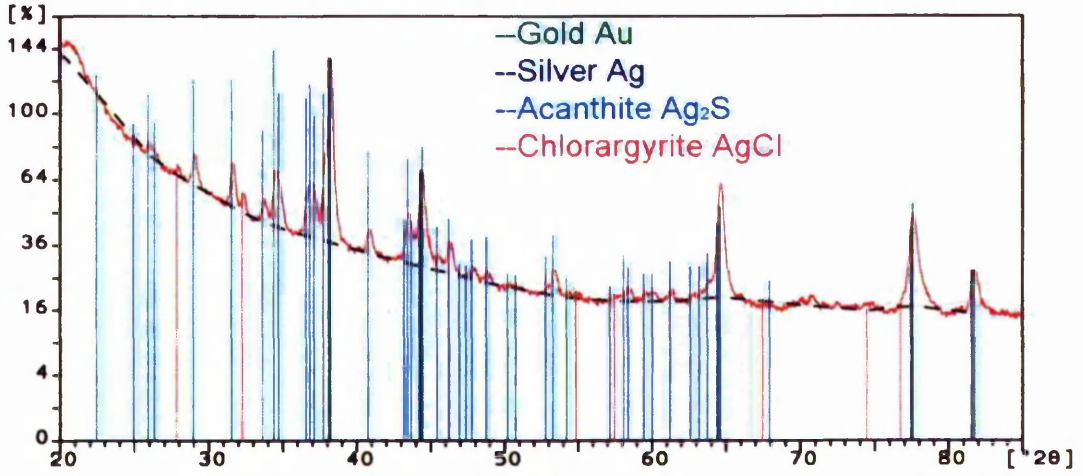

Figure 6.3.37. XRD pattern of metal thread corrosion on sample HCP 161A6

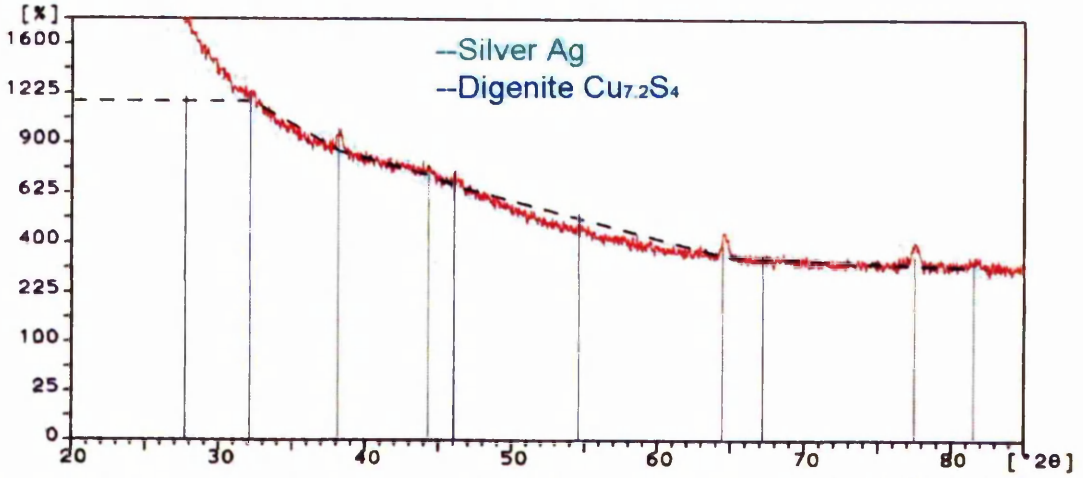

Figure 6.3.38. XRD pattern of metal thread corrosion on sample HCP 169A2

6.3.7. Investigation of Oddy test coupon corrosion by SEM/EDX, XPS and XRD

Oddy tests were conducted to study the influence of the degradation of differently dyed wool and silk on the corrosion of silver and copper.

Both thermal and light Oddy tests caused visible tarnishing on the Ag and Cu coupons incubated with the textile samples, but none on the control coupons. Ag and Cu coupons incubated with wool showed significantly more discolouration than those coupons incubated with silk. This was expected due to the higher levels of sulphur containing amino acids in wool than silk. Discolouration was more obvious on Ag than on Cu and most evident around the edges of the coupons. Thermal degradation of the undyed, alum mordanted and variously dyed fibres produced similar levels of tarnish on both Cu and Ag coupons with blue to black shades observed. However, greater variation was observed due to the photo-degradation of fibres. Figure 6.3.39 shows the light Oddy tested Cu and Ag coupons. The undyed wool was the only sample that caused complete blackening of the Cu coupon, while all other wools caused patchy black corrosion on Cu. Photodegradation of the silk samples caused no visible tarnish on Cu. Tarnish on the Ag coupons was observed at varying shades of yellow, green, red, purple, blue and black. There was a gradation of tarnish from yellow and red at the centre of the coupons, to blue or black at the edges of the metal coupons, suggesting that the different colours were caused by varying tarnish film thicknesses rather than chemical composition of corrosion products. Table 6.3.6 lists the observed tarnish colours on both sides of the silver coupons subjected to photodegradation of the differently dyed fibres. Although all fibres in the light Oddy test caused the tarnishing of Ag coupons, woad and madder dyed wool, and undyed silk appeared to cause the highest levels of tarnish. The tarnishing of the dyed wool samples may be due to greater light absorption of the dark shades increasing sulphur volatilisation, while with silk the nature of the effect is unclear. A possible explanation may be the degradation of the woollen warp threads, as the light Oddy tests were conducted using the model tapestry fabrics. The warp threads received no or less direct irradiation due to the tight weave structure and complete coverage of warp yarns by weft yarns, see Chapter 3.section 3.2.3. Weaving, however, undyed silk is more translucent than dyed silk which may have caused photodegradation of the warp yarns.

Table 6.3.6. Colour variation of tarnish on light Oddy tested silver coupons

Textile material		Side A*		Side B*	
Control		n.t.	n.t.	n.t.	n.t.
Silk	undyed	blue	purple	yellow	purple
	weld	red	blue	yellow	red
	woad	blue	yellow	yellow	blue
	madder	red	yellow	yellow	blue
	brazil	red	red	yellow	red
Wool	undyed	n.t.	black	green	green
	weld	green	green	green	green
	woad	blue	yellow	purple	yellow
	madder	blue	purple	red	black
	brazil	yellow	blue	green	green

* Dominant tarnish colour is stated first. n.t. = no tarnish

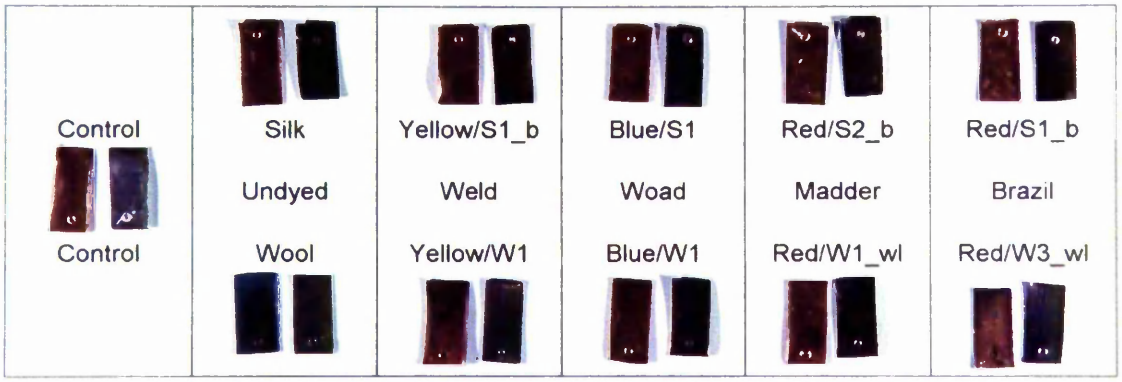

Figure 6.3.39. Light Oddy tested Cu and Ag coupons

SEM micrographs of corrosion morphologies on silver and copper are shown in Figure 6.3.40 (a-f). In areas with little corrosion the initial growths were found to develop along scratches and pits on the surface. Generally the corrosion growths on copper were more rounded and accumulated than corrosion on silver, which formed a more evenly distributed layer with uniformly sized corrosion crystals and little differences in height. In addition, one of the copper coupons associated with photodegradation of undyed wool showed regular longitudinal crystals, Figure 6.3.40 (f).

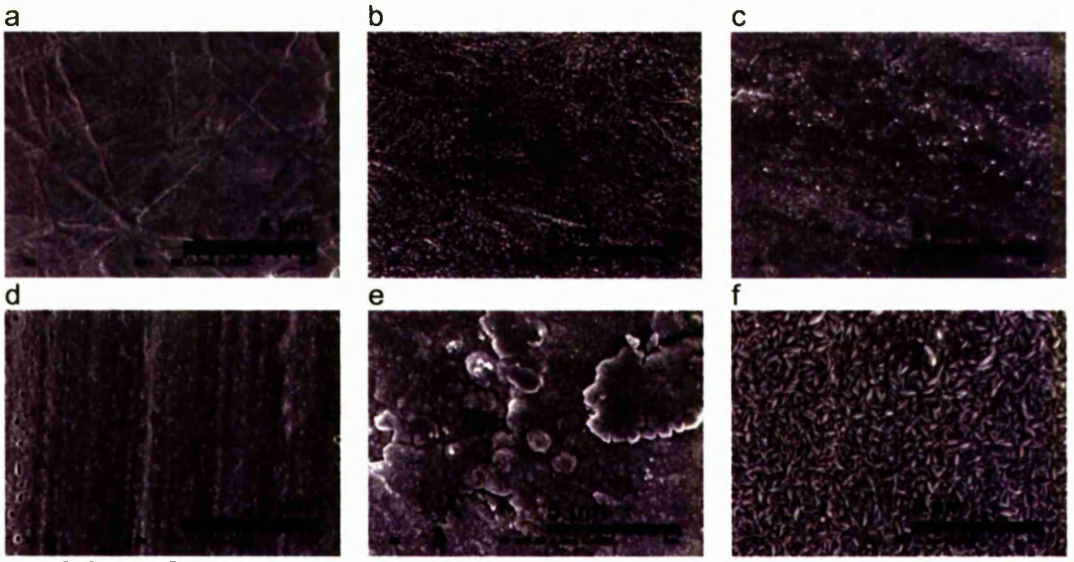

Figure 6.3.40. SEM micrographs of corrosion crystal morphology on thermal and light Oddy tested silver and copper coupons incubated with undyed wool. (a) Silver control, (b) Silver Oddy thermal, (c) Silver Oddy light, (d) Copper control, (e) Copper Oddy thermal, (f) Copper Oddy light

The surface chemical composition of most light and thermal Oddy tested Cu and Ag coupons was investigated by XPS. Up to three spectra were obtained from each sample and the average atomic ratios of oxygen, carbon and sulphur to metallic component are represented in Figures 6.3.41 to 6.3.44. The complete data sets of all XPS results of Ag and Cu coupons are listed in the appendix sections J.1. to J.6.

Low level contaminants were chlorine, nitrogen and tin as well as some silver on copper coupons and some copper on silver coupons probably due to cross contamination during the Oddy tests. The results represented in Figures 6.3.41 to 6.3.44 show that the relative levels of oxygen and carbon were significantly higher on Cu coupons than on Ag coupons and did not change considerably due to the accelerated tarnishing tests. The C/Ag and C/Cu ratios showed both increases and decreases for the tarnished coupons without any apparent trend, while the O/Ag and O/Cu ratios, in general, experienced a slight decrease for those coupons incubated with silk and wool as compared to the control samples. This can be attributed to the partial conversion of the protective oxide layer into corrosion products. Only the sulphur component showed significant increases due to accelerated tarnishing which were higher on silver than on copper, and were also higher due to the degradation of wool than silk with the exception of the light Oddy tested Ag coupons where the S/Ag ratios were similar for samples incubated with silk or wool. This agreed with the visual assessment of levels of tarnishing. Despite

the longer exposure time during thermal Oddy tests, the sulphur levels were higher on those metal coupons exposed to light irradiated wool and silk compared to thermally degraded wool and silk. This may be due to greater degradation of the fibres under the influence of light at room temperature as compared to thermal degradation at 60°C in darkness. However, due to instrumental requirements the light and thermal Oddy test set-ups were not identical and the difference in observed sulphur levels may be due to a volumetric effect. A further explanation is offered by Franey et al. whose work on humidity and temperature influences on sulphur corrosion has shown that the average water film thickness on silver above 30°C (at constant humidity of 18+/- 1 torr = 94 % RH at 21°C) is lower than three monolayers and therefore does not retain the bulk water properties necessary for water-enhanced sulphur corrosion formation [44]. In fact, Franey et al. suggest that sulphur corrosion reactions occur at different mechanisms at lower and higher temperatures with the first mechanism being water-dependent and the latter mechanism water-independent but temperature-dependent [44]. The maximum S/Ag ratios were observed on light Oddy tested silver coupons with many samples exhibiting S/Ag > 0.5 which would account for the complete sulfidation of the silver surface into acanthite. Therefore the higher S/Ag ratio suggests the presence of adsorbed sulphur compounds or additional corrosion products other than acanthite (Ag_2S).

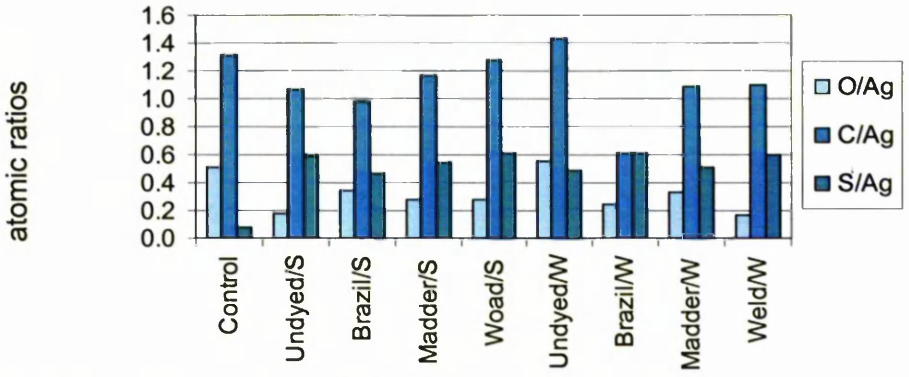

Figure 6.3.41. XPS results of light Oddy tested Ag coupons (S: silk, W: wool)

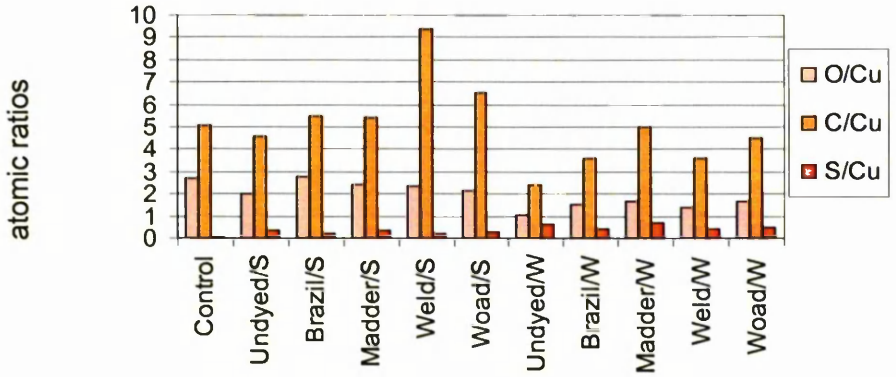

Figure 6.3.42. XPS results of light Oddy tested Cu coupons (S: silk, W: wool)

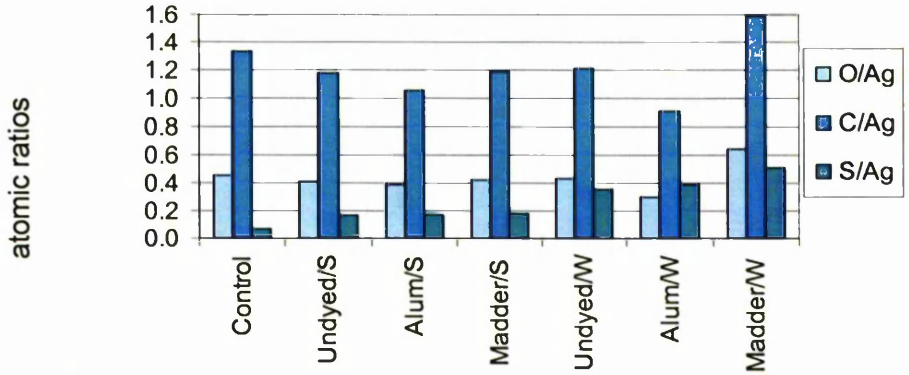

Figure 6.3.43. XPS results of thermal Oddy tested Ag coupons (S: silk, W: wool)

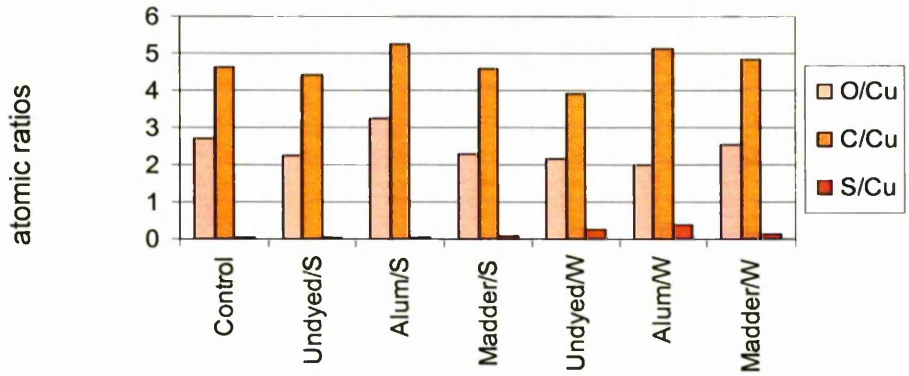

Figure 6.3.44. XPS results of thermal Oddy tested Cu coupons (S: silk, W: wool)

Figures 6.3.45 and 6.3.46 show the average total atomic % of the S(2p) component and the relative contributions from the two oxidation states S(II) and S(VI) attributed to sulfide and sulfate, respectively; the data sets showing S(2p) quantifications of all XPS analyses are listed in the appendix sections J.5 and J.6. As mentioned above, it can be seen that the overall amount of surface sulphur is higher on silver than on copper, higher on light Oddy tested samples compared to thermal Oddy tested samples and generally higher due to the degradation of wool as opposed to silk. However, especially the silver coupons incubated with silk in the light Oddy tests showed high levels of sulphur, similar to those observed on silver coupons incubated with wool. This was surprising due to the low content of sulphurous amino acids in silk (< 1 mol %) but may be due to the volatilisation of sulphur compounds from the woollen warp threads as discussed above. Nevertheless, it was expected to observe higher levels of sulphur due to irradiation of wool fabrics compared to silk fabrics, which was found to hold true for the copper samples, Figure 6.3.45. The relative amount of sulphur in it's higher oxidation state S(VI) was higher on most copper coupons as compared to silver coupons, and was attributed to copper sulfate corrosion products.

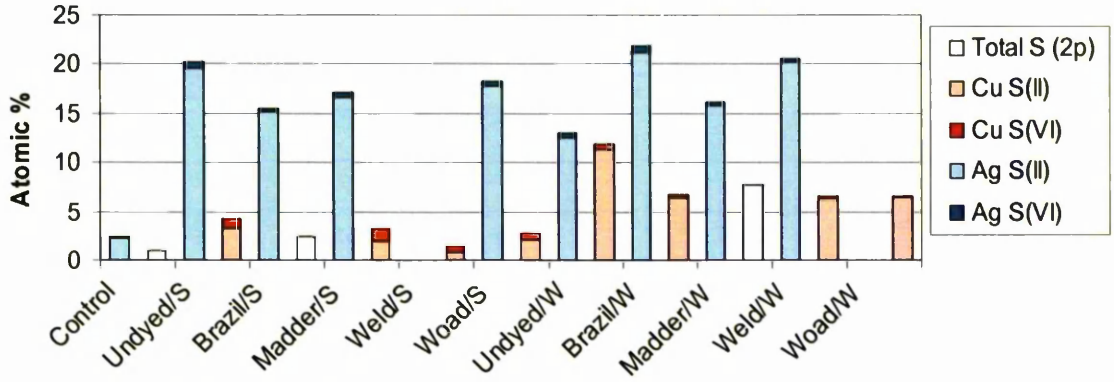

Figure 6.3.45. S (2p) peak components of light Oddy tested Ag and Cu coupons

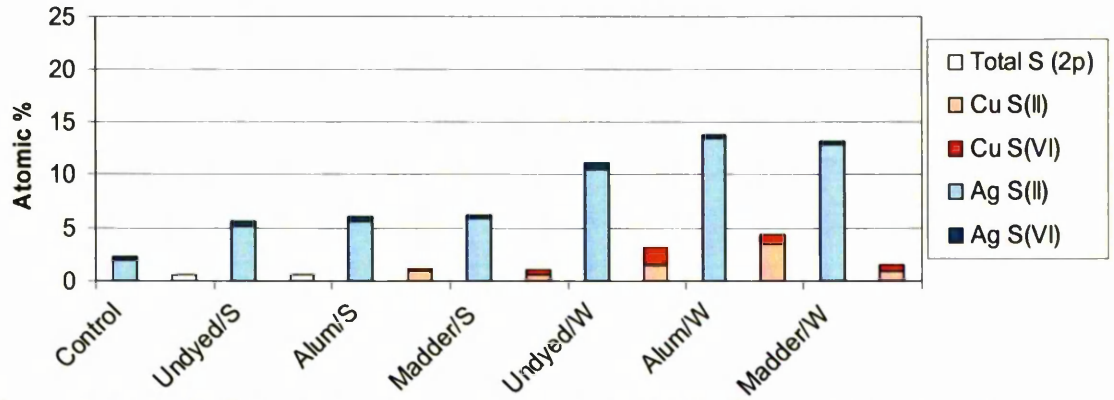

Figure 6.3.46. S (2p) peak components of thermal Oddy tested Ag and Cu coupons

The corrosion products on the Ag and Cu coupons incubated with undyed wool under thermal and light Oddy test conditions were analysed by X-Ray Diffraction (XRD). In each case the major signals obtained could be attributed to the pure metal crystal Ag or Cu. Both Ag coupons showed traces of the corrosion product acanthite Ag_2S, with the signals being stronger for the thermal Oddy tested sample, Figure 6.3.47.

The thermal and light Oddy tested Cu coupons incubated with undyed wool showed different corrosion crystal morphologies, Figure 6.3.40 (e) and (f). Accordingly XRD analysis confirmed the presence of different corrosion products on the two samples, Figures 6.3.49 and 6.3.50. The rounded crystals on the thermal Oddy tested Cu sample were identified as cuprite Cu_2O, while chalcocite Cu_2S and traces of tenorite CuO were detected on the light Oddy tested Cu sample which exhibited regular elongated corrosion crystals. However, the occurrence of elongated crystals on the Cu coupons incubated with undyed wool is atypical as they were not observed on any other light or thermal Oddy tested Cu coupons incubated with wool.

Figure 6.3.49 shows the diffraction pattern for silver in addition to copper and cuprite, this contamination originated from silver paint which was used to electrically connect the sample with the sample holder in SEM analysis.

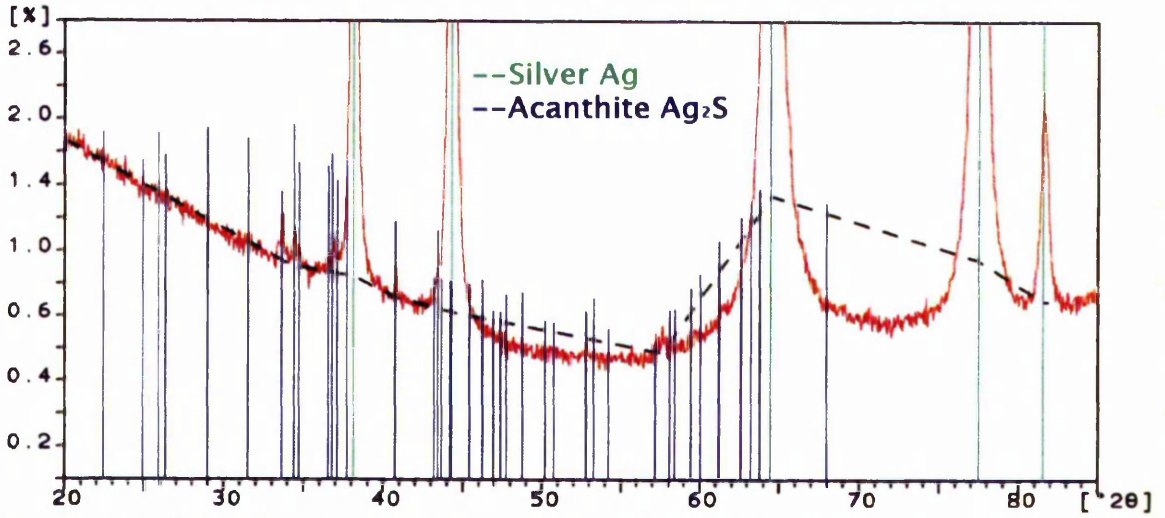

Figure 6.3.47. XRD pattern of Ag coupon accelerated tarnished under thermal Oddy test conditions with undyed wool

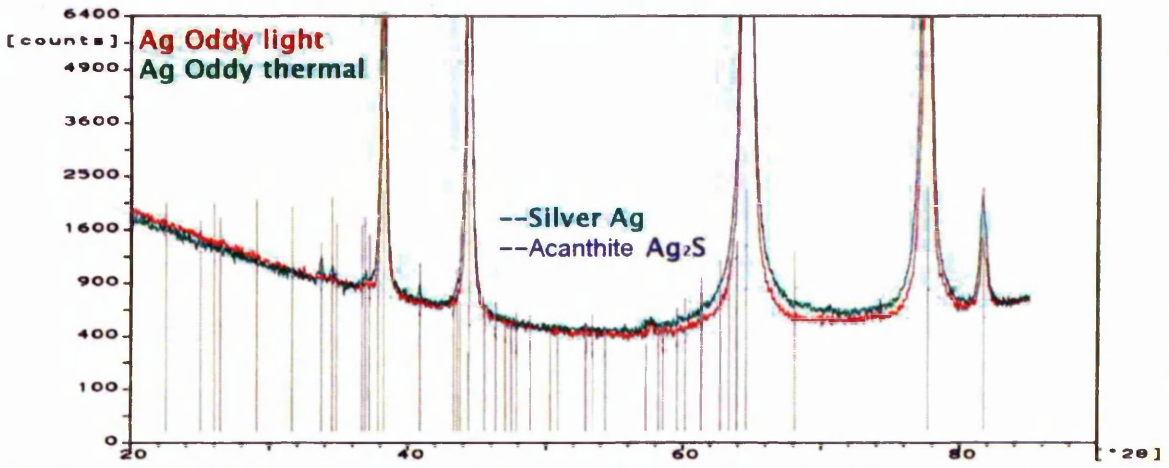

Figure 6.3.48. XRD patterns overlay of accelerated tarnished Ag coupons

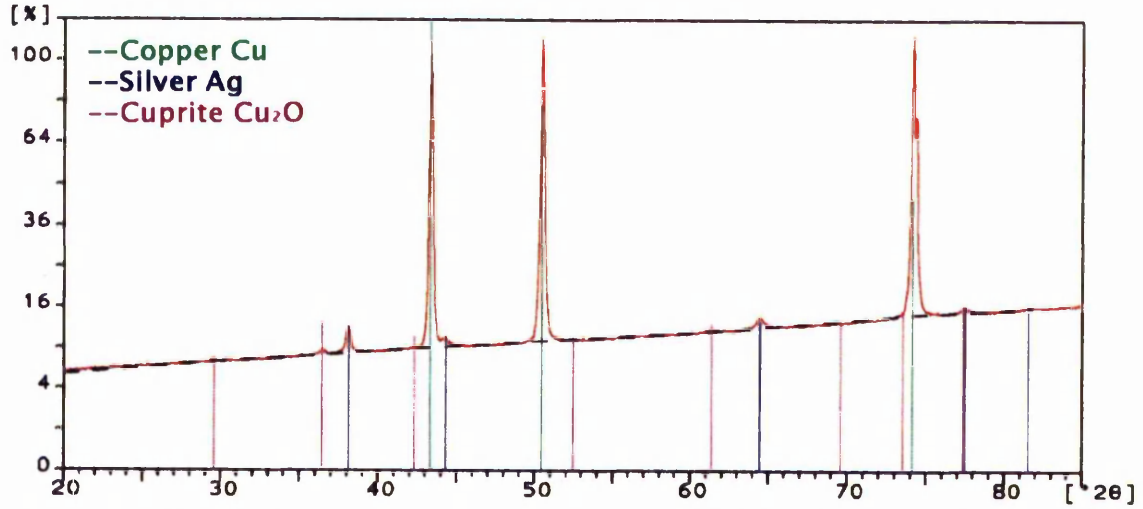

Figure 6.3.49. XRD pattern of Cu coupon accelerated tarnished under thermal Oddy test conditions with undyed wool

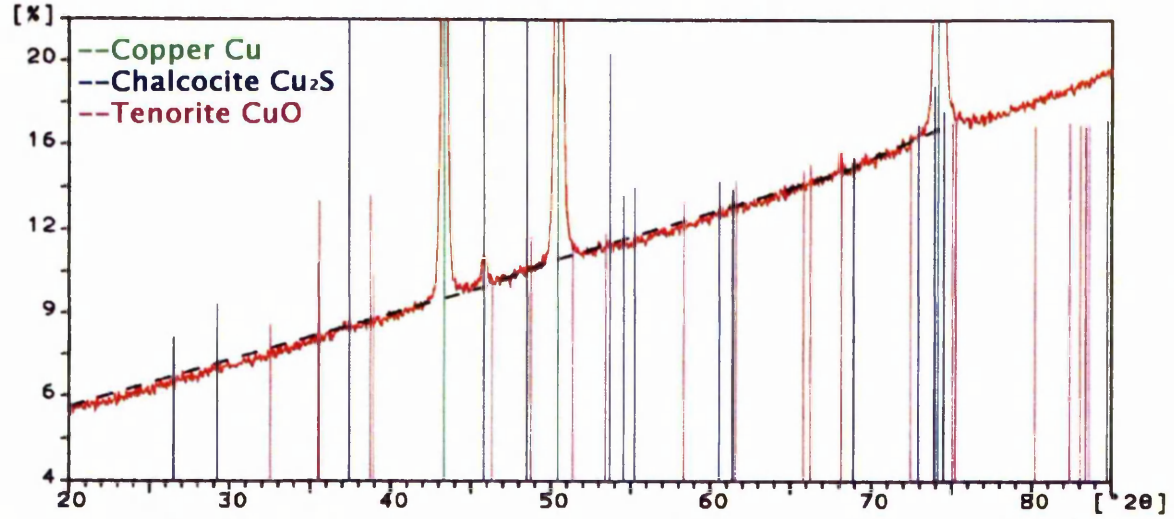

Figure 6.3.50. XRD pattern of Cu coupon accelerated tarnished under light Oddy test conditions with undyed wool

6.3.8. Investigation of detergent residues on metals

Precious metal threads form an integral part of many of the most valuable historic textiles in museum collections. Conservation treatments of textiles frequently include washing with detergents in aqueous solutions. Since most metallic decorations cannot be removed from the textile without substantial damage, one has to consider the possible implications of washing procedures on metal threads or similar metallic decorations. Insufficient drying after treatment in aqueous solutions may increase corrosion formation while other non-aqueous solvents may cause the weakening of metal interfaces [36]. Surfactants reduce the surface tension of water and thereby aid the wetting process of the fibres. However, if surfactants are not completely rinsed off the treated textile, left over residues may facilitate the diffusion of gaseous or particulate atmospheric contamination and deteriorating pollutants [68].

The evaluation of cleaning procedures and choice of detergents has received much attention in conservation science [68-72]. A combination of non-ionic and anionic detergents is generally considered most effective [70]. Residues of detergents are commonly monitored in the rinsing solution using the 'methylene blue method' or UV-vis spectrophotometry [59, 73]. Recent studies applied XPS and SIMS to investigate the residues of surfactants in-situ on wool and cashmere fibres and found that both non-ionic and anionic detergents adsorb onto the textile [74-76].

This study aims to investigate the residues of detergents on clean and corroded metals using ToF-SIMS analysis. The choice of detergents, their concentration and treatment temperature was based on cleaning procedures used at the Textile Conservation Studio at Hampton Court Palace [59]. The detergents used were Sodium Dodecyl Sulfate (SDS) and the nonylphenol ethoxylate Tergitol-NP9 (T-NP9), Scheme 6.3.1.

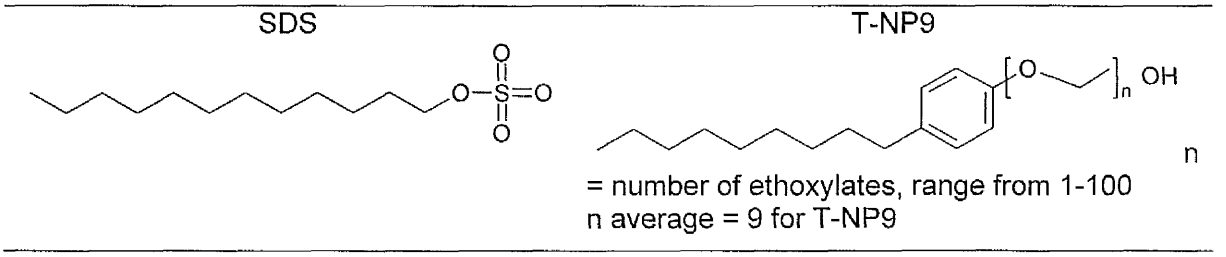

Scheme 6.3.1. Chemical structures of Sodium Dodecyl Sulfate and Tergitol-NP9

Characteristic ToF-SIMS peaks for the anionic surfactant Sodium Dodecyl Sulfate were attributed to the ionised alkyl sulfate residue $CH_3(CH_2)_{11}OSO_3^-$ at m/z 265- as well as S, SH, SO^-, SO_3^-, SO_4^- and HSO_4^- residues, as seen in the negative ion spectrum of the pure detergent, Figure 6.3.51. The SDS spectrum in positive ion mode yielded mainly a large peak for Na^+.

The ToF-SIMS spectrum of Tergitol-NP9 showed a major peak at m/z 45^+ attributed to the monoethoxylate (EO^+); further ethoxy derivative, phenol or hydrocarbon peak clusters occurred at m/z 57^+, 71^+, 89^+, 107^+, 121^+ and 135^+, Table 6.3.7. The peak for the dehydroxylated nonylphenol monoethoxylate molecule (n=1-OH) was present at m/z 247^+ ($NPEO^+$) followed by a 'fingerprint pattern' of cationised nonylphenol ethoxylates with a maximum at m/z 611^+ for a chain length of eight ethoxylates and potassium cation (NP8EO/ K^+). Derivative peaks with 44 amu increments represent the longer, respectively shorter, ethoxylate chains and extend from m/z 303^+ (n = 1) to 1183^+ (n = 21), see Figure 6.3.53. The negative ion spectrum of T-NP9 exhibited mainly hydrocarbon peaks as well an intense signal at m/z 219^- attributable to the nonylphenoxide anion (NPO^-), Table 6.3.7 and Figure 6.3.54.

Table 6.3.7. ToF-SIMS peak assignments for T-NP9

m/z	Assignment		m/z	Assignment	
45^+	$HOCH_2CH_2^+$	(EO^+)	121^+	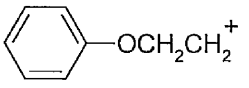	
57^+	$C_4H_9^+$		135^+	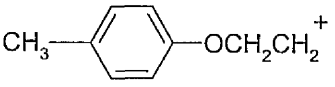	
71^+	$C_5H_{11}^+$		219^-	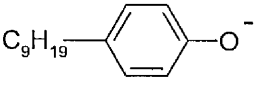	(NPO^-)
89^+	$(OCH_2CH_2)_2H^+$		247^+	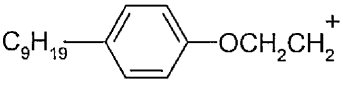	($NPEO^+$)
107^+	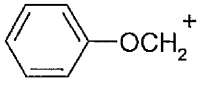		611^+	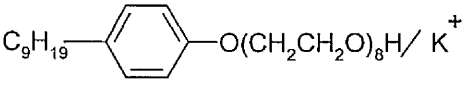	(NP8EO/ K^+)

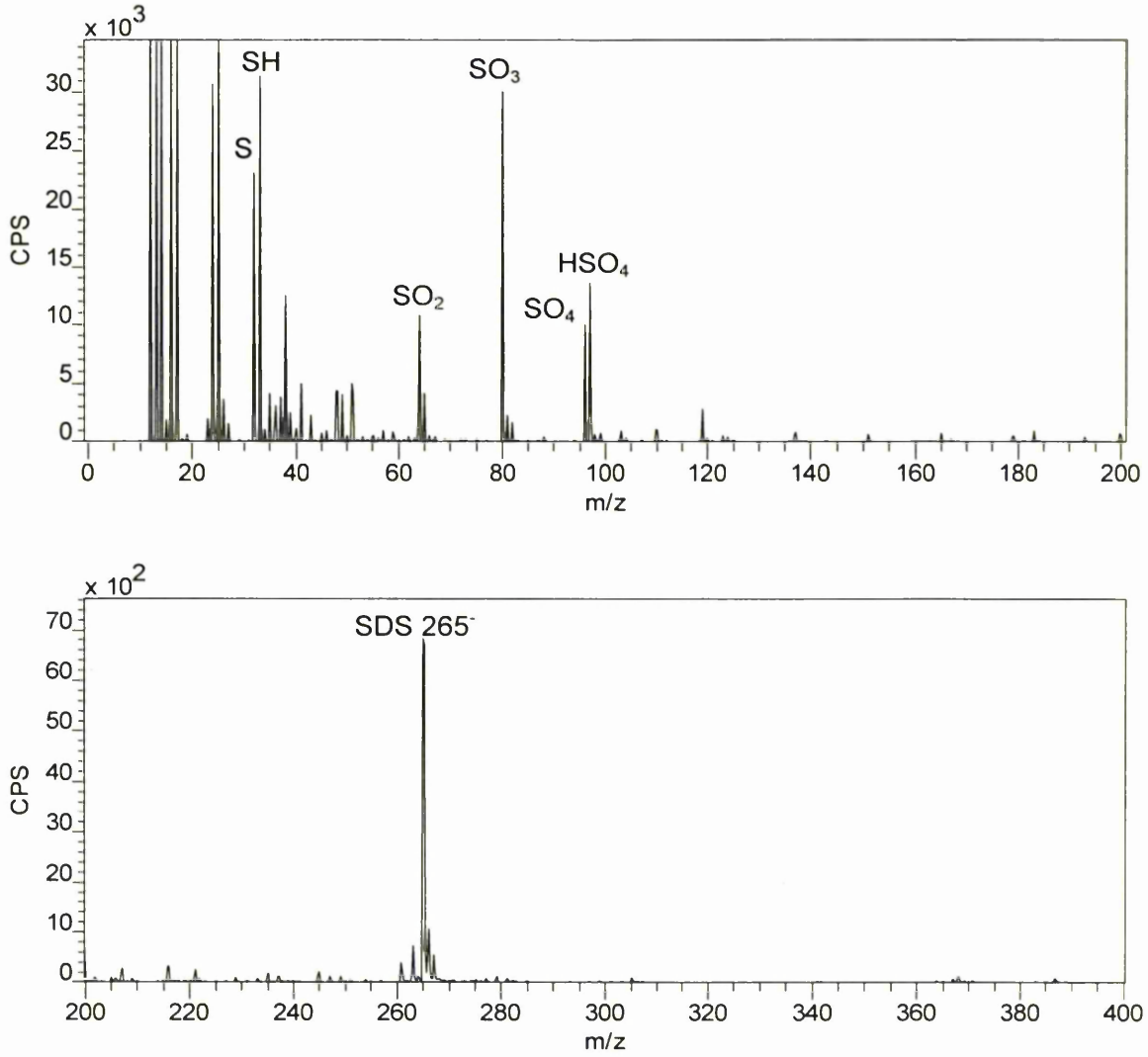

Figure 6.3.51. ToF-SIMS negative ion spectrum of SDS detergent

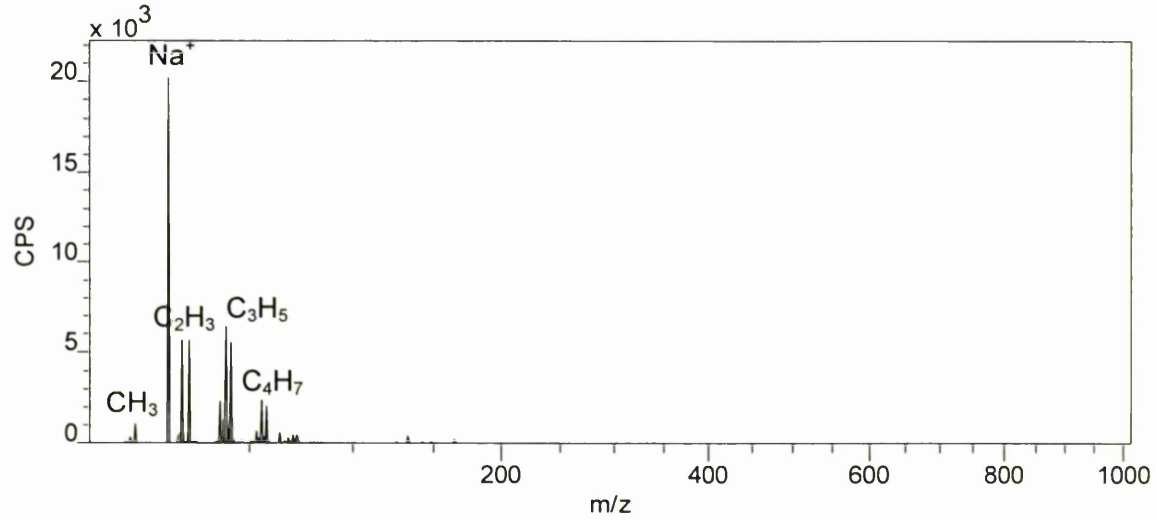

Figure 6.3.52. ToF-SIMS positive ion spectrum of SDS detergent

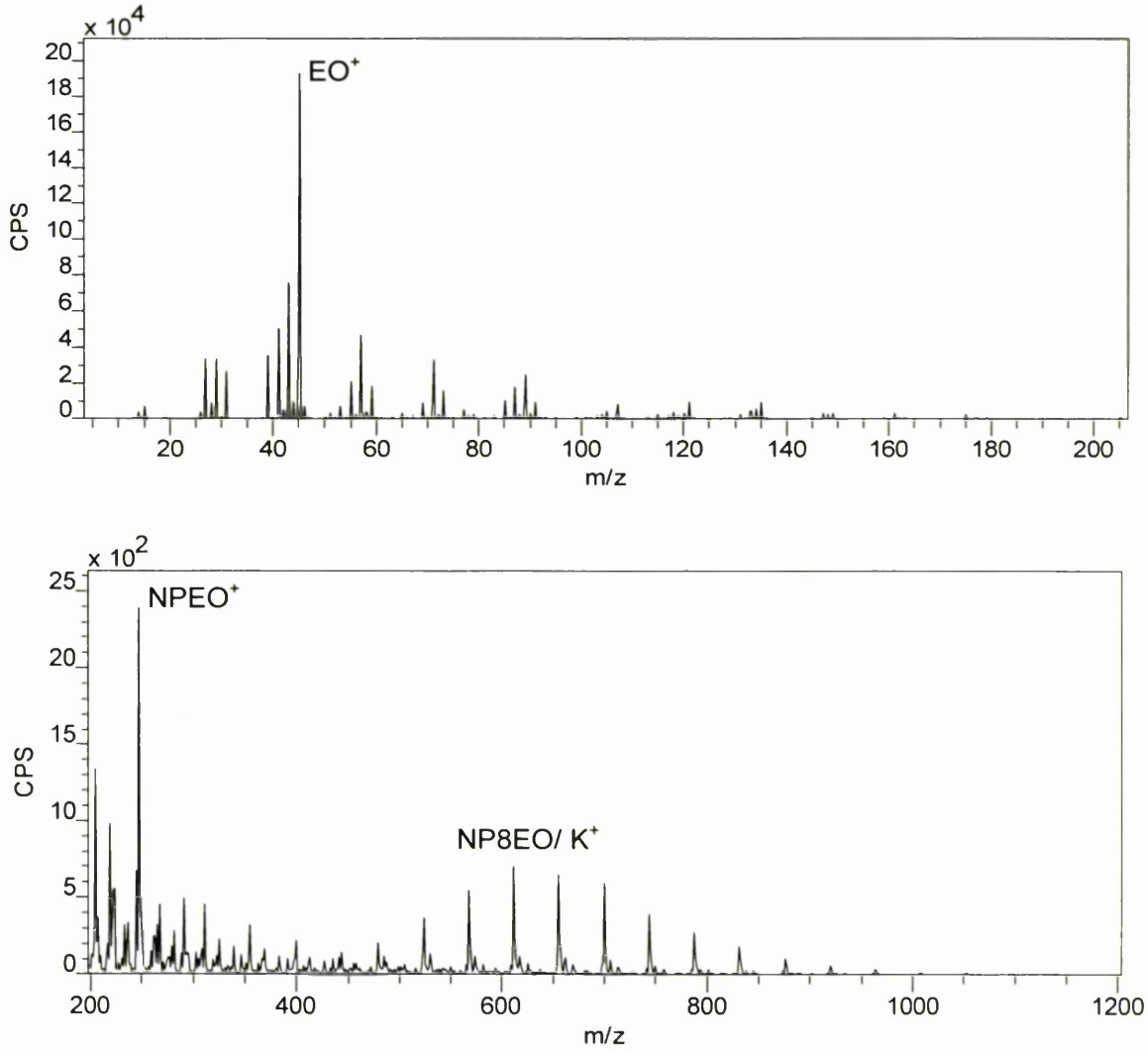

Figure 6.3.53. ToF-SIMS positive ion spectrum of T-NP9 detergent

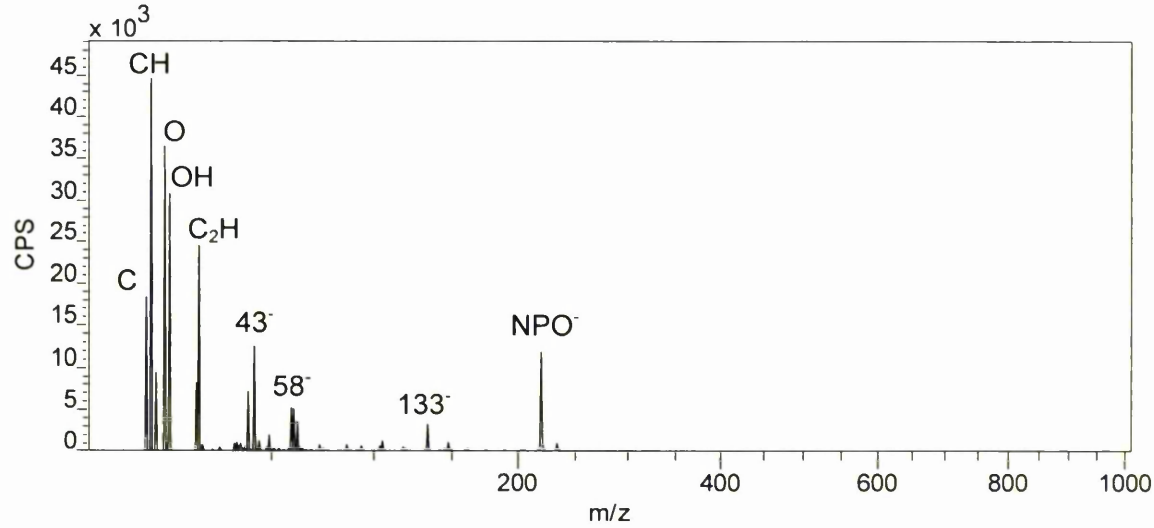

Figure 6.3.54. ToF-SIMS negative ion spectrum of T-NP9 detergent

All ToF-SIMS spectra of detergent treated metal coupons and metal threads are shown in the appendix sections K.1. to K.3; some representative spectra are also shown below to illustrate the peaks discussed in the text. Table 6.3.8 gives an overview of the major species detected on each sample; Table 6.3.9 to Table 6.3.11 provide semi-quantification of surface residues using the equation $1000*I_{(A)} / I_{(Total)}$, where I = peak area of (A): peak of interest and (Total): m/z 0-1000.

ToF-SIMS analysis of SDS treated metal coupons and metal threads generally showed a strong SDS signal at m/z 265^- as well as signals at m/z 293^-, 321^- and 349^- attributed to longer alkyl sulfate chain residues, i.e. $C_nH_{n+1}OSO_3^-$ (where n = 14, 16 and 18, respectively), this is illustrated on the example of sample 'SDS 98% clean Cu', Figure 6.3.55. These longer chain residues were not detected in the pure SDS spectrum indicating either a rearrangement of the alkyl sulfate chains in solution or a preferential adsorption of the longer chains onto the metal surfaces, thereby raising their localised concentration above the detection limit. SDS surfactant was identified on the untreated metal thread PNM5_24 and may be a residue from conservation treatment, i.e. washing of the tapestry. This is consistent with ToF-SIMS analyses of historic wool samples where some residual detergent was also observed, see Chapter 5. Analysis of Wool and Silk: section 5.4.11. Sample 'H_2O clean Cu' also exhibited the m/z 265^- signal attributed to SDS detergent contamination, possibly originating from the glassware used for the treatment. The highest SDS peak was observed on the 'SDS 99% clean Ag' sample. However, this was not attributed to preferential adsorption of SDS onto silver over copper because the silver samples treated with the combination of SDS and Tergitol-NP9 did not exhibit the SDS peak at all. Therefore the variations in SDS intensities were most likely due to irregular localised adsorption, as was also suggested by the random adsorption patterns observed on Tergitol-NP9 and SDS treated metal threads, where two samples showed peaks for both detergents and two samples showed peaks for either Tergitol-NP9 or SDS, Table 6.3.8.

There is generally a two to three fold increase of the relative amount of SO_3^- on the SDS treated samples compared to the control samples (untreated and H_2O treated) or the Tergitol-NP9 treated samples which have not been in contact with SDS, Table 6.3.9. The adsorption of SO_3^- might have implications for further corrosion of the metal. However, the relative intensities of other surface sulphur species (S, SO_2, HSO_4) do not appear to increase with SDS adsorption. Furthermore, both SDS and nonyl phenol ethoxylate surfactants, in combination

with corrosion inhibitors such as vinyl and acrylic polymers, have found application in corrosion resistant coatings for metals [77-79]. Therefore, a corrosive effect of adsorbed sulfonate ions from SDS may be insignificant but should, nevertheless, not be ruled out.

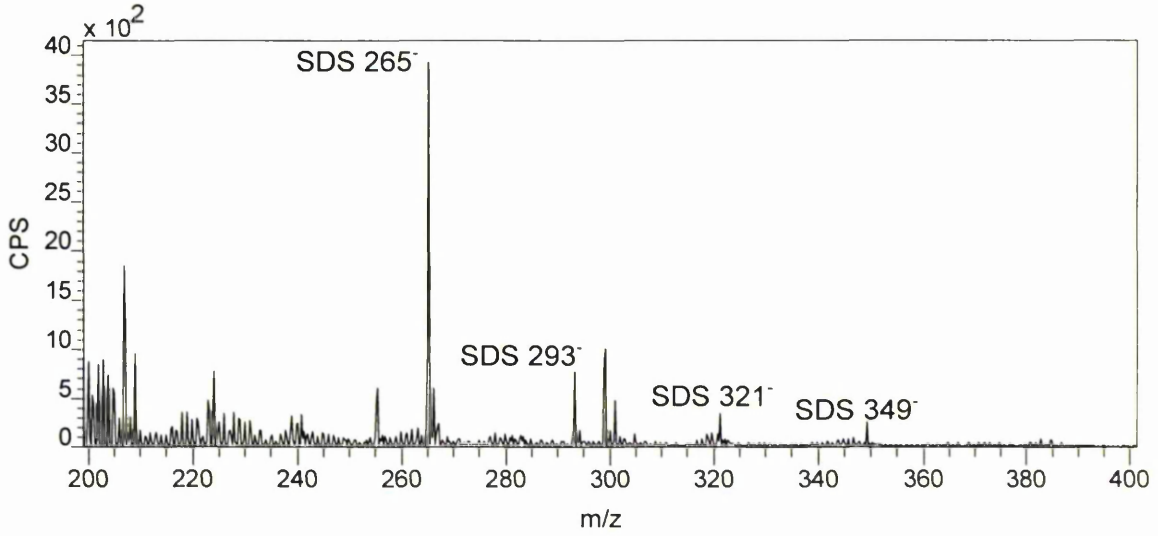

Figure 6.3.55. ToF-SIMS negative ion spectrum of sample 'SDS 98% clean Cu'

ToF-SIMS spectra of the Tergitol-NP9 treated metal samples did not exhibit the NPEO peak at m/z 247^+ or the fingerprint pattern around m/z 611^+, while the nonylphenoxide signal at m/z 219^- was present for all Tergitol-NP9 treated samples and semi-quantification indicated an up to 76 fold increase of signal intensity compared to the background level m/z 219^- signal of samples not treated with Tergitol-NP9, Table 6.3.8 and Table 6.3.10. An increase in the ethoxylate signal at m/z 45^+ was also noted for some Tergitol-NP9 treated samples which is in agreement with Brack et al. and Carr et al. who noted an increase in the m/z 45^+ ion on wool fibre surfaces due to ethoxylate adsorption of the non-ionic detergent [74, 75]. The absence of the high mass detergent peaks in the positive ion spectra indicates that the NPEO molecules do not adsorb strongly to the metal surface or are completely removed during the rinsing process while fragmented molecules, i.e. nonylphenoxide and , to a lesser extend, ethoxylates, show greater affinity to the metal surfaces.

ToF-SIMS spectra of the corroded silver coupons and the untreated metal threads in particular showed peaks attributed to silver chloride corrosion ($AgCl_2$) at m/z 177^-,179^- and 181^-. For the metal thread samples (Model, PNM2_17 and PNM5_24) $AgCl_2$ was found to reduce with detergent treatments while such apparent trend was not observed on the silver coupons, Table 6.3.10. The 'H_2O

corroded Ag' sample showed the highest relative intensity of $AgCl_2$ followed by samples 'SDS 99% corroded Ag' and 'Untreated clean Ag' despite the latter sample being visually clean, untarnished silver. However, $AgCl_2$ is not the main corrosion product as the Oddy tested coupons were exposed to high levels of sulphur during the degradation of wool which led to silver sulfides being formed, see section 6.3.7. Investigation of Oddy test coupon corrosion by SEM/EDX, XPS and XRD. The absence of metal sulfide or metal oxide peaks was unexpected and may be due to instability of these corrosion products during ionisation desorption under the analysis conditions applied. Furthermore, the electron affinity of chlorine (3.62 eV) is higher than that of sulphur (2.08 eV) and oxygen (1.46 eV) [65], which may lead to an over-representation of chlorine compounds in the negative ion mass spectra.

Signals identified as fatty acid contamination were observed on most samples with peaks attributed to palmitic acid ($C_{15}H_{31}COO^-$ at m/z 255^-) and to a lesser extent myristic acid ($C_{13}H_{27}COO^-$ at m/z 227^-), mono-unsaturated and saturated pentadecanoic acid ($C_{14}H_{27}COO^-$ at m/z 239^- and $C_{14}H_{29}COO^-$ at m/z 241^-), mono-unsaturated oleic acid ($C_{17}H_{33}COO^-$ at m/z 281^-) and stearic acid ($C_{17}H_{35}COO^-$ at m/z 283^-), Figure 6.3.56. Other contaminants included siloxane residues, with its characteristic peaks at m/z 73^+, 117^+, 147^+, 207^+, 221^+, 265^+, 267^+, 279^+ and 281^+ which were observed on almost all samples and polyethylene (m/z 105^+, 115^+, 128^+ and 165^+) which was identified in three spectra of metal threads only. The origin of these contaminants is unknown but they are present in a wide variety of applications and may have arisen from sample containers or cross contamination via laboratory beakers and surfaces. Large peaks for the halogens chlorine, iodine and bromine were observed on all silver coupon spectra, the copper coupon and metal thread spectra also showed peaks for chlorine but with lower relative intensity and peaks for iodine and bromine were weak or absent. Unidentified peaks included, most notably, m/z 223^- which was present in nearly every negative ion spectrum and m/z 299^-, 301^-, present on negative ion spectra of copper coupons only.

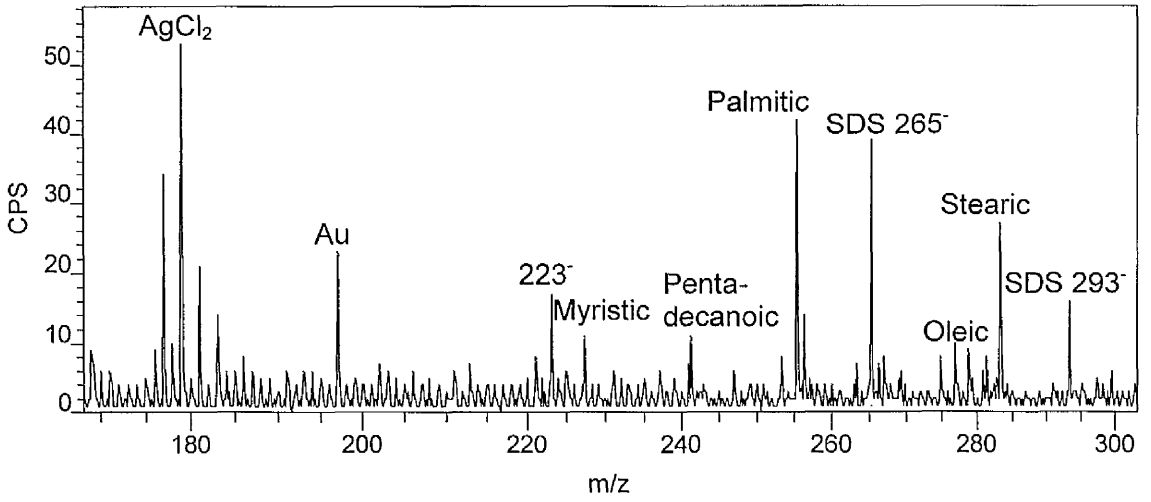

Figure 6.3.56. ToF-SIMS negative ion spectrum of metal thread 'untreated PNM5_24'

Table 6.3.8. ToF-SIMS peaks observed in negative and positive ion spectra*

Peak assignment / m/z / Sample	Ag	Cu	Au	SDS				NPO	$AgCl_2$	I / Br	Myristic	Pentadecanoic	Palmitic	Oleic	Stearic	Siloxane	Polyethylene
	107^+ 109^+	63^+ 65^+	197^-	265^-	293^-	321^-	349^-	219^-	177^- 179^- 181^-	127^- / 79^- 81^-	227^-	241^-	255^-	281^-	283^-	Si^+	PE^+
Untreated clean Cu	-	x	-	-	-	-	-	-	-	-	-	o	x	-	-	-	-
H_2O clean Cu	-	x	-	x	x	-	-	-	-	-	-	-	-	-	-	-	-
H_2Ol corroded Cu	-	x	-	-	-	-	-	-	-	-	-	o	x	-	o	x	-
SDS 98% clean Cu	-	x	-	x	x	x	x	-	-	-	-	-	x	-	-	-	-
SDS 99% clean Cu	-	x	-	x	x	x	x	-	-	-	-	-	x	x	x	-	-
SDS 99% corroded Cu	-	x	-	x	x	-	-	-	-	-	o	o	x	o	o	x	-
T-NP9 + SDS 99% clean Cu	-	x	-	x	-	-	-	x	-	-	x	x	x	x	x	-	-
T-NP9 + SDS 99% corroded Cu	-	x	-	x	x	-	-	x	-	-	x	x	x	x	x	x	-
T-NP9 clean Cu	-	x	-	-	-	-	-	o	-	-	-	-	-	-	-	-	-
T-NP9 corroded Cu	-	x	-	-	-	-	-	o	-	-	x	x	x	x	x	x	-
Untreated clean Ag	x	-	-	-	-	-	-	-	x	x	-	-	o	o	o	-	-
H_2O clean Ag	x	o	-	-	-	-	-	-	x	x	-	-	o	o	o	x	-
H_2O corroded Ag	x	-	-	-	-	-	-	-	x	x	-	-	o	-	-	x	-
SDS 98% clean Ag	x	-	-	-	-	x	x	-	x	x	o	o	x	x	-	-	-
SDS 99% clean Ag	x	o	-	x	x	o	x	-	x	x	-	-	x	x	x	x	-
SDS 99% corroded Ag	x	-	-	x	x	o	o	-	x	x	-	-	x	-	-	x	-
T-NP9 + SDS 99% clean Ag	x	-	-	o	x	-	-	x	x	x	o	-	x	x	x	-	-
T-NP9 + SDS 99% corroded Ag	x	o	-	o	o	-	x	x	-	x	o	-	x	-	o	x	-
T-NP9 clean Ag	x	-	-	-	-	-	-	o	x	x	-	-	o	o	o	-	-
T-NP9 corroded Ag	x	-	-	-	-	-	-	o	x	x	-	-	o	-	-	x	-
Untreated Model	x	o	x	-	-	-	-	-	x	-	-	-	x	x	-	x	-
SDS 99% Model	x	-	x	o	o	o	-	-	-	-	-	-	x	x	-	x	-
T-NP9 + SDS 99% Model	x	-	x	x	-	-	-	o	-	-	-	-	x	o	x	x	-
T-NP9 Model	x	-	x	x	x	o	-	o	-	-	-	-	x	o	x	x	-
Untreated PNM1_24	-	-	o	-	-	-	-	-	-	-	x	o	x	-	-	x	x
T-NP9 + SDS 99% PNM1_24	x	x	o	x	-	-	-	x	-	-	x	o	x	o	x	x	-
T-NP9 PNM1_24	-	-	-	-	-	-	-	-	-	-	-	-	x	-	-	x	x
Untreated PNM2_17	x	x	-	-	-	-	-	-	x	-	-	-	x	-	x	x	-
SDS 99% PNM2_17	-	-	-	-	x	-	-	-	-	-	-	-	x	o	-	x	x
T-NP9 + SDS 99% PNM2_17	x	x	o	-	-	-	-	x	-	-	x	x	x	-	x	-	-
T-NP9 PNM2_17	x	x	-	-	-	-	-	x	-	-	x	x	x	-	x	-	-
Untreated PNM5_24	x	x	x	x	x	o	-	-	x	-	x	x	x	o	x	x	-
SDS 99% PNM5_24	x	x	o	x	x	x	-	-	-	-	-	-	o	-	-	x	-
T-NP9 + SDS 99% PNM5_24	x	x	-	x	-	-	-	x	-	-	o	o	x	-	x	x	-
T-NP9 PNM5_24	x	x	-	-	-	-	-	x	-	-	x	o	x	-	x	x	-

*Peaks for hydrocarbons, sulphur and sulphur oxides, chlorine, and the ethoxylate ion (45^+) have been omitted from the table because they were present in every spectrum.

Si^+ (Siloxane) peaks are: m/z 73^+, 117^+, 147^+, 207^+, 221^+, 265^+, 267^+, 279^+ and 281^+

PE^+ (Polyethylene) peaks are: 105^+, 115^+, 128^+ and 165^+

x = peak was present; o = peak was present but obscured by background; - = peak was not present or at background level.

Table 6.3.9. Relative intensities of negative ion ToF-SIMS signals

Peak Assignment m/z / Sample	$1000*I_{(A)}/I_{(Total)}$ S 32^-	SO_2 64^-	SO_3 80^-	HSO_4 97^-	SDS 265^-	SDS 293^-	SDS 321^-	SDS 349^-
Untreated clean Cu	9.4	0.0	11.7	11.7	0.1	0.0	0.1	0.0
H_2O clean Cu	6.7	0.0	14.1	11.4	4.3	0.7	0.1	0.0
H_2O corroded Cu	3.7	1.5	4.9	7.6	0.1	0.1	0.1	0.0
SDS 98% clean Cu	6.2	0.0	19.1	13.9	6.5	1.6	0.9	0.6
SDS 99% clean Cu	4.5	0.0	**19.4**	9.6	3.8	0.8	0.8	0.7
SDS 99% corroded Cu	6.5	6.8	17.2	10.6	**7.7**	4.0	0.2	0.1
T-NP9 + SDS 99% clean Cu	7.6	0.0	7.3	9.8	3.3	0.3	0.0	0.0
T-NP9 + SDS 99% corroded Cu	4.5	3.1	10.2	11.2	5.2	0.9	0.2	0.1
T-NP9 clean Cu	5.2	0.0	5.7	7.6	0.1	0.0	0.0	0.0
T-NP9 corroded Cu	10.2	2.7	6.0	7.9	0.2	0.1	0.1	0.1
Untreated clean Ag	19.6	2.8	9.7	3.0	0.2	0.1	0.1	0.1
H_2O clean Ag	11.0	2.0	12.5	8.1	0.3	0.3	0.3	0.2
H_2O corroded Ag	14.4	2.8	4.6	2.9	0.1	0.0	0.0	0.0
SDS 98% clean Ag	19.1	4.4	**36.5**	8.1	0.6	0.3	1.8	5.3
SDS 99% clean Ag	13.9	3.9	30.6	10.6	**12.6**	1.5	0.4	0.8
SDS 99% corroded Ag	13.1	3.2	14.3	5.3	1.5	0.6	0.2	0.4
T-NP9 + SDS 99% clean Ag	19.7	3.3	14.5	5.8	1.6	1.0	0.3	0.2
T-NP9 + SDS 99% corroded Ag	16.7	3.4	14.3	12.4	0.7	0.5	0.4	1.9
T-NP9 clean Ag	11.0	2.7	5.6	4.7	0.1	0.1	0.1	0.0
T-NP9 corroded Ag	17.4	4.1	18.0	5.3	0.4	0.1	0.1	0.0
Untreated Model	4.9	0.4	2.0	2.0	1.6	1.3	0.2	0.2
SDS 99% Model	8.2	2.0	**10.2**	9.6	**17.6**	1.2	0.0	0.0
T-NP9 + SDS 99% Model	2.0	0.4	4.0	4.7	9.0	0.4	0.1	0.2
T-NP9 Model	3.9	1.1	8.0	8.1	6.7	7.2	0.1	0.2
Untreated PNM1_24	6.5	0.3	1.0	0.7	0.1	0.0	0.0	0.0
T-NP9 + SDS 99% PNM1_24	2.3	0.7	**3.1**	2.4	**2.1**	0.4	0.2	0.2
T-NP9 PNM1_24	6.2	1.3	2.8	2.2	0.1	0.1	0.1	0.1
Untreated PNM2_17	3.5	0.9	**5.5**	10.1	0.3	0.2	0.2	0.2
SDS 99% PNM2_17	10.0	0.7	1.0	0.8	0.1	0.1	0.0	0.0
T-NP9 + SDS 99% PNM2_17	7.5	0.7	3.2	5.5	0.2	0.3	0.3	0.1
T-NP9 PNM2_17	8.0	0.8	3.2	5.0	**0.3**	0.2	0.2	0.2
Untreated PNM5_24	4.7	0.8	3.2	4.6	2.2	1.0	0.3	0.1
SDS 99% PNM5_24	7.3	1.9	**15.5**	9.6	**13.1**	0.7	0.6	0.1
T-NP9 + SDS 99% PNM5_24	5.2	1.0	6.0	5.8	6.9	0.1	0.1	0.1
T-NP9 PNM5_24	6.2	0.5	3.8	5.1	0.4	0.3	0.3	0.2

Table 6.3.10. Relative intensities of negative ion ToF-SIMS signals

Peak Assignment m/z / Sample	$1000*I_{(A)}/I_{(Total)}$ CH 13^-	O 16^-	C_2H 25^-	Cl 35^-	$AgCl_2$ 179^-	Au 197^-	NP9 219^-	FA* 255^-
Untreated clean Cu	50.6	107.8	42.0	8.8	-	-	0.0	0.6
H_2O clean Cu	46.3	102.5	41.9	7.6	-	-	0.1	0.3
H_2O corroded Cu	66.9	113.8	42.5	19.0	-	-	0.0	1.3
SDS 98% clean Cu	55.7	104.6	39.4	12.9	-	-	0.0	1.0
SDS 99% clean Cu	68.2	84.2	44.7	7.9	-	-	0.0	2.2
SDS 99% corroded Cu	89.9	110.2	57.3	**67.1**	-	-	0.1	1.1
T-NP9 + SDS 99% clean Cu	45.2	80.4	38.2	5.1	-	-	1.2	0.4
T-NP9 + SDS 99% corroded Cu	94.6	94.6	57.8	10.9	-	-	**2.3**	2.8
T-NP9 clean Cu	42.3	82.2	38.5	10.4	-	-	0.3	0.4
T-NP9 corroded Cu	114.6	92.8	58.9	5.1	-	-	0.6	3.8
Untreated clean Ag	30.4	61.0	27.7	60.3	9.7		0.1	0.9
H_2O clean Ag	67.1	116.3	40.6	30.0	2.5		0.1	0.7
H_2O corroded Ag	67.1	90.3	37.8	**103.8**	**13.7**		0.0	1.2
SDS 98% clean Ag	33.1	57.8	29.6	46.8	3.7		0.1	2.3
SDS 99% clean Ag	63.7	78.9	45.0	40.2	3.4		0.1	4.5
SDS 99% corroded Ag	63.5	104.2	36.5	79.2	10.6		0.1	1.1
T-NP9 + SDS 99% clean Ag	34.2	63.0	33.0	50.8	4.0		**1.1**	1.1
T-NP9 + SDS 99% corroded Ag	56.2	80.6	39.4	18.4	2.2		0.9	1.8
T-NP9 clean Ag	58.0	104.8	40.0	62.4	4.6		0.3	0.6
T-NP9 corroded Ag	37.1	72.3	34.6	51.8	4.2		0.3	0.8
Untreated Model	166.8	174.4	67.8	**38.7**	**11.1**	2.8	0.0	4.2
SDS 99% Model	194.2	317.2	63.2	2.4	0.2	4.0	0.1	2.5
T-NP9 + SDS 99% Model	93.0	135.5	48.1	9.0	0.7	17.7	0.3	18.0
T-NP9 Model	100.0	200.3	48.9	10.5	1.5	8.4	**1.2**	10.0
Untreated PNM1_24	188.3	310.6	56.1	13.6	0.0	0.1	0.0	0.0
T-NP9 + SDS 99% PNM1_24	216.2	144.8	60.4	5.3	0.4	0.4	**0.4**	3.0
T-NP9 PNM1_24	135.8	258.1	57.0	**19.0**	**0.5**	0.3	0.1	0.4
Untreated PNM2_17	108.6	158.0	44.4	**26.4**	**3.1**	0.8	0.3	1.9
SDS 99% PNM2_17	217.5	192.1	93.5	10.2	0.1	0.2	0.1	0.3
T-NP9 + SDS 99% PNM2_17	108.7	148.3	51.1	9.6	1.0	0.5	**1.4**	2.4
T-NP9 PNM2_17	106.9	151.7	50.6	10.8	0.9	0.5	1.3	2.5
Untreated PNM5_24	157.2	162.6	42.2	**37.4**	**3.2**	1.1	0.2	2.2
SDS 99% PNM5_24	125.0	190.6	50.4	9.3	0.7	1.1	0.3	1.0
T-NP9 + SDS 99% PNM5_24	147.0	175.8	66.7	12.3	0.5	0.8	1.4	1.3
T-NP9 PNM5_24	101.5	117.7	47.9	25.3	1.0	1.2	**2.4**	3.8

FA* = Fatty acid (Palmitic acid)

Table 6.3.11. Relative intensities of positive ion ToF-SIMS signals

Peak Assignment m/z / Sample	1000*$I_{(A)}/I_{(Total)}$						Isotope ratios	
	CH_3	C_2H_3	C_3H_5	EO	Cu	Ag	Cu	Ag
	15^+	27^+	41^+	45^+	63^+	107^+	63/65	107/109
Untreated clean Cu	11.2	41.8	51.9	6.6	126.8	-	0.4	-
H_2O clean Cu	14.3	41.6	48.1	6.5	107.0	-	0.4	-
H_2O corroded Cu	7.9	39.2	47.9	1.8	183.2	-	0.3	-
SDS 98% clean Cu	10.2	39.1	51.6	3.6	134.6	-	0.4	-
SDS 99% clean Cu	8.3	43.1	60.4	4.5	115.4	-	0.5	-
SDS 99% corroded Cu	8.1	43.0	51.1	0.4	85.3	-	0.6	-
T-NP9 + SDS 99% clean Cu	12.7	44.3	48.2	**16.0**	132.6	-	0.4	-
T-NP9 + SDS 99% corroded Cu	6.6	37.9	48.6	2.0	150.2	-	0.3	-
T-NP9 clean Cu	13.3	44.2	48.5	11.6	121.1	-	0.4	-
T-NP9 corroded Cu	7.6	48.8	74.2	2.7	165.0	-	0.4	-
Untreated clean Ag	6.3	23.7	35.0	5.0	3.7	76.5	9.3	1.0
H_2O clean Ag	3.7	9.3	30.1	8.3	23.9	49.9	1.3	1.0
H_2O corroded Ag	3.2	15.6	27.4	3.1	3.8	72.4	7.2	0.9
SDS 98% clean Ag	5.7	27.9	45.7	5.3	15.9	52.4	2.9	1.0
SDS 99% clean Ag	5.5	20.3	32.7	**18.6**	6.2	78.2	5.3	1.0
SDS 99% corroded Ag	5.2	22.8	36.2	5.2	3.3	77.7	10.9	1.0
T-NP9 + SDS 99% clean Ag	2.9	12.3	20.2	2.8	8.9	59.9	2.3	0.9
T-NP9 + SDS 99% corroded Ag	6.0	22.4	36.2	7.6	2.8	70.8	13.0	1.0
T-NP9 clean Ag	4.7	24.2	37.2	5.7	71.9	96.9	0.5	0.9
T-NP9 corroded Ag	4.6	22.6	44.3	8.3	12.2	43.2	3.6	0.9
Untreated Model	4.5	23.0	41.4	1.2	17.5	23.7	2.4	1.1
SDS 99% Model	6.5	29.7	54.4	0.9	5.0	30.9	10.9	1.0
T-NP9 + SDS 99% Model	2.9	16.5	35.6	2.0	5.1	159.9	7.0	1.0
T-NP9 Model	2.9	11.8	25.2	**3.8**	9.8	91.8	2.6	1.1
Untreated PNM1_24	7.9	28.7	44.2	4.3	3.1	1.7	14.2	1.2
T-NP9 + SDS 99% PNM1_24	7.8	52.2	89.9	**5.8**	33.6	10.2	2.7	1.0
T-NP9 PNM1_24	7.9	27.3	40.3	4.3	3.9	1.1	10.3	1.0
Untreated PNM2_17	6.9	30.9	44.6	1.3	91.0	10.2	0.5	1.1
SDS 99% PNM2_17	9.6	33.0	48.1	4.1	1.0	0.2	49.7	1.2
T-NP9 + SDS 99% PNM2_17	6.9	36.3	51.2	13.5	91.6	58.3	0.6	1.1
T-NP9 PNM2_17	6.8	36.3	52.6	**14.7**	88.5	56.9	0.6	1.1
Untreated PNM5_24	4.7	29.3	52.8	2.1	42.7	31.8	1.2	1.1
SDS 99% PNM5_24	8.7	46.0	66.4	3.0	54.7	22.6	1.2	1.1
T-NP9 + SDS 99% PNM5_24	7.7	39.0	58.9	11.4	49.8	15.9	1.2	1.1
T-NP9 PNM5_24	6.3	35.5	53.8	**16.2**	58.8	55.5	0.9	1.1

6.4. Conclusions

Thorough documentation of metal threads and the interpretation of metal thread images allowed the identification of correlations between metal thread dimensions, indicating that manufacturers chose wider filaments for the spinning of coarser metal threads and the finest filaments for the spinning of threads with the smallest diameter and narrow winding. The relative amounts of coarse and fine metal threads and the number of double and triple wrapped threads observed in the investigated tapestries suggested a deliberate choice of the highest quality metal threads in the Spanish "Fables of Ovid" tapestries, while the varying levels of corrosion between the different tapestries signify their display and storage histories. Careful interpretation of the literature and measurements of the widths and winding directions of overlapping metal thread filaments suggested that some double wrapped threads were in fact single wrapped threads showing the joining of filaments due to discontinuous spinning. This has previously not been identified in the published literature on metal threads and resolves the speculations on fusing or hammering metal filaments together prior to spinning.

EDX, SIMS and XPS analyses provided evidence for copper ion migration from the bulk to the surfaces of metal filaments. This was most noticeable in metal filaments with a higher copper content which was found to vary from ~ 4 wt% to 15 wt% with no apparent trends between tapestries or groups of metal threads. EDX analyses singled out one metal thread with double sided gilding and comparison with compositions of previously identified restoration threads suggested that this particular sample was wrongly assigned during sampling, showing the merit of chemical analysis for the assistance of conservator's assessments of original or restored areas in textiles. Cross sectional analyses of metal threads showed the silver-copper bulk as a single phase alloy which may have been deliberately achieved to retain the metals flexibility in preference to the hardening of phase segregated metal alloys. The sections also showed the presence of pores in the alloy which were stretched longitudinally parallel to the axis of the filaments suggesting that the metal was rolled during manufacturing, this was supported by the observance of longitudinal striations on the surface of a metal filament. The pores on the edges of the filaments showed signs of compression due to cutting from the non-gilt side (interior) to the gilt side (exterior). This combination of rolling and cutting for the manufacture of metal threads contributes new information to the common hypotheses of manufacturing routes being divided into "beaten and cut"

and "cast, drawn and rolled". SIMS depth profiles and SEM images of metal thread cross sections showed that leaf gilding technique was employed and gilt layers were < 0.5 μm in thickness. To the author's knowledge this is the first time that such unambiguous evidence of leaf gilding on historic metal threads has been obtained.

Investigations of corrosion morphologies showed the presence of mainly rounded crystals growing on the surfaces of metal filaments and corrosion tunnelling causing the disintegration of the filament bulk. Corrosion delamination was observed on most samples and EDX spectra identified compositional variations between the delaminating and the underlying layers with most samples showing a layer of high silver and sulphur content detaching from a layer of high copper and carbon content. XPS analysis of corrosion products was hampered by high levels of carbon contaminations; nevertheless, various amounts of chlorine, oxygen as well as sulfide and sulfate compounds were detected. High resolution scans confirmed the presence of at least two chemical states for copper, with the main peak being attributed to compounds containing Cu, Cu_2S, CuS, CuCl or C_2O and a smaller peak of copper in a higher oxidation state with possible compounds being $CuCl_2$, CuO, $Cu(OH)_2$ or $CuSO_4$. SIMS spectra of metal filament surfaces showed the presence of various simple metal compounds with chlorine, sulphur, oxygen or carbon while larger molecules, especially metal-sulphates or carbonates, were not detected. This was attributed to ionisation desorption effects of the analysis technique rather than the absence of larger corrosion products. Unambiguous identification of corrosion products on metal threads was achieved, for the first time, using XRD. Due to the small sample dimensions XRD analysis of metal threads can be difficult and often fails. However, those metal threads of which XRD patterns were successfully obtained showed the presence of acanthite and chloragyrite and possibly digenite.

Silver and copper coupons were incubated with variously dyed wool and silk samples to study the influence of thermal and light degradation of the fibres on corrosion formation (Oddy tests). Under the conditions applied light degradation caused greater tarnishing than thermal degradation with the degradation of wool being more corrosive than the degradation of silk. There were no apparent differences in levels of corrosion due to the degradation of variously dyed fibrous samples in thermal Oddy tests while variations in levels of tarnishing observed among light Oddy tested samples were tentatively attributed to greater light

absorption, loss of gaseous sulphur species, and hence further degradation of the darker shades of wool fibres. SEM investigation of the corrosion morphologies showed rounded crystals on both silver and copper samples as well as longitudinal crystals on one copper sample which XRD analysis confirmed as different corrosion products. The rounded corrosion crystals were found to be acanthite on silver and cuprite on copper while the copper sample with longitudinal crystals showed the presence of chalcocite and tenorite. XPS analysis confirmed the increase in surface sulphur, especially due to the degradation of wool, with sulphur levels being generally higher on silver than on copper coupons which showed high levels of oxygen, as was consistent with the presence of oxygen containing corrosion products cuprite and tenorite. Sulphur to silver ratios on some silver samples exceeded 0.5 indicating the presence of additional corrosion products other than acanthite or adsorbed organic sulphur compounds. Sulphur was mainly present in the S^{2+} state but especially copper samples also showed sulphur in its higher oxidation state S^{6+} possibly attributable to copper sulphate formation.

Clean and corroded metal samples were treated with detergents representative of cleaning methods applied in textile conservation. ToF-SIMS analyses showed that both Sodium Dodecyl Sulfate and Tergitol-NP9 residues deposit on the surface indicated by obvious increases in SO_3^-, SDS, nonylphenoxide and ethoxylate levels on most detergent treated samples. However, the increases in signal intensities were not consistent throughout all samples with few samples showing no residual detergent signals, indicating that the detergent residues do not adsorb uniformly onto the metal surfaces and / or are partially removed by rinsing in deionised water. There were no obvious differences in adsorption levels onto silver or copper surfaces and clean or corroded surfaces. Adsorbed detergent residues may have implications for the future degradation of metals by increasing the surface sulphur levels, i.e. SO_3^- residues, and potentially enhancing the diffusion of atmospheric pollutants onto the metal surfaces.

6.5. References

1. Braun-Ronsdorf, M., 'Gold and Silver Fabrics from Medieval to Modern Times', *C.I.B.A. Review* **3** (1961) 2-16.

2. Hoke, E. and I. Petrascheck-Heim, 'Microprobe Analysis of Gilded Silver Threads from Mediaeval Textiles', *Studies in Conservation* **22** (1977) 49-62.

3. Indictor, N. and C. Blair, 'The Examination of Metal from Historic Indian Textiles Using Scanning Electron Microscope-Energy Dispersive X-Ray Spectrometry', *Textile History* **21** (2) (1990) 149-163.

4. Járó, M., 'Gold Embroidery and Fabrics in Europe: XI-XIV Centuries', *Gold Bulletin* **23** (2) (1990) 40-57.

5. Montegut, D., C. Adelson, R.J. Koestler, and N. Indictor, 'Examination of Metal Threads From Some XV/XVI Century Italian Textiles by Scanning Electron Microscopy-Energy Dispersive X-Ray Spectrometry', in *Materials Issues in Art and Archaeology III*, San Francisco, California, 27 April-1 May 1992, Materials Research Society 9800 McKnight Rd. Pittsburgh Pennsylvania 15237 USA, 309-317.

6. Hardin, I.R. and F.J. Duffield, 'Characterization of Metallic Yarns in Historic Persian Textiles by Microanalysis', in *Historic Textile and Paper Materials. ACS Symposium Series 212* 1986, ed. H.L. Needles and S.H. Zeronian, American Chemical Society, 231-252.

7. Darrah, J.A., 'Metal Threads and Filaments', in *Jubilee Conservation Conference; Recent Advances in the Conservation and Analysis of Artefacts*, University of London Institute of Archaeology 1987, ed. J. Black, Summer School Press, 211-221.

8. Indictor, N., R.J. Koestler, C. Blair, and A.E. Wardwell, 'The Evaluation of Metal Wrappings from Medieval Textiles Using Scanning Electron Microscopy-Energy Dispersive X-Ray Spectrometry', *Textile History* **19** (1) (1988) 3-19.

9. Indictor, N., R.J. Koestler, M. Wypyski, and A.E. Wardwell, 'Metal Threads Made of Proteinaceous Substrates Examined by Scanning Electron Microscopy-Energy Dispersive X-Ray Spectrometry', *Studies in Conservation* **34** (1988) 171-182.

10. Montegut, D., N. Indictor, J. Summerfield, and A. Summerfield, 'Technical Examination of Metal Threads in Some Indonesian Textiles of West Sumatra', *Textile History* **27** (1) (1996) 101-114.

11. Járó, M., A. Toth, and E. Gondar, 'Determination of the Manufacturing Technique of a 10th Century Metal Thread', in *ICOM Committee for Conservation 9th Triennial Meeting (Preprints)*, Dresden 1990, 299-302.

12. Járó, M., E. Gondar, and A. Toth, 'Technical Revolutions in Producing Gold Threads Used for European Textile Decoration', in *Outils et ateliers d'orfèvres des temps anciens*, Château de Sait-Germain-el-Laye 1993, ed. C. Eluère, Société des Amis du Musée des Antiquités Nationales, 119-124.

13. Darrah, J.A., 'The Microscopical and Analytical Examination of Three Types of Metal Thread', in *International Restorer Seminar*, Veszprem, Hungary: National Centre of Museums, 1-10 July 1989, ed. M. Járó and I. Eri, 53-63.

14. Oddy, W.A., 'The Production of Gold Wire in Antiquity. Hand-Making Methods before the Introduction of the Draw-Plate', *Gold Bulletin* **10** (3) (1977) 79-87.

15. Járó, M., E. Gondar, and A. Toth, 'Reconstruction of Gilding Techniques Used for Medieval Membrane Threads in Museum Textiles', *Archeometry '90, Birkhaeuser Verlag Basel* (1990) 317-325.

16. Járó, M. and A. Toth, 'Scientific Identification of European Metal Thread Manufacturing Techniques of the 17th-19th Centuries', *Endeavour (UK)* **15** (4) (1991) 175-184.

17. Geijer, A. and E.B. Thomas, 'The Viminacium Gold Tapestry', in *Meddelanden fran Lunds*, Universitets Historika Museum, Lund (1964-65) 223-236.

18. King, E., 'Digging up the Romans', Museum of London http://www.museumoflondon.org.uk/MOLsite/learning/features_facts/digging/people/o1.html (2003).

19. Járó, M., 'The Manufacturing Technique of Gold Threads in the 11th Century Coronation Mantle and some 12-14th Century Coronation Vestments of the Holy Roman Empire', in *Precious Thread: The Manufacture, Trade and Usage of Gold and Silver Yarn in Medieval Society. Medieval Dress and Textile Society - Autumn Meeting*, The Courtauld Institute of Art, London, 22-23 October 2005, unpublished lecture.

20. Presbyter, T., *Shedula Diversarum Artium, 12th century*, Quoted in: Járó, M., 'Gold Embroidery and Fabrics in Europe: XI-XIV Centuries', Gold Bulletin 23 (2) (1990) 40-57.

21. Finch, K., in *Precious Thread: The Manufacture, Trade and Usage of Gold and Silver Yarn in Medieval Society. Medieval Dress and Textile Society - Autumn Meeting*, The Courtauld Institute of Arts, London, 22-23 October 2005, unpublished translation of: Sofus Larsen, 'Nordisk Guldspinding og Guldbroderi i den tidlige Middelalder', Ejnar Munksgaard, Copenhagen, 1939.

22. Trélat, P., 'Ad Opus Cyprense. The Production and Trade of Cypriot Textiles with Gold', in *Precious Thread: The Manufacture, Trade and Usage of Gold and Silver Yarn in Medieval Society. Medieval Dress and Textile Society - Autumn Meeting*, The Courtauld Institute of Arts, London, 22-23 October 2005, unpublished lecture.

23. Kohara, N., Y. Sasa, K. Sakurai, and M. Uda, 'A Note on the Characterization of Metal Threads in Historic Textiles Handed Down by the Ainu People (Japanese Embroidery, Fabric)', *Studies in Conservation* **43** (2) (1998) 109-113.

24. Reyer de, D., A.Y. Jeantet, S. Pilbout, A. Anglo, and M. Monnerot, 'Les Lamelles des Fils Metallique Organiques dans les Textiles Medievaux: Approche Methodologique de leur Origine Biologique', *Studies in Conservation* **47** (2002) 122-133.

25. Monnas, L., 'Gold Thread of Lucca in the Middle Ages', in *Precious Thread: The Manufacture, Trade and Usage of Gold and Silver Yarn in Medieval Society. Medieval Dress and Textile Society - Autumn Meeting*, The Courtauld Institute of Arts, London, 22-23 October 2005, unpublished lecture.

26. Skals, I., 'Technical and Analytical Notes: Metal Thread with Animal-Hair Core', *Studies in Conservation* **36** (1991) 240-242.

27. Budney, M. and D. Tweedle, 'The Early Medieval Textiles at Maaseik, Belgium', *The Antiquaries Journal* **LXV** (II) (1985) 353-389.

28. Goodway, M. and J.S. Odell, 'The Metallurgy of 17th- and 18th- Century Music Wire', in *A Monograph Series in Honor of Frank Hubbard, The Historical Harpsichord*, (ed.) H. Schott, Pendragon Press, Stuyvesant, NY (1992).

29. Járó, M., T. Gal, and A. Toth, 'The Characterization and Deterioration of Modern Metallic Threads', *Studies in Conservation* **45** (2) (2000) 95-105.

30. Járó, M., 'The Investigation of the Metal Embroidery Threads of the Hungarian Coronation Mantle by SEM and Physical Methods of Analysis', in *ICOM 7th Triennial Meeting*, Copenhagen, 10-14 September 1984 1984, 84.1.22-84.1.24.

31. Tronner, K., A.G. Nord, J. Sjöstedt, and H. Hydman, 'Extremely Thin Gold Layers on Gilded Silver Threads', *Studies in Conservation* **47** (2002) 109-116.

32. Garside, P., *Investigations of Analytical Techniques for the Characterisation of Natural Textile Fibres Towards Informed Conservation*, Ph.D., University of Southampton, Southampton, (2002).

33. Rogerson, C., 'Report: 15th Century Tapestry Woven Altar Frontal', Textile Conservation Centre, Hampton Court Palace, University of Southampton, East Molesey (1999) 6-26.

34. Hacke, A.M., C.M. Carr, A. Brown, and D. Howell, 'Investigation into the Nature of Metal Threads in a Renaissance Tapestry and the Cleaning of Tarnished Silver by UV/Ozone (UVO) Treatment', *Journal of Materials Science* **38** (2003) 3307-3314.

35. Hacke, A.M., C.M. Carr, and A. Brown, 'Characterisation of Metal Threads in Renaissance Tapestries', in *AHRB annual conference for textile conservation*, Winchester, UK 2004.

36. Indictor, N. and M. Ballard, 'The Effects of Ageing on Textiles that Contain Metal: Implications for Analyses', in *International Restorer Seminar*, Veszprem, Hungary: National Centre of Museums, 1-10 July 1989, ed. M. Járó and I. Eri, 67-75.

37. Kentish Barnes, W., 'Gold and Silver Threads, their Origins and their Developments', in *Precious Thread: The Manufacture, Trade and Usage of Gold and Silver Yarn in Medieval Society. Medieval Dress and Textile Society - Autumn Meeting*, The Courtauld Institute of Arts, London, 22-23 October 2005, unpublished lecture.

38. Howell, D., R. Mitchell, C.M. Carr, and J. Walton, 'X-ray Photoelectron Spectroscopy (XPS) and Time-of-Flight Secondary Ion Mass Spectrometry (ToF-SIMS) Study of the Tarnishing of Metal-Coated Textiles', *Journal of the Textile Institute* **90** (3) (1999) 50-59.

39. Indictor, N. and R.J. Koestler, 'The Identification and Characterization of Metal Wrappings in Historic Textiles Using Microscopy and Energy Dispersive X-Ray Spectrometry: Problems Associated with Identification and Characterization', *Scanning Electron Microscopy*(2) (1986) 491-7.

40. Nord, A.G. and K. Tronner, 'A Note on the Analysis of Gilded Metal Embroidery Threads', *Studies in Conservation* **45** (4) (2000) 274-279.

41. Humphrey, D., 'Gold and Silver Production in Northern Europe c. 1350-1550', in *Precious Thread: The Manufacture, Trade and Usage of Gold and Silver Yarn in Medieval Society. Medieval Dress and Textile Society - Autumn Meeting*, The Courtauld Institute of Arts, London, 22-23 October 2005, unpublished lecture.

42. Járó, M., 'Re-Corrosion of Silver and Gilt Silver Threads on Museum Textiles after Treatment', in *International Restorer Seminar*, Veszprem, Hungary: National Centre of Museums, 1-10 July 1989, ed. M. Járó and I. Eri, 95-98.

43. Dubus, M., C. Moulherat, L. Robinet, and H. Spencer, 'Influence of the 2003 Heatwave on the Corrosion of Silver in Museums', in *6th Indoor Air Quality Meeting (IAQ2004)*, Padova, Italy, 10-12 November 2004, http://www.isac.cnr.it/iaq2004/abstract/dubus.PDF.

44. Franey, J.P., G.W. Kammlott, and T.E. Graedel, 'The Corrosion of Silver by Atmospheric Sulfurous Gases', *Corrosion Science* **25** (2) (1985) 133-143.

45. Leygraf, C. and T.E. Graedel, *Atmospheric Corrosion*, John Wiley & Sons, Inc. (2000) 1-354.

46. Graedel, T.E., J.P. Franey, and G.W. Kammlott, 'Carbonyl Sulfide: Potential Agent of Atmospheric Sulfur Corrosion', *Science* **212** (1981) 663-664.

47. Sipos, E. and E. Gondar, 'Effect of Different Treatments on Textiles with Metal Threads', in *International Restorer Seminar*, Veszprem, Hungary: National Centre of Museums, 1-10 July 1989, ed. M. Járó and I. Eri, 83-86.

48. Bennett, H.E., R.L. Peck, D.K. Burge, and J.E. Bennett, 'Formation and Growth of Tarnish on Evaporated Silver Films', *Journal of Applied Physics* **40** (1969) 3351-3360.

49. Járó, M. and A. Toth, 'Deterioration of Metal Threads and Other Metallic Decorations Made of Gold, Silver or Gilt Silver on Museums Textiles. Problems of their Conservation', in *Metal 95 : Proceedings of the International Conference on Metals Conservation* 1995, ed. I.D. MacLeod, S.L. Pennec, and L. Robbiola, 201-208.

50. Eggert, G., M. Weichert, H. Euler, and B. Barbier, 'Some News about Black Spots', in *Proceedings of the International Conference on Metals Conservation*, Canberra, Australia, 4-8 October 2004, ed. J. Ashton and D. Hallam, 142-148.

51. Weichert, M., G. Eggert, A.M. Jones, and H.A. Ankersmit, 'Trees, Bunches, Cauliflowers - A Closer Look at Sulphurous Corrosion on Copper Alloys and Minerals ('Black Spots')', in *Proceedings of the International Conference on Metals Conservation*, Canberra, Australia, 4-8 October 2004, ed. J. Ashton and D. Hallam, 149-154.

52. Drott, J., 'Growth of Silver Sulphide Whiskers', *Acta Metallurgica* **8** (1960) 19-22.

53. Dubus, M., M. Aucoutrier, and B. Moignard, 'Atmospheric Corrosion Monitoring on Silver in Museums', in *5th meeting of the Indoor Air Pollution Working Group (IAQ 2003)*, University of East Anglia, School of Environmental Sciences, Norwich, April 28th-29th 2003, ed. M. Ryhl-Svendsen, http://www.iaq.dk/iap/iaq2003/2003_15.htm.

54. van Langh, R., H.A. Ankersmit, and I. Joosten, 'The Delamination of Silver Sulphide Layers', in *Proceedings of the International Conference on Metals Conservation*, Canberra, Australia, 4-8 October 2004, ed. J. Ashton and D. Hallam, 137-141.

55. Bathy, G., 'Restoration of the Turkish-age Treasure Find from Ozora', in *International Restorer Seminar*, Veszprem, Hungary: National Centre of Museums, 1-10 July 1989, ed. M. Járó and I. Eri, 115-117.

56. Howell, D., 'Experiments with Chemical Cleaning for Metal Threads', in *International Restorer Seminar*, Veszprem, Hungary: National Centre of Museums, 1-10 July 1989, ed. M. Járó and I. Eri, 87-89.

57. Degrigny, C., E. Tanguy, R. Le Gall, V. Zafiropulos, and G. Marakis, 'Laser Cleaning of Tarnished Silver and Copper Threads in Museum Textiles', *Journal of Cultural Heritage* **4** (Supplement 1) (2003) 152-156.

58. Járó, M., A. Toth, and M. Kiss-Bendefy, 'Investigation of Metal Threads and Metallic Decorations of a Sixteenth-Century Bonnet', in *International Perspective on Textile Conservation Papers from the ICOM-CC*, London 1998, ed. Á. Tímár-Balázsy.

59. Cartwright, H. and A. Colombini, 'Detergent Monitoring during the Washing Process at the Textile Conservation Studios, Hampton Court Palace', in *Preprints of ICOM Committee for Conservation, 10th Triennial Meeting*, Washington, D.C. 1993, ed. J. Bridgland, 293-298.

60. Encarta® World English Dictionary, Bloomsbury Publishing Plc (2005).

61. Enguita, O., A. Climent-Font, G. Garcia, I. Montero, M.E. Fedi, M. Chiari, and F. Lucarelli, 'Characterization of Metal Threads Using Differential PIXE Analysis', *Nuclear Instruments and Methods in Physics Research Section B: Beam Interactions with Materials and Atoms* **189** (1-4) (2002) 328-333.

62. Beck, L., S. Bosonnet, S. Reveillon, D. Eliot, and F. Pilon, 'Silver Surface Enrichment of Silver-Copper Alloys: A Limitation for the Analysis of Ancient Silver Coins by Surface Techniques', *Nuclear Instruments and Methods in Physics Research Section B: Beam Interactions with Materials and Atoms* **226** (1-2) (2004) 153-162.

63. Selwyn, L., 'Corrosion Chemistry of Gilded Silver and Copper', in *Gilded Metals: History, Technology and Conservation*, St. Paul, Minnesota, USA 1995, ed. T. Drayman-Weisser, Archetype Publications, 21-47.

64. Moulder, J.F., W.F. Stickle, P.E. Sobol, and K. Bomben, *Handbook of X-Ray Photoelectron Spectroscopy*, Perkin-Elmer Corporation Physical Electronics Division (1992).

65. Wilson, R.G., F.A. Stevie, and C.W. Magee, *Secondary Ion Mass Spectrometry. A Pratical Handbook for Depth Profiling and Bulk Impurity Analysis*, John Wiley & Sons (1989) App. B.14.

66. Hallett, K., D. Thickett, D.S. McPhail, and R.J. Chater, 'Application of SIMS to Silver Tarnish at the British Museum', *Applied Surface Science* **203** (2003) 789-792.

67. Dowsett, M.G., A. Adriaens, M. Soares, H. Wouters, V.V.N. Palitsin, R. Gibbons, and R.J.H. Morris, 'The Use of Ultra-Low-Energy Dynamic SIMS in the Study of the Tarnishing of Silver', *Nuclear Instruments & Methods in Physics Research Section B-Beam Interactions with Materials and Atoms* **239** (1-2) (2005) 51-64.

68. Tímár-Balázsy, Á. and D. Eastop, *Chemical Principles of Textile Conservation*, Butterworth-Heinemann (1998) 128 / 242-247.

69. Rice, J.W., 'Principles of Textile Conservation Science, No. VII: Characteristics of Detergents for Cleaning Historic Textiles', *Textile Museum Journal* (1966).

70. Patterson, H.T. and T.H. Grindstaff, 'Soil Release by Textile Surfactants', in *Fiber Science Series*, (ed.) M.J. Schick, (1975-1977) 448-494.

71. Tse, S. and D. Derschau von, 'The Science of Conservation: Surfactant Residue and Rinsing Procedures for Historic Textiles', *CCI Newsletter* **No. 27** (June) (2001).

72. Hofenk de Graaff, J.H., 'Some Recent Developments in the Cleaning of Ancient Textiles', in *Science and Technology in the Service of Conservation, Preprint of the Contributions*, International Institute for Conservation, London, UK 1982, ed. N.S. Brommelle and G. Thomson, 93-99.

73. Rhee, H. and M.W. Ballard, 'Residues of Surfactants on Silk', in *Preprints of ICOM Committee for Conservationof, 10th Triennial Meeting*, Washington, D.C. 1993, ed. J. Bridgland, 327-329.

74. Brack, N., R. Lamb, D. Pham, and P. Turner, 'Nonionic Surfactants and the Wool Fibre Surface', *Colloids and Surfaces, A: Physicochemical and Engineering Aspects* **146** (1-3) (1999) 405-415.

75. Carr, C.M., R. Mitchell, and D. Howell, 'Surface Chemical Investigation into the Cleaning Procedure of Ancient Tapestry Materials', *Journal of Materials Science* **39** (2004) 7317-7325.

76. Volooj, S., C.M. Carr, R. Mitchell, and J.C. Vickerman, 'Time-of-Flight Secondary Ion Mass Spectrometry (ToF-SIMS) Analysis of the Bleaching of Keratin Fibres and the Application of Cationic Alkyl Protein Softeners to Bleached Cashmere', *Surface and Interface Analysis* **29** (7) (2000) 422-430.

77. Clarke, N. and S.G. Grundy, 'Nonionic Surfactant-Containing Aqueous Acrylic Coating for Metals', in PCT Int. Appl. patent, (Laporte Industries Ltd., UK). (1993) 14.

78. Shah, S.S., T.G. Braga, A.B.A. Oude, and J. Mathew, 'Corrosion Inhibition on Metal Surface Using Bilayer-Forming Surfactants with Polymerization', in U.S. patent, (Petrolite Corp., USA). (1995) 13.

79. Sowa, F.J., 'Coating Metals such as Silver to Prevent Tarnishing', in U.S. patent (1944).

Summary

The research for this thesis was carried out within the context of a European project on the Monitoring of Damage in Historic Tapestries (MODHT) comprising partners from universities, conservation and museum research institutions and historic palaces, and focused on the following three main areas:

Applicability of ToF-SIMS for the identification of natural dyes

The most widely used identification methods for dyes rely on the chemical extraction of the dyes prior to analysis and may require sampling amounts impermissible by conservators and curators. There is, therefore, an interest in non-extractive methods capable of either *in-situ* dye identification or identification from micro samples, e.g. single fibres. In this research project the surface sensitive analysis technique ToF-SIMS was applied, for the first time, to the analysis of a wide range of natural dyes. The study emphasized the potential of the technique for identification of dyes through desorption ionisation of whole chromophoric species from dried films of dyebaths and dyes applied to a paper substrate. However, the analysis of dyes on textiles was largely unsuccessful with the exception of the identification of indigo on wool. The work also highlighted the drawbacks of the technique such as its sensitivity to contamination, the overlapping mass to charge ratios of different chromophoric species and the changes induced by dyebath conditions leading to indistinct 'fingerprint' patterns.

Mechanical, morphological and surface chemical investigations of wool and silk

Preceding the investigations eighteen tapestries dating from the early 15th to the 17th centuries were sampled for historic wool, silk and metal threads and forty-two wool and silk model tapestry fabrics were produced to closely resemble historic tapestries in terms of dyestuffs and dyeing procedures, wool and silk yarn specifications and weave structure. The model tapestry fabrics were accelerated light aged to the equivalent of 400 years exposure to sunlight behind window glass and were used for mechanical and chemical investigations by all MODHT project partners.

The mechanical, morphological and surface chemical properties of wool and silk were studied with the aim of establishing markers of damage and investigating the changes induced through mordanting and dyeing processes, as well as accelerated ageing and natural ageing.

The surface and fracture morphologies of historic wool and silk fibres and model tapestry fabrics were investigated by SEM. Overall, fracture morphologies were found to have comparable distributions in unaged, accelerated aged and historic samples. Similarly, the surface morphologies of unaged and historic fibres were often indistinguishable rendering SEM analyses an unfeasible tool for objective fibre damage assessment. Characteristic surface cracking structures were identified on accelerated aged fibres and, in the case of silk, were also observed on historic fibres. For wool the cracking structures were distinctly different, with mainly transverse cracks being observed in historic wool and longitudinal cracks forming due to accelerated ageing.

Dyeing procedures were found to significantly affect the initial tensile properties of wool but the effects were largely lost after accelerated ageing, while for silk the opposite was observed with dyeing procedures not altering the initial tensile properties to a great extent but influencing the rate of degradation induced by accelerated ageing. Weld, dyer's greenweed and oak gall dyeings reduced the initial tensile strength and strain of wool. Metal ion mordanting and dyeing also strongly affected the tensile properties, with alum imparting a strengthening effect to wool but not to silk and the ferrous sulphate black dyeings causing initial weakening but appearing photo-protective in conjunction with oak gall tannin and degradative with alder bark tannin.

The loss in tensile strain in wool following dyeing procedures was reflected in a decreasing surface carbon to oxygen ratio as measured by XPS. The extent of surface sulphur oxidation was suggested as another marker of damage for wool showing rough correlations with tensile strain values obtained from tests of unaged and accelerated aged yarns and historic fibres.

ToF-SIMS analyses of the wool fibre surfaces showed that the historic fibres were depleted of the major wool lipid 18MEA while accelerated ageing caused only the partial reduction of 18MEA on the model tapestry fabrics. In addition to the commonly recognised lipid peaks, two further peak series were identified on many wool surfaces and attributed to unsaturated and saturated fatty acids. Analyses with a cluster primary ion source (Bi_3^+) indicated a higher resistance to light ageing of oxygen ester bound fatty acids compared to the thioester bound 18MEA.

Analyses of metal thread composition, manufacture and corrosion

The investigation of almost 200 metal thread samples of five tapestries showed that all samples, with the exception of some restoration threads, were of the same

type with silver or silvergilt filaments wrapped around a silk core. Various rare and intricate double and triple wrapped threads were detected with especially high relative amounts in the Spanish tapestry series "Fables of Ovid".

Image analyses and compositional investigations of metal threads led to a wealth of new information on their manufacturing techniques. A correlation between metal thread dimensions, i.e. diameter, filament width and spacing was established. Some double wrapped threads were identified as filament overlaps caused during spinning resolving the issue of methods for the joining of filaments. The commonly acknowledged manufacturing routes "beaten and cut" and "cast, drawn and rolled" were questioned as evidence for rolling and cutting was detected in the same filaments. Cross sectional analyses identified the silver copper bulk as a single phase alloy with extremely thin (< 0.5 μm) leaf gilt layers.

Corrosion morphologies were mainly rounded crystals with corrosion delamination and corrosion tunnelling observed. The investigations of corrosion composition indicated copper ion migration from the bulk to the surfaces of metal filaments and the occurrence of silver-sulphur rich corrosion layers flaking off the surface of copper –carbon rich corrosion layers. Chlorine and oxygen rich corrosion formation was also observed and XPS analysis indicated the presence of sulfides as well as sulfates. Acanthite, chloragyrite and possibly digenite were identified by X-ray Diffraction of metal thread surfaces.

Oddy tests indicated relatively uniform corrosion formation on silver and copper due to the thermal degradation of variously dyed wool and silk, while photo-degradation of the differently dyed samples caused greater variations in corrosion levels. Corrosion crystals were rounded on both silver and copper surfaces, identified as acanthite and cuprite, respectively, with the exception of one copper sample exhibiting elongated crystals, identified as chalcocite and tenorite.

Investigations of the adsorption of anionic and non-ionic detergents on metal coupons and metal thread surfaces indicated the deposition of the dodecyl sulphate and Tergitol-NP9 residues following cleaning treatment procedures commonly used in textile conservation.

Further Work

- As ToF-SIMS instrumentation is continually improving, further research into the applicability of the technique for dye identification may eventually provide a practical, non-extractive alternative to current extractive methods. Especially the analysis of fibre cross sections may prove successful if further development and testing of embedding resins could eliminate the contaminations encountered in this study.
- The tensile properties of black dyed wool and silk yarns would need further investigation to elucidate the possible synergistic / additive effects of tannins and chromophores with ferrous sulphate and copper sulphate on the degradation or photo-protection of the fibres. A study into this general area is currently led by Dr Vincent Daniels at the Victoria and Albert Museum.
- XPS analysis of historic wool fibre surfaces showed a high degree of surface sulphur oxidation, with most samples having a relative % of S(VI) > 80% and some samples showing 100% surface sulphur oxidation. Even though these samples also showed very low strain values in tensile strength tests they still had some remaining strength. It follows that XPS analysis of wool surfaces could not reveal any further degradation, thereby limiting the sensitivity of the method. Additional XPS spectra may need to be obtained from sample cross sections in order to determine bulk sulphur oxidation as well as surface sulphur oxidation. This may enhance the differences detected between samples and thus improve correlations with mechanical properties.
- Further FEG-SEM / EDX cross sectional analyses of a wider variety of metal threads could advance the current knowledge on manufacturing techniques, i.e. evidence for rolling, cutting and gilding methods. Analysis of metal thread samples with a bulk copper content exceeding 9 wt% would elucidate whether the manufacture of a single phase alloy was deliberate to retain the metals flexibility or whether the samples investigated in this thesis exhibited a single phase alloy because of the ability of silver to include up to 9 wt% copper in a single phase.

Appendices

A. ToF-SIMS spectra of Dyestuffs

A.1. Madder

Alizarin synthetic chromophore negative ion spectrum : Cs^+ primary ion source

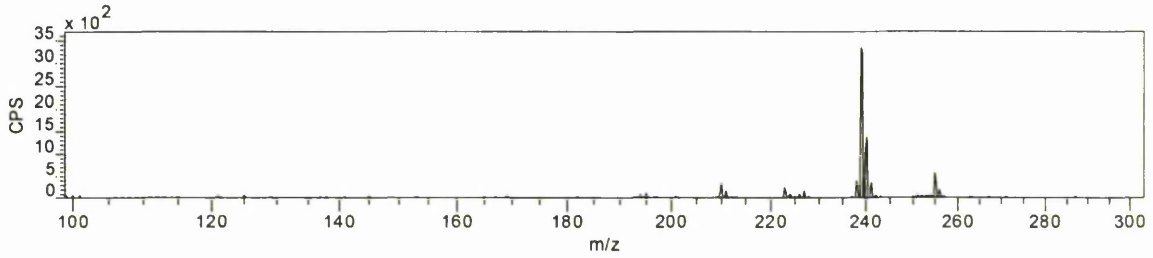

Alizarin synthetic chromophore positive ion spectrum : Cs^+ primary ion source

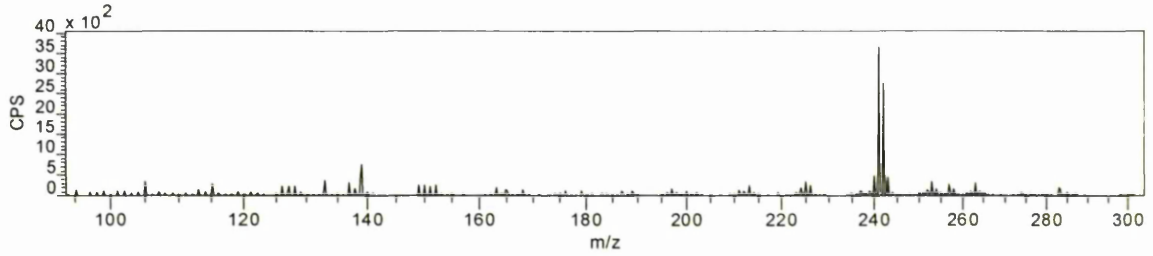

Madder dyebath (a) negative ion spectrum : Cs^+ primary ion source

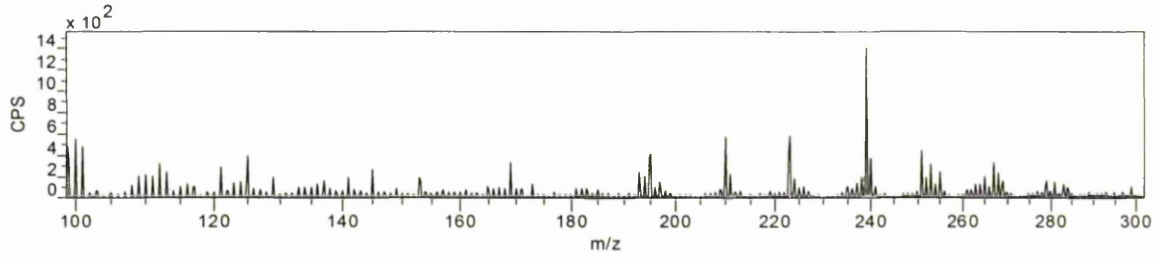

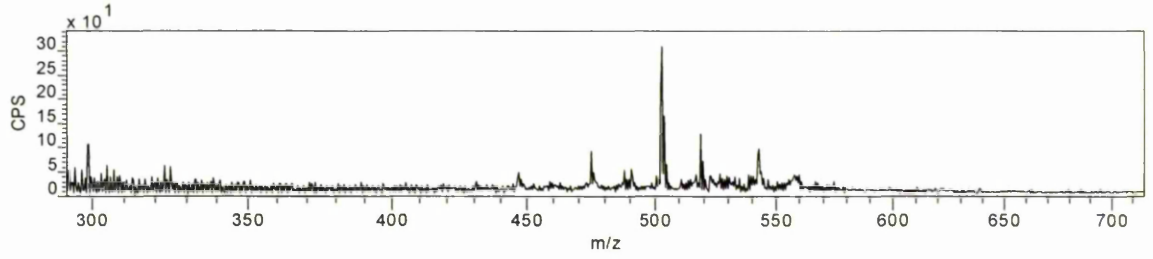

Madder dyebath (b) negative ion spectrum : Cs^+ primary ion source

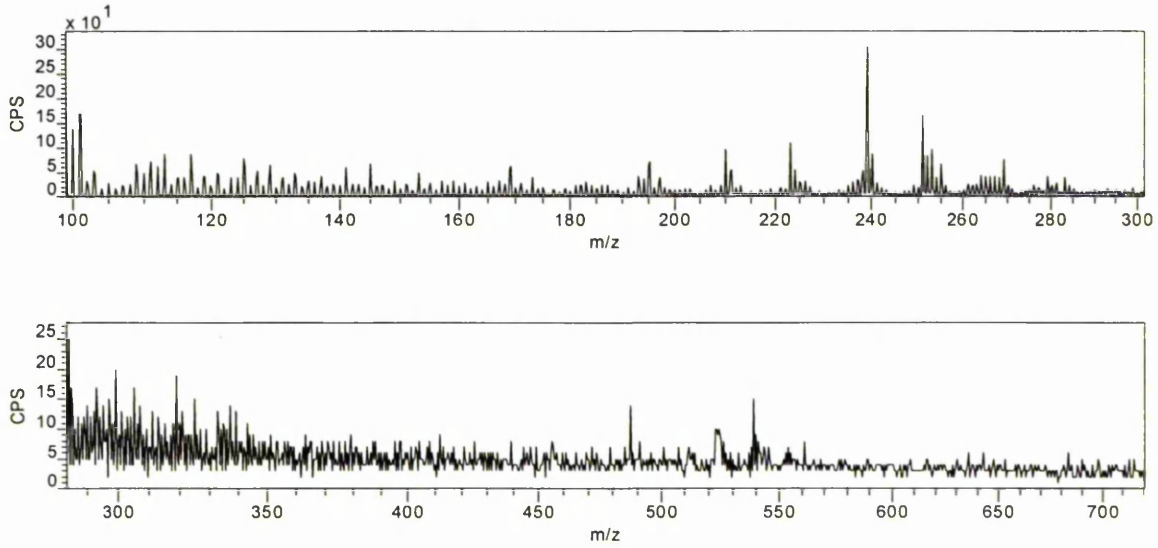

Madder dyebath (b) after exhaustion onto wool negative ion spectrum : Cs^+ primary ion source

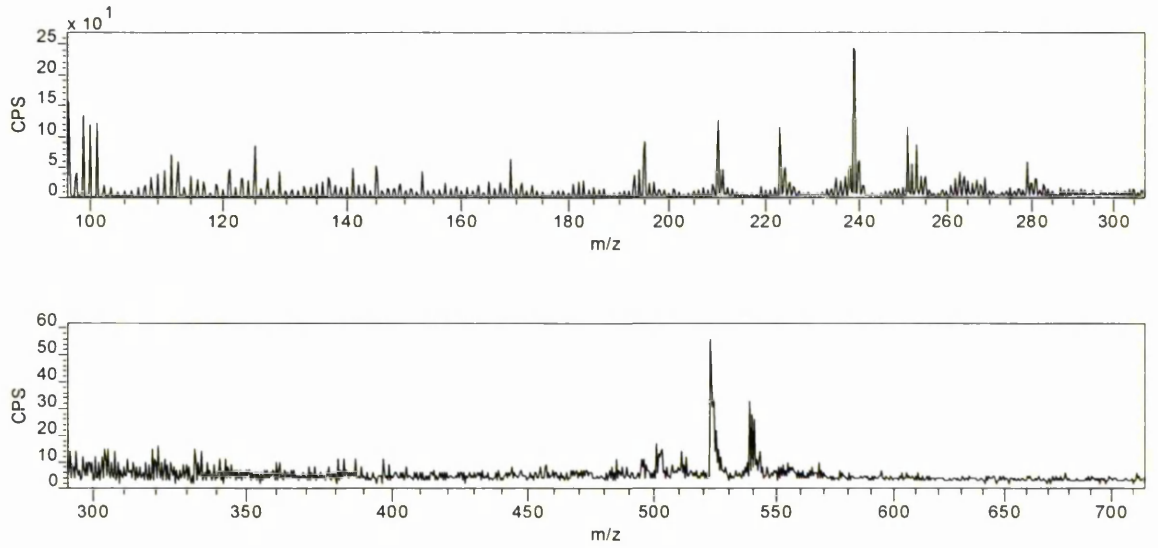

Madder dyebath (b) after exhaustion onto alum mordanted wool negative ion spectrum : Cs^+ primary ion source

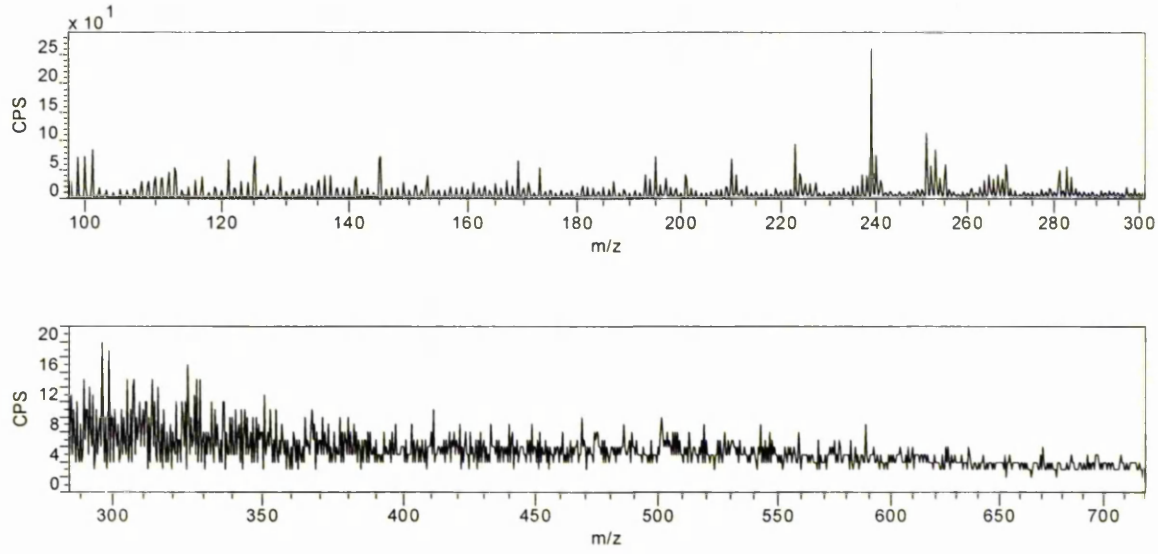

Madder dye on filter paper negative ion spectrum : Cs^+ primary ion source

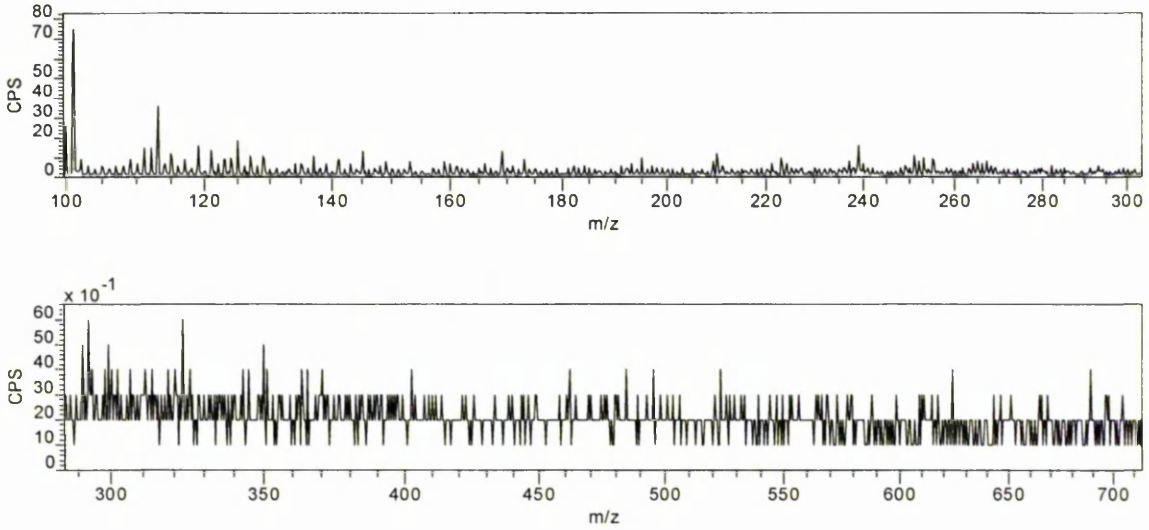

Madder dye on alum filter paper negative ion spectrum : Cs^+ primary ion source

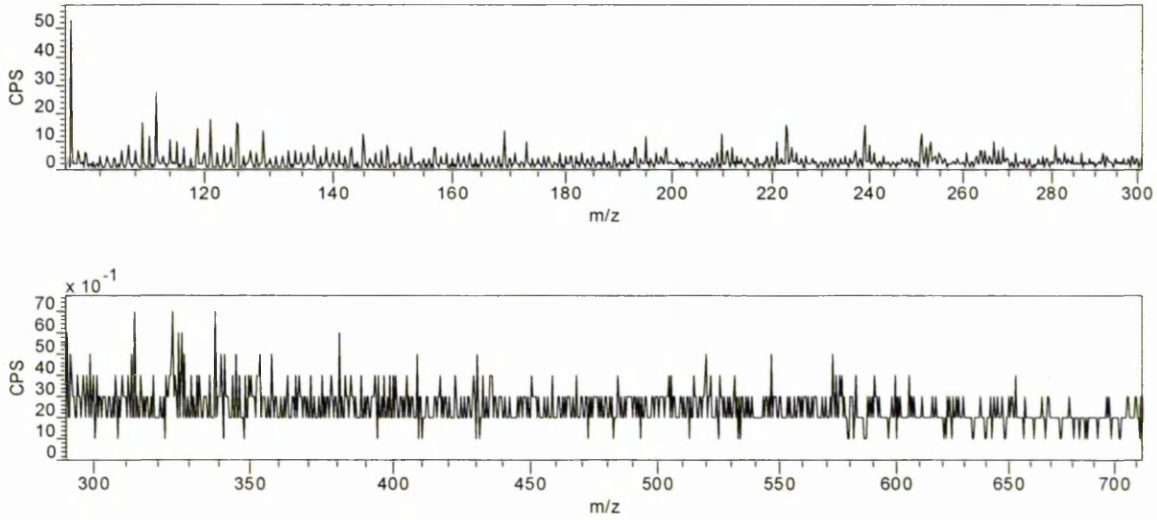

Madder/lye dyebath (a) negative ion spectrum : Cs^+ primary ion source

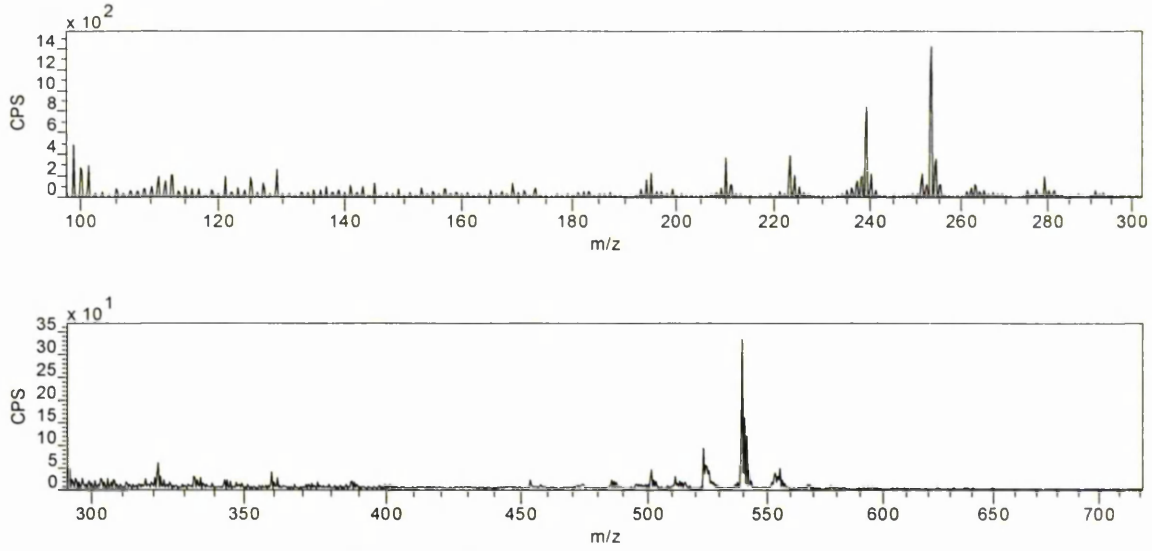

Madder/lye dyebath (b) negative ion spectrum : Cs^+ primary ion source

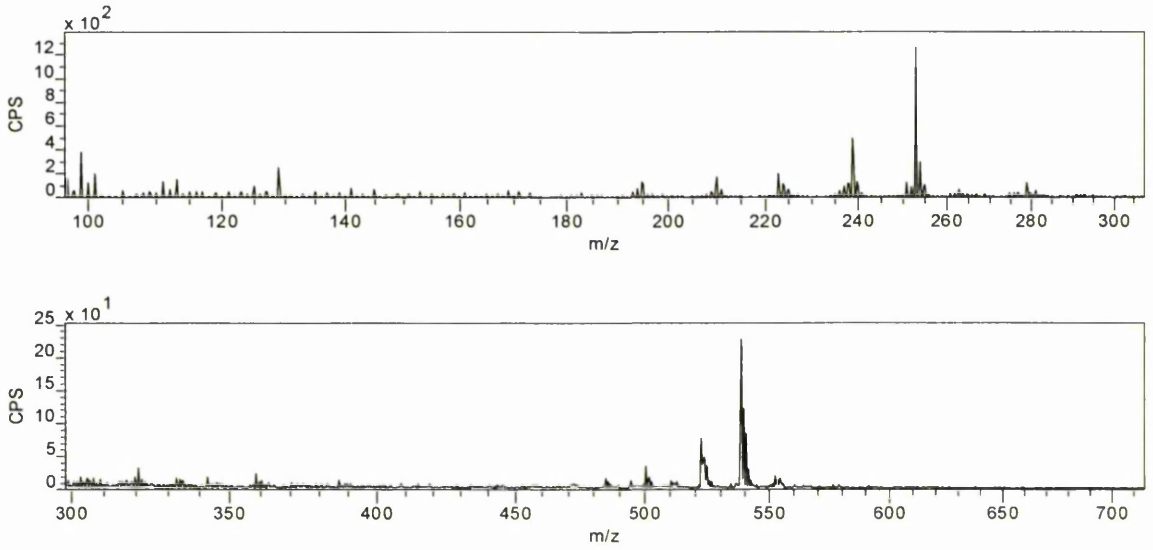

Madder/lye dyebath (b) after exhaustion onto wool negative ion spectrum : Cs^+ primary ion source

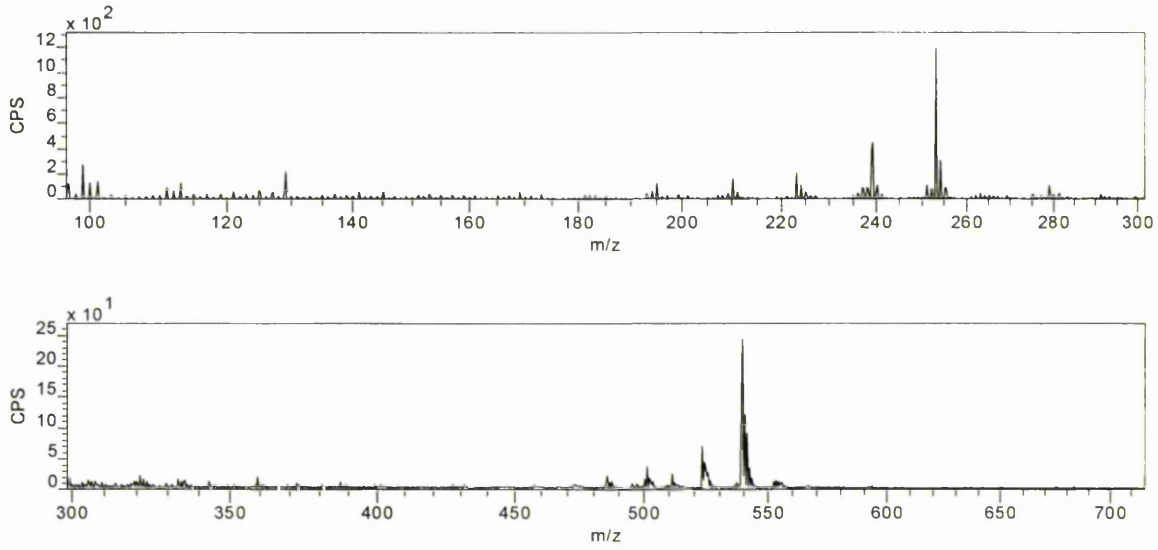

Madder/lye dyebath (b) after exhaustion onto alum mordanted wool negative ion spectrum : Cs^+ primary ion source

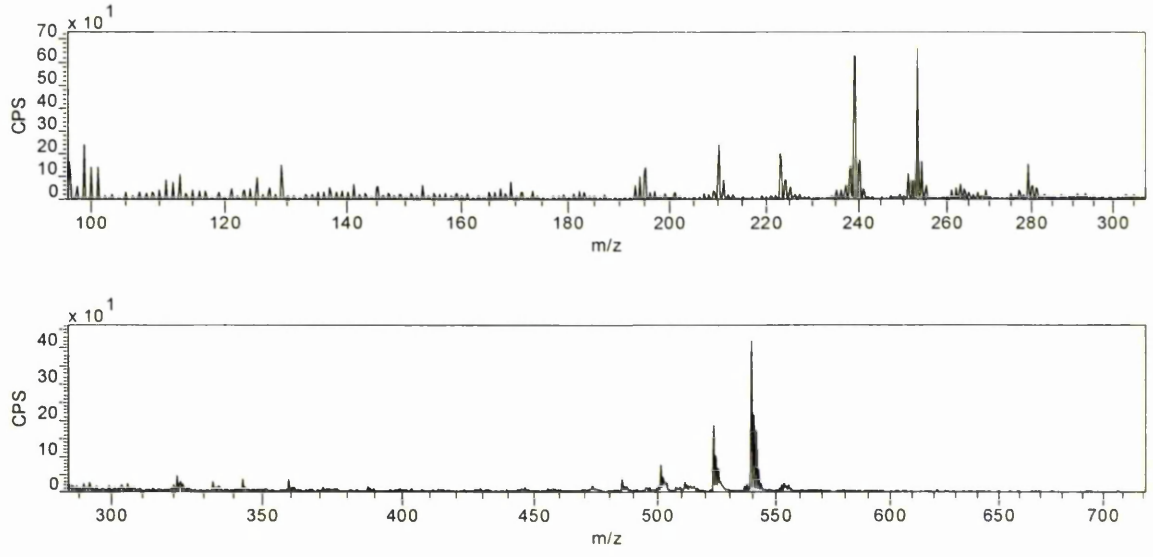

Madder/lye dye on filter paper negative ion spectrum : Cs^+ primary ion source

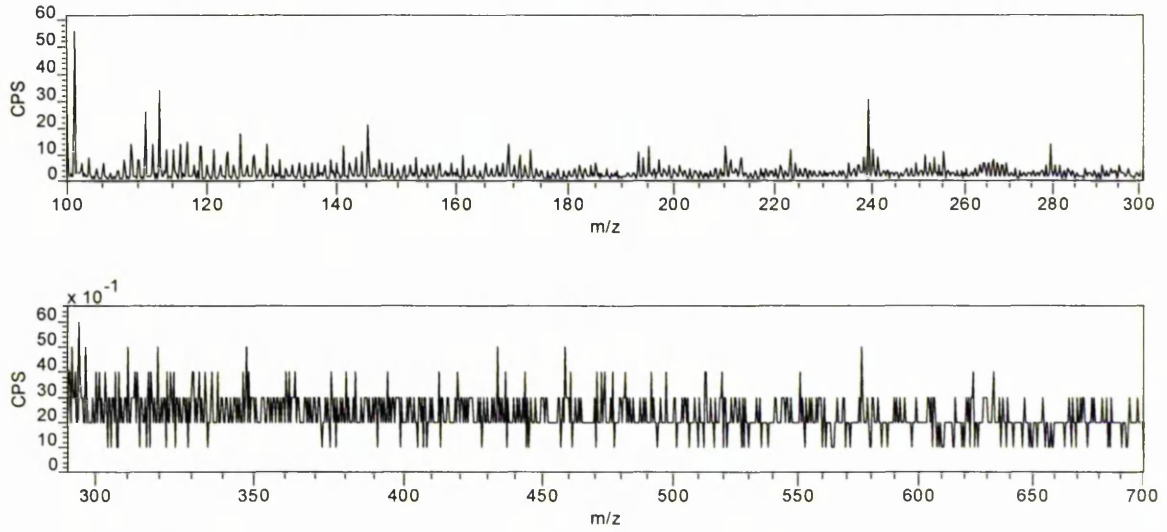

Madder/lye dye on alum filter paper negative ion spectrum : Cs^+ primary ion source

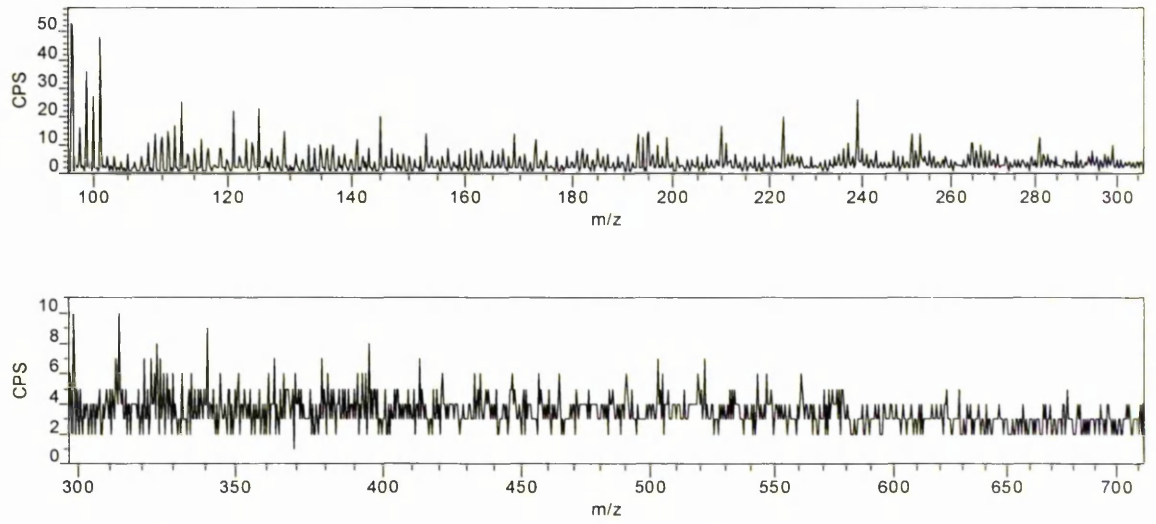

Madder dyed silk (Red/S2_b) negative ion spectrum : Cs^+ primary ion source

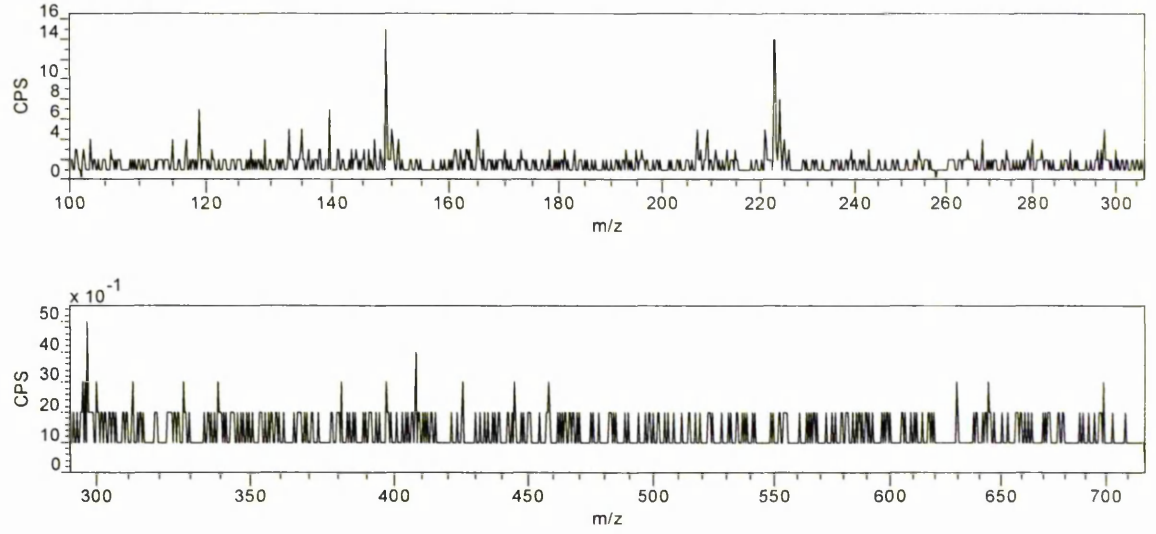

Madder dyed wool (Red/W1) negative ion spectrum : Cs^+ primary ion source

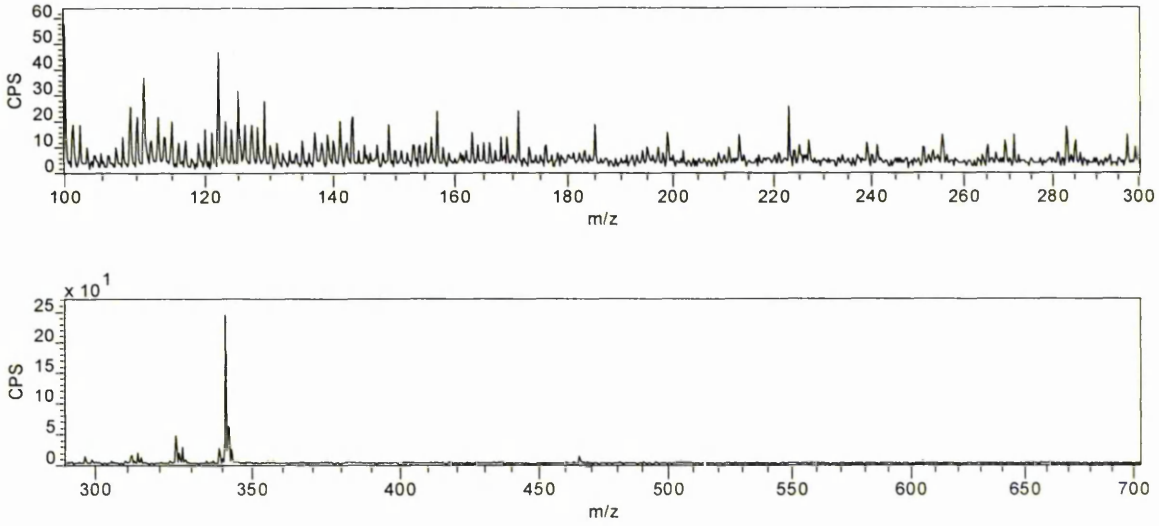

Madder dyed wool cross section negative ion spectrum : Au_1^+ primary ion source

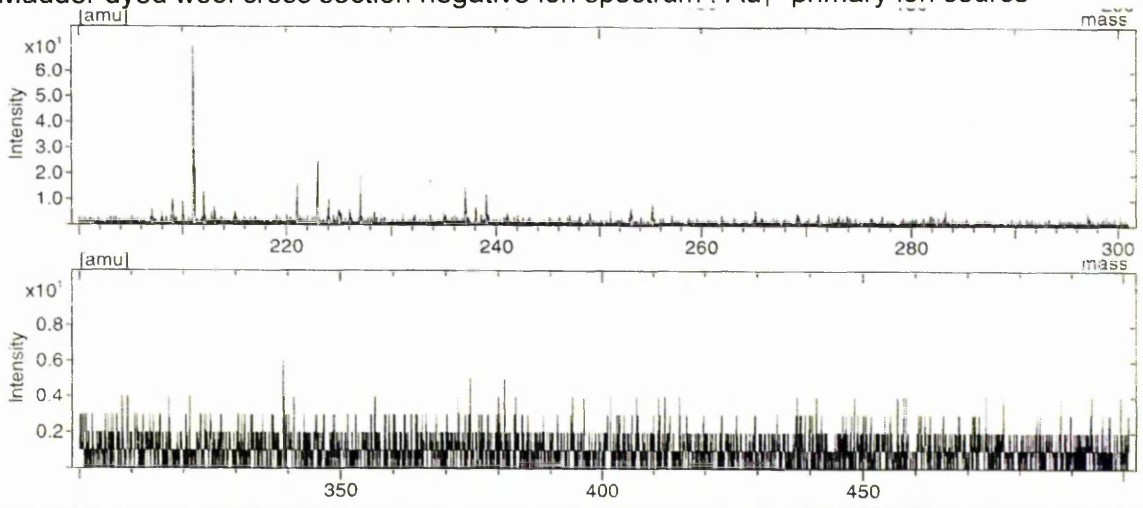

Madder dyebath negative ion spectrum : Au_1^+ primary ion source

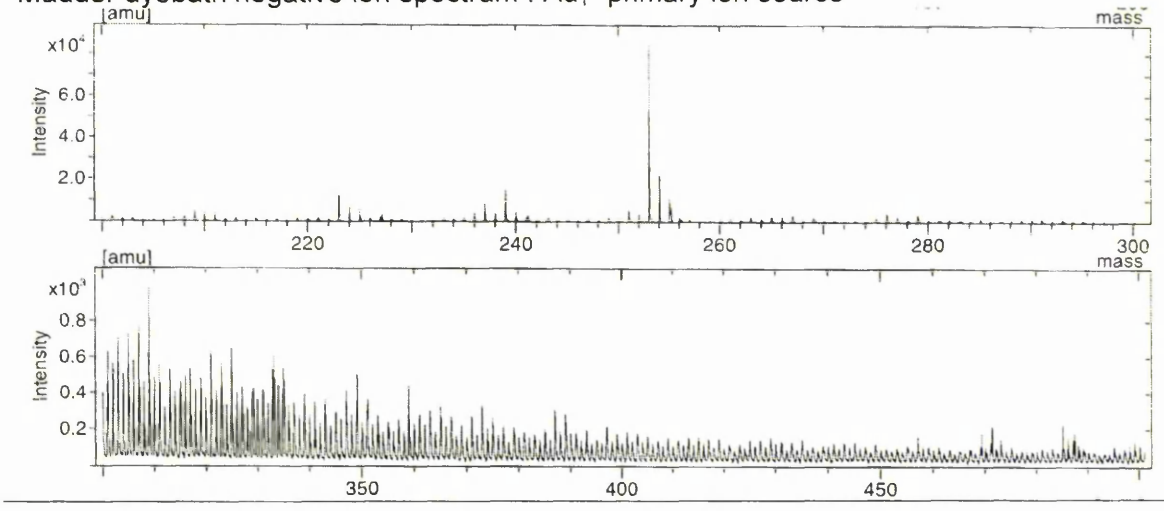

Madder/lye dyebath negative ion spectrum : Au_1^+ primary ion source

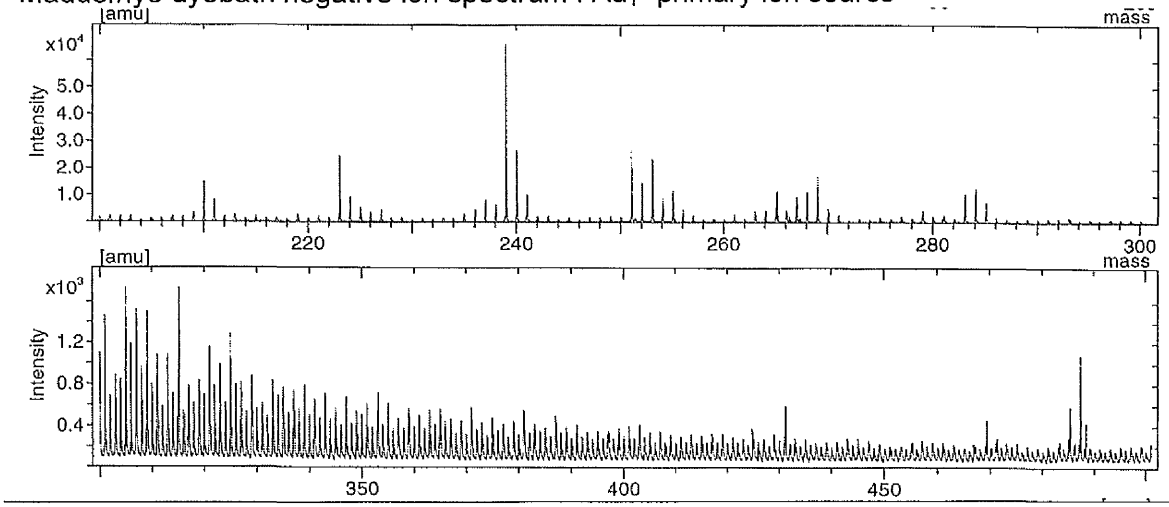

A.2. Cochineal

Carminic acid synthetic chromophore negative ion spectrum : Cs^+ primary ion source

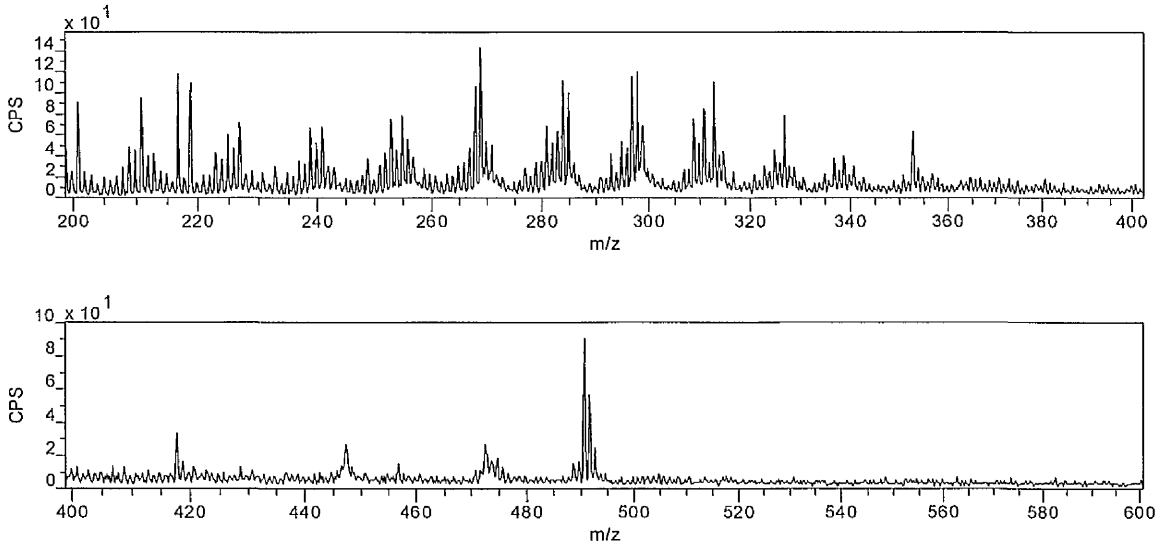

Cochineal dyebath negative ion spectrum : Cs^+ primary ion source

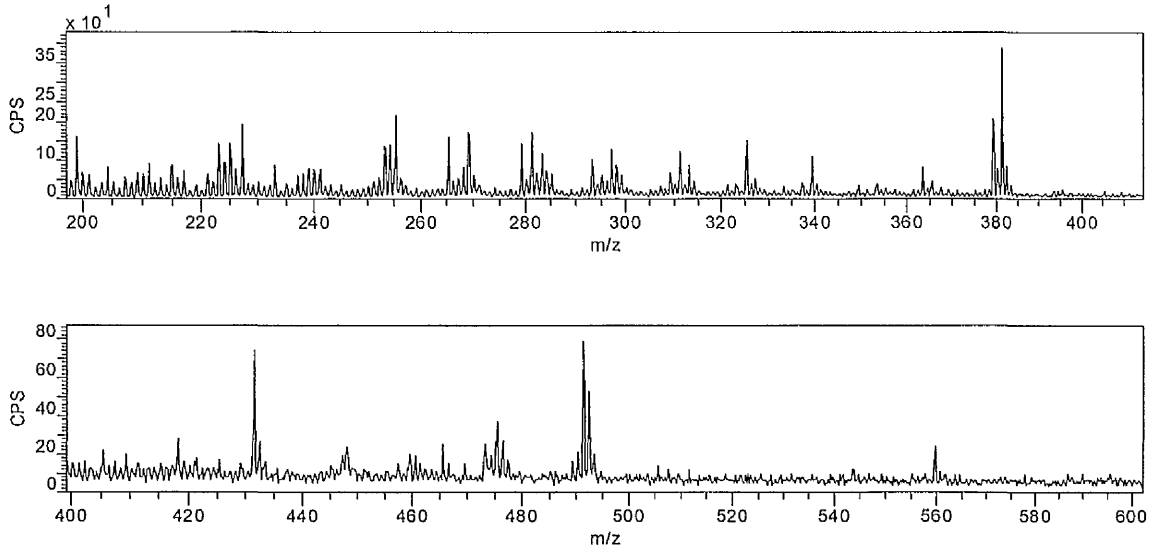

Cochineal dye on filter paper negative ion spectrum : Cs^+ primary ion source

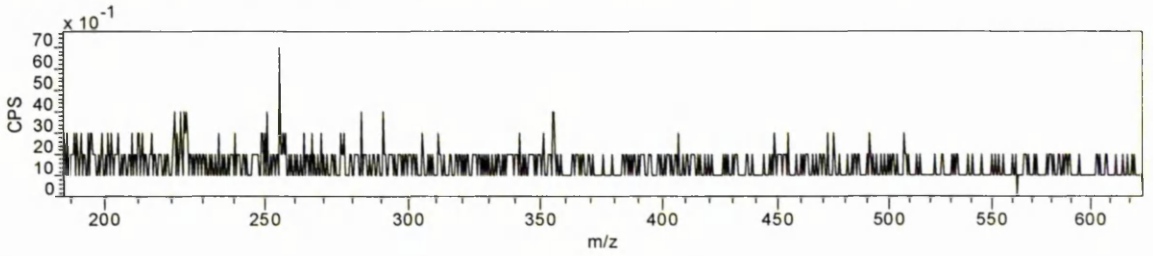

Cochineal dye on alum filter paper negative ion spectrum : Cs^+ primary ion source

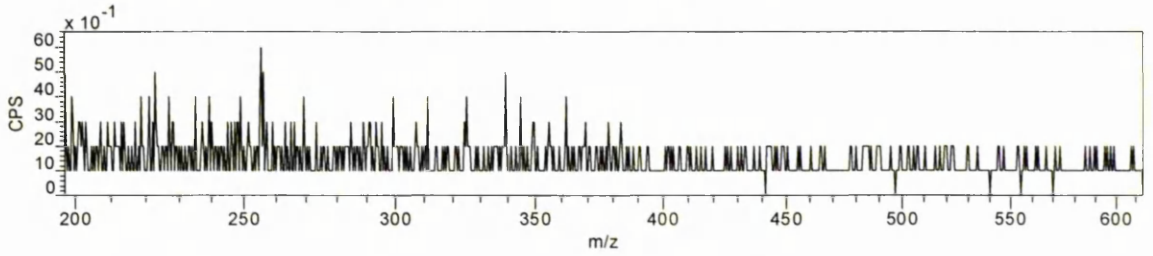

Cochineal/lye dye on filter paper negative ion spectrum : Cs^+ primary ion source

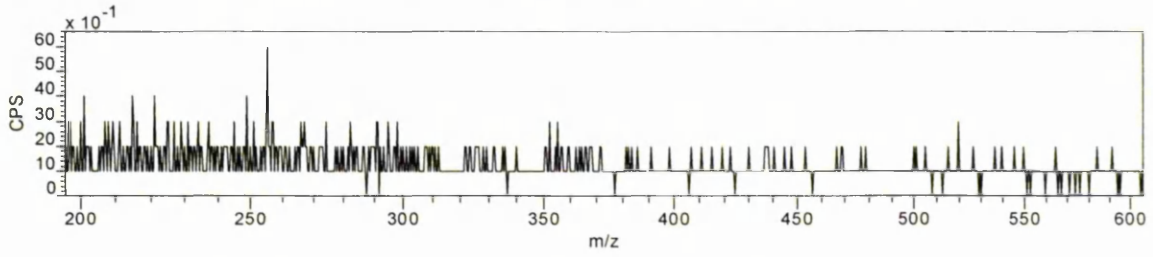

Cochineal/lye dye on alum filter paper negative ion spectrum : Cs^+ primary ion source

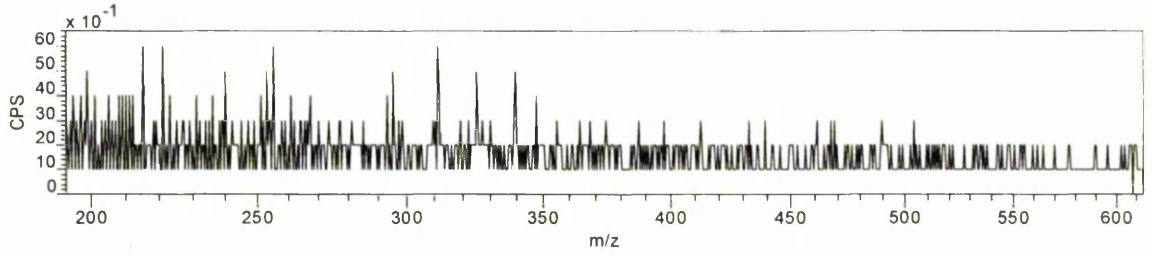

Cochineal dyed silk (Red/S3) negative ion spectrum : Cs^+ primary ion source

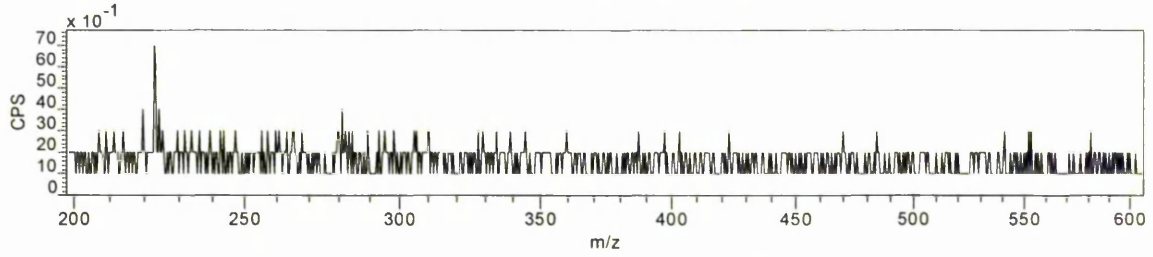

Cochineal dyed wool (Red/W4) negative ion spectrum : Cs^+ primary ion source

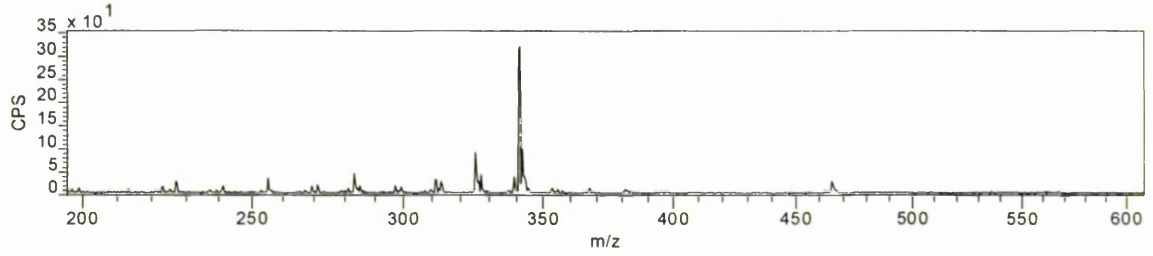

A.3. Brazilwood

Brazilwood dyebath negative ion spectrum : Cs^+ primary ion source

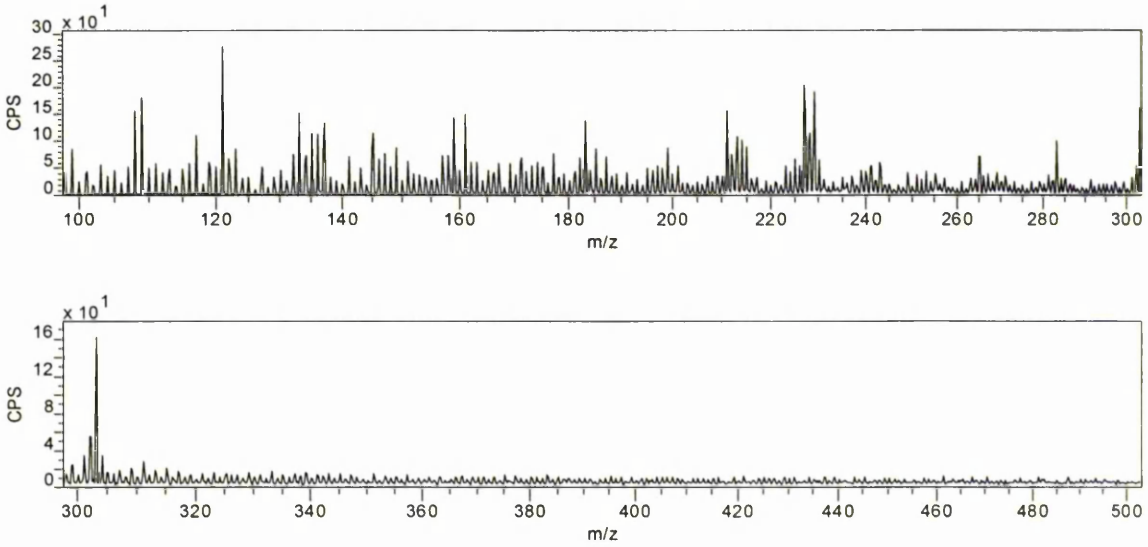

Brazilwood/lye dyebath negative ion spectrum : Cs^+ primary ion source

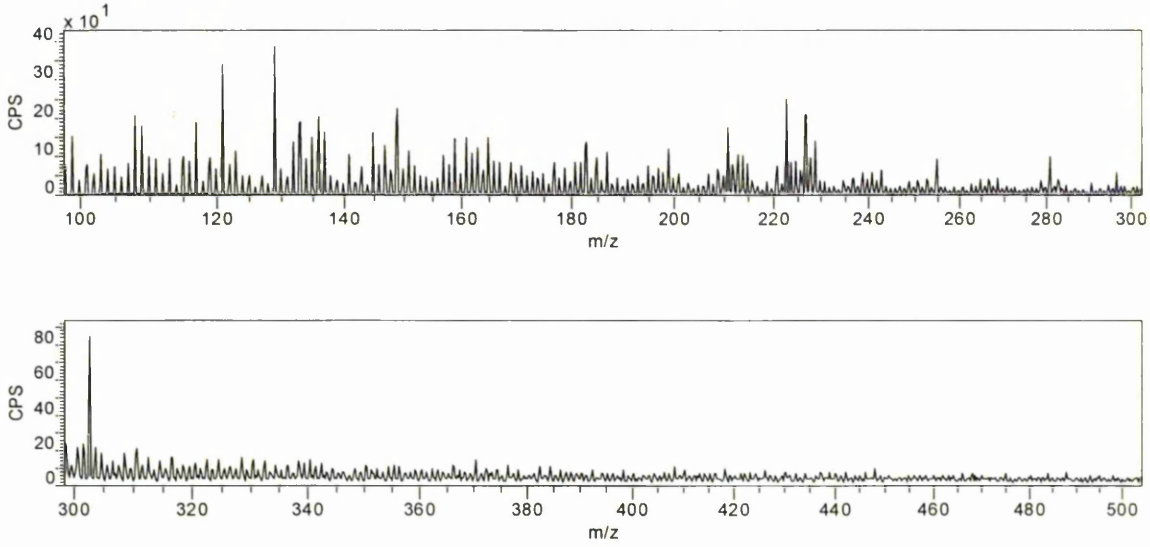

A.4. Dyer's Greenweed

Dyer's greenweed dyebath (a) negative ion spectrum : Cs^+ primary ion source

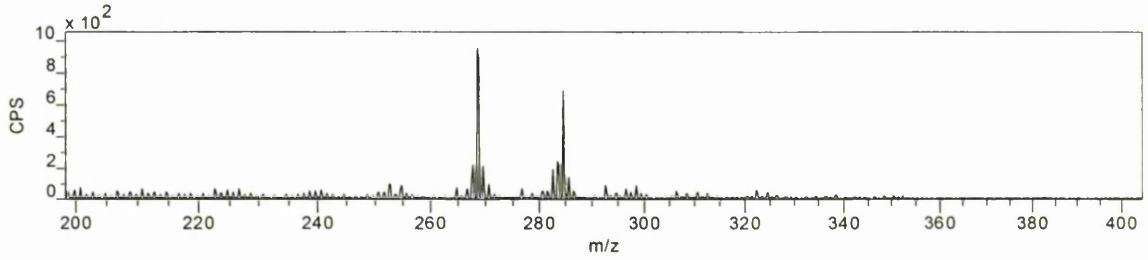

Dyer's greenweed dyebath (a) positive ion spectrum : Cs^+ primary ion source

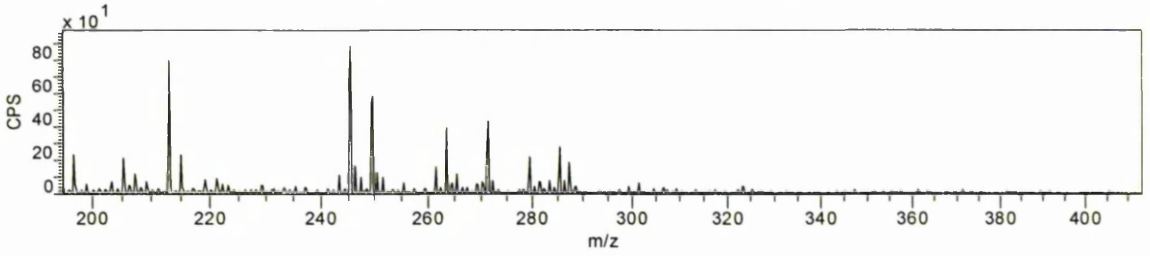

Dyer's greenweed dyebath (b) negative ion spectrum : Cs^+ primary ion source

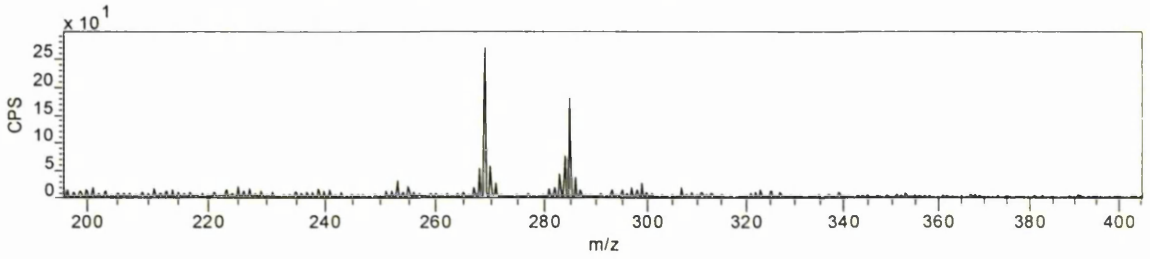

Dyer's greenweed dyebath (b) positive ion spectrum : Cs^+ primary ion source

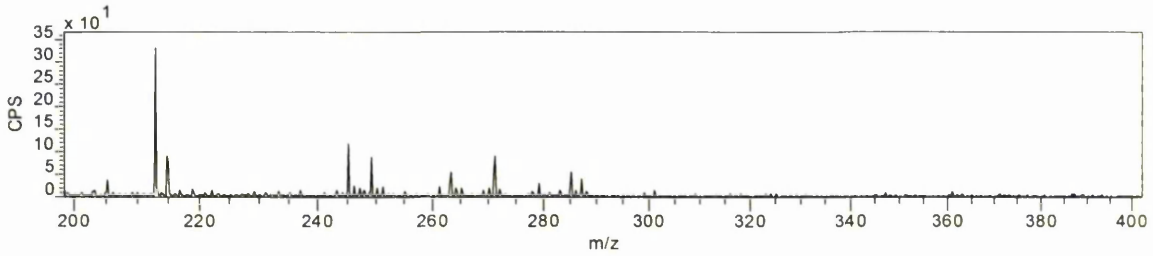

Dyer's greenweed dyebath (b) after exhaustion onto wool negative ion spectrum : Cs^+ primary ion source

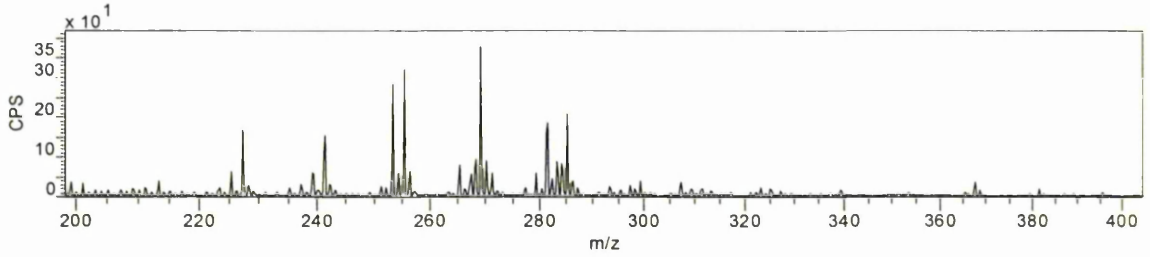

Dyer's greenweed dyebath (b) after exhaustion onto wool positive ion spectrum : Cs^+ primary ion source

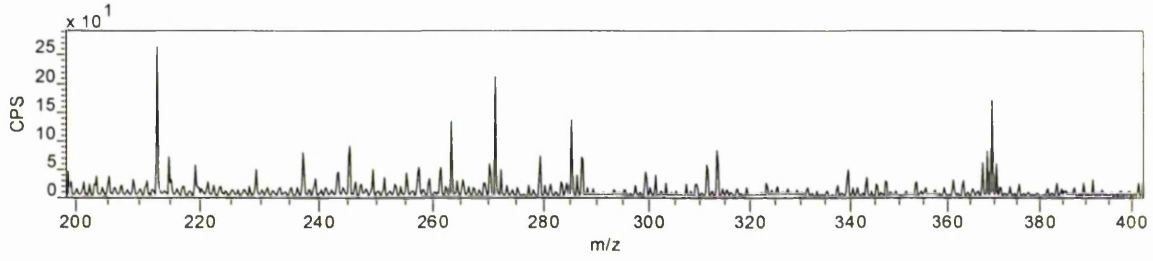

Dyer's greenweed dyebath (b) after exhaustion onto alum wool negative ion spectrum : Cs^+ primary ion source

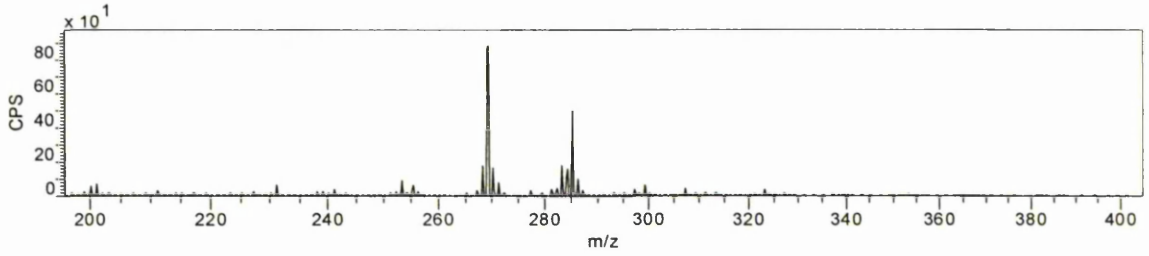

Dyer's greenweed dyebath (b) after exhaustion onto alum wool positive ion spectrum : Cs^+ primary ion source

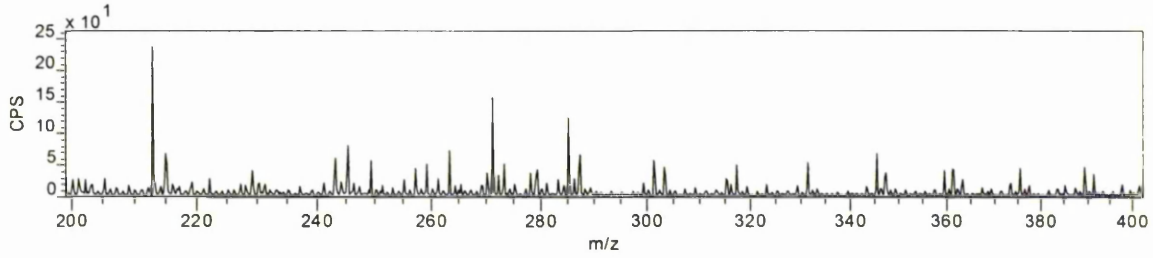

Dyer's greenweed/lye dyebath (a) negative ion spectrum : Cs^+ primary ion source

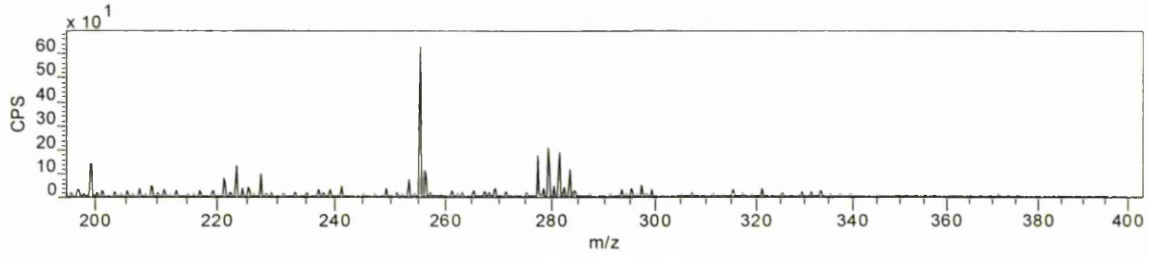

Dyer's greenweed/lye dyebath (a) positive ion spectrum : Cs^+ primary ion source

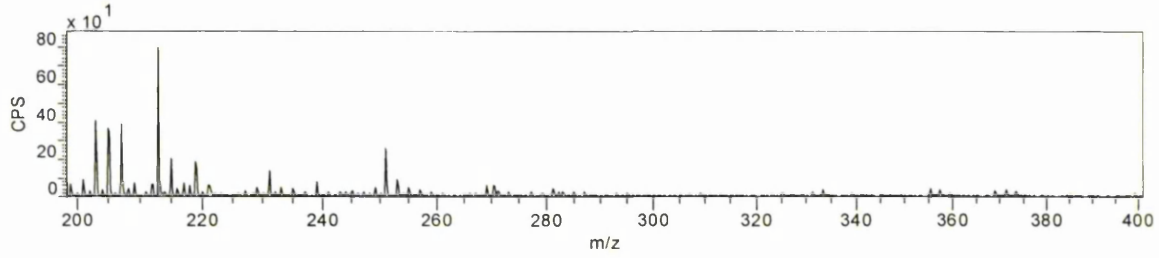

Dyer's greenweed/lye dyebath (b) negative ion spectrum : Cs^+ primary ion source

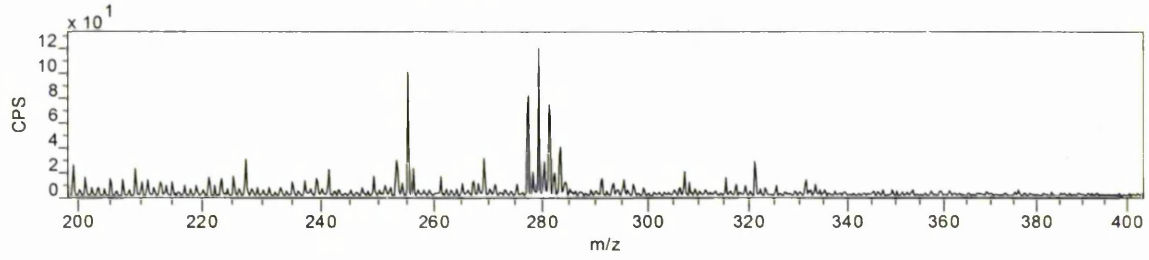

Dyer's greenweed/lye dyebath (b) positive ion spectrum : Cs^+ primary ion source

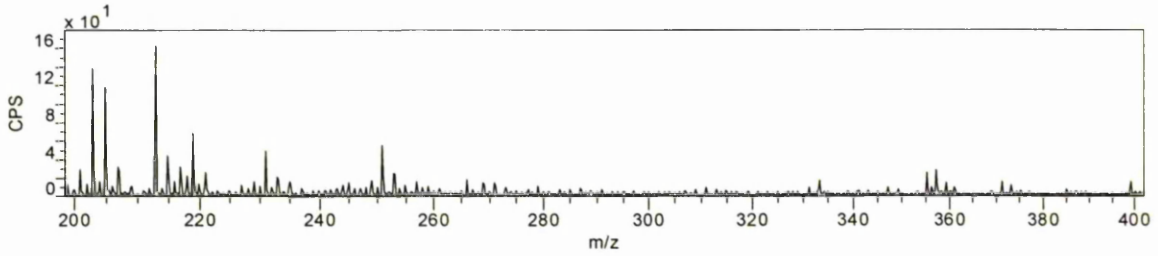

Dyer's greenweed/lye dyebath (b) after exhaustion onto wool negative ion spectrum : Cs^+ primary ion source

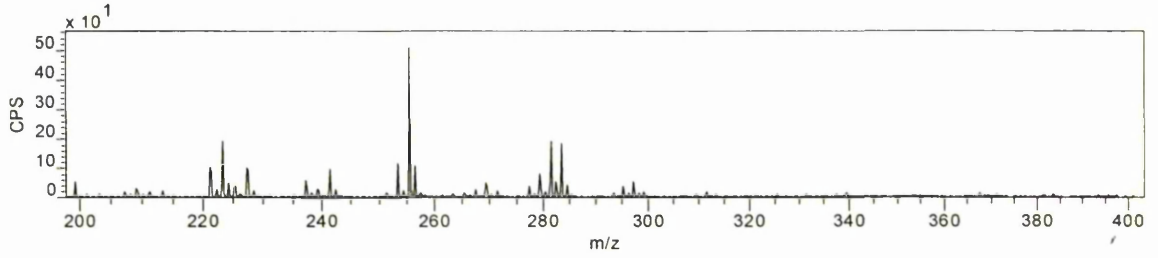

Dyer's greenweed/lye dyebath (b) after exhaustion onto wool positive ion spectrum : Cs^+ primary ion source

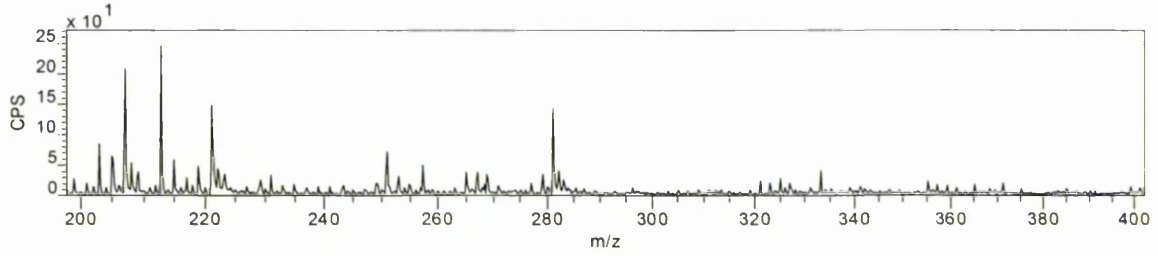

Dyer's greenweed/lye dyebath (b) after exhaustion onto alum wool negative ion spectrum : Cs^+ primary ion source

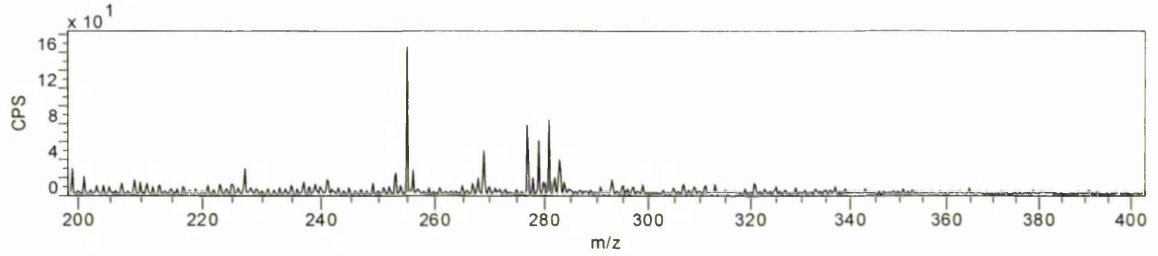

Dyer's greenweed/lye dyebath (b) after exhaustion onto alum wool positive ion spectrum : Cs^+ primary ion source

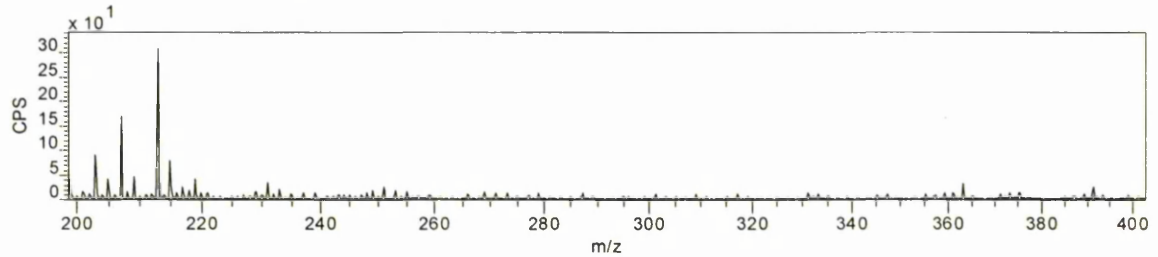

Dyer's greenweed dyebath negative ion spectrum : Au_1^+ primary ion source

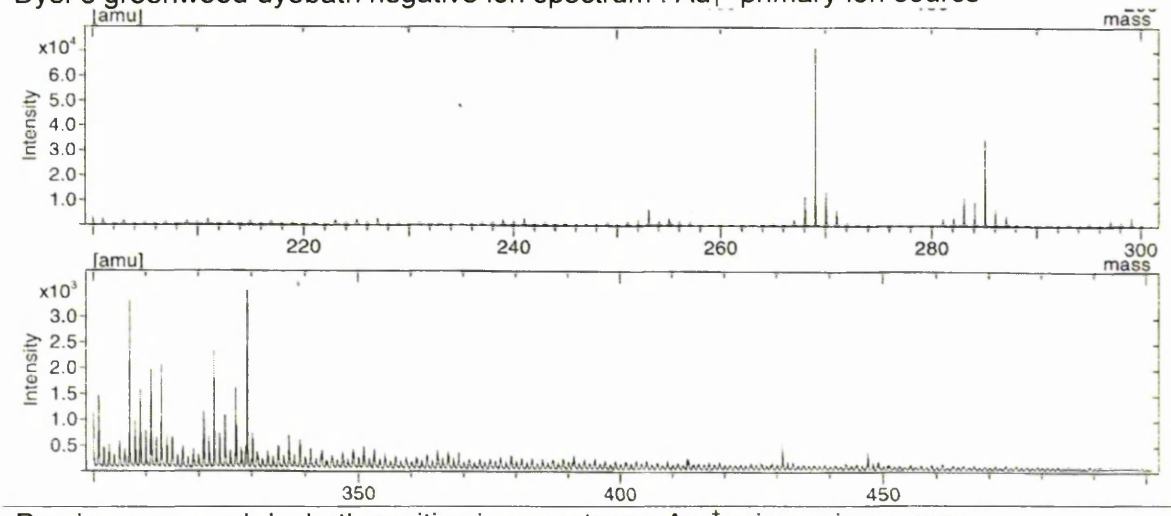

Dyer's greenweed dyebath positive ion spectrum : Au_1^+ primary ion source

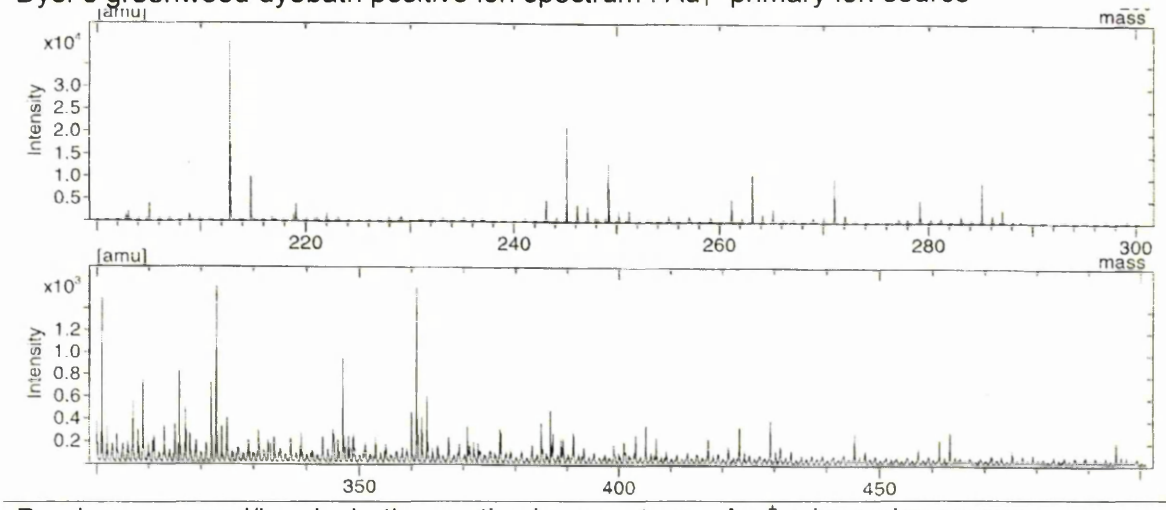

Dyer's greenweed/lye dyebath negative ion spectrum : Au_1^+ primary ion source

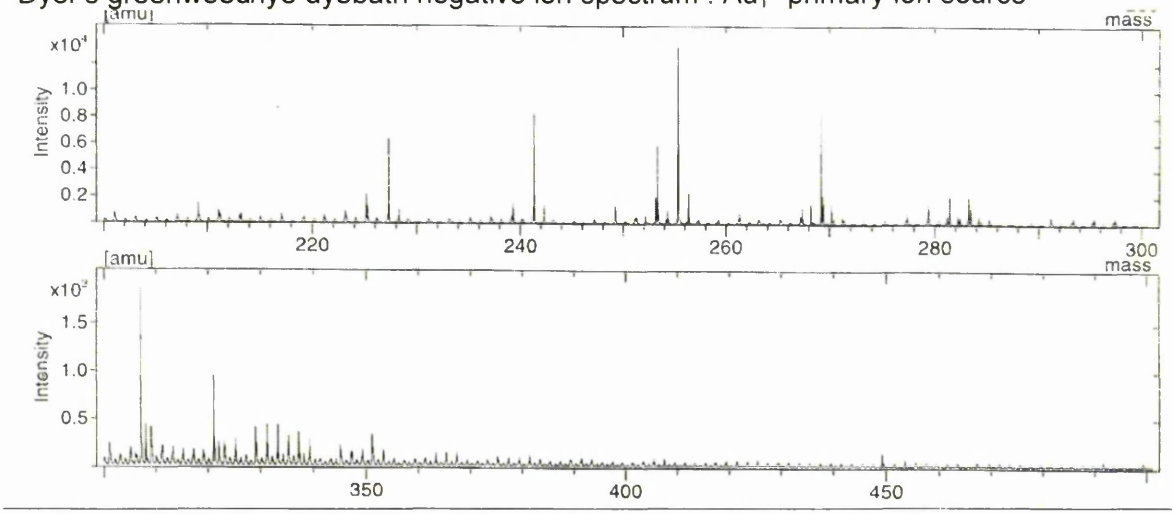

Dyer's greenweed/lye dyebath positive ion spectrum : Au_1^+ primary ion source

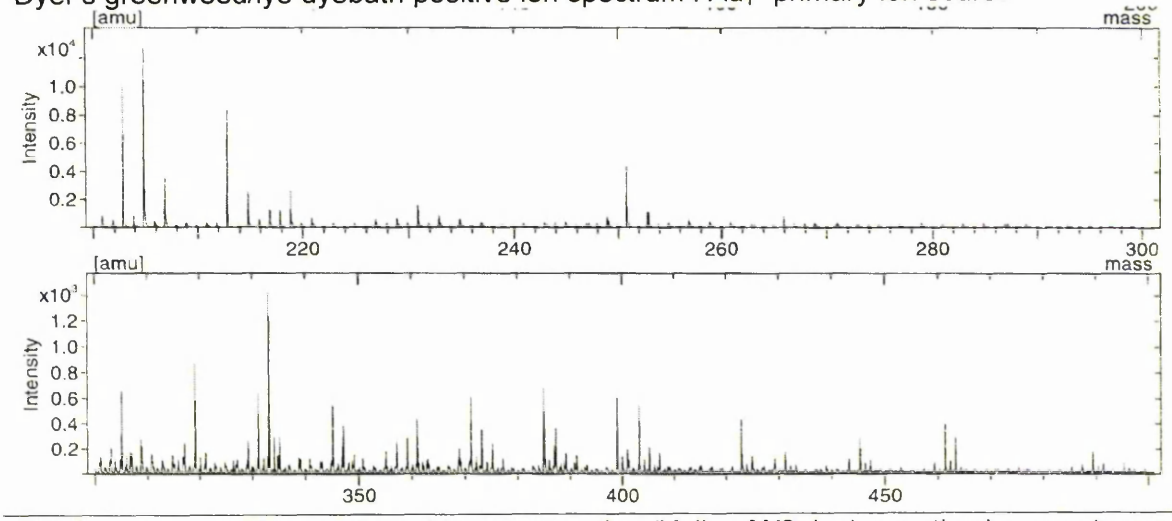

Dyer's greenweed/lye dyed wool in cross section (Yellow/W2_lye) negative ion spectrum : Au_1^+ primary ion source

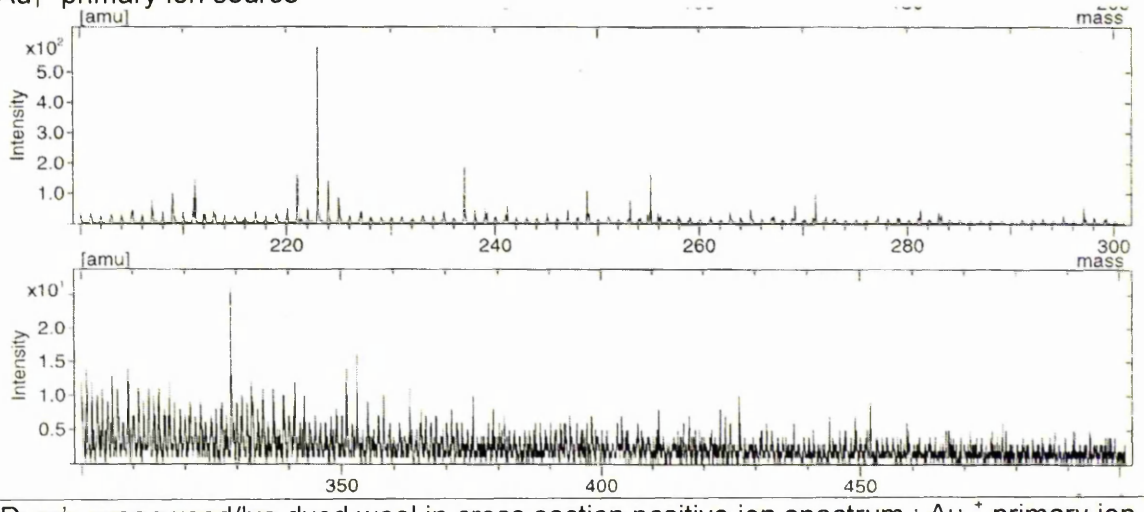

Dyer's greenweed/lye dyed wool in cross section positive ion spectrum : Au_1^+ primary ion source

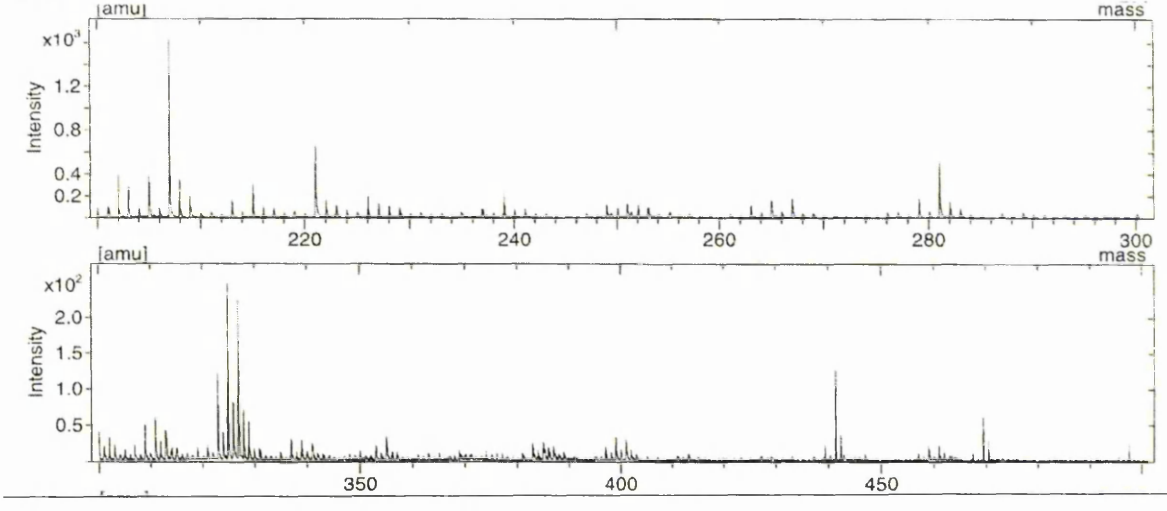

A.5. Weld

Weld dye on filter paper negative ion spectrum : Cs^+ primary ion source

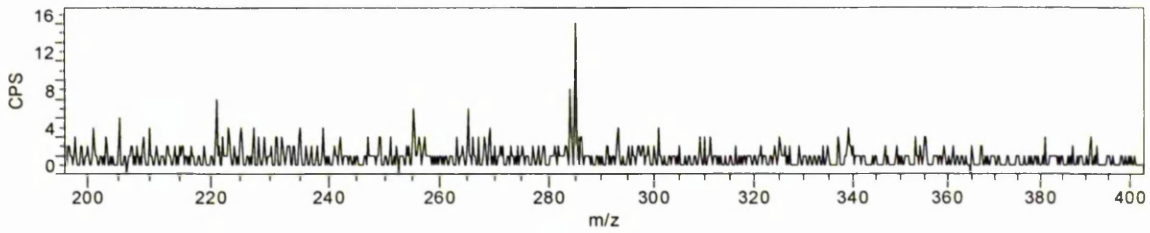

Weld dye on filter paper positive ion spectrum : Cs^+ primary ion source

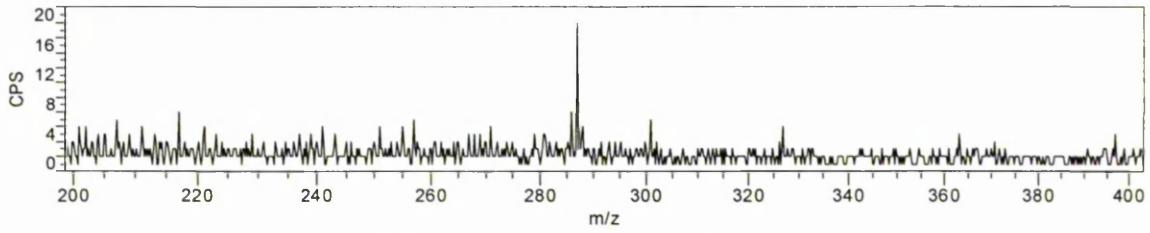

Weld dye on alum filter paper negative ion spectrum : Cs^+ primary ion source

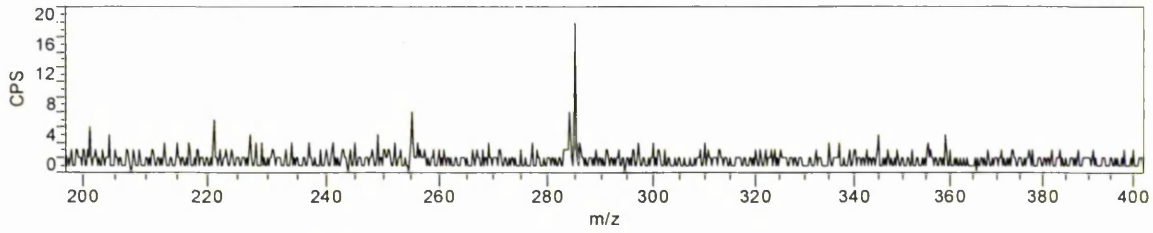

Weld dye on alum filter paper positive ion spectrum : Cs^+ primary ion source

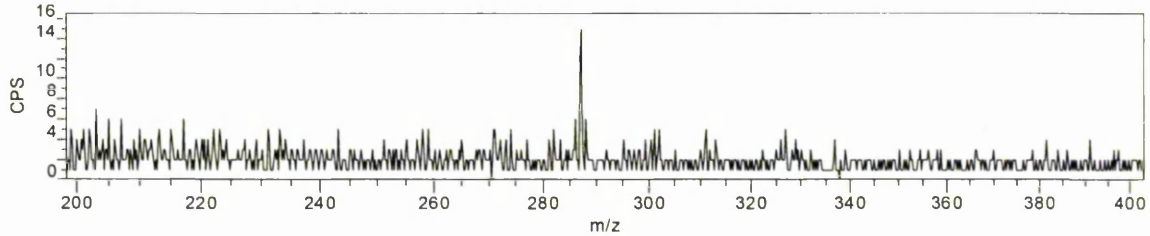

Weld/lye on filter paper negative ion spectrum : Cs^+ primary ion source

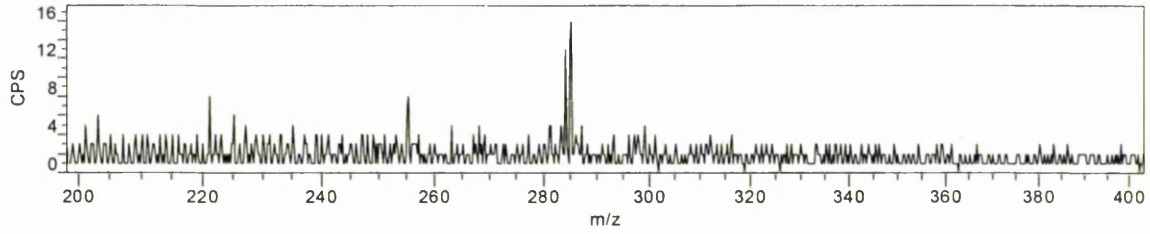

Weld/lye on filter paper positive ion spectrum : Cs^+ primary ion source

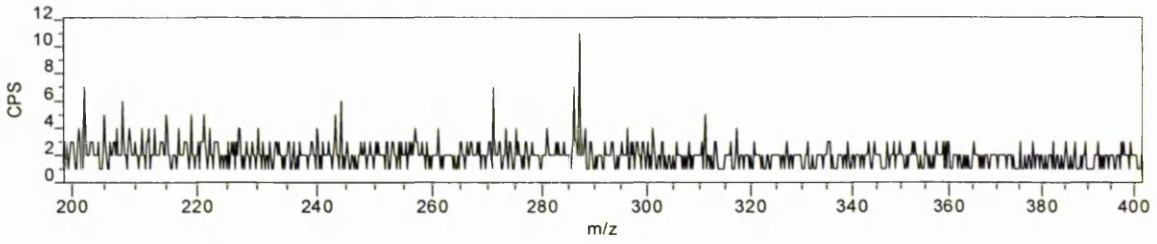

Weld/lye on alum filter paper negative ion spectrum : Cs^+ primary ion source

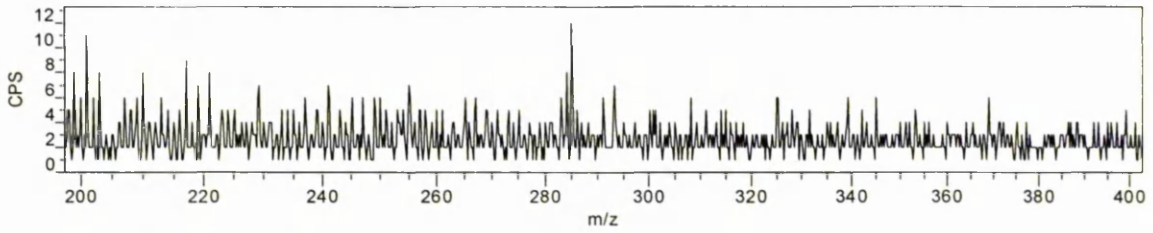

Weld/lye on alum filter paper positive ion spectrum : Cs^+ primary ion source

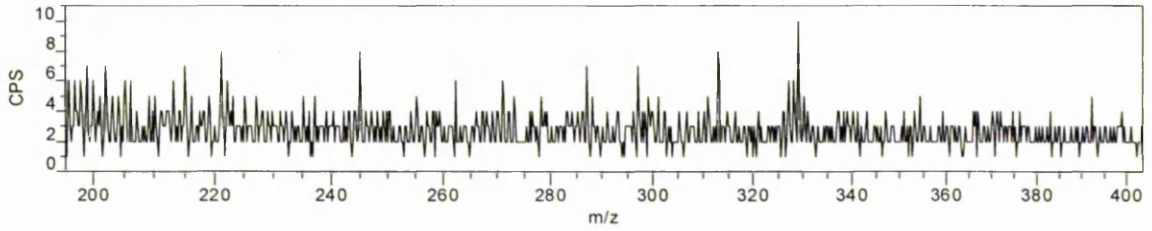

Weld dyed wool (Yellow/W1) negative ion spectrum : Cs^+ primary ion source

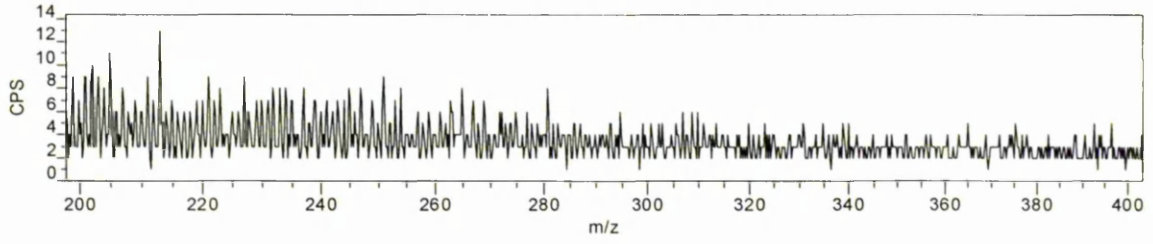

Weld dyed wool (Yellow/W1) positive ion spectrum : Cs^+ primary ion source

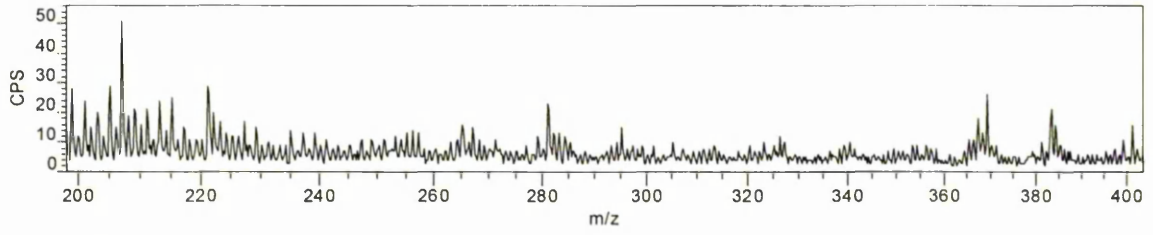

A.6. Young fustic

Young fustic dyebath (a) negative ion spectrum : Cs^+ primary ion source

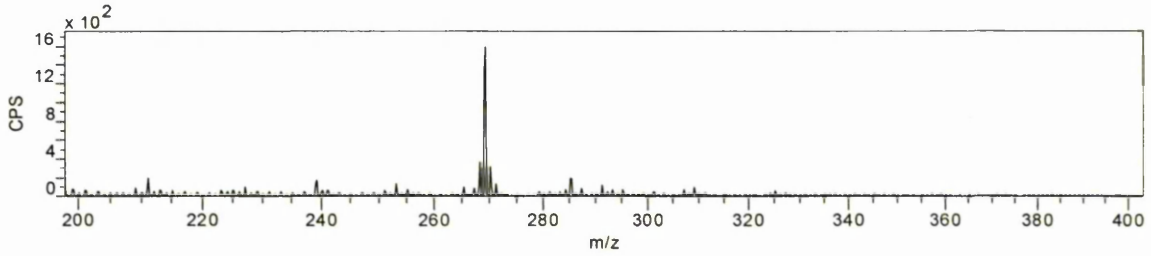

Young fustic dyebath (a) positive ion spectrum : Cs^+ primary ion source

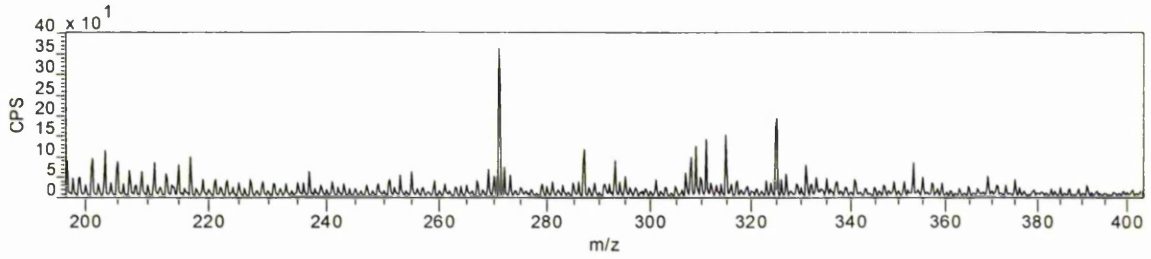

Young fustic dyebath (b) negative ion spectrum : Cs^+ primary ion source

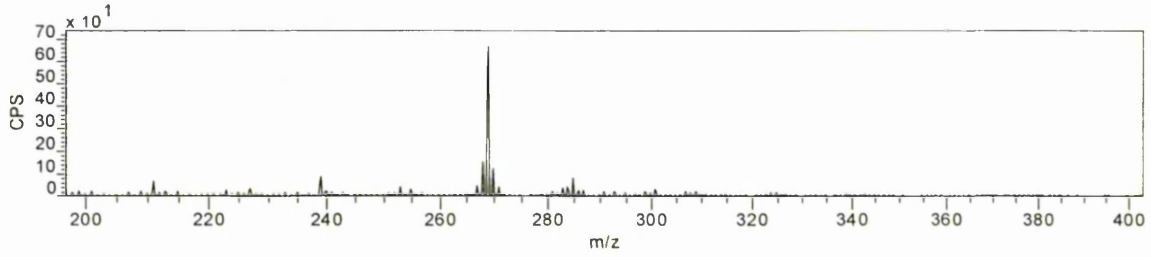

Young fustic dyebath (b) positive ion spectrum : Cs^+ primary ion source

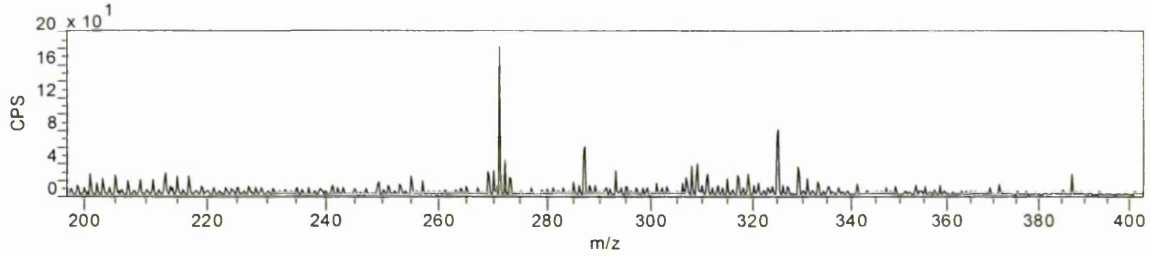

Young fustic dyebath (b) after exhaustion onto wool negative ion spectrum : Cs^+ primary ion source

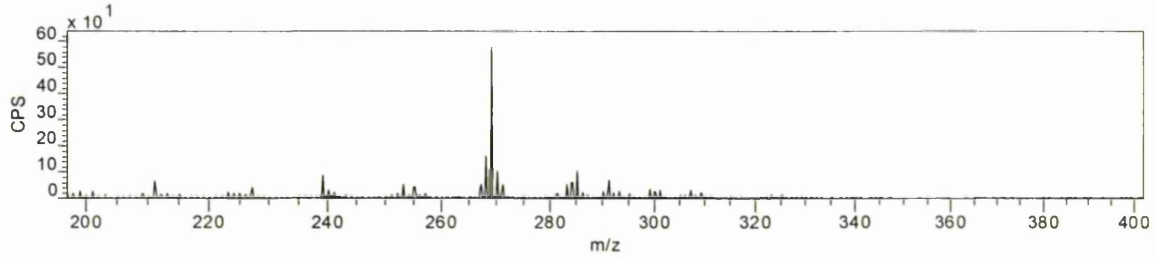

Young fustic dyebath (b) after exhaustion onto wool positive ion spectrum : Cs^+ primary ion source

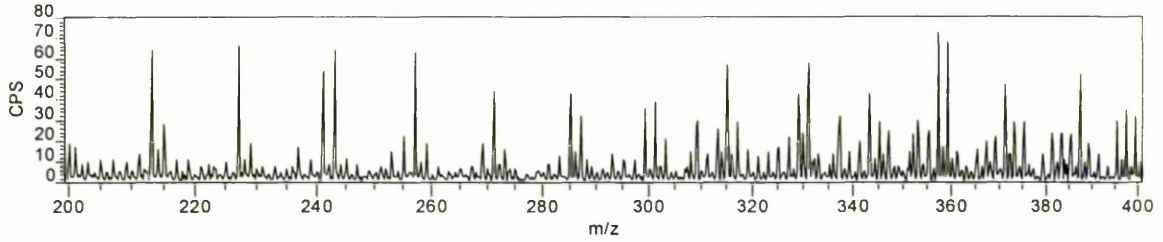

Young fustic dyebath (b) after exhaustion onto alum mordanted wool negative ion spectrum : Cs^+ primary ion source

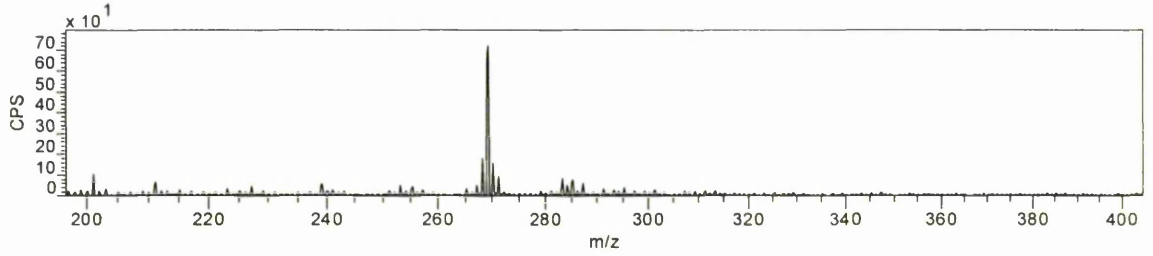

Young fustic dyebath (b) after exhaustion onto alum mordanted wool positive ion spectrum : Cs^+ primary ion source

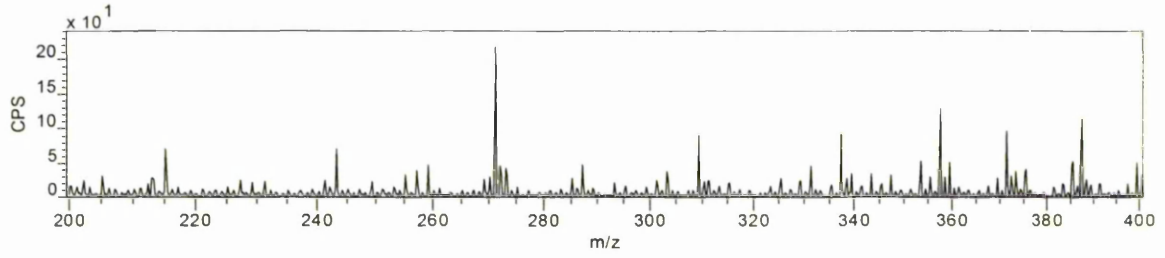

A.7. Oak gall

Oak gall bath negative ion spectrum : Cs^+ primary ion source

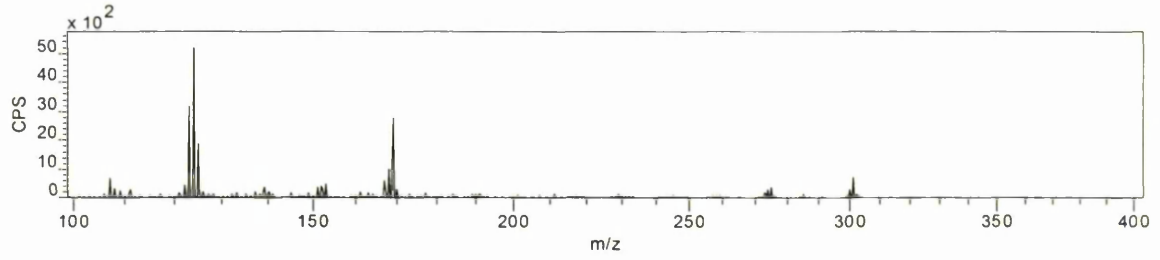

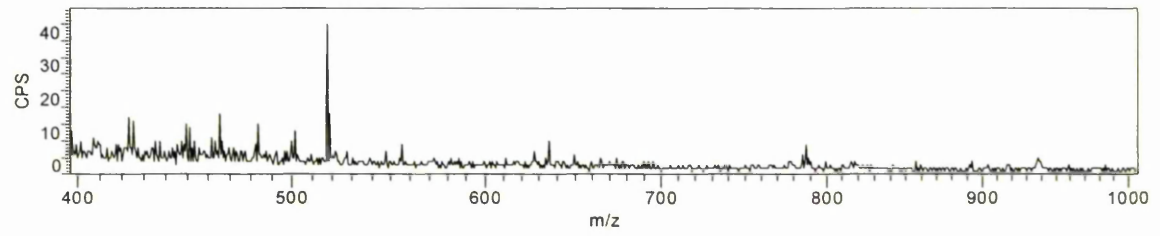

Oak gall bath positive ion spectrum : Cs^+ primary ion source

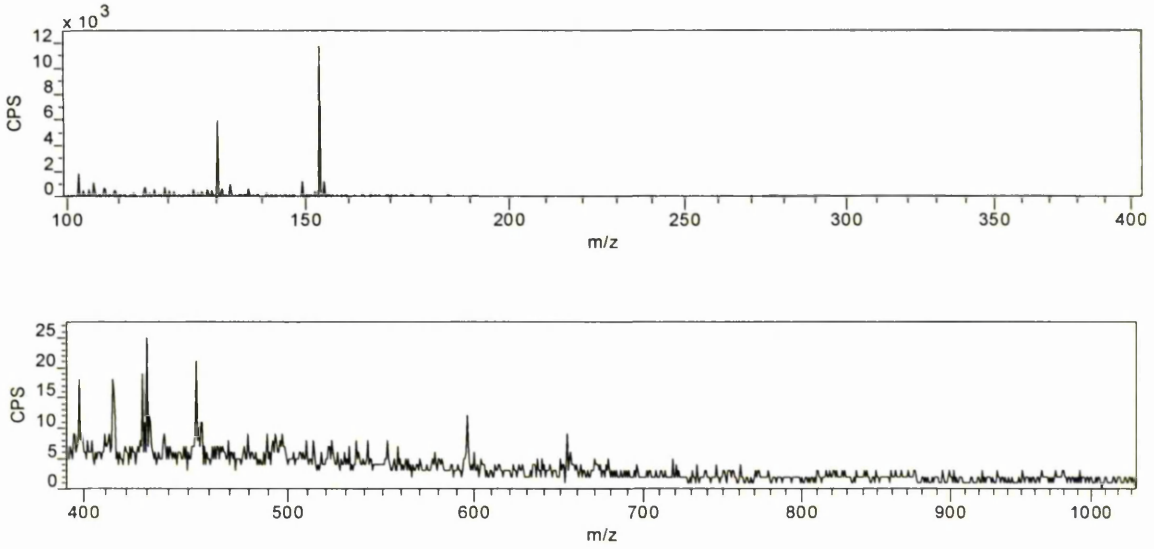

Oak gall on filter paper negative ion spectrum : Cs^+ primary ion source

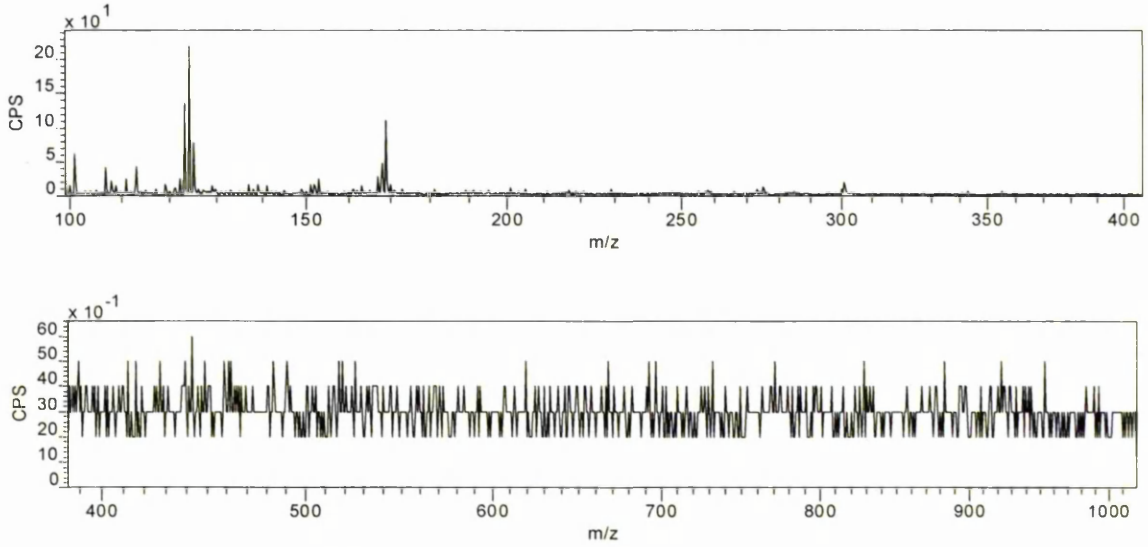

Oak gall on filter paper positive ion spectrum : Cs^+ primary ion source

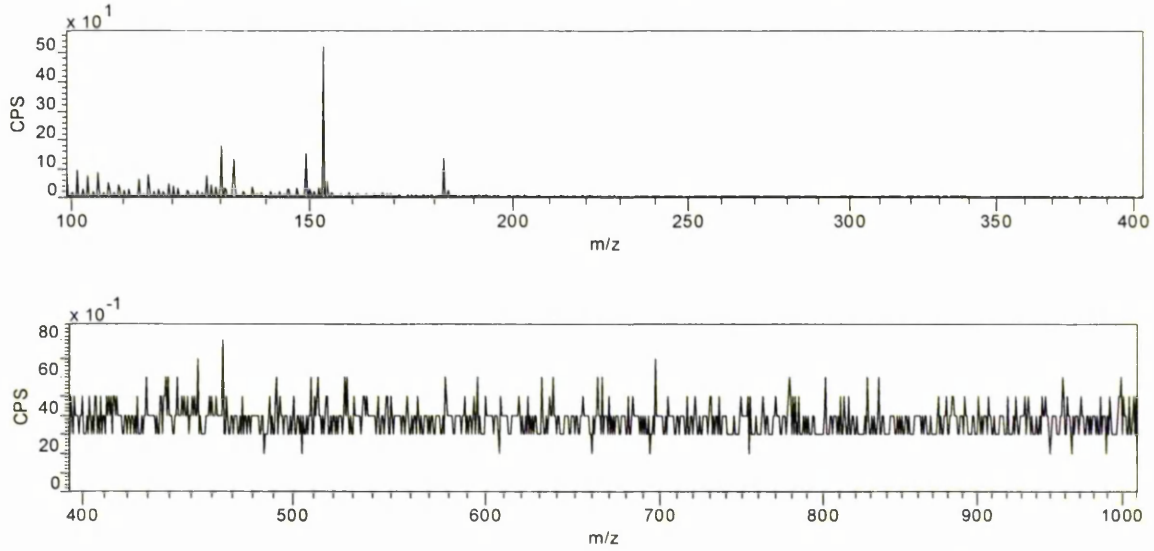

Oak gall + $FeSO_4$ on filter paper negative ion spectrum : Cs^+ primary ion source

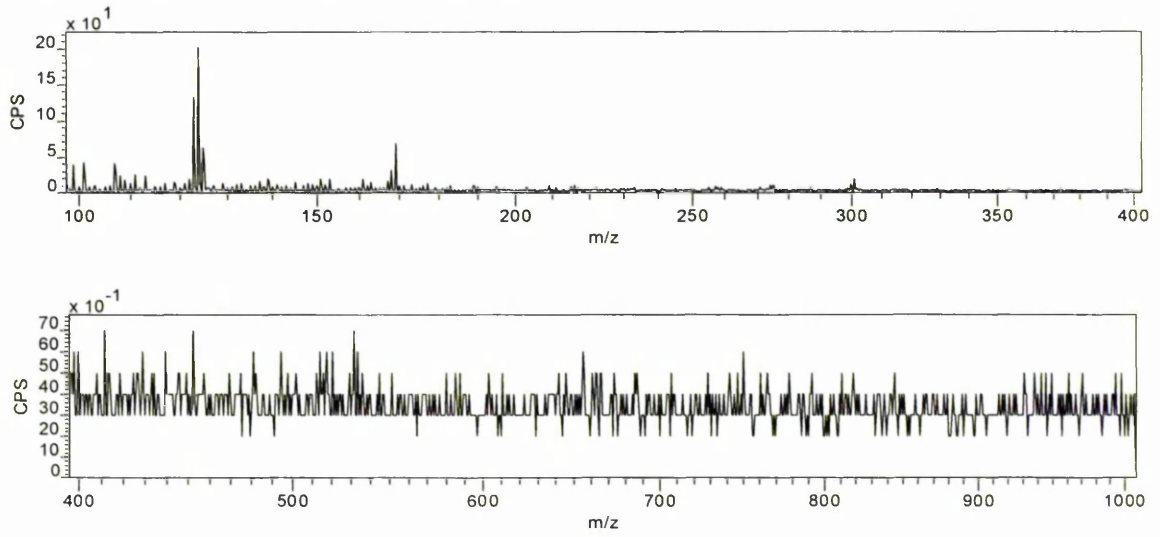

Oak gall + $FeSO_4$ on filter paper positive ion spectrum : Cs^+ primary ion source

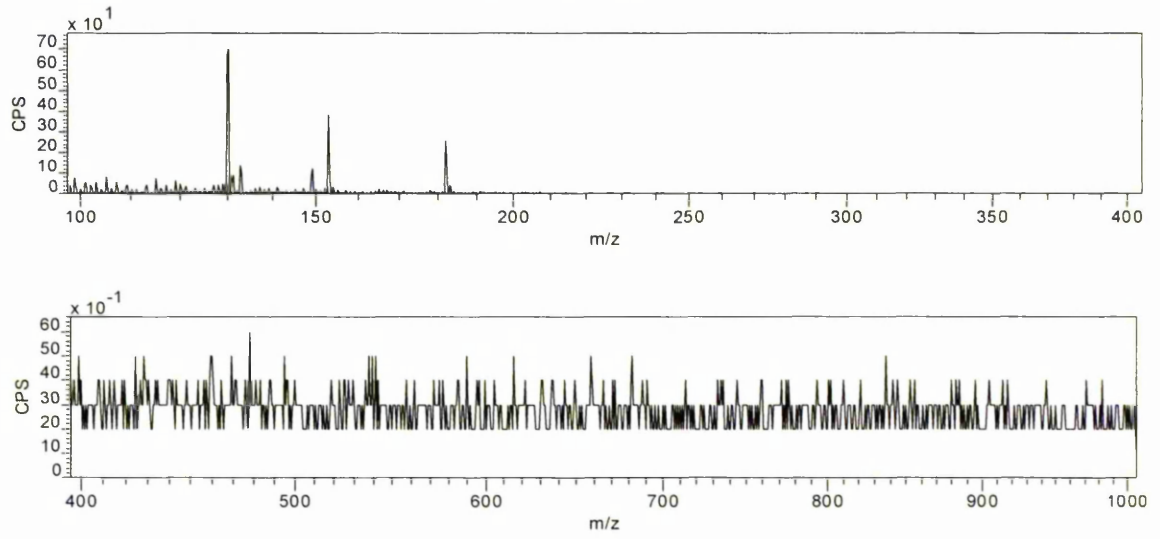

A.8. Alder bark

Alder bark bath negative ion spectrum : Cs^+ primary ion source

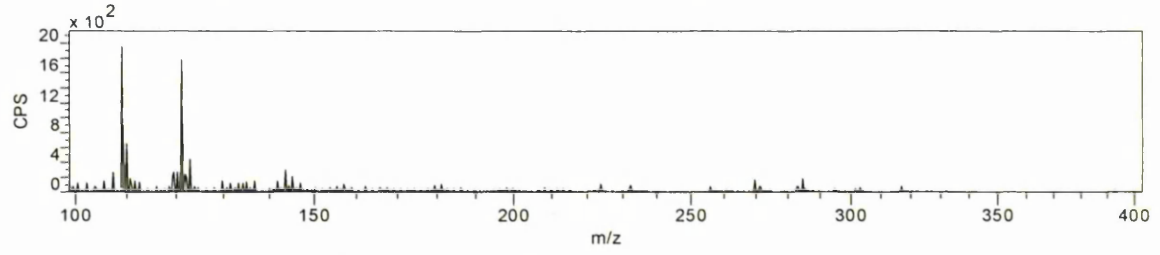

Alder bark bath positive ion spectrum : Cs^+ primary ion source

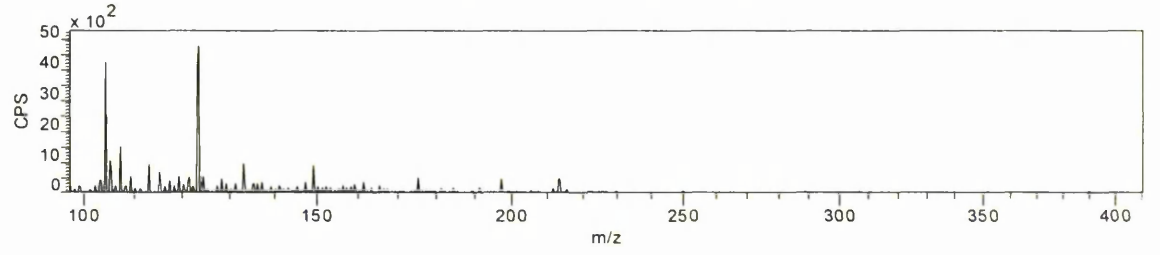

A.9. Woad

Dibromoindigo synthetic chromophore negative ion spectrum : Cs^+ primary ion source

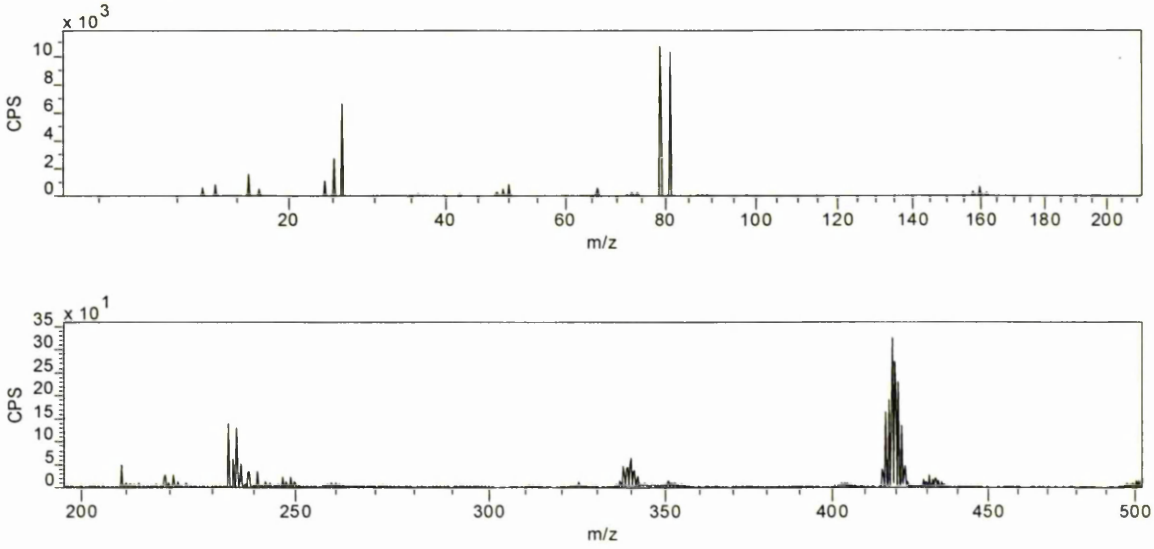

Dibromoindigo synthetic chromophore positive ion spectrum : Cs^+ primary ion source

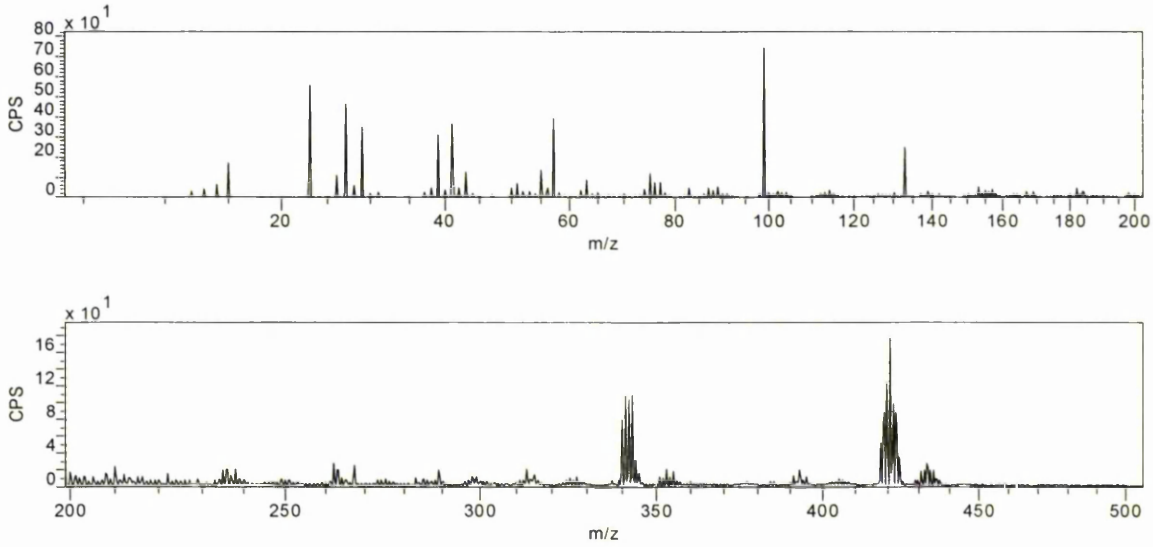

Woad powder dispersion negative ion spectrum : Au_1^+ primary ion source

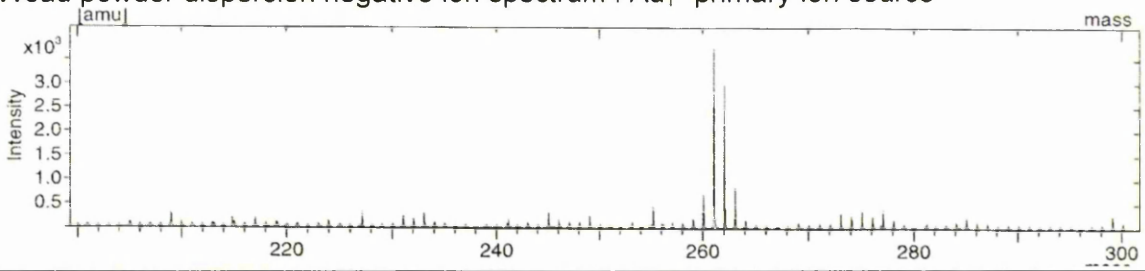

Woad powder dispersion positive ion spectrum : Au_1^+ primary ion source

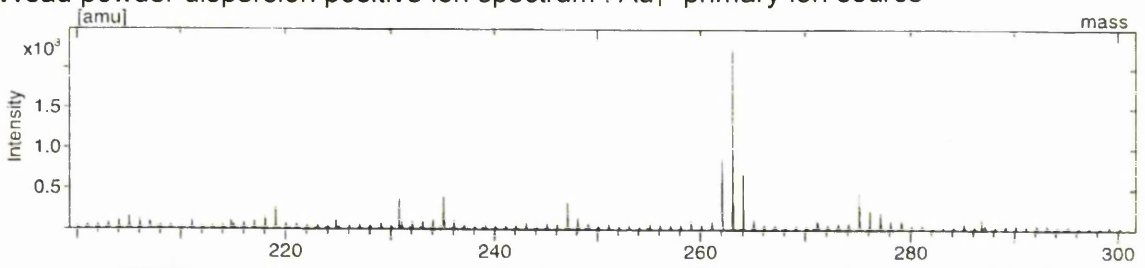

Woad dyed wool (Blue/W1) negative ion spectrum : Cs^+ primary ion source

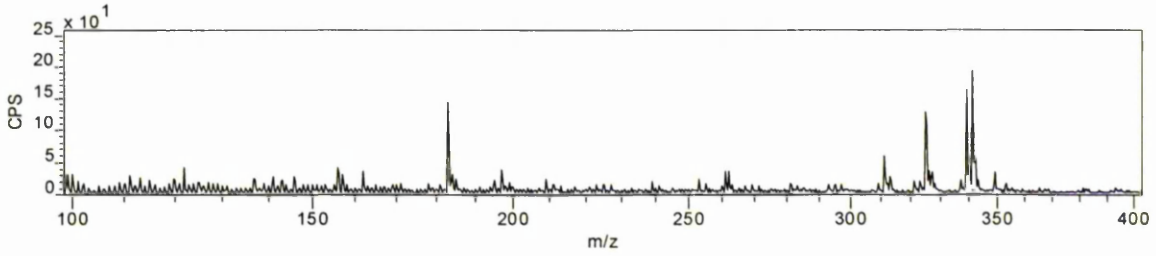

Woad dyed wool (Blue/W1) positive ion spectrum : Cs^+ primary ion source

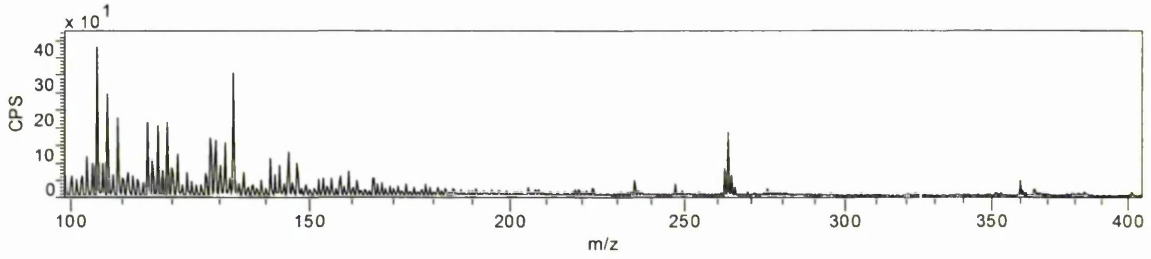

Woad and weld dyed wool (Green/W2) negative ion spectrum : Cs^+ primary ion source

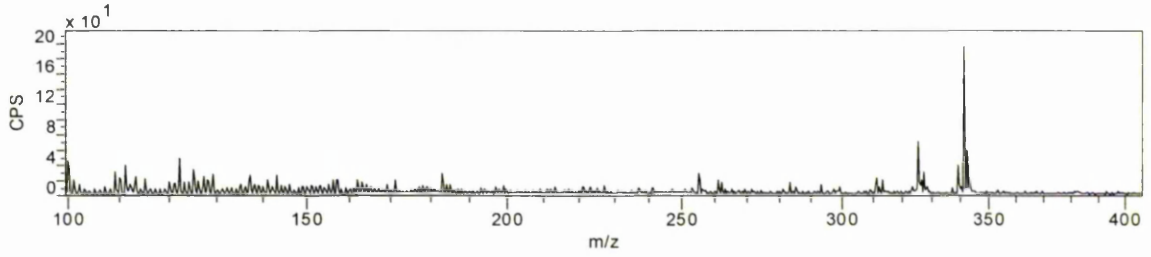

Woad and weld dyed wool (Green/W2) positive ion spectrum : Cs^+ primary ion source

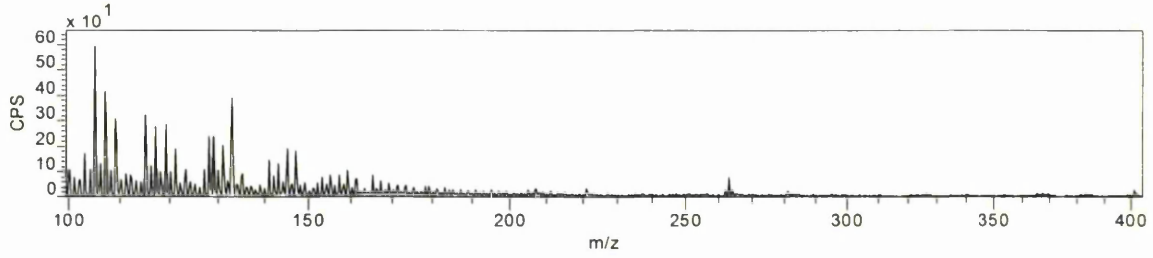

Woad dyed wool accelerated aged (Blue/W1_ag) negative ion spectrum : Cs^+ primary ion source

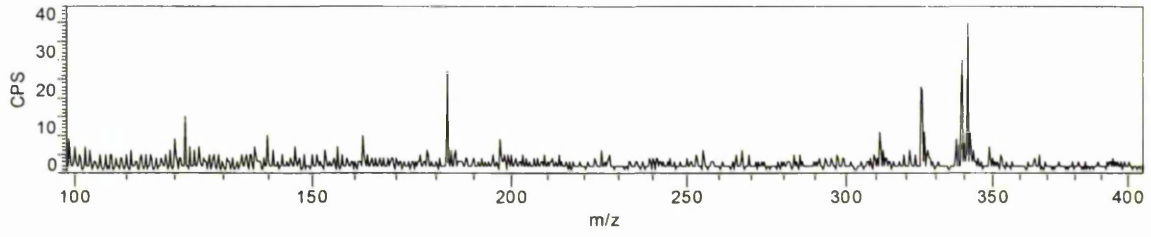

Woad dyed wool accelerated aged (Blue/W1_ag) positive ion spectrum : Cs^+ primary ion source

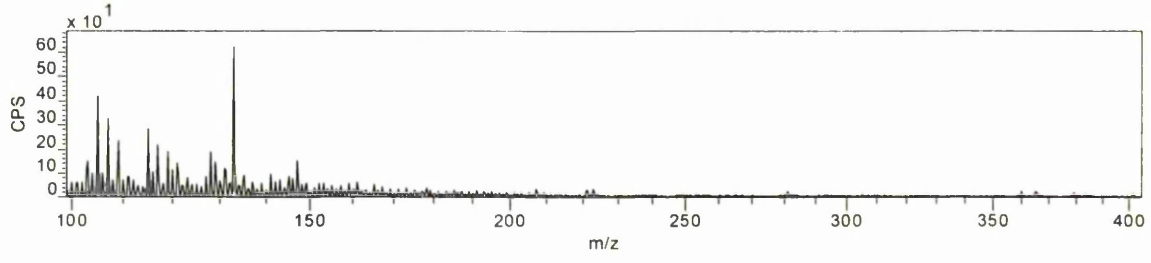

Woad dyed wool cross section negative ion spectrum : Au_1^+ primary ion source

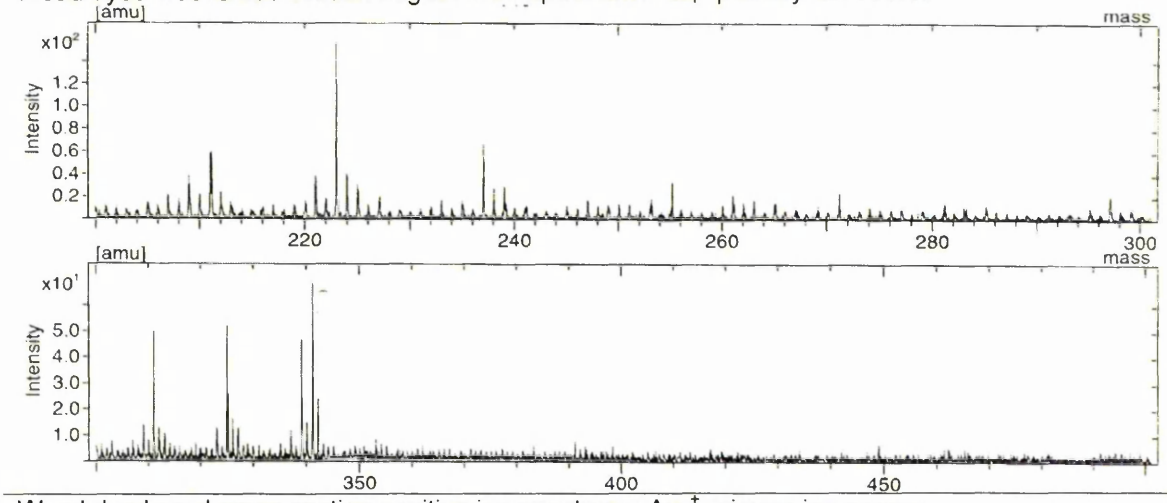

Woad dyed wool cross section positive ion spectrum : Au_1^+ primary ion source

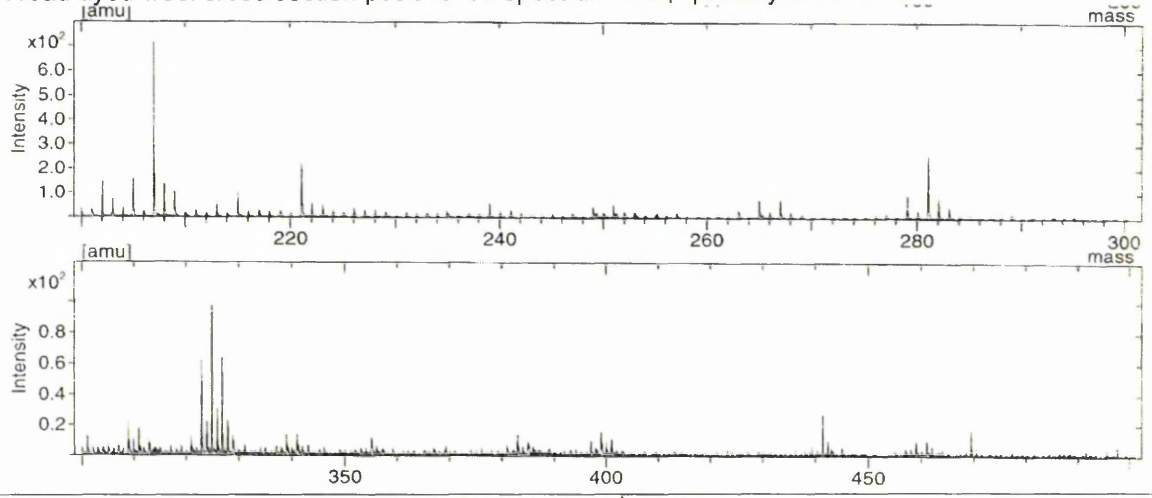

Woad dyed silk (Blue/S1) negative ion spectrum : Cs^+ primary ion source

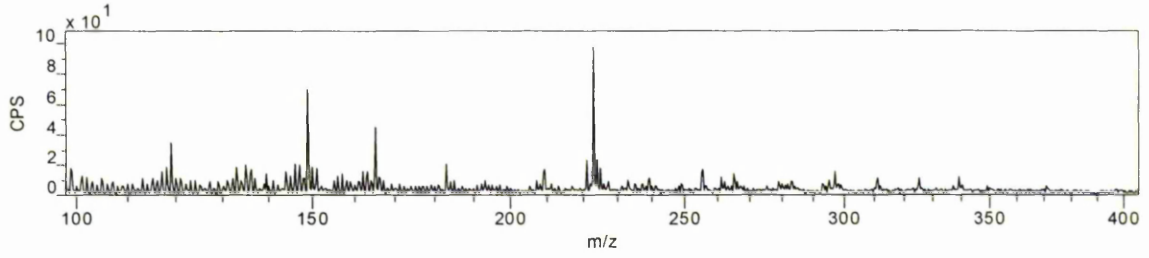

Woad dyed silk (Blue/S1) positive ion spectrum : Cs^+ primary ion source

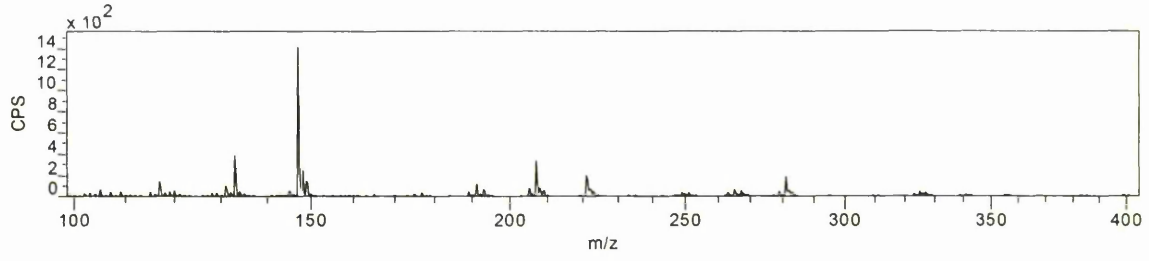

B. XPS data of unaged wool

B.1. Atomic % and ratios of unaged wool

Sample	Atomic %											Ratios			
	O (1s)	N (1s)	C (1s)	S (2p)	Al (2p)	P (2p)	Si (2p)	Ca (2p)	Cu (2p)	Fe (2p)	Sn (3d)	C/O	C/N	C/S	N/S
Undyed	11.98	8.65	75.78	3.21			0.40					6.33	8.76	23.64	2.70
Undyed	10.47	7.10	78.36	3.36			0.72					7.48	11.04	23.35	2.11
Undyed	11.80	7.44	76.53	3.36			0.87					6.49	10.29	22.76	2.21
Undyed	11.12	7.41	78.06	3.42			0.00					7.02	10.53	22.85	2.17
Blank dyed	12.36	7.37	77.01	2.55	0.00		0.32	0.39				6.23	10.45	30.21	2.89
Blank dyed_wl	13.78	6.59	76.31	1.76	0.05		0.49	1.02				5.54	11.57	43.26	3.74
Alum	18.62	6.12	67.25	3.56	4.19		0.26					3.61	11.00	18.87	1.72
Alum	18.59	5.90	67.37	3.53	4.46		0.15					3.62	11.41	19.08	1.67
Alder bark	13.83	7.24	75.32	2.58	0.06		0.64	0.33				5.45	10.40	29.21	2.81
Oak gall	14.23	5.05	78.36	2.36								5.51	15.52	33.26	2.14
Oak gall	12.36	7.06	76.87	3.71								6.22	10.89	20.75	1.91
Oak gall	17.83	6.04	72.90	3.23								4.09	12.07	22.56	1.87
Black/W1	15.07	6.86	74.46	2.74	0.14		0.14	0.20		0.40		4.94	10.86	27.18	2.50
Black/W2	23.77	4.97	67.35	1.65			0.20			2.07		2.83	13.56	40.87	3.01
Black/W2	21.11	5.94	68.66	2.20	0.01		0.18	0.00		1.93		3.25	11.57	31.25	2.70
Black/W2	18.17	5.69	72.44	2.62	0.00		0.14	0.00		0.92		3.99	12.72	27.62	2.17
Black/W3	16.54	7.40	71.78	2.96	0.00		0.26	0.04		1.02		4.34	9.70	24.22	2.50
Black/W4	16.52	6.95	73.00	2.56			0.41	0.16	0.08	0.34		4.42	10.51	28.57	2.72
Black/W4	16.03	6.66	73.86	2.41			0.30	0.09	0.13	0.53		4.61	11.09	30.62	2.76
Black/W4	16.64	7.14	72.37	2.87			0.28	0.06	0.08	0.57		4.35	10.14	25.25	2.49
Black/W4	16.65	7.69	71.87	2.72			0.38	0.07	0.15	0.48		4.32	9.35	26.39	2.82

Sample	Atomic %											Ratios			
	O (1s)	N (1s)	C (1s)	S (2p)	Al (2p)	P (2p)	Si (2p)	Ca (2p)	Cu (2p)	Fe (2p)	Sn (3d)	C/O	C/N	C/S	N/S
Blue/W1	14.05	8.18	73.38	3.28	0.41			0.70				5.22	8.97	22.39	2.50
Blue/W1	13.90	8.21	73.75	3.09	0.37			0.69				5.31	8.98	23.90	2.66
Green/W1	17.80	7.86	68.27	2.93	1.70	0.42		0.75				3.84	8.68	23.32	2.69
Green/W1	17.06	7.74	69.10	3.11	1.48	0.40	0.37	0.75				4.05	8.93	22.25	2.49
Green/W2	15.63	6.33	73.27	2.38	0.55	0.13	0.90	0.81				4.69	11.57	30.81	2.66
Green/W2	15.76	6.79	72.50	2.62	0.51	0.13	0.90	0.79				4.60	10.68	27.67	2.59
Green/W2	11.91	6.23	77.04	3.30	0.36		0.31	0.86				6.47	12.36	23.38	1.89
Red/W1	14.89	8.60	72.36	3.19	0.36		0.42	0.19				4.86	8.42	22.70	2.70
Red/W1	12.97	6.75	76.59	2.58	0.42		0.46	0.23				5.91	11.35	29.64	2.61
Red/W1_wl	13.98	8.22	73.50	3.13	0.33	0.08	0.42	0.35				5.26	8.94	23.45	2.62
Red/W1_wl	14.96	7.93	72.81	3.00	0.36	0.10	0.49	0.36				4.87	9.18	24.27	2.64
Red/W2	12.65	5.82	75.81	2.96	1.99		0.31	0.47				5.99	13.02	25.65	1.97
Red/W2_wl	16.79	6.55	72.70	2.58	0.62		0.22	0.56				4.33	11.10	28.23	2.54
Red/W3_wl	17.01	5.52	71.90	2.27	1.65		1.08	0.58				4.23	13.03	31.75	2.44
Red/W4	11.60	5.80	78.54	3.24			0.82					6.77	13.55	24.22	1.79
Red/W5	13.85	7.64	75.32	2.74	0.40						0.05	5.44	9.86	27.47	2.78
Red/W5	13.43	7.62	75.63	2.84	0.45						0.05	5.63	9.93	26.64	2.68
Yellow/W1	18.11	7.28	68.10	3.02	2.69	0.09	0.31	0.41				3.76	9.36	22.53	2.41
Yellow/W1	18.82	7.27	67.34	2.90	2.85	0.13	0.27	0.42				3.58	9.26	23.22	2.51
Yellow/W1	13.51	6.19	73.64	3.48	2.27		0.31	0.60				5.45	11.90	21.16	1.78
Yellow/W2	14.12	6.97	74.20	2.86	0.53	0.21	0.51	0.61			0.00	5.25	10.64	25.98	2.44
Yellow/W2	14.05	6.73	74.88	2.73	0.60	0.12	0.35	0.54			0.01	5.33	11.13	27.46	2.47

B.2. Relative % of C(1s) peak components and component ratios of unaged wool

Sample	Relative % of C(1s) peak components				Component ratios	
	Hydrocarbon 185 ev	Carbon-nitrogen ~186.3 eV	Carbonyl ~188 eV	Carboxyl ~189 eV	CH/CN	CH/CO
Undyed	67.1	19.1	11.6	2.2	3.5	4.9
Undyed	59.8	23.0	13.6	3.6	2.6	3.5
Undyed	61.6	23.0	13.2	2.2	2.7	4.0
Undyed	62.2	22.4	13.2	2.3	2.8	4.0
Blank dyed	69.1	17.5	11.6	1.9	4.0	5.2
Blank dyed_wl	58.7	25.9	11.6	3.8	2.3	3.8
Alum	63.6	22.3	11.7	2.4	2.9	4.5
Alum	62.4	23.4	11.5	2.7	2.7	4.4
Alder bark	67.8	19.7	11.3	1.1	3.4	5.5
Oak gall	61.2	20.3	15.2	3.3	3.0	3.3
Oak gall	44.3	33.6	15.9	6.2	1.3	2.0
Black/W1	64.9	20.0	12.6	2.5	3.3	4.3
Black/W2	37.7	27.5	25.5	9.2	1.4	1.1
Black/W2	37.9	27.8	25.5	8.8	1.4	1.1
Black/W3	54.9	27.1	12.8	5.3	2.0	3.0
Black/W4	60.6	23.3	13.3	2.8	2.6	3.8
Black/W4	54.4	26.5	14.3	4.8	2.1	2.8
Black/W4	54.3	25.6	13.7	6.4	2.1	2.7
Blue/W1	61.0	21.5	12.6	4.9	2.8	3.5
Green/W1	47.1	29.9	16.5	6.5	1.6	2.0
Green/W1	52.6	28.1	15.0	4.3	1.9	2.7
Green/W2	52.7	25.4	16.2	5.7	2.1	2.4
Green/W2	58.0	25.0	12.6	4.4	2.3	3.4
Green/W2	66.8	19.8	11.5	1.9	3.4	5.0
Red/W1	59.1	24.9	12.2	3.8	2.4	3.7
Red/W1_wl	45.8	29.7	17.4	7.1	1.5	1.9
Red/W1_wl	59.5	24.0	13.0	3.5	2.5	3.6
Red/W2	59.2	24.7	12.3	3.7	2.4	3.7
Red/W2_wl	46.7	26.8	20.0	6.6	1.7	1.8
Red/W3_wl	64.0	23.2	10.3	2.5	2.8	5.0
Red/W4	65.9	21.0	11.2	1.9	3.1	5.0
Red/W5	57.2	25.5	13.0	4.3	2.2	3.3
Red/W5	49.1	31.6	15.0	4.3	1.6	2.5
Yellow/W1	56.9	24.9	13.6	4.7	2.3	3.1
Yellow/W1	59.1	20.6	14.7	5.6	2.9	2.9
Yellow/W2	63.9	21.5	12.5	2.1	3.0	4.4
Yellow/W2	46.0	29.9	16.8	7.2	1.5	1.9

B.3. Relative % of S(2p) peak components of unaged wool

Sample	High resolution		Wide scans		Average	
	S^{2+}	S^{6+}	S^{2+}	S^{6+}	S^{2+}	S^{6+}
Undyed	90.8	9.2	86.5	13.5	88.7	11.3
Undyed	87.2	12.8	87.7	12.3	87.5	12.5
Undyed	90.3	9.7	93.7	6.3	92.0	8.0
Undyed	88.4	11.6	88.9	11.1	88.6	11.4
Blank dyed	88.1	11.9	87.1	12.9	87.6	12.4
Blank dyed_wl	81.1	18.9	82.0	18.0	81.5	18.5
Alum	63.6	36.4	60.6	39.4	62.1	37.9
Alum	60.4	39.6	59.0	41.0	59.7	40.3
Alder bark	86.2	13.8	81.9	18.1	84.1	15.9
Oak gall			100.0	0.0	100.0	0.0
Oak gall	85.6	14.4	89.7	10.3	87.6	12.4
Oak gall	89.9	10.1	88.8	11.2	89.4	10.6
Oak gall	92.5	7.5	90.5	9.5	91.5	8.5
Black/W1	91.1	8.9	90.8	9.2	90.9	9.1
Black/W2	72.5	[illegible]	77.9	22.1	77.9	22.1
Black/W2	67.4	32.6	[illegible]	20.9	67.4	32.6
Black/W2	41.1	58.9	75.1	24.9	41.1	58.9
Black/W3	88.0	12.0	87.7	12.3	87.8	12.2
Black/W4	84.6	[illegible]	77.9	22.1	78.0	22.1
Black/W4	82.9	17.1			82.9	17.1
Black/W4	88.9	[illegible]	82.2	17.8	82.2	17.8
Black/W4	90.5	[illegible]	85.1	14.9	85.1	14.9
Blue/W1	80.9	19.1	78.3	21.7	79.6	20.4
Blue/W1	80.3	19.7	77.5	22.5	78.9	21.1
Green/W1	79.6	20.4	78.4	21.6	79.0	21.0
Green/W1	80.4	19.6	78.7	21.3	79.5	20.5
Green/W2	77.8	22.2	79.6	20.4	78.7	21.3
Green/W2	84.8	15.2	81.5	18.5	83.2	16.8
Green/W2	86.7	13.3	84.3	15.7	85.5	14.5
Red/W1	89.2	10.8	88.4	11.6	88.8	11.2
Red/W1	85.2	14.8	[illegible]	[illegible]	85.2	14.8
Red/W1_wl	86.8	13.2	87.8	12.2	87.3	12.7
Red/W1_wl	88.8	11.2	83.8	16.2	86.3	13.7
Red/W2	90.2	9.9	88.1	11.9	89.1	10.9
Red/W2_wl	74.3	[illegible]	[illegible]	13.5		
Red/W3_wl	73.7	26.3	75.0	25.0	74.3	25.7
Red/W4	90.8	9.2	86.6	13.4	88.7	11.3
Red/W5	88.4	11.6	84.3	15.7	86.3	13.7
Red/W5	88.4	11.6	83.9	16.1	86.1	13.9
Yellow/W1	81.8	18.2	[illegible]	24.9	81.8	15.2
Yellow/W1	84.8	15.2	83.7	16.3	84.2	15.8
Yellow/W1	81.8	18.2	82.1	17.9	82.0	18.0
Yellow/W2	88.7	11.3	83.9	16.1	86.3	13.7
Yellow/W2	81.7	18.3			81.7	18.3

[illegible] peak [illegible] between high resolution and wide scans [illegible] shaded in gray

C. XPS data of accelerated aged wool

C.1. Atomic % and Ratios of accelerated aged wool

Sample	Atomic %										Ratios			
	O (1s)	N (1s)	C (1s)	S (2p)	Al (2p)	P (2p)	Si (2p)	Ca (2p)	Cu (2p)	Fe (2p)	Sn (3d)	C/O	C/N	C/S	N/S
Undyed	17.40	10.29	69.87	1.94			0.51					4.02	6.79	36.03	5.31
Undyed	18.04	9.92	69.10	1.88			1.06					3.83	6.97	36.72	5.27
Undyed	18.77	9.81	68.15	2.59			0.69					3.63	6.95	26.30	3.78
Undyed	18.87	9.54	69.50	1.94			0.15					3.68	7.29	35.88	4.92
Blank dyed	22.99	10.98	62.53	1.44	0.00		1.93	0.14				2.72	5.70	43.30	7.60
Blank dyed	23.43	11.03	61.66	1.52	0.02		2.25	0.10				2.63	5.59	40.62	7.26
Alum	28.65	8.43	54.13	3.76	4.66		0.38					1.89	6.42	14.40	2.24
Alder bark	22.82	9.20	66.09	1.41	0.00		0.37	0.11				2.90	7.18	46.88	6.53
Alder bark	22.59	8.99	66.11	1.57	0.25		0.43	0.07				2.93	7.35	42.13	5.73
Oak gall	20.46	7.51	70.66	1.37								3.45	9.41	51.46	5.47
Oak gall	23.43	6.72	69.40	0.44								2.96	10.32	156.66	15.17
Oak gall	18.93	7.73	71.94	1.39								3.80	9.30	51.61	5.55
Oak gall (back)	14.40	7.03	75.38	3.19								5.23	10.72	23.65	2.21
Black/W1	25.72	10.58	60.93	1.86	0.03		0.25	0.13		0.51		2.37	5.76	32.78	5.69
Black/W1	26.10	10.32	60.47	1.95	0.24		0.17	0.19		0.56		2.32	5.86	31.04	5.30
Black/W2	19.61	6.03	69.65	2.44			0.22			2.05		3.55	11.55	28.53	2.47
Black/W2	19.90	5.95	69.69	2.59			0.32			1.56		3.50	11.71	26.96	2.30
Black/W2	20.37	5.39	70.46	2.25			0.18			1.35		3.46	13.08	31.32	2.40
Black/W2	20.85	5.83	69.37	2.23			0.19			1.54		3.33	11.91	31.15	2.62
Black/W2	26.84	9.64	59.69	2.22	0.23		0.29	0.06		1.02		2.22	6.19	26.90	4.34
Black/W2	26.17	10.11	60.13	2.09	0.07		0.23	0.13		1.08		2.30	5.95	28.78	4.84

Sample	Atomic %											Ratios			
	O (1s)	N (1s)	C (1s)	S (2p)	Al (2p)	P (2p)	Si (2p)	Ca (2p)	Cu (2p)	Fe (2p)	Sn (3d)	C/O	C/N	C/S	N/S
Black/W3	24.10	12.11	61.09	1.78	0.00		0.28	0.00		0.64		2.54	5.05	34.24	6.79
Black/W4	23.79	9.34	63.75	2.08			0.35	0.07	0.20	0.42		2.68	6.83	30.60	4.48
Black/W4	16.26	7.03	73.09	2.67			0.29	0.13	0.12	0.42		4.50	10.40	27.33	2.63
Black/W4	19.92	8.66	67.95	2.49			0.28	0.10	0.23	0.38		3.41	7.85	27.29	3.48
Black/W4	21.40	8.81	66.30	2.15			0.52	0.05	0.23	0.53		3.10	7.52	30.84	4.10
Black/W4	23.51	8.90	64.32	1.97			0.49	0.09	0.34	0.39		2.74	7.23	32.58	4.51
Black/W4 (back)	16.56	6.83	72.75	2.68			0.38	0.13	0.15	0.52		4.39	10.65	27.13	2.55
Blue/W1	22.90	11.38	62.99	1.75	0.50			0.48				2.75	5.53	36.05	6.52
Blue/W1	22.62	11.37	63.48	1.73	0.38			0.42				2.81	5.58	36.65	6.57
Green/W1	26.45	11.88	56.81	1.88	1.64	0.45	0.46	0.44				2.15	4.78	30.20	6.31
Green/W1	25.59	11.53	58.13	1.81	1.55	0.47	0.50	0.42				2.27	5.04	32.15	6.38
Green/W2	23.45	10.16	64.40	0.89	0.90			0.20				2.75	6.34	72.36	11.42
Red/W1	20.15	8.33	67.27	2.24	0.18		1.42	0.42				3.34	8.07	30.02	3.72
Red/W1	22.57	10.58	63.67	1.24	0.43		1.42	0.09				2.82	6.02	51.30	8.53
Red/W1	22.99	11.16	63.32	1.38	0.31		0.68	0.16				2.75	5.67	46.02	8.11
Red/W1_wl	21.61	12.11	64.07	1.50	0.21	0.06	0.33	0.12				2.96	5.29	42.83	8.10
Red/W1_wl	20.64	12.21	64.86	1.57	0.23	0.07	0.30	0.12				3.14	5.31	41.29	7.77
Red/W1_wl (back)	16.74	7.90	71.31	2.85	0.31	0.09	0.34	0.47				4.26	9.03	25.07	2.78
Red/W1_wl (back)	16.24	7.85	71.60	3.20	0.31	0.08	0.29	0.42				4.41	9.12	22.37	2.45
Red/W2	20.91	9.96	66.38	1.52	1.24							3.17	6.67	43.81	6.57
Red/W2_wl	25.99	10.52	61.08	1.28	0.61		0.25	0.28				2.35	5.81	47.90	8.25
Red/W2_wl	26.20	10.41	61.04	1.30	0.65		0.27	0.13				2.33	5.86	47.06	8.03
Red/W3	24.69	10.26	61.50	1.58	1.34		0.43	0.20				2.49	6.00	38.83	6.48

Sample	Atomic %										Ratios			
	O (1s)	N (1s)	C (1s)	S (2p)	Al (2p)	P (2p)	Si (2p)	Ca (2p)	Cu (2p)	Fe (2p)	Sn (3d)	C/O	C/N	C/S	N/S
Red/W3_wl	20.48	8.61	66.27	2.41	1.82		0.26	0.13				3.24	7.69	27.46	3.57
Red/W4	17.98	8.15	71.75	1.15			0.98					3.99	8.80	62.66	7.12
Red/W5	20.87	8.62	68.61	1.37	0.51						0.02	3.29	7.96	50.19	6.30
Red/W5	20.54	8.64	68.89	1.47	0.44						0.03	3.35	7.98	46.90	5.88
Red/W5 (back)	14.57	7.97	74.20	2.94	0.28						0.05	5.09	9.31	25.28	2.71
Yellow/W1	24.20	10.16	58.92	2.07	3.83		0.58	0.25				2.44	5.80	28.44	4.90
Yellow/W2	22.61	7.72	66.41	1.55	0.59	0.13	0.61	0.38			0.01	2.94	8.60	42.93	4.99
Yellow/W2 (back)	15.95	6.78	72.52	2.79	0.68	0.12	0.51	0.63			0.03	4.55	10.70	25.97	2.43
Yellow/W2 (back)	15.90	7.11	72.15	2.71	0.76	0.19	0.52	0.66			0.02	4.54	10.15	26.66	2.63

C.2. Relative % of C (1s) peak components and component ratios of accelerated aged wool

Sample	Relative % of C(1s) peak components				Component ratios	
	Hydrocarbon 185 ev	Carbon-nitrogen ~186.3 eV	Carbonyl ~188 eV	Carboxyl ~189 eV	CH/CN	CH/CO
Undyed	43.0	28.8	21.1	7.1	1.5	1.5
Undyed	49.0	28.4	18.6	4.0	1.7	2.2
Undyed	46.0	27.7	18.9	7.4	1.7	1.7
Undyed	47.7	26.3	19.3	6.7	1.8	1.8
Alder bark	42.7	32.4	17.0	7.9	1.3	1.7
Oak gall	45.0	29.8	18.4	6.7	1.5	1.8
Oak gall	47.5	28.5	18.5	5.4	1.7	2.0
Oak gall	50.7	27.9	15.6	5.9	1.8	2.4
Oak gall (back)	50.2	28.8	16.0	5.0	1.7	2.4
Black/W1	44.0	29.2	21.4	5.4	1.5	1.6
Black/W1	42.5	29.2	22.1	6.3	1.5	1.5
Black/W2	43.7	30.6	18.3	7.4	1.4	1.7
Black/W2	44.4	30.6	18.6	6.3	1.5	1.8
Black/W2	46.3	30.5	16.0	7.2	1.5	2.0
Black/W2	46.3	29.3	17.2	7.2	1.6	1.9
Black/W2	36.0	25.7	26.3	12.0	1.4	0.9
Black/W3	39.2	29.6	23.7	7.5	1.3	1.3
Black/W3	41.8	29.1	23.7	5.4	1.4	1.4
Black/W4	45.0	27.8	17.6	9.6	1.6	1.7
Black/W4	42.0	30.6	18.8	8.6	1.4	1.5
Black/W4	47.4	28.7	17.4	6.6	1.7	2.0
Black/W4	47.2	29.2	17.4	6.2	1.6	2.0
Black/W4	53.1	27.1	13.9	5.9	2.0	2.7
Black/W4	51.8	27.8	15.7	4.7	1.9	2.5
Blue/W1	34.7	29.6	25.7	10.0	1.2	1.0
Green/W1	37.8	29.4	25.6	7.2	1.3	1.2
Green/W1	32.0	29.1	28.2	10.7	1.1	0.8
Green/W2	44.2	28.8	22.5	4.5	1.5	1.6
Red/W1	57.9	22.6	14.6	5.0	2.6	3.0
Red/W1	47.9	27.3	19.7	5.1	1.8	1.9
Red/W1_wl	46.1	27.5	19.4	7.0	1.7	1.7
Red/W1_wl	41.5	28.4	21.8	8.3	1.5	1.4
Red/W1_wl (back)	48.5	30.0	15.3	6.2	1.6	2.3
Red/W1_wl (back)	45.8	22.5	21.2	10.5	2.0	1.4
Red/W2_wl	41.2	30.8	21.8	6.1	1.3	1.5
Red/W2_wl	40.4	31.5	21.8	6.3	1.3	1.4
Red/W3_wl	45.1	27.8	19.7	7.5	1.6	1.7
Red/W3_wl (back)	52.8	26.2	15.4	5.6	2.0	2.5
Red/W4	58.3	29.1	11.1	1.6	2.0	4.6
Red/W5	49.2	28.1	15.6	7.1	1.8	2.2
Red/W5 (back)	56.0	24.5	14.5	5.0	2.3	2.9
Yellow/W1	42.3	29.1	22.1	6.5	1.5	1.5
Yellow/W2	53.9	25.7	14.9	5.5	2.1	2.6
Yellow/W2 (back)	55.1	25.7	14.4	4.9	2.1	2.9
Yellow/W2 (back)	49.4	31.2	13.8	5.6	1.6	2.5

C.3. Relative % of S (2p) peak components of accelerated aged wool

Sample	High resolution		Wide scans		Average	
	S^{2+}	S^{6+}	S^{2+}	S^{6+}	S^{2+}	S^{6+}
Undyed	28.1	71.9	31.5	68.5	29.8	70.2
Undyed	27.1	72.9	25.0	75.0	26.1	73.9
Undyed	23.2	76.8	25.7	74.3	24.5	75.5
Undyed	24.1	75.9	28.1	71.9	26.1	73.9
Blank dyed	26.2	73.8	28.4	71.6	27.3	72.7
Blank dyed	17.7	82.3	27.8	72.2		
Alum			8.7	91.3	8.7	91.3
Alder bark	25.4	74.6	37.4	62.6	25.4	74.6
Alder bark			47.5	52.5		
Oak gall	34.9	65.1	[illegible]	72.2	34.9	65.1
Oak gall	47.6	52.4			47.6	52.4
Oak gall	32.4	67.6	34.1	65.9	33.3	66.7
Oak gall (back)	78.2	21.8	78.0	22.0	78.1	21.9
Black/W1	30.7	69.3	[illegible]	64.[illegible]	30.7	69.3
Black/W1			31.2	68.8	31.2	68.8
Black/W2	85.4	14.6	81.0	19.0	83.2	16.8
Black/W2	85.9	14.1	84.8	15.2	85.4	14.6
Black/W2	87.2	12.8	[illegible]	[illegible]	87.2	12.8
Black/W2	87.6	12.4	81.8	18.2	84.7	15.3
Black/W2	25.4	74.6		[illegible]	25.4	74.6
Black/W2			[illegible]	[illegible]		
Black/W3	22.6	77.4	[illegible]	[illegible]	22.6	77.4
Black/W4	[illegible]	[illegible]	29.8	70.2	29.8	70.2
Black/W4	31.6	68.4	[illegible]	[illegible]	31.6	68.4
Black/W4	83.4	16.6			83.4	16.6
Black/W4	85.1	14.9	84.7	15.3	84.9	15.1
Black/W4	[illegible]	[illegible]	66.7	33.3	66.7	33.3
Black/W4	[illegible]	[illegible]	58.0	42.0	58.0	42.0
Black/W4 (back)			80.5	19.5	80.5	19.5
Blue/W1	22.4	77.6			22.5	77.6
Blue/W1			23.9	76.1	23.9	76.1
Green/W1	24.8	75.2	22.1	77.9	23.4	76.6
Green/W1	19.2	80.8	21.8	78.2	20.5	79.5
Green/W2	22.1	77.9	20.2	79.8	21.2	78.8
Red/W1	59.3	40.7	55.4	44.6	57.3	42.7
Red/W1	20.0	80.0	[illegible]	[illegible]	20.0	80.0
Red/W1	24.8	75.2	24.5	75.5	24.7	75.3
Red/W1_wl	28.7	71.3	24.7	75.3	26.7	73.3
Red/W1_wl	31.7	68.3	27.1	72.9	29.4	70.6
Red/W1_wl (back)	75.9	24.1	71.5	28.5	73.7	26.3
Red/W2			21.4	78.6	21.4	78.6
Red/W2_wl	20.4	79.6	[illegible]	[illegible]	20.4	79.6
Red/W2_wl	22.9	77.1	[illegible]		22.9	77.1
Red/W3_wl	20.1	79.9	22.9	77.1	21.5	78.5
Red/W3_wl (back)	58.8	41.2	60.7	39.3	59.7	40.3
Red/W4	28.2	71.8	24.8	75.2	26.5	73.5
Red/W5			31.5	68.5	31.5	68.5
Red/W5	35.5	64.5	30.7	69.3	33.1	66.9
Red/W5 (back)	83.5	16.5	83.2	16.8	83.3	16.7
Red/Wl_wl (back)	67.7	32.3	64.4	35.6	66.0	34.0
Yellow/W1	24.6	75.4	20.7	79.3	22.6	77.4
Yellow/W2	33.9	66.1	31.7	68.3	32.8	67.2
Yellow/W2 (back)	81.0	19.0			81.0	19.0
Yellow/W2 (back)	83.4	16.6	78.8	21.2	81.1	18.9

D. XPS data of historic wool

D.1. Atomic % and Ratios of historic wool

Sample	Comment*	Atomic %																Ratios			
		O (1s)	N (1s)	C (1s)	S (2p)	Na (1s)	Ca (2p)	Si (2p)	Al (2p)	K (2p)	P (2p)	Pb (4f)	Ag (3d)	Fe (2p)	Cu (2p)	Zn (2p)	Cl (2p)	Mg (2s)	C/O	C/N	C/S	N/S
BRU 1a_8	a	22.2	5.7	64.4	1.2		1.2	3.6	1.4		0.29	0.03							2.9			
BRU 1a_8	a	19.3	5.1	67.6	1.2		1.0	4.0	1.3		0.24	0.01							3.5	13.3	54.8	4.1
BRU 1a_8	a	21.9	6.4	64.8	1.4		1.3	2.4	1.6		0.34	0.02							3.0	10.1	47.7	4.7
BRU 2_23	h	29.9	4.9	55.7	2.6	0.8	2.0	2.9	0.7									0.54	1.9	11.4	21.1	1.8
BRU 2_23	h	30.4	5.2	55.2	2.3	0.5	2.3	2.9	0.7									0.45	1.8	10.6	23.6	2.2
BRU 3_15	m	20.9	2.9	69.9	2.0		0.9	3.5											3.3	24.2	34.9	1.4
BXL 1_5		30.8	2.7	52.2	4.9	0.9	2.6	2.1	0.8	2.83	0.16	0.03							1.7	19.1	10.7	0.6
BXL 1_5		30.7	2.8	51.6	4.8	1.1	2.7	2.3	0.9	2.74	0.22	0.02							1.7	18.2	10.8	0.6
HCP 112_C4		21.1	7.2	67.0	2.0		0.2	1.1	0.7					0.54					3.2	9.3	32.9	3.5
HCP 112_C4		21.0	6.7	67.7	1.9		0.3	1.3	0.5					0.58					3.2	10.1	36.3	3.6
HCP 115_C4	h	25.8	6.0	63.5	2.0			2.7											2.5	10.6	31.2	3.0
HCP 126_C1		21.5	4.9	68.2	1.2		0.3	2.6	1.1			0.04	0.09						3.2	14.0	57.5	4.1
HCP 126_C1		21.1	5.0	68.1	1.2		0.3	2.7	1.4			0.03	0.06						3.2	13.5	56.7	4.2
HCP 126_C1		23.0	0.6	74.7	0.3		0.1	0.7	0.5			0.15							3.2	129.7	277.8	2.1
HCP 126_C1		21.4	1.1	75.3	0.3		0.1	1.1	0.7			0.07							3.5	66.6	283.2	4.3
HCP 133_C1		22.92	0.663	74.71	0.305		0.079	0.67	0.472		0.147		0.031						3.3	112.7	245.0	2.2
HCP 133_C1		21.36	1.301	75.35	0.23		0.057	1.027	0.6		0.075								3.5	57.9	327.6	5.7
HCP 157_B6		27.1	1.4	62.3	0.5	0.7	0.5	1.0	5.7			0.15				0.37	0.27		2.3	43.6	130.1	3.0
HCP 157_B6		26.4	1.2	65.5	0.4	0.6	0.3	0.9	4.1			0.12				0.18	0.26		2.5	54.2	167.6	3.1
HCP 18_G4	h	20.6	3.8	71.9	1.4		0.2	1.3					0.68						3.5	18.7	49.7	2.7
HCP 33_G4		19.4	7.1	67.1	2.5		0.5	1.6	1.6				0.14						3.5	9.4	26.3	2.8
HCP 33_G4		20.5	6.4	67.9	2.0		0.6	1.2	1.0		0.28		0.11						3.3	10.6	34.2	3.2
HCP 45_F4		22.3	5.3	67.2	1.6		0.3	2.2	0.9		0.05	0.01		0.30					3.0	12.8	43.1	3.4

Sample	Comments*	Atomic %															Ratios			
		O (1s)	N (1s)	C (1s)	S (2p)	Na (1s)	Ca (2p)	Si (2p)	Al (2p)	K (2p)	P (2p)	Pb (4f)	Ag (3d)	Fe (2p)	Cu (2p)	Zn (2p)	Cl (2p)	Mg (2s)	C/O	C/N	C/S	N/S
HCP 45_F4		21.4	5.7	67.3	1.7		0.3	2.3	0.8		0.13	0.01	0.10	0.12					3.1	11.7	38.9	3.3
HCP 56_E1		20.6	6.7	67.9	1.9		0.6	1.5	0.6		0.09	0.02	0.06	0.11					3.3	10.2	35.6	3.5
HCP 90_C4	h	26.2	5.2	63.5	1.8			3.4											2.4	12.3	35.8	2.9
HRP 1_1	h	17.8	5.9	70.0	2.0		1.3	2.0	1.1										3.9	11.9	34.2	2.9
HRP 1_1	h	18.5	6.0	69.3	2.3		1.7	1.7	0.5										3.8	11.6	30.3	2.6
HRP 1_1	h	20.5	7.2	64.0	2.8		1.3	2.5	1.6										3.1	8.8	22.5	2.5
HRP 1_1	h	16.0	4.0	73.2	2.0		1.1	2.4	1.2										4.6	18.2	35.9	2.0
HRP 1_1	h	17.1	4.7	70.4	1.4		1.1	2.1	3.2										4.1	15.1	49.4	3.3
HRP 1_1	h	14.3	4.0	75.7	1.6		1.0	2.3	1.0										5.3	19.1	46.5	2.4
HRP 1_21	h	24.8	8.8	63.2	2.4		0.8												2.5	7.2	26.2	3.6
HRP 1_22	m	18.6	3.0	68.8	1.4		0.5	7.2	0.5										3.7	23.0	51.0	2.2
HRP 1_22	m	17.2	2.9	69.0	1.8		0.6	7.2	1.3										4.0	24.1	38.6	1.6
HRP 1_22	h	19.7	6.2	67.1	2.3		1.4	1.8	1.3						0.27				3.4	10.8	28.9	2.7
HRP 1_3	m	15.1	1.8	79.1	0.6		0.6	1.5	1.3										5.3	45.0	123.6	2.8
HRP 1_46	h	25.3	7.3	61.5	3.0		1.4	1.5											2.4	8.4	20.8	2.5
HRP 2_21	h	28.9	5.9	57.2	1.1		0.8	4.1	2.0										2.0	9.7	51.6	5.3
HRP 2_38	h	24.1	7.9	62.0	2.5		0.9	1.8	0.8										2.6	7.8	24.6	3.1
HRP 2_61	h	25.4	6.5	61.6	1.6		1.3	2.3	1.4										2.4	9.5	39.7	4.2
HRP 2_62	h	26.2	8.7	60.4	1.1		0.3	2.2	1.1										2.3	6.9	57.4	8.3
HRP 2_75	m	22.4	0.4	64.6	1.1		0.2	11.3											2.9	148.8	59.8	0.4
HRP 3_19	h	36.0	3.9	49.7	4.6	0.1	3.2	1.4	0.6									0.47				
HRP 3_19	h	33.9	3.4	52.7	3.5	0.3	2.8	1.5	1.3									0.64	1.6	15.5	15.0	1.0
PNM 2_27	h	34.7	3.8	53.7	2.0		2.3	2.1	0.7									0.72	1.5	14.2	26.6	1.9
PNM 2_27	h	33.4	4.0	55.0	2.1		2.6	2.0	0.7									0.32	1.6	13.9	26.8	1.9
PNM 5_15	h	25.4	4.2	62.8	1.6		2.0	3.0	0.7									0.26	2.5	14.9	38.9	2.6
PNM 5_15	h	28.4	4.9	59.1	2.0	0.3	2.3	1.9	0.9									0.21	2.1	12.1	29.5	2.4

Sample	Comments*	Atomic %																Ratios			
		O (1s)	N (1s)	C (1s)	S (2p)	Na (1s)	Ca (2p)	Si (2p)	Al (2p)	K (2p)	P (2p)	Pb (4f)	Ag (3d)	Fe (2p)	Cu (2p)	Zn (2p)	Cl (2p)	Mg (2s)	C/O	C/N	C/S	N/S
PNM 7_7	h	30.5	6.4	53.2	3.4	0.3	1.7	2.0	1.2									1.25	1.7	8.2	15.6	1.9
PNM 7_7	h	30.2	6.6	54.9	3.4	0.6	1.4	1.5	0.9									0.51	1.8	8.4	16.0	1.9
PNM 9_13	h	30.1	6.1	56.5	3.0	0.3	2.6	0.9	0.4									0.11	1.9	9.3	19.1	2.0
PNM 9_13	h	30.4	5.4	56.7	3.0	0.2	2.9	0.8	0.4									0.11	1.9	10.5	18.9	1.8
PNM 9_20	h	31.3	6.2	55.9	2.4	0.7	1.0	1.4	0.6									0.51	1.8	9.0	23.5	2.6
PNM 9_20	h	32.1	5.7	55.7	2.2	0.7	1.0	1.4	0.5									0.66	1.7	9.7	25.2	2.6

Comments* a: acetone extracted
h: heptane extracted
m: mounted on adhesive tape

D.2. Relative % of C (1s) peak components and Component ratios of historic wool

Sample	Relative % of C(1s) peak components					Component ratios	
	Comments*	Hydrocarbon 185 ev	Carbon-nitrogen ~186.3 eV	Carbonyl ~188 eV	Carboxyl ~189 eV	CH/CN	CH/CO
BRU1a_8	a	54.7	26.2	12.9	6.2	2.1	2.9
BRU1a_8	a	54.2	27.2	13.3	5.4	2.0	2.9
BRU1a_8	a	53.2	27.6	14.0	5.2	1.9	2.8
BRU2_23	h	54.9	27.3	12.9	4.9	2.0	3.1
BRU3_15	m	79.2	10.9	7.5	2.4	7.3	8.0
BXL1_5		66.5	19.3	9.7	4.6	3.4	4.7
BXL1_5		61.8	19.5	13.7	5.0	3.2	3.3
HCP 115_C4	h	41.5	30.4	19.6	8.5	1.4	1.5
HCP 126 C1		59.14	24.26	12.29	4.305	2.4	3.6
HCP 133_C1		44.55	33.21	18.4	3.839	1.3	2.0
HCP 157_B6		57.77	24.25	13.45	4.532	2.4	3.2
HCP 18_G4	h	63.5	21.3	10.1	5.1	3.0	4.2
HCP 33_G4		52.9	27.2	13.5	6.5	1.9	2.7
HCP 33_G4		54.8	24.4	14.2	6.7	2.2	2.6
HCP 45_F4		54.6	25.2	13.7	6.5	2.2	2.7
HCP 56_E1		42.1	32.0	17.2	8.7	1.3	1.6
HCP 90_D4	h	38.9	28.3	23.7	9.1	1.4	1.2
HRP1_1		46.9	30.5	12.9	9.6	1.5	2.1
HRP1_1		51.2	25.8	16.2	6.7	2.0	2.2
HRP1_1		64.8	20.8	10.8	3.6	3.1	4.5
HRP1_1	h	48.3	29.3	14.7	7.7	1.6	2.2
HRP1_1	h	56.2	24.3	13.6	6.0	2.3	2.9
HRP1_1	h	50.7	29.0	13.6	6.7	1.7	2.5
HRP1_22	m	71.2	16.0	7.2	5.6	4.4	5.6
HRP1_22	h	62.3	21.9	14.1	1.7	2.8	4.0
HRP1_3	m	70.5	18.6	7.0	3.9	3.8	6.5
HRP1_46	h	42.5	32.5	17.9	7.1	1.3	1.7
HRP2_21	h	47.5	28.4	16.2	7.9	1.7	2.0
HRP2_38	h	50.7	27.0	12.7	9.6	1.9	2.3
HRP2_62	h	47.8	29.3	18.5	4.4	1.6	2.1
HRP2_75	m	85.9	6.0	3.2	4.8	14.3	10.6
HRP3_19	h	57.2	25.2	13.3	4.3	2.3	3.2
HRP3_19	h	53.5	26.6	13.2	6.8	2.0	2.7
PNM2_27	h	59.2	23.9	12.9	3.9	2.5	3.5
PNM2_27	h	55.1	25.7	13.1	6.2	2.1	2.9
PNM5_15	h	44.9	32.3	14.9	7.9	1.4	2.0
PNM5_15	h	58.2	23.2	13.0	5.7	2.5	3.1
PNM7_7	h	54.5	24.7	15.5	5.4	2.2	2.6
PNM9_13	h	46.5	31.2	15.8	6.5	1.5	2.1
PNM9_20	h	49.0	28.2	13.1	9.6	1.7	2.2
PNM9_20	h	51.3	27.3	16.0	5.4	1.9	2.4

Comments* a: acetone extracted
h: heptane extracted
m: mounted on adhesive tape

D.3. Relative % of S (2p) peak components of historic wool

Sample	Comments*	High resolution S^{2+}	High resolution S^{6+}	Wide scans S^{2+}	Wide scans S^{6+}	Average S^{2+}	Average S^{6+}
BXL1_5		3.7	96.3	0.0	100.0	1.9	98.1
BXL1_5		0.0	100.0	0.7	99.3	0.3	99.7
BRU1a_8	a	24.4	75.6	21.6	78.4	23.0	77.0
BRU1a_8	a	26.1	73.9	23.1	76.9	24.6	75.4
BRU1a_8	a	20.1	79.9	25.4	74.6	22.7	77.3
HRP1_21	h			25.0	75.0	25.0	**75.0**
HRP1_46	h	36.6	63.4	23.1	76.9	36.6	**63.4**
HRP2_21	h	26.4	73.6	22.1	77.9	24.3	**75.7**
HRP2_38	h	22.4	77.6	21.7	78.3	22.0	**78.0**
HRP2_61	h	33.3	66.7	48.2	51.8	33.3	**66.7**
HRP2_62	h	22.1	77.9	14.3	85.7	22.1	**77.9**
HCP 18_G4	h	35.6	64.4	33.3	66.7	34.5	**65.5**
HCP 90_D4	h			32.9	67.1	32.9	**67.1**
HCP 115_C4	h	41.3	58.7	16.2	83.8	16.2	**83.8**
BRU3_15	m	2.4	97.6	6.0	94.0	4.2	**95.8**
HRP1_3	m	17.4	82.6	0.0	100.0	17.4	**82.6**
HCP 112_C4				55.3	44.7		
HCP 112_C4				23.8	76.2	23.8	**76.2**
HCP 45_F4				27.5	72.5	27.5	72.5
HCP 45_F4		25.2	74.8	24.4	75.6	24.8	75.2
HCP 56_E1		25.7	74.3	23.9	76.1	24.8	**75.2**
HRP1_1		17.0	83.0	43.5	56.5	17.0	83.0
HRP1_1		22.8	77.2	20.5	79.5	21.6	78.4
HRP1_1		33.3	66.7	25.9	74.1	33.3	66.7
HRP1_1	h	19.1	80.9	19.7	80.3	19.4	80.6
HRP1_1	h	21.1	78.9	17.1	83.0	19.1	80.9
HRP1_1	h			19.8	80.2	19.8	80.2
HRP1_22	m	26.1	73.9	24.5	75.5	25.3	74.7
HRP1_22	m			25.4	74.6	25.4	74.6
HRP1_22	h	23.3	76.7	25.5	74.5	24.4	**75.6**
HCP 33_G4		34.7	65.3	34.4	65.6	34.6	65.4
HCP 33_G4		34.9	65.1	25.1	74.9	25.1	74.9
HCP 157_B6		17.8	82.2	24.0	76.0	17.8	**82.2**
HCP 157_B6				0.0	100.0		
HCP 126_C1		29.2	70.8	25.0	75.0	27.1	**72.9**
HCP 126_C1				21.2	78.8		
HCP 133_C1		20.0	80.0	23.1	76.9	21.6	**78.4**
HCP 133_C1				13.1	86.9	100.0	
PNM9_20	h	14.4	85.6	11.7	88.3	13.0	87.0
PNM9_20	h	80.3	19.4	11.7	88.3	11.7	88.3
PNM7_7	h	18.7	81.3	19.4	80.6	19.0	81.0
PNM7_7	h			12.7	87.3	12.7	87.3
PNM9_13	h	10.5	89.5	9.0	91.0	9.8	90.2
PNM9_13	h			5.7	94.3	5.7	94.3
BRU2_23	h	17.0	83.0	13.0	87.0	15.0	85.0
BRU2_23	h			12.4	87.6	12.4	87.6
PNM5_15	h	18.6	81.4	14.4	85.6	16.5	83.5
PNM5_15	h	19.3	80.7	13.6	86.4	19.3	80.7
PNM2_27	h	6.8	93.2	8.1	91.9	7.4	92.6
PNM2_27	h	8.6	91.4	4.9	95.1	6.8	93.2
HRP3_19	h	2.0	98.0	1.0	99.0	1.5	98.5
HRP3_19	h	3.3	96.7	2.2	97.8	2.8	97.2

Components with disparity between high resolution and wide scans were not averaged; instead the noisier peak was disregarded and the numbers shown in gray

Comments*

a: acetone extracted
h: heptane extracted
m: mounted on adhesive tape

E. ToF-SIMS spectra of wool

E.1. Spectra acquired with a Cs^+ primary ion source

Undyed wool unaged positive ion spectrum : Cs^+ primary ion source

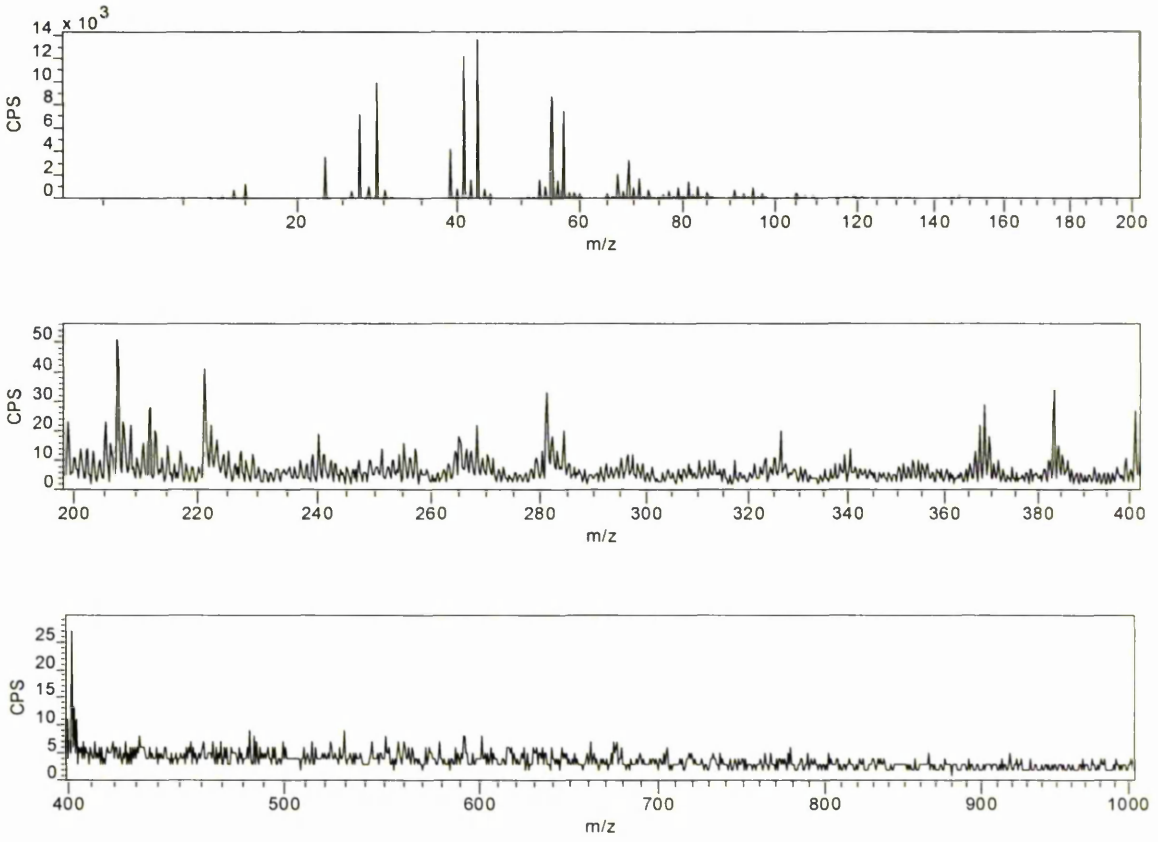

Undyed wool unaged negative ion spectrum : Cs^+ primary ion source

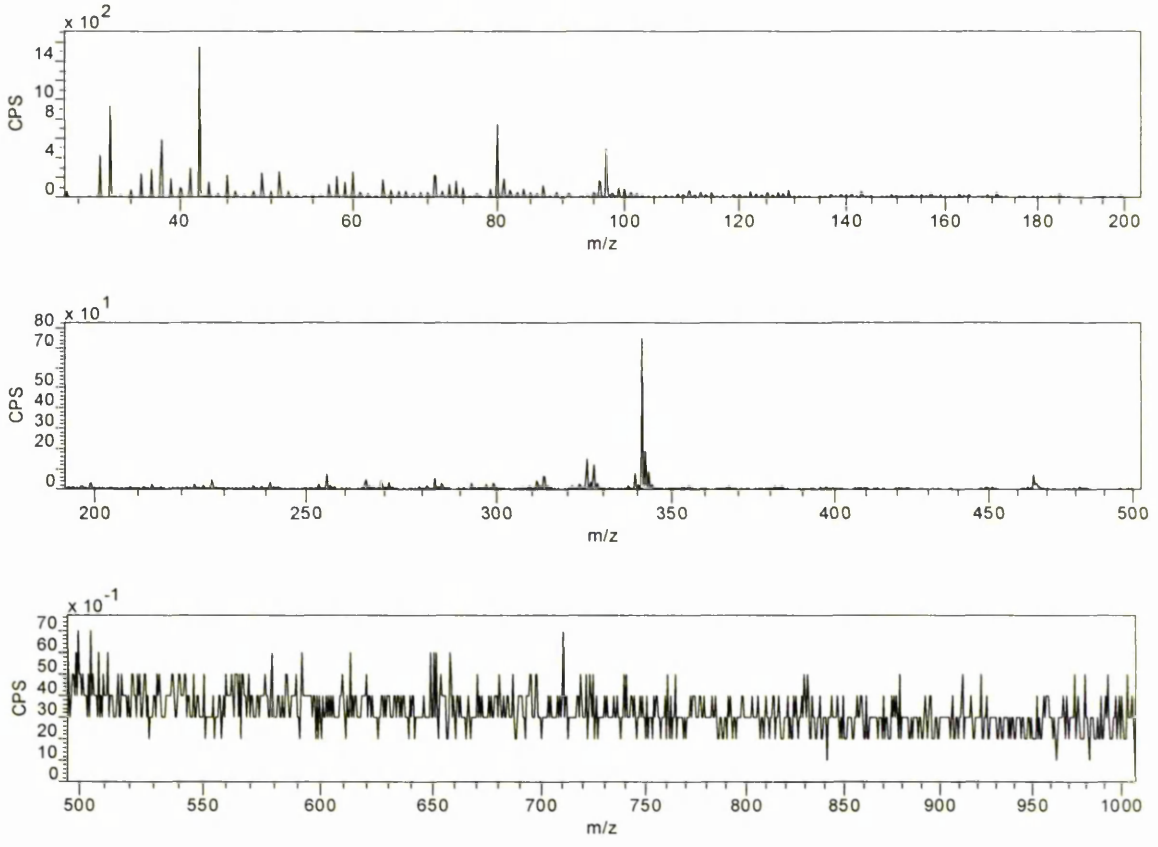

Undyed wool unaged positive ion spectrum : Cs^+ primary ion source

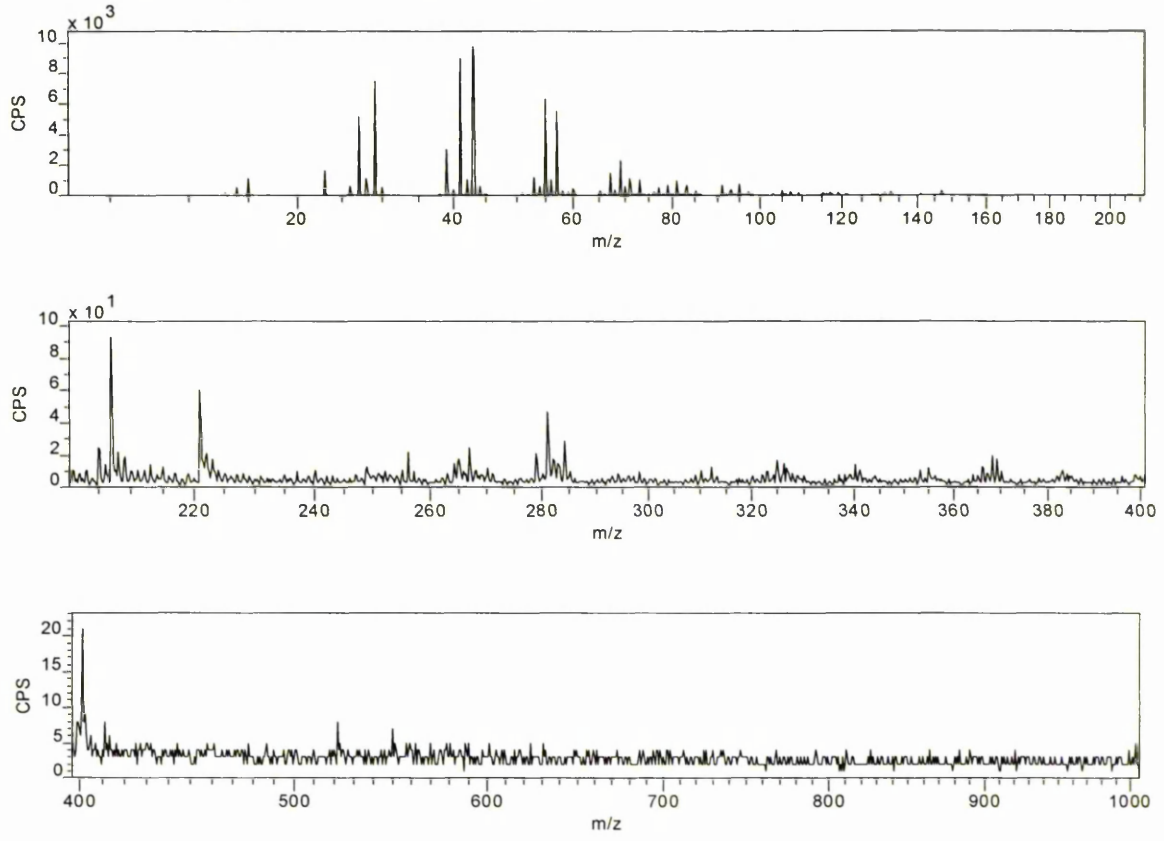

Undyed wool unaged negative ion spectrum : Cs^+ primary ion source

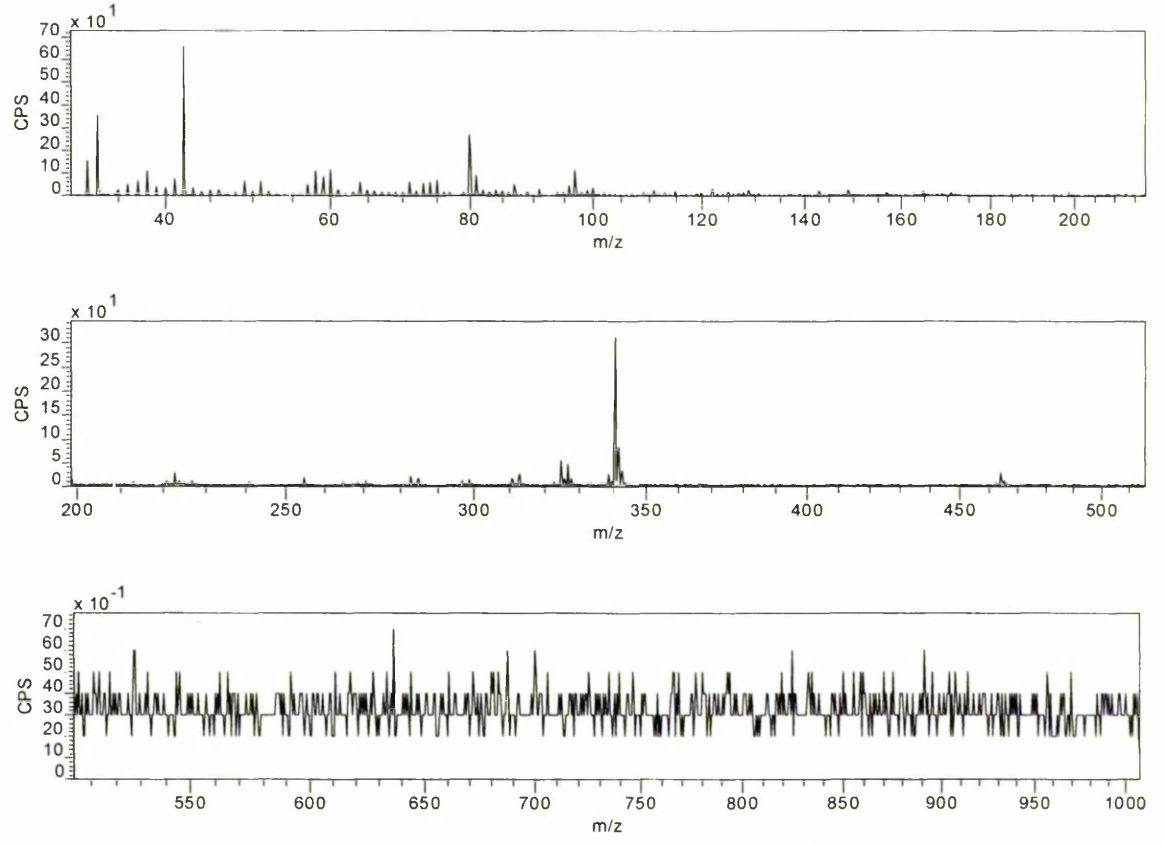

Undyed wool accelerated aged positive ion spectrum : Cs^+ primary ion source

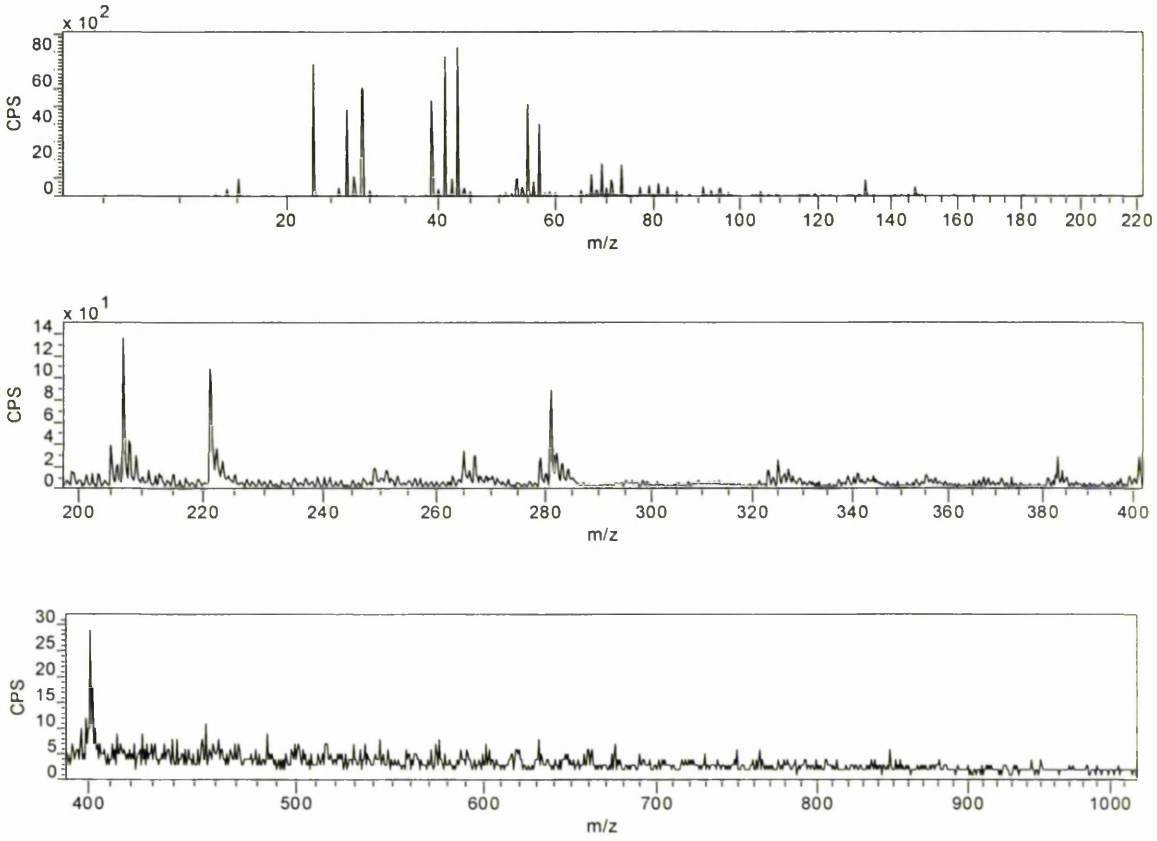

Undyed wool accelerated aged negative ion spectrum : Cs^+ primary ion source

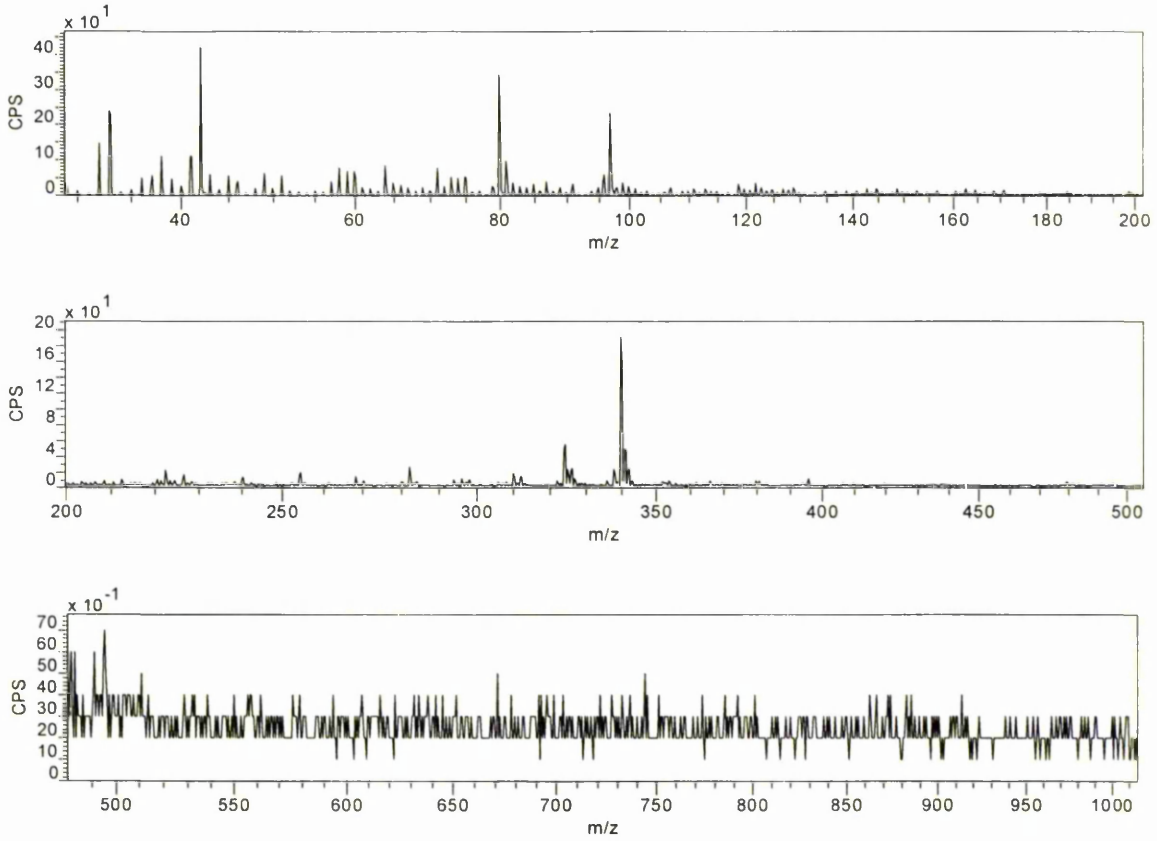

Alum mordanted wool unaged positive ion spectrum : Cs^+ primary ion source

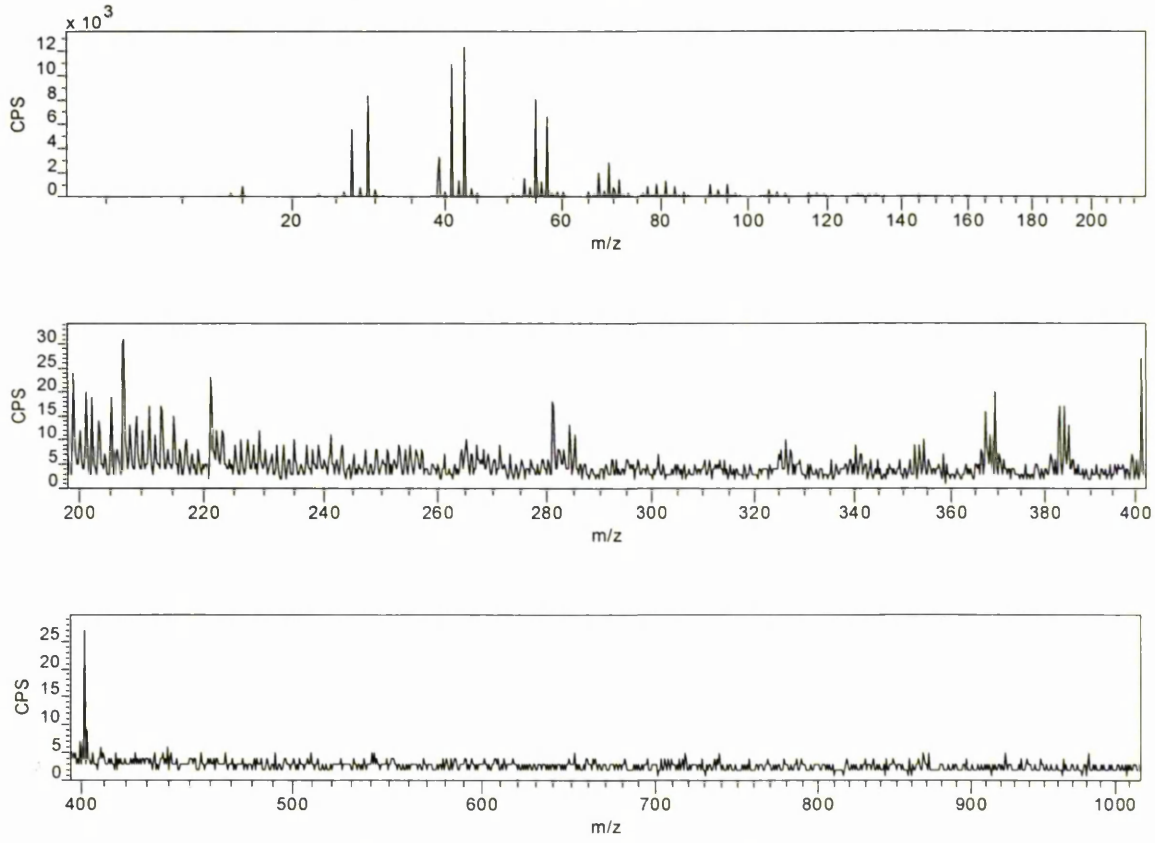

Alum mordanted wool unaged negative ion spectrum : Cs^+ primary ion source

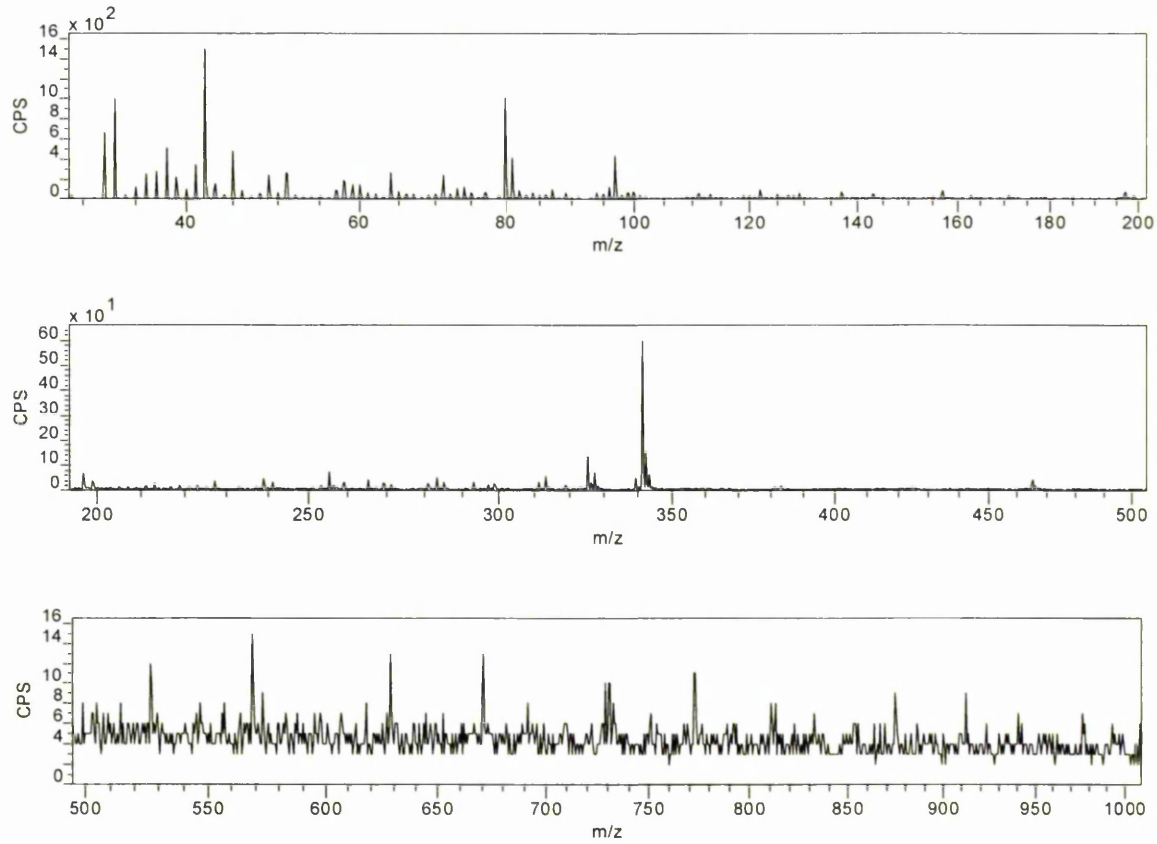

Alum mordanted wool accelerated aged positive ion spectrum : Cs^+ primary ion source

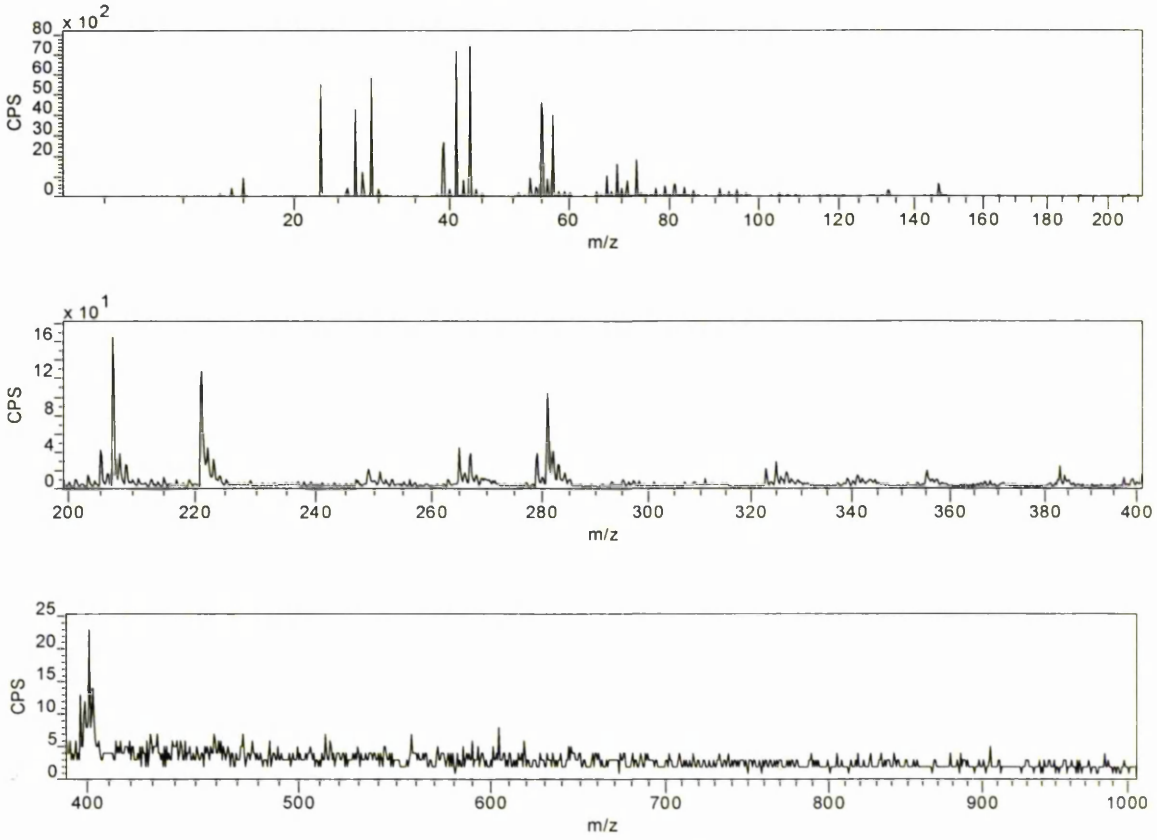

Alum mordanted wool accelerated aged negative ion spectrum : Cs^+ primary ion source

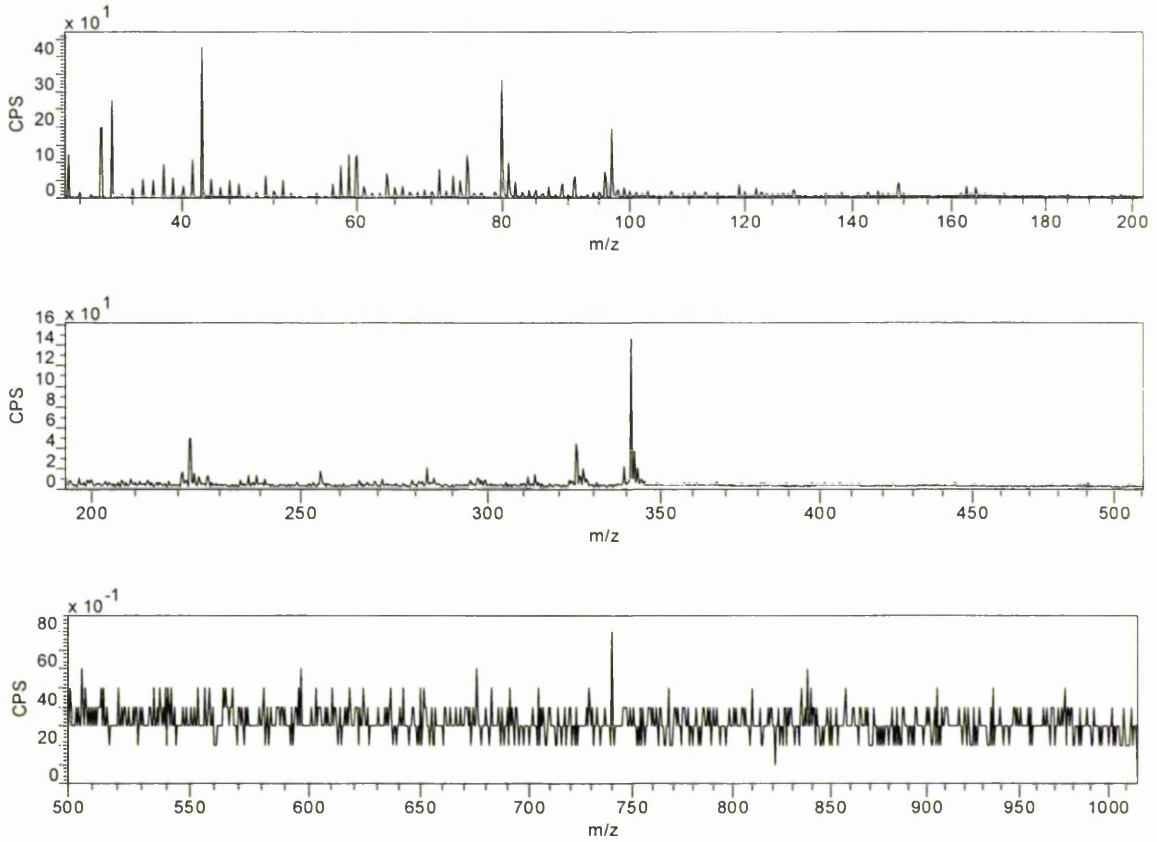

Blue/W1 unaged positive ion spectrum : Cs^+ primary ion source

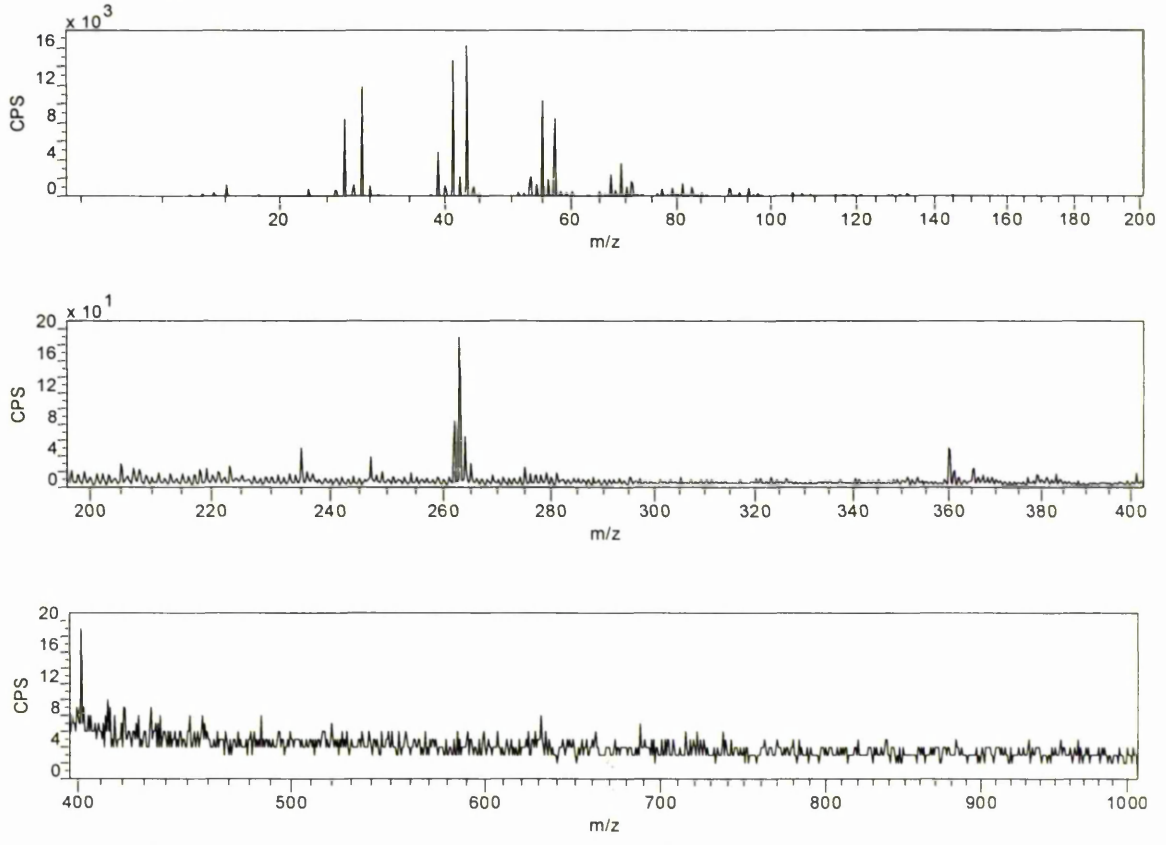

Blue/W1 unaged negative ion spectrum : Cs^+ primary ion source

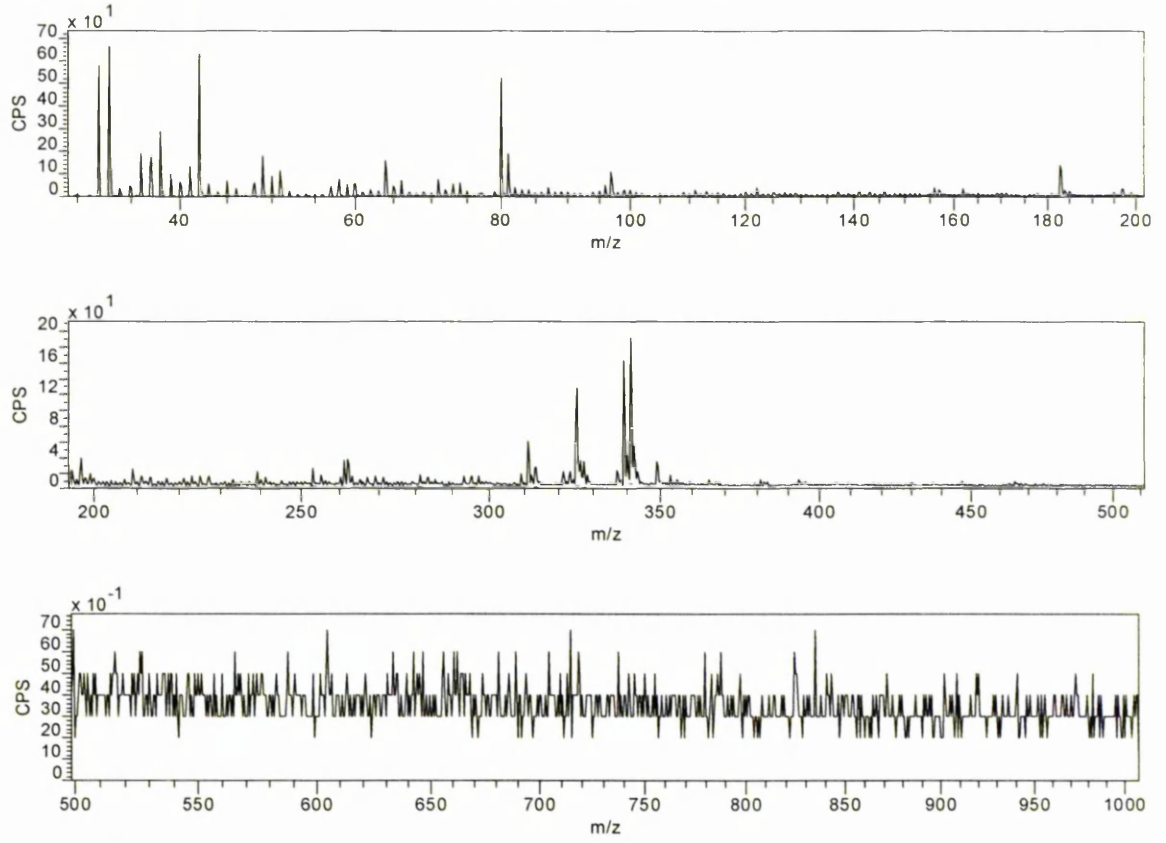

Blue/W1 accelerated aged positive ion spectrum : Cs^+ primary ion source

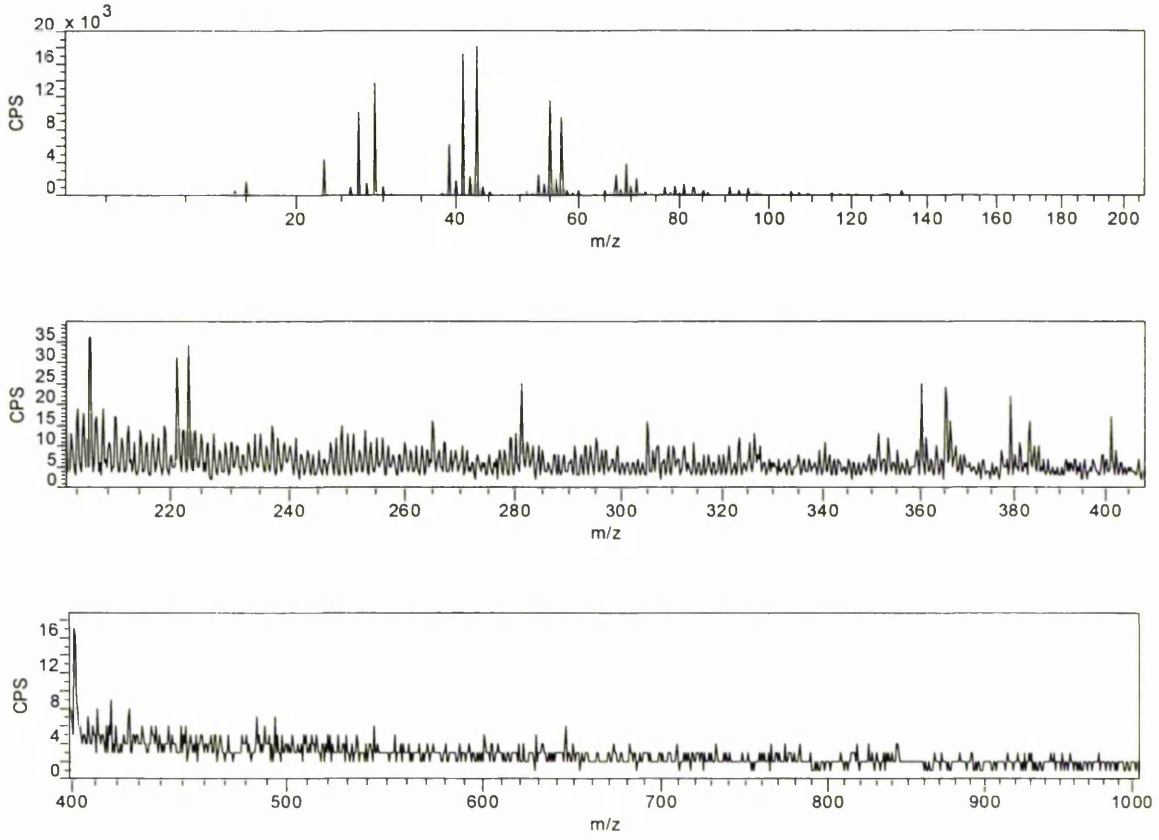

Blue/W1 accelerated aged negative ion spectrum : Cs^+ primary ion source

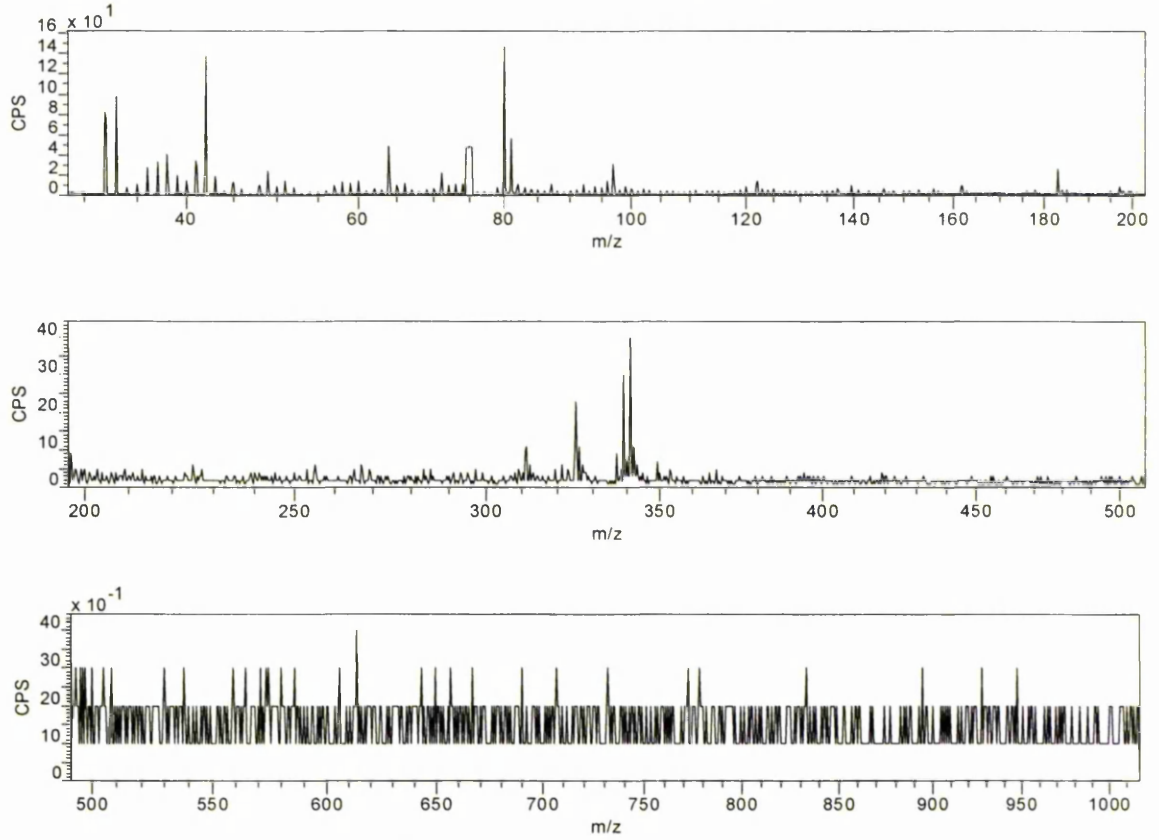

Red/W4 unaged positive ion spectrum : Cs^+ primary ion source

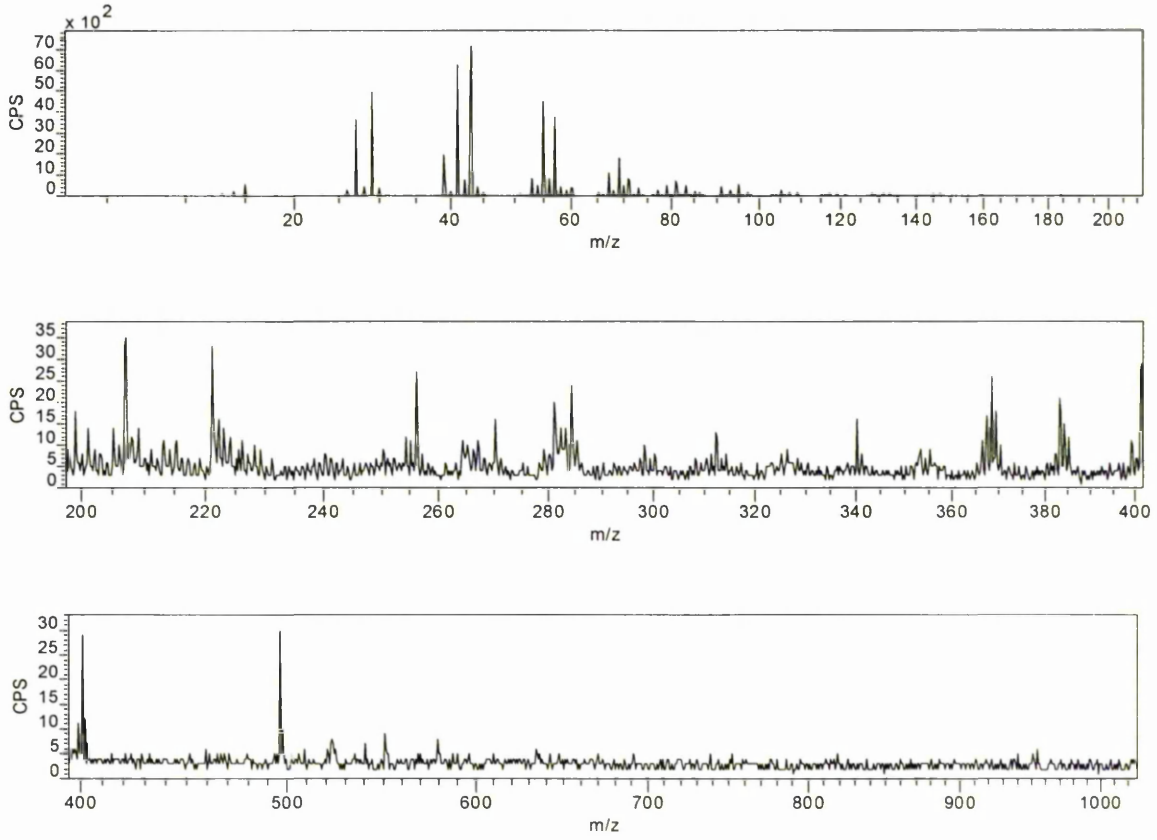

Red/W4 unaged negative ion spectrum : Cs^+ primary ion source

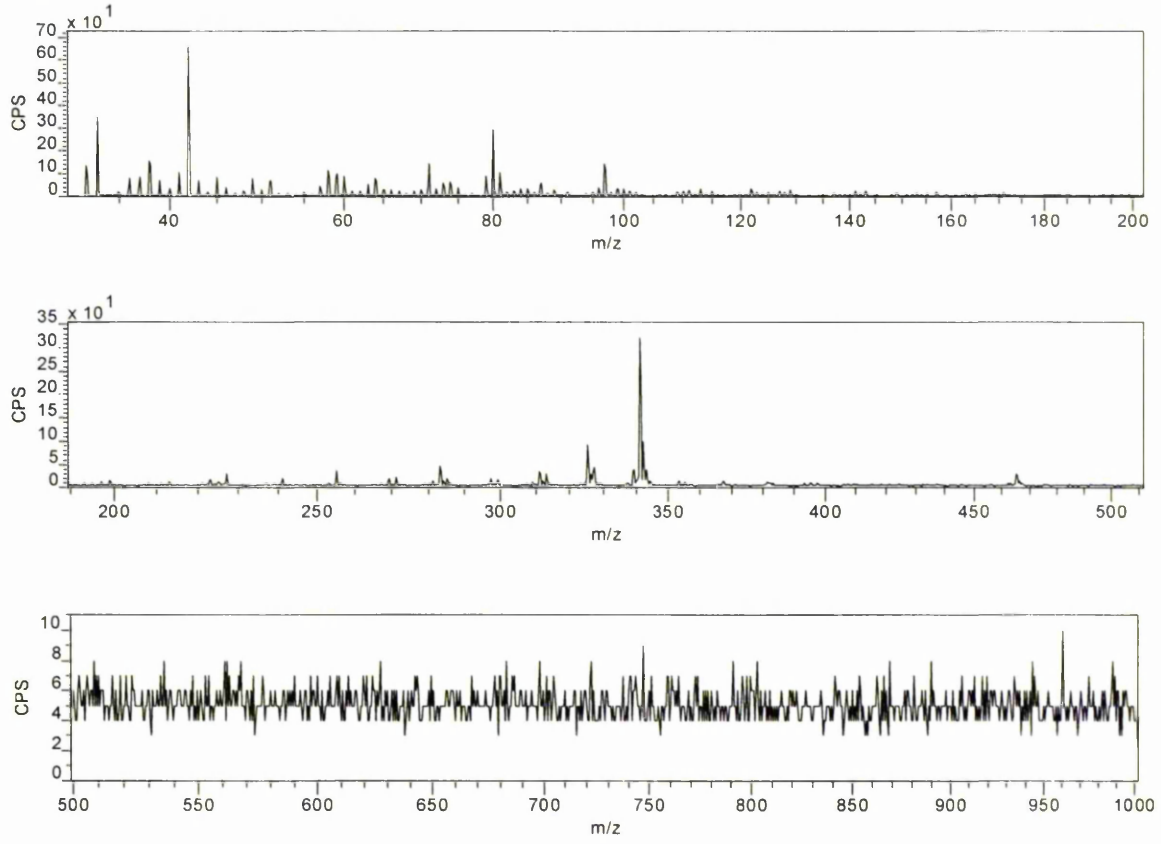

Red/W4 accelerated aged positive ion spectrum : Cs^+ primary ion source

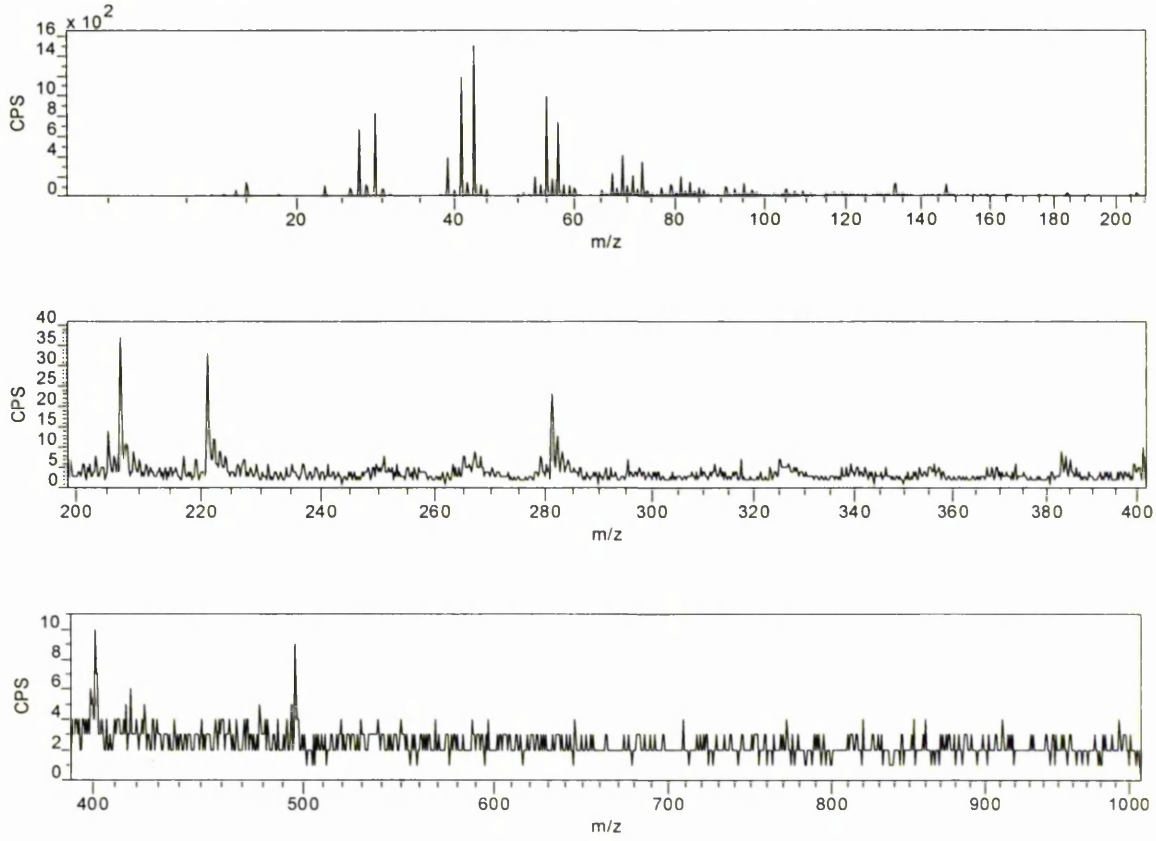

Red/W4 accelerated aged negative ion spectrum : Cs^+ primary ion source

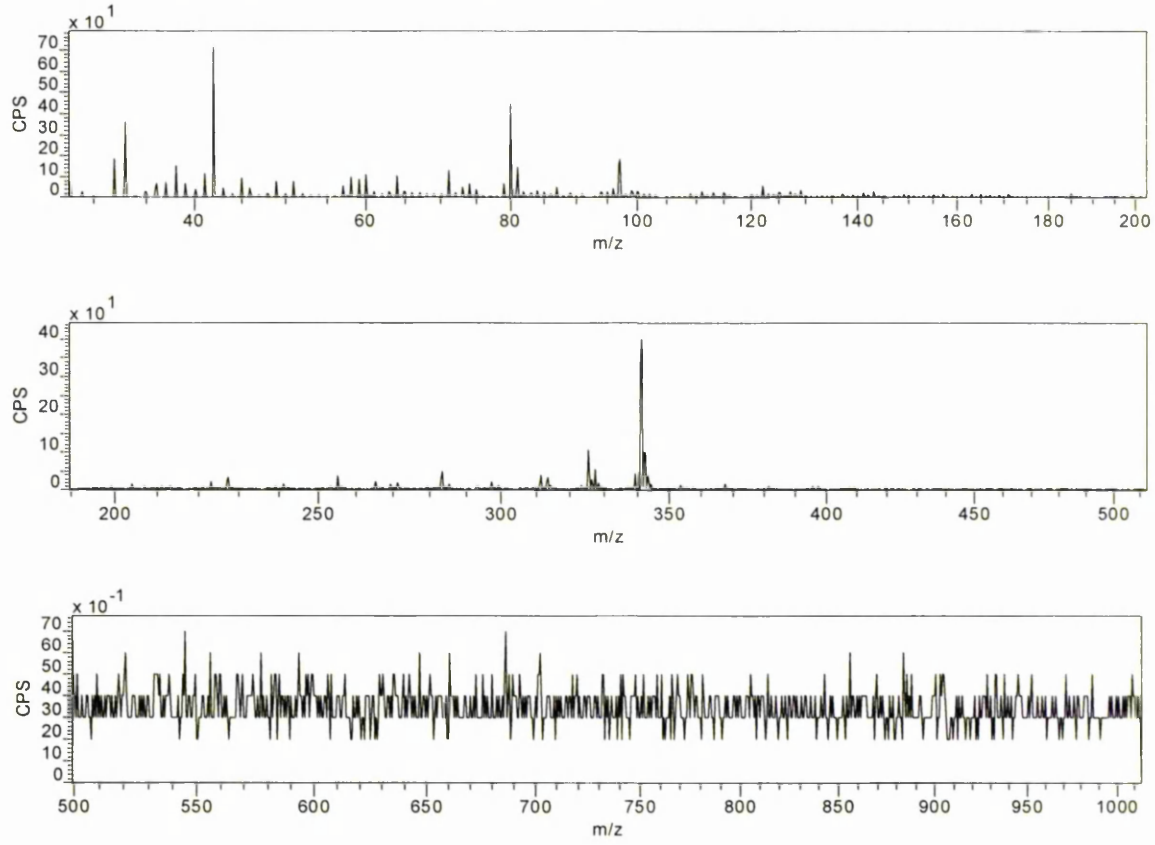

Red/W1 unaged positive ion spectrum : Cs^+ primary ion source

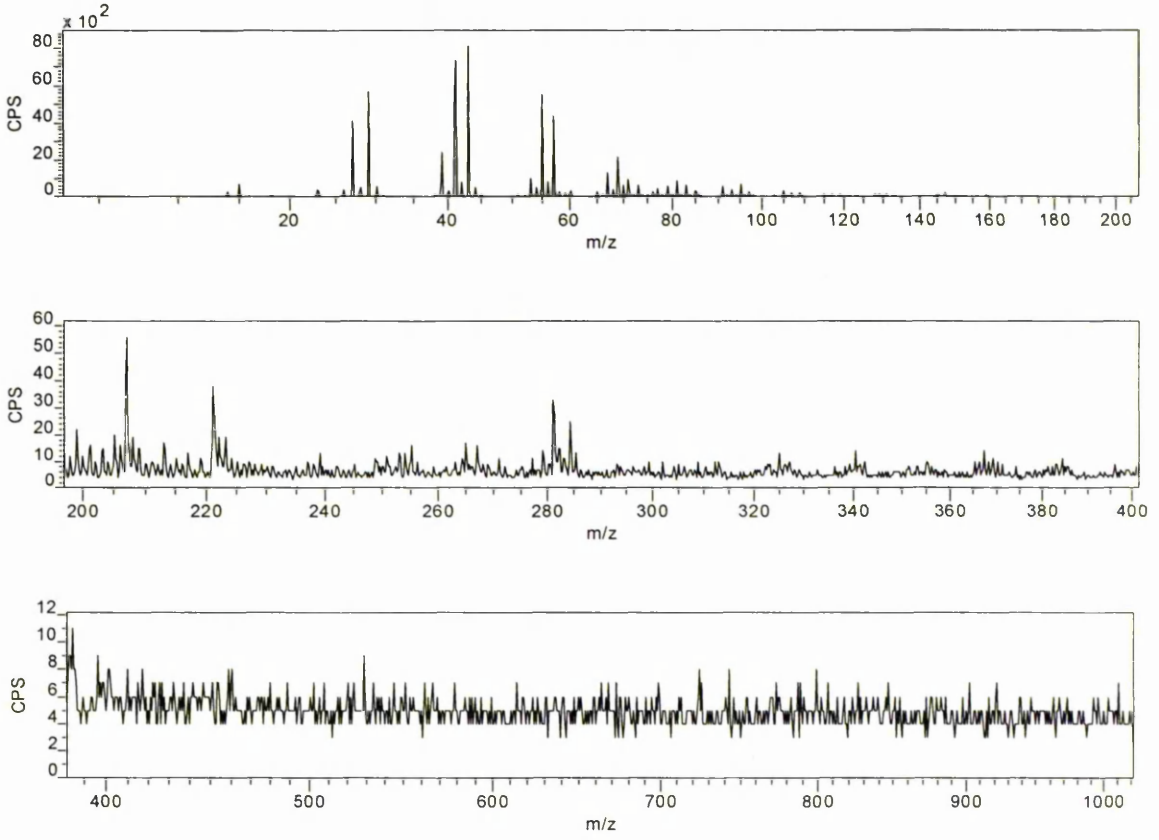

Red/W1 unaged negative ion spectrum : Cs^+ primary ion source

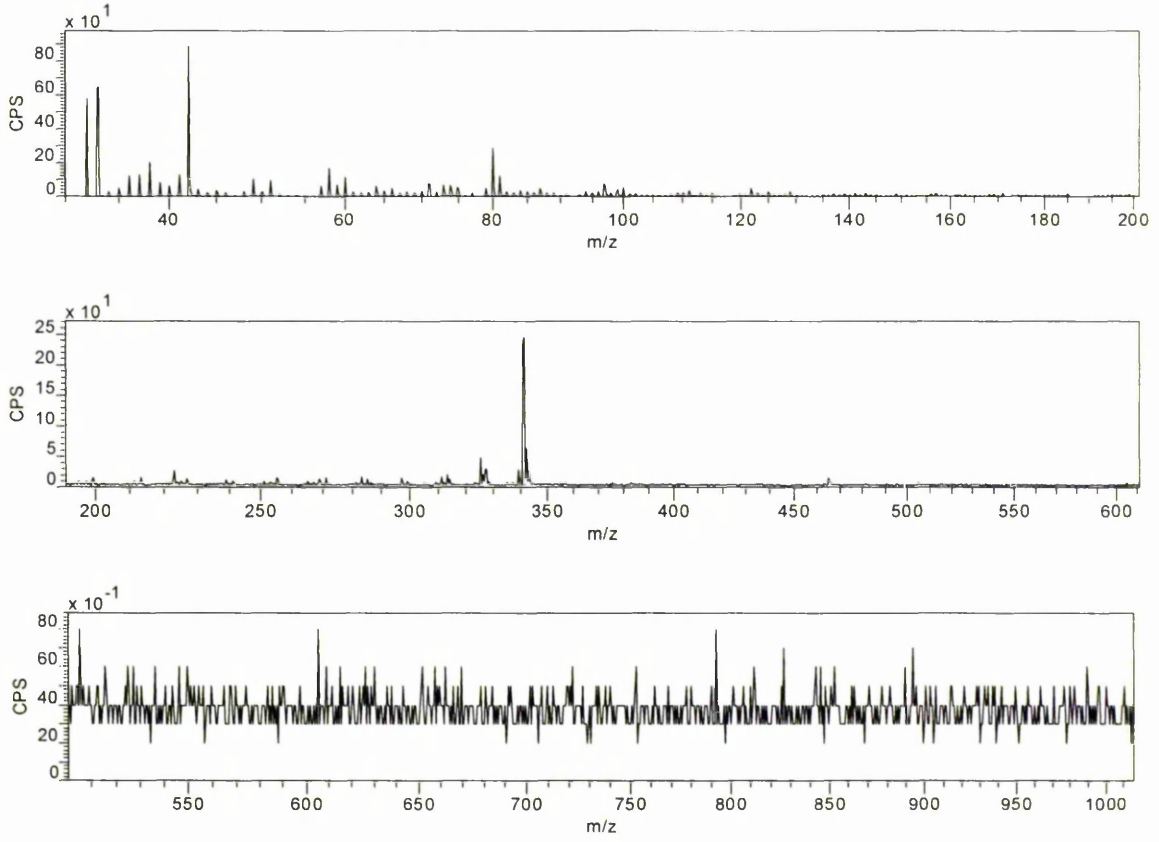

Red/W1_wl unaged positive ion spectrum : Cs^+ primary ion source

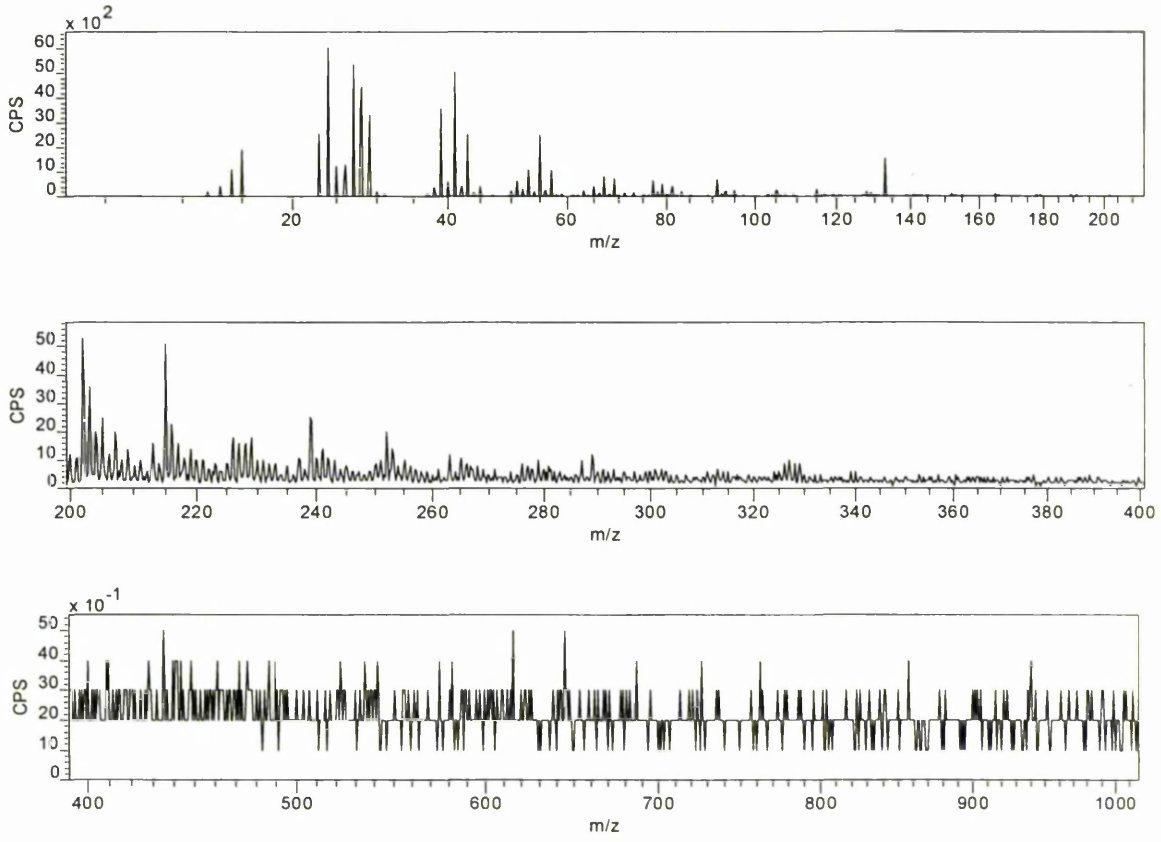

Red/W1_wl unaged negative ion spectrum : Cs^+ primary ion source

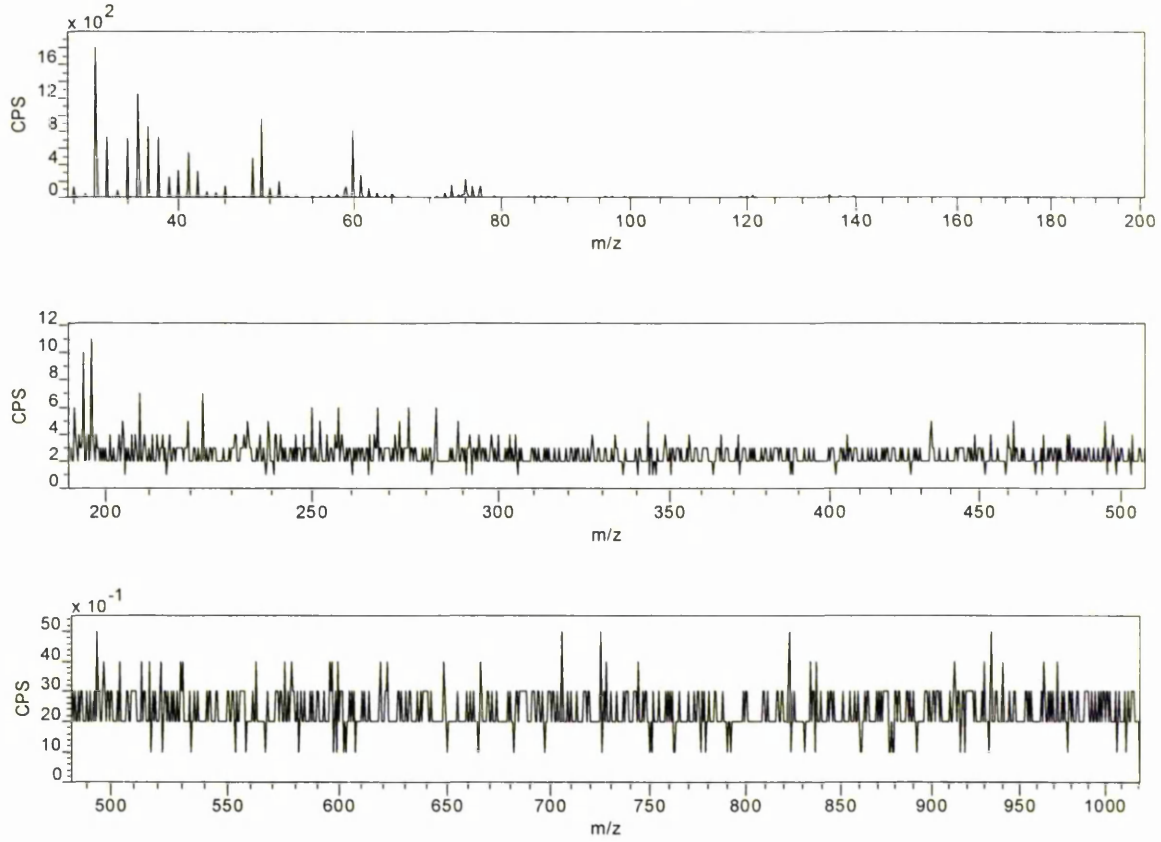

Yellow/W1 unaged positive ion spectrum : Cs^+ primary ion source

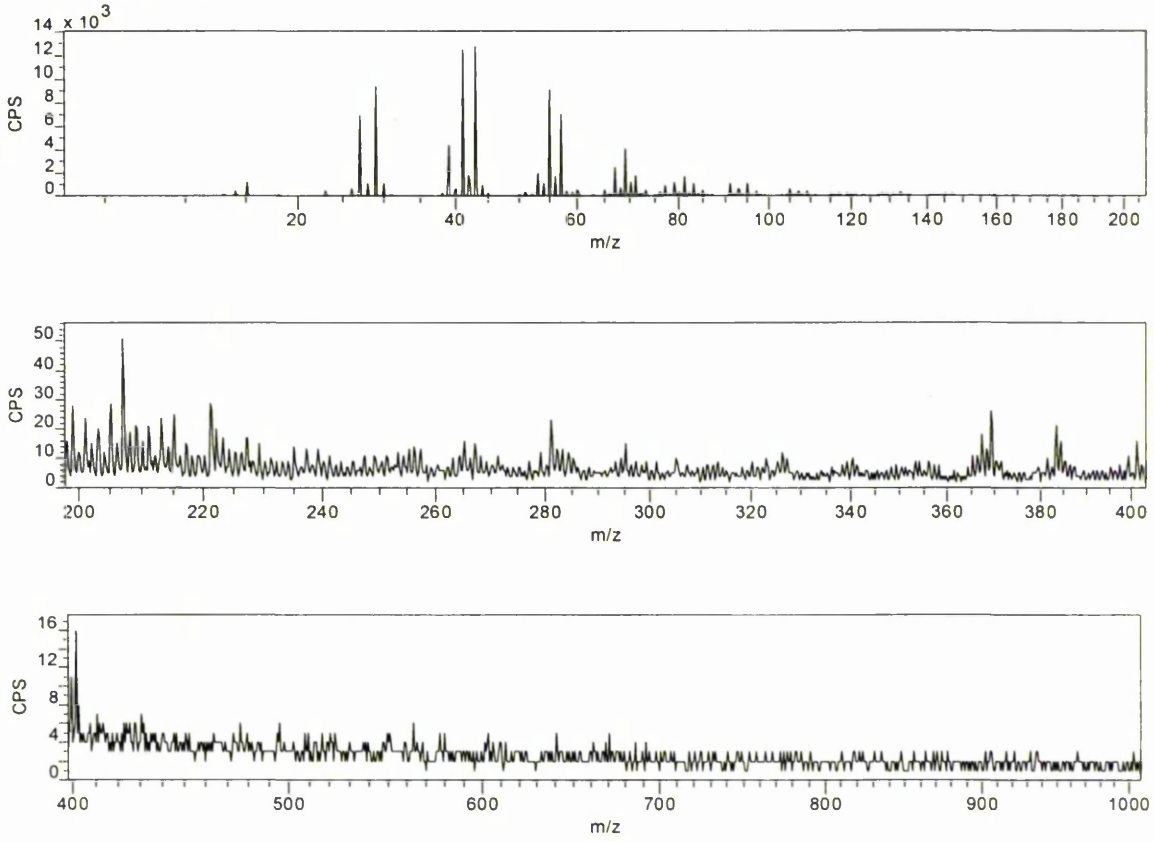

Yellow/W1 unaged negative ion spectrum : Cs^+ primary ion source

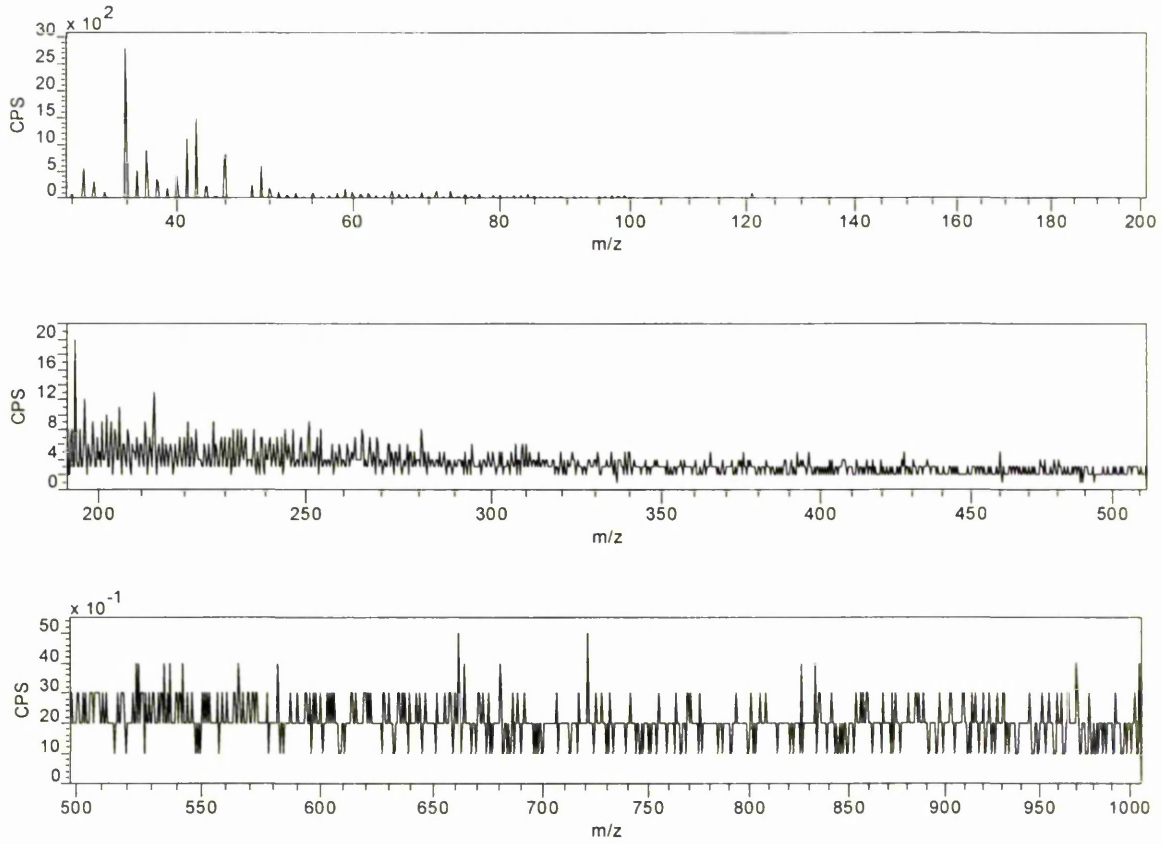

Green/W2 unaged positive ion spectrum : Cs^+ primary ion source

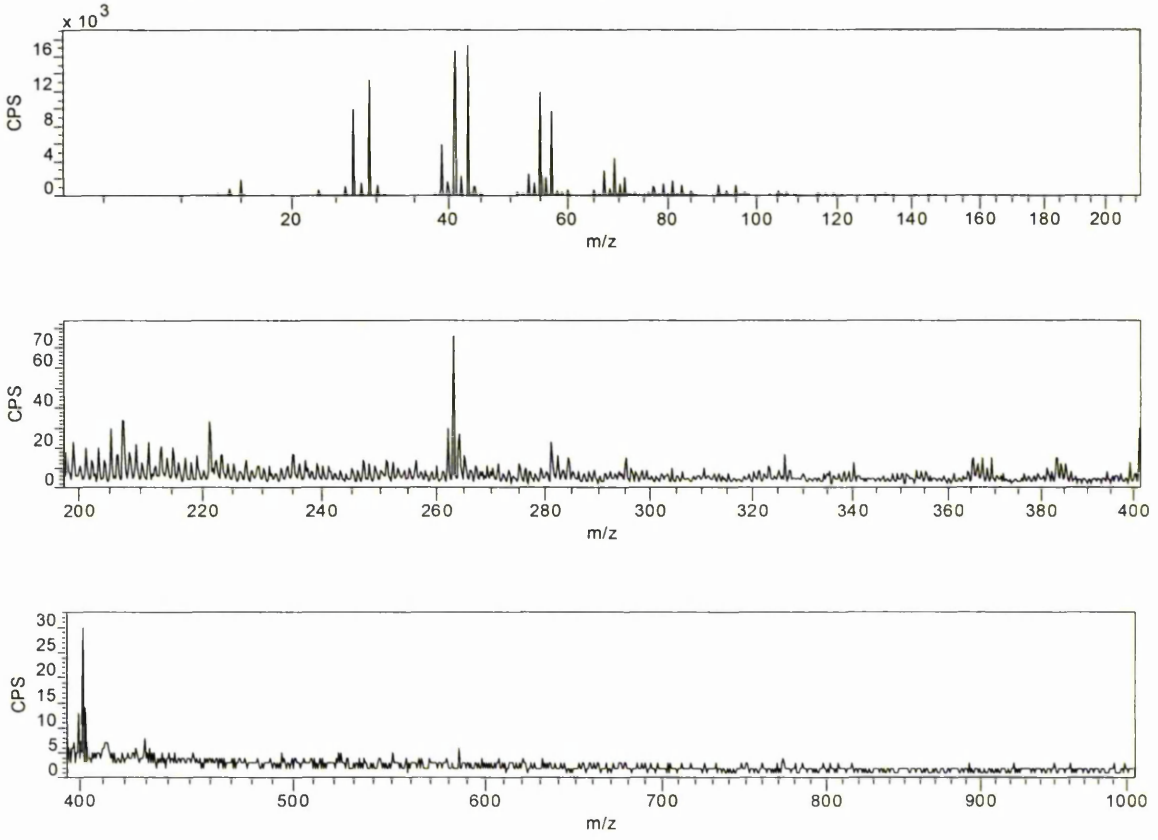

Green/W2 unaged negative ion spectrum : Cs^+ primary ion source

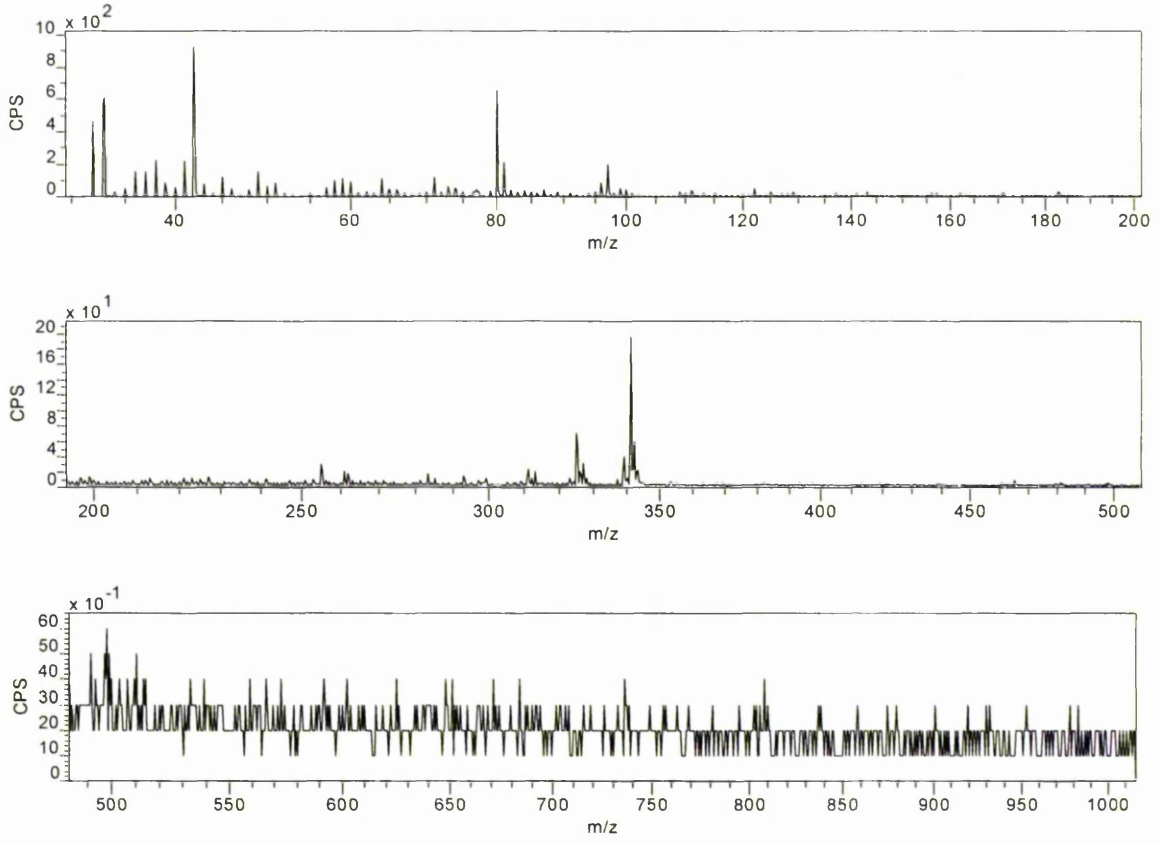

Historic wool HCP_90D4 positive ion spectrum : Cs^+ primary ion source

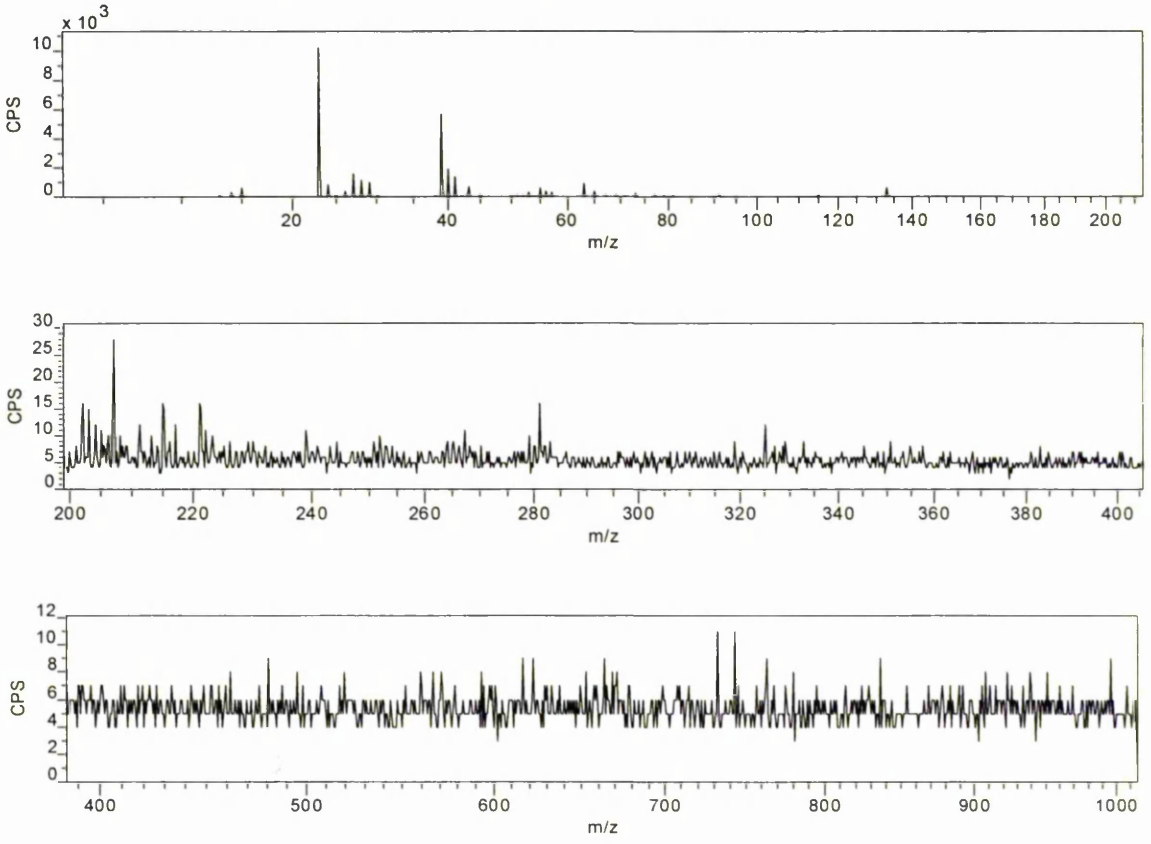

Historic wool HCP_90D4 negative ion spectrum : Cs^+ primary ion source

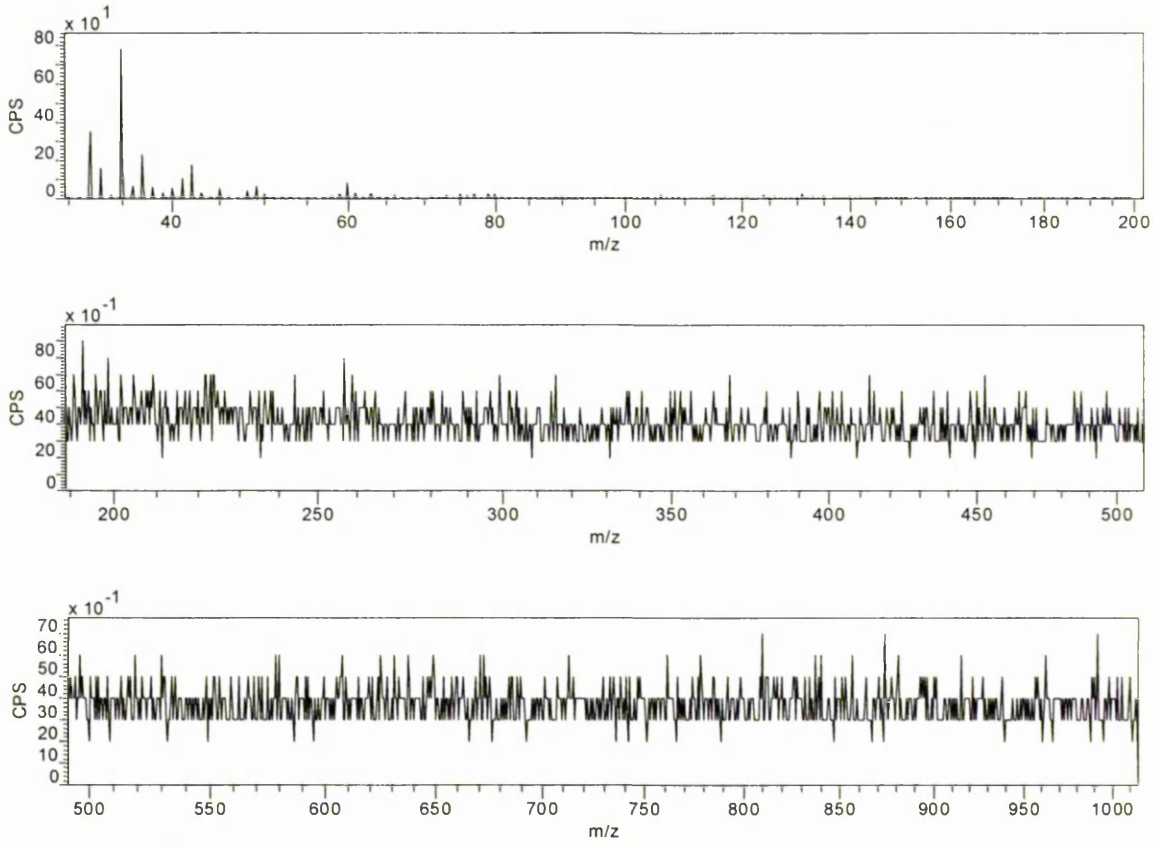

Historic wool HRP2_61 positive ion spectrum : Cs^+ primary ion source

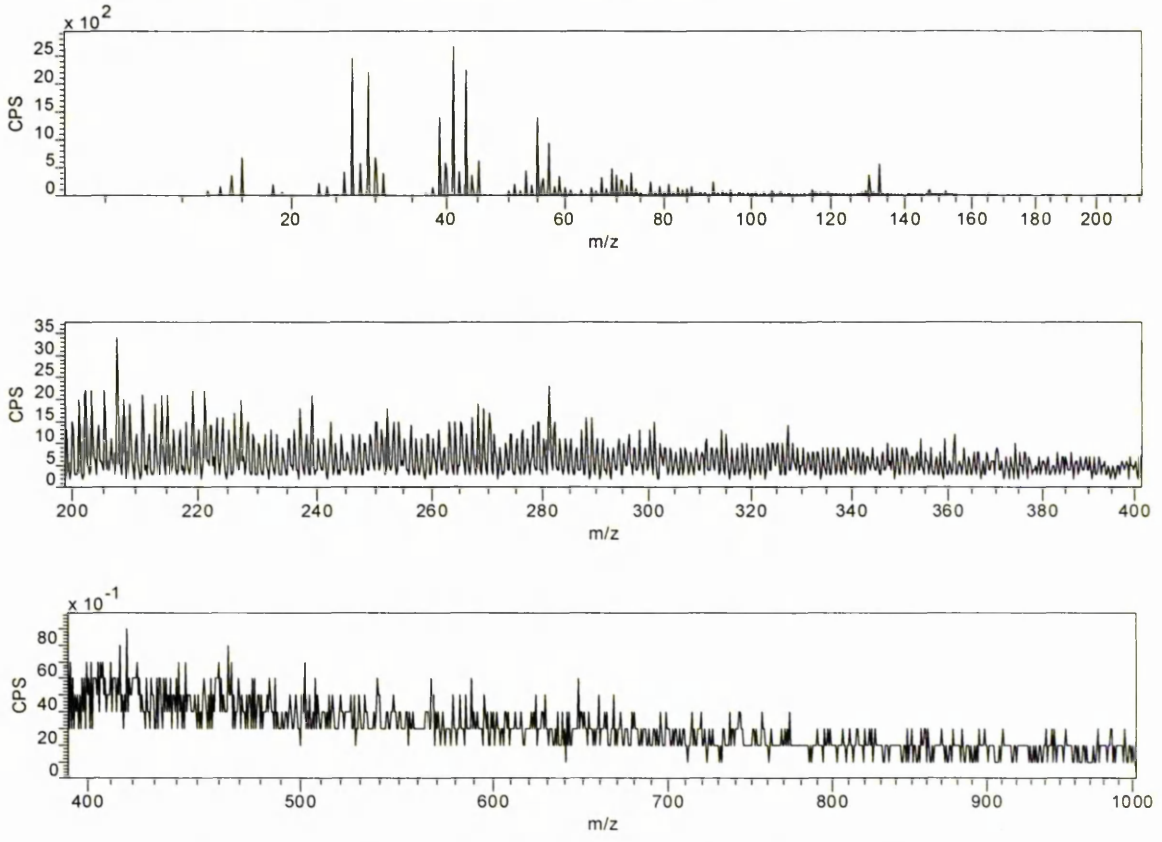

Historic wool HRP2_61 negative ion spectrum : Cs^+ primary ion source

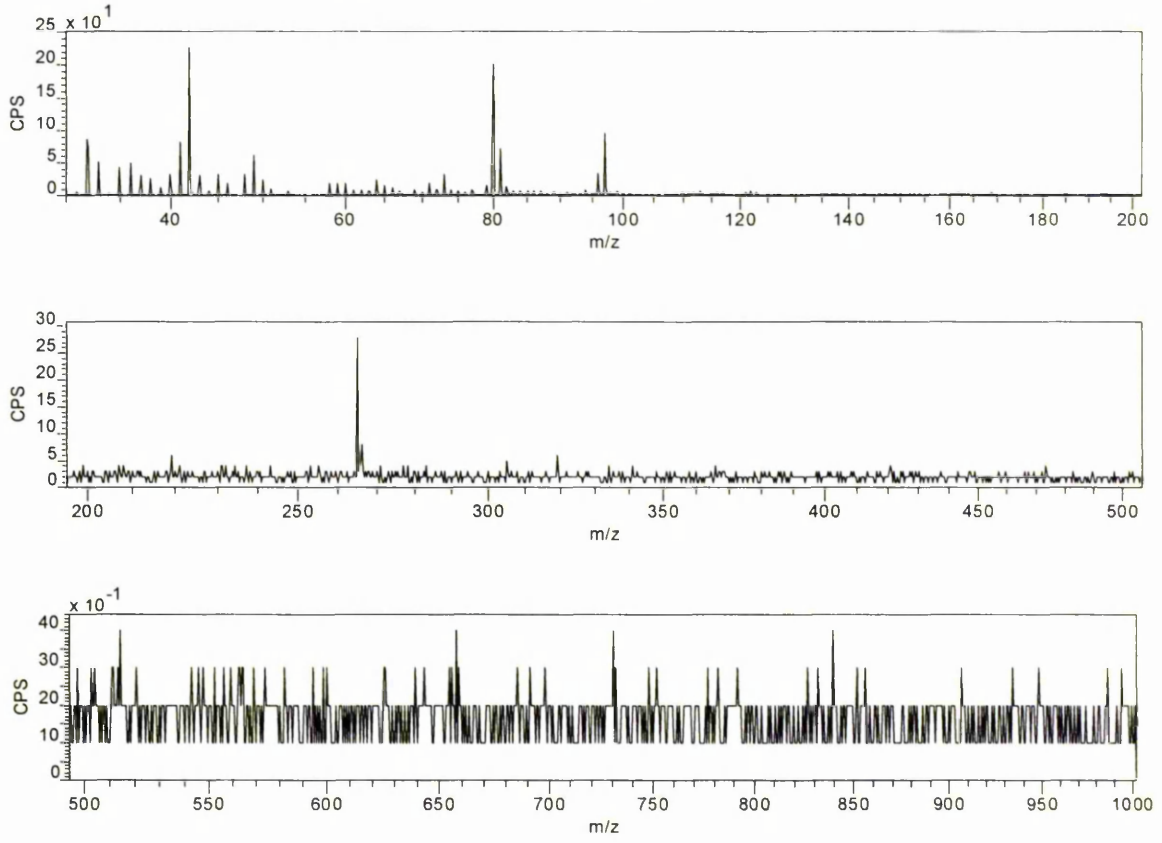

Historic wool HRP1_21 positive ion spectrum : Cs^+ primary ion source

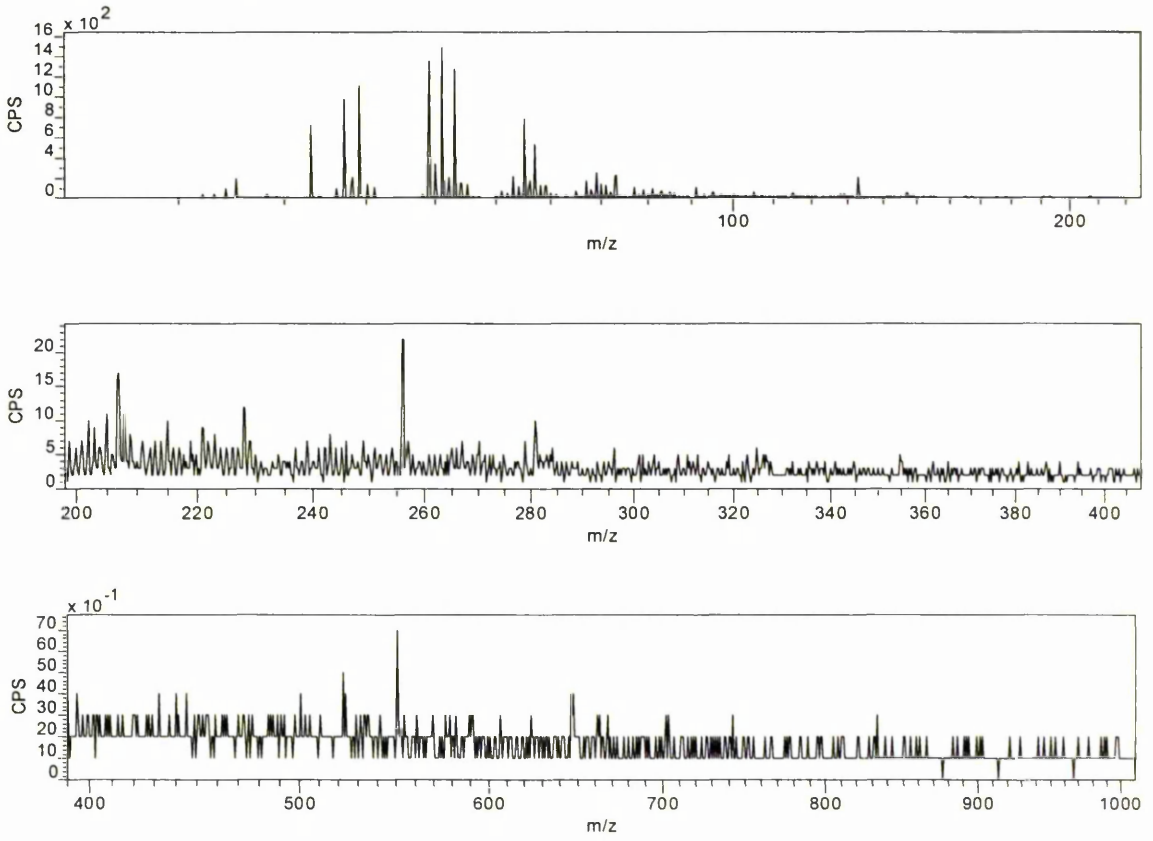

Historic wool HRP1_21 negative ion spectrum : Cs^+ primary ion source

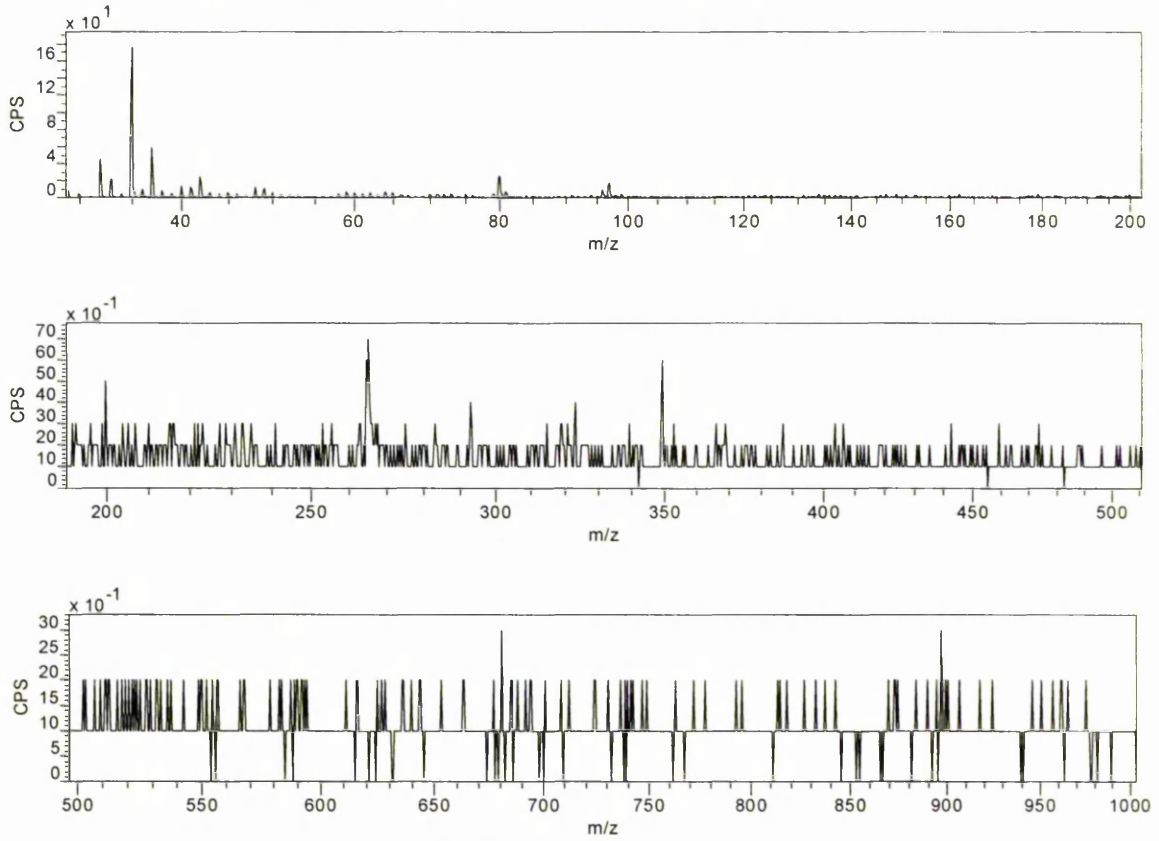

E.2. Spectra acquired with a Bi_3^+ primary ion source

Undyed wool unaged positive ion spectrum : Bi_3^+ primary ion source

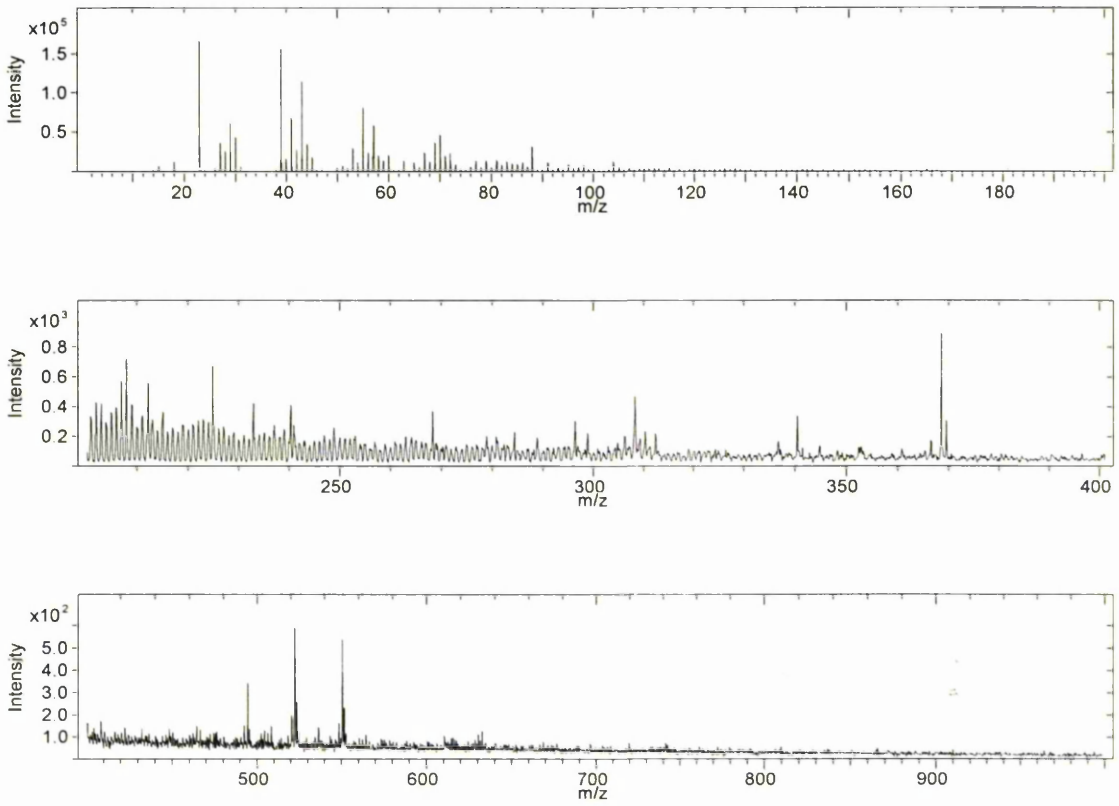

Undyed wool unaged negative ion spectrum : Bi_3^+ primary ion source

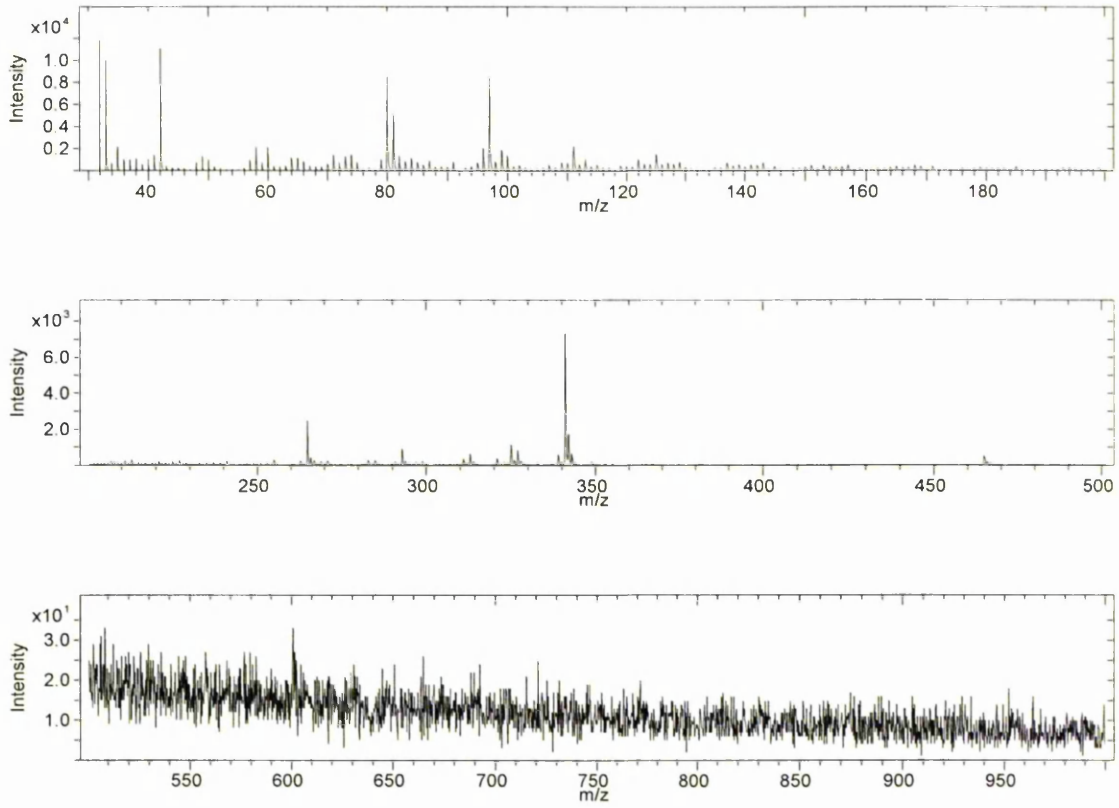

Undyed wool accelerated aged positive ion spectrum : Bi_3^+ primary ion source

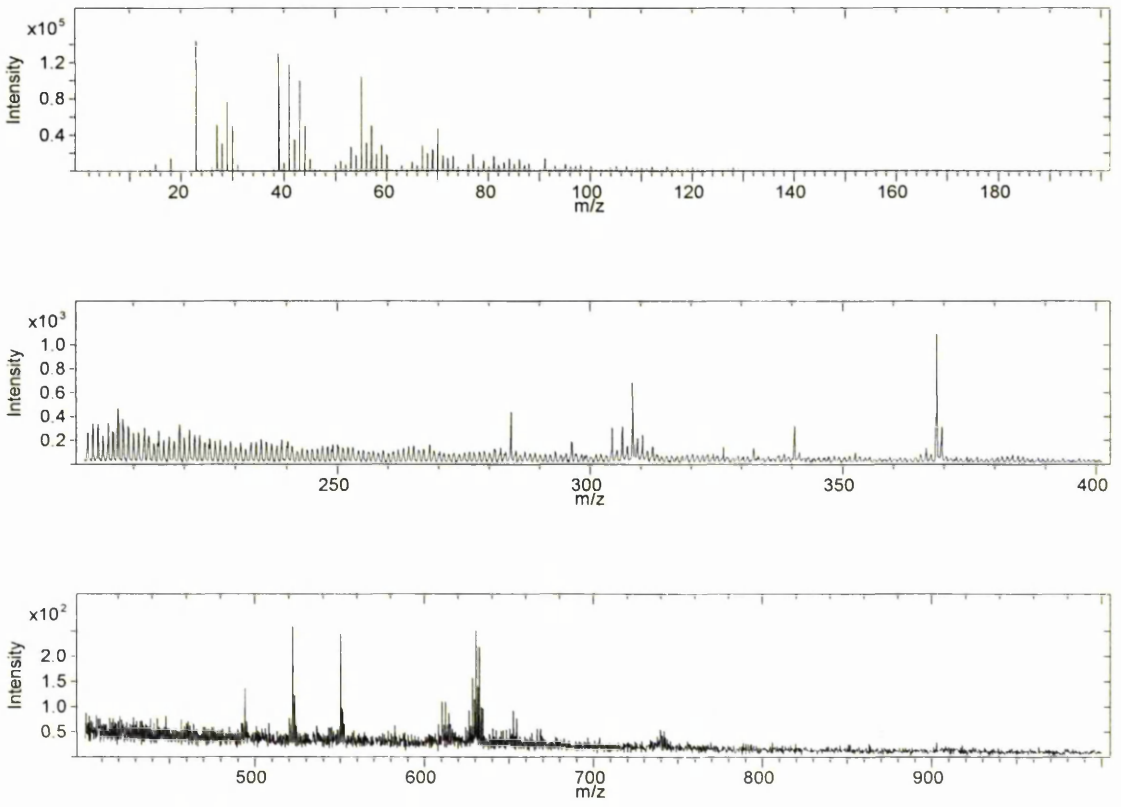

Undyed wool accelerated aged negative ion spectrum : Bi_3^+ primary ion source

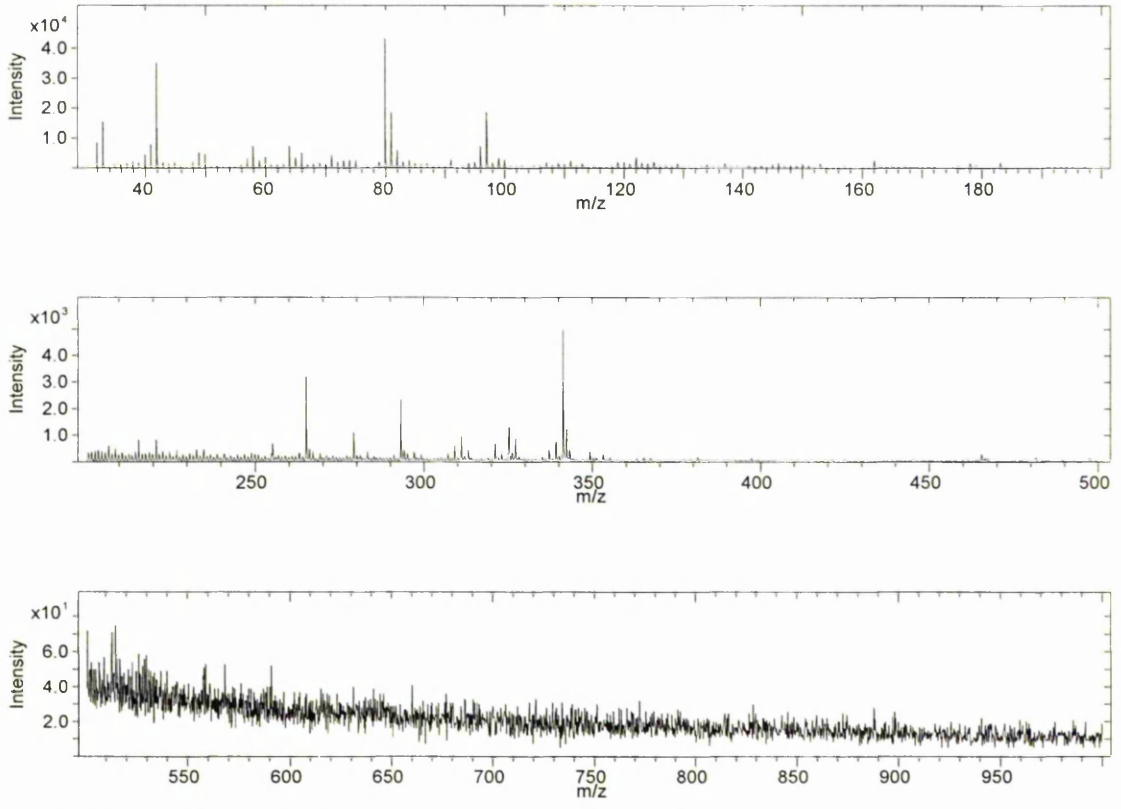

Yellow/W1 unaged positive ion spectrum : Bi_3^+ primary ion source

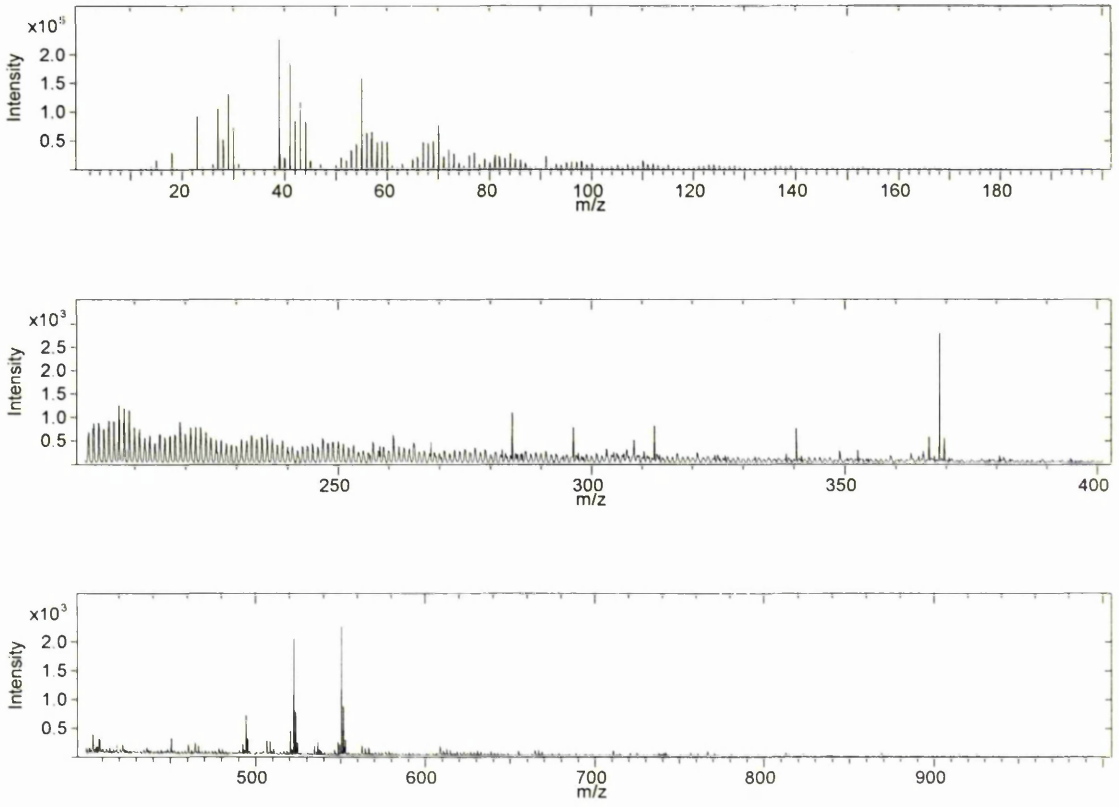

Yellow/W1 unaged negative ion spectrum : Bi_3^+ primary ion source

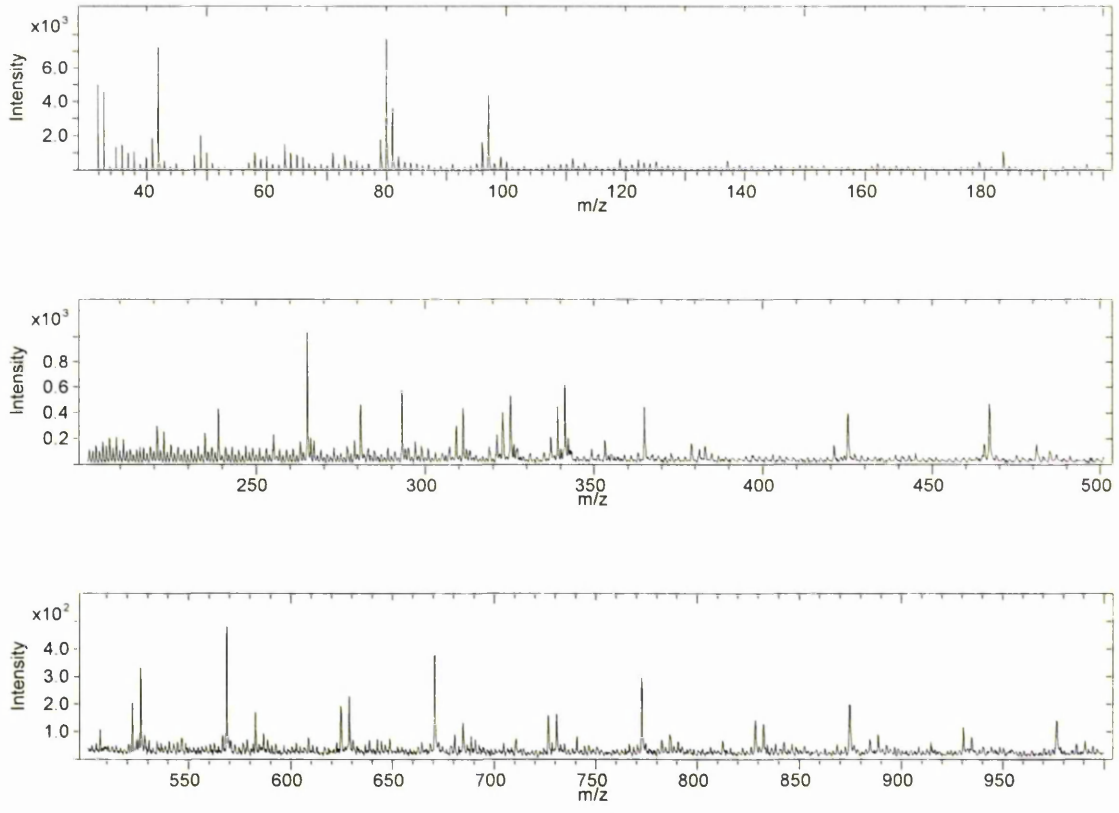

Yellow/W1 accelerated aged positive ion spectrum : Bi_3^+ primary ion source

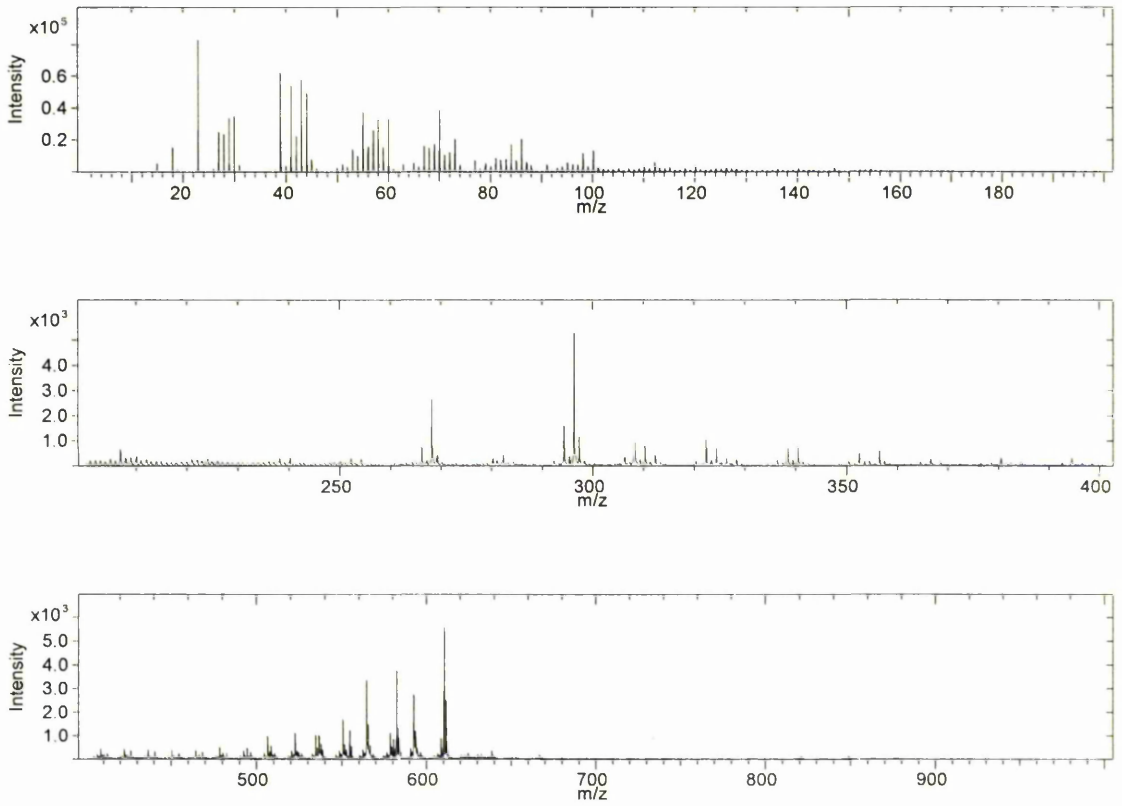

Yellow/W1 accelerated aged negative ion spectrum : Bi_3^+ primary ion source

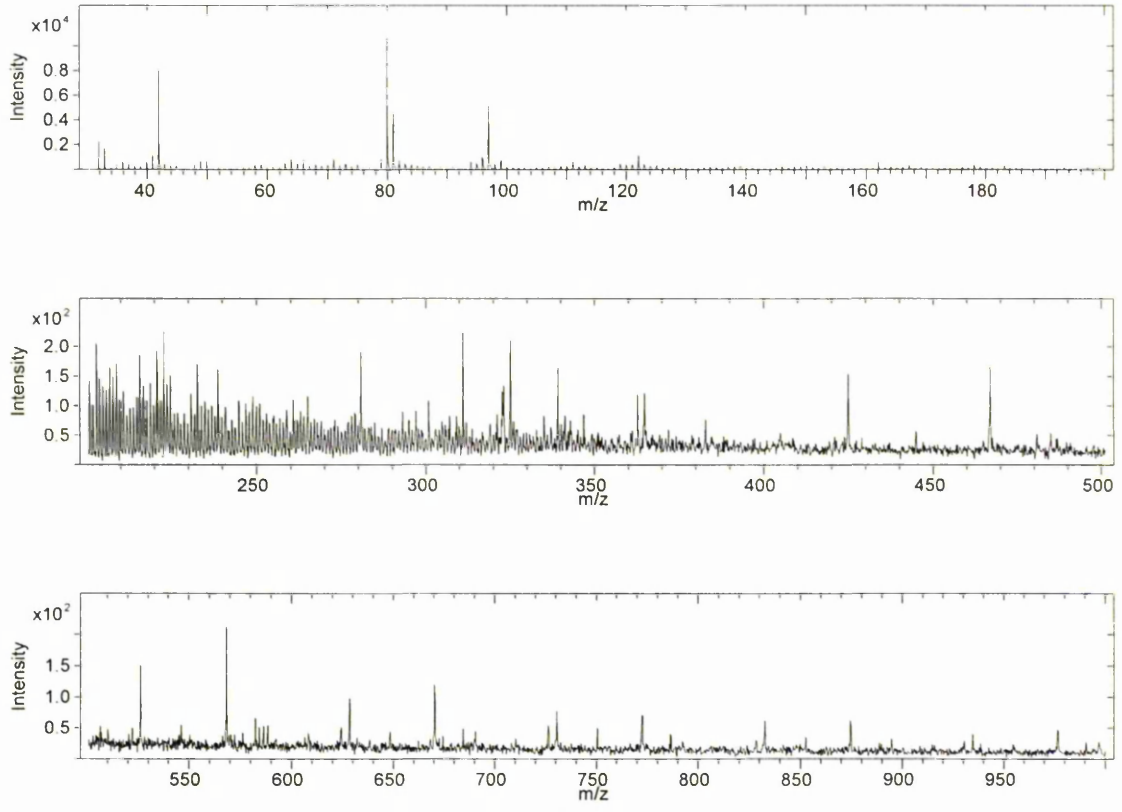

Red/W1_wl unaged positive ion spectrum : Bi_3^+ primary ion source

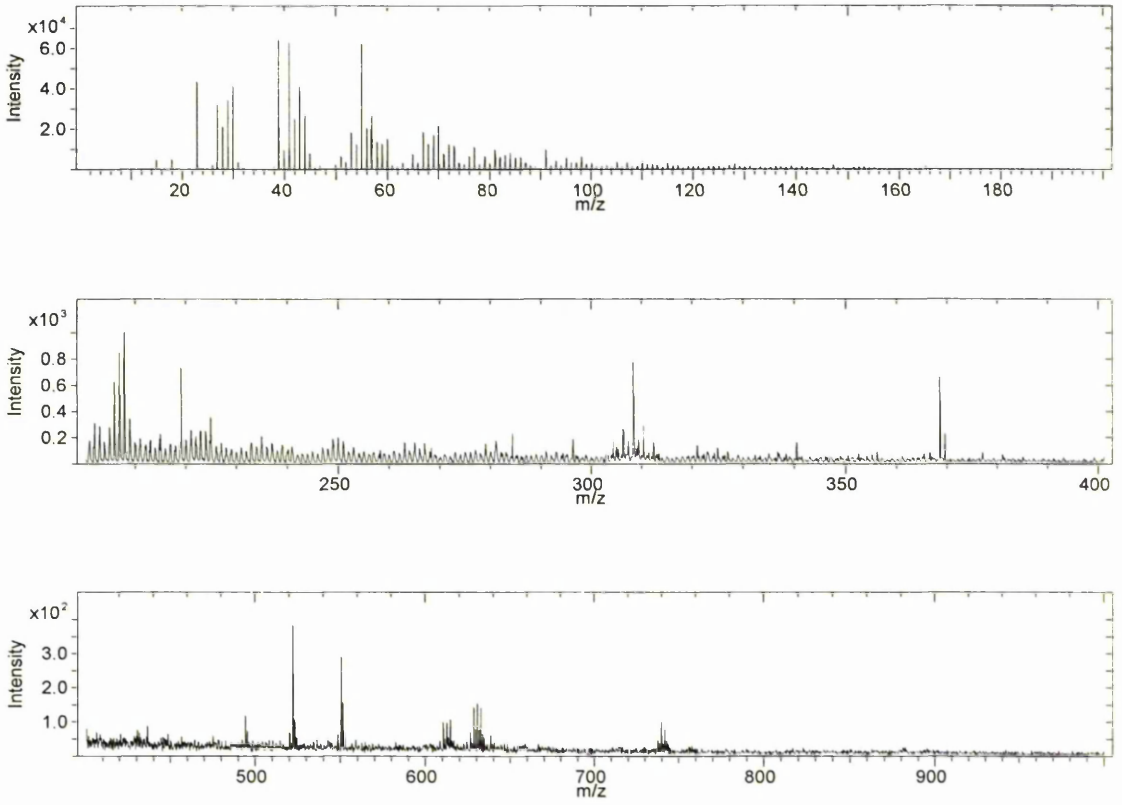

Red/W1_wl unaged negative ion spectrum : Bi_3^+ primary ion source

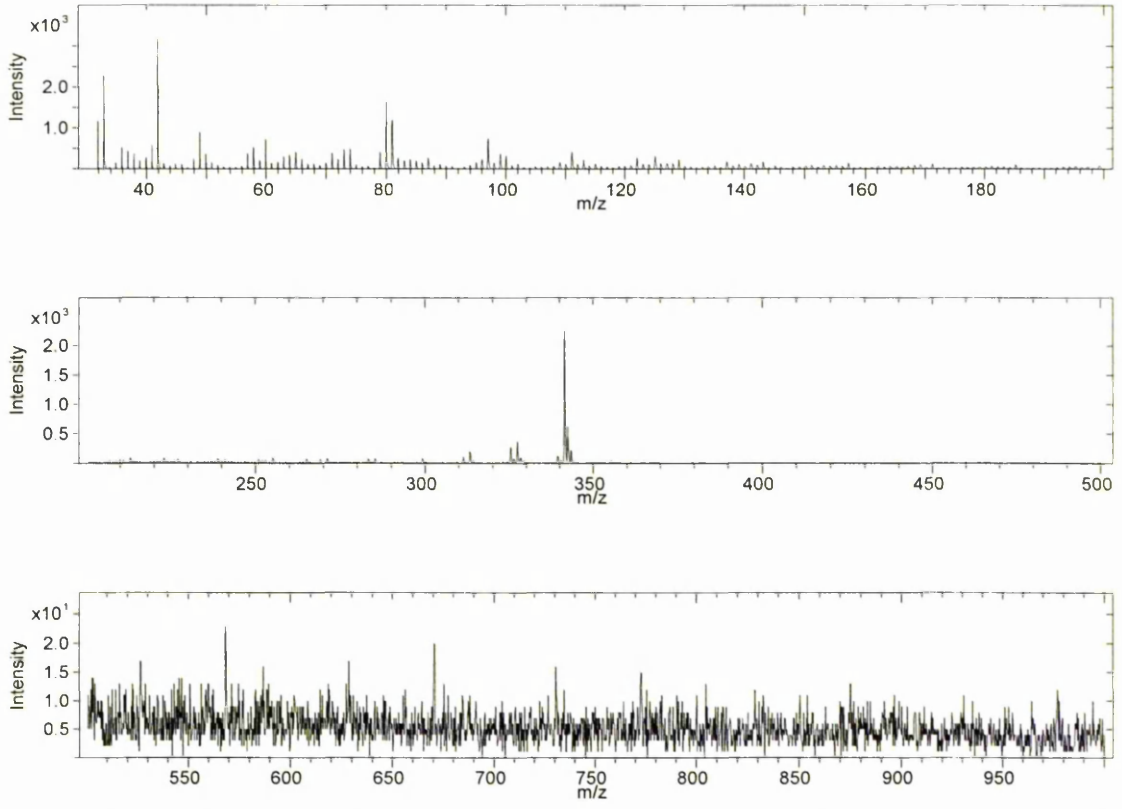

Red/W1_wl accelerated aged positive ion spectrum : Bi_3^+ primary ion source

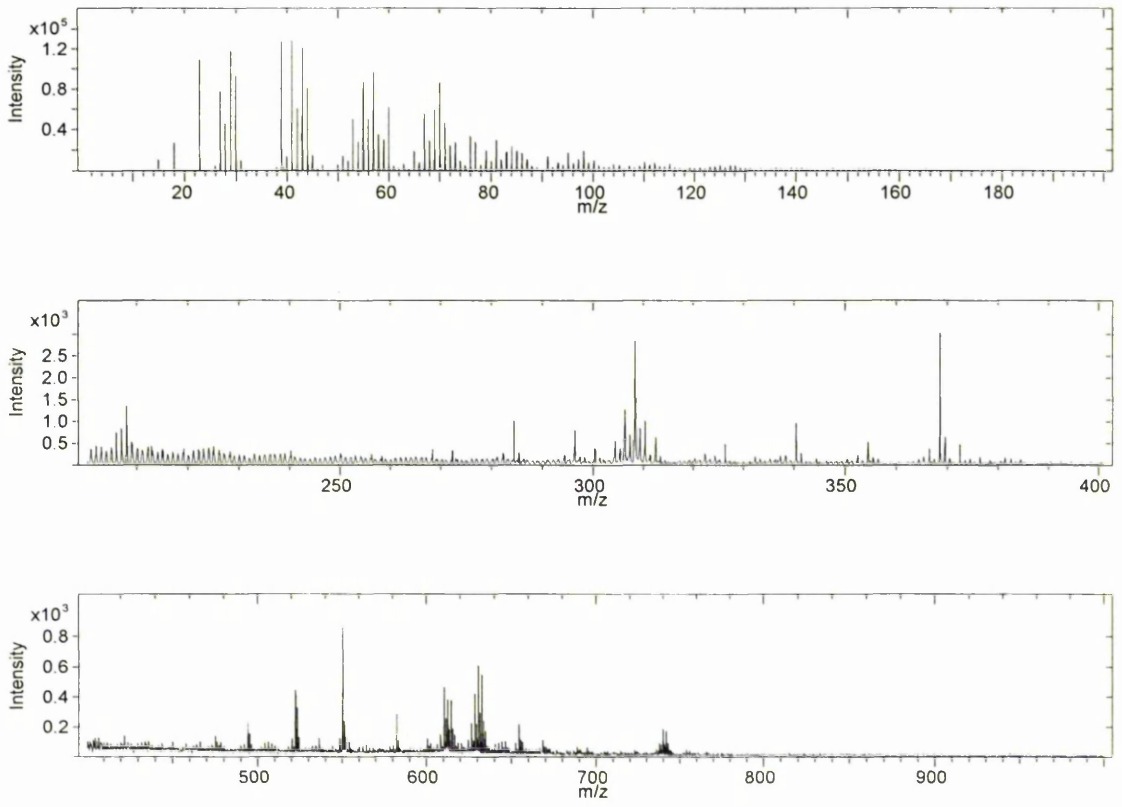

Red/W1_wl accelerated aged negative ion spectrum : Bi_3^+ primary ion source

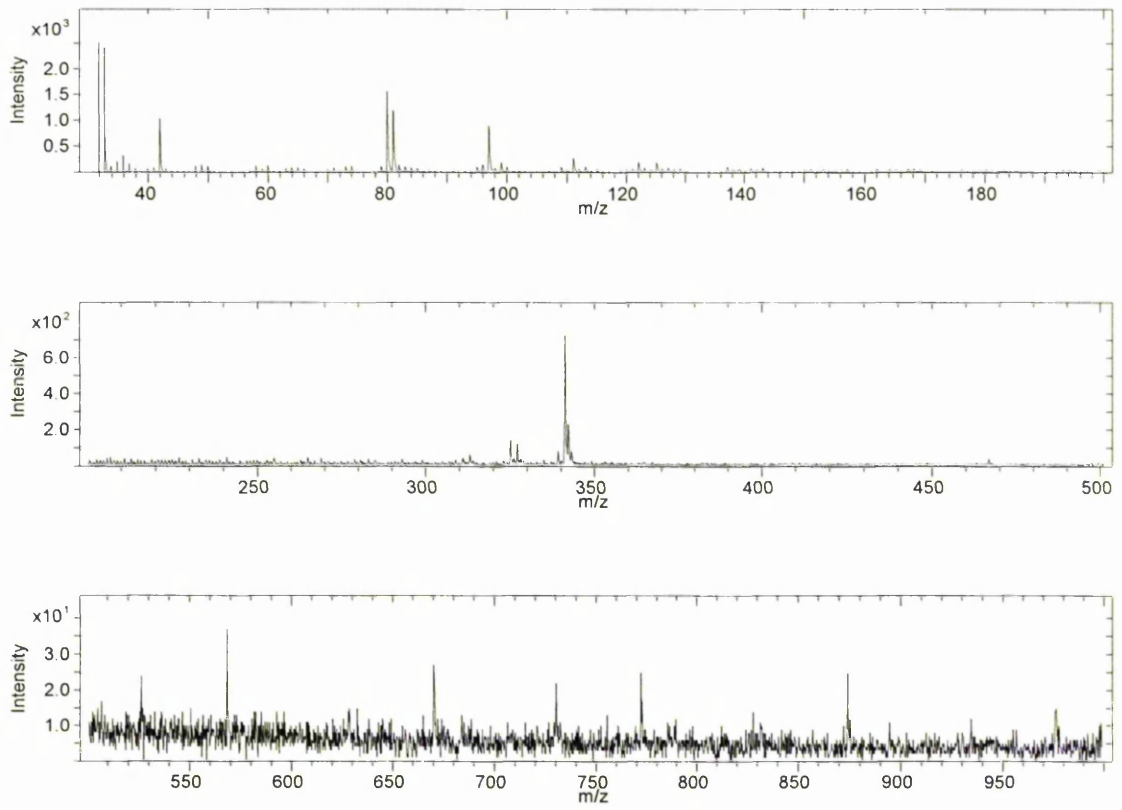

Red/W1 accelerated aged positive ion spectrum : Bi_3^+ primary ion source

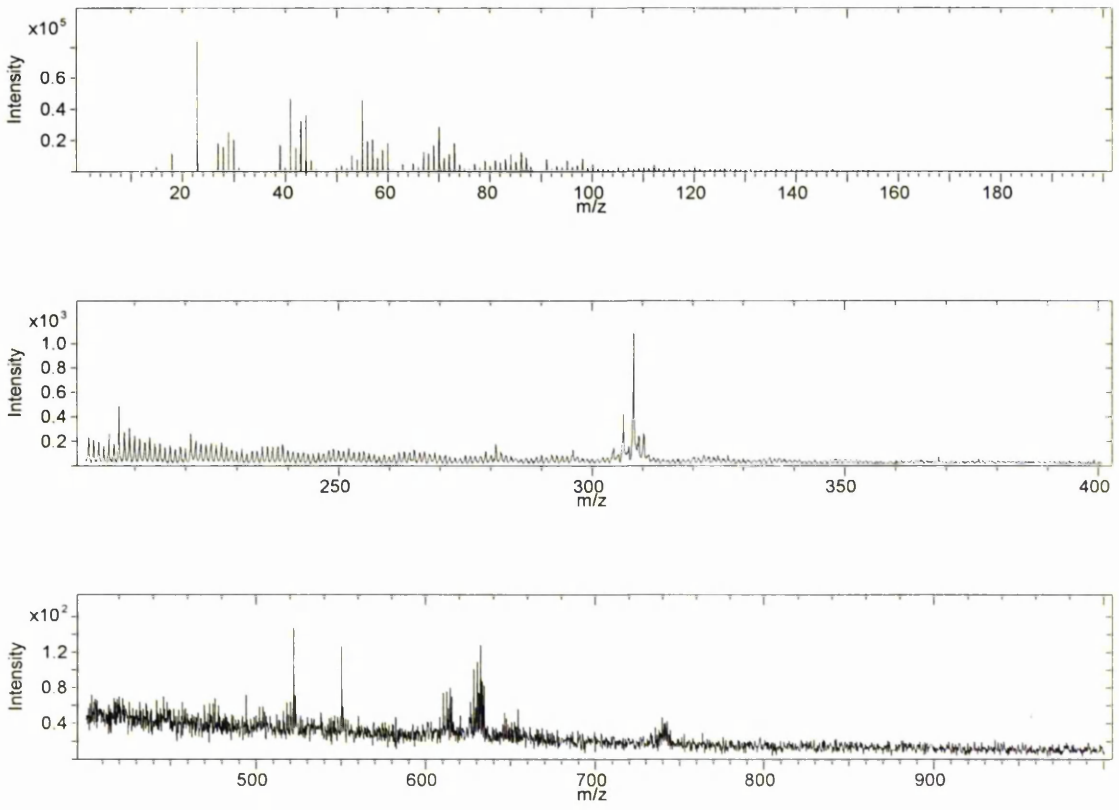

Red/W1 accelerated aged negative ion spectrum : Bi_3^+ primary ion source

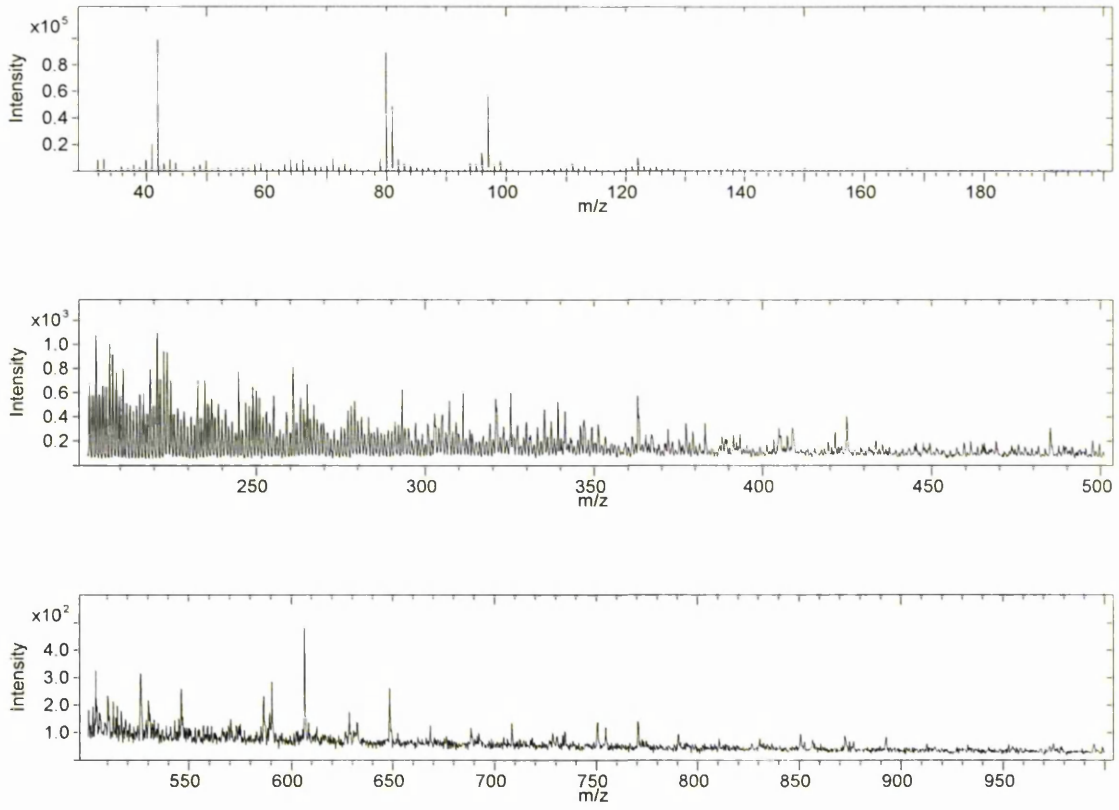

Green/W2 accelerated aged positive ion spectrum : Bi_3^+ primary ion source

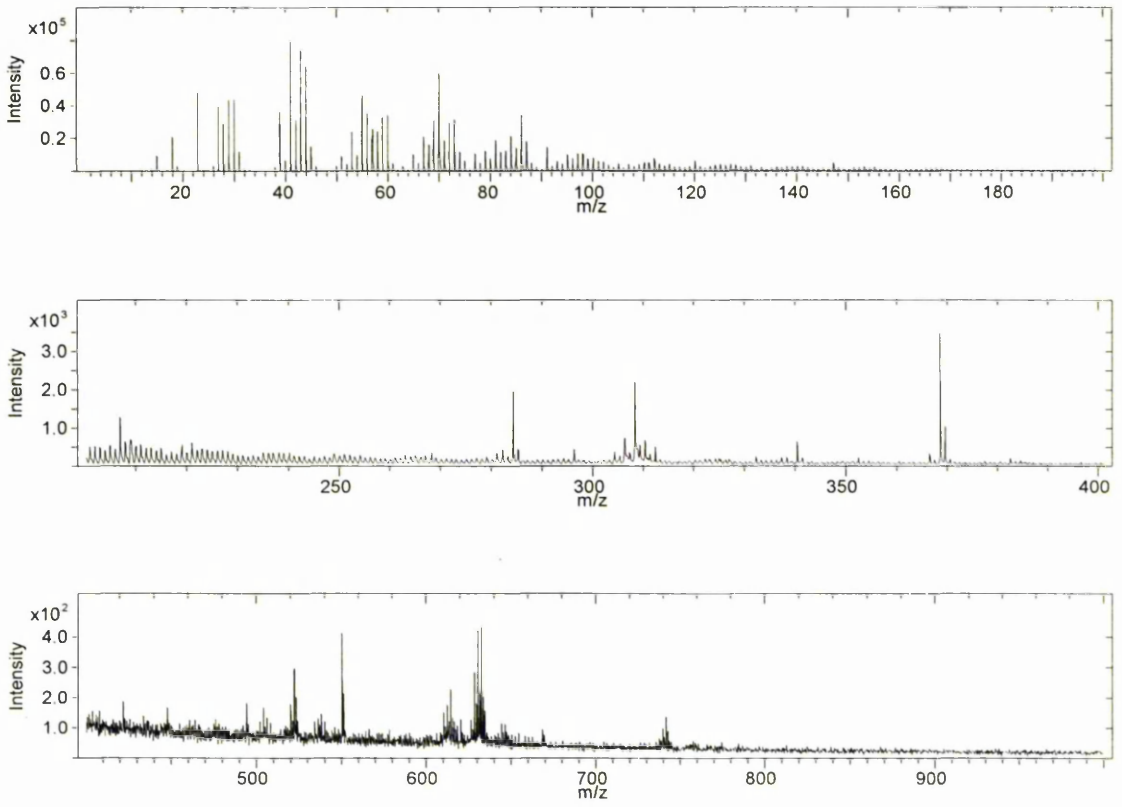

Green/W2 accelerated aged negative ion spectrum : Bi_3^+ primary ion source

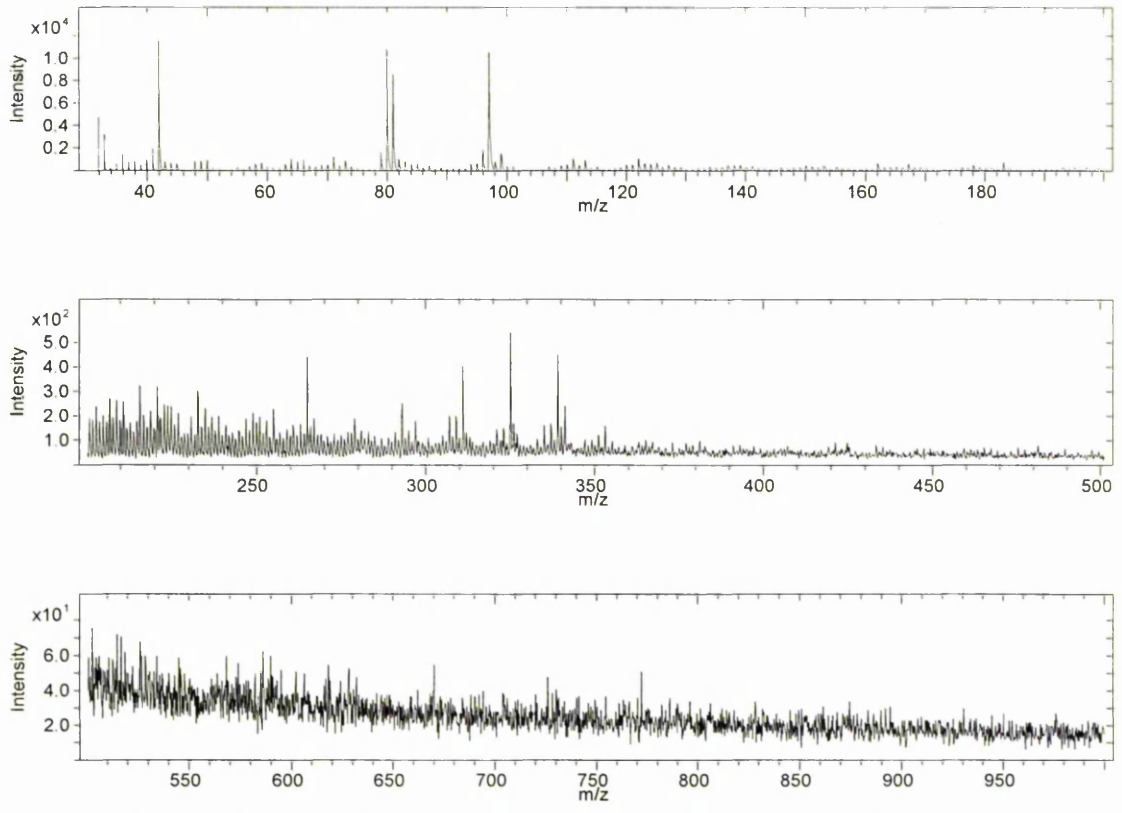

Historic wool HRP1_1 positive ion spectrum : Bi_3^+ primary ion source

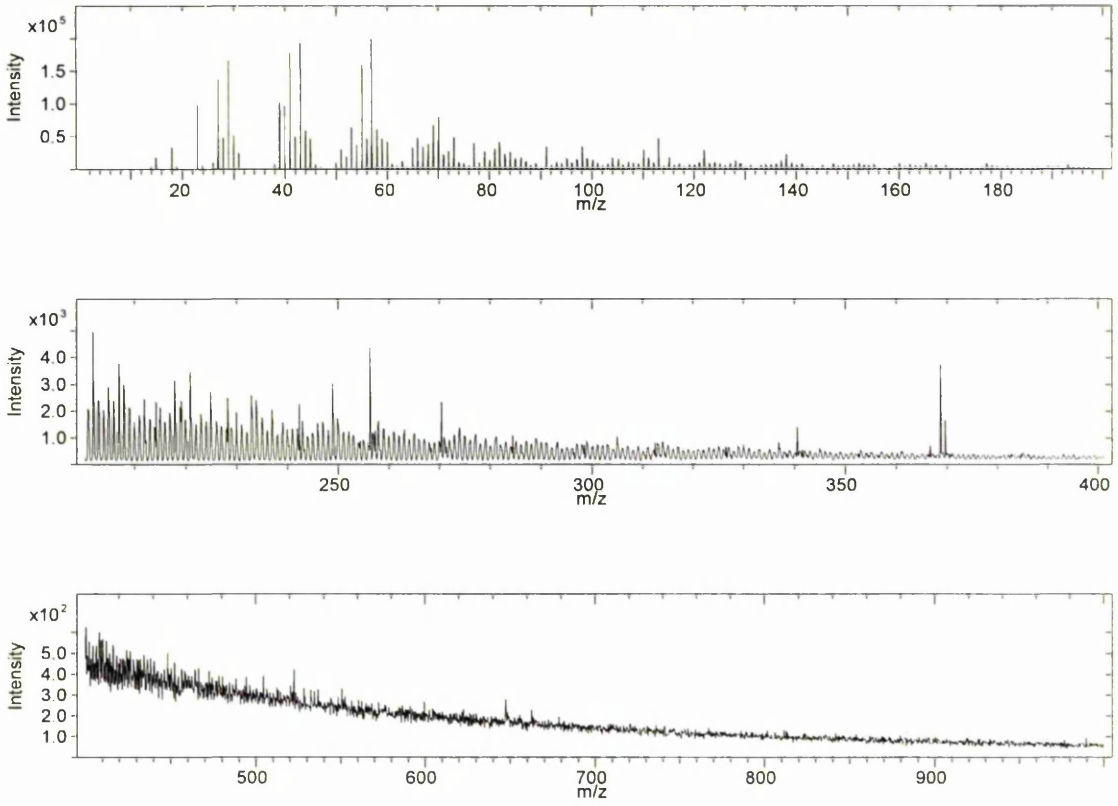

Historic wool HRP1_1 negative ion spectrum : Bi_3^+ primary ion source

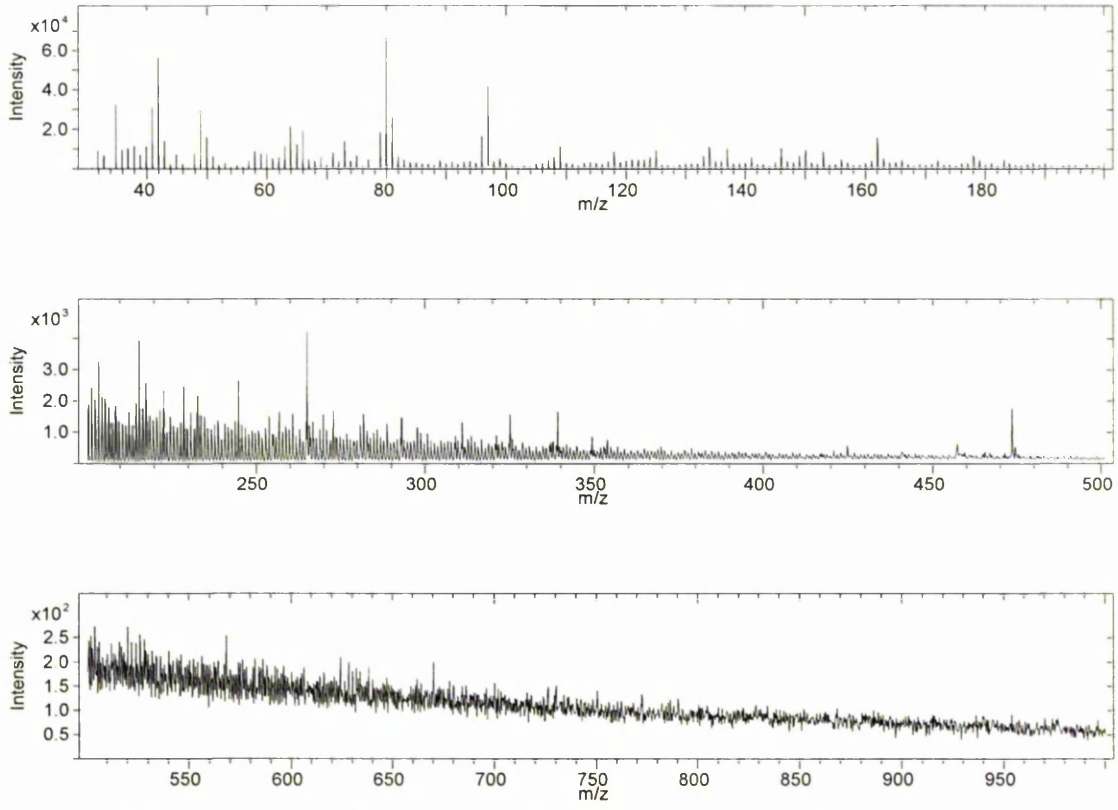

Historic wool HCP_115C4 positive ion spectrum : Bi_3^+ primary ion source

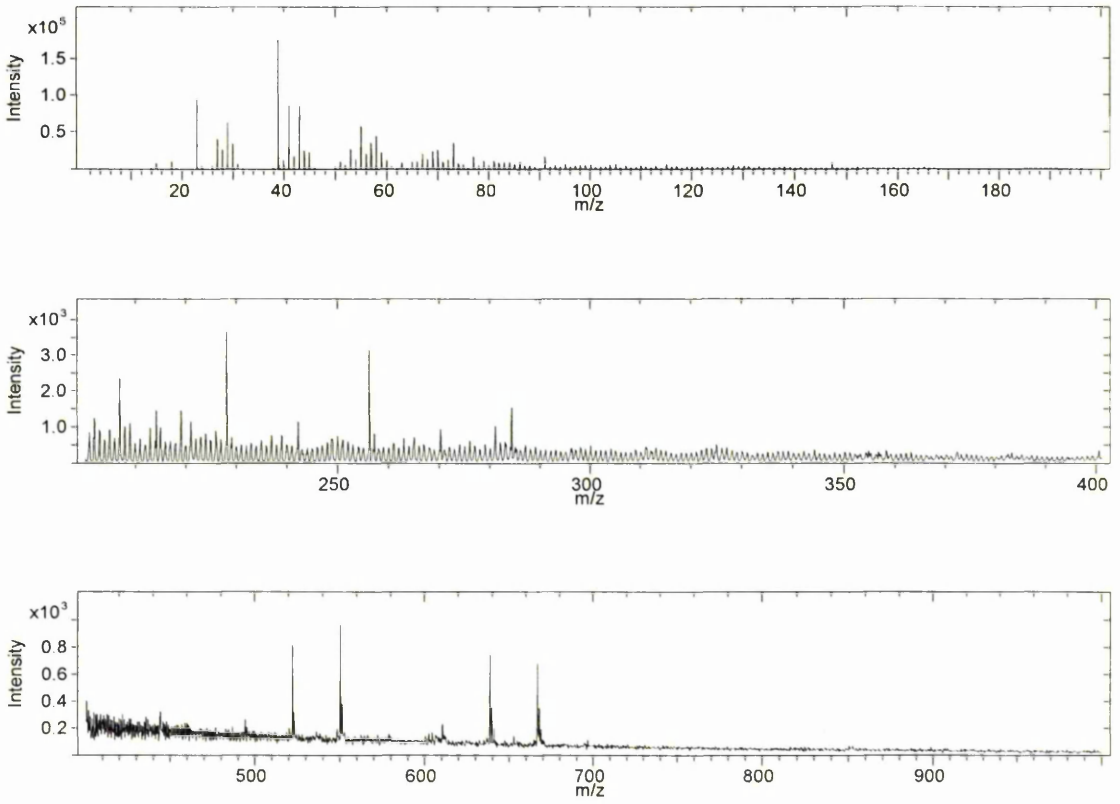

Historic wool HCP_115C4 negative ion spectrum : Bi_3^+ primary ion source

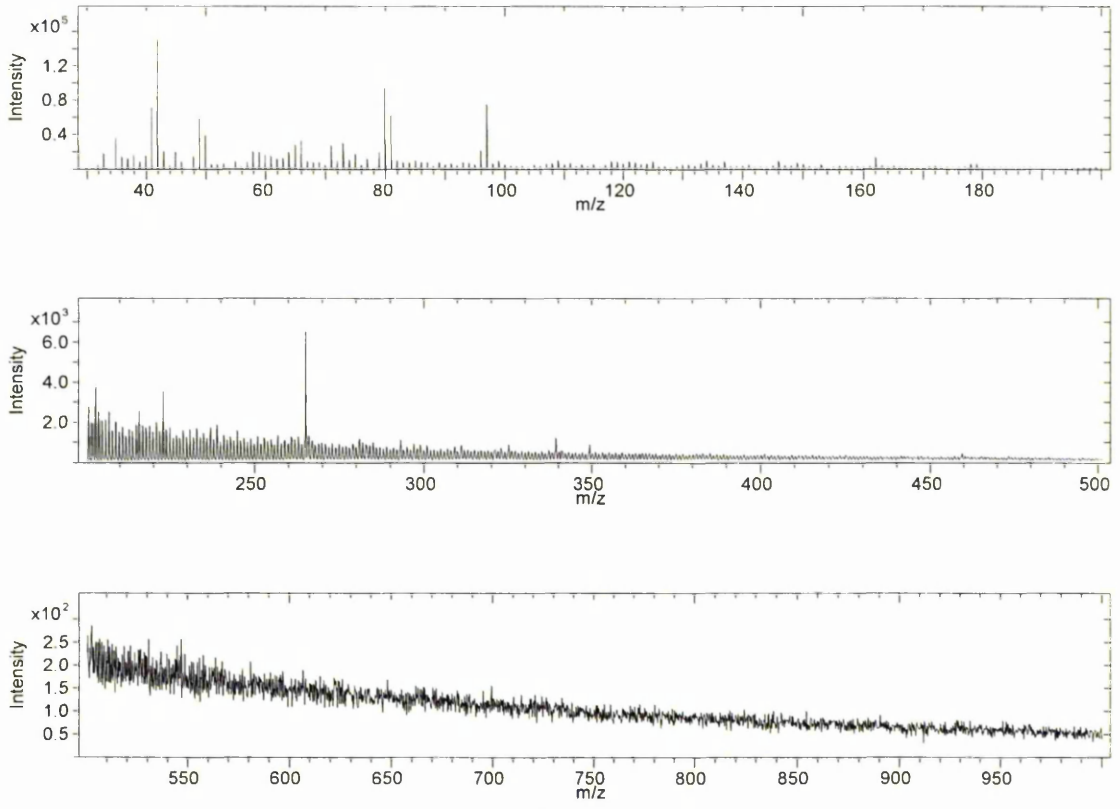

F. Images of double and triple wrapped metal threads

F.1. Double wrapped threads


HCP 67E6


HCP 136C6


HCP 153B6


HCP 103D6


HCP 73E4


HCP _X_


HCP 167A3


HCP 43F6


HCP 64E6


HCP 96E6


HCP 28G6


HCP 94D6


PNM 1_46


PNM 1_10

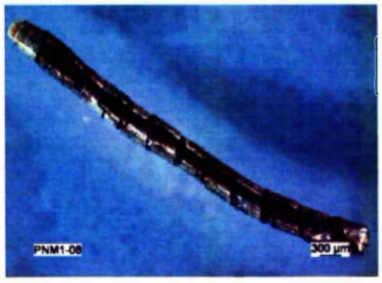
PNM 1_08

PNM 1_49

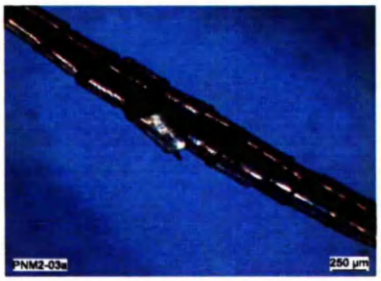

PNM 2_03

PNM 2_16

PNM 5_04

F.2. Triple wrapped threads

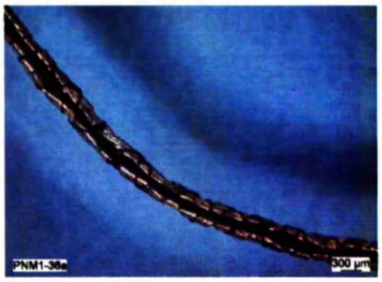

PNM 1_36

PNM 5_03

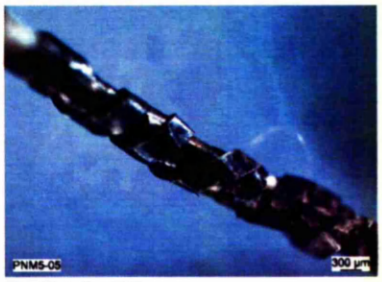

PNM 5_05

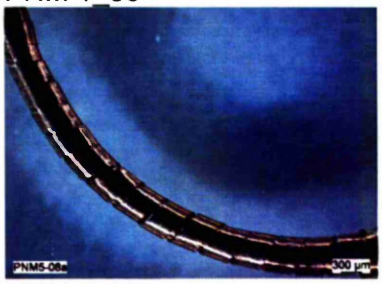

PNM 5_08

G. EDX data of metal threads

Accurate EDX ZAF quantification requires a polished, flat and homogenous sample. Metal thread filaments are neither flat nor homogenous, therefore all analysis results have been rounded to the nearest integer to avoid the impression of absolute accuracy of results. A blank space means the element was not detected or, in the case of carbon and oxygen, was not included in the quantification. Zero denotes the element was detected at < 0.5 wt.%. Contaminant elements detected at low levels, i.e. maximum 3 wt.%, have been omitted from the results table; these comprise Mg, Al and Si detected on most samples, N detected on < 2% of samples and K, Ca, Na, P or Hf detected on < 1% of samples.

Group *: L: Gilt large diameter; Lc: Gilt large diameter corroded; M: Gilt medium diameter; Mc: Gilt medium diameter corroded; S: Gilt small diamter; Sc: Gilt small diameter corroded; Ag: Silver; 2x: Double wrapped; 3x: Triple wrapped; R: Restoration.

Side **: e: Exterior; i: Interior; x: Cross section.

Mag. ***: Magnification of analysis area; k = *1000.

Comment +: c: Corrosion; g: Gold layer; s: SIMS crater.

Acc. vol. ++: Accelerating voltage in kV; the higher the kV the higher the depth of analysis.

Sample	Group *	Side **	Mag. ***	Comment +	Acc. vol. ++	Weight %							100*n / (Ag+Cu+Au)		
						Ag L	Cu L/K	Au M/L	C K	O K	S K	Cl K	n=Ag	n=Cu	n=Au
HCP 49F5	L	e	500		7	33	5	40	13	3	1	2	42	7	51
HCP 49F5	L	e	500		30	57	4	22	10	4	1	1	68	5	27
HCP 49F5	L	e	20k	c	7	17	4	74	4	1	0		18	4	78
HCP 49F5	L	e	4k	c	7	64	19	1	11	2	2		77	22	1
HCP 49F5	L	e	4k	c	7	36	12	19	17	6	4	3	54	18	28
HCP 49F5	L	e	4k	g	7	17	3	73	6	1			18	3	79
HCP 49F5	L	e	4k	c	7	72	7		5	2	9	4	91	9	0
HCP 49F5	L	e	6k	c	7	64	5	1	10	5	5	10	91	7	2
HCP 49F5	L	i	500		7	68	9		11	8	2	2	89	11	0
HCP 49F5	L	i	500		7	59	9		18	6	5	2	86	14	0
HCP 49F5	L	i	500		30	71	5		11	10	1	0	93	7	0
HCP 6E5	L	e	300		7	40	9	10	30	6	3	2	68	15	17
HCP 6E5	L	e	300		7	53	4	10	20	5	2	6	79	6	15
HCP 6E5	L	e	300		30	66	9	5	13	4	2	0	82	11	7
HCP 6E5	L	e	300		30	48	8	16	16	4	1	6	67	11	22
HCP 6E5	L	e	5k	c	7	22	10	28	32	5	0	3	37	16	46
HCP 6E5	L	e	5k	g	7	23	6	56	12	1		2	27	7	66
HCP 6E5	L	e	7k	g	7	22	7	55	13	2	1	1	26	8	66
HCP 6E5	L	i	300		30	77	7		10	3	0	1	92	8	0
HCP 6E5	L	i	300		30	67	9		17	3	1	1	88	12	0
HCP 6E5	L	i	400		7	54	8		26	6	1	4	87	13	0
HCP 6E5	L	i	400		7	45	12		31	6	2	4	79	21	0
HCP 6E5	L	i	10k	c	7	73	10		9	1	7	0	88	12	0
HCP 6E5	L	i	10k	c	7	44	16		33	2	5	0	73	27	0
HCP 71E5	L	e	300		7	35	3	43	15	3	0	1	43	3	54
HCP 71E5	L	e	300		7	32	3	47	13	3	0	1	39	4	57
HCP 71E5	L	e	300		10	39	3	41	12	3		1	47	3	50

Sample	Group *	Side **	Mag. ***	Comment +	Acc. vol. ++	Weight %							100*n / (Ag+Cu+Au)		
						Ag L	Cu L/K	Au M/L	C K	O K	S K	Cl K	n=Ag	n=Cu	n=Au
HCP 71E5	L	e	300		15	48	4	32	11	4		0	57	5	38
HCP 71E5	L	e	300		15	49	3	32	12	4		0	58	4	38
HCP 71E5	L	e	300		20	58	2	26	10	3			67	3	30
HCP 71E5	L	e	300		30	64	3	17	10	4			76	4	20
HCP 71E5	L	e	300		30	67	5	18	6	3	0		75	6	19
HCP 71E5	L	e	300		30	65	7	19	6	3	0		71	8	20
HCP 71E5	L	e	25k	c	7	81	3		12	1	2	0	97	3	0
HCP 71E5	L	e	4k	g	7	24	3	61	11	1			27	3	70
HCP 71E5	L	i	300		7	60	3		24	7	1	5	96	4	0
HCP 71E5	L	i	300		7	62	3		21	7	1	6	95	5	0
HCP 71E5	L	i	300		7	69	3		17	6	1	4	96	4	0
HCP 71E5	L	i	300		7	64	3		18	6	1	6	95	5	0
HCP 71E5	L	i	300		10	66	4		16	7	1	5	95	5	0
HCP 71E5	L	i	300		15	70	2		15	7	1	4	97	3	0
HCP 71E5	L	i	300		15	69	4		15	7	1	4	95	5	0
HCP 71E5	L	i	300		20	73	3		13	7	0	3	96	4	0
HCP 71E5	L	i	300		30	81	5		7	3	0	2	94	6	0
HCP 71E5	L	i	300		30	83	6		6	4	0	1	93	7	0
HCP 71E5	L	i	30k	c	7	74	0		8	0	0	17	99	1	0
HCP 95D6	L	e	400		7	30	3	56	7	2		1	34	3	63
HCP 95D6	L	e	400		7	29	4	56	8	2			33	4	63
HCP 95D6	L	e	400		10	32	3	55	7	2		0	35	3	61
HCP 95D6	L	e	400		15	40	5	45	7	2		0	45	6	50
HCP 95D6	L	e	400		15	41	4	45	7	2		0	45	4	50
HCP 95D6	L	e	400		20	46	5	37	7	3	1		52	6	42
HCP 95D6	L	e	400		30	59	8	24	5	2	0	0	65	9	26
HCP 95D6	L	e	400		30	57	9	27	5	2			61	10	29
HCP 95D6	L	e	10k	g	7	22	3	69	5	1		0	23	3	74
HCP 95D6	L	e	3k	g	7	25	3	64	6	1		0	27	4	69
HCP 95D6	L	e	6k	c	7	53	16	5	12	7	4	1	72	21	7
HCP 95D6	L	i	400		7	83	4		7	4	0	1	95	5	0
HCP 95D6	L	i	400		7	80	4		8	4	1	3	95	5	0
HCP 95D6	L	i	400		7	82	5		7	4	0	2	95	5	0
HCP 95D6	L	i	400		10	83	4		7	4	0	1	96	4	0
HCP 95D6	L	i	400		15	83	4		6	4	0	1	95	5	0
HCP 95D6	L	i	400		15	83	4		6	4	0	1	95	5	0
HCP 95D6	L	i	400		20	84	3		6	4	0	1	96	4	0
HCP 95D6	L	i	400		30	83	4		7	3	0	1	95	5	0
HCP 95D6	L	i	400		30	83	4		7	3	0	0	95	5	0
HCP 161A6	Lc	e	500		7	75	3	10	6	3	1	2	86	3	11
HCP 161A6	Lc	e	500		30	82	7	4	3	1	0		88	8	5
HCP 161A6	Lc	e	500		30	79	5	8	5	2	1	0	86	5	9
HCP 161A6	Lc	e	7k	g	7	22	3	66	6	1			24	3	72
HCP 161A6	Lc	i	500		7	68	5		13	5	9		93	7	0
HCP 161A6	Lc	i	500		30	70	14		10	4	2		83	17	0
HCP 161A6	Lc	i	500		30	75	11		7	6	1		87	13	0
HCP 161A6	Lc	i	10k	c	7	81	2		5	1	11		98	2	0
HCP 161A6	Lc	i	10k	c	7	64	7		18	2	9		90	10	0
HCP 161A6	Lc	i	7k	c	7	82	1		3	1	12		98	2	0
HCP 161A6	Lc	i	7k	c	7	70	12		5	9	4		86	14	0
HCP 72E4	Lc	e	500		7	27	8	9	44	7	2	2	61	19	20
HCP 72E4	Lc	e	500		7	20	7	15	48	7	2	1	48	17	35

Sample	Group *	Side **	Mag. ***	Comment +	Acc. vol. ++	Weight %							100*n / (Ag+Cu+Au)		
						Ag L	Cu L/K	Au M/L	C K	O K	S K	Cl K	n=Ag	n=Cu	n=Au
HCP 72E4	Lc	e	500		7	18	7	16	48	8	2	1	43	18	39
HCP 72E4	Lc	e	500		10	20	6	22	43	7	1	1	42	12	47
HCP 72E4	Lc	e	500		15	23	5	26	38	6	1	0	43	9	48
HCP 72E4	Lc	e	500		15	24	4	26	39	7	1	0	44	7	49
HCP 72E4	Lc	e	500		20	29	5	23	35	7	0	0	51	8	41
HCP 72E4	Lc	e	500		30	40	4	12	35	7	1	1	71	8	21
HCP 72E4	Lc	e	500		30	39	4	18	31	7	0	0	64	6	29
HCP 72E4	Lc	e	2k	c	7	16	10		60	7	2	4	61	39	0
HCP 72E4	Lc	e	2k	c	7	17	11		57	5	4	4	60	40	0
HCP 72E4	Lc	e	4k	g	7	79	4	11	5	1	0	0	84	5	11
HCP 72E4	Lc	e	4k	g	7	29	7	33	26	2	2	1	42	11	47
HCP 72E4	Lc	i	500		7	32	7		47	10	1	1	82	18	0
HCP 72E4	Lc	i	500		7	23	7		56	11	2	1	76	24	0
HCP 72E4	Lc	i	500		10	41	6		40	9	1	1	86	14	0
HCP 72E4	Lc	i	500		15	47	6		35	9	1	1	88	12	0
HCP 72E4	Lc	i	500		15	48	5		35	9	1	1	91	9	0
HCP 72E4	Lc	i	500		20	61	8		23	6	1	1	89	11	0
HCP 72E4	Lc	i	500		30	52	4		32	8	1	1	92	8	0
HCP 72E4	Lc	i	500		30	56	7		29	6	1	1	89	11	0
BXL 2_04	M	e	600		7	19	7	20	29	17	2	3	41	16	43
BXL 2_04	M	e	600		7	32	10	31	15	8	2	1	44	13	43
BXL 2_04	M	e	600		7	26	9	40	14	7	2	1	34	13	53
BXL 2_04	M	e	600		30	44	5	18	18	14	1	1	66	7	27
BXL 2_04	M	e	600		30	39	5	21	20	12	1	1	60	8	32
BXL 2_04	M	e	4k	g	7	32	7	44	10	4	1	1	38	8	53
BXL 2_04	M	e	4k	g	7	26	6	53	9	3	1	0	30	7	62
BXL 2_04	M	i	600		7	57	14		14	9	4	0	80	20	0
BXL 2_04	M	i	600		7	48	14		18	12	4	2	77	23	0
BXL 2_04	M	i	600		7	42	19		21	13	4	1	69	31	0
BXL 2_04	M	i	600		30	63	7		13	13	1	0	90	10	0
BXL 2_04	M	i	600		30	66	7		13	11	1	0	90	10	0
BXL 2_19	M	e	500		7	23	17	4	32	16	4	2	52	39	10
BXL 2_19	M	e	500		7	55	8	10	16	5	3	1	76	10	14
BXL 2_19	M	e	500		30	13	4	30	43	7	2	1	27	9	64
BXL 2_19	M	e	500		30	47	6	17	16	6	2		67	8	25
BXL 2_19	M	e	500		30	31	9	18	22	12	3	0	53	15	31
BXL 2_19	M	e	10k	c	7	58	16	1	21	3	2		78	21	1
BXL 2_19	M	e	10k	c	7	76	1	3	6	1	12	0	94	1	4
BXL 2_19	M	e	10k	c	7	26	19	4	35	9	3	2	53	38	9
BXL 2_19	M	e	10k	c	7	66	4	9	9	1	9	1	83	5	12
BXL 2_19	M	e	10k	c	7	67	5	9	8	1	8	0	82	6	12
BXL 2_19	M	e	10k	c	7	20	5	53	13	3	1	2	25	6	69
BXL 2_19	M	i	500		7	46	19		19	11	3	1	71	29	0
BXL 2_19	M	i	500		30	68	5		13	12	1		93	7	0
BXL 2_19	M	i	500		30	68	5		13	13	1		93	7	0
BXL 2_19	M	i	500		30	63	7		15	12	1	3	90	10	0
BXL 2_19	M	i	500		30	63	8		15	12	1	2	89	11	0
BXL 2_19	M	i	500		30	72	7		12	9	1		91	9	0
BXL 2_19	M	i	500		30	65	6		14	12	1	3	92	8	0
BXL 2_19	M	i	500		30	65	4		16	12	1	3	94	6	0
BXL 2_19	M	i	500		30	58	9		19	10	2	1	86	14	0
BXL 2_19	M	i	500		30	63	6		19	12	1		92	8	0

Sample	Group *	Side **	Mag. ***	Comment +	Acc. vol. ++	Weight %							100*n / (Ag+Cu+Au)		
						Ag L	Cu L/K	Au M/L	C K	O K	S K	Cl K	n=Ag	n=Cu	n=Au
BXL 2_19	M	i	500		30	73	6		10	10	1		92	8	0
BXL 2_19	M	i	10k	c	7	49	15		19	11	1	1	76	24	0
BXL 2_19	M	i	10k	c	7	61	16		12	7	1	1	79	21	0
BXL 2_19	M	i	10k	c	7	54	17		18	5	5	0	76	24	0
BXL 2_22	M	e	600		7	20	8	41	17	10	1	2	30	12	59
BXL 2_22	M	e	600		7	24	7	42	16	9	1	2	33	10	58
BXL 2_22	M	e	600		7	26	6	46	14	8	0	0	33	8	59
BXL 2_22	M	e	600		30	47	6	24	15	7	0	0	61	7	32
BXL 2_22	M	e	600		30	42	4	33	13	8	0	0	53	5	42
BXL 2_22	M	e	4k	g	7	17	5	59	11	3	1	2	21	6	73
BXL 2_22	M	i	600		7	67	8		12	8	2	2	89	11	0
BXL 2_22	M	i	600		7	62	9		14	9	3	3	88	12	0
BXL 2_22	M	i	600		7	59	10		14	9	3	2	85	15	0
BXL 2_22	M	i	600		30	78	6		6	7	1	0	93	7	0
BXL 2_22	M	i	600		30	72	5		10	9	1		93	7	0
BXL 2_36	M	e	600		7	28	12	11	25	15	3	4	55	23	22
BXL 2_36	M	e	600		7	48	8	17	11	9	2	2	65	11	24
BXL 2_36	M	e	600		7	27	5	37	16	9	3	2	39	8	54
BXL 2_36	M	e	600		30	49	4	19	15	12	0	1	68	6	26
BXL 2_36	M	e	600		30	46	5	19	16	12	1	0	66	7	27
BXL 2_36	M	e	4k	g	7	11	2	78	7	1			12	3	85
BXL 2_36	M	i	600		7	45	13		20	12	3	5	78	22	0
BXL 2_36	M	i	600		7	51	13		18	10	3	3	79	21	0
BXL 2_36	M	i	600		7	39	19		22	13	3	2	67	33	0
BXL 2_36	M	i	600		30	71	4		10	11	1	1	95	5	0
BXL 2_36	M	i	600		30	65	6		15	11	1	0	92	8	0
HCP 46F6	M	e	600		7	22	7	46	18	5	1	1	30	9	62
HCP 46F6	M	e	600		10	34	5	48	9	3	0	1	39	6	55
HCP 46F6	M	e	600		20	52	4	33	7	2	1	0	58	5	37
HCP 46F6	M	e	600		30	65	5	18	7	3	1		74	6	20
HCP 46F6	M	e	600		30	69	5	14	8	3	1		79	5	16
HCP 46F6	M	e	600		30	70	4	12	7	4	0		81	5	14
HCP 46F6	M	e	600		30	70	5	13	7	3	0		80	6	15
HCP 46F6	M	e		c	7	19	13	49	17	2	2		23	16	61
HCP 46F6	M	e		c	7	16	9	58	14	2	1		20	11	70
HCP 46F6	M	i	600		7	63	11		11	12	1	2	85	15	0
HCP 46F6	M	i	600		10	83	5		4	5	1	2	94	6	0
HCP 46F6	M	i	600		20	75	5		8	10	0	0	93	7	0
HCP 46F6	M	i	600		30	76	6		8	10	0		93	7	0
HCP 46F6	M	i	600		30	70	5		9	14	1	0	94	6	0
HCP 46F6	M	i	600		30	67	6		11	12	1	0	92	8	0
HCP 46F6	M	i	600		30	74	5		8	11	0		93	7	0
HCP 51F5	M	e	500		7	36	4	44	11	2	1	2	43	4	53
HCP 51F5	M	e	500		30	56	4	27	8	3	1	0	64	5	31
HCP 51F5	M	e	6k	g	7	31	3	59	5	1	1	1	33	3	64
HCP 51F5	M	i	500		7	54	7		25	6	0	8	89	11	0
HCP 51F5	M	i	500		30	73	4		13	5	0	2	94	6	0
PNM 1_03	M	e	400		7	27	9	45	11	5	2	1	34	11	56
PNM 1_03	M	e	400		10	30	7	44	11	6	2	0	37	9	54
PNM 1_03	M	e	400		20	46	7	31	10	6	1		55	8	37
PNM 1_03	M	e	400		30	55	7	23	9	6	1		65	8	27
PNM 1_03	M	e	2.5k		30	52	4	24	13	6			65	5	30

Sample	Group *	Side **	Mag. ***	Comment +	Acc. vol. ‡	Weight %							100*n / (Ag+Cu+Au)		
						Ag L	Cu L/K	Au M/L	C K	O K	S K	Cl K	n=Ag	n=Cu	n=Au
PNM 1_03	M	e	2.5k		30	53	4	24	13	7			65	5	30
PNM 1_03	M	e	2.5k		30	67	6	11	9	4			79	8	13
PNM 1_03	M	e	2.5k		30	52	4	24	10	6		1	65	5	30
PNM 1_03	M	e	2.5k		30	64	6	9	12	8		0	81	7	12
PNM 1_03	M	e	2.5k		30	41	5	33	14	4		0	52	7	41
PNM 1_03	M	i	400		7	66	13		10	9	1	2	84	16	0
PNM 1_03	M	i	400		10	68	12		9	9	1	1	85	15	0
PNM 1_03	M	i	400		20	72	11		9	8	0	0	87	13	0
PNM 1_03	M	i	400		30	73	10		9	7	0		88	12	0
PNM 1_03	M	i		c	10	72	11		10	4	1	1	87	13	0
PNM 1_38	M	e			10	22	10	33	23	11			33	16	51
PNM 1_38	M	e			10	20	12	35	23	9			30	18	52
PNM 1_38	M	e			25	64	4	12	11	8		0	80	5	16
PNM 1_38	M	e			25	67	5	8	8	9		0	83	6	10
PNM 1_38	M	e		s	25	82	9		6	1			90	10	0
PNM 1_38	M	i			25	79	8		5	6	0		91	9	0
PNM 1_38	M	i			25	75	10		7	7	0		89	11	0
PNM 1_38	M	i		s	25	84	10		4				90	10	0
PNM 2_17	M	e	500		7	40	5	29	14	8	3	1	54	7	39
PNM 2_17	M	e	500		7	38	6	33	12	7	2	1	49	8	43
PNM 2_17	M	e	500		7	35	6	38	11	7	1	1	44	7	48
PNM 2_17	M	e	500		30	50	5	11	10	21	2		75	8	17
PNM 2_17	M	e	500		30	56	5	17	1	20	1		72	6	22
PNM 2_17	M	e	4k	g	7	22	5	61	8	3	1	0	25	6	69
PNM 2_17	M	i	500		7	70	8		10	8	1	1	90	10	0
PNM 2_17	M	i	500		7	68	9		10	9	1	2	88	12	0
PNM 2_17	M	i	500		7	67	10		10	8	2	2	87	13	0
PNM 2_17	M	i	500		10	73	7		6	10	1	2	91	9	0
PNM 2_17	M	i	500		15	85	3		3	8	1	0	97	3	0
PNM 2_17	M	i	500		15	40	54		3	2	0	0	42	58	0
PNM 2_17	M	i	500		20	73	6		6	15	1		92	8	0
PNM 2_17	M	i	500		30	63	5		6	26	0		93	7	0
PNM 2_17	M	i	500		30	60	4		8	27			94	6	0
PNM 5_06	M	e	500		7	29	4	53	10	3		1	34	5	61
PNM 5_06	M	e	500		8	31	4	51	10	3		1	36	5	59
PNM 5_06	M	e	500		9	32	5	49	11	4		0	37	5	57
PNM 5_06	M	e	500		10	33	5	47	11	4		1	39	5	56
PNM 5_06	M	e	500		15	42	5	40	11	3			48	5	46
PNM 5_06	M	e	500		20	50	4	33	10	3			57	5	38
PNM 5_06	M	e	500		20	50	4	33	10	4			58	4	38
PNM 5_06	M	e	500		25	57	4	27	9	3			65	5	31
PNM 5_06	M	e	500		25	57	4	27	9	3			65	4	31
PNM 5_06	M	e	500		30	60	4	23	9	3		0	69	5	26
PNM 5_06	M	e	500		30	61	4	23	9	3		0	70	4	26
PNM 5_06	M	i	500		7	72	8		9	6	2	3	90	10	0
PNM 5_06	M	i	500		10	75	7		8	6	1	3	91	9	0
PNM 5_06	M	i	500		20	76	6		9	7	1	1	93	7	0
PNM 5_06	M	i	500		20	77	5		9	7	1	1	94	6	0
PNM 5_06	M	i	500		30	76	5		10	7		1	93	7	0
PNM 5_06	M	i	500		30	76	6		10	7		1	93	7	0
PNM 5_06	M	x			20	91	9						91	9	0
PNM 5_06	M	x			20	92	8						92	8	0

Sample	Group *	Side **	Mag. ***	Comment +	Acc. vol. ++	Weight %							100*n / (Ag+Cu+Au)		
						Ag L	Cu L/K	Au M/L	C K	O K	S K	Cl K	n=Ag	n=Cu	n=Au
PNM 5_06	M	x			20	87	11				2		89	11	0
PNM 5_06	M	x			20	88	12						88	12	0
PNM 5_06	M	x			20	86	12				2		88	12	0
PNM 5_06	M	x			20	84	14				2		86	14	0
PNM 5_06	M	x			20	87	11				2		89	11	0
PNM 5_06	M	x			20	65	7		27				90	10	0
PNM 5_06	M	x			20	74	12				14		86	14	0
PNM 5_06	M	x			20	45	2	54					45	2	54
PNM 5_06	M	x			20	12	0	5	54	28			67	2	31
PNM 5_06	M	x			20	46	1		41	10	1		98	2	0
PNM 5_06	M	x			20	93	7				1		93	7	0
PNM 5_06	M	x			20	93	7						93	7	0
PNM 5_06	M	x			20	92	7				1		93	7	0
PNM 5_06	M	x			20	91	9				1		91	9	0
PNM 5_06	M	x			20	93	7				1		93	7	0
PNM 5_06	M	x			20	90	6		4				94	6	0
PNM 5_06	M	x			20	87	8				5		91	9	0
PNM 5_06	M	x			20	31	1	68					31	1	68
PNM 5_06	M	x			20	36	1	31	19	13			53	1	46
PNM 5_06	M	x			20	87	1		8	3	1		99	1	0
PNM 5_26	M	e	1k		7	33	7	34	17	8	1	0	45	10	45
PNM 5_26	M	e	1k		7	18	6	60	10	5	1	0	21	7	72
PNM 5_26	M	e	1k		30	64	5	11	11	7	1		80	6	14
PNM 5_26	M	e	1k		30	61	5	20	7	5	1		71	6	23
PNM 5_26	M	i	600		7	66	11		12	8	2	1	86	14	0
PNM 5_26	M	i	600		7	49	15		18	11	3	3	76	24	0
PNM 5_26	M	i	600		30	73	6		11	8	0		92	8	0
PNM 5_30	M	e	500		7	27	5	54	8	3	2	0	32	6	62
PNM 5_30	M	e	500		30	54	6	22	11	6	0	0	65	7	27
PNM 5_30	M	e	19k	c	7	13	11	46	26	4	1		18	15	67
PNM 5_30	M	e	1k	c	7	17	5	60	12	4	1	1	21	6	74
PNM 5_30	M	e	4k	g	7	17	3	74	4	1	1	1	18	3	79
PNM 5_30	M	i	500		7	58	12		13	11	3	2	83	17	0
PNM 5_30	M	i	500		30	76	7		8	7	1		92	8	0
PNM 5_41	M	e	500		7	37	8	38	11	7			45	9	46
PNM 5_41	M	e	500		30	53	6	27	7	6			62	7	31
PNM 5_41	M	e	5k	g	7	11	4	74	8	3			13	5	83
PNM 5_41	M	i	500		7	75	8		7	7	1	1	90	10	0
PNM 5_41	M	i	500		30	80	7		6	5	0	0	92	8	0
BXL 2_05	Mc	e	600		7	65	9	2	12	6	4	0	85	12	2
BXL 2_05	Mc	e	600		7	67	8	4	10	6	3	0	85	10	5
BXL 2_05	Mc	e	600		7	44	9	20	14	7	3	1	61	12	27
BXL 2_05	Mc	e	600		30	63	6	9	13	7	2	0	81	7	11
BXL 2_05	Mc	e	600		30	55	8	12	15	8	2	0	73	10	16
BXL 2_05	Mc	e	4k	g	7	26	6	53	9	3	1	1	30	7	62
BXL 2_05	Mc	e	4k	g	7	20	4	68	5	1	0	1	21	5	74
BXL 2_05	Mc	e	6k	c	7	76	2	1	7	1	11	1	96	3	2
BXL 2_05	Mc	i	600		7	66	9		10	8	3	2	87	13	0
BXL 2_05	Mc	i	600		7	64	10		11	8	6		87	13	0
BXL 2_05	Mc	i	600		7	53	13		15	11	6	2	80	20	0
BXL 2_05	Mc	i	600		30	68	8		11	9	2		90	10	0
BXL 2_05	Mc	i	600		30	69	8		11	9	1		90	10	0

Sample	Group *	Side **	Mag. ***	Comment +	Acc. vol. ++	Weight %							100*n / (Ag+Cu+Au)		
						Ag L	Cu L/K	Au M/L	C K	O K	S K	Cl K	n=Ag	n=Cu	n=Au
BXL 2_06	Mc	e	600		7	51	12	5	17	9	4	1	75	18	7
BXL 2_06	Mc	e	600		7	25	7	42	15	8	2	2	34	9	57
BXL 2_06	Mc	e	600		7	27	6	46	12	5	2	0	35	8	58
BXL 2_06	Mc	e	600		30	52	5	29	9	4	2		60	6	34
BXL 2_06	Mc	e	600		30	47	5	30	9	7	2		57	7	37
BXL 2_06	Mc	e	4k	g	7	20	4	64	8	2	1	2	23	4	73
BXL 2_06	Mc	e	4k	g	7	12	5	71	8	2	1	1	14	5	81
BXL 2_06	Mc	i	600		7	61	9		15	9	2	2	88	12	0
BXL 2_06	Mc	i	600		7	58	9		16	10	2	3	87	13	0
BXL 2_06	Mc	i	600		7	65	9		13	8	2	1	87	13	0
BXL 2_06	Mc	i	600		30	72	6		10	9	1		93	7	0
BXL 2_06	Mc	i	600		30	70	5		13	9	1		93	7	0
HCP 169A2	Mc	e	400		7	59	4	10	9	5	2	11	81	6	14
HCP 169A2	Mc	e	400		7	55	4	12	11	6	1	10	77	6	17
HCP 169A2	Mc	e	500		30	71	7	3	8	3	1	6	88	9	3
HCP 169A2	Mc	e	500		30	66	5	14	6	3	1	5	78	6	17
HCP 169A2	Mc	e	600		30	74	4		15	4	1	1	95	5	0
HCP 169A2	Mc	e	600		30	64	5		20	6	2	1	93	7	0
HCP 169A2	Mc	e	10k	g	7	34	4	52	6	1	0	3	38	4	58
HCP 169A2	Mc	e	10k	g	7	30	6	54	6	1	0	2	33	7	60
HCP 169A2	Mc	e	1k	c	7	54	13	2	17	6	6	1	78	19	3
HCP 169A2	Mc	e	1k	c	7	64	6		11	5	1	13	91	9	0
HCP 169A2	Mc	e	1k	c	7	37	20		28	4	2	8	64	36	0
HCP 169A2	Mc	e	4k	c	7	65	3		9	8	4	12	95	5	0
HCP 169A2	Mc	e		g	7	12	8	63	13	3	0		14	10	76
HCP 169A2	Mc	e		c	7	61	4		21	2	11	0	94	6	0
HCP 169A2	Mc	e		c	7	54	5		24	7	9	1	92	8	0
HCP 169A2	Mc	e		c	7	36	6		37	10	0	9	86	14	0
HCP 169A2	Mc	e		c	7	50	7		27	8	2	6	88	12	0
HCP 169A2	Mc	e		c	7	53	9		30	4	2	2	85	15	0
HCP 169A2	Mc	i	500		30	60	13		14	3	5	4	83	17	0
HCP 169A2	Mc	i	500		30	78	7		8	3	2	1	91	9	0
HCP 169A2	Mc	i	600		7	62	11		16	5	5	2	85	15	0
HCP 169A2	Mc	i	600		7	50	18		19	4	6	2	73	27	0
HCP 169A2	Mc	i	20k	c	7	84	4		10	1	1		96	4	0
HCP 169A2	Mc	i	20k	c	7	77	4		8	1	8	2	95	5	0
HCP 169A2	Mc	i	7k	c	30	70	10		8	2	9	0	87	13	0
HCP 119C3	S	e	500		7	53	4	12	14	3	1	12	77	5	17
HCP 119C3	S	e	500		7	27	5	47	13	3	1	3	35	6	59
HCP 119C3	S	e	500		30	56	4	25	9	3	0	1	66	4	30
HCP 119C3	S	e	10k	c	7	45	22		18	5	8	1	67	33	0
HCP 119C3	S	e	5k	g	7	19	4	67	7	1	0	0	21	5	74
HCP 119C3	S	i	500		7	50	16		16	12	2	2	76	24	0
HCP 119C3	S	i	500		7	43	19		19	14	2	2	69	31	0
HCP 119C3	S	i	500		30	66	6		12	12	1	0	91	9	0
HCP 31G5	S	e	500		7	46	4	33	12	3	1	1	55	5	40
HCP 31G5	S	e	500		7	25	2	63	6	1	1	1	27	3	70
HCP 31G5	S	e	500		10	34	28	23	10	2	1	1	40	33	27
HCP 31G5	S	e	500		10	48	4	30	11	3	1	1	58	5	37
HCP 31G5	S	e	500		15	52	6	27	11	3	0		62	7	32
HCP 31G5	S	e	500		20	58	4	22	10	4	1	0	70	4	26
HCP 31G5	S	e	500		30	66	4	16	9	3	0		77	4	19

Sample	Group *	Side **	Mag. ***	Comment +	Acc. vol. ++	Weight %							100*n / (Ag+Cu+Au)		
						Ag L	Cu L/K	Au M/L	C K	O K	S K	Cl K	n=Ag	n=Cu	n=Au
HCP 31G5	S	e	500		30	62	4	24	6	1	0		69	4	27
HCP 31G5	S	e	5k	g	7	20	2	72	5	1	0		21	2	77
HCP 31G5	S	i	500		7	58	11		16	12	1	1	84	16	0
HCP 31G5	S	i	500		7	55	12		17	14	1	1	83	17	0
HCP 31G5	S	i	500		10	65	9		12	11	1	1	88	12	0
HCP 31G5	S	i	500		15	68	8		10	11	1	1	90	10	0
HCP 31G5	S	i	500		15	70	7		10	12			91	9	0
HCP 31G5	S	i	500		20	74	5		10	10	0	0	94	6	0
HCP 31G5	S	i	500		30	71	5		11	11	0		94	6	0
HCP 96D6	S	e	500		7	25	6	48	13	3	1	2	32	7	61
HCP 96D6	S	e	500		30	54	5	29	8	2	1	0	62	5	33
HCP 96D6	S	e	5k	g	7	10	3	77	6	1	1	1	11	3	85
HCP 96D6	S	i	500		7	50	16		18	12	1	2	76	24	0
HCP 96D6	S	i	500		30	71	6		10	9	0	0	93	7	0
PNM 1_06	S	e			25	51	3	22	15	8		1	67	5	29
PNM 1_06	S	e			25	56	4	13	17	9	2	1	77	5	18
PNM 1_06	S	i			25	45	6		32	13	2	1	89	11	0
PNM 1_24	S	e	500		7	25	6	48	13	6	2	1	32	7	61
PNM 1_24	S	e	500		30	48	5	28	10	7			59	6	35
PNM 1_24	S	e	14k	c	7	22	7	13	29	16	5	3	52	17	31
PNM 1_24	S	e	5k	g	7	18	4	62	8	3	2	0	22	5	73
PNM 1_24	S	i	500		7	70	10		9	9	1	1	88	12	0
PNM 1_24	S	i	500		7	66	11		11	10	1	1	86	14	0
PNM 1_24	S	i	500		30	74	7		8	9	1		92	8	0
PNM 2_02	S	e	500		7	32	11	20	24	9	3	2	51	17	32
PNM 2_02	S	e	500		7	26	10	29	23	9	2	2	40	16	44
PNM 2_02	S	e	500		7	28	7	39	16	7	1	1	38	9	53
PNM 2_02	S	e	4k	g	7	18	15	43	16	5	2		24	19	56
PNM 2_02	S	e	4k	g	7	35	7	47	7	3	1	1	40	8	53
PNM 2_02	S	i	500		7	60	12		14	10	1	2	83	17	0
PNM 2_02	S	i	500		7	50	13		20	10	2	4	79	21	0
PNM 2_02	S	i	500		30	53	5		19	22	1	0	91	9	0
PNM 2_02	S	i	500		30	61	5		13	18	1	3	93	7	0
PNM 2_02	S	i	500		30	65	5		11	19	1	0	93	7	0
PNM 2_06	S	e	500		7	32	7	2	30	18	3	7	78	18	5
PNM 2_06	S	e	500		7	28	11	10	29	14	3	5	58	22	20
PNM 2_06	S	e	500		7	29	7	11	28	14	3	6	62	15	23
PNM 2_06	S	e	500		7	37	18	13		21	5	7	54	26	19
PNM 2_06	S	e	500		10	29	10	16	25	12	4	4	53	18	29
PNM 2_06	S	e	500		15	31	10	19	22	13	3	2	52	17	31
PNM 2_06	S	e	500		30	41	6	15	16	19	2	1	67	9	24
PNM 2_06	S	e	500		30	45	7	15	16	14	2	1	67	10	23
PNM 2_06	S	e	500		30	45	7	16	16	14	2	1	67	10	23
PNM 2_06	S	e	3.5k	c	7	38	6	5	26	11	3	9	78	12	10
PNM 2_06	S	e	4k	g	7	32	9	44	9	3	3	0	37	11	52
PNM 2_06	S	i	500		7	49	16		19	7	5	3	76	24	0
PNM 2_06	S	i	500		7	61	20			9	6	4	75	25	0
PNM 2_06	S	i	500		30	56	7		10	24	3	0	88	12	0
PNM 2_06	S	i	500		30	55	9		12	20	3	1	86	14	0
PNM 2_06	S	i	500		30	58	7		10	23	2	0	90	10	0
PNM 2_19	S	e			10	19	15	21	31	13		0	35	27	38
PNM 2_19	S	e			10	19	14	26	28	12		1	32	23	45

Sample	Group *	Side **	Mag. ***	Comment +	Acc. vol. ++	Weight %							100*n / (Ag+Cu+Au)		
						Ag L	Cu L/K	Au M/L	C K	O K	S K	Cl K	n=Ag	n=Cu	n=Au
PNM 2_19	S	e			25	52	6	13	15	10	3	1	73	9	18
PNM 2_19	S	e		s	25	81	9	4	4	1			87	9	4
PNM 2_19	S	e			25	57	7	12	10	8	3	1	75	9	16
PNM 2_19	S	i			25	66	5		14	9	2	0	92	8	0
PNM 5_24	S	e	800	s	10	86	11		3				89	11	0
PNM 5_24	S	e	800	s	10	86	11		3				89	11	0
PNM 5_24	S	e	800	s	15	85	11		3				88	12	0
PNM 5_24	S	e	800	s	15	84	12		4				87	13	0
PNM 5_24	S	e	800	s	15	86	10		4				89	11	0
PNM 5_24	S	e	800	s	15	87	10		3				90	10	0
PNM 5_24	S	e	800	s	20	84	9		5	1			90	10	0
PNM 5_24	S	e	800	s	25	84	11		4				89	11	0
PNM 5_24	S	e	800		30	61	5	13	16	4			77	7	16
PNM 5_24	S	e	800		30	63	5	11	14	6			79	7	14
PNM 5_24	S	e	800		30	67	6	13	9	5			78	7	15
PNM 5_24	S	e	800		30	72	6	11	7	4			81	7	12
PNM 5_24	S	e	800		30	64	6	14	11	4			76	7	17
PNM 5_24	S	e	800		30	60	6	16	12	6			73	7	20
PNM 5_24	S	e	800		30	64	6	16	10	4			74	7	19
PNM 5_24	S	e	800		30	63	6	16	11	4			74	7	19
PNM 5_24	S	e	800		30	62	7	15	11	5			74	9	17
PNM 5_24	S	e	800		30	59	5	12	17	7			78	7	15
PNM 5_24	S	e	800	s	30	85	9		4				91	9	0
PNM 5_24	S	e			10	48	10	15	16	5	6		66	14	20
PNM 5_24	S	e			10	24	13	30	24	9		0	36	19	45
PNM 5_24	S	e			25	67	4	17	7	4	0		76	5	19
PNM 5_24	S	e		s	25	86	8		4	1			91	9	0
PNM 5_24	S	i	600		30	83	9		6	2	1		90	10	0
PNM 5_24	S	i	600		30	78	6		10	5	0		93	7	0
PNM 5_24	S	i	600		30	75	6		11	8	1		93	7	0
PNM 5_24	S	i	600		30	71	6		14	9	1		93	7	0
PNM 5_24	S	i	600		30	77	9		8	6	1		90	10	0
PNM 5_24	S	i	600		30	77	8		8	6	1		91	9	0
PNM 5_24	S	i	600		30	80	7		7	5	1		92	8	0
PNM 5_24	S	i	600		30	81	7		8	4	0		92	8	0
PNM 5_24	S	i	600		30	79	7		9	5	1		92	8	0
PNM 5_24	S	i	600		30	71	6		16	7	0		92	8	0
PNM 5_24	S	i			10	81	8		7	2	2		91	9	0
PNM 5_24	S	i			25	77	6		9	6			93	7	0
PNM 5_24	S	i			25	78	6		7	6	1		92	8	0
BXL 2_15	Sc	e			10	77	0	8	6	2	5		90	0	10
BXL 2_15	Sc	e			10	65		14	11	4	5	1	82	0	18
BXL 2_15	Sc	e		s	25	89	2	1	3	4	1		97	2	1
BXL 2_15	Sc	e			25	81		4	5	6	2		95	0	5
BXL 2_15	Sc	e			25	64			20	5	10		100	0	0
BXL 2_15	Sc	i			25	62	2	4	19	5	6	0	91	3	6
HCP 140B6	Ag	e	500		7	87	1		5	2	4	0	99	1	0
HCP 140B6	Ag	e	500		7	86	3		6	3	1	0	97	3	0
HCP 140B6	Ag	e	500		10	85	4		5	2	1	0	95	5	0
HCP 140B6	Ag	e	500		15	86	4		5	3	1	0	96	4	0
HCP 140B6	Ag	e	500		15	85	5		5	3	0	0	95	5	0
HCP 140B6	Ag	e	500		20	85	4		6	3	0	0	96	4	0

Sample	Group *	Side **	Mag. ***	Comment +	Acc. vol. ++	Weight %							100*n / (Ag+Cu+Au)		
						Ag L	Cu L/K	Au M/L	C K	O K	S K	Cl K	n=Ag	n=Cu	n=Au
HCP 140B6	Ag	e	500		30	85	5		6	3	0		95	5	0
HCP 140B6	Ag	i	500		7	79	4		8	3	3	1	95	5	0
HCP 140B6	Ag	i	500		30	82	5		6	4	1		94	6	0
HCP 140B6	Ag	i	700	c	7	82	3		7	2	4	0	97	3	0
HCP 140B6	Ag	i	2k	c	7	92	2		3	1	1		98	2	0
HCP 140B6	Ag	i	3k	c	7	77	2		8	2	9	1	97	3	0
PNM 1_01	Ag	e	500		30	75	4		11	8	2	0	95	5	0
PNM 1_01	Ag	e	500		30	56	3		21	14	5	1	95	5	0
PNM 1_01	Ag	e	500		30	75	4		11	8	1	0	95	5	0
PNM 1_01	Ag	e	500		30	74	5		10	8	2	0	93	7	0
PNM 1_01	Ag	e	500		30	72	5		12	9	3		94	6	0
PNM 1_01	Ag	i	500		30	81	4		9	6	1		95	5	0
PNM 1_01	Ag	i	500		30	76	5		11	6	2		94	6	0
PNM 1_01	Ag	i	500		30	70	6		10	11	3		92	8	0
PNM 1_01	Ag	i	500		30	77	5		10	7	2		94	6	0
PNM 1_01	Ag	i	500		30	69	5		13	8	5		93	7	0
PNM 2_18	Ag	e	500		30	65	8		15	10	2		89	11	0
PNM 2_18	Ag	e	500		30	68	8		13	9	2		90	10	0
PNM 2_18	Ag	e	500		30	54	6		26	12	2		89	11	0
PNM 2_18	Ag	e	500		30	70	7		13	9	1		91	9	0
PNM 2_18	Ag	e	500		30	73	8		10	7	2		90	10	0
PNM 2_18	Ag	i	500		30	76	8		9	6	1		91	9	0
PNM 2_18	Ag	i	500		30	76	7		9	7	1		91	9	0
PNM 2_18	Ag	i	500		30	67	7		15	8	3		90	10	0
PNM 2_18	Ag	i	500		30	73	8		10	7	2		90	10	0
PNM 2_18	Ag	i	500		30	69	9		11	7	3		88	12	0
PNM 2_18	Ag	i	500		30	72	9		10	7	3		89	11	0
PNM 2_18	Ag	i	500		30	71	8		10	6	4		90	10	0
PNM 2_18	Ag	i	500		30	70	8		11	7	3		90	10	0
PNM 2_18	Ag	i	500		30	69	10		11	7	3		88	12	0
PNM 2_18	Ag	i	500		30	67	9		14	7	3		88	12	0
PNM 5_09	Ag	e	500		7	72	8		9	6	3	1	90	10	0
PNM 5_09	Ag	e	500		30	76	7		8	6	1	0	91	9	0
PNM 5_09	Ag	i	500		7	68	8		10	7	2	4	89	11	0
PNM 5_09	Ag	i	500		30	79	6		7	5	1	0	93	7	0
HCP 28G6	2x	x			20	96	4						96	4	0
HCP 28G6	2x	x			20	96	3				2		97	3	0
HCP 28G6	2x	x			20	71	6			10	12	1	93	7	0
HCP 28G6	2x	x			20	45	2	53					45	2	53
PNM 1_36	3x	x			20	92	8					1	92	8	0
PNM 1_36	3x	x			20	93	5				2	0	95	5	0
PNM 1_36	3x	x			20	34	3	63					34	3	63
BXL 2_14	R	e	500		7	80	1	6	4	2	4	2	92	1	7
BXL 2_14	R	e	500		30	79	1	1	7	3	4	1	97	2	1
BXL 2_14	R	e	500		30	73	1	10	6	4	3	1	87	1	12
BXL 2_14	R	e	15k	g	7	21	1	72	4	1	1	0	22	1	77
BXL 2_14	R	e	2k	c	7	77	1		5	2	8	7	99	1	0
BXL 2_14	R	e	6k	c	7	74	0		6	3	9	6	100	0	0
BXL 2_14	R	i	500		7	73	2	1	9	3	9	3	97	2	1
BXL 2_14	R	i	500		7	71	1	4	9	3	8	3	93	2	6
BXL 2_14	R	i	500		30	68	2	2	12	4	10	1	95	3	2
BXL 2_14	R	i	500		30	66	2	7	10	4	8	1	89	2	9

Sample	Group *	Side **	Mag. ***	Comment +	Acc. vol. ++	Weight %							100*n / (Ag+Cu+Au)		
						Ag L	Cu L/K	Au M/L	C K	O K	S K	Cl K	n=Ag	n=Cu	n=Au
BXL 2_14	R	i	13k	g	7	73	2	1	9	3	9	3	97	2	1
BXL 2_24	R	x			20	3	0		78	19	0		93	7	0
BXL 2_24	R	x			20	13			72	13	1		100	0	0
						Ag L	Cu L/K	Zn L/K	C K	O K	S K	Cl K	n=Ag	n=Cu	n=Zn
BXL 2_07	R	e	500		7		45	21	21	11	2	1	0	68	32
BXL 2_07	R	e	500		7		51	27	11	7	1	1	0	65	35
BXL 2_07	R	e	500		30		73	11	10	3	1	0	0	86	14
BXL 2_07	R	e	500		30		73	11	10	3	1	0	0	86	14
BXL 2_07	R	e	37k	c	7		14	31	32	18	2	1	0	32	68
BXL 2_07	R	i	500		7		43	22	24	9	1	1	0	67	33
BXL 2_07	R	i	500		30		62	10	20	5	0	0	0	86	14
BXL 2_07	R	i	500		30		65	11	17	5	0	0	0	85	15

H. Positive dynamic SIMS depth profiles of metal threads

H.1. HCP_68E6 exterior

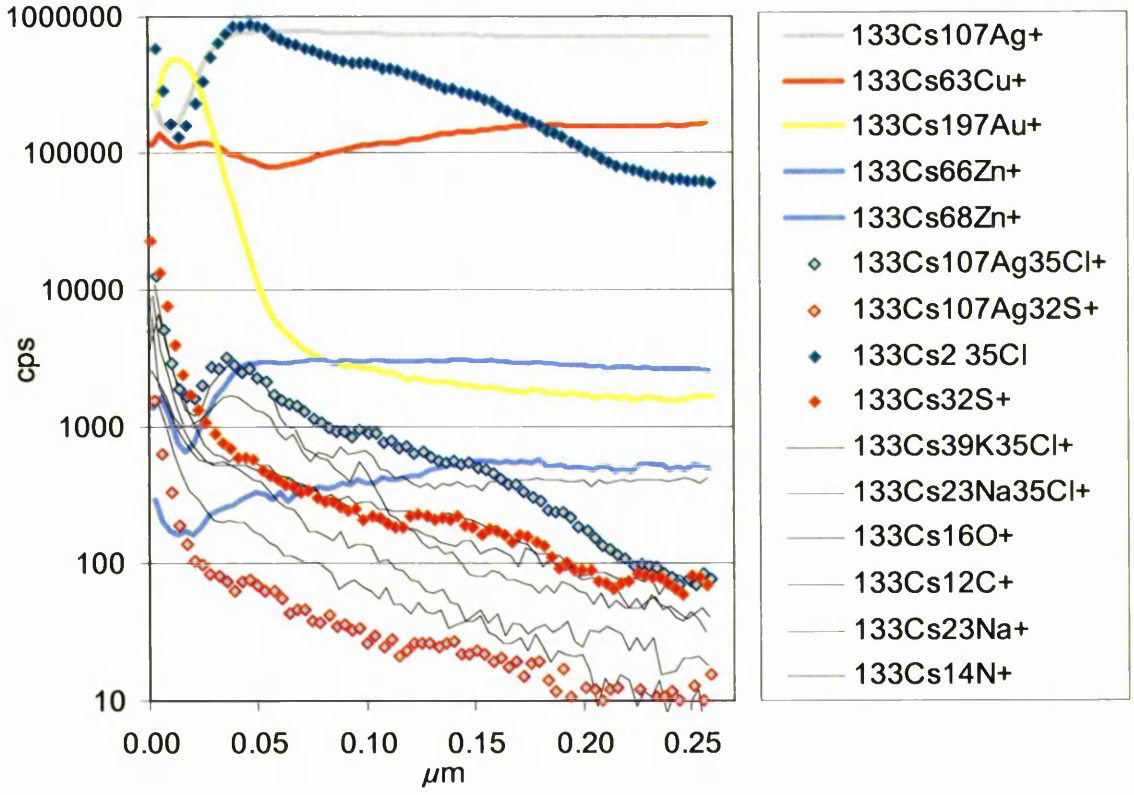

H.2. HCP_68E6 interior

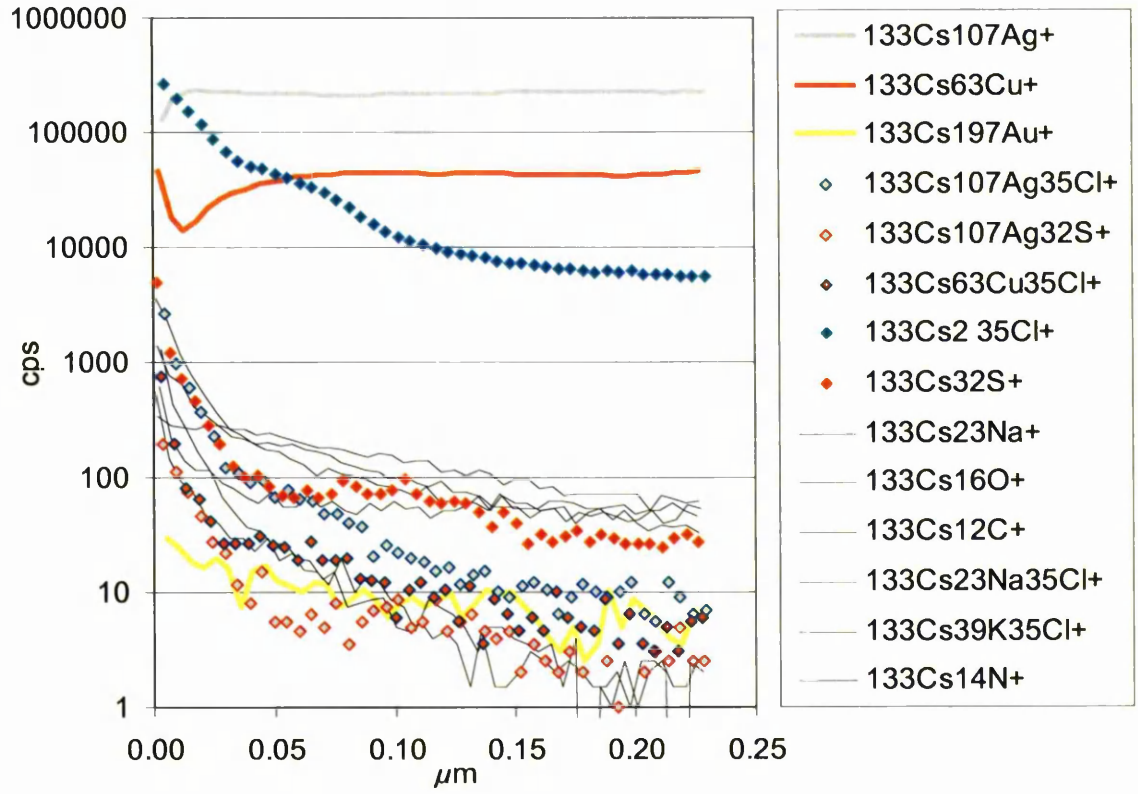

H.3. HCP_120C3 exterior

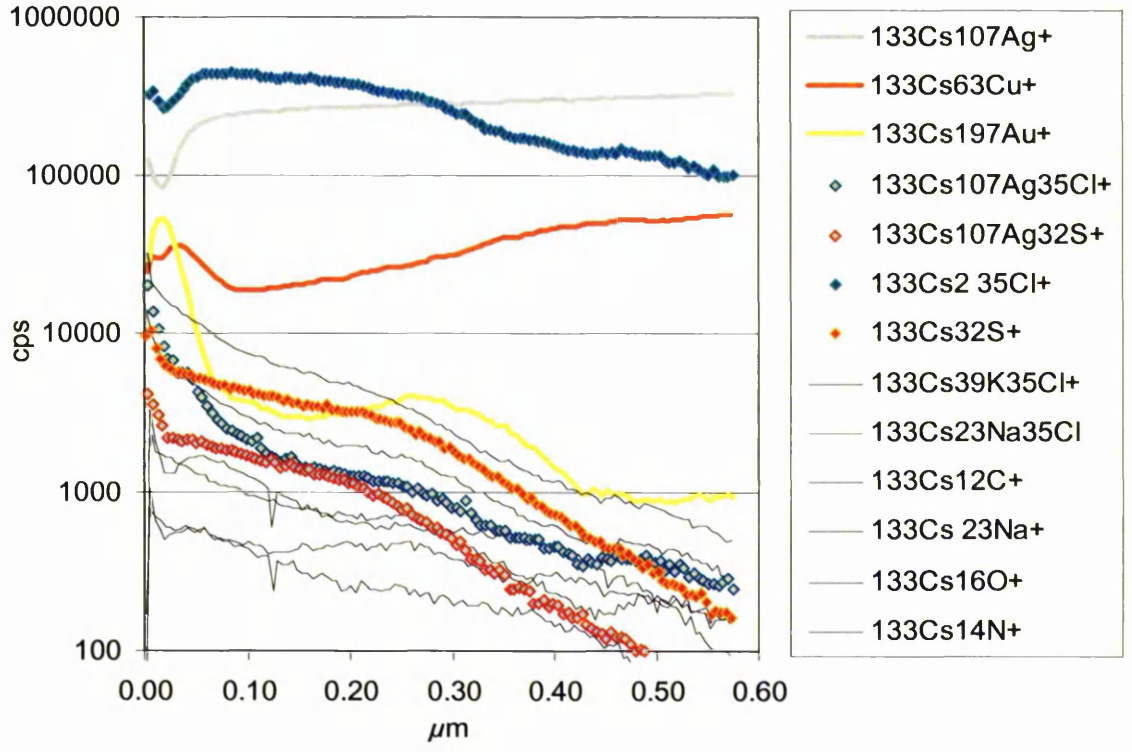

H.4. HCP_120C3 interior

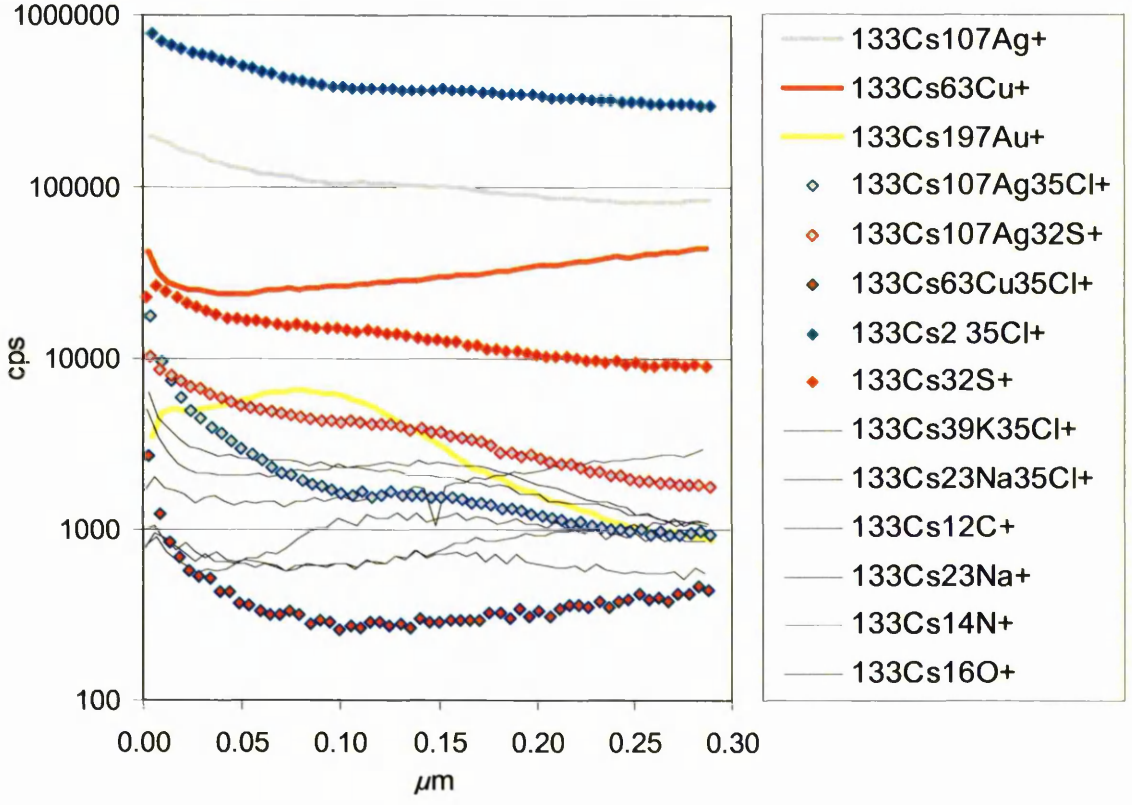

H.5. PNM1_38 exterior

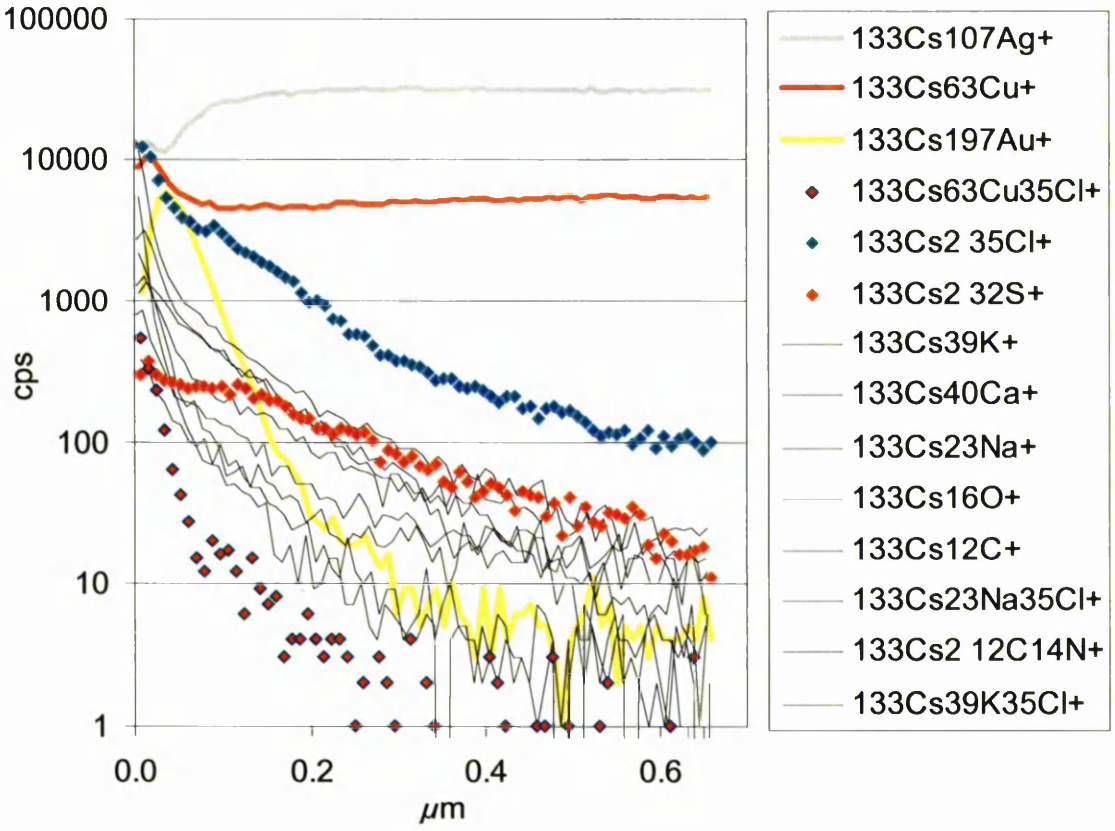

H.6. PNM1_38 interior

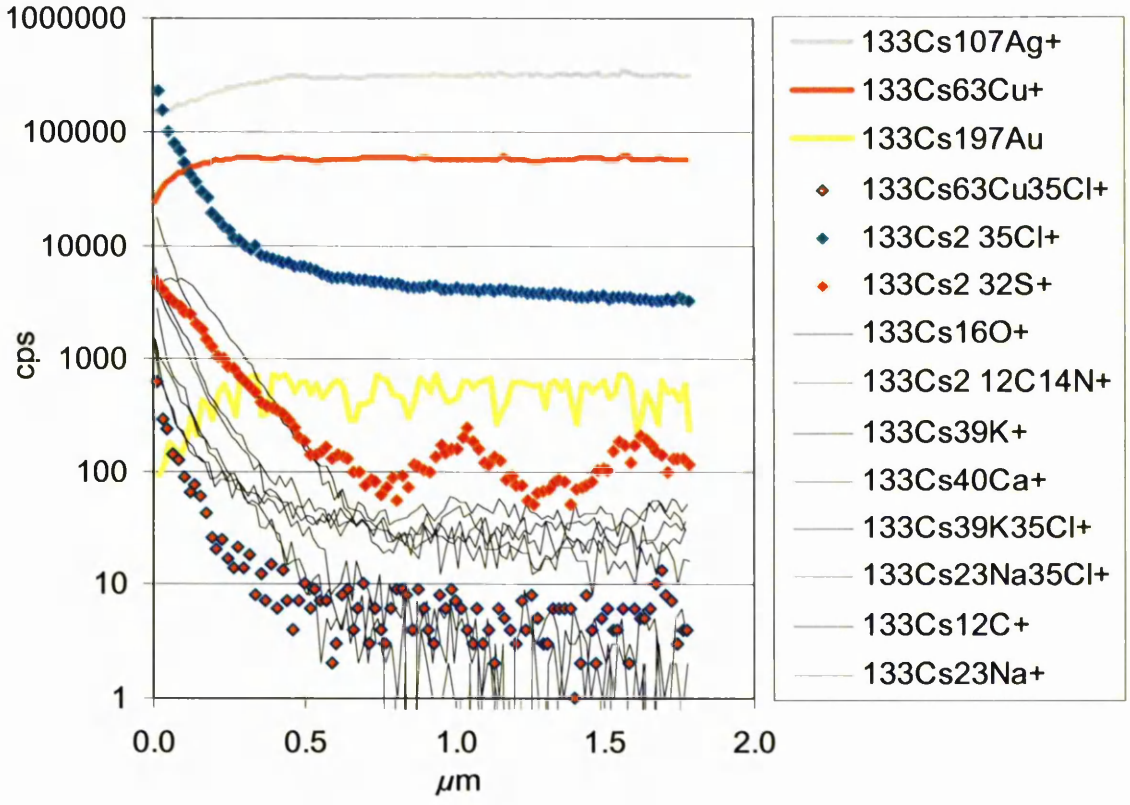

H.7. PNM2_19 exterior

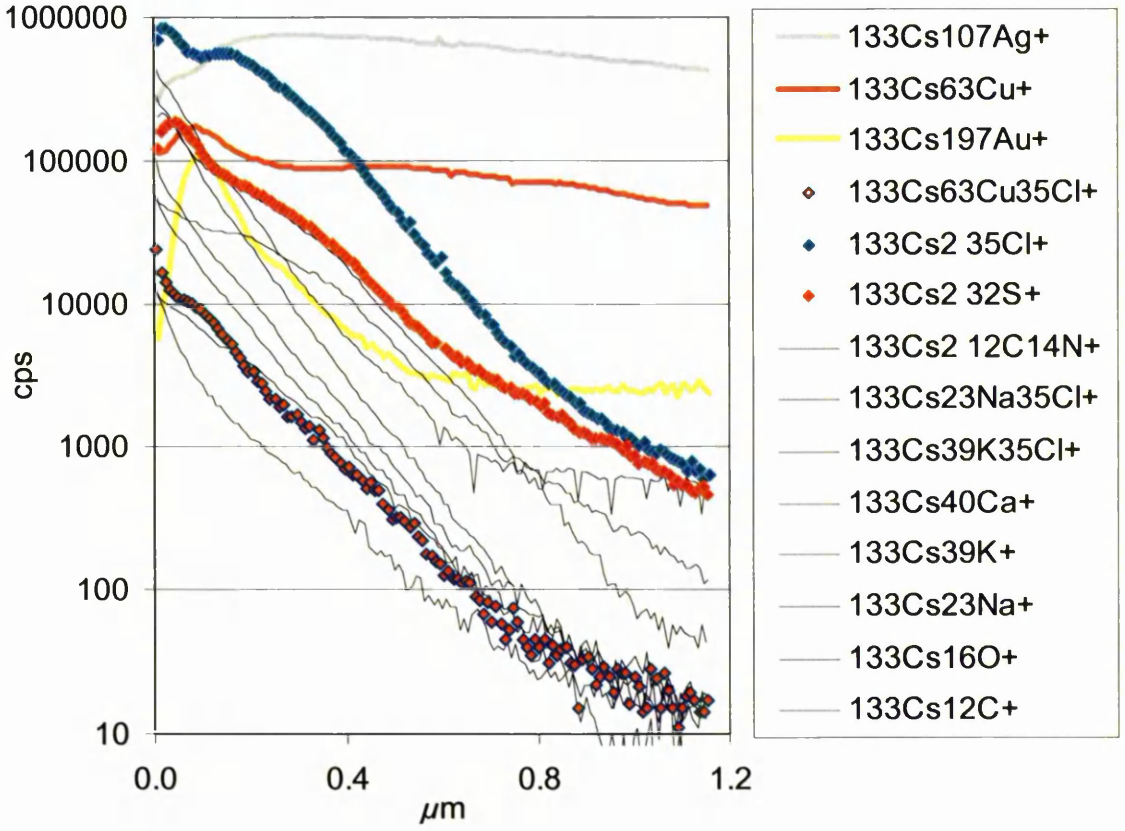

H.8. PNM5_24 exterior

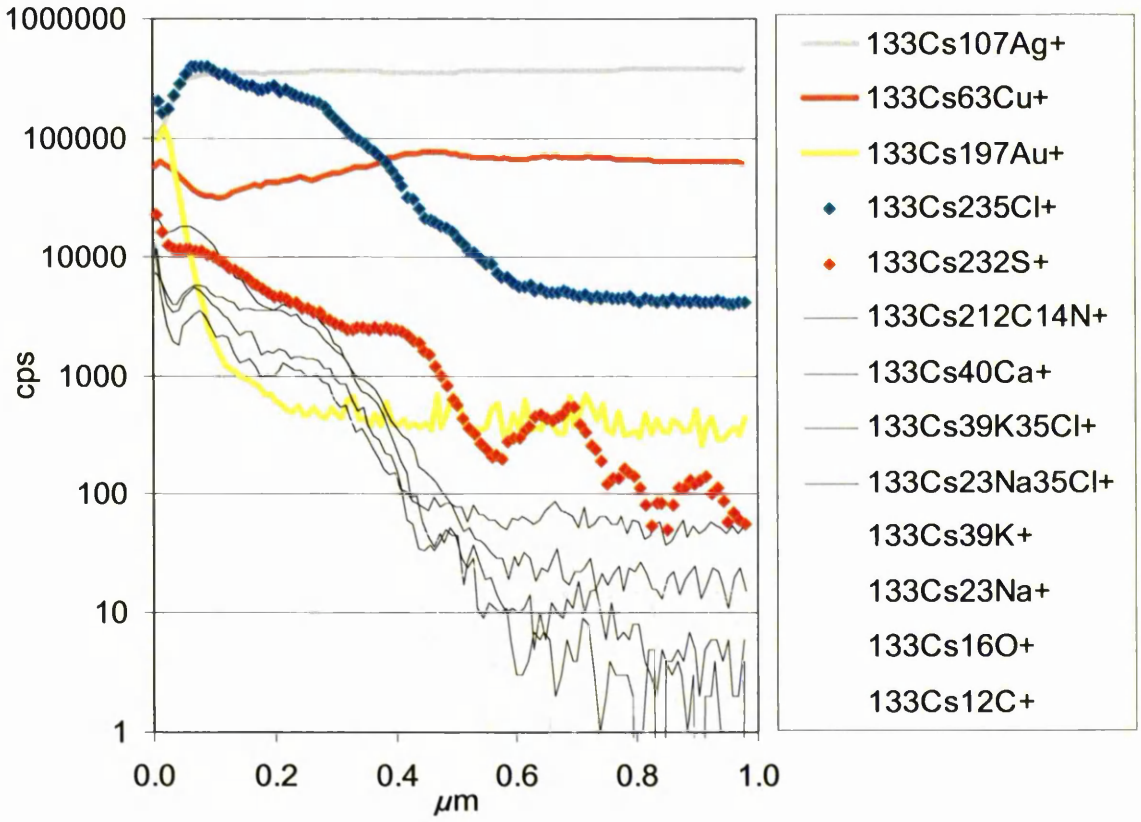

H.9. BXL2_15 exterior

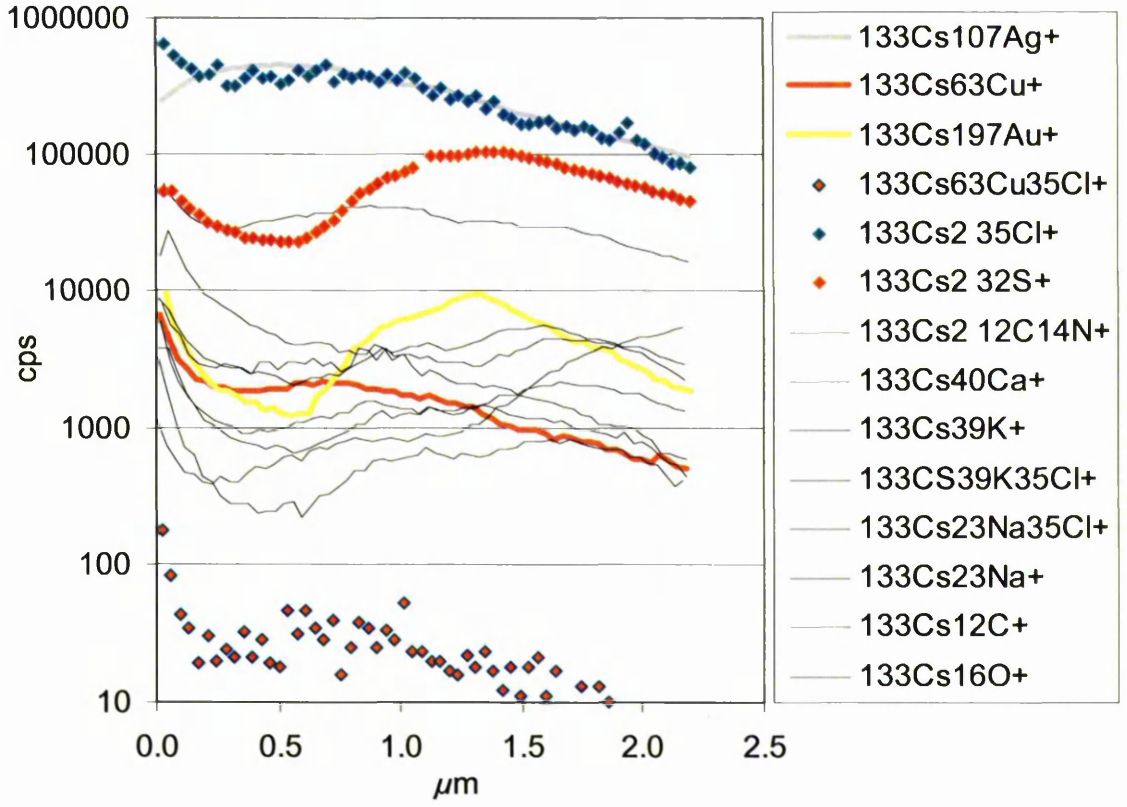

I. XRD patterns of metal threads

I.1. HCP_21G3

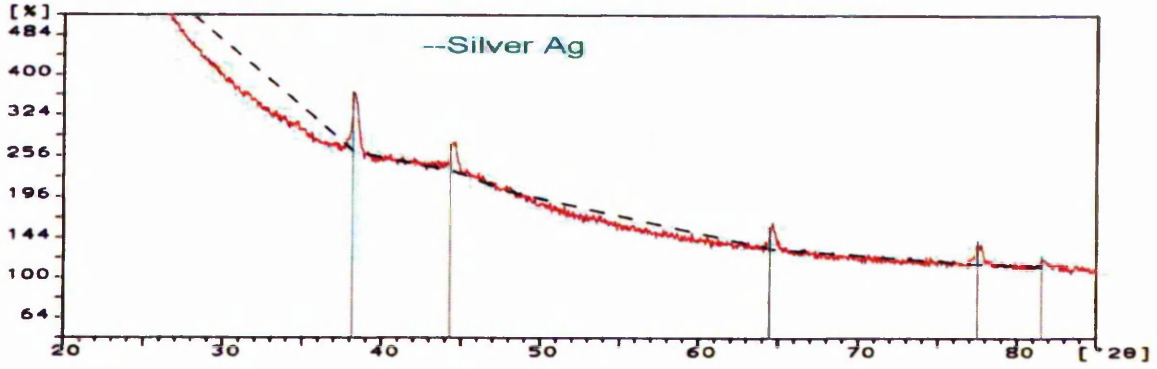

I.2. PNM1_21

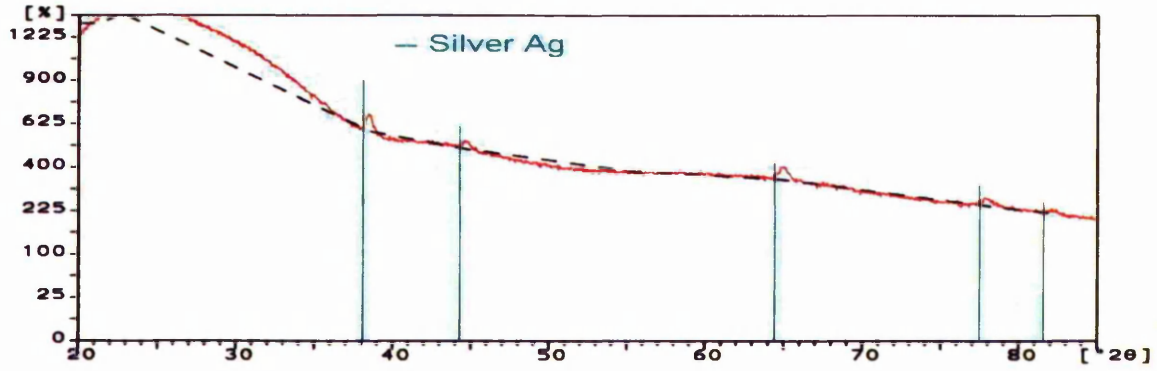

I.3. PNM2_04

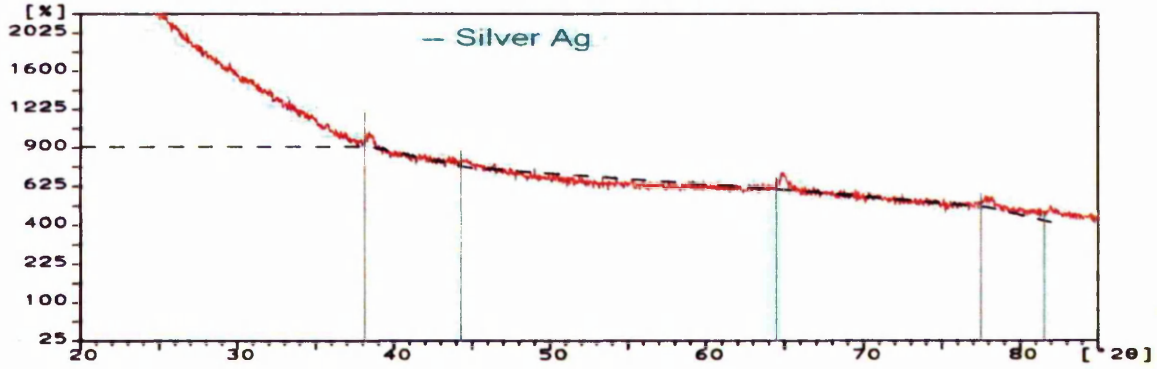

I.4. BXL2_11

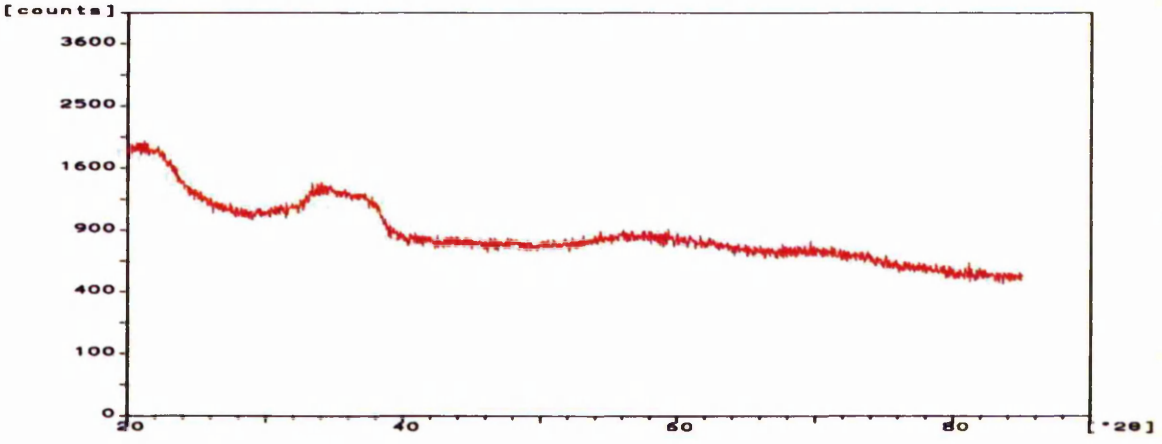

J. XPS data of Oddy tested Ag and Cu coupons

J.1. Atomic % of light Oddy tested Ag coupons

Sample		Atomic %							
		Ag (3d)	Cu (2p)	O (1s)	C (1s)	S (2p)	Sn (3d)	N (1s)	Cl (2p)
-	Control	31.65	0.27	16.10	41.43	2.55	2.28	2.42	3.31
Silk	Undyed	34.10	3.27	5.93	36.37	20.20	0.03	0.00	0.11
	Brazilwood	33.63	1.81	11.76	33.07	15.51	1.98	0.86	1.39
	Madder	31.40	4.12	9.17	34.54	17.09	1.63	0.62	1.44
	Madder	31.03	3.75	8.31	38.01	16.60	0.90	0.00	1.41
	Woad	29.67	4.24	8.36	38.03	18.27	0.37	0.31	0.76
Wool	Undyed	26.83	4.74	15.00	38.42	13.01	1.26	0.00	0.75
	Brazilwood	37.90	2.60	15.31	21.88	21.83	0.26	0.13	0.09
	Brazilwood	40.11	3.49	4.08	26.06	26.04	0.11	0.10	0.00
	Madder	32.41	2.03	9.51	35.81	16.13	1.40	0.05	2.65
	Madder	31.25	1.50	11.68	33.68	16.17	0.63	2.60	2.49
	Weld	32.61	3.70	5.22	36.51	20.49	0.41	0.00	1.07
	Weld	34.25	2.33	5.69	37.25	19.28	0.11	0.09	1.01

J.2. Atomic % of light Oddy tested Cu coupons

Sample		Atomic %							
		Cu (2p)	Ag (3d)	O (1s)	C (1s)	S (2p)	Sn (3d)	N (1s)	Cl (2p)
-	Control	10.88	0.12	29.12	55.39	1.00	1.14	2.23	0.12
Silk	Undyed	12.24	0.11	24.39	56.18	4.04	1.32	1.41	0.30
	Brazilwood	10.20	0.05	28.42	55.79	2.35	1.15	1.93	0.13
	Madder	10.57	0.00	25.58	57.21	3.34	0.73	2.44	0.13
	Weld	7.55	0.00	17.72	70.63	1.47	0.99	1.49	0.15
	Woad	9.65	0.24	20.65	63.07	2.86	1.48	2.02	0.03
Wool	Undyed	19.43	0.03	20.23	47.03	11.90	0.00	0.99	0.40
	Brazilwood	15.01	0.08	22.60	54.53	6.75	0.10	0.93	0.00
	Madder	11.61	0.18	18.97	58.39	7.77	0.45	2.15	0.48
	Weld	15.38	0.00	21.66	55.19	6.56	0.21	0.84	0.16
	Woad	12.84	0.01	21.48	58.38	6.62	0.00	0.67	0.00

J.3. Atomic % of thermal Oddy tested Ag coupons

Sample		Atomic %							
		Ag (3d)	Cu (2p)	O (1s)	C (1s)	S (2p)	Sn (3d)	N (1s)	Cl (2p)
-	Control	34.34	0.00	16.02	40.66	2.39	3.55	1.96	1.08
	Control	31.37	0.00	14.31	46.95	2.21	1.65	1.55	1.96
	Control	33.43	0.02	14.61	44.10	2.45	2.35	0.97	2.06
Silk	Undyed	32.13	0.39	15.73	40.91	6.67	1.89	0.72	1.57
	Undyed	36.15	0.19	12.70	39.79	4.69	2.72	1.42	2.34
	Alum	36.07	0.00	13.71	38.81	6.07	2.42	1.28	1.63
	Alum	37.95	0.00	13.24	36.80	6.53	2.61	1.72	1.16
	Alum	35.12	0.00	15.41	39.41	5.08	2.46	2.04	0.49
	Madder	33.44	0.56	14.47	40.78	5.60	1.50	1.66	1.99
	Madder	34.30	0.41	14.17	40.06	6.62	1.50	1.73	1.22
Wool	Undyed	28.19	1.27	14.63	39.06	12.04	2.18	1.08	1.55
	Undyed	34.45	0.56	12.22	37.14	10.15	2.27	1.32	1.89
	Alum	39.77	0.10	11.27	33.58	10.43	1.74	0.84	2.27
	Alum	34.04	0.97	12.21	34.08	16.20	1.24	0.37	0.90
	Alum	36.95	0.32	9.38	33.33	16.92	1.27	0.70	1.14
	Madder	25.08	1.45	17.95	40.60	12.35	1.05	0.65	0.88
	Madder	26.24	1.77	15.35	40.95	13.82	0.93	0.25	0.69

J.4. Atomic % of thermal Oddy tested Cu coupons

Sample		Atomic %							
		Cu (2p)	Ag (3d)	O (1s)	C (1s)	S (2p)	Sn (3d)	N (1s)	Cl (2p)
-	Control	11.88	0.00	31.57	51.91	0.59	1.16	2.79	0.10
	Control	11.42	0.00	30.86	53.37	0.62	1.19	2.56	0.00
	Control	11.21	0.00	30.61	54.17	0.42	1.20	2.37	0.02
Silk	Undyed	11.45	0.00	29.03	55.47	0.63	1.11	2.24	0.07
	Undyed	13.69	0.05	27.58	55.76	0.63	0.44	1.80	0.05
	Alum	11.42	0.00	38.41	49.48	0.24	0.04	0.31	0.11
	Alum	11.32	0.03	36.50	51.24	0.34	0.02	0.57	0.00
	Alum	8.51	0.00	26.10	63.41	1.22	0.02	0.74	0.00
	Madder	12.58	0.00	28.55	55.72	1.42	0.72	0.85	0.11
	Madder	12.03	0.00	28.17	57.02	0.81	0.73	1.12	0.11
Wool	Undyed	12.47	0.06	26.85	55.50	2.97	0.39	1.72	0.05
	Undyed	14.26	0.04	31.34	49.27	3.35	0.13	1.60	0.00
	Alum	11.06	0.00	23.23	59.43	3.90	0.45	1.70	0.24
	Alum	11.23	0.00	22.33	59.00	5.14	0.36	1.82	0.13
	Alum	12.33	0.00	23.06	58.86	4.39	0.11	1.25	0.00
	Madder	11.44	0.00	29.87	56.49	1.51	0.13	0.47	0.09
	Madder	11.89	0.00	29.31	56.35	1.60	0.15	0.57	0.12

J.5. Relative % of S (2p) peak component of light Oddy tested Ag and Cu coupons

Sample		Ag Oddy light			Cu Oddy light		
		S (2p) total atomic %	Relative % S^{2+}	Relative % S^{6+}	S (2p) total atomic %	Relative % S^{2+}	Relative % S^{6+}
	Control	2.5	87.6	12.4	1.0	*	*
Silk	Undyed/S	20.2	97.0	3.0	4.0	74.7	25.3
	Brazil/S	15.5	97.2	2.8	2.4	*	*
	Madder/S	17.1	97.1	2.9	3.3	59.3	40.7
	Weld/S	*	97.4	2.6	1.5	55.4	44.6
	Woad/S	18.3	96.9	3.1	2.9	77.4	22.6
Wool	Undyed/W	13.0	96.0	4.0	11.9	95.5	4.5
	Brazil/W	21.8	96.9	3.1	6.8	94.0	6.0
	Madder/W	16.1	98.0	2.0	7.8	*	*
	Weld/W	20.5	98.4	1.6	6.6	96.1	3.9
	Woad/W	*	99.9	0.1	6.6	97.6	2.4

* : no analysis data due to faulty or noisy spectra

J.6. Relative % of S (2p) peak component of thermal Oddy tested Ag and Cu coupons

Sample		Ag Oddy thermal			Cu Oddy thermal		
		S (2p) total atomic %	Relative % S^{2+}	Relative % S^{6+}	S (2p) total atomic %	Relative % S^{2+}	Relative % S^{6+}
	Control	2.4	79.9	20.1	0.6	*	*
	Control	2.2	84.6	15.4	0.6	*	*
	Control	2.5	82.3	17.7	0.4	*	*
Silk	Undyed	6.7	93.6	6.4	0.6	*	*
	Undyed	4.7	89.1	10.9	0.6	*	*
	Alum	6.5	*	*	0.2	*	*
	Alum	5.1	*	*	0.3	*	*
	Alum	6.1	93.6	6.4	1.2	73.7	26.4
	Madder	5.6	93.9	6.1	1.4	62.2	37.8
	Madder	5.6	*	*	1.4	56.9	43.1
	Madder	6.6	93.5	6.5	0.8	55.8	44.2
	Madder	6.6	93.9	6.1	0.8	62.7	37.3
Wool	Undyed	12.0	96.4	3.6	3.0	61.9	38.1
	Undyed	10.1	94.1	5.9	3.4	39.2	60.8
	Alum	10.4	97.3	2.8	3.9	80.1	19.9
	Alum	16.2	*	*	5.1	80.1	19.9
	Alum	16.9	97.9	2.1	4.4	78.9	21.1
	Madder	12.3	99.0	1.0	1.5	60.3	39.7
	Madder	12.3	98.0	2.0	1.5	46.9	53.1
	Madder	13.8	98.0	2.0	1.6	53.3	46.7
	Madder	13.8	98.4	1.6	1.6	55.5	44.5

* : no analysis data due to faulty or noisy spectra

K. ToF-SIMS spectra of detergent treated metal coupons and metal threads

K.1. ToF-SIMS spectra of silver coupons

Negative ion ToF-SIMS spectrum of 'Untreated clean Ag'

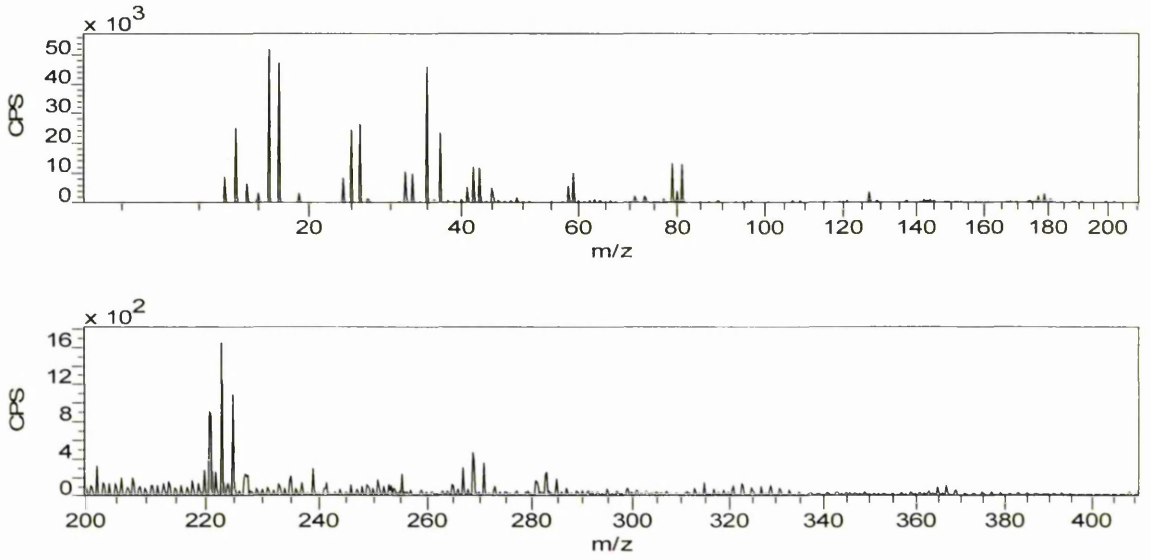

Positive ion ToF-SIMS spectrum of 'Untreated clean Ag'

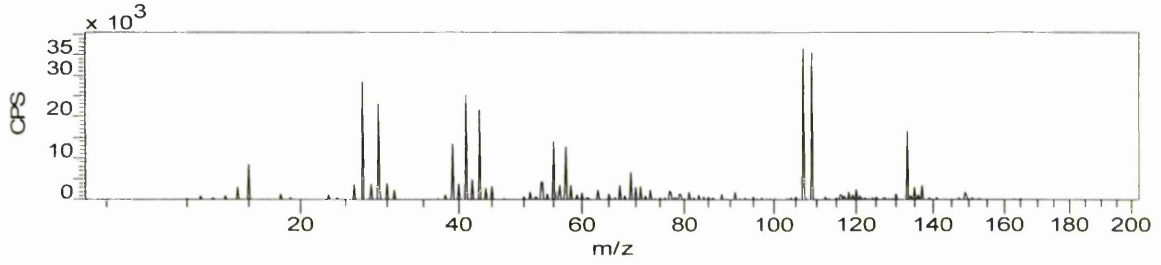

Negative ion ToF-SIMS spectrum of 'H_2O clean Ag'

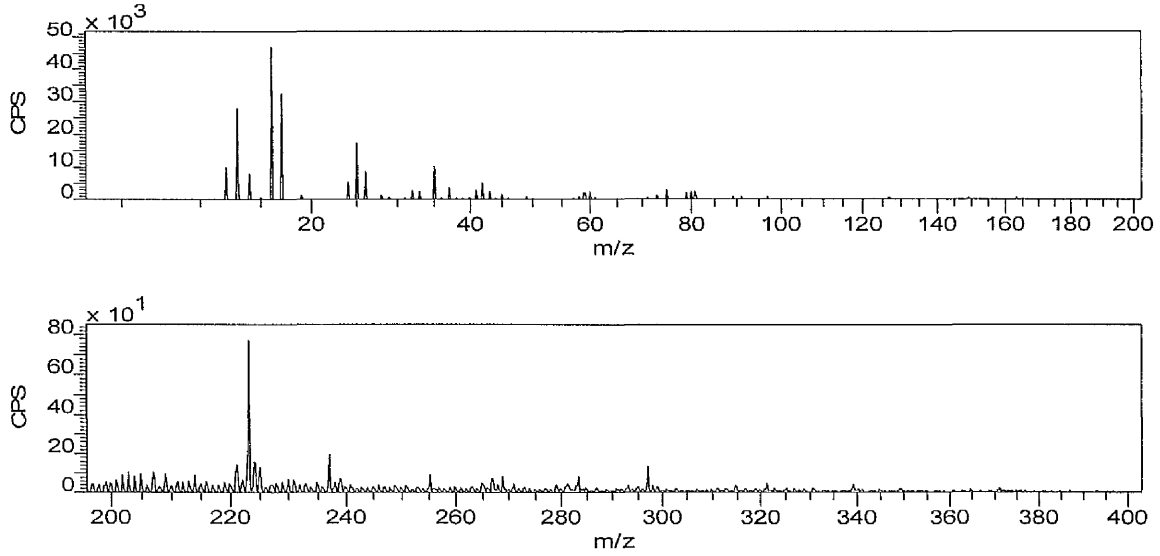

Positive ion ToF-SIMS spectrum of 'H_2O clean Ag'

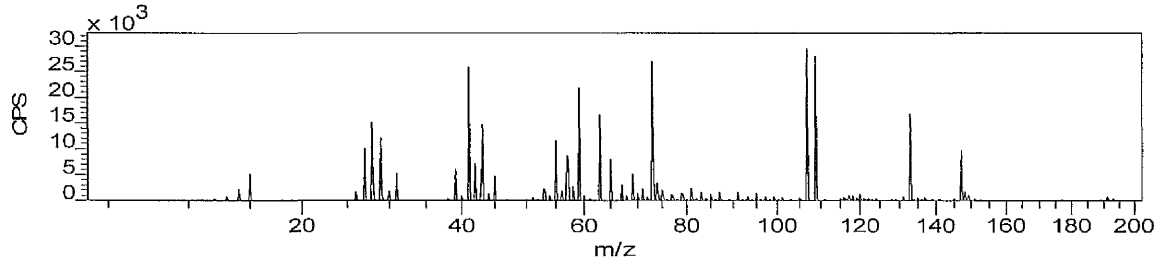

Negative ion ToF-SIMS spectrum of 'H_2O corroded Ag'

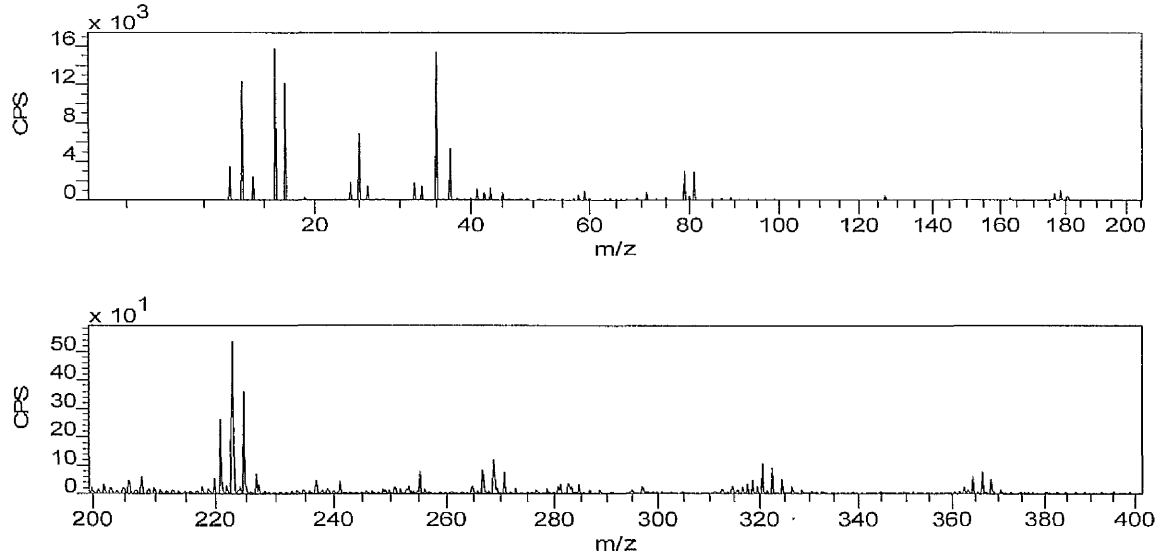

Positive ion ToF-SIMS spectrum of 'H_2O corroded Ag'

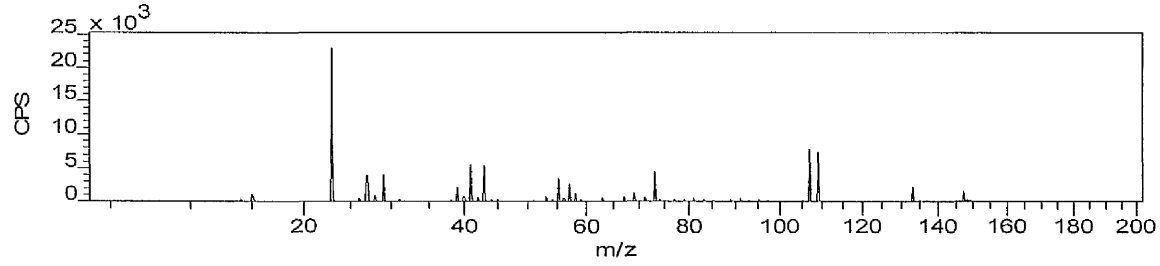

Negative ion ToF-SIMS spectrum of 'SDS 98% clean Ag'

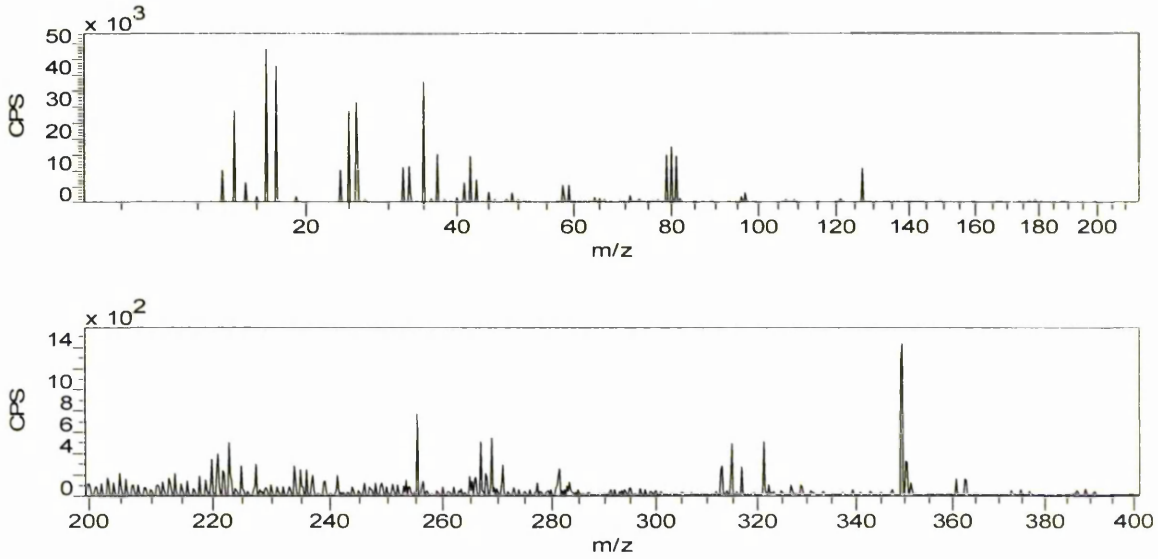

Positive ion ToF-SIMS spectrum of 'SDS 98% clean Ag'

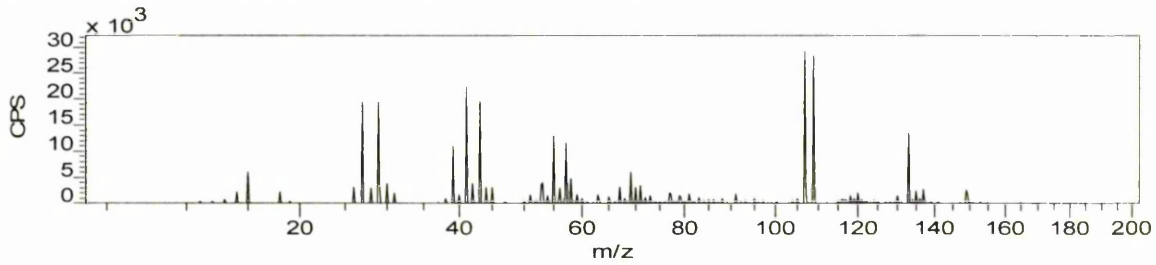

Negative ion ToF-SIMS spectrum of 'SDS 99% clean Ag'

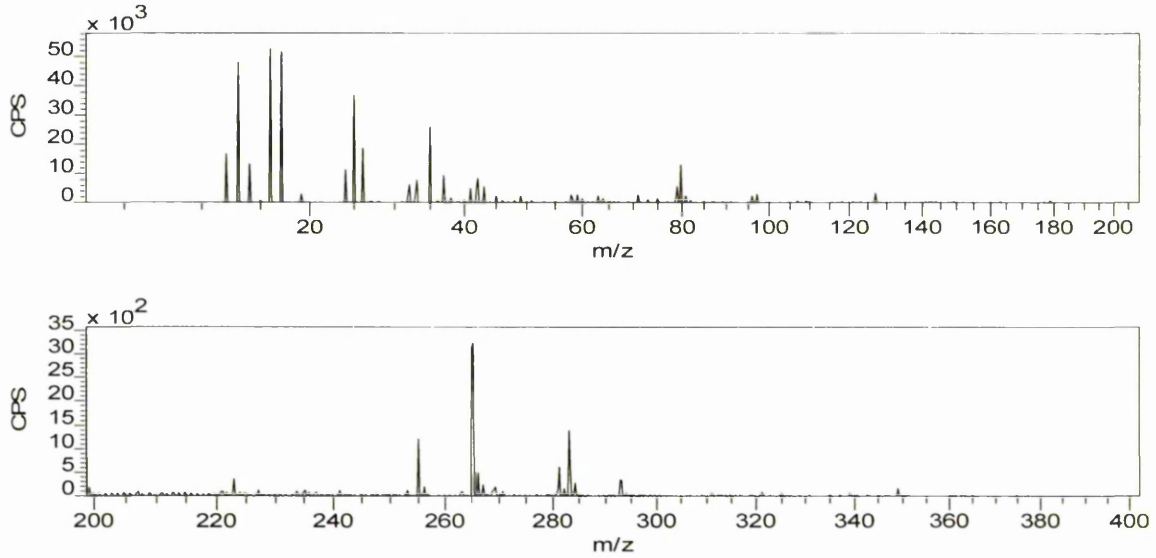

Positive ion ToF-SIMS spectrum of 'SDS 99% clean Ag'

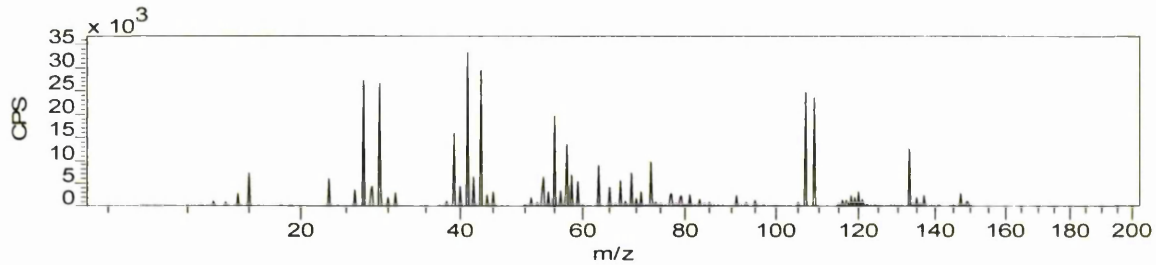

Negative ion ToF-SIMS spectrum of 'SDS 99% corroded Ag'

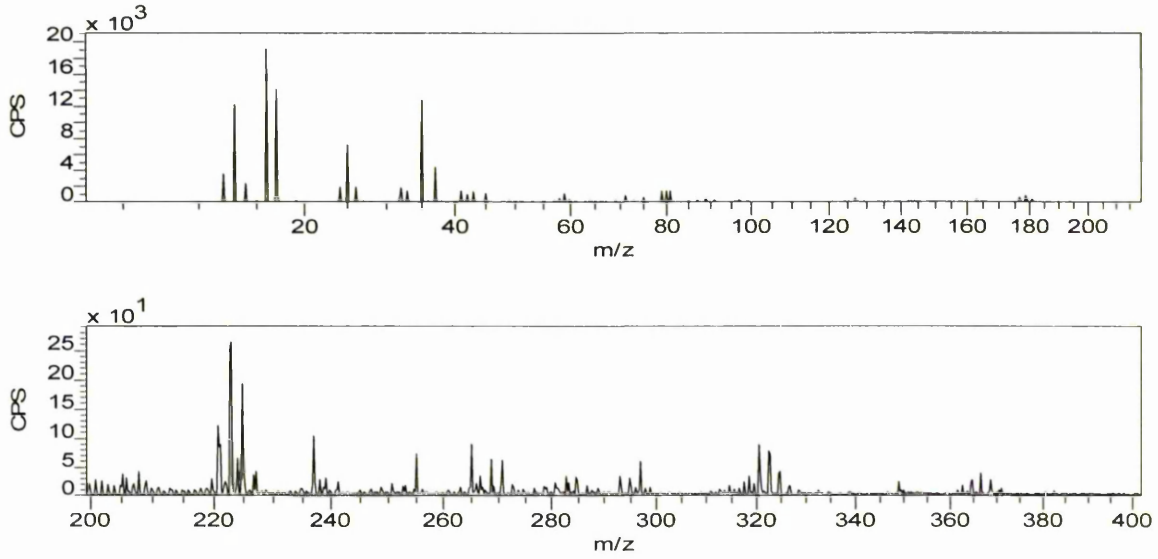

Positive ion ToF-SIMS spectrum of 'SDS 99% corroded Ag'

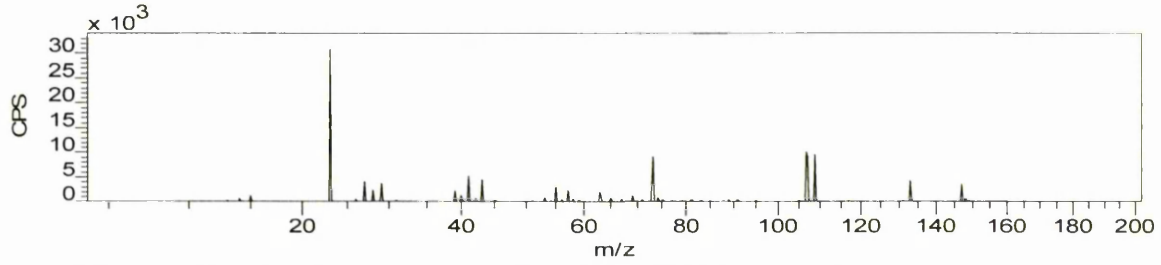

Negative ion ToF-SIMS spectrum of 'T-NP9 + SDS 99% clean Ag'

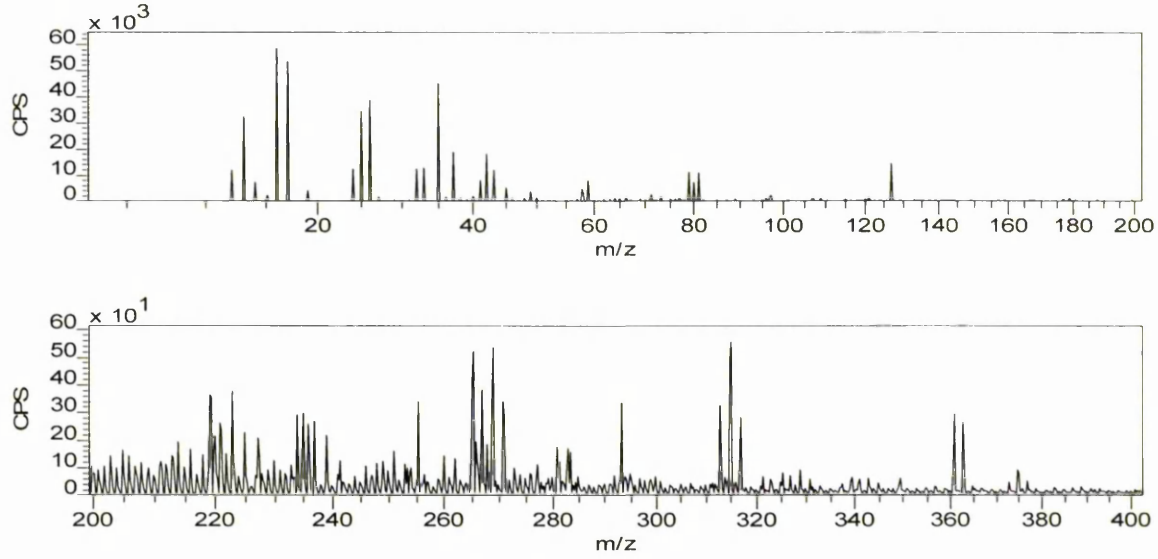

Positive ion ToF-SIMS spectrum of 'T-NP9 + SDS 99% clean Ag'

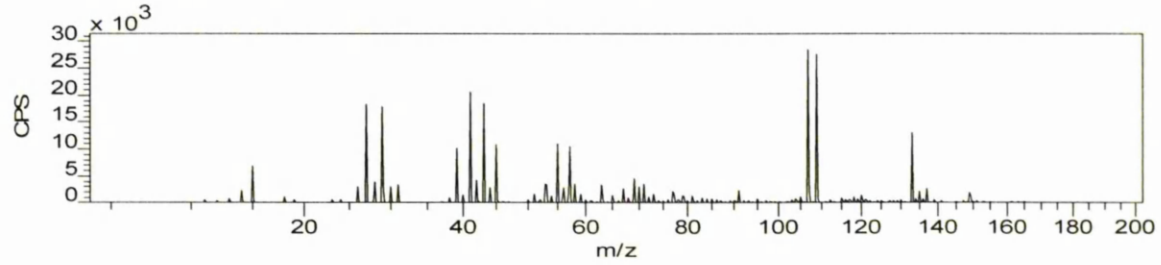

Negative ion ToF-SIMS spectrum of 'T-NP9 + SDS 99% corroded Ag'

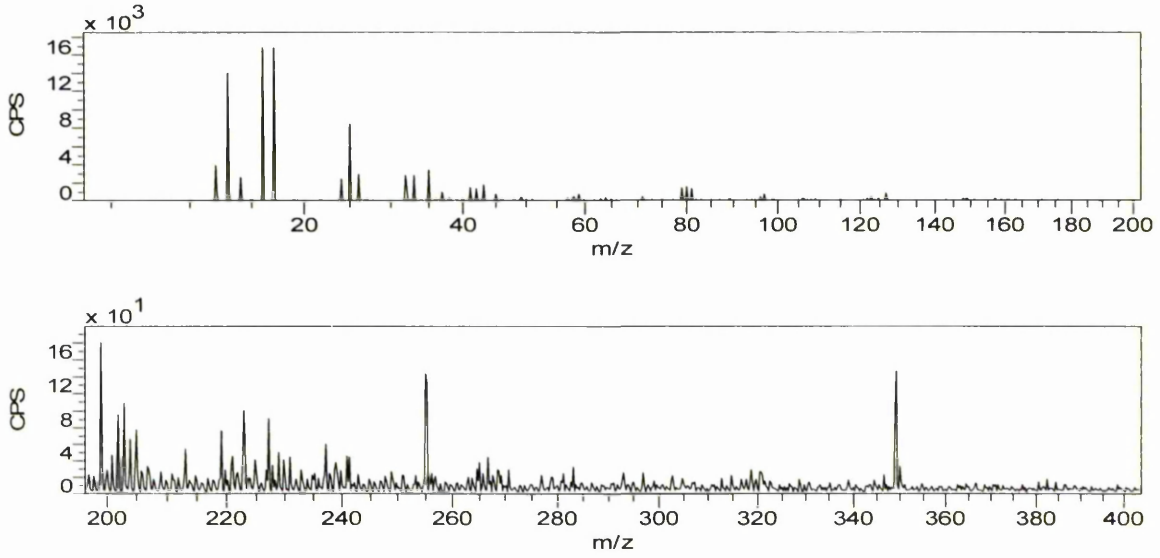

Positive ion ToF-SIMS spectrum of 'T-NP9 + SDS 99% corroded Ag'

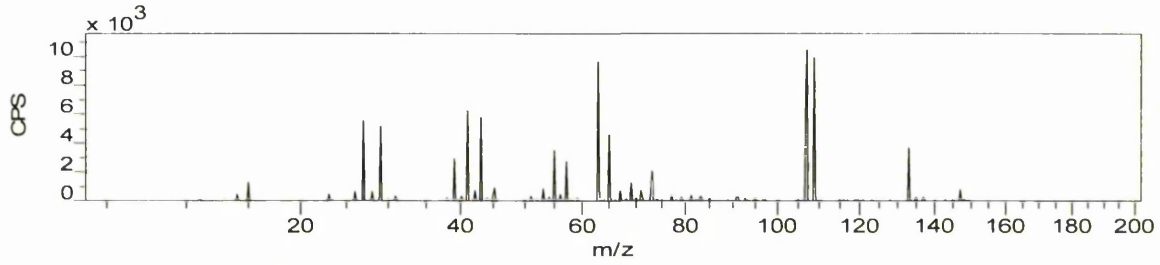

Negative ion ToF-SIMS spectrum of 'T-NP9 clean Ag'

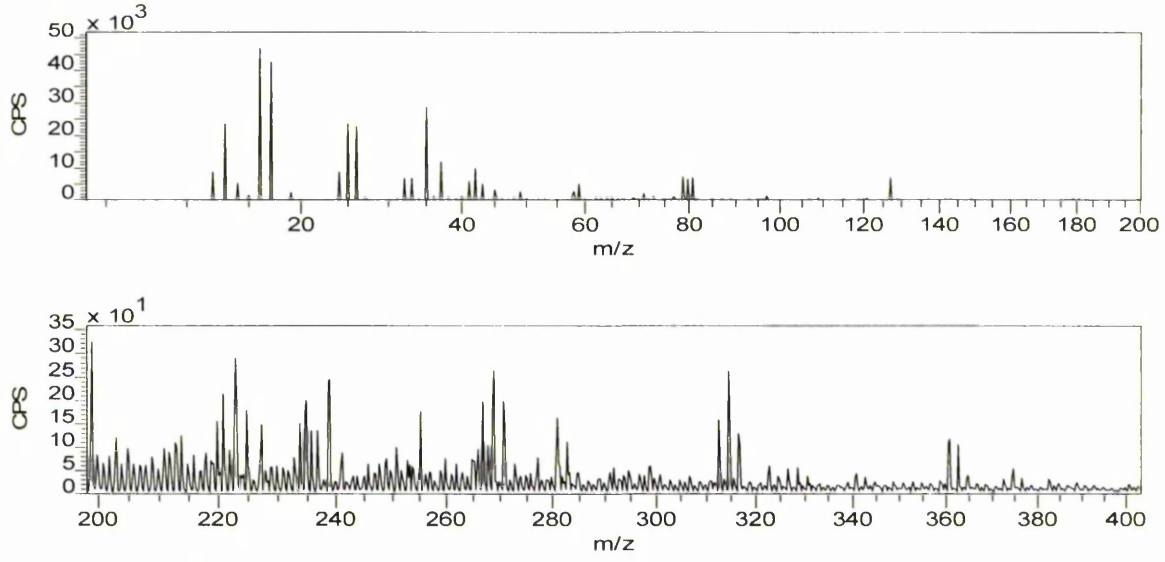

Positive ion ToF-SIMS spectrum of 'T-NP9 clean Ag'

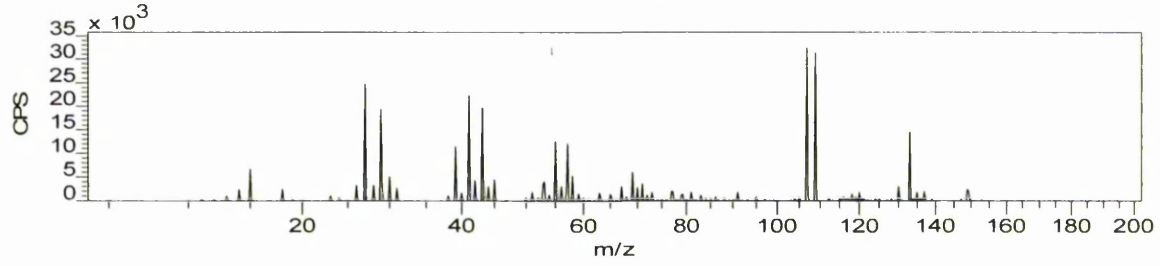

Negative ion ToF-SIMS spectrum of 'T-NP9 corroded Ag'

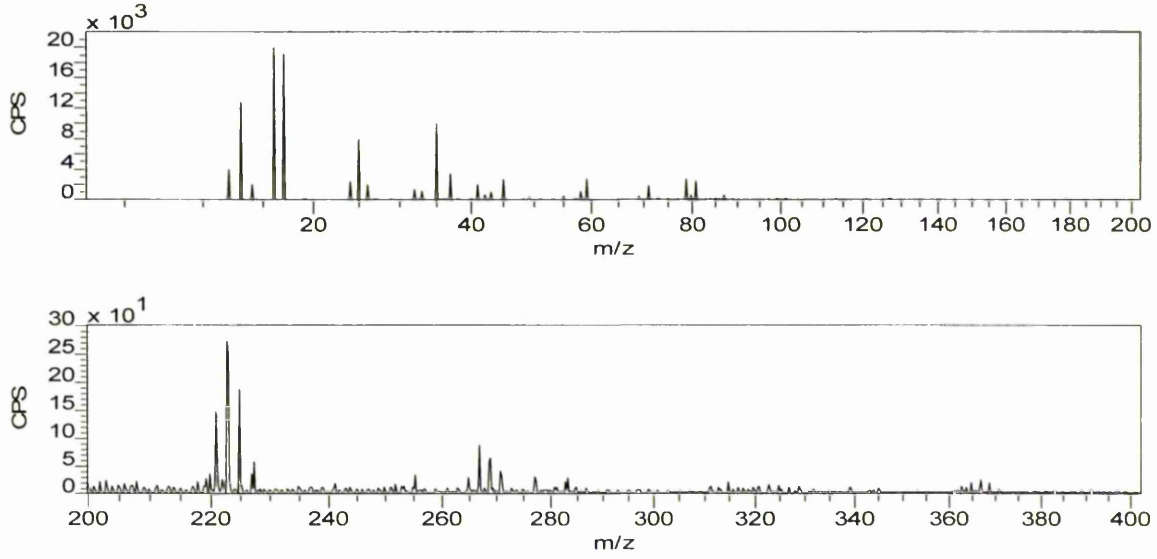

Positive ion ToF-SIMS spectrum of 'T-NP9 corroded Ag'

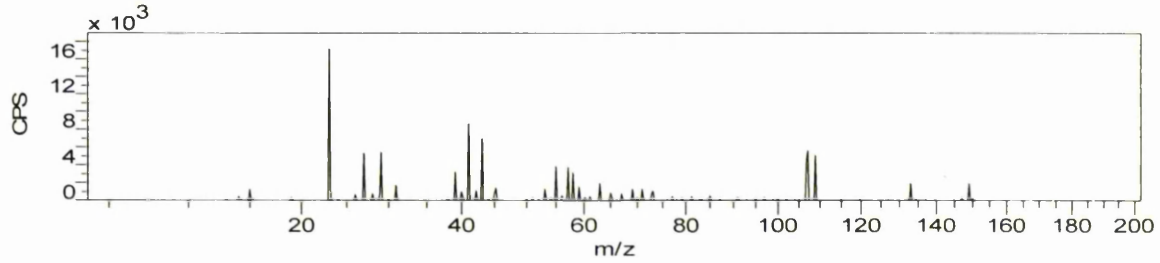

K.2. ToF-SIMS spectra of copper coupons

Negative ion ToF-SIMS spectrum of 'Untreated clean Cu'

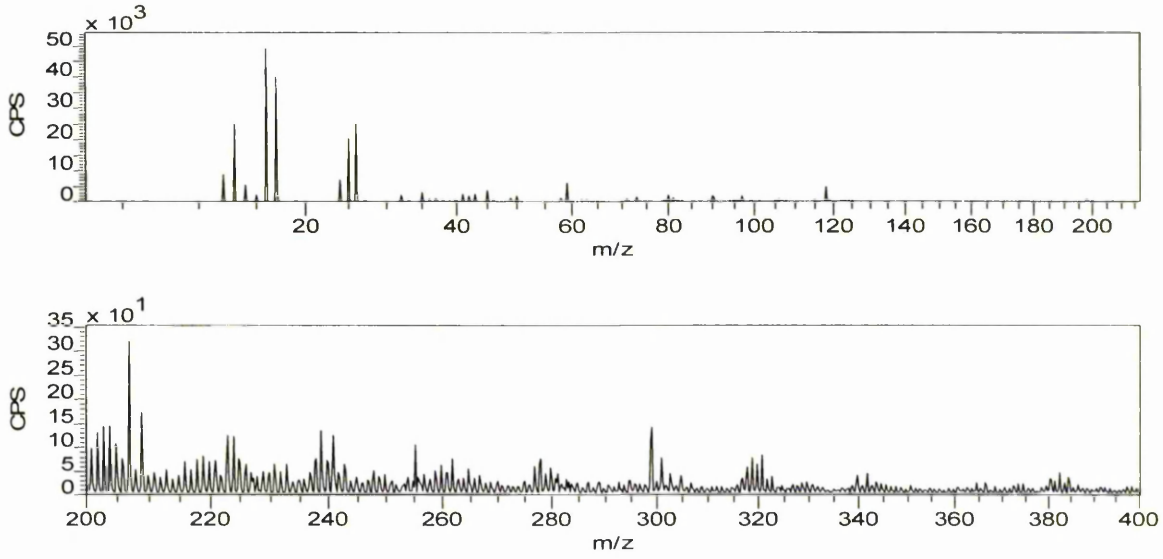

Positive ion ToF-SIMS spectrum of 'Untreated clean Cu'

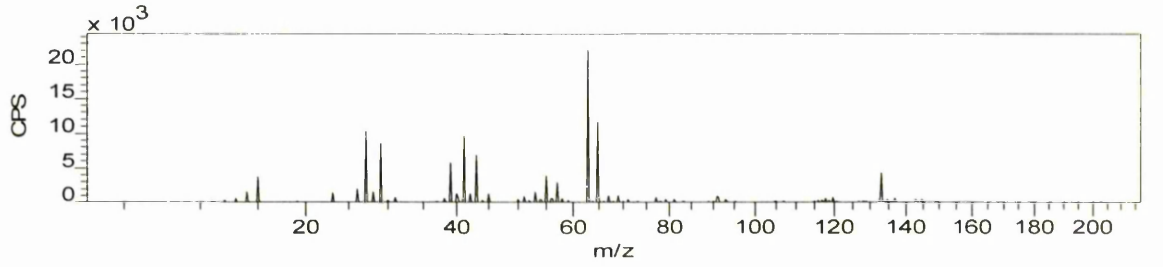

Negative ion ToF-SIMS spectrum of 'H_2O clean Cu'

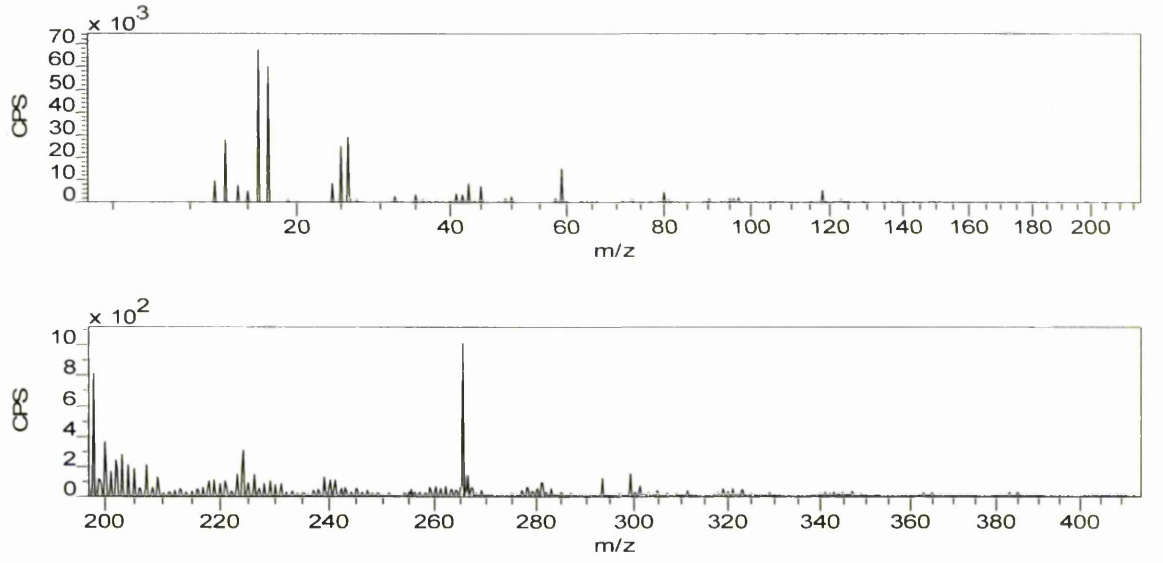

Positive ion ToF-SIMS spectrum of 'H_2O clean Cu'

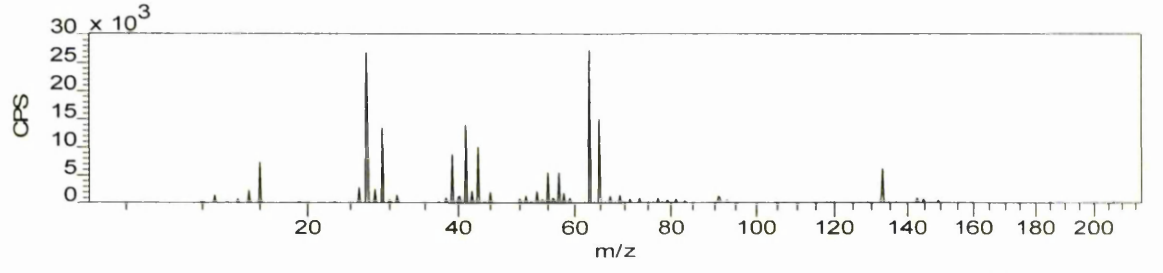

Negative ion ToF-SIMS spectrum of 'H_2O corroded Cu'

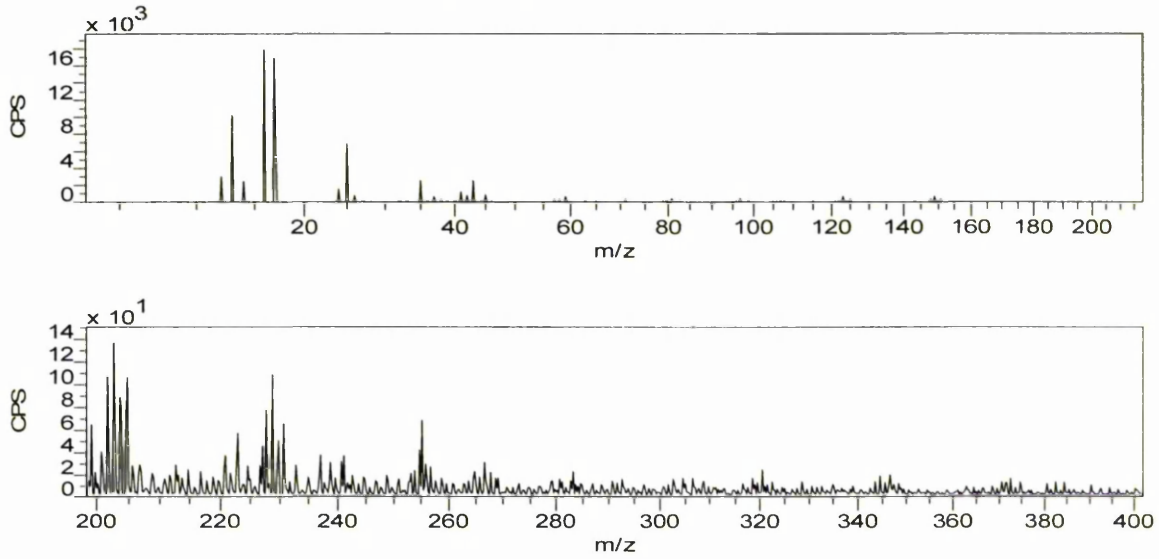

Positive ion ToF-SIMS spectrum of 'H_2O corroded Cu'

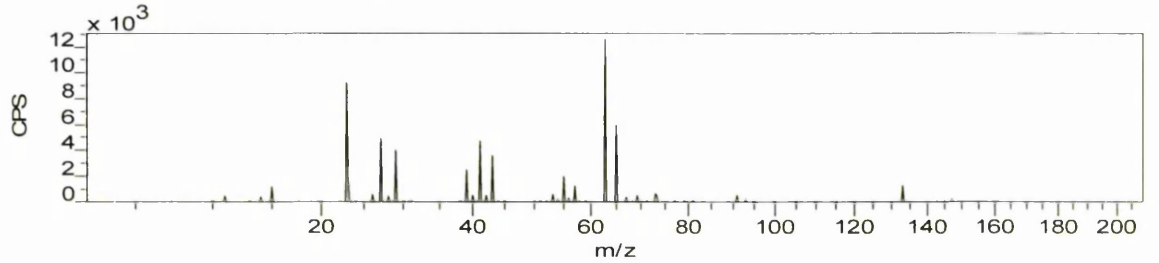

Negative ion ToF-SIMS spectrum of 'SDS 98% clean Cu'

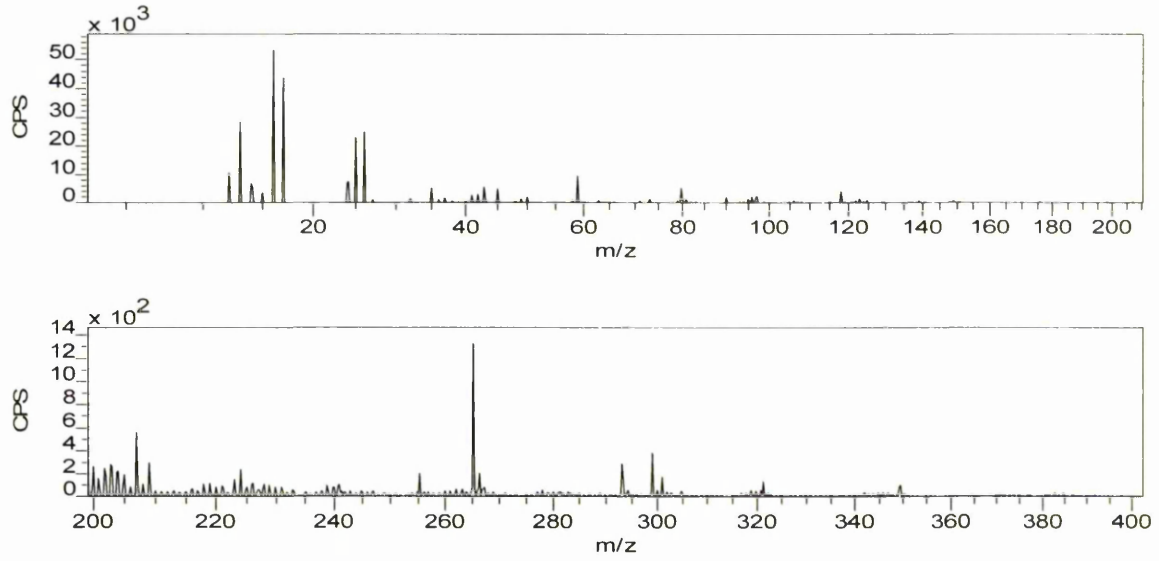

Positive ion ToF-SIMS spectrum of 'SDS 98% clean Cu'

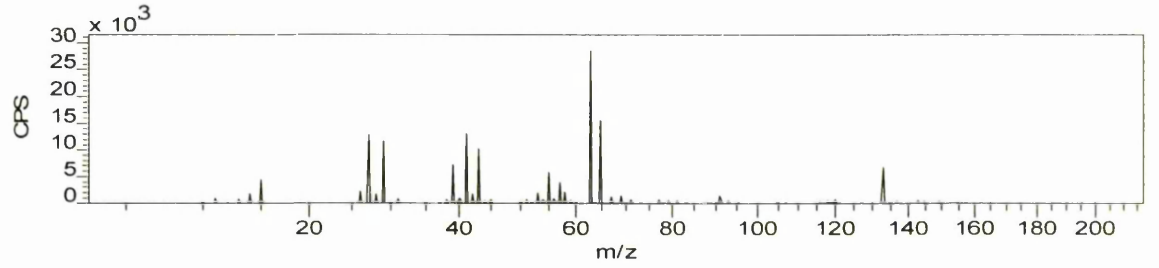

Negative ion ToF-SIMS spectrum of 'SDS 99% clean Cu'

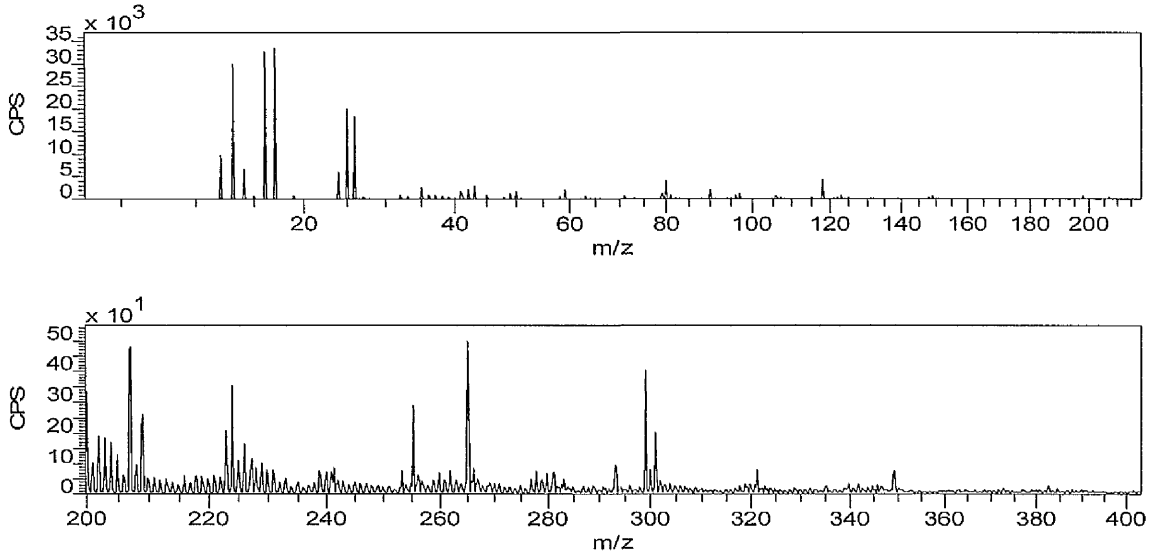

Positive ion ToF-SIMS spectrum of 'SDS 99% clean Cu'

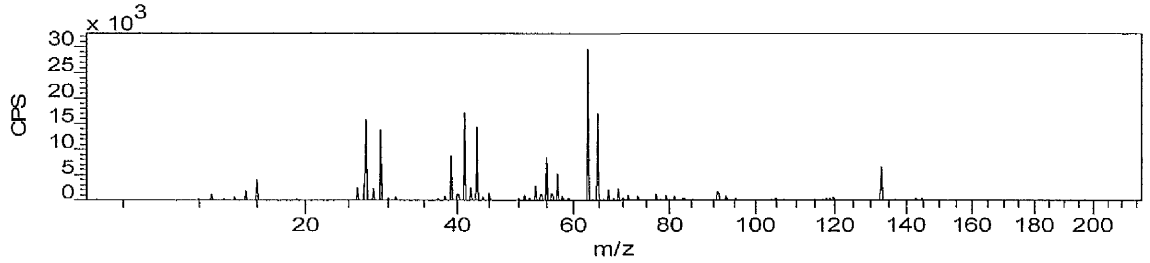

Negative ion ToF-SIMS spectrum of 'SDS 99% corroded Cu'

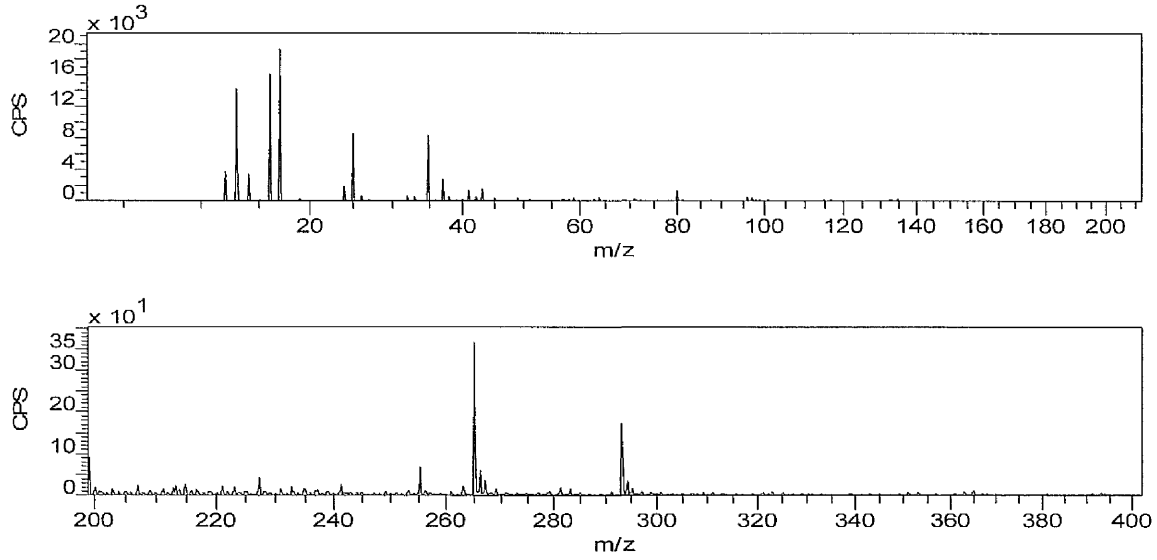

Positive ion ToF-SIMS spectrum of 'SDS 99% corroded Cu'

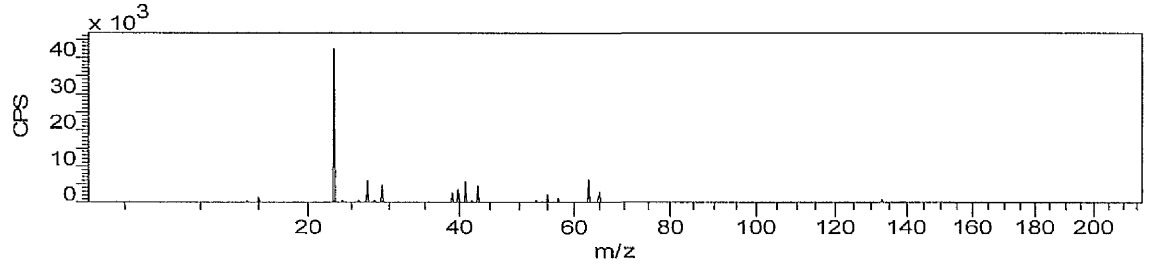

Negative ion ToF-SIMS spectrum of 'T-NP9 + SDS 99% clean Cu'

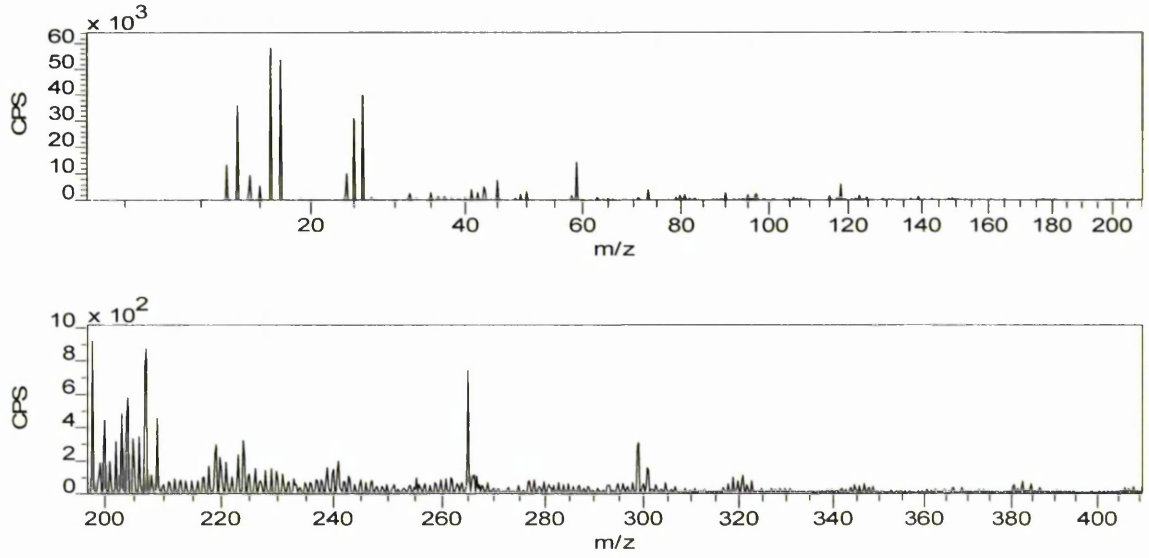

Positive ion ToF-SIMS spectrum of 'T-NP9 + SDS 99% clean Cu'

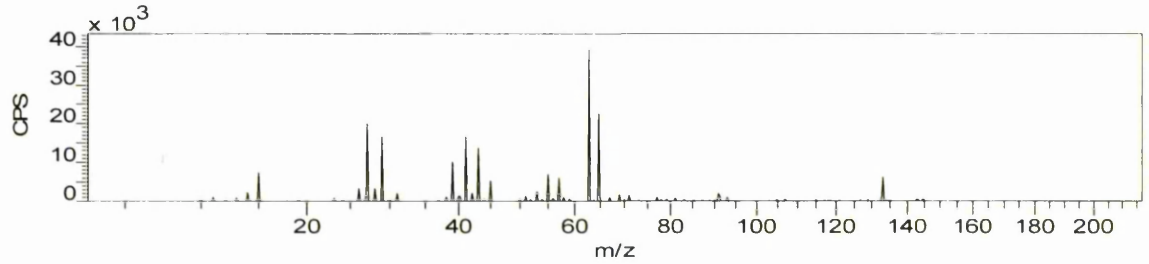

Negative ion ToF-SIMS spectrum of 'T-NP9 + SDS 99% corroded Cu'

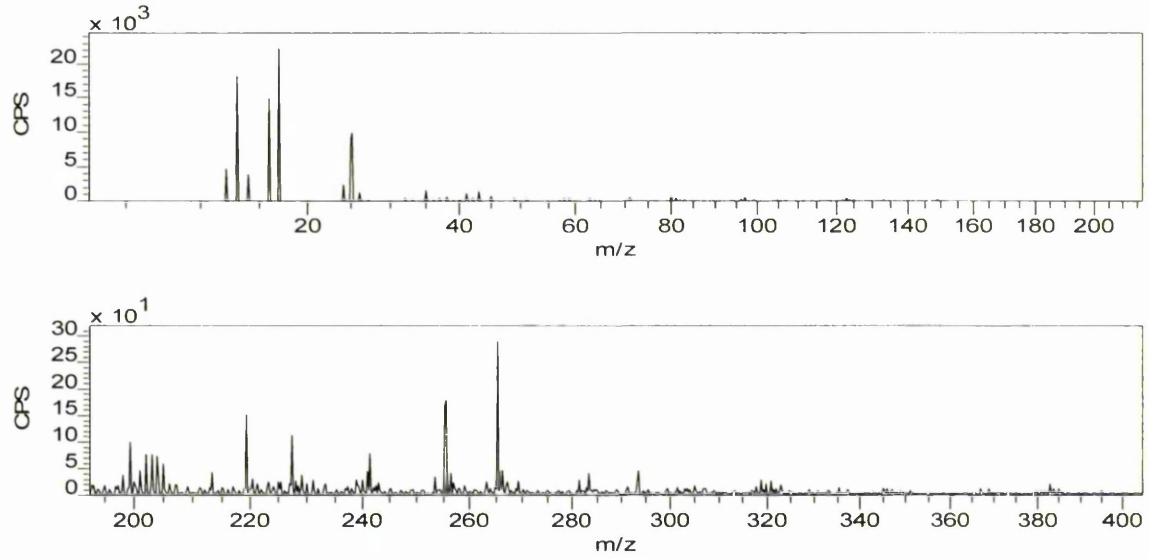

Positive ion ToF-SIMS spectrum of 'T-NP9 + SDS 99% corroded Cu'

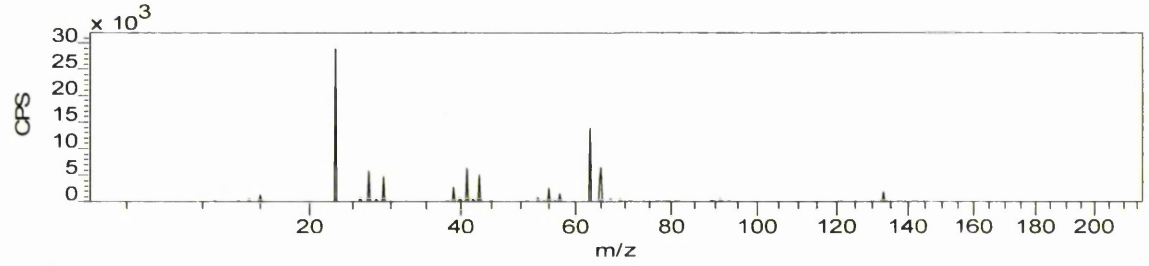

Negative ion ToF-SIMS spectrum of 'T-NP9 clean Cu'

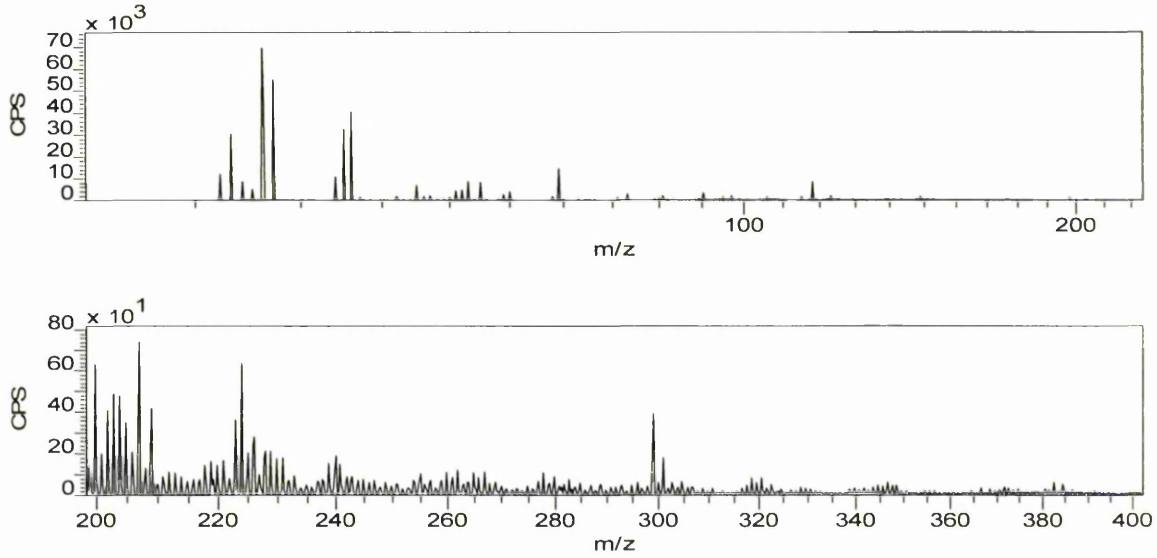

Positive ion ToF-SIMS spectrum of 'T-NP9 clean Cu'

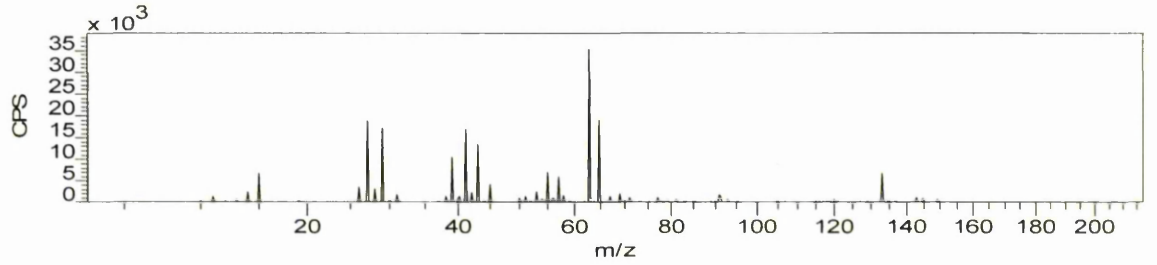

Negative ion ToF-SIMS spectrum of 'T-NP9 corroded Cu'

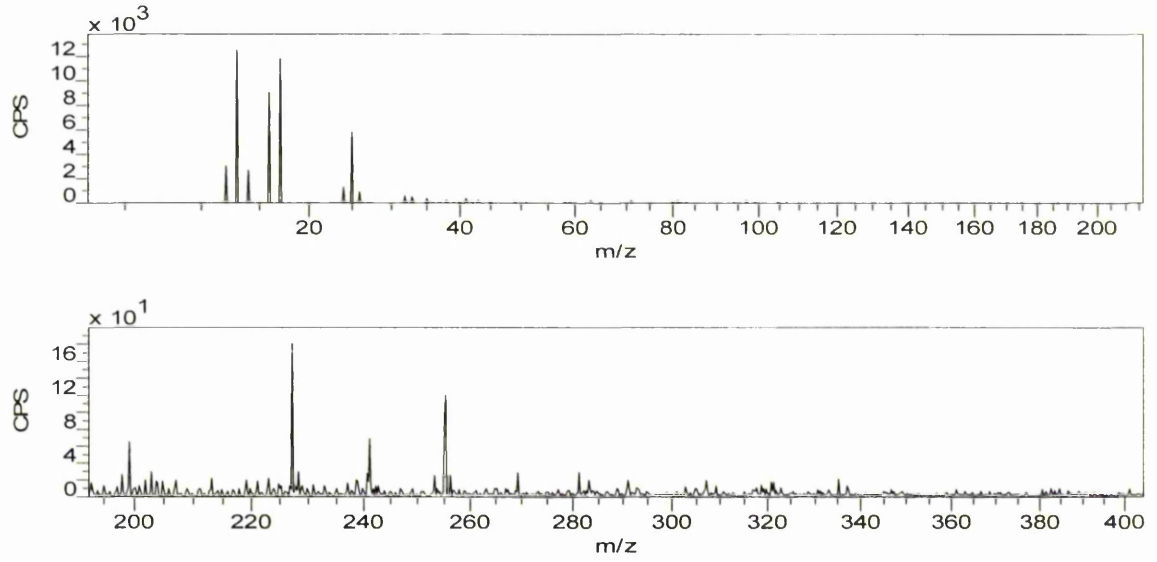

Positive ion ToF-SIMS spectrum of 'T-NP9 corroded Cu'

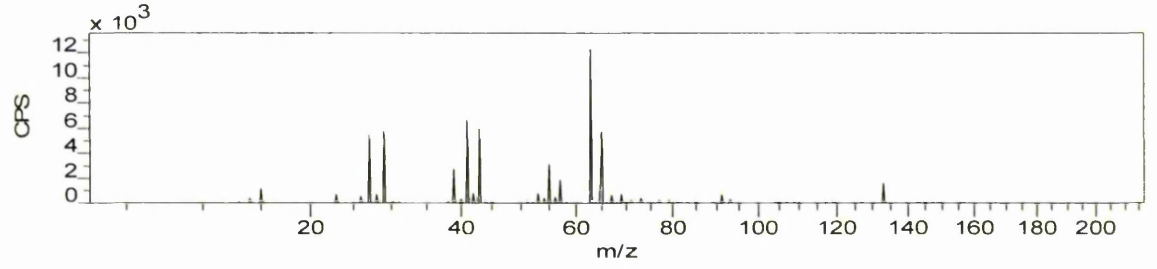

K.3. ToF-SIMS spectra of metal threads

Negative ion ToF-SIMS spectrum of 'Untreated Model'

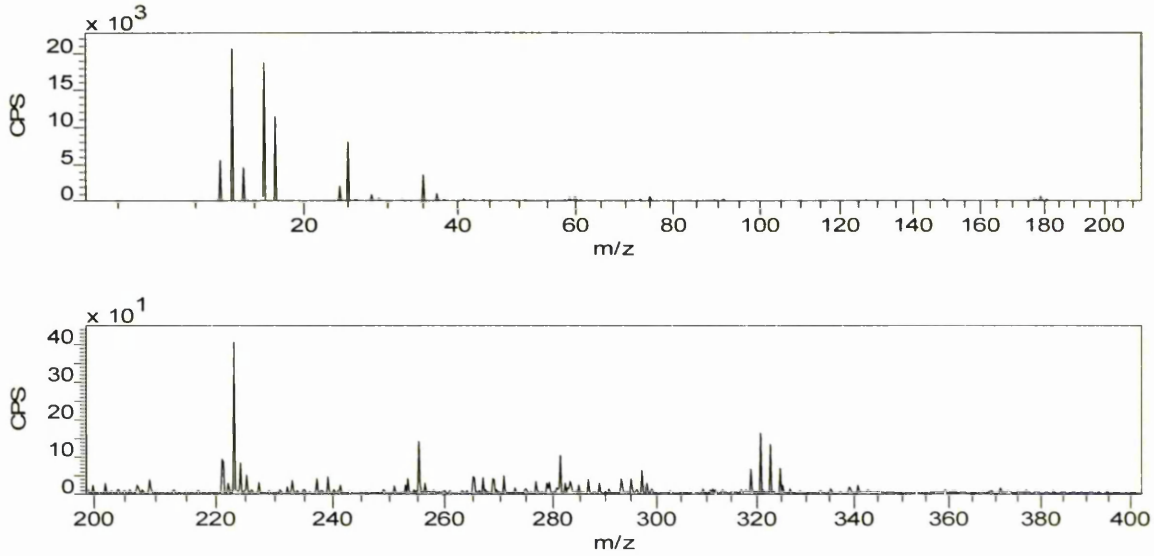

Positive ion ToF-SIMS spectrum of 'Untreated Model'

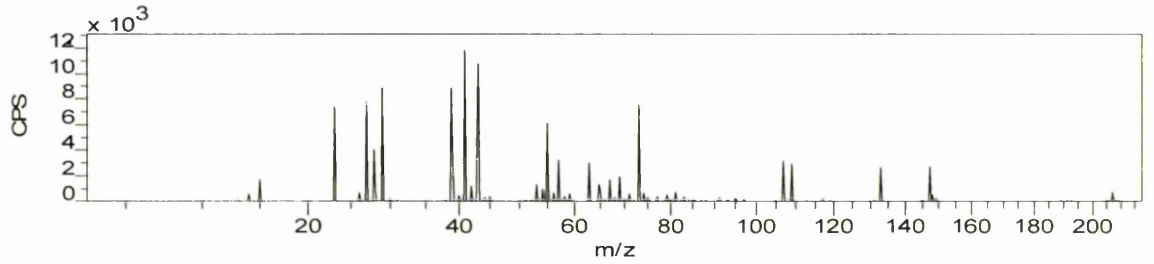

Negative ion ToF-SIMS spectrum of 'SDS 99% Model'

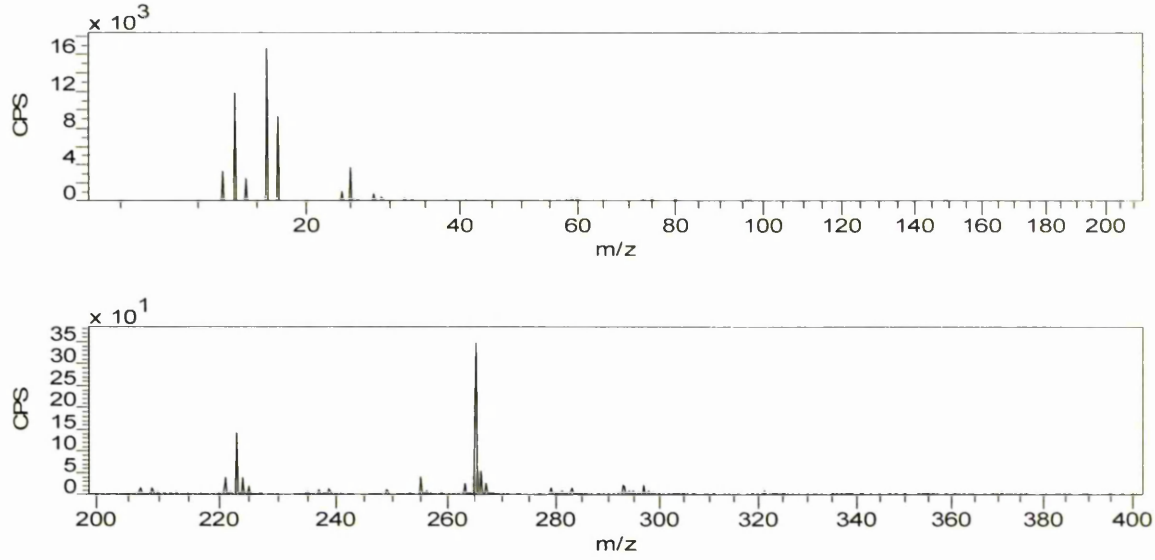

Positive ion ToF-SIMS spectrum of 'SDS 99% Model'

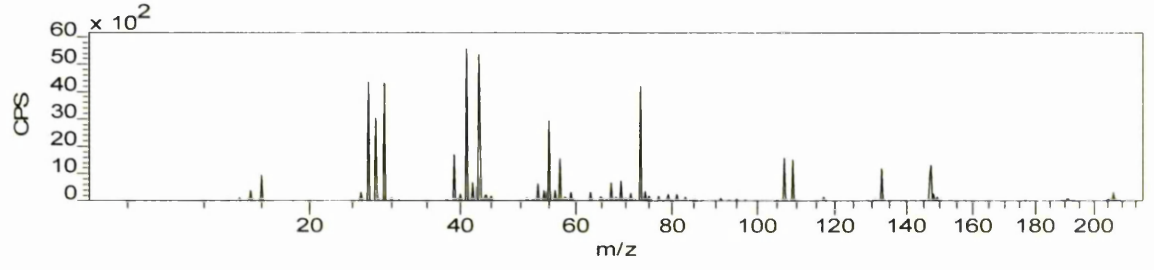

Negative ion ToF-SIMS spectrum of 'T-NP9 + SDS 99% Model'

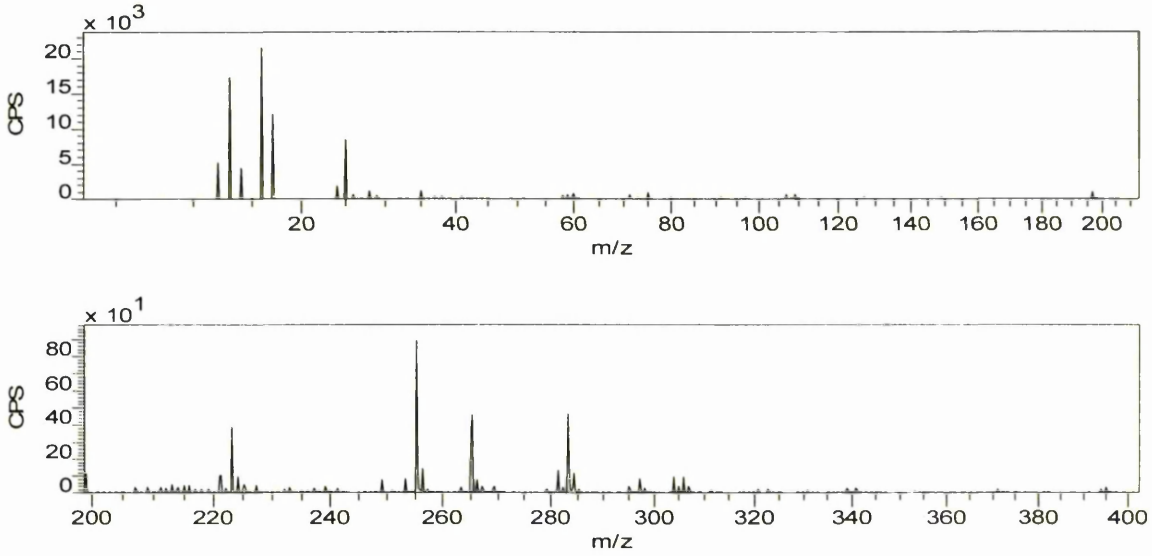

Positive ion ToF-SIMS spectrum of 'T-NP9 + SDS 99% Model'

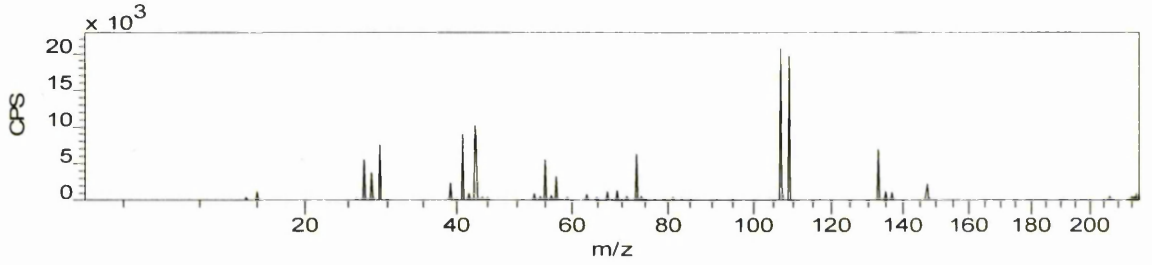

Negative ion ToF-SIMS spectrum of 'T-NP9 Model'

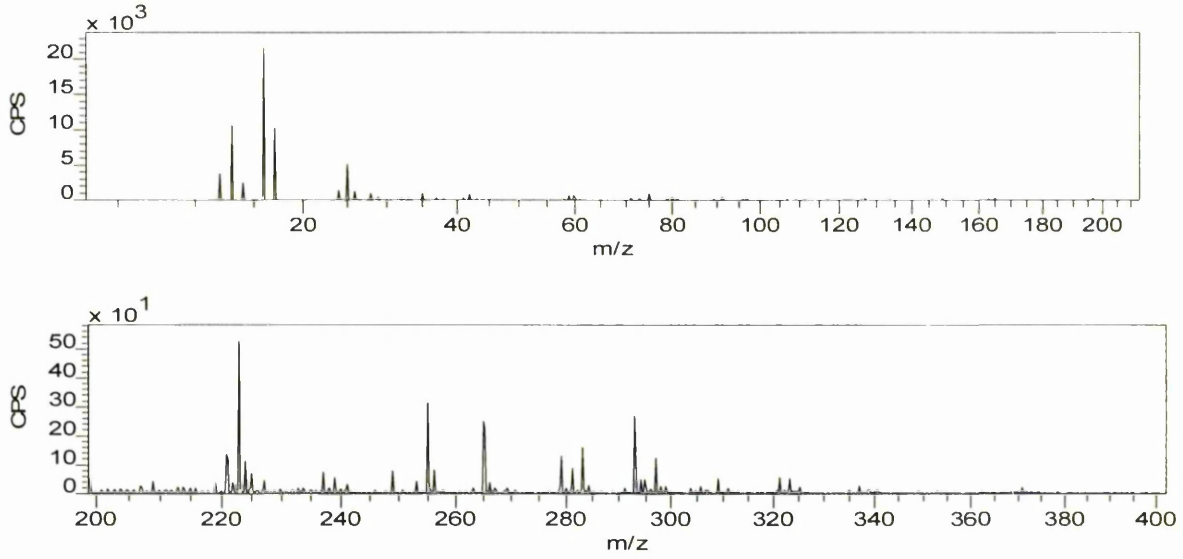

Positive ion ToF-SIMS spectrum of 'T-NP9 Model'

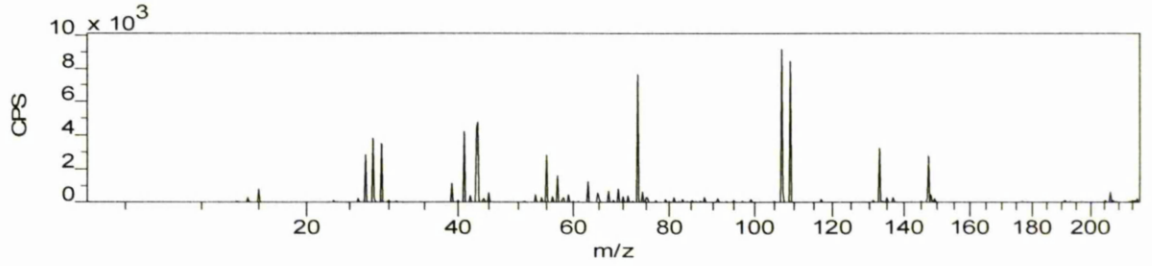

Negative ion ToF-SIMS spectrum of 'Untreated PNM1_24'

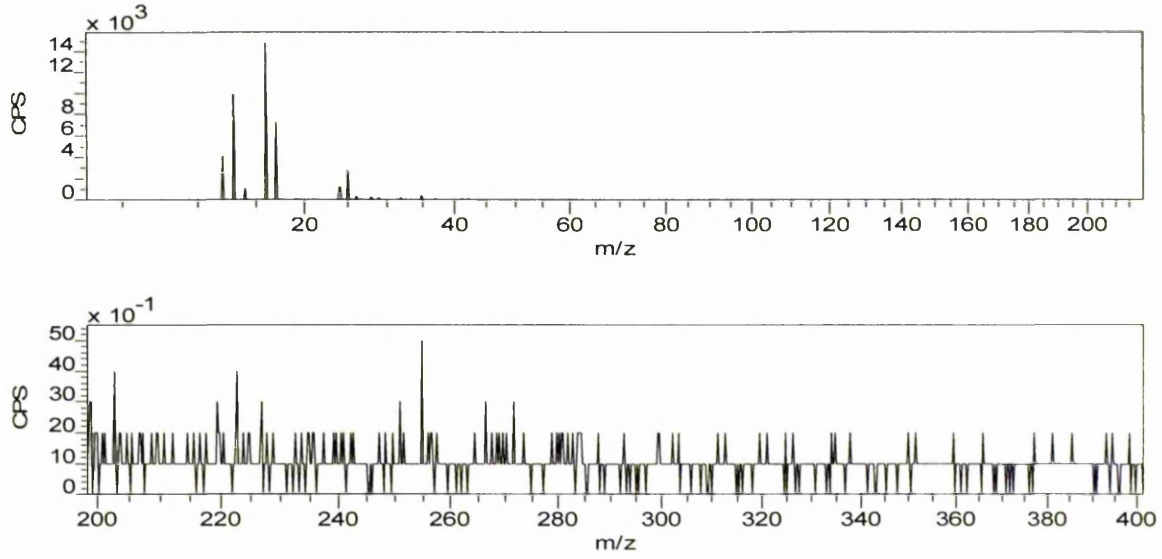

Positive ion ToF-SIMS spectrum of 'Untreated PNM1_24'

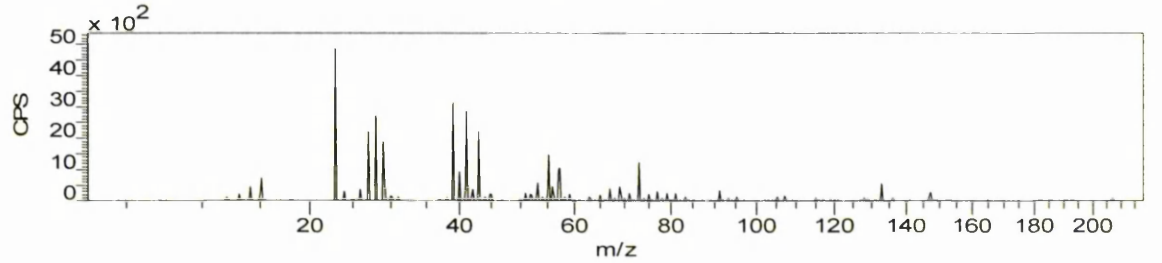

Negative ion ToF-SIMS spectrum of 'T-NP9 + SDS 99% PNM1_24'

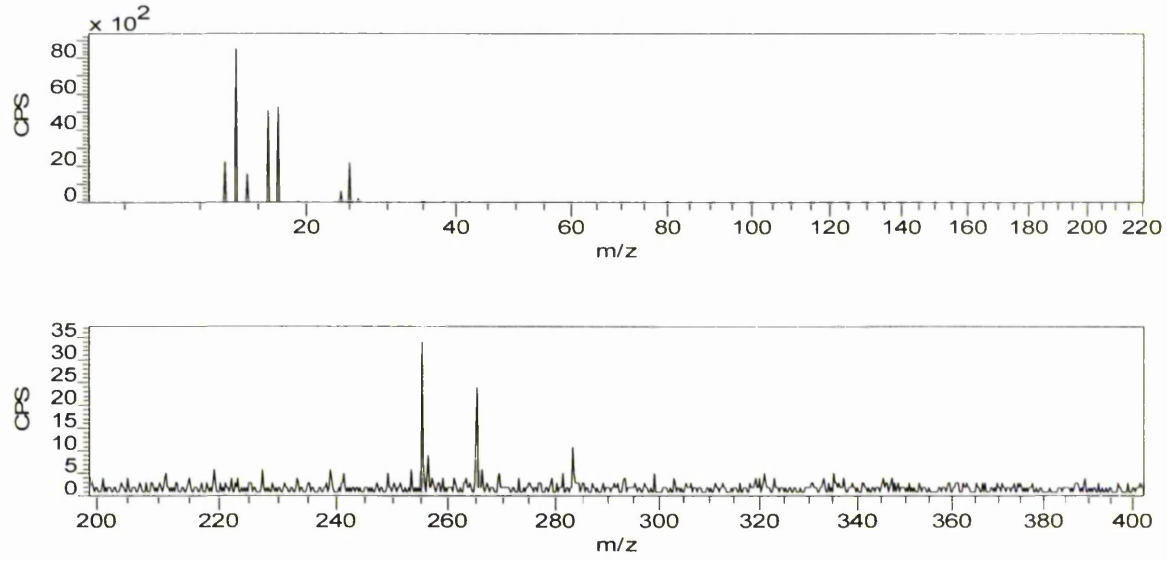

Positive ion ToF-SIMS spectrum of 'T-NP9 + SDS 99% PNM1_24'

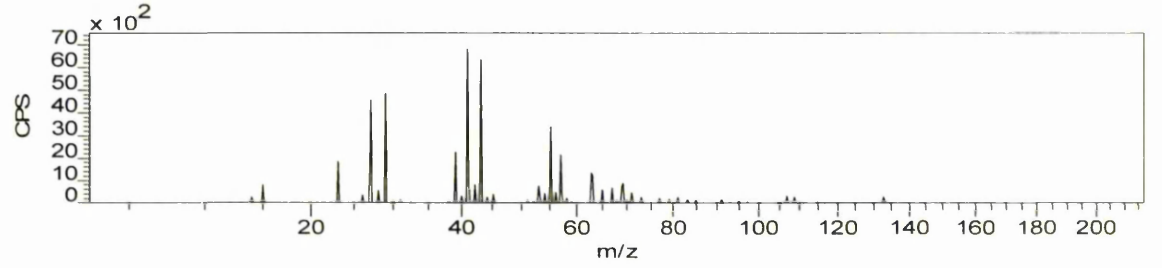

Negative ion ToF-SIMS spectrum of 'T-NP9 PNM1_24'

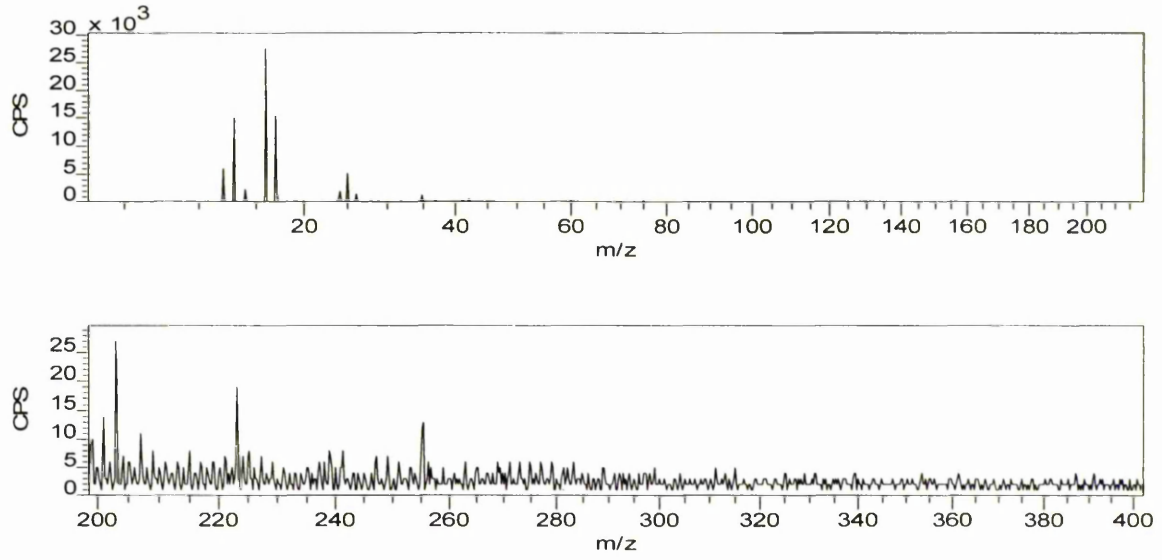

Positive ion ToF-SIMS spectrum of 'T-NP9 PNM1_24'

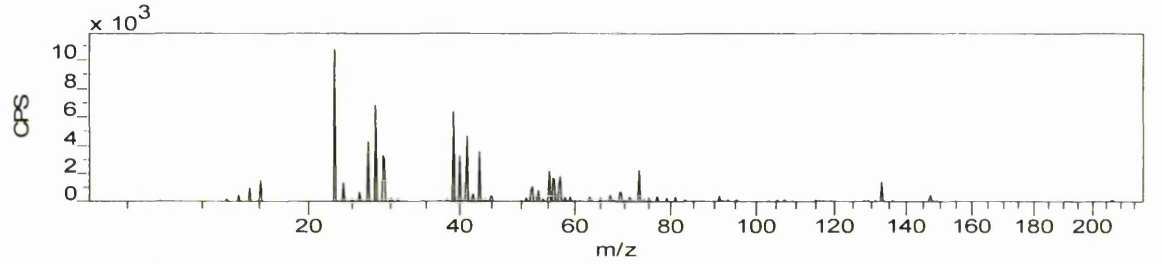

Negative ion ToF-SIMS spectrum of 'Untreated PNM2_17'

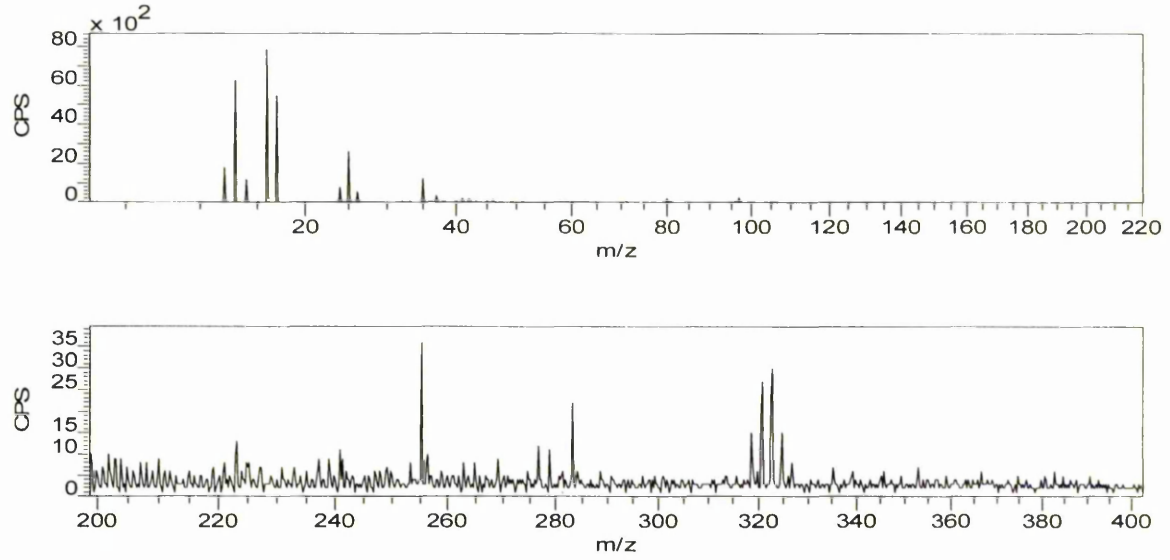

Positive ion ToF-SIMS spectrum of 'Untreated PNM2_17'

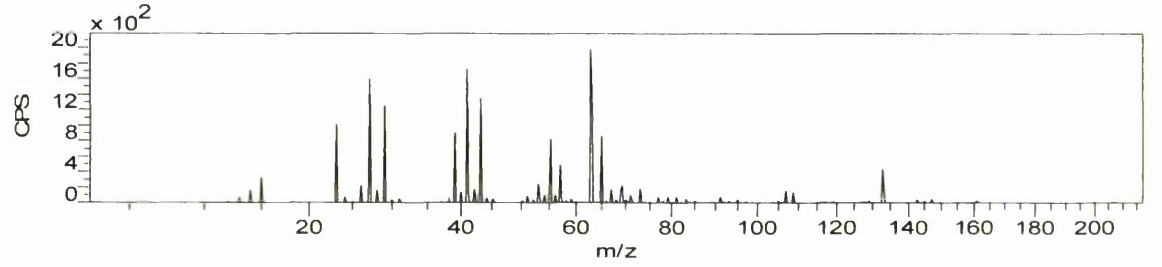

Negative ion ToF-SIMS spectrum of 'SDS 99% PNM2_17'

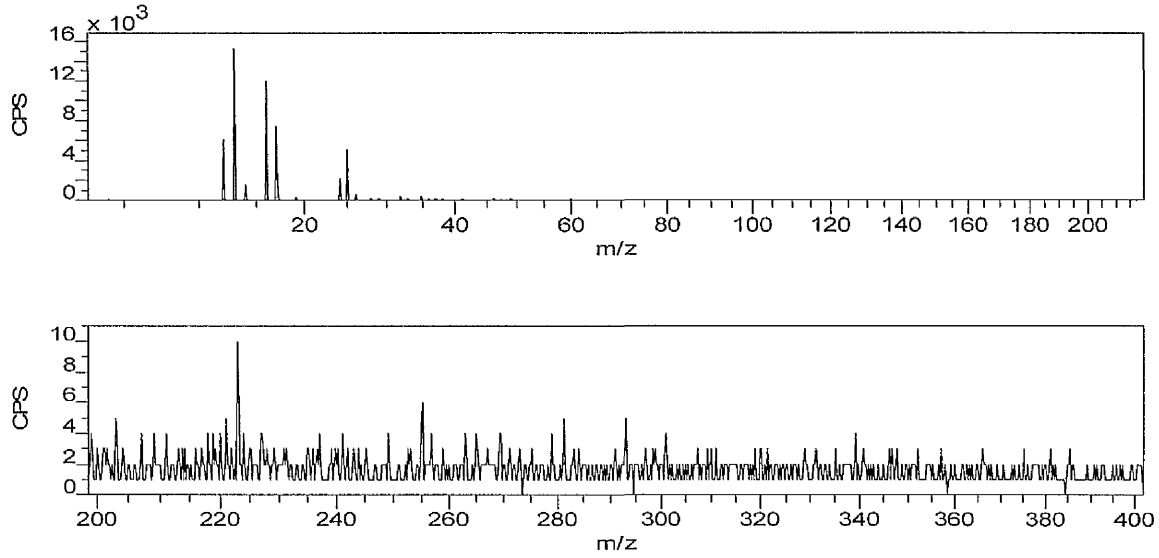

Positive ion ToF-SIMS spectrum of 'SDS 99% PNM2_17'

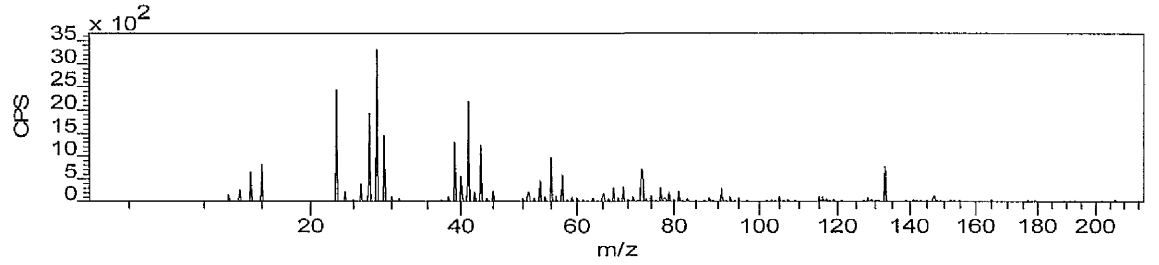

Negative ion ToF-SIMS spectrum of 'T-NP9 + SDS 99% PNM2_17'

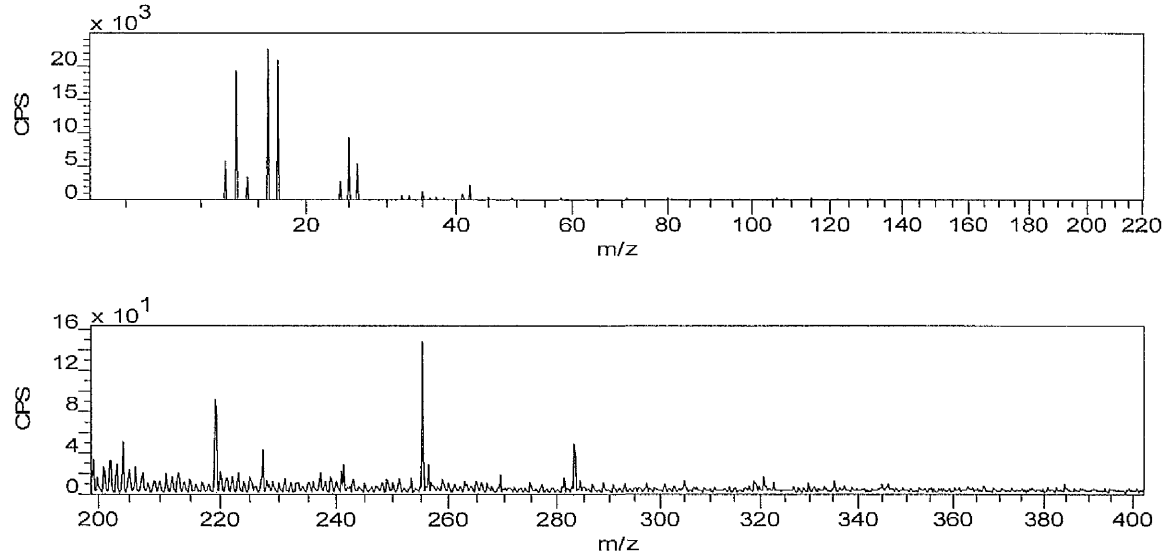

Positive ion ToF-SIMS spectrum of 'T-NP9 + SDS 99% PNM2_17'

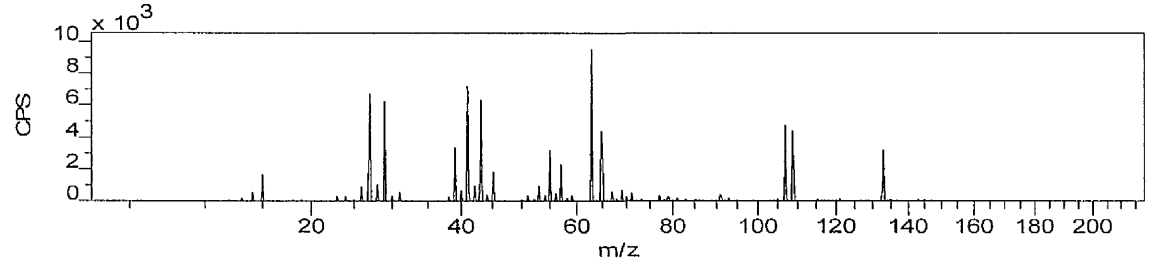

Negative ion ToF-SIMS spectrum of 'T-NP9 PNM2_17'

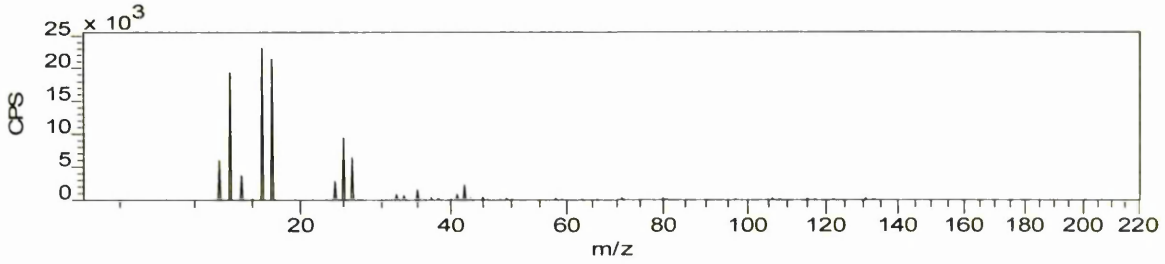

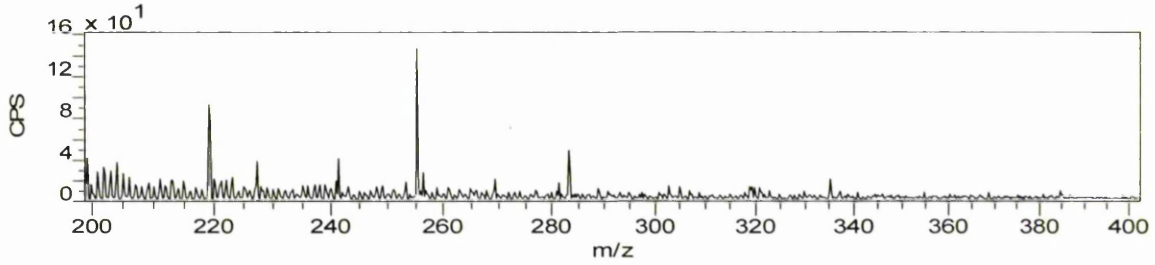

Positive ion ToF-SIMS spectrum of 'T-NP9 PNM2_17'

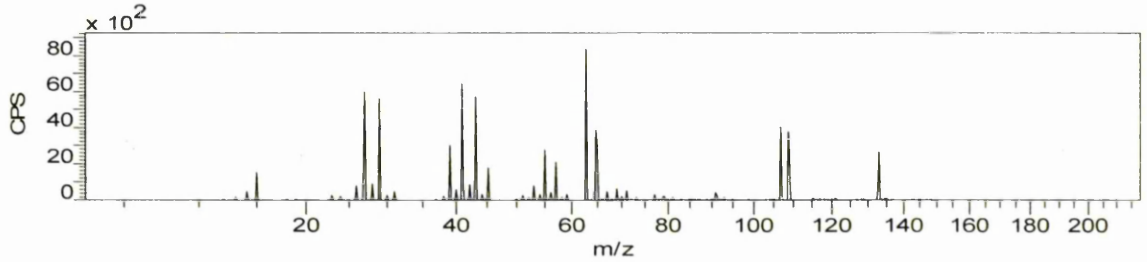

Negative ion ToF-SIMS spectrum of 'Untreated PNM5_24'

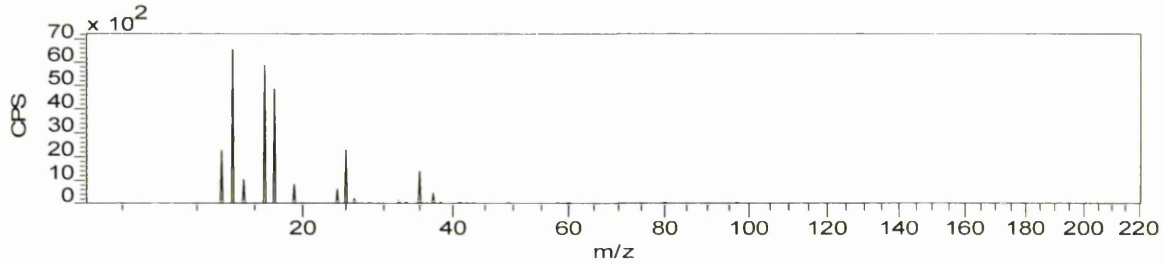

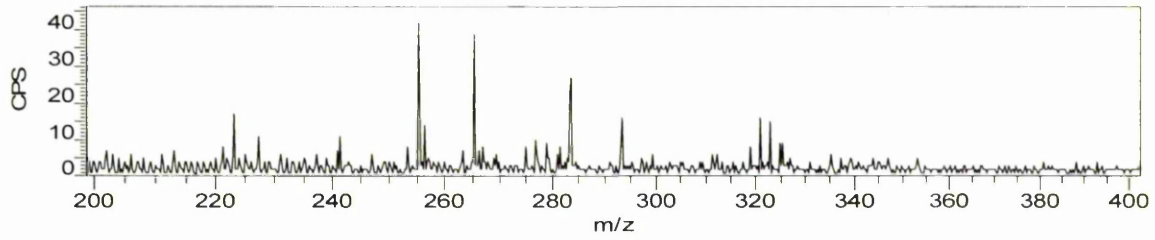

Positive ion ToF-SIMS spectrum of 'Untreated PNM5_24'

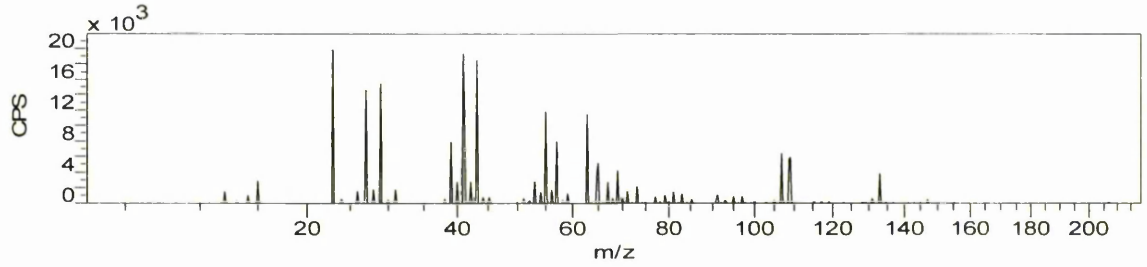

Negative ion ToF-SIMS spectrum of 'SDS 99% PNM5_24'

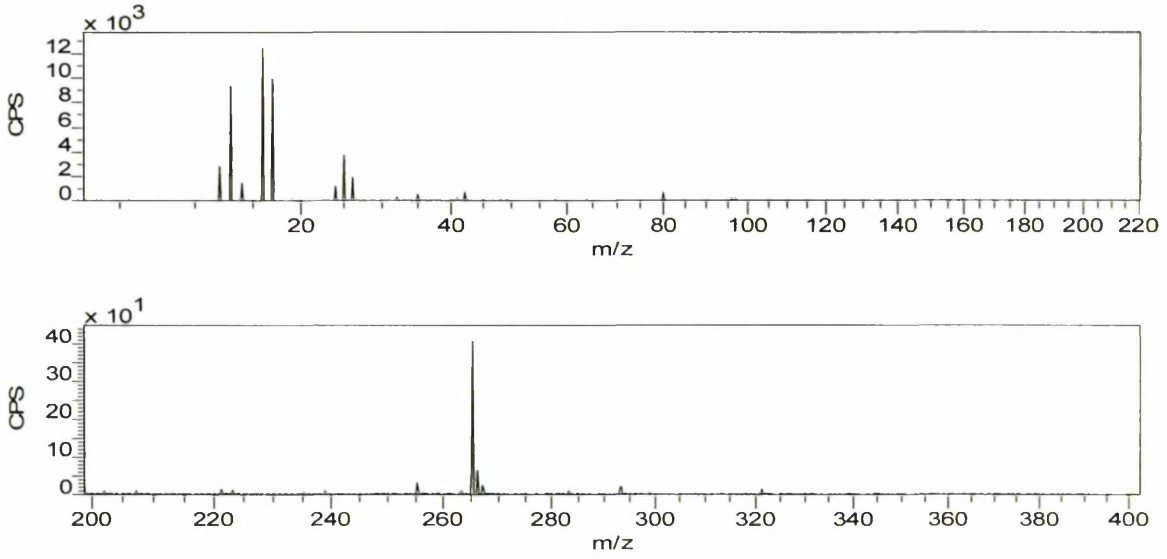

Positive ion ToF-SIMS spectrum of 'SDS 99% PNM5_24'

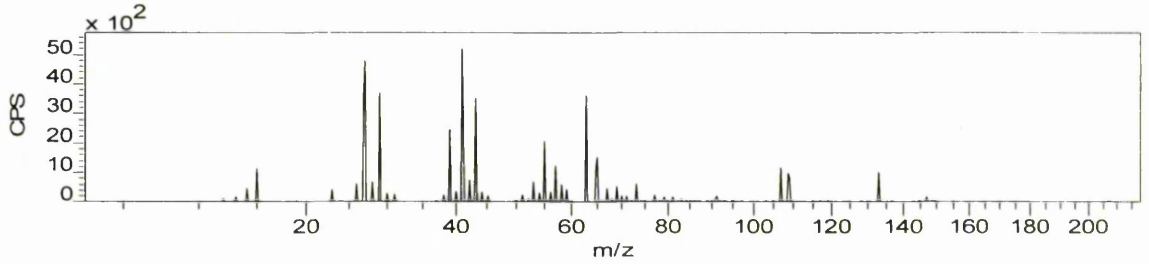

Negative ion ToF-SIMS spectrum of 'T-NP9 + SDS 99% PNM5_24'

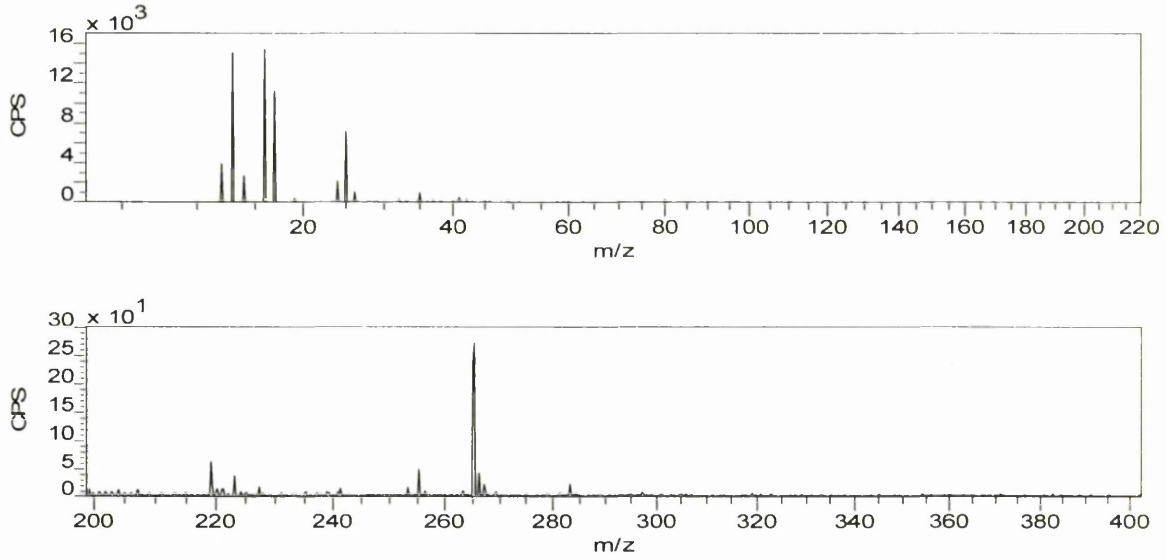

Positive ion ToF-SIMS spectrum of 'T-NP9 + SDS 99% PNM5_24'

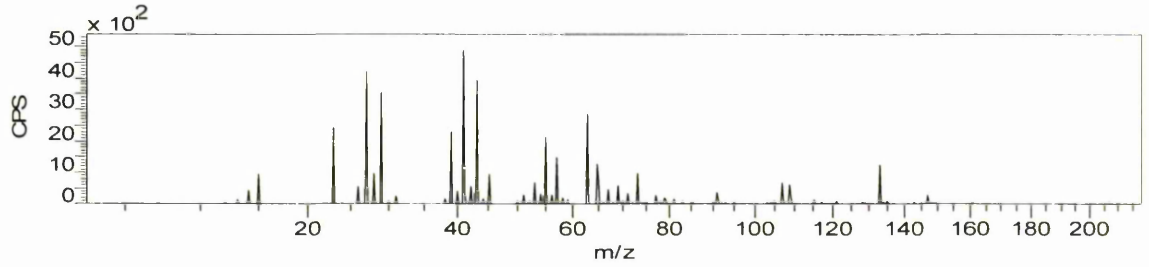

Negative ion ToF-SIMS spectrum of 'T-NP9 PNM5_24'

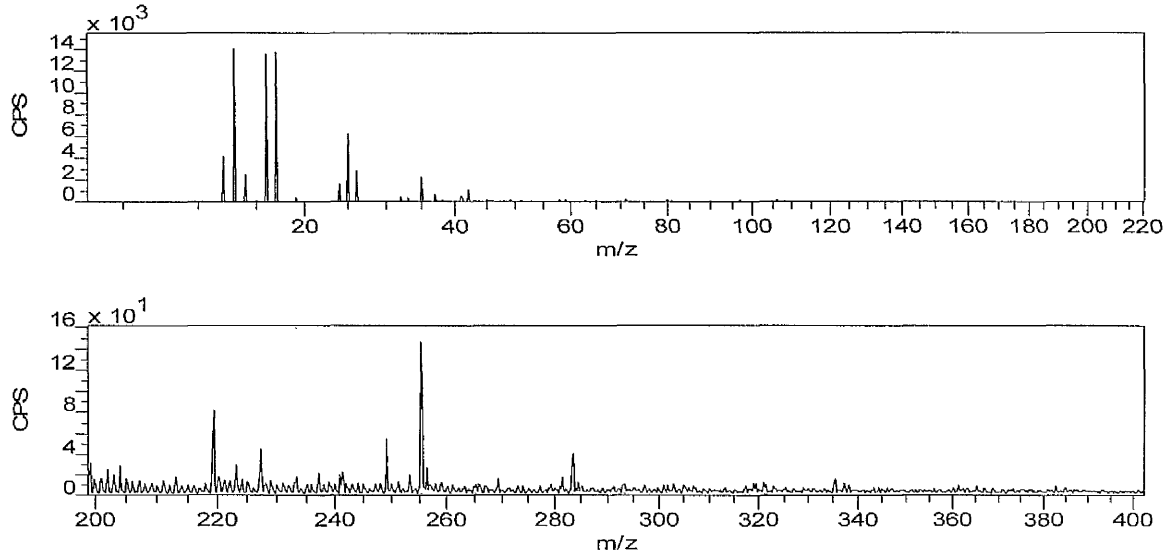

Positive ion ToF-SIMS spectrum of 'T-NP9 PNM5_24'